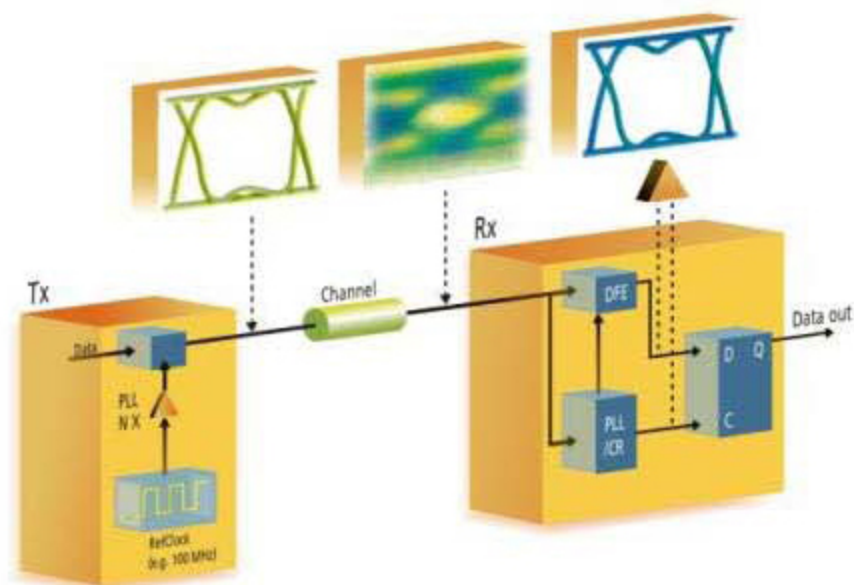


Jitter, Noise, and Signal Integrity at High-Speed



Mike Peng Li

Prentice Hall Modern Semiconductor Design Series
Prentice Hall Signal Integrity Library

Book: Jitter, Noise, and Signal Integrity at High-Speed

No part of any chapter or book may be reproduced or transmitted in any form by any means without the prior written permission for reprints and excerpts from the publisher of the book or chapter. Redistribution or other use that violates the fair use privilege under U.S. copyright laws (see 17 USC107) or that otherwise violates these Terms of Service is strictly prohibited. Violators will be prosecuted to the full extent of U.S. Federal and Massachusetts laws.

Information Theory Computer Science Mike Peng Li Prentice Hall Jitter, Noise, and Signal Integrity at High-Speed

Copyright

An Imprint of Pearson Education

Many of the designations used by manufacturers and sellers to distinguish their products are claimed as trademarks. Where those designations appear in this book, and the publisher was aware of a trademark claim, the designations have been printed with initial capital letters or in all capitals.

The author and publisher have taken care in the preparation of this book, but they make no expressed or implied warranty of any kind and assume no responsibility for errors or omissions. No liability is assumed for incidental or consequential damages in connection with or arising from the use of the information or programs contained herein.

The publisher offers excellent discounts on this book when ordered in quantity for bulk purchases or special sales, which may include electronic versions and/or custom covers and content particular to your business, training goals, marketing focus, and branding interests. For more information, please contact:

U.S. Corporate and Government Sales
800-382-3419
corpsales@pearsontechgroup.com

For sales outside the United States, please contact:

International Sales
international@pearsoned.com

Library of Congress Cataloging-in-Publication Data:

Li, Mike Peng.

Jitter, noise, and signal integrity at high-speed / Mike Peng Li.

p. cm.

ISBN 0-13-242961-6 (hardback : alk. paper) 1. Telecommunication—Traffic. 2. High performance computing. I. Title.

TK5102.985.L56 2007

621.382—dc22

2007036914

Copyright © 2008 Pearson Education, Inc.

All rights reserved. Printed in the United States of America. This publication is protected by copyright, and permission must be obtained from the publisher prior to any prohibited reproduction, storage in a retrieval system, or transmission in any form or by any means, electronic, mechanical, photocopying, recording, or likewise. For information regarding permissions, write to:

Pearson Education, Inc.
Rights and Contracts Department
501 Boylston Street, Suite 900
Boston, MA 02116

ISBN-13: 978-0-13-242961-0

Text printed in the United States on recycled paper at Courier in Westford, Massachusetts.

First printing: November 2007

Credits

Editor-in-Chief

Mark Taub

Publishing Partner

Bernard Goodwin

Managing Editor

Gina Kanouse

Project Editor

Jovana San Nicolas-Shirley

Copy Editor

Gayle Johnson

Indexer

Lisa Stumpf

Proofreader

Water Crest Publishing

Editorial Assistant

Michelle Housley

Cover Designer

Louisa Adair

Composition

ContentWorks

Graphics

Jake McFarland

Laura Robbins

Dedication

To Mercia, Eric, George, and my parents.

Book: Jitter, Noise, and Signal Integrity at High-Speed

No part of any chapter or book may be reproduced or transmitted in any form by any means without the prior written permission for reprints and excerpts from the publisher of the book or chapter. Redistribution or other use that violates the fair use privilege under U.S. copyright laws (see 17 USC107) or that otherwise violates these Terms of Service is strictly prohibited. Violators will be prosecuted to the full extent of U.S. Federal and Massachusetts laws.

Information Theory Computer Science Mike Peng Li Prentice Hall Jitter, Noise, and Signal Integrity at High-Speed

Prentice Hall Modern Semiconductor Design Series

James R. Armstrong and F. Gail Gray

VHDL Design Representation and Synthesis

Mark Gordon Arnold

Verilog Digital Computer Design: Algorithms into Hardware

Jayaram Bhasker

A VHDL Primer, Third Edition

Mark D. Birnbaum

Essential Electronic Design Automation (EDA)

Eric Bogatin

Signal Integrity: Simplified

Douglas Brooks

Signal Integrity Issues and Printed Circuit Board Design

Ken Coffman

Real World FPCA Design with Verilog

Alfred Crouch

Design-for-Test for Digital IC's and Embedded Core Systems

Dennis Derickson and Marcus Müller (Editors)

Digital Communications Test and Measurement

Greg Edlund

Timing Analysis and Simulation for Signal Integrity Engineers

Daniel P. Foty

MOSFET Modeling with SPICE: Principles and Practice

Tom Granberg

Handbook of Digital Techniques for High-Speed Design

Nigel Horspool and Peter Gorman

The ASIC Handbook

William K. Lam

Hardware Design Verification: Simulation and Formal Method-Based Approaches

Mike Peng Li
Jitter, Noise, and Signal Integrity at High-Speed

Farzad Nekoogar and Faranak Nekoogar
From ASICs to SOCs: A Practical Approach

Farzad Nekoogar
Timing Verification of Application-Specific Integrated Circuits (ASICs)

Samir Palnitkar
Design Verification with

David Pellerin and Scott Thibault
Practical FPCA Programming in C

Christopher T. Robertson
Printed Circuit Board Designer's Reference: Basics

Chris Rowen
Engineering the Complex SOC

Madhavan Swaminathan and A. Ege Engin
Power Integrity Modeling and Design for Semiconductors and Systems

Wayne Wolf
FPCA-Based System Design

Wayne Wolf
Modern VLSI Design: System-on-Chip Design, Third Edition

Bob Zeidman
Verilog Designer's Library

Book: Jitter, Noise, and Signal Integrity at High-Speed

No part of any chapter or book may be reproduced or transmitted in any form by any means without the prior written permission for reprints and excerpts from the publisher of the book or chapter. Redistribution or other use that violates the fair use privilege under U.S. copyright laws (see 17 USC107) or that otherwise violates these Terms of Service is strictly prohibited. Violators will be prosecuted to the full extent of U.S. Federal and Massachusetts laws.

Information Theory Computer Science Mike Peng Li Prentice Hall Jitter, Noise, and Signal Integrity at High-Speed

Preface

Moore's Law continues to guide the semiconductor technology road map. As the feature size of integrated circuits (ICs) reaches 65 nm today, and moves to 45, 32, and 22 nm in the near future, it will give IC systems more functionality and data-handling capability. A complex and functionality-rich system needs fast input/output (I/O) to be efficient. As a result, we see that the I/O speed keeps increasing as the number of transistors keeps increasing for advanced IC systems.

Although decreasing feature size and increasing I/O speed enable better system capability and performance, they also introduce technological challenges. One of the most important challenges is jitter as I/O speed increases, because the unit interval (UI), the total available jitter budget for a link, must decrease accordingly to ensure a reasonable bit error rate (BER) for a link system. Another very important challenge as the feature size decreases is to constrain the power density and power consumption within limits, implying that low-power design is necessary. As a result, noise becomes a critical challenge, because it needs to be reduced for low-power/low-voltage signals to maintain a reasonable signal-to-noise ratio (SNR). When the same channel material is maintained while the data rate increases, the data signal is attenuated and degraded more due to the same loss channel property and much-increased high-frequency contents associated with the higher data rate. The signal integrity (SI) due to signal attenuation and degradation is manifested by deterministic jitter and noise. Jitter, noise, and SI challenges get magnified when I/O link data rate increase is achieved by using the same channel material, a common approach used by most of the high-speed I/O standards for cost-effective considerations.

Today, most high-speed I/Os are designed around 5 to 6 Gbps rates for computer-centric applications where copper-based channels are used the most, including standards such as PCI Express II (5 Gbps), Serial ATA III (6 Gbps), and FB DIMM I (3.2, 4.0, and 4.8 Gbps). The next generation of those standards will likely double in data rate and will be at 8 to 12 Gbps rates. For network-centric applications, most current designs are at 8 to 10 Gbps rates, such as Fibre Channel 8x (8.5 Gbps), Gigabit Ethernet (GBE) 10 x (10 Gbps), and SONET OC-192 (10 Gbps), where optical fiber-based channels are used the most. The next generation of network I/O link will likely double or quadruple to 17 to 40 Gbps. At 10 Gbps, the UI is 100 ps, and at 40 Gbps, the UI is only 25 ps. To maintain a good BER (10^{-12}), the random jitter in I/O links at those data rates has to be in sub-ps or less, and that is a very daunting and challenging task. It is conceivable that, in the future, the jitter, noise, and SI challenges will become even harder at higher data rates.

In the past 20 years or so, many books have been published on signal integrity. However, the coverage of jitter, noise, and BER is rather brief and narrow in those books. Only two books have been dedicated to jitter, but that was 15 to 17 years ago, and the contents are outdated in comparison with the today's knowledge and understanding of jitter, noise, and SI.

Significant progress had created new theories and algorithms for in jitter, noise, and signal integrity in the past ten years. As far as jitter theorems and analysis, jitter components such as deterministic jitter (DJ) and random jitter (RJ) and associated math models have been developed as a better metric for jitter quantification. On the jitter-tracking part, jitter transfer function has been used extensively to determine outputs and tolerances for jitter, noise, and signaling quantitatively. Statistical signal analysis methods based on probability density function (PDF), cumulative distribution function (CDF), and the corresponding convolution operation are replacing the conventional simple, unsophisticated, and less accurate peak-to-peak and RMS metrics. Linear time-invariant (LTI) theorems are used regularly, coupling with the statistical signaling and circuit theorems, to determine jitter, noise, and signaling performance for both the link system and the subsystems within it.

At the same time, significant advancements also happened in high-speed networks and computer I/O links in terms of architectures and data rate speed. In general, the architectures developed in those standards are all serial at multiple Gbps, with its clock timing being extracted at the receiver side by a clock recovery circuit (CRC). The CRC also tracks and reduces low-frequency jitter at the receiver input to maintain a good overall BER performance for the receiver or system. Various clock and data recovery methods and circuits have been developed, including ones based on phase-locked loop (PLL), phase interpolator (PI), and oversampling (OS). Each clock recovery implies a different jitter transfer function and tracking capability and characteristics. To mitigate or compensate for signal degradation due to the lossy channel, extensive and advanced equalization techniques and circuits have been developed, including linear

equalization (LE) and decision feedback equalization (DFE). Accordingly, new theorems, algorithms, designs, and test methods have been developed to accommodate the emerging challenges imposed by new architectures, data rates, clock recovery, and equalization for the latest multiple-Gbps high-speed I/O links.

Innovations and breakthroughs have been developed in the past ten years, including theory, algorithm, methodologies for understanding, modeling, and analyzing jitter, noise, and SI. Link architectures, theory, algorithm, and circuits for mitigating them also have been developed. However, no book has focused on all the latest advancements in jitter, noise, and SI in a systematic and cohesive manner. This book was written to fill in this gap.

This book intends to give a concurrent, comprehensive, systematic, and in-depth review and discussion of fundamentals of, new theories about, and algorithms on jitter, noise, and SI, as well as their modeling, testing, and analysis methodologies within the contexts of clock and I/O link signaling. This book covers important topics such as jitter and noise separation theories and algorithms; jitter transfer functions for output and tolerance; clock and PLL jitter; and modeling, analysis, and testing for the link system, covering its subsystems of transmitter, receiver, channel, reference clock, and PLL, with emphasis on jitter, noise, and SI aspects.

We start [Chapter 1](#) with overview of the basics on jitter, noise, and SI and communication link systems. The root cause mechanisms for various jitter, noise, and SI are discussed and the statistical handling for jitter and noise are introduced. Then, we progress to the discussion on jitter and noise components concept and definition and the rationales on why they are necessary and important. In conclusion, we bring the jitter, and noise, and SI discussion to the framework of a communication system.

With a big picture introduction on jitter, noise, SI, and link communication system in [Chapter 1](#), we will dive into the details on the necessary and relevant mathematical in [Chapter 2](#). Theories on relevant statistics, stochastic processes for jitter, noise, and SI, and linear time invariant (LTI) theory for link systems and signaling, and the theory for combining statistics with LTI are introduced in this chapter.

In [Chapters 3](#) and [4](#), we apply the statistical and stochastic theory introduced in [Chapter 2](#) to quantify jitter, noise, SI, and BER in terms of appropriate PDF and CDF, as well spectrum function of power spectrum density (PSD). In [Chapter 3](#), we give quantitative description for each jitter or noise component in terms of PDF and PSD, along with the relationship between component PDFs to the total PDF, and component PSDs to the total PSD. In [Chapter 4](#), we discuss jitter and noise jointly in a two-dimensional (2-D) frame. The mathematical representations for the joint PDF of jitter and noise (e.g., eye-contour), and joint jitter and noise CDF (e.g., BER contour) are presented.

[Chapters 5](#) and [6](#) are dedicated to jitter and noise separation to various layers of components. In [Chapter 5](#), we present the jitter separation to its components of deterministic jitter (DJ) and random jitter (RJ) based on jitter PDF or CDF function using the widely used Tailfit method. In [Chapter 6](#), we introduce jitter separation based on real-time function or autocorrelation function of jitter to its first and second layer jitter components of data dependent jitter (DDJ), duty-cycle distortion (DCD), inter-symbol interference (ISI), periodic jitter (PJ), bounded uncorrelated jitter (BUJ), and RJ. Jitter spectrum or PSD estimation via Fourier transformation (FT) is introduced. Both time and frequency domain separation techniques are presented.

With the fundamental knowledge on statistical jitter, noise, and SI, as well as theories and algorithms for construct the total jitter or noise PDF or PSD to total PDF or PSD, or separating total jitter or noise PDF or PSD to its component PDF or PSD, we are ready to solve the practical problems. At high frequencies, clock and PLL jitter become the major limiting factor for their performance and we will dedicate the first application to jitter in clocks and PLLs. [Chapter 7](#) focuses on clock jitter. We start with clock jitter definition and reveal its impacts to both synchronous and asynchronous systems. Next, we introduce three different jitter types of phase jitter, period jitter, and cycle-to-cycle jitter, along with their physical meanings, usage model, and interrelationship in both time and frequency domain. In the end, we discuss the relationship and mapping math models between phase jitter and phase noise, a conventional metric for the performance of a clock or PLL in frequency domain that is widely used in microwave and radio frequency (RF) fields. [Chapter 8](#) is dedicated to jitter and noise in PLLs. First, LTI model for PLL in both time and frequency domain are introduced, along with functional and parametric analysis methods. Second, generic jitter and noise analysis and modeling methods are introduced using autocorrelation function in time domain and PSD function in frequency domain. Third, comprehensive and detailed modeling and analysis are presented for jitter, noise, and transfer functions for both 2nd and 3rd order PLLs.

[Chapters 9](#), [10](#), and [11](#) are dedicated to the jitter, noise, and SI in a high-speed link, covering three important aspects of physical mechanisms, modeling and simulation methods, and test and verification methods. [Chapter 9](#) focuses on jitter, noise, and SI physical mechanisms for the purpose of establishing a good understanding. Subsystem architecture including transmitter, receiver, channel, and reference clock and physical mechanisms for jitter, noise, and SI within each are presented. [Chapter 10](#) devotes to quantitative modeling and analysis for high-speed link system and its subsystems. Modeling methods based on LTI theorem are developed for the subsystems and the entire system through LTI cascading. Subsystem models of jitter, noise, and signaling for transmitter, receiver, and channel are presented. Importance elements of equalization and clock recovery are included in the modeling. Both linear and DFE equalizations are covered. [Chapter 11](#) dedicates to testing and analysis for the high-speed link system and its subsystems. Testing requirements and methods for link subsystems of transmitter, receiver, channel, reference clock, and PLL are presented. Latest testing methods of reference receiver that is composed of both reference clock recovery and equalization for jitter, noise, and signaling output, as well as worst case jitter, noise, and signaling generation methods for receiver tolerance testing are presented. At the end of this chapter, link system level test method such as loopback is introduced and trade-offs between on-chip built-in-self-test (BIST) and off-chip external test is discussed.

[Chapter 12](#) gives the summary of the book, discusses the trend, outlook, and challenges for jitter, noise, and SI in the future.

This book is written for readers such as engineers and managers working on high-speed circuits, devices, and systems for industry. A wide range of engineers can benefit from reading this book, including design engineers, test engineers, application engineers, and system engineers who are already in or about to enter the field of jitter, noise, signal integrity, and high-speed links. It is also written for researchers, professors, and students who are either in this field or plan to enter it. This book aims to give you a comprehensive understanding of jitter, noise, and signal integrity, as well as high-speed link signaling and performance.

Book: Jitter, Noise, and Signal Integrity at High-Speed

No part of any chapter or book may be reproduced or transmitted in any form by any means without the prior written permission for reprints and excerpts from the publisher of the book or chapter. Redistribution or other use that violates the fair use privilege under U.S. copyright laws (see 17 USC107) or that otherwise violates these Terms of Service is strictly prohibited. Violators will be prosecuted to the full extent of U.S. Federal and Massachusetts laws.

Information Theory Computer Science Mike Peng Li Prentice Hall Jitter, Noise, and Signal Integrity at High-Speed

Acknowledgments

I would like to thank many individuals who have given their encouragement and support in different ways, at different times, directly or indirectly, to help the writing and production of this book.

In particular, I would like to thank the following individuals from whom I have benefited during the process of growing and advancing my skills and capabilities as a graduate student, researcher, scientist, engineer, technical leader, and technical executive, either under their mentoring or through team, work, or professional-society interactions with them. They are Prof. Shui Wang (University of Science and Technology of China), Prof. James Horwitz (University of Texas, Arlington), Prof. Gordon Emslie (Oklahoma State University, Stillwater), Dr. Kevin Hurley (University of California, Berkeley), Prof. Robert Lin (University of California, Berkeley), Dr. Burnie West (Credence (retired), Milpitas, CA), Mr. Dennis Petrich (Wavecrest, Eden Prairie, MN), Mr. John Hamre (Wavecrest, Eden Prairie, MN), Prof. Tim Cheng (University of California, Santa Barbara), Prof. Gordon Roberts (McGill University, Canada), Prof. Mani Soma (Washington University, Seattle), Prof. David Keezer (Georgia Institute of Technology, Atlanta), Dr. Wenliang Chen (TI, Richardson, TX), Mr. Masashi Shimanouchi (Credence, Milpitas, CA), Dr. Takahiro Yamaguchi (Advantest, Japan), Dr. Yi Cai (LSI, Allentown, PA), Mr. Mark Marlett (LSI, Milpitas, CA), Mr. Gerry Talbot (AMD, Boxborough, MA), Mr. Andy Martwick (Intel, Hillsborough, OR), Mr. TM Mak (Intel, Santa Clara, CA), and Dr. LT Wang (SynTest, Sunnyvale, CA).

I sincerely thank Mr. Dennis Leisz, Chief Executive Officer and president of Wavecrest, also my former supervisor, for his passion and vision for technology and innovation. I also thank him for his long-term support, encouragement, and friendship.

Many of my publications relevant to this book were coauthored or co-invented with Mr. Jan Wilstrup, and I am deeply grateful. I value the stimulating and intriguing discussions, debates, and challenges between us during the course of developing those widely cited papers and patents. The collaboration and discussion with Jan helped sharpen and deepen my view of and thoughts on the subjects presented in this book.

Thanks also to the Prentice Hall editors and staff, including Bernard Goodwin, Publishing Partner, and Michelle Housley, Editorial Assistant, for their persistence, timely editorial support, schedule tracking, encouragement, and patience offered in developing the book drafts and production manuscript.

Finally, I would like to sincerely thank my family for their long-term support and encouragement when I was writing this book. This book would not be possible without their solid and persistent support. I would like to give my deepest gratitude to my wife, Xiaoyan (Mercia), for covering my family duties on many occasions and for her understanding and tolerance of my absences from family activities when I had to spend weekends and evenings writing this book during the past four years. I am indebted to my sons, Eric and George, because I missed many of their afterschool activities (which I intend to make up for before it is too late), but they showed superior understanding. Last, I would like to give big thanks and gratitude to my parents for their support of and inspiration for my intellectual exploration I have been pursuing ever since my boyhood.

Book: Jitter, Noise, and Signal Integrity at High-Speed

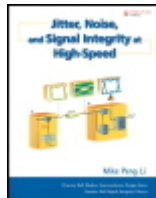
No part of any chapter or book may be reproduced or transmitted in any form by any means without the prior written permission for reprints and excerpts from the publisher of the book or chapter. Redistribution or other use that violates the fair use privilege under U.S. copyright laws (see 17 USC107) or that otherwise violates these Terms of Service is strictly prohibited. Violators will be prosecuted to the full extent of U.S. Federal and Massachusetts laws.

Information Theory Computer Science Mike Peng Li Prentice Hall Jitter, Noise, and Signal Integrity at High-Speed

About the Author

Dr. Mike Li was the Chief Technology Officer (CTO) with Wavecrest. He is now a Principle Architecture/Distinguished Engineer with Altera. Dr. Li pioneered the jitter separation method (Tailfit); deterministic jitter (DJ), random jitter (RJ), and total jitter (TJ) concept and theory formation; and the jitter transfer function (JTF) concept, theory, and application for high-speed serial link analysis. He has set and contributed to standards for jitter, noise, and signal integrity for leading serial data communications, such as Fibre Channel, Gigabit Ethernet, Serial ATA, PCI Express, FB DIMM, and International Technology Roadmap for Semiconductors (ITRS). He has been the cochairman of the PCI Express jitter standard committee. Dr. Li has been involved in technical committees for IEEE- and IEC-sponsored technical conferences such as International Test Conference (ITC) and DesignCon. He is a frequent speaker, invited author/speaker, panelist, and session and panel chair on the subjects of jitter/noise and signal integrity, covering both design and testing. He has received many awards, including a design paper award from Designcon/IEC and a contribution award from PCI-SIG. He has been listed in Who's Who in America and Who's Who in the World since 2006.

Dr. Li has more than 15 years of experience in high-speed-related measurement instrumentation, testing, and analysis/modeling algorithms and tools, with applications in IC, microprocessor, clock, serial data communications for electrical and optical, and wireless communication. He has a BS in physics from the University of Science and Technology in China and an MSE in electrical engineering and a PhD in physics from the University of Alabama in Huntsville. He did his post-doctorate work at the University of California, Berkeley, where he worked as a research scientist on high-energy astrophysics before he joined industry. Dr Li has published more than 80 papers in refereed technical journals and conferences. He has filed 12 patents, with four granted and eight pending. He was the executive editor for *Design and Test for Multiple Gbps Communication Devices and Systems* and wrote two contributing chapters on jitter, signal integrity, and high-speed I/O design and testing for two books.



Jitter, Noise, and Signal Integrity at High-Speed

By [Mike Peng Li](#)

Publisher: **Prentice Hall**

Pub Date: **November 19, 2007**

Print ISBN-10: **0-13-242961-6**

Print ISBN-13: **978-0-13-242961-0**

Pages: **400**

Slots: **3.0**

[Table of Contents](#) | [Index](#)

Copyright

Prentice Hall Modern Semiconductor Design Series

Preface

Acknowledgments

About the Author

Chapter 1. Introduction

Section 1.1. Jitter, Noise, and Communication System Basics

Section 1.2. Sources of Timing Jitter, Amplitude Noise, and Signal Integrity

Section 1.3. Signal and Statistical Perspectives on Jitter and Noise

Section 1.4. System Perspective on Jitter, Noise, and BER

Section 1.5. Historical Overview of Jitter, Noise, BER, and Signal Integrity

Section 1.6. Overview of This Book

Endnotes

Chapter 2. Statistical Signal and Linear Theory for Jitter, Noise, and Signal Integrity

Part A: Probability, Statistics, Stochastic Signal

Section 2.1. Random Variables and Distribution

Section 2.2. Statistical Estimates

Section 2.3. Sampling and Estimation

Section 2.4. Statistical Random Process and Spectral Analysis

Part B: Linear System Theory

Section 2.5. An LTI System

Section 2.6. Statistical Estimators for an LTI System

Section 2.7. Power Spectrum Density (PSD) for an LTI System

Section 2.8. Summary

Endnotes

Chapter 3. Source, Mechanism, and Math Model for Jitter and Noise

Section 3.1. Deterministic Jitter (DJ)

Section 3.2. Random Jitter (RJ)

Section 3.3. Overall Jitter PDF and PSD

Section 3.4. Summary

Endnotes

Chapter 4. Jitter, Noise, BER (JNB), and Interrelationships

Section 4.1. Eye Diagrams and BER Basics

- Section 4.2. Jitter Total PDF and the Relationship to Its Component PDFs
 - Section 4.3. Noise Total PDF and the Relationship to Its Component PDFs
 - Section 4.4. The Joint PDF of Timing Jitter and Amplitude Noise
 - Section 4.5. BER and Jitter/Noise Relationship
 - Section 4.6. Summary
 - Endnotes
- Chapter 5. Jitter and Noise Separation and Analysis in the Statistical Domain
- Section 5.1. Rationale and Motivation for Jitter Separation
 - Section 5.2. Jitter Separation Based on PDF
 - Section 5.3. Jitter Separation Based on BER CDF
 - Section 5.4. Straightforward Dual-Dirac Jitter Separation Method
 - Section 5.5. Summary
 - Endnotes
- Chapter 6. Jitter and Noise Separation and Analysis in the Time and Frequency Domains
- Section 6.1. Time and Frequency Domain Representations
 - Section 6.2. DDJ Separation
 - Section 6.3. PJ, RJ, and BUJ Separation
 - Section 6.4. Pulse Width Shrinkage (PWS)
 - Section 6.5. Comparison of Various Time and Frequency Domain Jitter Separation Methods
 - Section 6.6. Summary
 - Endnotes
- Chapter 7. Clock Jitter
- Section 7.1. Clock Jitter
 - Section 7.2. Definitions of and Math Model for Various Jitter Types
 - Section 7.3. Clock Jitter Versus Phase Noise
 - Section 7.4. Summary
 - Endnotes
- Chapter 8. PLL Jitter and Transfer Function Analysis
- Section 8.1. PLL Introduction
 - Section 8.2. PLL Time and Frequency Domain Behavior
 - Section 8.3. PLL Functional and Parametric Analysis
 - Section 8.4. PLL Jitter and Noise Analysis
 - Section 8.5. A Second-Order PLL Analysis
 - Section 8.6. A Third-Order PLL Analysis
 - Section 8.7. Comparison with the Conventional PLL Analysis Methods
 - Section 8.8. Summary
 - Endnotes
- Chapter 9. Jitter and Signal Integrity Mechanisms for High-Speed Links
- Section 9.1. Link System Architecture and Components
 - Section 9.2. Transmitter
 - Section 9.3. Receiver
 - Section 9.4. Channel or Medium
 - Section 9.5. Reference Clock
 - Section 9.6. Overall Link Jitter Budget
 - Section 9.7. Summary
 - Endnotes
- Chapter 10. Modeling and Analysis for Jitter and Signaling Integrity for High-Speed Links
- Section 10.1. A Linear Time-Invariant (LTI) Approach
 - Section 10.2. Transmitter Modeling and Analysis
 - Section 10.3. Channel Modeling and Analysis
 - Section 10.4. Receiver Modeling and Analysis
 - Section 10.5. Summary
 - Endnotes
- Chapter 11. Testing and Analysis for Jitter and Signaling Integrity for High-Speed Links

Section 11.1. Link Signaling and Its Impact on Testing

Section 11.2. Transmitter Output Testing

Section 11.3. Channel and Channel Output Testing

Section 11.4. Receiver Testing

Section 11.5. Reference Clock Testing

Section 11.6. PLL Testing

Section 11.7. Loopback Testing

Section 11.8. Summary

Endnotes

Chapter 12. Book Summary and Future Challenges

Section 12.1. Book Summary

Section 12.2. Future Challenges

Endnotes

Index

Book: Jitter, Noise, and Signal Integrity at High-Speed

No part of any chapter or book may be reproduced or transmitted in any form by any means without the prior written permission for reprints and excerpts from the publisher of the book or chapter. Redistribution or other use that violates the fair use privilege under U.S. copyright laws (see 17 USC107) or that otherwise violates these Terms of Service is strictly prohibited. Violators will be prosecuted to the full extent of U.S. Federal and Massachusetts laws.

Information Theory Computer Science Mike Peng Li Prentice Hall Jitter, Noise, and Signal Integrity at High-Speed

1. Introduction

This chapter offers basic and high-level introductions to terminology, definitions, and concepts concerning jitter, noise, signal integrity, bit error rate, and working mechanisms for communication link systems. Sources and root causes of jitter, noise, and signal integrity then are discussed, followed by statistical and system views on jitter, noise, and signal integrity. Then we give a historical overview of the evolution of and advancement path for jitter, noise, and signal integrity. This chapter ends by discussing this book's organization and flow.

Book: Jitter, Noise, and Signal Integrity at High-Speed
Section: Chapter 1. Introduction

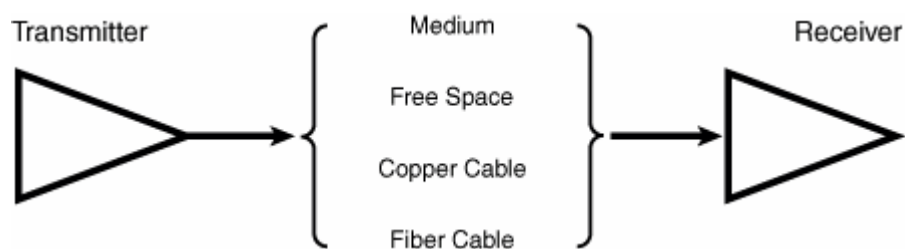
No part of any chapter or book may be reproduced or transmitted in any form by any means without the prior written permission for reprints and excerpts from the publisher of the book or chapter. Redistribution or other use that violates the fair use privilege under U.S. copyright laws (see 17 USC107) or that otherwise violates these Terms of Service is strictly prohibited. Violators will be prosecuted to the full extent of U.S. Federal and Massachusetts laws.

Information Theory Computer Science Mike Peng Li Prentice Hall Jitter, Noise, and Signal Integrity at High-Speed

1.1. Jitter, Noise, and Communication System Basics

The essence of communication is about transmitting and receiving a signal through a medium or channel. An early mathematical model for communication may be traced back to Claude Shannon's famous 1948 paper.^[1] Depending on what kind of medium is used to transmit and receive a signal, communication systems are grouped into three basic categories: fiber, copper, and wireless (or free space) (see Figure 1.1). The bandwidths typically are a few THz for fiber and a few GHZ for copper media. Considering the constraints of bandwidth, attenuation, and cost, fiber-based communication is often used for long-distance ($> 1 \text{ km}$), high-data-rate (up to $> 100 \text{ Gb/s}$ per channel) communication. Copper-based communication is used for medium-distance ($< 1 \text{ km}$) and medium-high data rates (1 Mb/s to a few Gb/s per channel). Wireless is used for medium distance ($\sim \text{km}$) and medium data rates (up to $\sim 100 \text{ Mb/s}$). The choice of a communication medium is largely determined by cost and application requirements. Clearly, fiber has the highest intrinsic bandwidth, so it can deliver the highest data rate possible for a single channel.

Figure 1.1. A simple communication system, including three basic building blocks: transmitter, medium, and receiver.

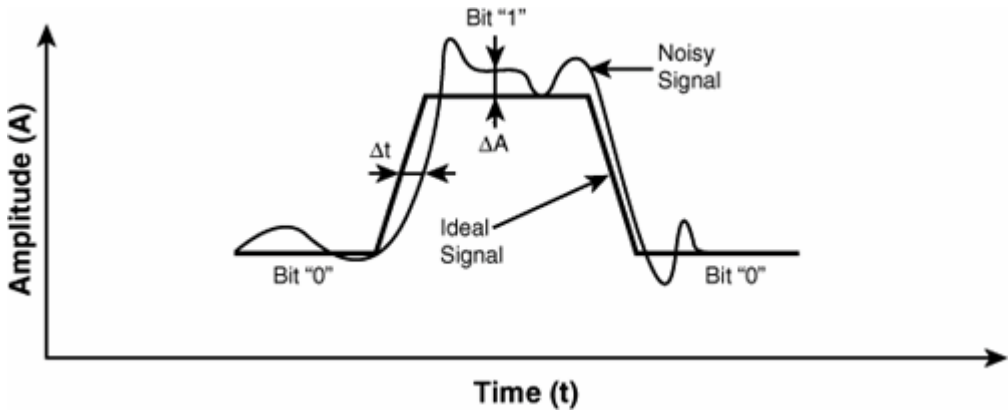


1.1.1. What Are Jitter, Noise, and Signal Integrity?

When a signal is transmitted and received, a physical process called noise is always associated with it. Noise is basically any undesired signals added to the ideal signal. In the context of digital communication, the information is encoded in logical bits of 1 and 0. An ideal signal may be represented by a trapezoid wave with a finite 0 to 1 rise time or 1 to 0 fall time. In the presence of noise, it is the sum of ideal signal, with the noise giving rise to the "net" or actual signal waveform. If no noise is added, the actual signal is identical to the ideal signal waveform. If the noise is added, the actual signal is deviated from the ideal signal, as shown in Figure 1.2.

Figure 1.2. An ideal signal versus a noisy signal for a digital waveform.

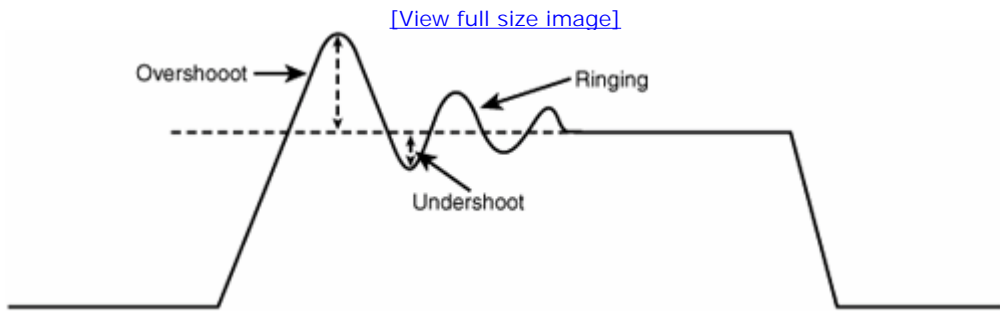
[\[View full size image\]](#)



The deviation of a noisy signal from its ideal can be viewed from two aspects: timing deviation and amplitude deviation. The amplitude of the digital signal for a copper-based system is the voltage, and for a fiber-based or radio frequency (RF) wireless system it is the power. The deviation of the signal amplitude (ΔA) is defined as the amplitude noise (or simply noise), and the deviation of time (Δt) is defined as the timing jitter (or simply jitter). Those definitions will be used throughout this book. The impacts of timing jitter and amplitude noise are not symmetrical, though. Amplitude noise is a constant function and can affect system performance all the time. Timing jitter affects system performance only when an edge transition exists.

Signal integrity generally is defined as any deviation from ideal waveform.^[2] As such, signal integrity contains both amplitude noise and timing jitter in a broad sense. However, certain signal integrity signatures such as overshoot, undershoot, and ringing (see Figure 1.3) may not be well covered by either noise or jitter alone.

Figure 1.3. Some signal integrity key signatures.



1.1.2. How Do Jitter and Noise Impact the Performance of a Communication System?

There is no doubt that jitter, noise, and signal integrity all impact the quality of a communication system. The following sections discuss and illustrate how jitter and noise cause a bit error and under what conditions this bit error occurs. Then the metric that is commonly used to quantify the bit error rate in a communication system is discussed.

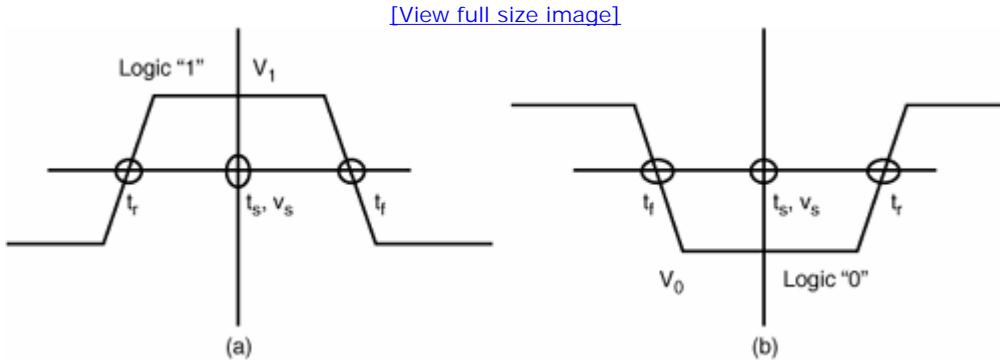
1.1.2.1. Bit Error Mechanisms

The impacts of timing jitter and amplitude noise can best be understood from the perspective of a receiver for a communication system.^[3] A receiver samples the incoming logical 1 pulse data at a sampling time of t_s and threshold voltage of v_s , as shown in Figure 1.4. For a jitter- and noise-free digital pulse, an ideal receiver samples the data at the center of the incoming pulse. In this context, clearly there is no need to talk about signal integrity, because its effects are covered by jitter and noise. Under such conditions, threshold crossing times for rising and falling edges satisfying the conditions of $t_r < t_s < t_f$ and $V_1 > v_s$ result in a logical 1 being detected, and the data bit is received correctly (see part (a) of Figure 1.4). In the presence of jitter and noise, the rising and falling edges can move along the time axis, and the voltage level can move along the amplitude axis. As such, the correct bit detection conditions for sampling time and voltage may not be satisfied, resulting in a bit error due to bit 1 being received/detected as bit 0. The violations of those sampling conditions can occur in three scenarios:

- The crossing time of the rising edge lags behind the sampling time, or $t_r > t_s$.
- The crossing time of the falling edge is ahead of the sampling time, or $t_f < t_s$.

- The logical 1 voltage is below the sampling voltage v_s , or $V_1 < v_s$.

Figure 1.4. A receiver sampling an incoming data bit 1 (a) and 0 (b), where t_r and t_f are the timings for the 50% crossing (or zero crossing timings) for the rising and falling edges, respectively, and t_s and v_s are the sampling time and voltage, respectively.



For a zero pulse or bit "0" detection, in the case of part (b) of Figure 1.4, the correct detection condition becomes $t_r < t_s < t_f$ and $V_0 < v_s$. Similarly, the violation of correct sampling condition causes a bit error because bit 0 is received as bit 1. The violation scenarios for timing are similar to those of bit 1 pulse (part (a) of Figure 1.4). However, the violation condition for voltage becomes $V_0 > v_s$.

1.1.2.2. Bit Error Rate (BER)

We have demonstrated how jitter and noise cause a digital system bit error with a simple example. Because a digital system transmits and receives many bits for a given time, the system's overall performance can best be described by the rate of bit failure—namely, the ratio of the total failed bits N_f to the total bits received N . This ratio is called the bit error rate (BER) or bit error ratio. Bit error ratio is a more precise definition because $BER = N_f/N$ and no normalization of time is as involved as most of the rate definition otherwise required.

BER is the bottom-line metric for determining a good communication system. At multiple Gb/s rates, the BER requirement for most communication standards such as Fibre Channel (FC), Gigabit Ethernet, SONET, and PCI Express is 10^{-12} or smaller. Larger BER degrades network or link efficiency and, worse, system latency. A simple implication of $BER = 10^{-12}$ is that with 10^{12} bits being transmitted/received, only one bit error is allowed. Clearly BER depends on data rate, jitter, and noise in the communication system. The definition of BER implies that BER is a counting statistic so that Poisson statistics may apply.

Book: Jitter, Noise, and Signal Integrity at High-Speed
Section: Chapter 1. Introduction

No part of any chapter or book may be reproduced or transmitted in any form by any means without the prior written permission for reprints and excerpts from the publisher of the book or chapter. Redistribution or other use that violates the fair use privilege under U.S. copyright laws (see 17 USC107) or that otherwise violates these Terms of Service is strictly prohibited. Violators will be prosecuted to the full extent of U.S. Federal and Massachusetts laws.

Information Theory Computer Science Mike Peng Li Prentice Hall Jitter, Noise, and Signal Integrity at High-Speed

1.2. Sources of Timing Jitter, Amplitude Noise, and Signal Integrity

Jitter and noise are deviations from an ideal signal. Jitter and noise can have many causes. The physical nature of various noise and jitter sources for a communication system can be classified into two major classes: intrinsic and nonintrinsic. The intrinsic type has to do with the physical properties of electrons and "holes" in electrical or semiconductor devices. The nonintrinsic type are design-related and may be eliminated. These types are discussed in detail in the following sections.

1.2.1. Intrinsic Noise and Jitter

Intrinsic noise is fundamentally caused by the randomness and fluctuation of electrons and "holes" existing in all the electronic/optical/semiconductor circuits/devices. Intrinsic noise can be minimized but cannot be completely removed from devices or systems. Therefore, this kind of noise puts a fundamental limit on device and system performance and dynamic range. Typical intrinsic noises in electrical-optical devices include thermal noise, shot noise, and flick noise.

1.2.1.1. Thermal Noise

Thermal noise is caused by the random motion of charge carriers under the thermal equilibrium condition. The kinetic energy of those randomly fluctuating charge carriers is proportional to their temperature, as well as to their mean-square velocity. The power spectrum density (PSD) of the thermal noise is white and apparently proportional to its temperature. Thermal noise places a fundamental limit on the signal-to-noise ratio (SNR) performance because it exists in all electric/optical/semiconductor devices having a nonzero absolute temperature. Johnson^[4] first discovered that the noise in a conductor depends on temperature and resistor under the thermal equilibrium condition. Nyquist^[5] shortly after developed a theory to explain Johnson's discovery based on the second law of thermodynamics. Because of their pioneering contributions, thermal noise is sometimes called Johnson noise or Nyquist noise.

1.2.1.2. Shot Noise

Shot noise is produced by individual quantized carrier flow (current) in a potential barrier with a random generation time or spatial distribution. In other words, shot noise is basically due to random flow fluctuation. Schottky^[6] first studied shot noise in vacuum tube diodes and later it was also found in P-N junction in a semiconductor transistor. Shot noise is directly proportional to DC bias current, as well as the charge of the carrier. Shot noise is typically larger than thermal noise in semiconductor devices.

1.2.1.3. Flick Noise

Flick noise is a phenomenon that is found to have a noise power spectrum inversely proportional to the frequency over a wide range of frequencies. Johnson was the first to observe flick noise in an electronic system.^[7] Flick noise can be found in all active devices, and some passive devices such as carbon resistors. DC current is necessary to produce flick noise. No universally accepted theory explains the cause and mechanism of flick noise, unlike the causes of thermal and shot noise. As a result, the quantitative study of flick noise is mostly empirical. It has been found that the PSD of flick noise is proportional to $1/f^\alpha$, where α is around 1. Because of this reason, flick noise is also called $1/f$ noise. One common interpretation of flick noise is the "trap and release" theory. It is believed that the flow of carriers due to the DC current can be trapped due to contamination and defects in devices. However, the "trap and release" process is random, giving rise to the flick noise that is most significant at low frequencies.^[8]

1.2.2. Translation of Noise to Timing Jitter

Noise is typically described using physical quantities or parameters. In communication, computer, and electronic systems, those quantities may include voltage, current, or power. We use the generic term of amplitude to represent those physical quantities. Assuming that the amplitude noise $\Delta A(t)$ is superimposed on the amplitude waveform of $A_0(t)$ so that the total waveform has the following form:

Equation 1.1

$$A(t) = A_0(t) + \Delta A(t)$$

the corresponding timing jitter can be estimated through the linear small-signal perturbation theory as the following:

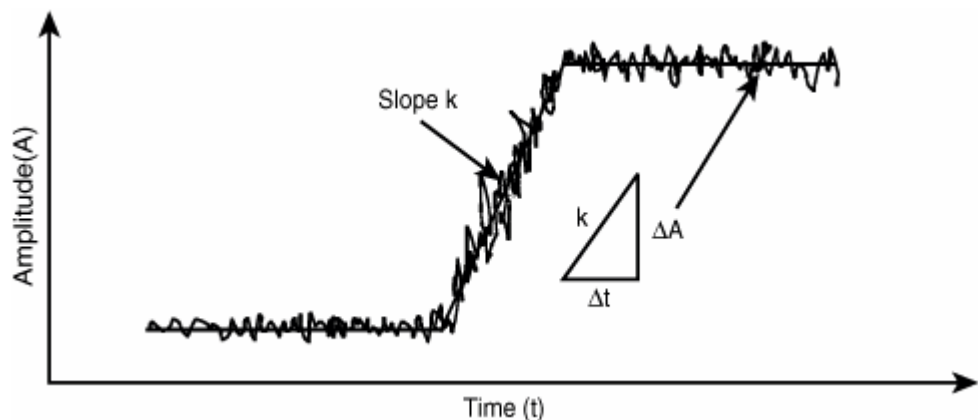
Equation 1.2

$$\Delta t(t) = \Delta v / \left(\frac{dA_0(t)}{dt} \right) = \Delta t / k$$

where $k = (dA_0(t)/dt)$ is the slope or slew rate of the waveform.

This linear amplitude noise to timing jitter conversion is shown in Figure 1.5.

Figure 1.5. Amplitude noise to timing jitter conversion through the linear perturbation model.



You can see that for amplitude noise ΔA , the corresponding timing jitter decreases as the slope increases, and vice versa. To maintain a smaller timing jitter conversion, a large slope or fast slew rate is favored. In the context of a digital signal, this implies a small rise/fall time.

1.2.3. Nonintrinsic Noise and Jitter

Nonintrinsic jitter and noise are design-related deviations. In other words, those types of jitter and noise can be controlled or fixed with appropriate design improvements. Commonly encountered nonideal design-related noise and jitter include periodic modulation (phase, amplitude, and frequency), duty cycle distortion (DCD), intersymbol interference (ISI), crosstalk, undesired interference such as electromagnetic interference (EMI) due to radiation, and reflection caused by unmatched media. The following sections discuss these noise sources and their root causes.

1.2.3.1. Periodic Noise and Jitter

Periodic noise or jitter is a type of signal that repeats every time period. It can be described mathematically by the following general equation:

Equation 1.3

$$\Delta t_p = f(2\pi \frac{t}{T_0} + \phi_0)$$

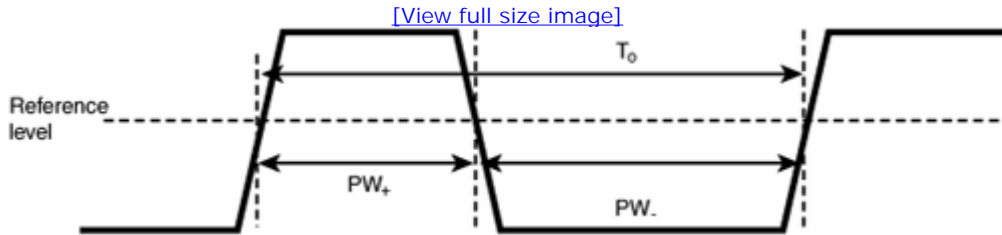
where T_0 is the period, t is the time, and ϕ_0 is the phase of the periodic signal. The period T_0 and frequency f_0 satisfy the reciprocal relationship of $T_0 = 1/f_0$. Although the notation and discussion are based on timing jitter, the same type of discussion can be applied to amplitude noise. The frequency-domain periodic function can be obtained through Fourier Transformation (FT), a subject that is discussed in Chapter 2, "Statistical Signal and Linear Theory for Jitter, Noise, and Signal Integrity."

Periodic jitter can be caused by various modulation mechanisms, such as amplitude modulation (AM), frequency modulation (FM), and phase modulation (PM). Moreover, the modulation function can have various shapes. Typical modulation shapes include sinusoidal, triangular, and sawtooth. It is apparent that a periodic amplitude noise causes period timing jitter, with the amplitude proportional inversely to the slope or slew rate of the edge transition, as discussed in section 1.3.2. In the computer environment, period noise/jitter can be caused by switching power supply, spread-spectrum clock (SSC), and period EMI sources.

1.2.3.2. Duty Cycle Distortion (DCD)

DCD is defined as the deviation in duty cycle from its normal value. Mathematically, a duty cycle is the ratio of pulse width to its period for a clock signal, as shown in Figure 1.6.

Figure 1.6. Illustration of period (T_0), pulse width PW_+ / PW_- (either positive or negative), and reference level for a periodic signal.



Duty cycle is defined as follows:

Equation 1.4

$$\eta_+ = \frac{PW_+}{T_0}, \quad \eta_- = \frac{PW_-}{T_0}$$

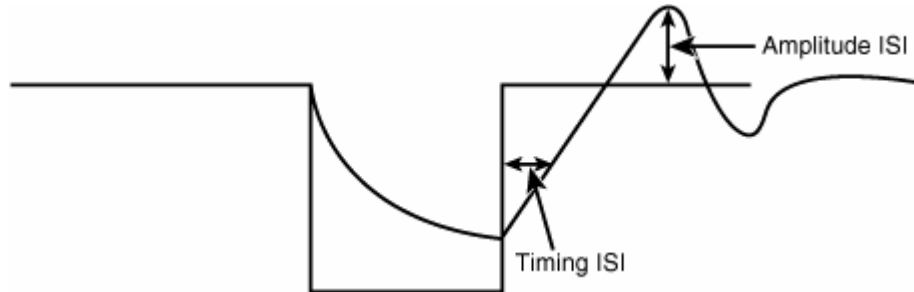
Most clocks have a nominal duty cycle of 50%. So either shorter pulse width or longer pulse width causes DCD. DCD can be caused by pulse width deviation, period deviation, or both. Furthermore, pulse width deviation can be caused by the deviation of reference signal level. Another DCD-causing mechanism is propagation delay if the clock is formed from rising and falling edges of two half-rate clocks and those two half-rate clocks undergo different propagation delays. Because a clock can have many periods, DCD must be looked at from the distribution point of view with many samples considered, and the average period should be used for the overall DCD estimation.

1.2.3.3. Intersymbol Interference (ISI)

ISI is related to data signal, but a clock signal does not have ISI by definition. A data signal is a generic digital signal form that does not have to have an edge transition in every UI or bit period, like the clock signal. The data signal can be kept at the same amplitude level for many UIs without an edge transition, whereas a clock signal cannot be. The type of data pattern used in digital communication critically depends on the coding scheme of the communication architecture.^[9] An important parameter for digital pattern is the run length, which is defined as the maximum length of consecutive 1s or 0s within a pattern. The run length determines the lowest frequency of the data pattern spectrum and therefore governs the frequency range for the test coverage. The long-haul fiber-optic communication standard SONET uses a scramble code scheme and can have a much longer run length (such as a run length of 23, 31) and therefore relatively low-frequency spectral content. A short-haul data communication standard such as Fibre Channel or Gigabit Ethernet uses block code (e.g., 8B10B coding) that has a shorter run length (e.g., a run length of 5) and relatively high-frequency spectral content.

In a lossy medium, the previous bits can cause both transition timing and amplitude level off the ideal values. In copper-based communication systems, this is due to the "memory" characteristics of the electronic devices used to switch bits between 1s and 0s. One example of this "memory" nature is the capacitive effect. Due to capacitive effect, each transition has a finite charge or discharge time. If the transition happens such that the next transition occurs before the previous transition reaches the designated level, deviation of both time and level occurs for the current bit. Such an effect can be cascaded. The ISI effect is shown in [Figure 1.7](#).

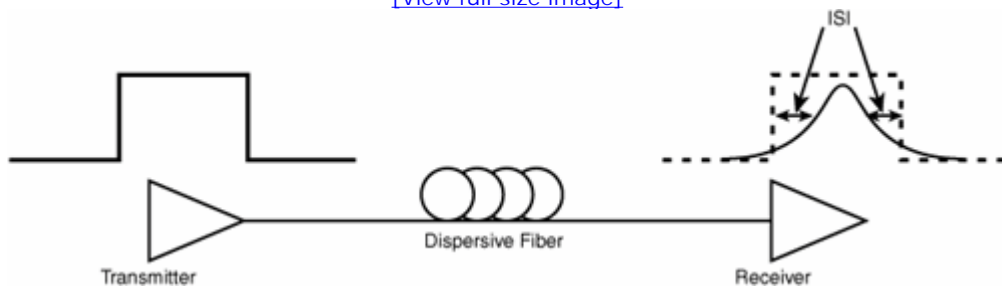
Figure 1.7. The ISI effect for both timing and amplitude.



Any pulse-width broadening or spreading effects cause ISI, and dispersion is a known physical phenomenon that causes a traveling pulse to be broadened or spread. As such, ISI is expected to occur in a fiber-based communication system too.^[10] For multimode fiber, the spread mechanism is called mode dispersion (MD), where a number of electromagnetic waves can exist in the multimode fiber waveguide, and the number of wave modes depends on the physical parameters of the multimode fiber, such as refraction index and geometry. Those different modes have different propagation times. The spread of the propagation times in multimode fiber cause the pulse to spread at the other end of the fiber. For a single-mode fiber, the dominant spread mechanism is the dispersion effects, including chromatic dispersion (CD) and polarization mode dispersion (PMD). The physical reason for CD is that the refraction index of the fiber material is wavelength-dependent. Therefore, the group velocity of the wave propagation inside the fiber is wavelength-dependent. Both laser source and modulation waveform have some spread in their spectrum. The combined spread spectrum of the input optical waveform, coupled with the CD effect, causes the optical pulse train to spread in the time domain, resulting in both timing and amplitude ISI. PMD is due to the birefringence, in which the refraction indexes along the two orthogonal axes are different, causing different propagation velocities. Again, the two different velocities for the two orthogonal modes of PMD eventually cause pulse train at the other end of the fiber to spread, resulting in ISI. [Figure 1.8](#) shows the dispersion effects on a pulse for an optical fiber.

Figure 1.8. ISI effects in a fiber-based communication link.

[\[View full size image\]](#)



1.2.3.4. Crosstalk

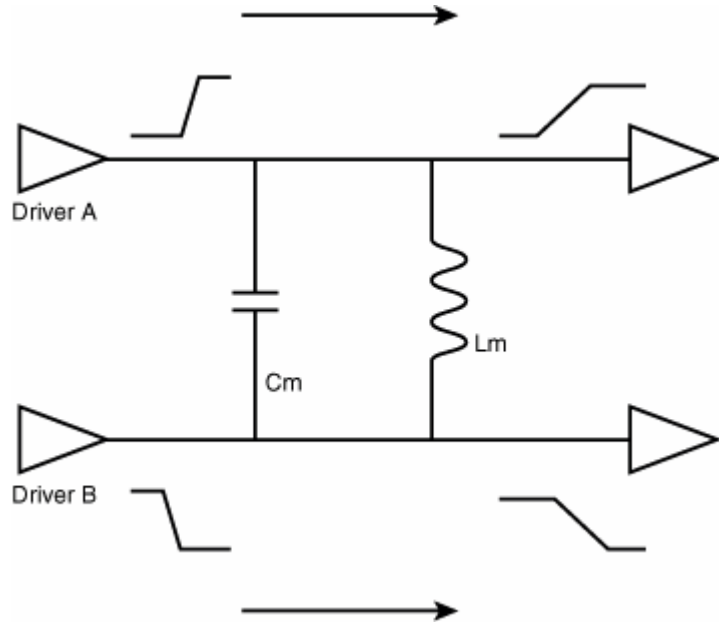
Two types of crosstalk are discussed here. One is associated with copper cables, and the other is associated with optical fibers.

1.2.3.4.1. Copper-Based Crosstalk

Crosstalk is basically an interference phenomenon. Crosstalk is generally involved in a parallel channel system in which signals are propagated concurrently and affect each other. For copper-based communication channels, crosstalk is caused by electromagnetic coupling. For integrated circuits (ICs) where the geometry and space between connects is relatively small, the capacitive coupling is the dominant mechanism.^{[11], [12]} When a signal transition happens in one channel, some of its energy leaks to the neighboring or adjacent channel through charge flow due to capacitive coupling, causing the signal level in that channel to fluctuate. For board-level circuits where the geometry is relatively large, inductive and capacitive coupling are both important. Inductive coupling follows Lentz's Law, in which changing the magnetic field flux generates an electrical field, and that electrical field, coupled with electrical charge, causes voltage fluctuation. In general, the effect of crosstalk can be modeled primarily as the voltage fluctuation or noise. However, it can affect the timing jitter directly as well. When two transmission lines are coupled capacitively, and when digital transitions occur simultaneously on two lines from the same end (the near end), the slew rate of the signals at the other end (the far end) is larger if the two transitions at the near end are in phase (have the same polarity) or is smaller if the two transitions are out of phase (have the

opposite polarity). Figure 1.9 shows the capacitive and inductive coupling mechanisms for crosstalk.

Figure 1.9. Schematic drawing of crosstalk caused by capacitive and inductive coupling. The crosstalk due to the simultaneous steps' response with opposite polarities slows down the slew rate of the step signals at the far end.



From the definitions of mutual capacitive and inductive constants C_m and L_m , the voltage noises due to capacitive and inductive coupling can be calculated according to the following equation:

Equation 1.5

$$V_{mc} = Z_v C_m \frac{dV_d}{dt}$$

where Z_v is the impedance of the impacted or victim line and dV_d/dt is the time derivative of the driving voltage. For inductive-induced voltage noise, we have

Equation 1.6

$$V_{mL} = L_m \frac{dI_d}{dt} = \frac{L_m}{Z_d} \frac{dV_d}{dt}$$

where Z_d is the impedance of the driving line, and dI_d/dt and dV_d/dt are driver current and voltage time derivatives or change rate, respectively.

You can see that crosstalk is proportional to the voltage or current slew rate. As the date rate or frequency keeps increasing, the rise time of the digital signal becomes smaller. Therefore, the slew rate and crosstalk-induced noise increase. As mentioned in previous sections, timing jitter due to crosstalk can be estimated through division of appropriated far-end signal slew rate.

1.2.3.4.2. Fiber-Based Crosstalk

Crosstalk can also happen in optical fiber-based communication systems, particularly in multiple-channel systems such as wavelength division multiplexing (WDM) systems.^[13] In a WDM or dense WDM (DWDM) system, crosstalk can happen through linear and/or nonlinear effects. Linear effects often refer to the leaking of photon energy from neighboring channels that have different wavelengths

to the concerned channel in the optical filters or demultiplexers, causing the amplitude noise fluctuation. Nonlinear effects include the following:

- Stimulated Raman Scattering (SRS), in which short-wavelength channels can amplify long-wavelength channels over a wide wavelength range
- Stimulated Brillouin Scattering (SBS), in which short-wavelength channels can amplify long-wavelength channels over a narrow wavelength range
- Four-wave mixing (FWM), in which a new wave or signal, or the fourth wave, is generated when three wavelengths from three WDM channels satisfy a certain relationship

Like copper-based crosstalk, fiber-based crosstalk causes amplitude noise for the transmitting signal and subsequently causes timing jitter through the slew rate conversion, in turn degrading system performance.

Book: Jitter, Noise, and Signal Integrity at High-Speed
Section: Chapter 1. Introduction

No part of any chapter or book may be reproduced or transmitted in any form by any means without the prior written permission for reprints and excerpts from the publisher of the book or chapter. Redistribution or other use that violates the fair use privilege under U.S. copyright laws (see 17 USC107) or that otherwise violates these Terms of Service is strictly prohibited. Violators will be prosecuted to the full extent of U.S. Federal and Massachusetts laws.

Information Theory Computer Science Mike Peng Li Prentice Hall Jitter, Noise, and Signal Integrity at High-Speed

1.3. Signal and Statistical Perspectives on Jitter and Noise

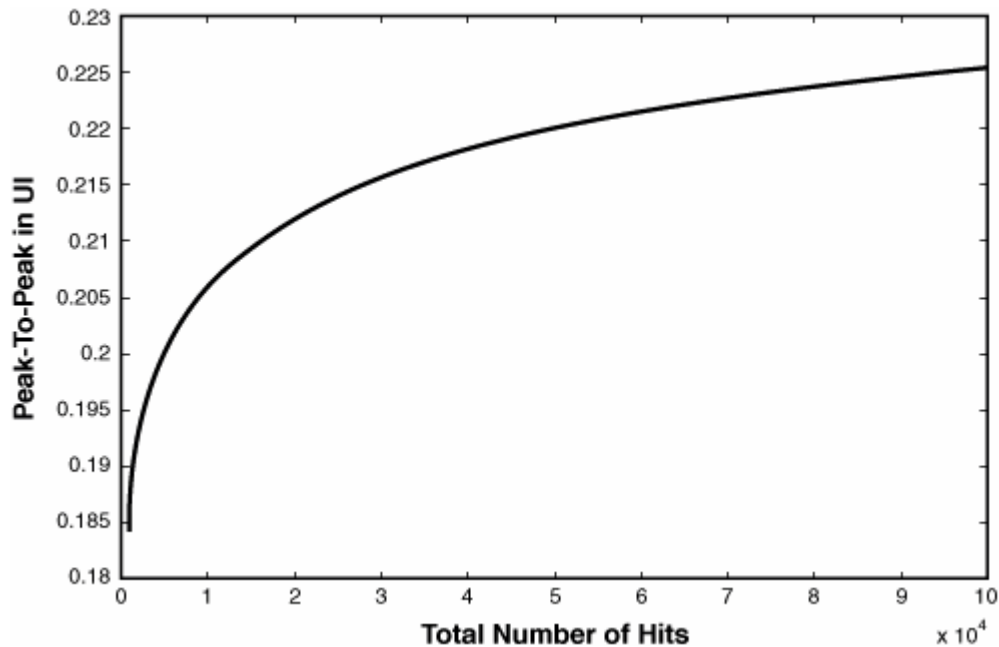
We will first talk about the limitations and drawbacks of peak-to-peak-based metrics for jitter. Then we will discuss why the jitter component method of quantifying jitter is better and more accurate and should be used to describe and quantify statistical processes such as jitter and noise.

1.3.1. Peak-to-Peak and Root-Mean-Square (RMS) Description

For many years, jitter was quantified by peak-to-peak value and/or standard deviation (1σ or rms) of the entire jitter histogram or distribution. It is now widely realized that this can be very misleading. In the presence of random and unbounded jitter or noise (such as thermal noise or shot noise), expected peak-to-peak value is a monotonically increasing function of statistical sample size. Peak-to-peak value is a useful parameter for bounded jitter or noise but not for unbounded ones. Similar problems occur with the standard deviation calculation. In the presence of bounded, non-Gaussian jitter or noise, the total jitter or noise histogram or distribution is not a Gaussian, and the statistical standard deviation or rms estimation does not equal the 1σ of the true Gaussian distribution. Therefore, the latter is the correct quantity to describe a Gaussian process or distribution. Using standard deviation or rms based on the total jitter or noise histogram statistics "inflates" the true 1σ value for Gaussian process.

To demonstrate the incorrect usage of statistical peak-to-peak in the presence of unbounded Gaussian jitter or noise, we start with a single Gaussian distribution via Monte Carlo method. We determine the peak-to-peak value for a given sample size N that is monotonically increasing and then plot the peak-to-peak value as a function of sample size. [Figure 1.10](#) shows the results, clearly demonstrating the monotonicity trend.

Figure 1.10. Peak-to-peak value plotted as a function of number of samples (N). The histogram distribution is a Gaussian, and the 1σ of the Gaussian equals 0.03 UI (bit clock period).



To demonstrate how different a statistical standard deviation or rms and 1σ of a Gaussian distribution can be, we assume that the histogram distribution has a bimodal distribution that is the superimposition of two identical Gaussians with different mean positions. Each peak corresponds to a single Gaussian mean position. Then standard deviation for such a bimodal distribution is 1.414 times (or 41.4% larger than) the true Gaussian 1σ value when they are well separated (10 σ apart).

As the goal becomes to completely grasp the jitter or noise process, as well as to quantify the overall distribution and its associated components and root causes, the simple parameter-based approach to jitter or noise becomes insufficient and invalid. What is needed is the distribution function such as probability density function (PDF) and its associated component PDFs. Those PDFs not only give the overall description for jitter or noise statistical process, but also give the corresponding root causes.

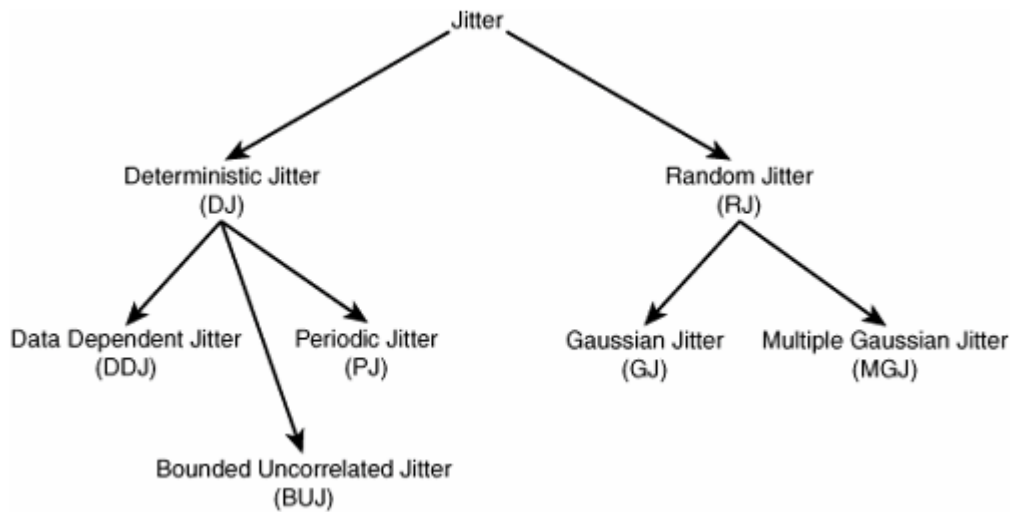
1.3.2. Jitter or Noise PDF and Components Description

Jitter or noise is a complex statistical signal and therefore can have many components associated with it. We will focus on jitter, but the same concept applies well to noise. In general, jitter can be split into two components: deterministic jitter (DJ) and random jitter (RJ). The amplitude of DJ is bounded, and that of RJ is unbounded and Gaussian. This classification scheme is the first step in jitter separation.^[14]

Jitter can be further separated after the first-layer splitting, as shown in Figure 1.11. Within deterministic jitter, jitter can be further classified into periodic jitter (PJ), data-dependent jitter (DDJ), and bounded uncorrelated jitter (BUJ). DDJ is the combination of DCD and ISI. BUJ can be caused by crosstalk. Within random jitter, jitter can be single-Gaussian (SG) or multiple-Gaussian (MG). Each jitter component has some specific corresponding root causes and characteristics. For example, the root cause of DJ can be a bandwidth-limited medium, reflection, crosstalk, EMI, ground bouncing, periodic modulations, or pattern dependency. The RJ source can be thermal noise, shot noise, flick noise, random modulation, or nonstationary interference.

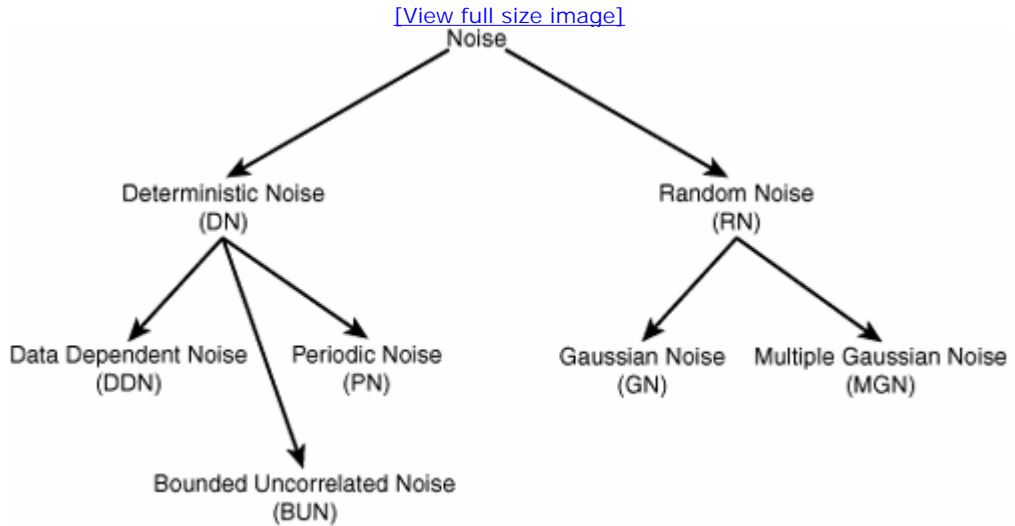
Figure 1.11. Jitter classification scheme from a signal statistical view.

[\[View full size image\]](#)



A similar type of noise component tree classification can be developed, as shown in [Figure 1.12](#).

Figure 1.12. Noise classification scheme from a signal statistical view.



Most of the component concepts for jitter and noise are symmetrical, except DCD, which does not have a noise counterpart. Also, the same type of jitter and noise component may or may not be correlated.

Book: Jitter, Noise, and Signal Integrity at High-Speed
Section: Chapter 1. Introduction

No part of any chapter or book may be reproduced or transmitted in any form by any means without the prior written permission for reprints and excerpts from the publisher of the book or chapter. Redistribution or other use that violates the fair use privilege under U.S. copyright laws (see 17 USC107) or that otherwise violates these Terms of Service is strictly prohibited. Violators will be prosecuted to the full extent of U.S. Federal and Massachusetts laws.

Information Theory Computer Science Mike Peng Li Prentice Hall Jitter, Noise, and Signal Integrity at High-Speed

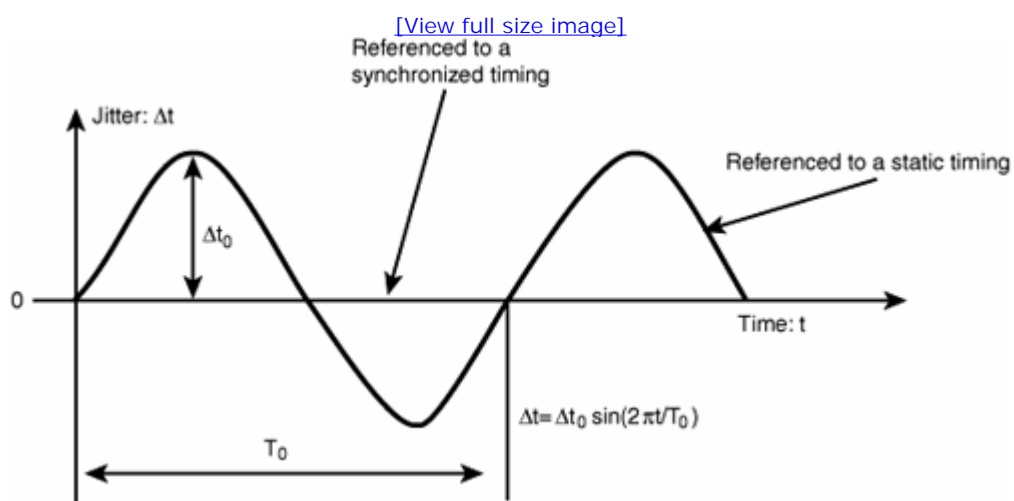
1.4. System Perspective on Jitter, Noise, and BER

This section briefly discusses jitter, noise, and BER within a high-speed linksystem. It also covers the role that clock recovery plays in providing the timing reference and in tracking low-frequency jitter, as well as jitter transfer functions.

1.4.1. The Importance of Reference

The beginning of this chapter defined jitter as any deviation from ideal timing. This definition is from the point of view of a "static timing reference" (see [Figure 1.13](#)). In other words, the ideal timing reference is a fixed timing point. This definition is very useful from concept and mathematical views, but it needs to be enhanced to be useful for the system application. Although it's true in a wide sense that jitter is any deviation from the ideal, if the properties of the reference are considered, the resulting jitter can be quite different. For example, a data signal with a sinusoidal timing jitter referenced to an ideal clock with a perfect period (i.e., zero-jitter) has a larger peak value than when it is referenced to the same clock but modulated with the same kind of sinusoidal, because the reference clock moves "in phase" with the data signal in this case.

Figure 1.13. The same jitter source results in two different jitter estimations with two different jitter references. One is a static ideal timing, and the other is a synchronized timing giving rise to zero jitter estimation.

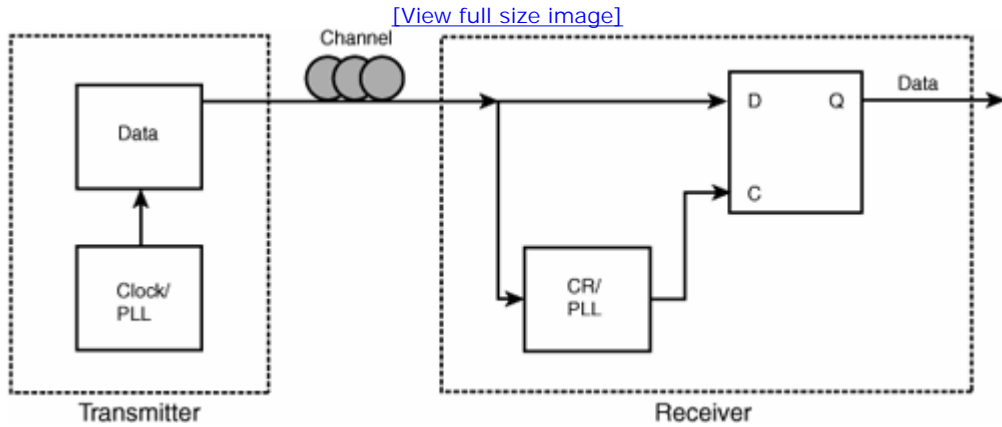


This is in analogy to Newton's law for motion. Whether or not an object moves critically depends on the reference. In parallel, we can fairly say that whether or not a signal has jitter depends on the reference signal used to determine the timing. For illustration purposes, we will focus on a timing reference signal in the context of serial data communication. However, the general concept applies to other systems.

1.4.2. Jitter Transfer Function in Serial Data Communication

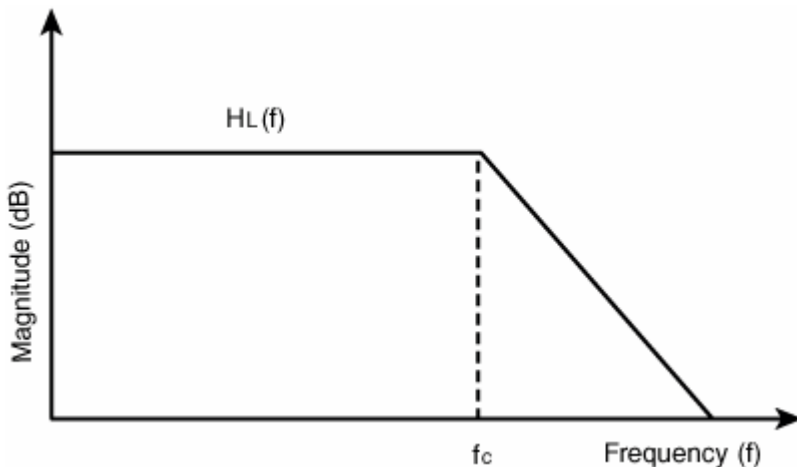
Serial data communication embeds the clock signal in its transmitting data bit stream. At the receiver side, this clock needs to be recovered through a clock recovery (CR) device where phase-locked loop (PLL) circuits are commonly used. It is well known that a PLL typically has certain frequency response characteristics. Therefore, when a receiver uses the recovered clock to time or retime the received data, the jitter seen by the receiver follows certain frequency response functions. [Figure 1.14](#) shows a typical serial link system with a transmitter (Tx), medium or channel, and receiver (Rx).

[Figure 1.14. A schematic block diagram for a serial link composed of three key elements: transmitter \(Tx\), medium \(or channel\), and receiver \(Rx\). Clock for Tx data generation and clock recovery \(CR\)/PLL for receiver are also shown.](#)



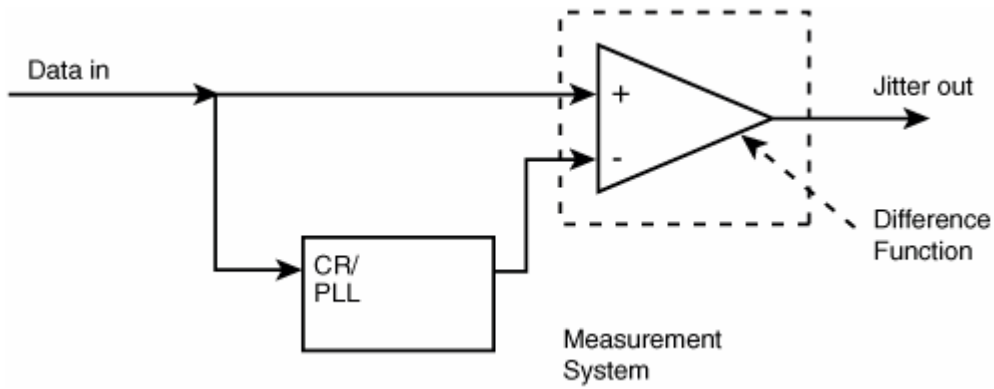
A PLL typically has a low-pass frequency response function $H_L(f)$, as shown in [Figure 1.15](#).

[Figure 1.15. A typical PLL magnitude frequency response.](#)



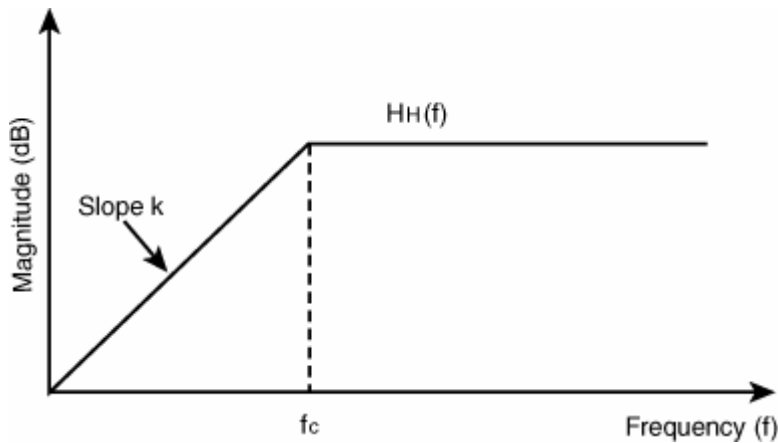
Any good estimation methodology should emulate the actual device behavior. In the case of receiver jitter, noise, and BER estimation/measurement, the model/measurement setup should estimate/measure the jitter as what a receiver sees. A receiver "sees" jitter on the data from its recovered clock.^[15] Therefore, it is a difference function from clock to data, as shown in [Figure 1.16](#).

[Figure 1.16. A jitter estimation/measurement system emulates jitter as seen by a serial data receiver. Note that the data latch function of "D" flip-flop in Figure 1.14 is replaced by the difference function to emulate the receiver jitter behavior.](#)



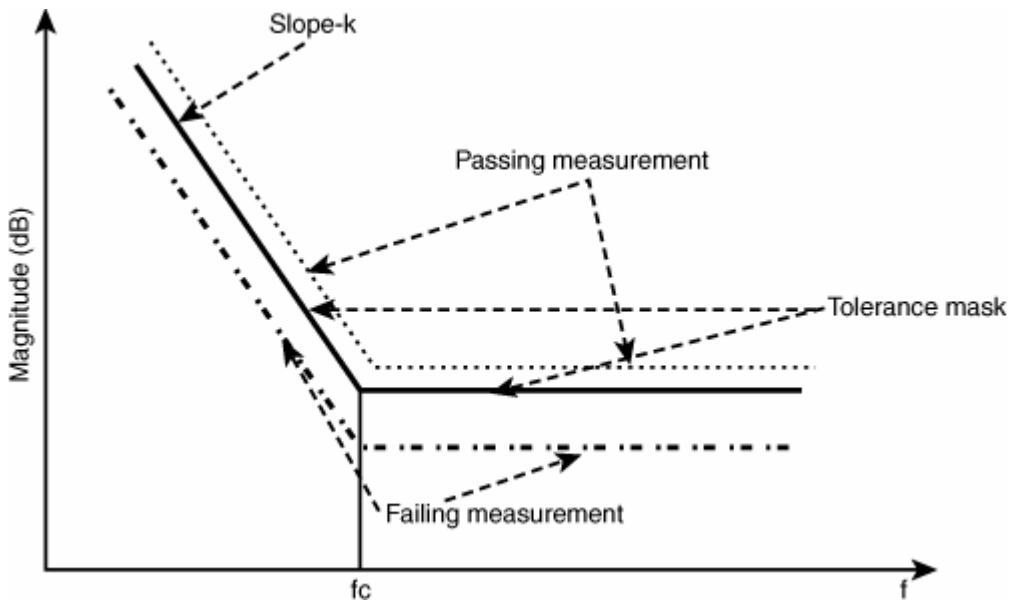
Because the clock recovery (or PLL) device has a low-pass transfer function $H_L(f)$, the jitter output has a high-pass transfer function of $H_H(f)$, as shown in Figure 1.17. $H_L(s) + H_H(s) = 1$, where s is a complex frequency.

Figure 1.17. Jitter frequency response as seen by a serial receiver or as measured by a difference function.



The high-pass jitter transfer function shown in Figure 1.17 suggests that a receiver can track more low-frequency jitter at frequencies of $f < f_c$ than at higher frequencies of $f > f_c$. This implies that a receiver can tolerate more low-frequency jitter than high-frequency jitter, with a jitter tolerance function being the reciprocal of the jitter output function, as shown in Figure 1.17. Figure 1.18 shows the jitter tolerance mask corresponding to the jitter transfer function in Figure 1.17.

Figure 1.18. The receiver jitter tolerance mask corresponding to the jitter transfer function shown in Figure 1.17.



Notice the same magnitude but different polarity slopes in [Figures 1.17](#) and [1.18](#) at frequencies at $f < f_c$. For a receiver tolerance test, a receiver should be able to tolerate more jitter than those defined in the [Figure 1.18](#) mask. So the mask is a minimum jitter magnitude as a function of frequency that a receiver must satisfy. When the mask has a second-order slope—namely, -40dB/decade —a receiver with a first-order jitter transfer function with a slope of 20 dB/decade does not meet the tolerance requirement. A second-order jitter transfer function may meet the tolerance requirement, and a third-order jitter transfer function with a 60 dB/decade slope will exceed the tolerance requirement.

The jitter transfer function is a very important element in estimating the relevant jitter in a serial link. Without this building block, it is not possible to estimate the relevant jitter for the system and related BER performance in a rational way. We will give detailed discussions by using the jitter transfer function when we discuss specific communication link technologies in the upcoming chapters.

Book: Jitter, Noise, and Signal Integrity at High-Speed
Section: Chapter 1. Introduction

No part of any chapter or book may be reproduced or transmitted in any form by any means without the prior written permission for reprints and excerpts from the publisher of the book or chapter. Redistribution or other use that violates the fair use privilege under U.S. copyright laws (see 17 USC107) or that otherwise violates these Terms of Service is strictly prohibited. Violators will be prosecuted to the full extent of U.S. Federal and Massachusetts laws.

Information Theory Computer Science Mike Peng Li Prentice Hall Jitter, Noise, and Signal Integrity at High-Speed

1.5. Historical Overview of Jitter, Noise, BER, and Signal Integrity

During the last two decades, two books were published with significant space dedicated to jitter analysis.^{[16], [17]} During that time, most communication architectures operated at a data rate of less than 1 Gb/s. Jitter was not as serious then as it is today, when most leading communication links are running at rates of 1 to 10 Gb/s.

The book by Trischitta & Varma^[16] in 1989 was mostly focused on the accumulated jitter in a network system and jitter related to some specific components in an optical network at the time, including regenerators, retimers, and multiplexers. The jitter handling in this book was tightly coupled with the link architecture of almost 20 years ago, so many of the concepts and theories in this book do not apply well to the serial link architectures developed after the 1990s.

The book by Takasaki^[17] in 1991 treated digital transmission design and jitter in the same context. This book is weighted more toward digital transmission, with only two chapters dedicated to jitter topics, covering jitter generation and accumulation. This book does discuss jitter classification in some way. The major point of Takasaki on jitter classification is that there are two types of jitter: random and systematic. However, it has no quantitative math model discussion on the jitter classification scheme. It also has no further discussion of the jitter component beyond random and systematic. The discussion of jitter accumulation is largely based on the repeater component in a network.

In the past 15 years, significant progress has been made in the field of understanding jitter, and related new theory, definition, analysis methods, and measurement tools. In particular, more rigorous definition of and theory about jitter and its associated jitter components have been developed (such as ^[15], ^[18], and ^[19], to name a few). Now jitter and noise component concepts have been widely accepted and adopted by many serial data communication standards. In fact, jitter and noise component concepts are required for determining the link jitter budget, for debugging and diagnostics for designing and testing most of the multiple Gb/s serial data links, and for setting standards. In addition, a generic jitter transfer function for a linear or quasi-linear system has recently been developed. Such a method can be applied to jitter analysis for most of the serial data communication links and standards ^[15], ^[20]. The combination of the statistical and system transfer function elements of a link system in estimating overall jitter, noise, BER (JNB), and signal integrity (SI) performance has put the research and application in those areas on a new historical plateau.

In light of that significant progress in JNB and SI, as well as the ever-increasing importance of their roles in > 1 Gb/s serial communication links in both network and PC applications, a new book summarizing that progress—with an emphasis on the latest definitions, theories, and applications, as well as simulation modeling, measurement, and analysis technologies—is apparently greatly needed.

Book: Jitter, Noise, and Signal Integrity at High-Speed
Section: Chapter 1. Introduction

No part of any chapter or book may be reproduced or transmitted in any form by any means without the prior written permission for reprints and excerpts from the publisher of the book or chapter. Redistribution or other use that violates the fair use privilege under U.S. copyright laws (see 17 USC107) or that otherwise violates these Terms of Service is strictly prohibited. Violators will be prosecuted to the full extent of U.S. Federal and Massachusetts laws.

Information Theory Computer Science Mike Peng Li Prentice Hall Jitter, Noise, and Signal Integrity at High-Speed

1.6. Overview of This Book

This book systematically presents the latest developments and advancements in jitter, noise, and BER (JNB) and SI. It guides you from the basic math, statistics, circuit, and system models to the final practical applications. It covers fundamental theory, to JNB and SI simulation/modeling, to JNB and SI diagnostics/debug and compliance testing, with an emphasis on two major applications: clock and serial data communications. It tries to keep a good balance and coupling between theory and practical applications.

As you have seen, this chapter is a high-level overview of JNB and SI basics. This chapter introduced the JNB component classification scheme, JNB interrelationship, root-cause mechanisms, JNB measurement references, clock recovery, and associated JNB transfer functions.

[Chapter 2](#) reviews and introduces the basic theories on statistics, linear time-invariant (LTI) systems, and digital signal processing that you need to quantitatively understand and model JNB and its related components. Also introduced in this chapter is the statistical signal process theory that is used to quantify the JNB spectrum and power spectrum density (PSD).

[Chapter 3](#) describes the jitter component in a quantitative manner. Detailed root causes and mathematical models and treatments for each jitter component are given. This chapter lays the necessary physical and mathematical foundation for jitter and noise to warrant the precision of the estimations. Jitter component math models can be applied to noise components similarly.

[Chapter 4](#) discusses jitter, noise, and BER correlatively from the view of statistical signal processing. It first discusses the jitter total PDF and its relationship with the PDFs of its component. It then discusses the noise total PDF and its relationship with the PDFs of its component. It also discusses the joint PDFs, with both jitter and noise being considered. Finally, it discusses the BER cumulative distribution function (CDF) and its relationship to both corresponding jitter and noise PDFs. Applications of two-dimensional eye diagram and BER contour are introduced.

[Chapter 5](#) focuses on jitter separation methods in the statistical distribution domain. Equipped with basic math knowledge, as well as the mechanism and physical nature of each jitter component, you will read about jitter separation. Jitter separation is an important step toward understanding and quantifying jitter components, because in reality the jitter that we observe or measure is a "compound" jitter with many components. Jitter separation methods based on jitter PDF and BER CDF are introduced. The "Tailfit" method in which random jitter PDF is quantified by a Gaussian distribution is first introduced for PDF-based jitter separation. Then the same method is applied to BER CDF-based distribution, in which the random jitter CDF is quantified by the integration of a Gaussian—namely, an error function.

[Chapter 6](#) discusses jitter separation methods in the time and frequency domain. Both spectrum (first moment) and PSD (second moment)-based jitter separation methods are introduced, and associated advantages and disadvantages of each method are given. This chapter also compares statistical PDF/CDF-based methods with spectrum and PSD-based jitter separation methods.

[Chapter 7](#) focuses on clock jitter because it is an important topic for all digital systems, so it deserves a dedicated treatment. New concepts of phase jitter, period jitter, cycle-to-cycle jitter, and their corresponding relationships are discussed. The mathematical relationship between phase jitter, period jitter, and cycle-to-cycle jitter is given in both time and frequency domain. Furthermore, phase jitter and its relationship to the conventional phase noise for quantifying the performance of clock or crystal oscillator in the frequency spectrum domain are also discussed.

[Chapter 8](#) focuses on PLL jitter because it is widely used in clock generation and clock recovery and is an important metric for any high-speed PLL. Jitter at the PLL output and its relationship with PLL building elements such as phase detector (PD), low-pass filter

(LPF), voltage control oscillator (VCO), and dividing/multiplying are discussed. Jitter as a function of PLL reference and internal noise sources and transfer functions is derived and applied to PLL and its jitter analysis for second-order, third-order, and general n th-order PLL implementations.

[Chapter 9](#) is dedicated to jitter, noise, and SI mechanisms and root-cause sources or mechanisms for a high-speed link system. Those mechanisms are discussed within the context of link architecture, including its subsystems of transmitter, receiver, channel, and reference clock. For the transmitter, reference clock jitter and voltage driver noise are discussed. For the receiver, jitter from clock recovery circuits and data sampler are the focus. For the channel, various losses in both copper- and optical-based channels are covered. For the reference clock, jitter due to PLL or crystal oscillator, as well as spread-spectrum clocking (SSC), are presented. This chapter also discusses the link jitter budget method using the RJ root-sum-square (RSS) method to ensure the link's interoperability and overall BER performance.

[Chapter 10](#) focuses on quantitative modeling and analysis for jitter, noise, and SI. Modeling and analysis methods are presented for link subsystems of transmitter, receiver, and channel within the framework of the LTI system theory. By using the cascading property of the LTI theorem, signal, jitter, and noise at the channel and receiver outputs are readily obtainable. Important subsystems of equalization and clock recovery are included in the modeling and analysis. For the equalization, both transmitter and receiver equalizations are considered. The modeling and analysis methods introduced in this chapter can give estimations for most advanced serial links today and are scalable to future link advancement given that they are LTI-based.

[Chapter 11](#) is dedicated to the various testing aspects of jitter, noise, and SI. It describes test implications and requirements for the link architectures/topologies operating mechanisms, with a focus on clock recovery and equalization. Testing requirements and methods for links with clock recovery and equalization are presented, covering transmitter, channel or medium, reference clock, and PLL. System test methods such as loopback test also are discussed.

[Chapter 12](#) is an executive summary and overview of the entire book. Future works and trends for JNB and SI at high speed as data rates keep increasing also are discussed.

Book: Jitter, Noise, and Signal Integrity at High-Speed
Section: Chapter 1. Introduction

No part of any chapter or book may be reproduced or transmitted in any form by any means without the prior written permission for reprints and excerpts from the publisher of the book or chapter. Redistribution or other use that violates the fair use privilege under U.S. copyright laws (see 17 USC107) or that otherwise violates these Terms of Service is strictly prohibited. Violators will be prosecuted to the full extent of U.S. Federal and Massachusetts laws.

Information Theory Computer Science Mike Peng Li Prentice Hall Jitter, Noise, and Signal Integrity at High-Speed

Endnotes

1. C. E. Shannon, "A Mathematical Theory of Communication," *Bell System Technical Journal*, vol. 27, pp. 379–423, 623–656, July, October, 1948.
2. H. Johnson and M. Graham, *High-Speed Digital Design: A Handbook of Black Magic*, Prentice-Hall, 1993.
3. A. B. Carlson, *Communication Systems: An Introduction to Signals and Noise in Electrical Communication*, Third Edition, McGraw-Hill, 1986.
4. J. B. Johnson, *Phys. Rev.*, vol. 32, pp. 97–109, 1928.
5. H. Nyquist, *Phys. Rev.*, vol. 32, pp. 110–113, 1928.
6. W. Schottky, *Ann. Phys.*, 57, 541, 1918.
7. J. B. Johnson, "Electronic Noise: The First Two Decades," *IEEE Spectrum*, vol. 8, pp. 42–46, 1971.
8. A. Van Der Ziel, *Noise in Solid State Devices and Circuits*, Wiley InterScience, 1986.
9. S. Lin and D. J. Costello, Jr., *Error Control Coding: Fundamentals and Applications*, Prentice-Hall, 1983.
10. G. P. Agrawal, *Fiber Optic Communication Systems*, a Wiley InterScience Publication, John Wiley & Sons, Inc., Second Edition, 1997.
11. S. H. Hall, G. W. Hall, and J. A. McCall, *High-Speed Digital System Design: A Handbook of Interconnect Theory and Design Practices*, a Wiley InterScience Publication, John Wiley & Sons, Inc., 2000.
12. M. Li, *Design and Test for Multiple Gbps Communication Devices and Systems*, International Engineering Consortium (IEC), 2005.
13. National Committee for Information Technology Standardization (NCITS), Working Draft for "Fiber Channel—Methodologies for Jitter Specification," Rev. 10, 1999.
14. R. E. Best, *Phase-Locked Loops: Design, Simulation, and Applications*, Fourth Edition, McGraw-Hill, 1999.
15. M. Li and J. Wilstrup, "Paradigm Shift for Jitter and Noise in Design and Test > 1 Gb/s Communication Systems," an invited paper, IEEE International Conference on Computer Design (ICCD), 2003.
16. P. R. Trischitta and E. L. Varma, *Jitter in Digital Transmission Systems*, 1989, Artech House.
17. Y. Takasaki, *Digital Transmission Design and Jitter Analysis*, 1991, Artech House.
18. J. Wilstrup, "A Method of Serial Data Jitter Analysis Using One-Shot Time Interval Measurements," IEEE International Test Conference (ITC), 1998.
19. M. Li, J. Wilstrup, R. Jessen, and D. Petrich, "A New Method for Jitter Decomposition Through Its Distribution Tail Fitting," IEEE International Test Conference (ITC), 1999.

20. M. Li, "Statistical and System Approaches for Jitter, Noise and Bit Error Rate (BER) Tests for High Speed Serial Links and Devices," IEEE International Test Conference (ITC), 2005.

Book: Jitter, Noise, and Signal Integrity at High-Speed

No part of any chapter or book may be reproduced or transmitted in any form by any means without the prior written permission for reprints and excerpts from the publisher of the book or chapter. Redistribution or other use that violates the fair use privilege under U.S. copyright laws (see 17 USC107) or that otherwise violates these Terms of Service is strictly prohibited. Violators will be prosecuted to the full extent of U.S. Federal and Massachusetts laws.

Information Theory Computer Science Mike Peng Li Prentice Hall Jitter, Noise, and Signal Integrity at High-Speed

2. Statistical Signal and Linear Theory for Jitter, Noise, and Signal Integrity

This chapter discusses statistical signal and linear system theory in two parts. Part A focuses on the relevant topics of random variables and distribution, statistical estimators, sampling theorem, statistical process, and spectral analysis. Part B focuses on linear time-invariant (LTI) theorem, statistical estimators, and power spectrum density (PSD) analysis within an LTI system. Those theorems will be used extensively throughout the rest of the book.

Book: Jitter, Noise, and Signal Integrity at High-Speed

Section: Chapter 2. Statistical Signal and Linear Theory for Jitter, Noise, and Signal Integrity

No part of any chapter or book may be reproduced or transmitted in any form by any means without the prior written permission for reprints and excerpts from the publisher of the book or chapter. Redistribution or other use that violates the fair use privilege under U.S. copyright laws (see 17 USC107) or that otherwise violates these Terms of Service is strictly prohibited. Violators will be prosecuted to the full extent of U.S. Federal and Massachusetts laws.

Information Theory Computer Science Mike Peng Li Prentice Hall Jitter, Noise, and Signal Integrity at High-Speed

Part A: Probability, Statistics, Stochastic Signal

We will introduce only statistical topics that are used and relevant to the rest of the chapters. We do not intend to cover details and treat statistical subjects very rigorously that can be found in other books and articles dedicated to statistics.

Book: Jitter, Noise, and Signal Integrity at High-Speed

Section: Chapter 2. Statistical Signal and Linear Theory for Jitter, Noise, and Signal Integrity

No part of any chapter or book may be reproduced or transmitted in any form by any means without the prior written permission for reprints and excerpts from the publisher of the book or chapter. Redistribution or other use that violates the fair use privilege under U.S. copyright laws (see 17 USC107) or that otherwise violates these Terms of Service is strictly prohibited. Violators will be prosecuted to the full extent of U.S. Federal and Massachusetts laws.

Information Theory Computer Science Mike Peng Li Prentice Hall Jitter, Noise, and Signal Integrity at High-Speed

2.1. Random Variables and Distribution

This section introduces random variables, probability, and probability distribution functions. Associated mathematical basics are also discussed.

2.1.1. Random Variables and Probability

This subsection discusses a mathematical description of the probability for a random variable or process. Properties for probability for random variables, their probability and joint probability functions, whether dependent or independent, are also given.

2.1.1.1. Basic Definition

Statistically, a random variable represents a phenomenon whose outcome cannot be predicted. It is easier to demonstrate the concept of a random variable through a statistical experiment. Suppose that in an experiment, an event A can have two only consequences—occur or not occur. One example of such an experiment is flipping a coin; each experiment can only result in either heads or tails. If the experiment is repeated N times, and event A occurs N_A times, the occurrence frequency of event A is defined as follows:

Equation 2.1

$$f(A) = \frac{N_A}{N}$$

If N approaches very large and f(A) yields or converges to the same limit, we say that the relative frequency approaches a probability for the occurrence of event A, and we define this probability as follows:

Equation 2.2

$$P(A) = \frac{N_A}{N} \quad \text{and } N \rightarrow \infty$$

A few properties are associated with probability P(A):

.

$$0 \leq P(A) \leq 1$$

$$P(A) + P(\bar{A}) = 1, \quad \bar{A} \text{ means NOT event A}$$

2.1.1.2. Joint Probability

Suppose two events, A and B, are involved in an experiment, and we repeat the experiment N times. If the number of events where A and B occur simultaneously is N_{AB} , the "and" joint probability of A and B is

Equation 2.3

$$P(AB) = \frac{N_{AB}}{N} \quad \text{and } N \rightarrow \infty$$

Here AB means "A•B," or "A and B."

The "or" probability—the probability that event A or B will occur—is given by

Equation 2.4

$$P(A+B) = P(A) + P(B) - P(AB)$$

If A and B are mutually exclusive—in other words, A and B cannot happen at the same time— $P(AB) = 0$ by definition, and we have

Equation 2.5

$$P(A+B) = P(A) + P(B)$$

2.1.1.3. Conditional Probability

Conditional probability deals with the occurrence probability of one event under the condition that another event has occurred. Mathematically, the probability that event B will occur under the condition that A has occurred is given by

Equation 2.6

$$P(B|A) = \frac{P(AB)}{P(A)}$$

[Equation 2.6](#) implies that $P(A)$ has to be > 0 . Another way to understand this equation is that conditional probability of $P(B|A)$ is invalid if $P(A) = 0$.

The definition of [equation 2.6](#) is interchangeable. In other words, the probability of event A occurring under the condition that B has occurred is given by

Equation 2.7

$$P(A|B) = \frac{P(AB)}{P(B)}$$

The common linkage between [equations 2.6](#) and [2.7](#) is the "and" joint probability $P(AB)$. From [equations 2.6](#) and [2.7](#), we get the following equations:

Equation 2.8

$$P(A|B) = \frac{P(B|A)P(A)}{P(B)} \quad \text{or} \quad P(B|A) = \frac{P(A|B)P(B)}{P(A)}$$

Equation 2.8 is very useful because it enables the reverse condition probability calculation. Suppose $P(A)$ and $P(B)$ are known. If $P(B|A)$ is given, $P(A|B)$ can be estimated based on this equation. Similarly, if $P(A|B)$ is given, $P(B|A)$ can be estimated. Equation 2.8 is also known as Bayes' Theorem.

2.1.1.4. Statistical Independence

With the definition of conditional probability accomplished, we are ready to discuss statistical independence. If the condition for a conditional probability does not affect the outcome of the conditional probability, or, in mathematical terms,

Equation 2.9

$$P(A|B) = P(A) \quad \text{or} \quad P(B|A) = P(B)$$

we say that events A and B are independent. Using equation 2.7, we have the following consequence for the "and" joint probability if A and B are independent:

Equation 2.10

$$P(AB) = P(A)P(B)$$

Equation 2.10 can be generalized to n independent events of the following equation:

Equation 2.11

$$P(A_1 A_2 A_3 \dots A_n) = P(A_1)P(A_2)P(A_3)\dots P(A_n)$$

Equation 2.11 says that the "and" joint probability of n independent statistical events equals the product of the probability of each independent event.

2.1.2. Distribution Functions

There are two types of random variables: discrete and continuous. Commonly encountered physical parameters such as analog voltage and current noise are continuous variables. Digital error rate and circuit failure rate are discrete variables. We will start with continuous variables and give a detailed derivation of the related theory. We then will extend similar results for the discrete variables. The major difference between a discrete variable and a continuous variable is that the summation for a discrete variable becomes integration for a continuous variable.

2.1.2.1. Probability Density Function (PDF)

Suppose that x is a random variable under consideration. For example, x can be voltage noise, current noise, or timing jitter. We define that the probability for x in the range of x to $x+dx$ is $p(x)dx$. Then we call $p(x)$ as the probability density function for the variable x because it represents the probability per unit x.

PDF obeys the following properties:

Equation 2.12

$$p(x) \geq 0, \quad \int_{-\infty}^{\infty} p(x)dx = 1$$

Apparently, the probability $P(a \leq x \leq b)$ for variable x in the interval between a and b is given by the following:

Equation 2.13

$$P(a \leq x \leq b) = \int_a^b p(x)dx$$

2.1.2.2. Cumulative Distribution Function (CDF)

CDF is the integration of the PDF function to a certain value. It is defined by the following equation:

Equation 2.14

$$P(X) = \int_{-\infty}^X p(x)dx$$

Here X is the variable for the CDF function $P(X)$. You can see that CDF $P(X)$ has a variable that is the upper limit of the PDF integral. Considering the relationships between [equations 2.12](#), [2.13](#), and [2.14](#), we have the following property for CDF:

Equation 2.15

$$P(b) - P(a) = \int_{-\infty}^b p(x)dx - \int_{-\infty}^a p(x)dx = \int_a^b p(x)dx = P(a \leq x \leq b)$$

A CDF function is bounded by

Equation 2.16

$$0 \leq P(X) \leq 1$$

Because PDF $p(x)$ is nonnegative, it follows that CDF $P(X)$ is a nondecreasing function. In other words, CDF always satisfies the following:

Equation 2.17

$$\frac{dP(X)}{dX} \geq 0$$

In addition, at the extreme values for X ($X = -\infty$ and $X = \infty$), the CDF values are

Equation 2.18

$$P(-\infty) = 0, \quad \text{and} \quad P(\infty) = 1$$

For illustration purposes, let's assume a uniform PDF of

Equation 2.19

$$p_u(x) = \begin{cases} \frac{1}{b-a} & \text{for } a \leq x \leq b \\ 0 & \text{others} \end{cases}$$

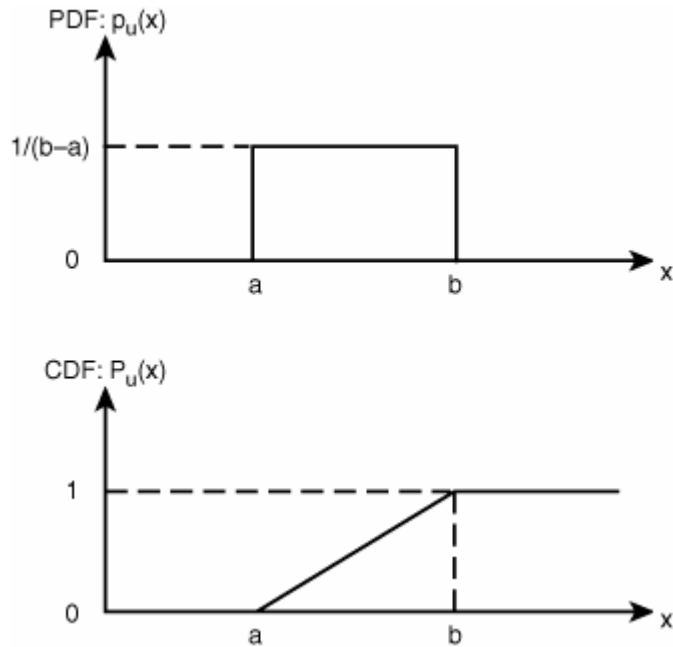
Then the corresponding CDF can be calculated based on [equation 2.14](#) as the following:

Equation 2.20

$$P_u(x) = \begin{cases} 0 & x < a \\ \frac{x-a}{b-a} & a \leq x \leq b \\ 1 & x > b \end{cases}$$

Graphically, this can be shown by [Figure 2.1](#).

Figure 2.1. A uniform PDF function and its corresponding CDF function.



2.1.2.3. Relationship Between PDF and CDF

PDF $p(x)$ and CDF $P(x)$ are related through differentiation or integration. If the PDF function $p(x)$ is known, you can calculate CDF $P(x)$ through the integration, as shown in [equation 2.14](#). Conversely, if CDF $P(x)$ is known, the PDF function $p(x)$ can be calculated through differentiation of the following:

Equation 2.21

$$p(x) = \frac{dP(x)}{dx}$$

[Equation 2.14](#) uses lowercase x for $p(x)$ and uppercase X for $P(X)$. Two variables are involved in an integration: dummy x and state

variable X. [Equation 2.21](#) uses only one variable notation for both the PDF and CDF functions because differentiation does not introduce two variables for math representation purposes. The variable interchange does not affect the nature of those distribution functions.

2.1.2.4. PDFs of Related Variables

An often-encountered problem in PDF estimation is that a PDF function $p_1(x)$ is known, and another random variable y is related to x through $y = f(x)$. What is the PDF $p_2(y)$ as a function of y ?

This is essentially a variable-mapping problem. If the relationship between y and x is one-to-one correspondence, or $y(x)$ is a monotonic function, the probability over a differential range of dx in x -variable space corresponds to the same probability over a similar differential range of dy . Mathematically, this means that

Equation 2.22

$$p_1(x)dx = p_2(y)dy$$

Because both $p_1(x)$ and $p_2(y)$ are nonnegative functions, we need to maintain dx/dy as a positive. Also, $y = f(x)$ is a monotonical function, the inverse solution exists, and we have $x = f^{-1}(y)$. With those two considerations, $p_2(y)$ can be estimated as

Equation 2.23

$$p_2(y) = p_1(x) \left| \frac{dx}{dy} \right| = p_1(f^{-1}(y)) \left| \frac{df^{-1}(y)}{dy} \right|$$

Conversely, if $p_1(x)$ needs to be estimated, the following equation provides the answer:

Equation 2.24

$$p_1(x) = p_2(y) \left| \frac{dy}{dx} \right| = p_2(f(x)) \left| \frac{df(x)}{dx} \right|$$

2.1.2.5. Multidimensional PDF and CDF

We have introduced PDF and CDF with only one statistical variable. The basic concept can be extended to n -dimensional with n variables. Suppose that x_1, x_2, \dots, x_n are n statistical variables and that $p(x_1, x_2, \dots, x_n)$ is the n -dimensional PDF function. And the probability over $x_1-x_1+dx_1, x_2-x_2+dx_2, \dots, x_n-x_n+dx_n$ is $p(x_1, x_2, \dots, x_n) dx_1 dx_2 \dots dx_n$. Given the n -dimensional PDF function $p(x_1, x_2, \dots, x_n)$, the corresponding CDF function can be estimated as follows:

Equation 2.25

$$P(X_1, X_2, \dots, X_n) = \int_{-\infty}^{x_1} \int_{-\infty}^{x_2} \dots \int_{-\infty}^{x_n} p(x_1, x_2, \dots, x_n) dx_1 dx_2 \dots dx_n$$

As in the case of one-dimensional, n -dimensional PDF and CDF functions have certain properties. For PDF function, we have nonnegative and unit area properties of

Equation 2.26

[\[View full size image\]](#)

$$p(x_1, x_2, \dots, x_n) \geq 0 \quad \text{and} \quad \int_{-\infty}^{\infty} \int_{-\infty}^{\infty} \dots \int_{-\infty}^{\infty} p(x_1, x_2, \dots, x_n) dx_1 dx_2 \dots dx_n = 1$$

For a CDF function, we have range and unit properties of

Equation 2.27

[View full size image]

$$0 \leq P(X_1, X_2, \dots, X_n) \leq 1, \quad \text{and} \quad P(-\infty, -\infty, \dots, -\infty) = 0, \quad \text{and} \quad P(\infty, \infty, \dots, \infty) = 1$$

Integration [equation 2.25](#) gives the relationship from PDF to CDF. If the CDF is known, the corresponding PDF can be calculated through the following differentiation operation:

Equation 2.28

$$p(x_1, x_2, \dots, x_n) = \frac{\partial^n}{\partial x_1 \partial x_2 \dots \partial x_n} P(x_1, x_2, \dots, x_n)$$

2.1.2.6. PDF and CDF for Independent Variables

If n statistical variables are independent, for X_1, X_2, \dots, X_n of CDF $P(X_1, X_2, \dots, X_n)$, we have

Equation 2.29

$$P(X_1, X_2, \dots, X_n) = P_1(X_1)P_2(X_2) \dots P_n(X_n)$$

It is also true that for n independent statistical variables of x_1, x_2, \dots, x_n for PDF $p(x_1, x_2, \dots, x_n)$, we have

Equation 2.30

$$p(x_1, x_2, \dots, x_n) = p_1(x_1)p_2(x_2) \dots p_n(x_n)$$

2.1.2.7. PDF for the Sum of Two Statistical Variables

Here's a commonly encountered and interesting problem: If the PDF of the joint probability for random variables of x and y is known as $f(x,y)$, what is the PDF function for the variable $z = x+y$? For example, if a signal amplitude has both noise from crosstalk (represented by x) and thermal noise (represented by y), and you want to find the PDF function for the sum of those two noise sources (represented by z), you want the same solution that we will discuss.

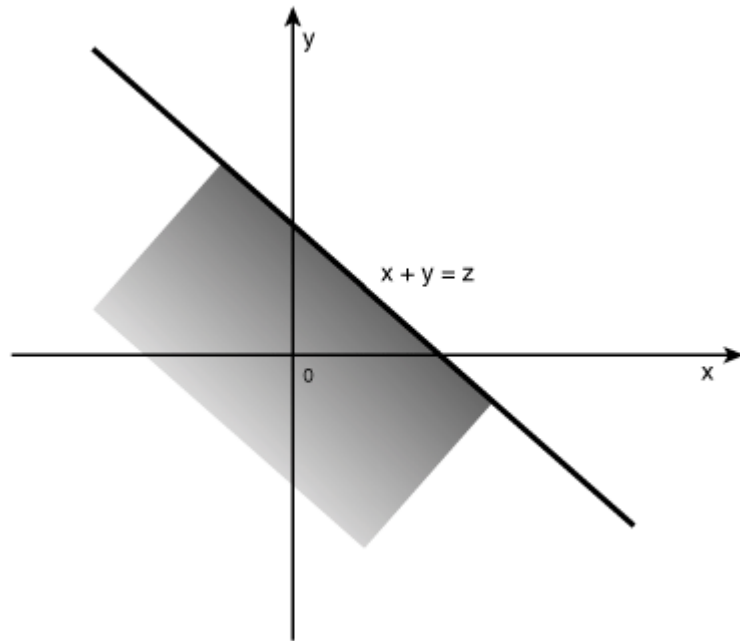
Let's first consider the CDF function $F(z)$ of $z = x+y$. $F(z)$ equals the integration of $f(x, y)$ over the region $x+y \leq z$, given by the following equation:

Equation 2.31

$$F(z) = \int \int_{x+y \leq z} f(x, y) dx dy$$

Figure 2.2 shows the integration region of $x+y \leq z$.

Figure 2.2. The integration region (represented by the shading) for $x+y \leq z$.



Integration by parts yields the following:

Equation 2.32

$$F(z) = \int_{-\infty}^{\infty} \left[\int_{-\infty}^{z-y} f(x, y) dx \right] dy$$

If we take the derivative for [equation 2.32](#), we get the following:

Equation 2.33

[\[View full size image\]](#)

$$\frac{dF(z)}{dz} = \frac{d}{dz} \left\{ \int_{-\infty}^{\infty} \left[\int_{-\infty}^{z-y} f(x, y) dx \right] dy \right\} = \int_{-\infty}^{\infty} \left[\frac{d}{dz} \int_{-\infty}^{z-y} f(x, y) dx \right] dy = \int_{-\infty}^{\infty} f(z-y, y) dy$$

$$\frac{dF(z)}{dz} = f_z(z)$$

Because $\frac{dF(z)}{dz} = f_z(z)$, where $f(z)$ is the PDF for z , we have the following equation for $f(z)$:

Equation 2.34

$$f_z(z) = \int_{-\infty}^{\infty} f(z-y, y) dy$$

Equation 2.34 gives the mathematical foundation for estimating PDF for a random variable that is the sum of the other two random variables. One particular scenario is worth further discussion. If x and y are two *independent* variables, $f(x,y)$ can be represented by

Equation 2.35

$$f(x,y) = f_x(x)f_y(y)$$

where $f_x(x)$ and $f_y(y)$ are PDFs for x and y , respectively. Substituting equation 2.35 into 2.34, we get

Equation 2.36

$$f_z(z) = \int_{-\infty}^{\infty} f_x(z-y)f_y(y)dy$$

using y as the integration variable. Similarly, if we use x as the integration variable, we get

Equation 2.37

$$f_z(z) = \int_{-\infty}^{\infty} f_x(x)f_y(z-x)dx$$

The right side of equations 2.36 and 2.37 defines a *convolution* of f_x with f_y . Therefore, we have found a rule that when two variables are independent, the PDF for the variable that is the sum of those two independent variables equals the convolution of the PDFs of the two independent variables. If we use $*$ to define a convolution, equations 2.36 and 2.37 can be equivalently written in a different form:

Equation 2.38

$$f_z = f_x * f_y = f_y * f_x$$

It turns out that equation 2.38 can be extended to a variable that is the sum of n independent variables. In other words, if $x_s = x_1 + x_2 + \dots + x_n$, x_1, x_2, \dots, x_n are independent, and their corresponding PDFs are $f_1(x_1), f_2(x_2), \dots, f_n(x_n)$, the PDF for x_s , f_s is

Equation 2.39

$$f_s = f_1 * f_2 * \dots * f_n$$

Note that the convolution is interchangeable in order, so equation 2.39 is just one way to represent the convolution of many functions.

The PDF for the sum of many independent variables expressed in equation 2.39 is very important, because it is used throughout the entire book for jitter and noise analysis, for their separation into variable independent components, or for estimation from independent component PDFs to the overall PDF for the variable that equals the sum of independent variables.

User name: CSU San Diego

Book: Jitter, Noise, and Signal Integrity at High-Speed

Section: Chapter 2. Statistical Signal and Linear Theory for Jitter, Noise, and Signal Integrity

No part of any chapter or book may be reproduced or transmitted in any form by any means without the prior written permission for reprints and excerpts from the publisher of the book or chapter. Redistribution or other use that violates the fair use privilege under U.S. copyright laws (see 17 USC107) or that otherwise violates these Terms of Service is strictly prohibited. Violators will be prosecuted to the full extent of U.S. Federal and Massachusetts laws.

Information Theory Computer Science Mike Peng Li Prentice Hall Jitter, Noise, and Signal Integrity at High-Speed

2.2. Statistical Estimates

We have discussed statistical distribution for a random variable. Although statistical distribution is necessary and important, some characteristics of the variable can be learned through its moments such as mean (or average) or standard deviation.

2.2.1. Expectation or Average

Suppose variable $g(x)$ has a corresponding PDF of $p(x)$. The statistical average or mean for $g(x)$ is defined by [equation 2.40](#):

Equation 2.40

$$\overline{g(x)} = E(g(x)) = \int_{-\infty}^{+\infty} g(x)p(x)dx$$

[Equation 2.40](#) is defined for a single random variable and can be easily extended to multiple variables. In the case when $g = g(x,y)$, the average or expectation can be estimated by [equation 2.41](#):

Equation 2.41

$$E(g(x,y)) = \int_{-\infty}^{+\infty} \int_{-\infty}^{\infty} g(x,y)p(x,y)dxdy$$

Of particular interest is that when x and y are independent and $g(x,y) = g_1(x)g_2(y)$, we have

Equation 2.42

[\[View full size image\]](#)

$$E(g_1(x)g_2(y)) = \int_{-\infty}^{+\infty} \int_{-\infty}^{\infty} g_1(x)g_2(y)p(x,y)dxdy = \int_{-\infty}^{+\infty} g_1(x)p_1(x)dx \int_{-\infty}^{+\infty} g_2(y)p_2(y)dy$$

[Equation 2.42](#) is in fact

Equation 2.43

$$E(g_1(x)g_2(y)) = E(g_1(x))E(g_2(y))$$

Equation 2.43 can be extended to n independent variables. Thus, we have a general rule that says the mean of a statistical variable that is the product of many statistically independent random variables equals the product of means for each independent variable. This is equivalent to the following equation:

Equation 2.44

$$E(g_1(x_1)g_2(x_2)\dots g_n(x_n)) = E(g_1(x_1))E(g_2(x_2))\dots E(g_n(x_n))$$

The mean or average has the following properties:

If c is a constant, $E(c) = c$

$E(cx) = cE(x)$

$E(x+y) = E(x)+E(y)$, where both x and y are random variables

2.2.2. Variance

We have discussed the statistical mean that represents the steady measure of the variable. Another related statistical measure is called variance, and it represents the spread of the random variable fluctuation around its mean value. The mathematical definition of the variance is given by the following:

Equation 2.45

$$Var(x) = E[(x - \bar{x})^2] = \int_{-\infty}^{+\infty} (x - \bar{x})^2 p(x) dx$$

It follows that

Equation 2.46

[View full size image]

$$Var(x) = \int_{-\infty}^{+\infty} (x^2 p(x) - x \bar{x} p(x) + \bar{x}^2 p(x)) dx = E(x^2) - 2\bar{x} \cdot \bar{x} + [\bar{x}]^2 = E(x^2) - [\bar{x}]^2$$

The variance can be shown to have the following properties:

If c is a constant, $Var(c) = 0$

$Var(cx) = c^2 Var(x)$

If x and y are independent random variables, $Var(x+y) = Var(x)+Var(y)$

The standard deviation or σ_x is defined as the square root of the variance:

Equation 2.47

$$\sigma_x = \sqrt{Var(x)}$$

2.2.3. Moments

Moments are an important statistical measure and are a generalization of some of the known statistical measures, such as mean and standard deviation. For a random variable x , its n th moment is defined as

Equation 2.48

$$E(x^n) = \int_{-\infty}^{+\infty} x^n p(x) dx$$

When $n = 1$, [equation 2.48](#) gives the definition for the mean $E(x)$ or average for x , as given by the following equation:

Equation 2.49

$$E(x) = \bar{x} = \int_{-\infty}^{+\infty} x p(x) dx$$

When $n = 2$, [equation 2.48](#) gives the second moment for x , or $E(x^2)$. $E(x^2)$ is of particular interest, because when x is a physical quantity such as voltage or current, $E(x^2)$ represents the average power.

The moment defined in [equation 2.48](#) is referenced to zero. Another important moment is the n th central moment; it is referenced to the mean of the random variable itself. It is given by the following:

Equation 2.50

$$E[(x - \bar{x})^n] = \int_{-\infty}^{+\infty} (x - \bar{x})^n p(x) dx$$

2.2.3.1. Second Central Moment and Variance

Of particular interest is the case when $n = 2$: the second central moment that is, in fact, the variance of x , or

Equation 2.51

$$E[(x - \bar{x})^2] = \int_{-\infty}^{+\infty} (x - \bar{x})^2 p(x) dx = Var(x)$$

2.2.3.2. Third Central Moment and Skewness

The third central moment is related to a statistical measure called skewness. Skewness specifies whether the distribution is symmetrical. It is defined by the following:

Equation 2.52

$$S_3(x) = \frac{E[(x - \bar{x})^3]}{\sigma_x^3}$$

If the distribution has a skewness of $S_3 = 0$, the distribution must be symmetrical. When $S_3 > 0$, the distribution is skewed toward the right or has a longer "right" tail in the distribution. Similarly, $S_3 < 0$ means that the distribution is skewed toward the left or has a longer "left" tail in the distribution.

2.2.3.3. Fourth Central Moment and Kurtosis

The fourth central moment is related to a statistical measure called kurtosis. Kurtosis implies the sharpness or peakness of a distribution, generally relative to a Gaussian distribution. The Kurtosis is defined as follows:

Equation 2.53

$$S_4(x) = \frac{E[(x - \bar{x})^4]}{\sigma_x^4}$$

2.2.4. The Chebyshev Inequality

A commonly encountered problem is estimating the probability limit when the distance of the random variable to its mean is larger than a certain value. The Chebyshev Inequality provides a direct answer to this question.

For any random variable, the following equations and inequalities always hold:

Equation 2.54

$$E(|y|^2) = \int_{-\infty}^{+\infty} |y|^2 p(y) dy \geq \int_{|y| \geq \varepsilon} |y|^2 p(y) dy \geq \varepsilon^2 \int_{|y| \geq \varepsilon} p(y) dy$$

for any positive value ε . The second inequality comes from $|y| \geq \varepsilon$. The preceding inequality can be written in another format:

Equation 2.55

$$P(|y| \geq \varepsilon) \leq \frac{E(|y|^2)}{\varepsilon^2}$$

We can substitute the preceding inequality with another shifted variable of $y = x - \bar{x}$ such that

$$P(|x - \bar{x}| \geq \varepsilon) \leq \frac{E((x - \bar{x})^2)}{\varepsilon^2}$$

Because $E((x - \bar{x})^2) = Var(x) = \sigma_x^2$, substituting this into equation 2.55, we have

Equation 2.56

$$P(|x - \bar{x}| \geq \varepsilon) \leq \frac{\sigma_x^2}{\varepsilon^2}$$

Equation 2.56 is called the Chebyshev Inequality. It can also have another form:

Equation 2.57

$$P(|x - \bar{x}| < \varepsilon) > 1 - \frac{\sigma_x^2}{\varepsilon^2}$$

The Chebyshev Inequality is very useful in estimating the probability of the dispersion for a random variable. For example, if we take $\varepsilon = 3\sigma_x$, using equation 2.57 we will have the following inequality:

Equation 2.58

$$P(|x - \bar{x}| < 3\sigma_x) > 0.888889$$

If we take $\varepsilon = 6\sigma_x$, the answer will be

Equation 2.59

$$P(|x - \bar{x}| < 6\sigma_x) > 0.972222$$

2.2.5. Correlation

So far, we have focused on statistical estimations for a single variable in most cases. An interesting scenario that we need to discuss is when the statistical distribution has multiple variables, particularly two variables.

Suppose that the joint probability distribution function for random x and y is $p(x,y)$. Then the expectations for x and y are

Equation 2.60

$$E(x) = \int_{-\infty}^{\infty} \int_{-\infty}^{\infty} x p(x,y) dx dy$$

and

$$E(y) = \int_{-\infty}^{\infty} \int_{-\infty}^{\infty} y p(x,y) dx dy$$

The variances for x and y are

Equation 2.61

$$Var(x) = E[(x - \bar{x})^2] = \int_{-\infty}^{+\infty} \int_{-\infty}^{\infty} (x - \bar{x})^2 p(x, y) dx dy$$

and

Equation 2.62

$$Var(y) = E[(y - \bar{y})^2] = \int_{-\infty}^{+\infty} \int_{-\infty}^{\infty} (y - \bar{y})^2 p(x, y) dx dy$$

With these renewed definitions for expectation and variance in the context of joint distribution, we are ready to define the covariance for x and y as

Equation 2.63

$$Cov(x, y) = E[(x - \bar{x})(y - \bar{y})] = \int_{-\infty}^{+\infty} \int_{-\infty}^{\infty} (x - \bar{x})(y - \bar{y}) p(x, y) dx dy$$

Expanding [equation 2.63](#), we get

Equation 2.64

$$Cov(x, y) = E(xy) - E(x)E(y)$$

If we consider the variance of the sum of two variables in a general case, we have

Equation 2.65

$$Var(x + y) = E[((x + y) - \bar{x} - \bar{y})^2] = E[(x - \bar{x})^2] + E[(y - \bar{y})^2] + 2E[(x - \bar{x})(y - \bar{y})]$$

Using the definitions for variance and covariance, [equation 2.65](#) can be written as

Equation 2.66

$$Var(x + y) = Var(x) + Var(y) + 2Cov(x, y)$$

If x and y are independent, we have $E(xy) = E(x)E(y)$. Using this property, we have $Cov(x, y) = E[(x - \bar{x})(y - \bar{y})] = E[(x - \bar{x})]E[(y - \bar{y})] = 0$. Therefore, [equation 2.66](#) becomes $Var(x+y) = Var(x) + Var(y)$.

You can see that the covariance is related to the dependence between x and y. The correlation coefficient between x and y is defined as

Equation 2.67

$$\rho_{xy} = \frac{Cov(x, y)}{\sqrt{Var(x)}\sqrt{Var(y)}}$$

The Cauchy-Schwarz inequality says

Equation 2.68

$$\text{Var}(x)\text{Var}(y) \geq [\text{Cov}(x, y)]^2$$

Therefore, we have

Equation 2.69

$$\rho_{xy}^2 = \frac{[\text{Cov}(x, y)]^2}{\text{Var}(x)\text{Var}(y)} \leq 1$$

As such, the correlation coefficient satisfies the following:

Equation 2.70

$$|\rho_{xy}| \leq 1, \quad \text{or} \quad -1 \leq \rho_{xy} \leq 1$$

We have shown that the range for the correlation coefficient is between -1 and 1 . When the coefficients are -1 or 1 , it can be shown that x and y are linearly related. When $\rho_{xy} = 0$, x and y are uncorrelated. However, we need to point out that when both x and y are uncorrelated, they may not necessarily be independent. Conversely, if x and y are independent, we will always have $\rho_{xy} = 0$, and x and y will always be unrelated.

These statistical correlation relationships and properties between two variables are very important math foundations in dealing with jitter and noise in the context of eye diagrams, discussed in later chapters.

URL <http://access.proquest.safaribooksonline.com/9780132429610/ch02lev1sec3>

User name: CSU San Diego

Book: Jitter, Noise, and Signal Integrity at High-Speed

Section: Chapter 2. Statistical Signal and Linear Theory for Jitter, Noise, and Signal Integrity

No part of any chapter or book may be reproduced or transmitted in any form by any means without the prior written permission for reprints and excerpts from the publisher of the book or chapter. Redistribution or other use that violates the fair use privilege under U.S. copyright laws (see 17 USC107) or that otherwise violates these Terms of Service is strictly prohibited. Violators will be prosecuted to the full extent of U.S. Federal and Massachusetts laws.

Information Theory Computer Science Mike Peng Li Prentice Hall Jitter, Noise, and Signal Integrity at High-Speed

2.3. Sampling and Estimation

This section deals with sampling and estimation, an important and necessary subject related to simulation and measurements of jitter, noise, and signal integrity. An inappropriate sampling or estimation method would cause inaccuracy in the subsequent measurement or analysis, or inaccurate or even wrong conclusions. It is necessary to understand the relevant basic math before we get into the detailed applications.

2.3.1. Sample Estimators and Convergence

In our discussion of the probability distribution, we either explicitly or implicitly assume that we have knowledge of its distribution function, and the estimations are drawn or derived from those known distribution functions. This is also called population distribution-based statistics. In practical applications, however, what we face is different. Often what we have are values of a statistical distribution or process through a number of experiments. We try to learn or derive the distribution function and estimators of the underlying statistical distribution through these sampling experiments. In other words, we are trying to learn or draw conclusions about the population statistics from the sampling statistics. This subsection first introduces the estimation methods for mean and variance based on statistical samples, rather than statistical probability distribution. Then we will introduce the law of large numbers and answer the question when an estimation based on samples approaches that of the distribution. After that we will introduce the central limiting theorem, which deals with the sampling distribution when the samples are drawn from various statistically independent processes.

2.3.1.1. Mean, Standard Deviation, and Peak-to-Peak Estimations

Suppose that x_1, x_2, \dots, x_N are experimental values for a random variable x in N independent and identical experiments. With those values, we can define the statistical estimators. The mean \bar{x} that describes a central tendency for x_i is given by

Equation 2.71

$$\bar{x} = \frac{1}{N} \sum_{i=1}^N x_i$$

The sample mean gives the estimation of the sample's "clustering" value but offers little information on the deviation from this central tendency. Another statistical estimator that offers information on the deviation from the central tendency called sampling variance or standard deviation is defined as follows:

Equation 2.72

$$Var(x_i) = \frac{1}{N-1} (x_i - \bar{x})^2$$

The standard deviation is simply the square root of the variance:

Equation 2.73

$$\sigma(x_i) = \sqrt{Var(x_i)}$$

Sometimes a sample estimator called range or peak-to-peak is also used. Caution must be exercised when a sample range is used. It can easily give unstable and inaccurate estimation because it uses only two extreme values from the N experiments and is subject to least constraints among the other two estimators we introduced.

The statistical range or peak-to-peak is defined as the following:

Equation 2.74

$$pk - pk(x_i) = Max(x_i) - Min(x_i)$$

where $Max(x_i)$ gives the maximum value and $Min(x_i)$ gives the minimum value among those N samples. It is clear that whether the estimator can converge to the value for the population statistical estimator depends on both the sample size and the nature of the population distribution. For example, if the population distribution is unbounded, such as a Gaussian, both the mean and standard deviation converge for a large sample size, but the peak-to-peak value does not.

2.3.1.2. Law of Larger Numbers

Section 2.2.4 discussed the Chebyshev Inequality. We will use it to derive another useful theorem called the law of larger numbers, which is helpful in answering the question of when the sampling mean will converge to the population mean.

Before deriving the law of larger numbers, we would like to define convergence. Suppose y_1, y_2, \dots, y_N are random variable series. If for any positive value of ϵ we always have

Equation 2.75

$$\lim_{N \rightarrow \infty} P\{|y_N - c| < \epsilon\} = 1$$

we say that y_N converges to a constant c .

Recall the Chebyshev Inequality of equation 2.57. In the current context, the random variable becomes

$$\bar{x}_N = \frac{1}{N} \sum_{i=1}^N x_i$$

The statistical expectation and variance are calculated as

Equation 2.76

$$E(\bar{x}_N) = E\left(\frac{1}{N} \sum_{i=1}^N x_i\right) = \frac{1}{N} \sum_{i=1}^N E(x_i) = \frac{1}{N} N \mu_x = \mu_x$$

and

Equation 2.77

$$Var(\bar{x}_N) = Var\left(\frac{1}{N} \sum_{i=1}^N x_i\right) = \frac{1}{N^2} \sum_{i=1}^N Var(x_i) = \frac{1}{N^2} N \sigma_x^2 = \sigma_x^2 / N$$

Substituting [equations 2.76](#) and [2.77](#) into [equation 2.57](#) gives us

Equation 2.78

$$P(|\bar{x}_N - \mu_x| < \varepsilon) > 1 - \frac{\sigma_x^2 / N}{\varepsilon^2}$$

If we let $N \rightarrow \infty$, the preceding probability will be to 1 because it cannot be larger than 1:

Equation 2.79

$$\lim_{N \rightarrow \infty} \{P(|\bar{x}_N - \mu_x| < \varepsilon)\} = 1$$

[Equation 2.77](#) suggests that as the sample size keeps increasing, the sampling mean approaches the population mean. As the sample size becomes very large, the population mean can be well represented by the sample mean.

The large number theorem has a direct implication for daily practice. Unless the sample size used to estimate the mean is very large, it does not converge to the population mean. In other words, if the sample size is not large enough, an error exists between the sample mean and the population mean. In practice, the number of samples can be identified when the sample mean is converged or unchanging when the sample size is larger than a threshold value.

2.3.1.3. Convergence of the Estimator

We have shown that as the sample size becomes very large, the sample mean approaches the population mean with a confidence probability of 1.

For the sample standard deviation and peak-to-peak, a similar theorem can be drawn. However, the speed of convergence is much slower compared to the mean estimator, particularly for peak-to-peak when the random variable distribution is unbounded.

2.3.2. Central Limiting Theory

In practical application, we are often confronted with the sum of many independent variables and what their distribution function will be.

Suppose that x_1, x_2, \dots, x_N are independent sequences of random variables that share the same probability distribution and each has the same mean μ and standard deviation σ . The central limit theorem says that the distribution of the sum variable $S_n = x_1 + x_2 + \dots + x_N$ approaches a Gaussian or normal if N becomes very large, regardless of the original distributions of the random variable, as long as it has a finite mean and a standard deviation (or variance).

The proof of the central limit theorem can be fairly straightforward if we introduce the characteristic function for a distribution function. For a distribution function of $p(x)$, its corresponding characteristic function is defined as follows:

Equation 2.80

$$\Phi(\omega) = E(e^{j\omega x}) = \int_{-\infty}^{\infty} e^{j\omega x} p(x) dx$$

This transformation from PDF $p(x)$ to characteristic function $\Phi(\omega)$ is in fact a Fourier transformation, so we should expect that all the properties for a Fourier pair should apply here. It can be shown that if $p(x) = \exp(-x^2/2)$, we will have

Equation 2.81

$$\Phi(\omega) = \int_{-\infty}^{\infty} e^{j\omega x} e^{-x^2/2} dx = e^{-\omega^2/2}$$

This implies that the characteristic function for a Gaussian (or normal) is a Gaussian (or normal) distribution in a dual domain.

Let us consider a normalized S_n variable of

Equation 2.82

$$S_N^* = \frac{S_N - N\mu}{\sqrt{N\sigma}}$$

Its character function is as follows:

Equation 2.83

$$\Phi_N^*(\omega) = E(e^{j\omega S_N^*}) = E(e^{j\omega \frac{S_N - N\mu}{\sqrt{N\sigma}}}) = [E(e^{j\omega \frac{x_1 - N\mu}{\sqrt{N\sigma}}})]^N$$

We have used independent and identical distribution properties in the last two steps to derive [equation 2.83](#). The exponential term inside the expectation estimation brackets can be calculated by using the Taylor expansion theorem of the following:

Equation 2.84

[\[View full size image\]](#)

$$\begin{aligned} E(e^{j\omega \frac{x_1 - \mu}{\sqrt{N\sigma}}}) &= E(1 + j\omega \frac{(x_1 - \mu)}{\sigma\sqrt{N}} + (j\omega)^2 \frac{(x_1 - \mu)^2}{2\sigma^2 N} + \dots) \\ &= E(1) + \frac{j\omega}{\sigma\sqrt{N}} E(x_1 - \mu) + \frac{(j\omega)^2}{2\sigma^2 N} E[(x_1 - \mu)^2] + \dots \\ &= 1 + \frac{j\omega}{\sigma\sqrt{N}} (0) + \frac{(j\omega)^2}{2\sigma^2 N} (\sigma^2) + \dots \end{aligned}$$

From [equations 2.83](#) and [2.84](#) we find the character function for the sum as follows:

Equation 2.85

$$\begin{aligned}\Phi_N^*(\omega) &= \left(1 + \frac{(j\omega)^2}{2N} + \dots\right)^N \\ &= e^{\frac{(j\omega)^2}{2}} = e^{\frac{-\omega^2}{2}}; \text{ as } N \rightarrow \infty\end{aligned}$$

Comparing [equation 2.81](#) to [equation 2.85](#) indicates that S_N^* has the same character function as that of a Gaussian or normal; therefore, its probability distribution function must also be Gaussian or normal.

Central limit theorem has a wide range of applications in solving practical problems. For example, the random noise observed in electronics is Gaussian because it is composed of many independent random noise events and, at a macroscopic level, it appears to always be a Gaussian. The same is true of random jitter, because it can be caused by many independent jitter events, with forming mechanisms of random noise-to-jitter conversion through the finite slew rate of the edge transition, amplitude-to-phase conversion, random frequency, or phase modulation.

URL <http://access.proquest.safaribooksonline.com/9780132429610/ch02lev1sec4>

User name: CSU San Diego

Book: Jitter, Noise, and Signal Integrity at High-Speed

Section: Chapter 2. Statistical Signal and Linear Theory for Jitter, Noise, and Signal Integrity

No part of any chapter or book may be reproduced or transmitted in any form by any means without the prior written permission for reprints and excerpts from the publisher of the book or chapter. Redistribution or other use that violates the fair use privilege under U.S. copyright laws (see 17 USC107) or that otherwise violates these Terms of Service is strictly prohibited. Violators will be prosecuted to the full extent of U.S. Federal and Massachusetts laws.

Information Theory Computer Science Mike Peng Li Prentice Hall Jitter, Noise, and Signal Integrity at High-Speed

2.4. Statistical Random Process and Spectral Analysis

We have discussed random variable distribution and its properties in previous sections without getting into the time dependency of those statistical distribution functions. Indeed, we implicitly assumed that the processes those distributions represent are static and time-independent. In reality, fluctuation of the motion of electrons in a semiconductor, or the random noise in an integrated circuit, are random processes and are in fact time-dependent in general. We therefore will discuss statistical process and its time dependence characteristics in this section.

2.4.1. PDF and CDF for a Statistical Random Process

Similar to the definition that we gave in [equation 2.13](#), the CDF and PDF relationship in the context of random process for variable X(t) is given by the following:

Equation 2.86

$$P(X(t_1), t_1) = \int_{-\infty}^{X(t_1)} p(x, t_1) dx$$

if X(t) is one-dimensional or one-variable-dependent. One-dimensional PDF or CDF can only give the statistical characteristics at a given time, not the relationship between different times.

However, this concept can be extended to n-dimensional at n different times for X(t). By analogy, the n-dimensional CDF and PDF for X(t) are defined as follows:

Equation 2.87

[\[View full size image\]](#)

$$P(X_1, X_2, \dots, X_n, t_1, t_2, \dots, t_n) = \int_{-\infty}^{X_1(t_1)} \int_{-\infty}^{X_2(t_2)} \dots \int_{-\infty}^{X_n(t_n)} p(x_1, x_2, \dots, x_n, t_1, t_2, \dots, t_n) dx_1 dx_2 \dots dx_n$$

2.4.2. Statistical Estimators for a Random Process

The commonly used statistical estimators for the process of a random variable X(t) are first-order moment, second-order moment, and correlation function. The first-order moment gives the mean and expectation. Together with the first-order moment, the second-order moment gives the variance or the standard deviation, similar to what was introduced in [section 2.2](#), but now it is time-dependent.

Correlation function is a necessary estimator for a random process, because it addresses the statistical relationship between two different times. The mathematical representations for those three estimators are given by the following equations.

First-order moment:

Equation 2.88

$$E(X(t)) = \bar{X}(t) = \int_{-\infty}^{+\infty} X p(X, t) dX$$

Second-order moment:

Equation 2.89

$$E(X^2(t)) = \bar{X}^2(t) = \int_{-\infty}^{+\infty} X^2 p(X, t) dX$$

Autocorrelation function:

Equation 2.90

$$R_x(t_1, t_2) = E[X(t_1)X(t_2)]$$

Another way to write the autocorrelation is to use their time difference as the state variable. Let's define $\tau = t_1 - t_2$ and set $t = t_2$. [Equation 2.90](#) can be rewritten to another equivalent form:

Equation 2.91

$$R_x(t, \tau) = E[X(t)X(t + \tau)]$$

Because autocorrelation function involves only two different time locations, a more explicit PDF function in terms of the statistical values for $X(t)$ at t_1 and t_2 is possible. Using the concept of two-dimensional PDF, as shown in [equation 2.87](#), we can rewrite [equation 2.91](#) as the following:

Equation 2.92

$$R_x(t_1, t_2) = E[X(t_1)X(t_2)] = \int_{-\infty}^{\infty} \int_{-\infty}^{\infty} x_1 x_2 p(x_1, x_2, t_1, t_2) dx_1 dx_2$$

The variance function is given by the following:

Equation 2.93

$$VAR_x(t) = E\{[X^2(t) - \bar{X}(t)]\} = E[X^2(t)] - \bar{X}^2(t)$$

If we set $t_1 = t_2 = t$ in [equation 2.90](#), we get

Equation 2.94

$$R_X(t,t) = E[X^2(t)]$$

Substituting [equation 2.94](#) for [equation 2.93](#), we get the following:

Equation 2.95

$$VAR_X(t) = R_X(t,t) - \bar{X}^2(t)$$

[Equation 2.95](#) is very important, because it gives the relationship between variance function, autocorrelation function, and mean function of a random process. Knowing two of them, the third one is uniquely determined.

Example 2.1: Let's show an example of how to use [equation 2.95](#) for a commonly encountered problem of a sinusoid process with a random phase given by $X(t) = A\cos(\omega t + \phi)$, where the random phase has a uniform distribution over 0 and 2π —namely, $p(f) = 1/2\pi$.

Solution: Based on [equation 2.88](#), we estimate the mean as the following:

$$\bar{X}(t) = \int_0^{2\pi} A \cos(\omega t + \phi) \frac{1}{2\pi} d\phi = 0$$

Similarly, according to [equation 2.92](#), the autocorrelation function is estimated as follows:

[View full size image]

$$\begin{aligned} E(X(t_1)X(t_2)) &= R_X(t_1, t_2) = \int_0^{2\pi} A \cos(\omega t_1 + \phi) A \cos(\omega t_2 + \phi) \frac{1}{2\pi} d\phi \\ &= \frac{A^2}{2} \cos[\omega(t_1 - t_2)] = \frac{A^2}{2} \cos \omega \tau = E(X(t)X(t + \tau)) = R_x(t, \tau) \end{aligned}$$

where $\tau = t_1 - t_2$. Again, if we set $t_1 = t_2 = t$ (implying $\tau = 0$), we have

$$R_X(t, t) = \bar{X}^2(t) = \frac{A^2}{2}$$

Consequently, the variance function according to [equation 2.95](#) is determined as follows:

$$VAR_X(t) = R_X(t, t) - \bar{X}^2(t) = \frac{A^2}{2}$$

In summary, the randomly phased sinusoid has a zero mean, and a constant square-mean, as well as a constant variance function.

2.4.3. Different Statistical Random Processes

In general, statistical random processes are complicated, and their statistical characteristics do not follow a certain pattern. However, in practical applications, statistical processes can be classified into several distinct types; each type has a set of unique statistical estimators.

2.4.3.1. Wide-Sense Stationary (WSS) Random Process

A WSS process is defined as having a constant mean (independent of time), and its autocorrelation function only depends on the time difference. Mathematically, this means that a WSS process has the following properties:

Equation 2.96

$$E[X(t)] = \text{const}$$

and

Equation 2.97

$$E[X^2(t)] < \infty, \quad \text{and} \quad R_{XX}(\tau) = E[X(t)X(t + \tau)]$$

A WSS process involves only one- ($p(x,t)$) and two-dimensional ($p(x_1,x_2,t_1,t_2)$) PDFs for a random process. [Equation 2.97](#) implies that the autocorrelation of the two-dimensional PDF for $X(t)$ depends only on the time difference of the PDF, because the time delay equals the time difference of $t_1 - t_2$. WSS enables some mathematical advantages in dealing with random process. For example, in autocorrelation function, you need to deal with only the time difference, without getting into the specific or absolute time point of the process. From a measurement point of view, WSS enables a lot of undersampling techniques, versus a strictly real-time measurement approach.

2.4.3.2. Strict-Sense Stationary (SSS) Random Process

The WSS process is constrained by only one- and two-dimensional PDFs, leaving other higher-dimension PDFs unconstrained. If a random process is stationary for all its PDFs, regardless of its dimension, we call this process a strict sense stationary random process. Mathematically, the definition of an SSS random process is given by the following:

Equation 2.98

$$p(x_1, x_2, \dots, x_n; t_1, t_2, \dots, t_n) = p(x_1, x_2, \dots, x_n; t_1 + \tau, t_2 + \tau, \dots, t_n + \tau)$$

This means that the PDF for an SSS random process does not change with the time shifting. It can be shown that if the SSS process condition of [equation 2.98](#) is satisfied, the conditions for a WSS process of [equations 2.96](#) and [2.97](#) are automatically satisfied. In other words, if a random process is SSS, it must be WSS too, but the opposite is not necessarily true.

2.4.3.3. Ergodic Random Process

In practical applications, a commonly encountered problem is what is the relationship between the averages along the time axis versus the ensemble average ([equation 2.92](#)) using samples obtained from variable time locations. The mean or average definitions we have introduced so far are all ensemble averages because the estimation is based on samples. We will introduce time average for a random process first and then discuss its relationship with the ensemble average.

The time average for the first-order random process $X(t)$ is given by the following:

Equation 2.99

$$\langle X(t) \rangle = \lim_{T \rightarrow \infty} \left[\frac{1}{2T} \int_{-T}^{+T} X(t) dt \right]$$

The time average for the second-order random process $X(t)$ is given by the following:

Equation 2.100

$$\langle X^2(t) \rangle = \lim_{T \rightarrow \infty} \left[\frac{1}{2T} \int_{-T}^{+T} X^2(t) dt \right]$$

The time average for the autocorrelation function for a random process $X(t)$ is given by the following:

Equation 2.101

$$\langle X(t)X(t+\tau) \rangle = \lim_{T \rightarrow \infty} \left[\frac{1}{2T} \int_{-T}^{+T} X(t)X(t+\tau) dt \right]$$

The corresponding ensemble averages for [equations 2.99](#), [2.100](#), and [2.101](#) are [equations 2.88](#), [2.89](#), and [2.90](#). With the introduction of time average and ensemble average for random process $X(t)$, we are ready to introduce the ergodic process.

If all the time averages equal the corresponding ensemble averages for any order or form of statistical estimators, the process is considered an ergodic process.

Example 2.2: Find the time average for the same randomly phased sinusoid introduced in [example 2.1](#):

$$\begin{aligned} \langle X(t) \rangle &= \lim_{T \rightarrow \infty} \left[\frac{1}{2T} \int_{-T}^{+T} A \cos(\omega t + \phi) dt \right] \\ &= \lim_{T \rightarrow \infty} \frac{A \cos \phi \sin \omega T}{\omega T} = 0 \end{aligned}$$

and

$$\begin{aligned} \langle X(t)X(t+\tau) \rangle &= \lim_{T \rightarrow \infty} \left\{ \frac{1}{2T} \int_{-T}^{+T} A \cos(\omega t + \phi) A \cos[\omega(t+\tau) + \phi] dt \right\} \\ &= \frac{A^2}{2} \cos \omega \tau \end{aligned}$$

Solution: If we compare the time averages with the ensemble averages shown in [example 2.1](#), we find that

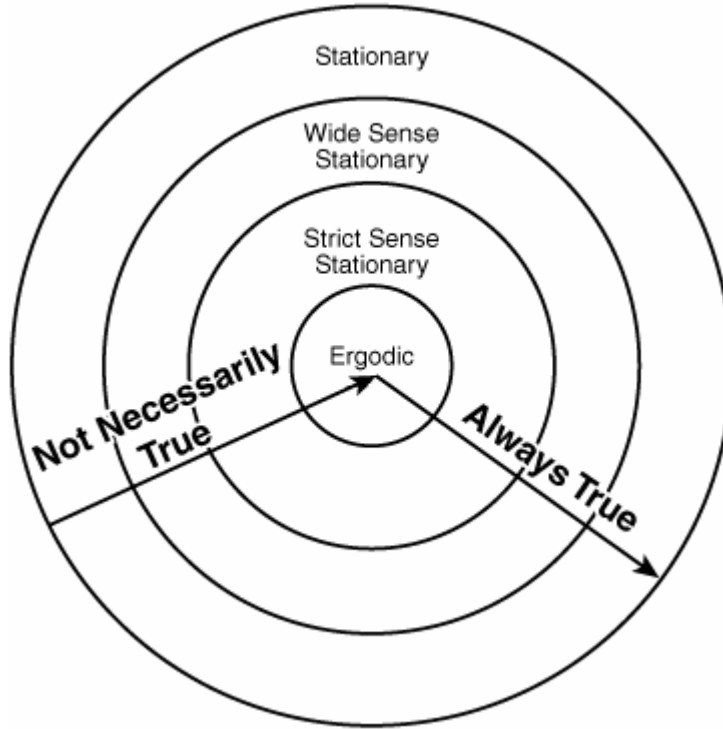
$$\begin{aligned} \bar{X}(t) &= E[X(t)] = \langle X(t) \rangle \text{ and} \\ R_X(\tau) &= E[X(t)X(t+\tau)] = \langle X(t)X(t+\tau) \rangle \end{aligned}$$

The ensemble averages and time averages are equal, suggesting that the random phase sinusoid is indeed an ergodic random process.

2.4.3.4. Relationships Between Different Random Processes

We have introduced and discussed various random processes, and they are clearly interrelated. At the highest level, the random processes are classified as stationary and nonstationary. Most of the discussions have concentrated on stationary processes because the nonstationary process is still a mathematical challenge and an ongoing research topic. The stationary process has several levels of constraints, and each set of them gives rise to a type of process, as shown in the previous sections. Their relationships are shown in Figure 2.3.

Figure 2.3. The interrelationship between different stationary random processes.



This diagram indicates that if an inner process is true, its corresponding outer annulus is always true. Conversely, if an outer annulus process is true, its corresponding inner circle stationary process is not necessarily true.

2.4.4. Signal Power and Power Spectrum Density (PSD)

If the random process $X(t)$ represents a physical signal in practice, such as the voltage rate for an electrical signal wave or power rate of an optical signal wave, it must be finite. Mathematically, this means that we have a Fourier integral pair of the following:

Equation 2.102

$$F_X(\omega) = \int_{-\infty}^{+\infty} X(t)e^{-j\omega t} dt$$

In general, $F_X(\omega)$ is a complex variable. According to the Parseval theorem, $X(t)$ and $F_X(\omega)$ also satisfy the following:

Equation 2.103

$$\int_{-\infty}^{+\infty} |X(t)|^2 dt = \frac{1}{2\pi} \int_{-\infty}^{+\infty} |F_X(\omega)|^2 d\omega$$

This equation demonstrates the energy conservation law. In other words, the power density sums in the time and frequency domains from $-\infty$ to ∞ are the same. Clearly, $|F_X(\omega)|^2$ represents the power density in the frequency domain.

2.4.4.1. PSD Definition

In practical application, what we are most interested in is the $X(t)$ process within a finite interval of $[-T, T]$, and we can define its corresponding frequency spectrum within this time range as follows:

Equation 2.104

$$F_X(\omega, T) = \int_{-T}^{+T} X(t) e^{-j\omega t} dt$$

Applying Parseval theorem for this truncated function $X(t)$ results in

Equation 2.105

$$\int_{-T}^{+T} |X(t)|^2 dt = \frac{1}{2\pi} \int_{-\infty}^{+\infty} |F_X(\omega, T)|^2 d\omega$$

Taking both the time and ensemble average for [equation 2.105](#), we have

Equation 2.106

$$\lim_{T \rightarrow \infty} E\left[\frac{1}{2T} \int_{-T}^{+T} |X(t)|^2 dt\right] = \frac{1}{2\pi} \int_{-\infty}^{+\infty} \lim_{T \rightarrow \infty} E\left[\frac{1}{2T} |F_X(\omega, T)|^2\right] d\omega$$

The left side is the average power for random process $X(t)$. The kernel within the right side integral in the frequency domain represents the PSD function $S_X(\omega)$ for $X(t)$. Apparently, we have

Equation 2.107

$$S_X(\omega) = \lim_{T \rightarrow \infty} E\left[\frac{1}{2T} |F_X(\omega, T)|^2\right] d\omega$$

Because

Equation 2.108

$$|F_X(\omega, T)|^2 = F_X(\omega, T) F_X^*(\omega, T) = F_X(\omega, T) F_X(-\omega, T)$$

Clearly, PSD $S_X(\omega)$ is an even and positive function of frequency.

2.4.4.2. PSD and the Wiener-Kinchine Theorem

From [equation 2.107](#), we have learned that the PSD of a random process equals the average power density. We want to further explore what determines the average power density. [Equation 2.107](#) can be rewritten as follows:

Equation 2.109

$$S_x(\omega) = \lim_{T \rightarrow \infty} \frac{1}{2T} E\left[\int_{-T}^T X(t_1) e^{-j\omega t_1} dt_1 \right] \left[\int_{-T}^T X(t_2) e^{-j\omega t_2} dt_2 \right]$$

Exchanging the order of expectation and double integration operation, we get the following:

Equation 2.110

$$\begin{aligned} S_x(\omega) &= \lim_{T \rightarrow \infty} \frac{1}{2T} \int_{-T}^T \int_{-T}^T E\{X(t_1)X(t_2)\} e^{-j\omega(t_2-t_1)} dt_1 dt_2 \\ &= \lim_{T \rightarrow \infty} \frac{1}{2T} \int_{-T}^T \int_{-T}^T R_x(t_2 - t_1) e^{-j\omega(t_2-t_1)} dt_1 dt_2 \end{aligned}$$

Let's do the following variable transformation of $\tau_1 = t_1 + t_2$ and $\tau_2 = -t_1 + t_2$. The double integration region changes from a square to a diamond. Then [equation 2.110](#) becomes

Equation 2.111

$$\begin{aligned} S_x(\omega) &= \lim_{T \rightarrow \infty} \frac{1}{T} \int_0^{2T} R_x(\tau_2) e^{-j\omega\tau_2} d\tau_2 \int_0^{2T-\tau_2} d\tau_1 \\ &= \lim_{T \rightarrow \infty} \frac{1}{T} \int_0^{2T} (2T - \tau_2) R_x(\tau_2) e^{-j\omega\tau_2} d\tau_2 \\ &= \lim_{T \rightarrow \infty} \int_0^{2T} \left(2 - \frac{\tau_2}{T}\right) R_x(\tau_2) e^{-j\omega\tau_2} d\tau_2 \end{aligned}$$

When $T \rightarrow \infty$, $(2 - \tau_2/T) \rightarrow 2$. Setting the integration dummy variable τ_2 as τ , and using the even property of autocorrelation function R_x , and $T \rightarrow \infty$, we get the following:

Equation 2.112

$$S_x(\omega) = \int_{-\infty}^{\infty} R_x(\tau) e^{-j\omega\tau} d\tau$$

[Equation 2.112](#) reveals that the PSD of a random process equals the Fourier transformation of its autocorrelation function for a stationary random process. Because $S_x(\omega)$ and $R_x(\tau)$ follow the Fourier relationship, the time-domain $R_x(\tau)$ can also be easily represented by its corresponding $S_x(\omega)$ through inverse Fourier transformation of the following:

Equation 2.113

$$R_x(\tau) = \frac{1}{2\pi} \int_{-\infty}^{\infty} S_x(\omega) e^{j\omega\tau} d\omega$$

The relationships represented by [equations 2.112](#) and [2.113](#) were first discovered by Wiener and Kinchine and therefore are often called the Wiener-Kinchine theorem. Because both $S_x(\omega)$ and $R_x(\tau)$ are even functions, they are both real functions.

Example 2.3: For white noise having a constant PSD of $S_x(\omega) = S_0$, find out its corresponding autocorrelation function $R_x(\tau)$.

Solution: Using [equation 2.113](#), we substitute the expression of $S_x(\omega)$ into it and obtain the following:

$$\begin{aligned} R_x(\tau) &= \frac{1}{2\pi} \int_{-\infty}^{\infty} S_0 e^{j\omega\tau} d\omega \\ &= S_0 \delta(\tau) \end{aligned}$$

This example demonstrates that the autocorrelation function is a white noise source and a Dirac delta function.

URL <http://access.proquest.safaribooksonline.com/9780132429610/ch02lev1sec5>

User name: CSU San Diego

Book: Jitter, Noise, and Signal Integrity at High-Speed

Section: Chapter 2. Statistical Signal and Linear Theory for Jitter, Noise, and Signal Integrity

No part of any chapter or book may be reproduced or transmitted in any form by any means without the prior written permission for reprints and excerpts from the publisher of the book or chapter. Redistribution or other use that violates the fair use privilege under U.S. copyright laws (see 17 USC107) or that otherwise violates these Terms of Service is strictly prohibited. Violators will be prosecuted to the full extent of U.S. Federal and Massachusetts laws.

Information Theory Computer Science Mike Peng Li Prentice Hall Jitter, Noise, and Signal Integrity at High-Speed

Part B: Linear System Theory

The linear system of interest here has the following two important properties:

- If a system input $x(t)$ produces an output $y(t)$, when the system input is $x(t+\tau)$, the output will be $y(t+\tau)$.
- If input $x_1(t)$ produces output $y_1(t)$, and input $x_2(t)$ produces output $y_2(t)$, the input of linear combination of $(a_1x_1(t)+a_2x_2(t))$ produces output $(a_1y_1(t)+a_2y_2(t))$.

A system with those properties is often called linear time-invariant (LTI). This section first introduces the concept of impulse response for a linear system. Then it discusses how to use this impulse response function to completely describe linear system behavior.

URL <http://access.proquest.safaribooksonline.com/9780132429610/ch02lev1sec6>

User name: CSU San Diego

Book: Jitter, Noise, and Signal Integrity at High-Speed

Section: Chapter 2. Statistical Signal and Linear Theory for Jitter, Noise, and Signal Integrity

No part of any chapter or book may be reproduced or transmitted in any form by any means without the prior written permission for reprints and excerpts from the publisher of the book or chapter. Redistribution or other use that violates the fair use privilege under U.S. copyright laws (see 17 USC107) or that otherwise violates these Terms of Service is strictly prohibited. Violators will be prosecuted to the full extent of U.S. Federal and Massachusetts laws.

Information Theory Computer Science Mike Peng Li Prentice Hall Jitter, Noise, and Signal Integrity at High-Speed

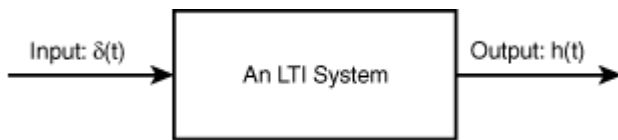
2.5. An LTI System

This section defines transfer function for an LTI system and how it links the output and input signals in both the time and frequency domains.

2.5.1. Time-Domain Analysis

For a linear system, an important system behavior or characteristic is its output response when an impulse signal $\delta(t)$ is applied at its input, as shown in [Figure 2.4](#).

Figure 2.4. The impulse response function for an LTI system when the input is a Dirac delta function.



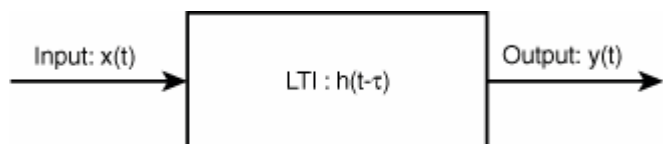
The impulse function $\delta(t)$ is something called a Dirac delta function, and its mathematical definition is given by the following:

Equation 2.114

$$\delta(t) = \begin{cases} \infty, & \text{when } t = 0 \\ 0, & \text{when } t \neq 0 \end{cases} \quad \text{and} \quad \int_{-\infty}^{+\infty} \delta(t) dt = 1$$

Due to the LTI properties, the output signal $y(t)$ is the sum of product of input signal $x(t)$ with the shifted impulse response function $h(t-\tau)$, where τ is the time shifting, as shown in [Figure 2.5](#), when an input signal $x(t)$ is applied.

Figure 2.5. A linear time-invariant system represented by its time-domain shifted impulse response function, input $x(t)$, and output $y(t)$.



Mathematically, this means that output signal $y(t)$ can be expressed as follows:

Equation 2.115

$$y(t) = \sum_{i=-\infty}^{\infty} x(i\Delta t)h(t - i\Delta t)\Delta t$$

Let's take the limit and let $\Delta t \rightarrow 0$. We get the following:

Equation 2.116

$$y(t) = \lim_{\Delta t \rightarrow 0} \left(\sum_{i=-\infty}^{\infty} x(i\Delta t)h(t - i\Delta t)\Delta t \right) = \int_{-\infty}^{\infty} x(\tau)h(t - \tau)d\tau$$

Equation 2.116 indicates that the output of an LTI system is the *convolution* between its input signal and its impulse response function. Another way to represent this relation is the following:

Equation 2.117

$$y(t) = x(t) * h(t)$$

where $*$ denotes the convolution operation. Note that convolution poses the associative property.

2.5.2. Frequency-Domain Analysis

With the convolution relationship defined in equation 2.117, we are ready to discuss its frequency domain relationship. Let's use a Laplace transformation for this equation. We get the following:

Equation 2.118

$$\text{Lap}(y(t)) = \text{Lap}(x(t) * h(t))$$

where Lap denotes Laplace transformation. For a given function $x(t)$, $\text{Lap}(x(t))$ is defined as

Equation 2.119

$$\text{Lap}(x(t)) = \int_{-\infty}^{\infty} x(t)e^{-st}dt$$

where s is a complex frequency. Define the Laplace transformation for $y(t)$ as

Equation 2.120

$$Y(s) = \int_{-\infty}^{\infty} y(t)e^{-st}dt$$

Using this definition, [equation 2.118](#) becomes

Equation 2.121

[[View full size image](#)]

$$\begin{aligned}
 Y(s) &= \int_{-\infty}^{\infty} (x(t) * h(t)) e^{-st} dt = \int_{-\infty}^{\infty} [\int_{-\infty}^{\infty} x(\tau)h(t-\tau)d\tau]e^{-st} dt \\
 &= \int_{-\infty}^{\infty} x(\tau)[\int_{-\infty}^{\infty} h(t-\tau)e^{-st} dt]d\tau = [\int_{-\infty}^{\infty} x(\tau)e^{-s\tau} d\tau][\int_{-\infty}^{\infty} h(t)e^{-st} dt] \\
 &= X(s)H(s)
 \end{aligned}$$

Clearly:

Equation 2.122

$$X(s) = \int_{-\infty}^{\infty} x(t)e^{-st} dt$$

and

Equation 2.123

$$H(s) = \int_{-\infty}^{\infty} h(t)e^{-st} dt$$

$X(s)$ and $H(s)$ are the Laplace transformations for $x(t)$ and $h(t)$, respectively. Thus, in the complex frequency s -domain, the input $X(s)$, transfer function $H(s)$, and output $Y(s)$ are related through a simple *linear* product relationship of the following:

Equation 2.124

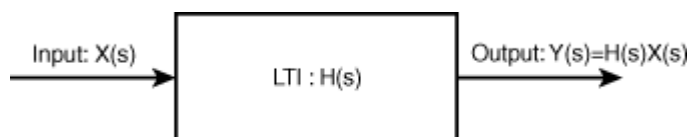
$$Y(s) = X(s)H(s)$$

$H(s)$ is often termed the transfer function for the LTI system that determines its behavior.

If two of the three functions in [equation 2.114](#) are known, the third function can be uniquely determined. This is also true for the time-domain convolution relationship of [equation 2.117](#). Theoretically, the time-domain convolution/deconvolution operation and the frequency-domain multiplication/division operation are equivalent approaches to determining the third function from the two known. However, in practice, time-domain convolution/deconvolution is less intuitive and straightforward.

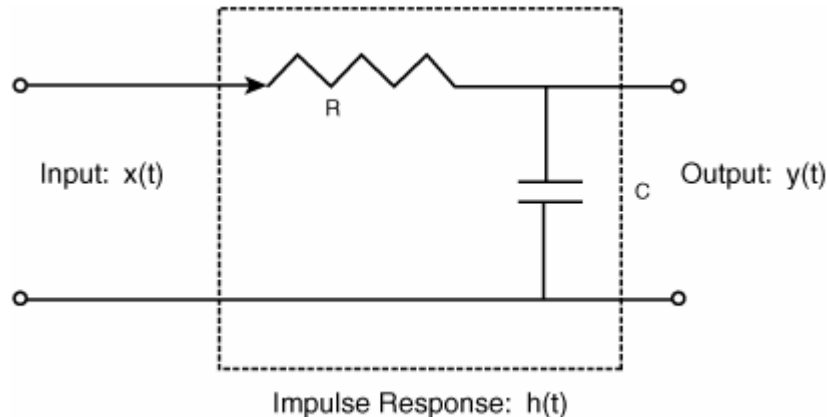
[Figure 2.6](#) shows the relationship block diagram between $X(s)$, $H(s)$, and $Y(s)$.

Figure 2.6. An LTI system represented by its complex frequency s-domain response function $H(s)$, input $X(s)$, and output $Y(s)$.



Example 2.4: Figure out the transfer function for an RC circuit, as shown in Figure 2.7.

Figure 2.7. An RC circuit with its input as $x(t)$, output as $y(t)$, and impulse response as $h(t)$.



Solution: Because the sum of voltage over the resistor and capacitor equals the input voltage, we have the following equation:

$$R(C \frac{dy(t)}{dt}) + y(t) = x(t)$$

Let $RC = 1/\alpha$, and apply the Laplace transformation to both sides of the equation. The result is as follows:

$$\frac{1}{\alpha} sY(s) + Y(s) = X(s)$$

Then we find the transfer function in the s-domain:

$$H(s) = \frac{Y(s)}{X(s)} = \frac{1}{\frac{s}{\alpha} + 1} = \frac{\alpha}{s + \alpha}$$

Applying the inverse Laplace transformation to $H(s)$, we obtain the time-domain impulse response function of the RC circuit:

$$h(t) = L^{-1}[H(s)] = \begin{cases} \alpha e^{-\alpha t}, & t \geq 0 \\ 0, & t < 0 \end{cases}$$

2.5.3. LTI Properties

Three key properties are related to an LTI system. We will discuss them in both the time and frequency domains.

2.5.3.1. Commutative Property

Because convolution satisfies the commutative property, so does the LTI system. In the time domain, we have

Equation 2.125

$$y(t) = x(t) * h(t) = h(t) * x(t)$$

In the frequency domain, it is even more obvious, because we have

Equation 2.126

$$Y(s) = X(s)H(s) = H(s)X(s)$$

2.5.3.2. Distributive Property

If two LTI systems are added together, the total transfer function is $[h_1(t)+h_2(t)]$. Therefore, in the time domain, we have the following:

Equation 2.127

$$y(t) = x(t) * (h_1(t) + h_2(t)) = x(t) * h_1(t) + x(t) * h_2(t)$$

In the frequency domain, we have a similar multiplication property:

Equation 2.128

$$Y(s) = X(s)(H_1(s) + H_2(s)) = X(s)H_1(s) + X(s)H_2(s)$$

2.5.3.3. Associative Property

If the LTI system transfer function equals two convoluting transfer functions, the following associative property in the time domain is obvious:

Equation 2.129

$$y(t) = x(t) * (h_1(t) * h_2(t)) = (x(t) * h_1(t)) * h_2(t)$$

In the frequency domain, we have

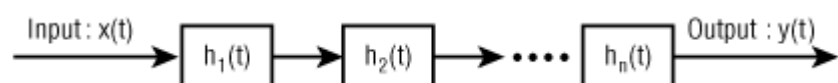
Equation 2.130

$$Y(s) = X(s)(H_1(s)H_2(s)) = (X(s)H_1(s))H_2(s)$$

2.5.3.4. Cascading Property

In practical application, an LTI system consists of many LTI subsystems, as shown in [Figure 2.8](#).

Figure 2.8. An LTI system consists of n cascading sub-LTI systems.



The overall system transfer function in the time domain is as follows:

Equation 2.131

$$h_t(t) = h_1(t) * h_2(t) * \dots * h_n(t)$$

and input/output follows this relationship:

Equation 2.132

$$y(t) = x(t) * h_t(t)$$

Similarly, the frequency domain overall transfer function is as follows:

Equation 2.133

$$H_t(s) = H_1(s)H_2(s)\dots H_n(s)$$

and the input/output relation in frequency domain is

Equation 2.134

$$Y(s) = X(s)H_t(s)$$

URL <http://access.proquest.safaribooksonline.com/9780132429610/ch02lev1sec7>

User name: CSU San Diego

Book: Jitter, Noise, and Signal Integrity at High-Speed

Section: Chapter 2. Statistical Signal and Linear Theory for Jitter, Noise, and Signal Integrity

No part of any chapter or book may be reproduced or transmitted in any form by any means without the prior written permission for reprints and excerpts from the publisher of the book or chapter. Redistribution or other use that violates the fair use privilege under U.S. copyright laws (see 17 USC107) or that otherwise violates these Terms of Service is strictly prohibited. Violators will be prosecuted to the full extent of U.S. Federal and Massachusetts laws.

Information Theory Computer Science Mike Peng Li Prentice Hall Jitter, Noise, and Signal Integrity at High-Speed

2.6. Statistical Estimators for an LTI System

This subsection discusses statistical estimators such as mean, autocorrelation function, and variance of the LTI output and its relationship to the transfer function and input signal. We will start with the mean.

2.6.1. Mean

Recall [equation 2.117](#), the output and input relationship for an LTI system. If we take the mean for both sides of the equation, we get the following:

Equation 2.135

$$\begin{aligned} E[y(t)] &= E\left[\int_{-\infty}^{\infty} x(t-\tau)h(\tau)d\tau\right] \\ &= \int_{-\infty}^{\infty} E[x(t-\tau)]h(\tau)d\tau \\ &= \bar{x} \int_{-\infty}^{\infty} h(\tau)d\tau \end{aligned}$$

Thus, the mean relationship between input and output is the following:

Equation 2.136

$$\bar{y} = \bar{x} \int_{-\infty}^{\infty} h(\tau)d\tau$$

[Equation 2.136](#) implies that the output mean equals the input mean times the integral of the impulse response function for an LTI system.

2.6.2. Autocorrelation Function

Recall the autocorrelation function definition of [equation 2.91](#) that gives the relationship between the input signal and output signal by using the commutative property between expectation and integral operations:

Equation 2.137

$$\begin{aligned}
 R_y(t, t + \tau) &= E[y(t)y(t + \tau)] \\
 &= E\left[\int_{-\infty}^{\infty} x(t - \zeta_1)h(\zeta_1)d\zeta_1 \int_{-\infty}^{\infty} x(t + \tau - \zeta_2)h(\zeta_2)d\zeta_2\right] \\
 &= E\left[\int_{-\infty}^{\infty} \int_{-\infty}^{\infty} x(t - \zeta_1)x(t + \tau - \zeta_2)h(\zeta_1)h(\zeta_2)d\zeta_1 d\zeta_2\right] \\
 &= \int_{-\infty}^{\infty} \int_{-\infty}^{\infty} E[x(t - \zeta_1)x(t + \tau - \zeta_2)]h(\zeta_1)h(\zeta_2)d\zeta_1 d\zeta_2 \\
 &= \int_{-\infty}^{\infty} \int_{-\infty}^{\infty} R_x(t - \zeta_1, t + \tau - \zeta_2)h(\zeta_1)h(\zeta_2)d\zeta_1 d\zeta_2
 \end{aligned}$$

For a WSS process where the autocorrelation function depends on only the time difference, not the starting time t , we can drop the time variable t and obtain the autocorrelation function relationship as follows:

Equation 2.138

$$R_y(\tau) = \int_{-\infty}^{\infty} \int_{-\infty}^{\infty} R_x(\zeta_2 - \zeta_1 - \tau)h(\zeta_1)h(\zeta_2)d\zeta_1 d\zeta_2$$

[Equations 2.137](#) and [2.138](#) give the relationships between output autocorrelation function and input autocorrelation function through the double integration knowing the impulse response of the LTI system.

2.6.3. Square-Mean

The square-mean of the output is ready to be estimated using [equation 2.138](#) for a WSS statistical process. Starting with the definition of the square-mean, we have

Equation 2.139

$$\begin{aligned}
 \overline{y^2} &= E[y(t)y(t)] = R_y(0) \\
 &= \int_{-\infty}^{\infty} \int_{-\infty}^{\infty} R_x(\zeta_2 - \zeta_1)h(\zeta_1)h(\zeta_2)d\zeta_1 d\zeta_2
 \end{aligned}$$

[Equation 2.139](#) suggests that the square-mean is the integration of the product between input autocorrelation function and impulse response functions.

Example 2.5: For an input white noise to an RC circuit having an impulse response function, as shown in [example 2.4](#), find the autocorrelation function and square-mean at its output.

Solution: [Example 2.3](#) showed that the autocorrelation function for white noise is $R_x(\tau) = S_0\delta(\tau)$.

Substituting this formula into [equation 2.138](#) and using the transfer function for the RC circuit derived in [example 2.4](#), we have

$$\begin{aligned}
R_y(\tau) &= \int_{-\infty}^{\infty} \int_{-\infty}^{\infty} S_0 \delta(\zeta_2 - \zeta_1 - \tau) h(\zeta_1) h(\zeta_2) d\zeta_1 d\zeta_2 \\
&= \int_{-\infty}^{\infty} S_0 h(\zeta_1) d\zeta_1 \int_{-\infty}^{\infty} \delta(\zeta_2 - \zeta_1 - \tau) h(\zeta_2) d\zeta_2 \\
&= \int_{-\infty}^{\infty} S_0 h(\zeta_1) h(\zeta_1 + \tau) d\zeta_1
\end{aligned}$$

For $\tau \geq 0$, we have

$$\begin{aligned}
R_y(\tau) &= \int_0^{\infty} S_0 \alpha e^{-\alpha \zeta_1} \alpha e^{-\alpha(\zeta_1 + \tau)} d\zeta_1 \\
&= S_0 \alpha^2 e^{-\alpha \tau} \int_0^{\infty} e^{-2\alpha \zeta_1} d\zeta_1 \\
&= \frac{S_0 \alpha}{2} e^{-\alpha \tau}
\end{aligned}$$

For $\tau < 0$, let $\zeta_1 + \tau = \zeta$. We have the following:

$$\begin{aligned}
R_y(\tau) &= \int_0^{\infty} S_0 \alpha e^{-\alpha \zeta} \alpha e^{-\alpha(\zeta - \tau)} d\zeta \\
&= S_0 \alpha^2 e^{\alpha \tau} \int_0^{\infty} e^{-2\alpha \zeta} d\zeta \\
&= \frac{S_0 \alpha}{2} e^{\alpha \tau}
\end{aligned}$$

Therefore, when we have the $R_y(\tau)$ of the entire range of τ :

$$R_y(\tau) = \frac{S_0 \alpha}{2} e^{-\alpha|\tau|}, \text{ for } -\infty < \tau < \infty$$

the square-mean is ready to be calculated as follows:

$$\overline{y^2} = R_y(0) = \frac{S_0 \alpha}{2}$$

URL <http://access.proquest.safaribooksonline.com/9780132429610/ch02lev1sec8>

User name: CSU San Diego

Book: Jitter, Noise, and Signal Integrity at High-Speed

Section: Chapter 2. Statistical Signal and Linear Theory for Jitter, Noise, and Signal Integrity

No part of any chapter or book may be reproduced or transmitted in any form by any means without the prior written permission for reprints and excerpts from the publisher of the book or chapter. Redistribution or other use that violates the fair use privilege under U.S. copyright laws (see 17 USC107) or that otherwise violates these Terms of Service is strictly prohibited. Violators will be prosecuted to the full extent of U.S. Federal and Massachusetts laws.

Information Theory Computer Science Mike Peng Li Prentice Hall Jitter, Noise, and Signal Integrity at High-Speed

2.7. Power Spectrum Density (PSD) for an LTI System

This section focuses on PSD estimation for an LTI system and its relationship to the input signal and system transfer function.

2.7.1. Output PSD

Section 2.4.4.2 introduced the Wiener-Kinchine theorem, revealing a Fourier relationship between autocorrelation function and PSD. What we will introduce is how the output PSD of a random process for an LTI system relates to its input PSD. We will start with equation 2.138 by dropping the dummy variable t under the assumption that the statistical process is a WSS. We get the following:

Equation 2.140

$$R_y(\tau) = \int_{-\infty}^{\infty} d\zeta_1 \int_{-\infty}^{\infty} R_x(\zeta_2 - \zeta_1 - \tau) h(\zeta_1) h(\zeta_2) d\zeta_2$$

Applying the Fourier transformation to both sides of equation 2.140, we get the following:

Equation 2.141

[View full size image]

$$\int_{-\infty}^{\infty} R_y(\tau) e^{j\omega\tau} d\tau = \int_{-\infty}^{\infty} \left[\int_{-\infty}^{\infty} d\zeta_1 \int_{-\infty}^{\infty} R_x(\zeta_2 - \zeta_1 - \tau) h(\zeta_1) h(\zeta_2) d\zeta_2 \right] e^{j\omega\tau} d\tau$$

According to the Wiener-Kinchine theorem of equation 2.112, the left side is the PSD for y. The integrals on the right side of the equation are exchangeable. Thus, we get the following:

Equation 2.142

$$S_y(\omega) = \int_{-\infty}^{\infty} \int_{-\infty}^{\infty} \left[\int_{-\infty}^{\infty} R_x(\zeta_2 - \zeta_1 - \tau) e^{j\omega\tau} d\tau \right] h(\zeta_1) h(\zeta_2) d\zeta_1 d\zeta_2$$

After doing the replacement of $t = \zeta_2 - \zeta_1 - \tau$ and using the even property of Rx, we get the following:

Equation 2.143

$$\begin{aligned}
 S_y(\omega) &= \int_{-\infty}^{\infty} \int_{-\infty}^{\infty} \left[\int_{-\infty}^{\infty} R_x(t) e^{j\omega t} dt \right] e^{-j\omega(\zeta_2 - \zeta_1)} h(\zeta_1) h(\zeta_2) d\zeta_1 d\zeta_2 \\
 &= \int_{-\infty}^{\infty} \int_{-\infty}^{\infty} S_x(\omega) e^{-j\omega(\zeta_2 - \zeta_1)} h(\zeta_1) h(\zeta_2) d\zeta_1 d\zeta_2 \\
 &= S_x(\omega) \left[\int_{-\infty}^{\infty} e^{j\omega \zeta_1} h(\zeta_1) d\zeta_1 \right] \left[\int_{-\infty}^{\infty} e^{-j\omega \zeta_2} h(\zeta_2) d\zeta_2 \right]
 \end{aligned}$$

Recall the definition of a transformation in the complex s frequency domain of [equation 2.143](#). Using $s = j\omega$, we reach the following relationship:

Equation 2.144

$$S_y(\omega) = S_x(\omega) H(-j\omega) H(j\omega)$$

Because $H(-j\omega) = H^*(j\omega)$, we can rewrite [equation 2.144](#) into another form:

Equation 2.145

$$\begin{aligned}
 S_y(\omega) &= S_x(\omega) H^*(j\omega) H(j\omega) \\
 &= |H(j\omega)|^2 S_x(\omega)
 \end{aligned}$$

[Equation 2.145](#) reveals that the PSD of the output signal equals the PSD of the input signal multiplied by the magnitude square of the system transfer function. Again, if you know either two of those variables, you can determine the third. However, unlike the signal itself, the PSD of the output signal does not depend on the phase of the transfer function. This is not a total surprise, because the autocorrelation function does not depend on the signal's phase. As such, PSD, its Fourier transformation, is phase-independent.

2.7.2. Output Autocorrelation Function

According to the Wiener-Kinchine theorem, autocorrelation function and PSD are Fourier pairs. Therefore, the autocorrelation function can be calculated via inverse Fourier transformation given by [equation 2.113](#). Substituting [equation 2.145](#) into [equation 2.113](#) gives us

Equation 2.146

$$\begin{aligned}
 R_y(\tau) &= \frac{1}{2\pi} \int_{-\infty}^{\infty} S_y(\omega) e^{j\omega\tau} d\omega \\
 &= \frac{1}{2\pi} \int_{-\infty}^{\infty} |H(j\omega)|^2 S_x(\omega) e^{j\omega\tau} d\omega
 \end{aligned}$$

Accordingly, the square-mean for y , using the relationship established in [equation 2.133](#), gives us the following:

Equation 2.147

$$\overline{y^2} = R_y(0) = \frac{1}{2\pi} \int_{-\infty}^{\infty} |H(j\omega)|^2 S_x(\omega) d\omega$$

URL <http://access.proquest.safaribooksonline.com/9780132429610/ch02lev1sec9>

User name: CSU San Diego

Book: Jitter, Noise, and Signal Integrity at High-Speed

Section: Chapter 2. Statistical Signal and Linear Theory for Jitter, Noise, and Signal Integrity

No part of any chapter or book may be reproduced or transmitted in any form by any means without the prior written permission for reprints and excerpts from the publisher of the book or chapter. Redistribution or other use that violates the fair use privilege under U.S. copyright laws (see 17 USC107) or that otherwise violates these Terms of Service is strictly prohibited. Violators will be prosecuted to the full extent of U.S. Federal and Massachusetts laws.

Information Theory Computer Science Mike Peng Li Prentice Hall Jitter, Noise, and Signal Integrity at High-Speed

2.8. Summary

Part I of this chapter introduced basic probability, statistical, and random signal theories and gave some examples. Part II introduced the basic signal and linear system theories, which required some concepts and theories from Part I, and gave some examples. These theories are necessary and fundamental for us to deal with jitter, noise, and BER in a communication system in a thorough and quantitative manner. These mainstream, well-established theories are used extensively in the following chapters.

Our intent was to present basic statistical and system theorems related to jitter, noise, BER, and signal, not to comprehensively present those topics with full coverage and in-depth discussion. Many good books have been published on these topics; we refer you to some of them for further reading. For example, [1], [2], [3], and [4] have good discussions and reviews of probability, statistics, and stochastic process. [5], [6], [7], and [8] have good reviews of signal, noise, and linear system theory.

URL <http://access.proquest.safaribooksonline.com/9780132429610/ch02lev1sec10>

User name: CSU San Diego

Book: Jitter, Noise, and Signal Integrity at High-Speed

Section: Chapter 2. Statistical Signal and Linear Theory for Jitter, Noise, and Signal Integrity

No part of any chapter or book may be reproduced or transmitted in any form by any means without the prior written permission for reprints and excerpts from the publisher of the book or chapter. Redistribution or other use that violates the fair use privilege under U.S. copyright laws (see 17 USC107) or that otherwise violates these Terms of Service is strictly prohibited. Violators will be prosecuted to the full extent of U.S. Federal and Massachusetts laws.

Information Theory Computer Science Mike Peng Li Prentice Hall Jitter, Noise, and Signal Integrity at High-Speed

Endnotes

1. A. W. Drake, *Fundamentals of Applied Probability Theory*, McGraw-Hill, 1967.
2. S. M. Kay, *Fundamentals of Statistical Signal Processing: Estimation Theory*, Prentice-Hall, 1993.
3. A. Papoulis, *Probability, Random Variables, and Statistical Processes*, Third Edition, McGraw-Hill, 1991.
4. P. Z. Peebles, Jr., *Probability, Random Variables, and Random Signal Principles*, Third Edition, McGraw-Hill, 1993.
5. J. A. Cadzow and H. F. Van Landingham, *Signals and Systems*, Prentice-Hall, 1985.
6. W. B. Davenport and W. L. Root, *An Introduction to the Theory of Random Signals and Noise*, IEEE Press, 1987.
7. A. V. Oppenheim, A. S. Willsky, and S. H. Nawab, *Signals & Systems*, Prentice Hall, 1996.
8. F. J. Taylor, *Principles of Signals and Systems*, McGraw-Hill, 1994.

URL <http://access.proquest.safaribooksonline.com/9780132429610/ch02lev1sec11>

User name: CSU San Diego

Book: Jitter, Noise, and Signal Integrity at High-Speed

No part of any chapter or book may be reproduced or transmitted in any form by any means without the prior written permission for reprints and excerpts from the publisher of the book or chapter. Redistribution or other use that violates the fair use privilege under U.S. copyright laws (see 17 USC107) or that otherwise violates these Terms of Service is strictly prohibited. Violators will be prosecuted to the full extent of U.S. Federal and Massachusetts laws.

Information Theory Computer Science Mike Peng Li Prentice Hall Jitter, Noise, and Signal Integrity at High-Speed

3. Source, Mechanism, and Math Model for Jitter and Noise

Chapter 1, "Introduction," introduced the basic jitter and noise sources and their causing mechanisms in a qualitative way. Chapter 2, "Statistical Signal and Linear Theory for Jitter, Noise, and Signal Integrity," introduced the necessary statistical signaling and linear system theorems. Now we are ready to discuss jitter and noise components in a quantitative way to enable advanced discussions of jitter separation in time, frequency, and statistical domains in later chapters. The jitter and noise component models will be treated in terms of statistical PDFs, and also in terms of their corresponding time series and frequency domain spectrum or PSD. We will focus first on the jitter and its component discussion, and then similar concepts will be established for noise components.

URL <http://access.proquest.safaribooksonline.com/9780132429610/ch03>

User name: CSU San Diego

Book: Jitter, Noise, and Signal Integrity at High-Speed

Section: Chapter 3. Source, Mechanism, and Math Model for Jitter and Noise

No part of any chapter or book may be reproduced or transmitted in any form by any means without the prior written permission for reprints and excerpts from the publisher of the book or chapter. Redistribution or other use that violates the fair use privilege under U.S. copyright laws (see 17 USC107) or that otherwise violates these Terms of Service is strictly prohibited. Violators will be prosecuted to the full extent of U.S. Federal and Massachusetts laws.

Information Theory Computer Science Mike Peng Li Prentice Hall Jitter, Noise, and Signal Integrity at High-Speed

3.1. Deterministic Jitter (DJ)

Recall [Figure 1.11](#) in [Chapter 1](#), which classifies various jitter components and their relationships with higher-level deterministic and random jitter. The three basic deterministic jitter types are data-dependent jitter (DDJ), periodic jitter (PJ), and bounded uncorrelated jitter (BUJ). DDJ is composed of duty cycle distortion (DCD) and ISI. DCD is a special type of DDJ when the data pattern is a clock like pattern.

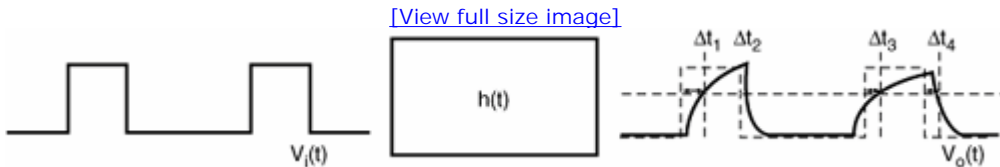
3.1.1. Data-Dependent Jitter (DDJ)

The following sections focus on DDJ because it is the most commonly encountered DJ type and its effect is significant as data rates increase. Also, it is the dominant limiting factor for the link channel or medium at multiple Gbps rates, especially for copper-based channel materials. We will first establish the DDJ formation mechanism and theory for quantitative estimation. Then we will discuss its two subcomponents of ISI and DCD.

3.1.1.1. General Theory

DDJ is due to the "memory" of any lossy electrical or optical system such that the bit transition time (or zero-crossing time) of the current bit depends on the transition times of the previous bits. Equivalently, the current bit transition times affect the future bit transition times. DDJ can be modeled through an LTI system in which an ideal data pattern is the input to the LTI system. DDJ is calculated from the output waveform via its deviation of the edge transition times from the corresponding ideal edge transition times. [Figure 3.1](#) shows DDJ modeling and estimation through an LTI system.

Figure 3.1. DDJ modeling and estimation through an LTI system.



This figure shows a data pattern input signal with ideal rise/fall times (zero rise/fall time) to an LTI system. If an LTI system has a non-Dirac delta impulse response function, the output pattern $V_o(t)$ has time deviations from its ideal transition times at a given threshold level. Examples are a 50% voltage level for a single-ended signal, or 0 voltage for a differential signal, assuming that there is no DC bias. Those time deviations of $\Delta t_1, \Delta t_2, \Delta t_3$, and Δt_4 , as shown in [Figure 3.1](#), are DDJs. From the LTI theory introduced in [Chapter 2](#), we know that

Equation 3.1

$$V_o(t) = V_i(t) * h(t)$$

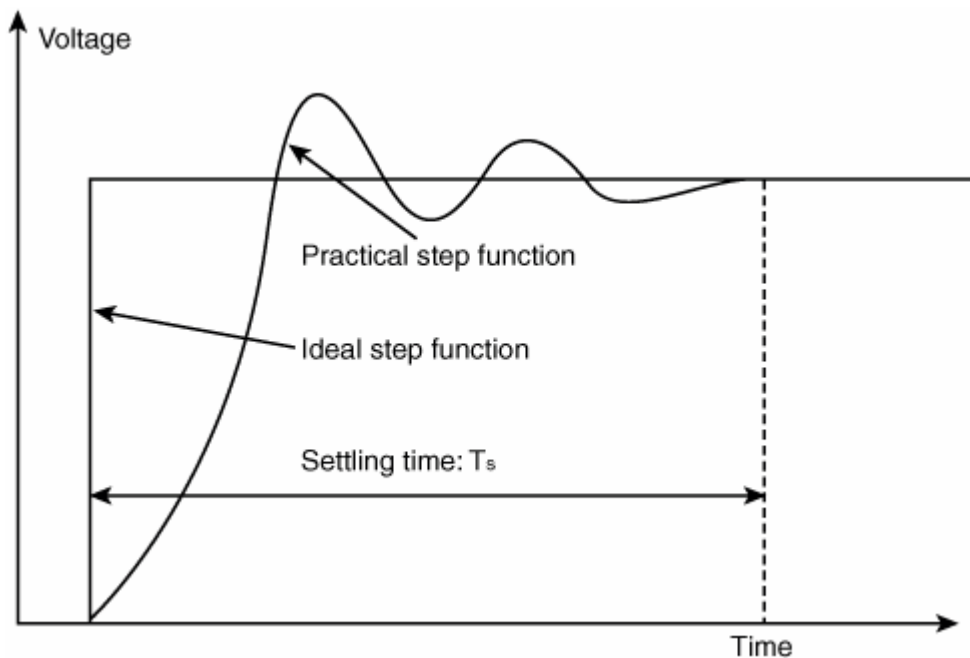
You can see that DDJ has the following properties:

- DDJ depends on the impulse response of the system that generates the pattern.
- DDJ depends on the input pattern $V_i(t)$.
- DDJ is a distribution with its sample size equal to the number of transitions of the data patent.
- If the LTI system is perfect or non-lossy—namely, $V_o(t) = V_i(t)$, and no DDJ or zero DDJ is introduced by the system.

Theoretically, to maintain exactly the same waveform between input signal and output signal, the impulse response of the LTI system needs to be a Dirac delta function, meaning an ideal step response (the integral of the impulse response) with zero rise time, or infinite bandwidth. If the Dirac delta condition cannot be met, the edge transition deviates from the ideal, and DDJ occurs. In general, the impact of the LTI transfer function on the DDJ can be viewed in both time and frequency domains. In the time domain, the step response gives a good indication of the DDJ. Similarly, in the frequency domain, the frequency response function for both magnitude and phase of the LTI leads the estimation of DDJ. As discussed in section 2.5 of Chapter 2, the time domain and frequency domain are equivalent and transformable through Laplace/inverse Laplace transformation. Whether to use the time domain or frequency domain is just a matter of convenience. For instance, DDJ is a time-domain phenomenon, so it is relatively easier or more convenient to develop a qualitative relationship between DDJ and step response function characteristic parameters.

For a step response, as shown in Figure 3.2, the settling time T_s gives a good indication for the DDJ, although the exact estimation depends on the exact pattern and the shape of the step response function.

Figure 3.2. Ideal step function, practical step function, and associated settling time.



The settling time gives a good indication of DDJ. In general, the longer the settling time, the larger the DDJ is for a given pattern. Further readings on LTI application in DDJ estimation can be found in [1], [2], and [3].

3.1.1.2. DDJ Estimation for an RC LTI System

We will illustrate how to estimate the DDJ for a single pulse when the LTI system transfer function is an RC circuit, as illustrated in section 2.6.2 of Chapter 2. Here we assume an RC constant of $\tau = RC$. The step response for an RC circuit is given by the following equation:

Equation 3.2

$$U_o(t) = 1 - e^{-t/\tau}$$

The DDJ time displacement at the 50% voltage level according to the definition shown in [Figure 3.1](#) can be calculated as follows:

Equation 3.3

$$\Delta t_{DDJ} = -\tau \ln(1-50\%) = 0.6931 \tau$$

Clearly, the DDJ in this case is proportional to the RC constant τ . In the case of an RC first-order system, the rise time is also proportional to the RC constant. In this context, we may say that DDJ is also proportional to the rise time of the RC circuit.

This problem can also be viewed in the frequency domain. According to the transfer function developed in [Example 2.4 of Chapter 2](#), the transfer function of an RC circuit is as follows:

Equation 3.4

$$|H(\omega)| = \frac{1}{\sqrt{1 + (\omega\tau)^2}}$$

The 3 dB bandwidth for such a transfer function can be estimated as follows:

Equation 3.5

$$f_{3dB} = \frac{0.2757}{\tau}$$

Combining [equations 3.3](#) and [3.5](#) and eliminating τ yields the following:

Equation 3.6

$$\Delta t_{DDJ} = \frac{0.191}{f_{3dB}}$$

In this case, the DDJ is inversely proportional to the 3 dB bandwidth of the RC circuit.

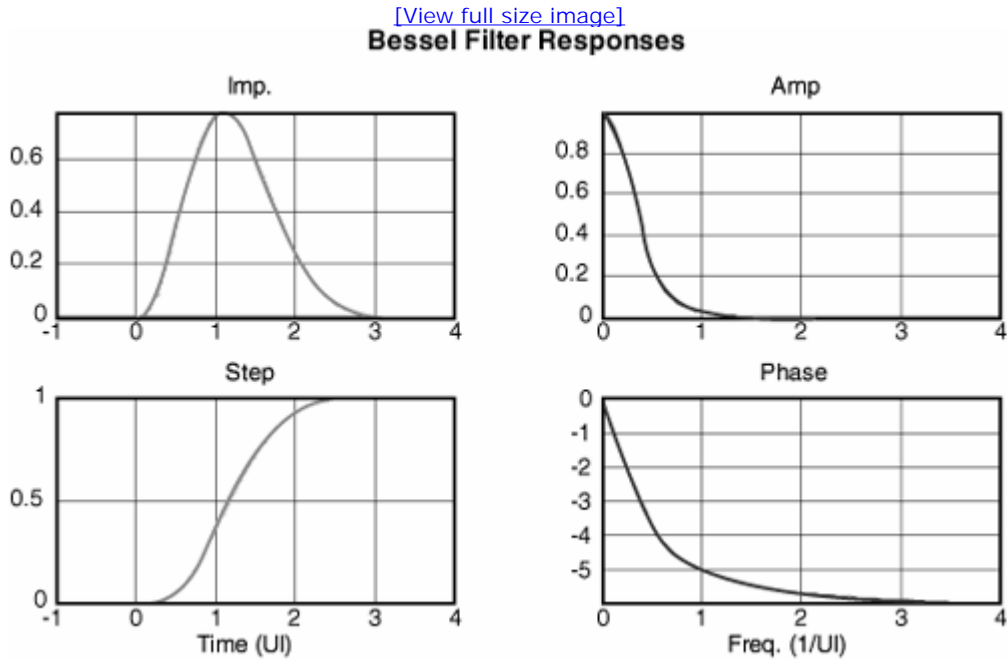
For a data pattern containing many transition bits, a general analytical form for DDJ is hard to obtain. We have to rely on [equation 3.1](#) and the DDJ definition shown in [Figure 3.1](#) to obtain the DDJ estimation numerically. The next section shows some simulation results.

3.1.1.3. Simulations

We have pointed out that the DDJ depends on both the data pattern and the impulse/step response of the channel or medium that the signal passes through. A critical parameter that determines the magnitude of DDJ is the pattern's run length (the longest UI span of consecutive 1s or 0s). The longer the run length, the larger the maximum DDJ is. Because DDJ is estimated from the waveform, and it is derived from a collection of all the data pattern's edge transitions, it is best viewed in the form of an eye diagram in a cumulative or statistical manner. Here the simulation model is based on the theory established in [section 3.1.1.1](#).

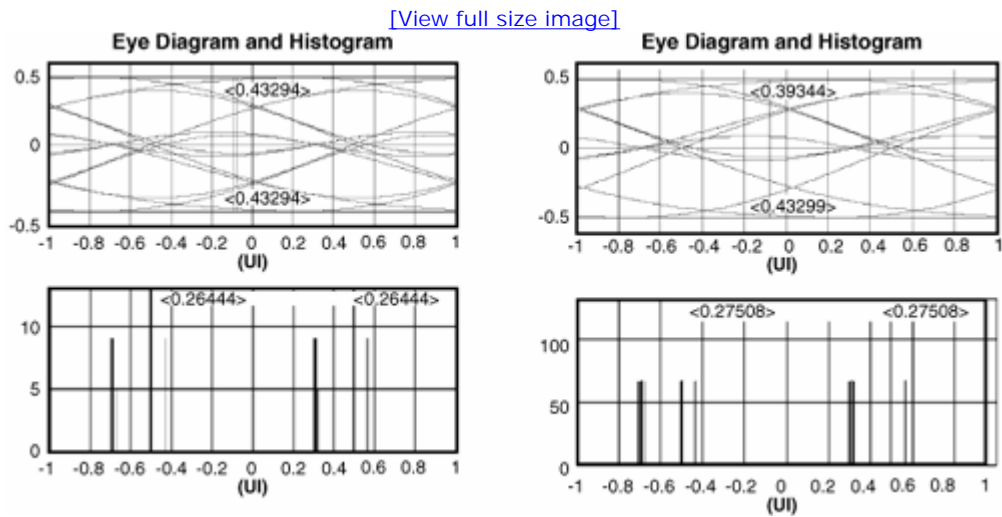
First, we will show pattern effect on the DDJ. The LTI transfer function that we use in this example is a fourth-order Bessel function. Its impulse, step, frequency-domain magnitude, and phase response functions are shown in [Figure 3.3](#). We chose the Bessel filter because it is the standard receiver model for many communication standards, such as Fibre Channel and Gigabit Ethernet.^[4]

Figure 3.3. The impulse (upper left), step (lower left), frequency magnitude (upper right), and frequency phase (lower right) response functions for a fourth-order Bessel function. The 3 dB bandwidth is $0.3 * (1/\text{UI})$.



We studied two patterns of K28.5 and PRBS $2^{10} - 1$ and they are the commonly used testing patterns for multiple Gbps data communication links. The DDJ for those two patterns are shown in Figure 3.4. K28.5 has a run length of 5 UI and a total of 20 bits. PRBS $2^{10} - 1$ has a run length of 10 UI and a total of 1024 bits. The eye opening for the PRBS $2^{10} - 1$ is smaller than the K28.5, as we may expect due to the longer run length for PRBS $2^{10} - 1$. The DDJs are 0.2644 UI and 0.2751 UI for K28.5 and PRBS $2^{10} - 1$, respectively.

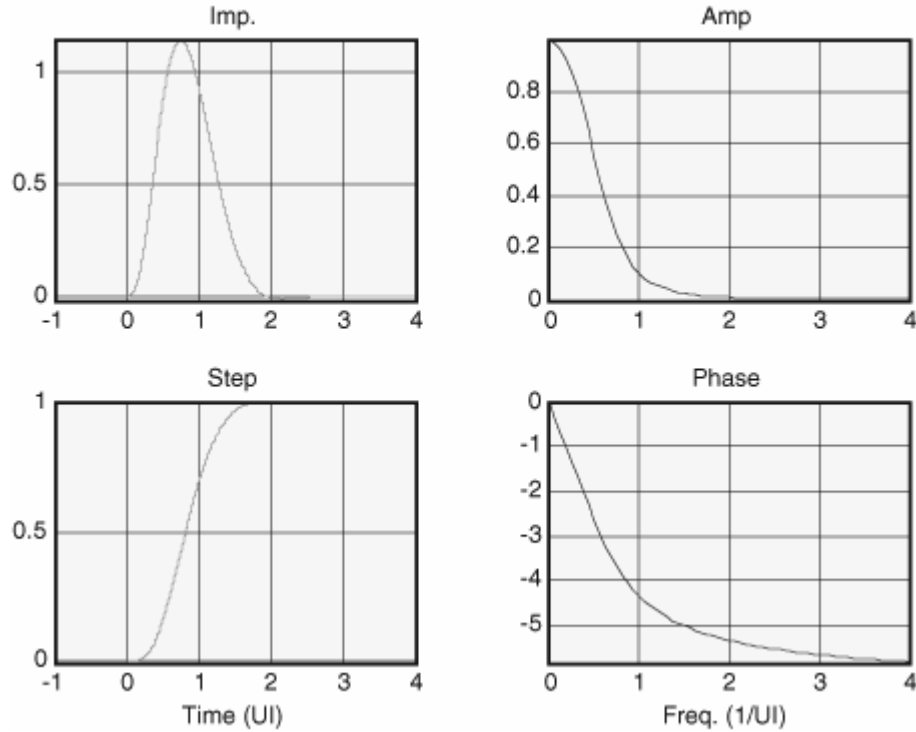
Figure 3.4. Eye diagrams for data pattern of K28.5 (a) and PRBS $2^{10} - 1$ (b), for the same LTI transfer function of the fourth-order Bessel-Thompson shown in Figure 3.3.



Second, we will show the effect of the LTI system bandwidth on the DDJ. The data pattern used is a PRBS $2^{10} - 1$, and the LTI system response function is still a fourth-order Bessel function. However, the bandwidth is $0.6 * (1/\text{UI})$ in this case. Its time and frequency domain response functions are shown in Figure 3.5.

Figure 3.5. The same as Figure 3.3, but with a 3 dB bandwidth of $0.6 * (1/\text{UI})$.

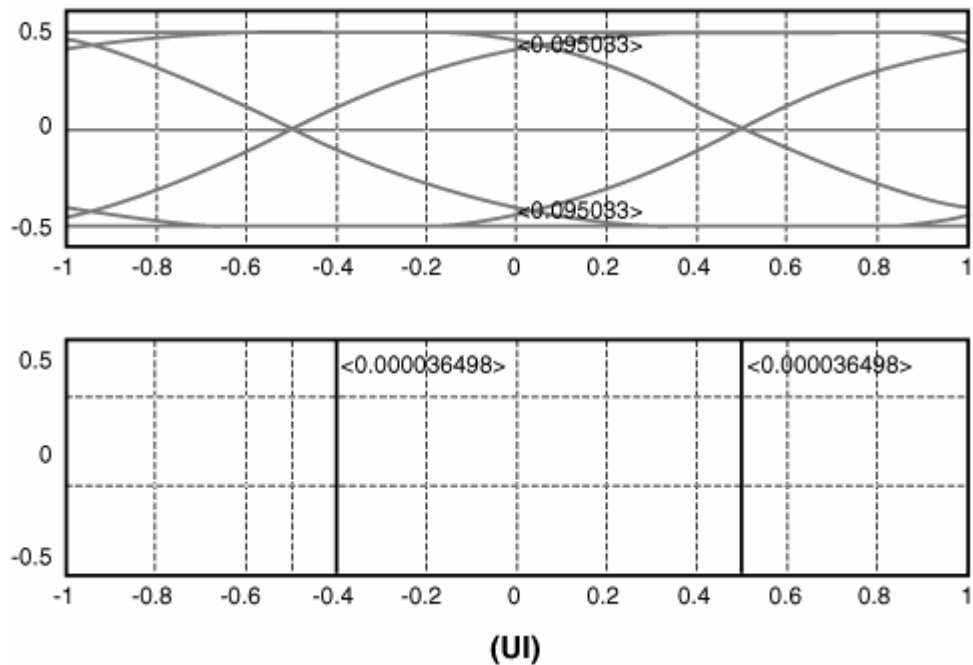
Bessel Filter Responses



The eye diagram and DDJ histogram corresponding to Figure 3.5 are shown in Figure 3.6. For the $0.6 * (1/\text{UI})$ bandwidth, the DDJ value is 0.00036 UI , much smaller than the DDJ of 0.275 UI for the case when the bandwidth is $0.3 * (1/\text{UI})$. As may be expected, the smaller the bandwidth, the larger the rise time, and so are the eye closure and DDJ.

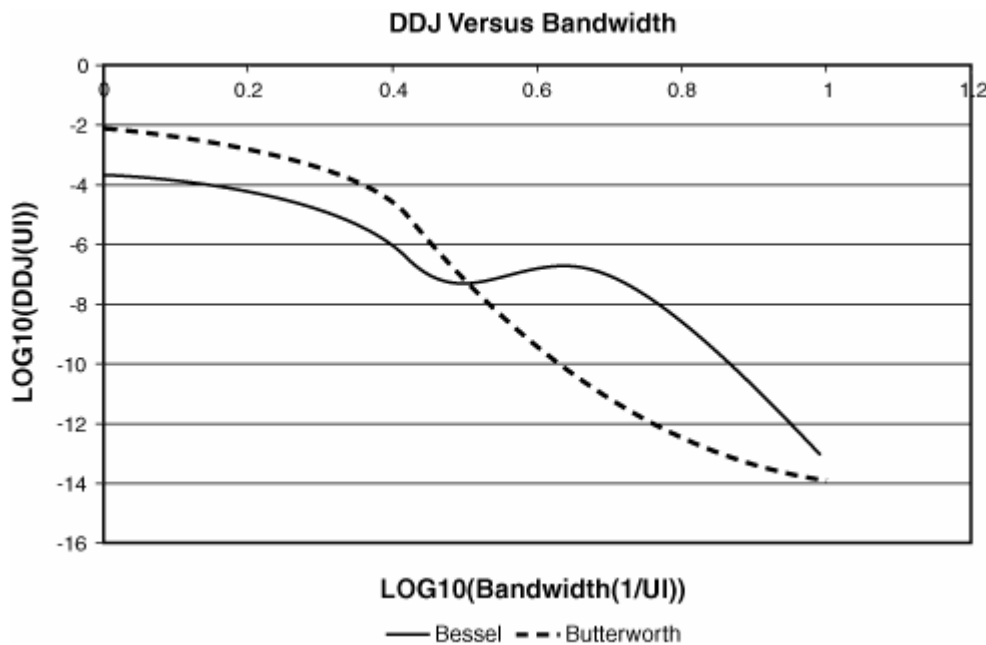
Figure 3.6. The same as in Figure 3.4, part (b), but with a higher 3 dB bandwidth $0.6 * (1/\text{UI})$. Notice the smaller DDJ and eye closure.

Eye Diagram and Histogram



It will be interesting to see how the DDJ changes as a function of bandwidth for a given pattern and system transfer function type. We extend the exercise of this DDJ-versus-bandwidth relation study by including more data points. The results are shown in Figure 3.7.

Figure 3.7. DDJ as a function of bandwidth for a PRBS $2^7 - 1$ pattern. The solid-line curve is for a fourth-order Bessel transfer function, and the dashed-line curve is for a fourth-order Butterworth transfer function.

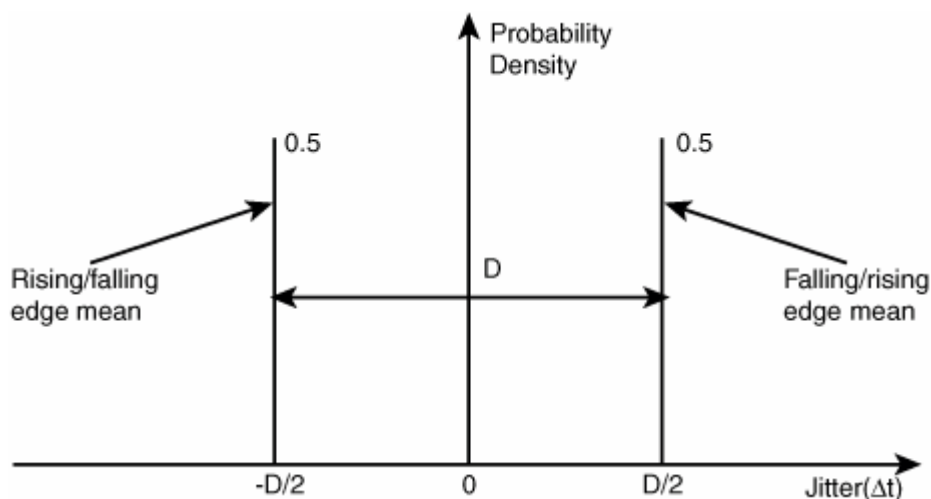


As might be expected, DDJ decreases as bandwidth increases in general, although we do observe a small ripple effect in the 0.5–0.6 (1/UI) range for the Bessel transfer function. The curve is not linear in the log-log plot, suggesting that it is not an exponential function. It is worth pointing out that for different patterns or different LTI transfer function types, the DDJ-versus-bandwidth function is different.

3.1.1.4. Duty Cycle Distortion

Duty Cycle Distortion (DCD) jitter is only for clock patterns of repeating 0101 bits. It is the mean deviation of the clock pulse (either positive or negative) from its ideal. Theoretically, the LTI method introduced in [section 3.1.1.1](#) is also applicable to DCD estimation, but the pattern used needs to be a clock pattern. One common root cause of DCD is the variation of the reference signal for the clock high and clock low logic generation, as shown in [Chapter 1](#). Another cause is the transport delays for clocks synthesized with many substrate clocks. The DCD jitter is determined by two mean values of rising edge and falling edge. Thus, DCD can best be modeled by the dual-Dirac delta function shown in [Figure 3.8](#).

Figure 3.8. A dual-Dirac delta function representing the DCD jitter PDF function.



Mathematically, this dual-Dirac function can be represented as follows:

Equation 3.7

$$f_{DCD}(\Delta t) = \frac{1}{2} [\delta(\Delta t - \frac{D}{2}) + \delta(\Delta t + \frac{D}{2})]$$

3.1.1.5. Intersymbol Interference (ISI)

ISI is another component of DDJ. ISI is caused by timing spread of various pulses with different run lengths within the pattern. More specifically, ISI is largely associated with the edge transitions surrounded by uneven pulses. Referring to [Figure 3.2](#), the largest interference can be expected between a short pulse (1 bit period or unit interval (UI)) and a long pulse with opposite polarity (several bit periods or UIs) or vice versa. For example, a bit sequence of 011111 or 100000 is expected to have the largest ISI for a pattern with 5 UI run length. Here the interference is defined as the residual difference between the actual waveform and the ideal waveform, and ISI is proportional to the residual difference. ISI depends on both data pattern and channel or medium system response function. As a result, an ISI PDF function has no fixed and closed form. However, the convolution rule still holds for DDJ components of ISI and DCD, as long as they are independent, and that is generally true for DCD and ISI, because they are caused by different mechanisms. If the DDJ and DCD PDFs are both known, the ISI PDF can be estimated using the following inverse convolution, or deconvolution, operation:

Equation 3.8

$$f_{ISI}(\Delta t) = Con^{-1}(f_{DDJ} / f_{DCD})$$

$Con^{-1}()$ represents deconvoluting f_{DCD} from f_{DDJ} to get f_{ISI} . Most publications on the DDJ and ISI do not differentiate between DDJ and ISI. Few publications deal with DCD and ISI separation.^[4] Those that do take a more ad hoc or qualitative approach.

3.1.1.6. A General Model for DDJ

Because DDJ is closely related to the run length of a data pattern, and there are only limited run-length permutations for a given pattern, the DDJ value will be finite and discrete. Based on this, we can establish a general DDJ math model for its PDF. This method can also extend to cover the ISI and DCD generic PDF models. The following is the generic form for a DDJ PDF:

Equation 3.9

$$f_{DDJ}(\Delta t) = \sum_{i=1}^N P_i^{DDJ} \delta(\Delta t - D_i^{DDJ})$$

P_i^{DDJ} is the probability for the DDJ value of D_i^{DDJ} . Clearly, P_i^{DDJ} needs to satisfy the following probability property:

Equation 3.10

$$\sum_{i=1}^N P_i^{DDJ} = 1$$

ISI and DCD PDFs can also be written in the generic form of [equation 3.9](#), but with fewer discrete values if the same resolution is used. For example, if we write the ISI PDF like this:

Equation 3.11

$$f_{ISI}(\Delta t) = \sum_{j=1}^M P_j^{ISI} \delta(\Delta t - D_j^{ISI})$$

$$P_j^{ISI} \sum_{j=1}^N P_j^{ISI} = 1$$

a similar condition to [equation 3.10](#) can be found for P_j^{ISI} as $\sum_{j=1}^N P_j^{ISI} = 1$. Because the peak-to-peak value of DDJ is always larger or equal to that of ISI, we always have the following inequality of

Equation 3.12

$$\max(D_i^{DDJ}) - \min(D_i^{DDJ}) \geq \max(D_j^{ISI}) - \min(D_j^{ISI})$$

The same kind of sum of delta function method can be applied for DCD distribution, so we will not repeat the derivation here. For the DCD with a dual-Dirac delta function PDF, it is in fact a special case of DDJ with $N = 2$ and $P_k^{DCD} = 0.5$.

3.1.2. Periodic Jitter (PJ)

Periodic jitter is a repeating jitter signal at a certain period or frequency. From a signal perspective, it is the same as any periodic signal in terms of frequency and phase, but its amplitude is jitter in units of timing. PJ can be viewed as bounded uncorrelated narrow-band jitter.

3.1.2.1. PDF for a Single PJ

For illustration purposes, periodic jitter is assumed to be sinusoidal. It can be described mathematically by the following:

Equation 3.13

$$\Delta t = A \cos(\omega t + \phi_0)$$

ω is the angular frequency and ϕ_0 is the initial phase. The conclusions established can apply well to other PJs with different profiles, such as triangle, sawtooth, or trapezoid.

Let us define the overall phase for this sinusoidal as $\Phi = \omega t + \phi_0$. Then [equation 3.13](#) can be rewritten as

Equation 3.14

$$\Delta t = A \cos \Phi$$

Phase Φ has a uniform distribution if it is observed over a few periods. Its PDF is given by

Equation 3.15

$$f_\Phi(\Phi) = \frac{1}{2\pi} \quad \text{for } 0 \leq \Phi \leq 2\pi$$

We need to find the PDF for PJ based on [equations 3.14](#) and [3.15](#) by using the inverse variable PDF estimation method of equation [\(2.23\)](#). The inverse function of Δt is $\Phi = \cos^{-1}(\Delta t / A)$. The PDF for PJ Δt is given by

Equation 3.16

$$f_{PJ}(\Delta t) = \left(\frac{d\Phi(\Delta t)}{d\Delta t} \right) f_\Phi = \left(\frac{d(\cos^{-1}(\Delta t / A))}{d\Delta t} \right) f_\Phi$$

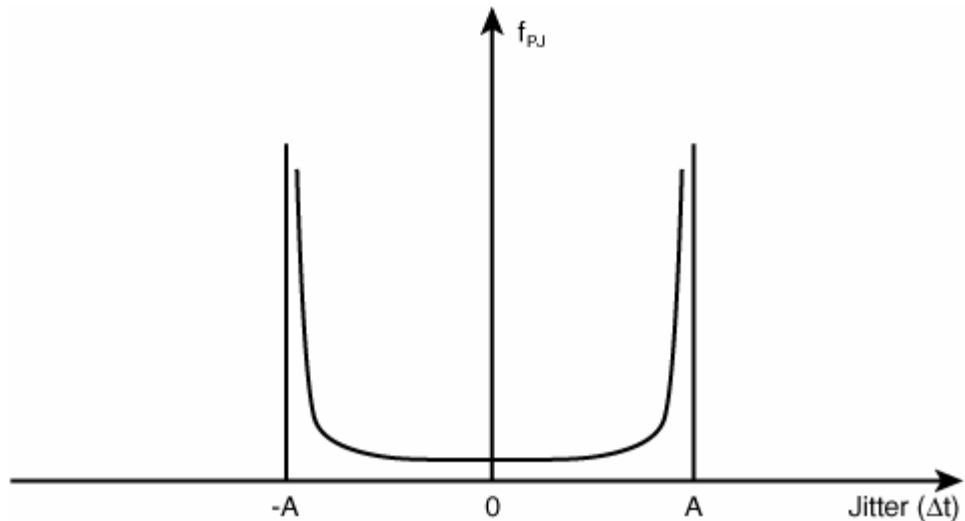
Substituting the PDF of the phase and carrying out the derivative operation, we find that the PDF for the single PJ is as follows:

Equation 3.17

$$f_{PJ}(\Delta t) = \frac{1}{\pi\sqrt{1-(\Delta t/A)^2}}, \quad -A \leq \Delta t \leq A \\ 0, \text{ otherwise}$$

This PDF for a single sinusoidal is shown in [Figure 3.9](#).

Figure 3.9. The PDF for a single sinusoidal PJ.



An approximation of a PJ PDF can be a dual-Dirac delta function of the following:

Equation 3.18

$$f_{PJ}(\Delta t) \approx \frac{1}{2}[\delta(\Delta t - A) + \delta(\Delta t + A)]$$

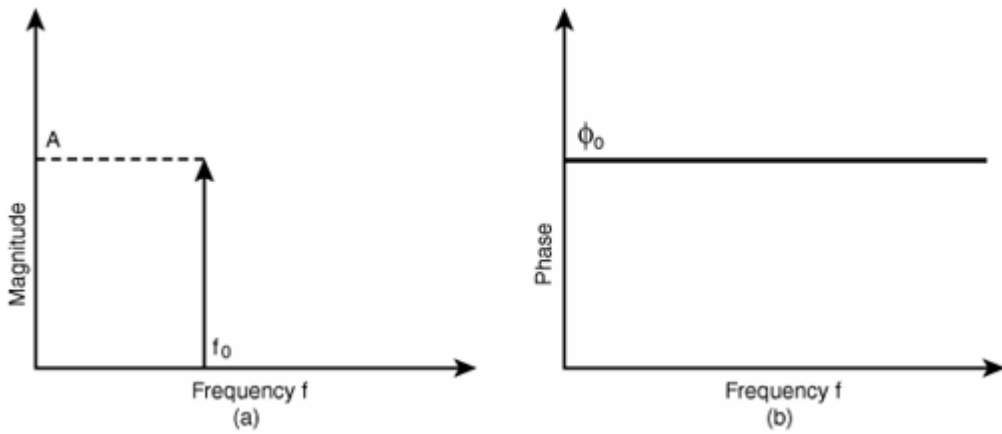
This approximation makes the PJ PDF convolution operation with other types of PDFs easy to carry out.

3.1.2.2. Spectrum for a Single PJ

If we take the Fourier Transformation (FT) for [equation 3.13](#), we get the spectrum for the single PJ. The spectrum is a complex function and therefore has two parts: magnitude and phase functions. Because we are dealing with a single frequency (or tone) sinusoidal with a constant phase, the complex spectrum has both magnitude and phase response functions, as shown in [Figure 3.10](#).

Figure 3.10. The complex spectrum magnitude (a) and phase (b) for a single sinusoidal PJ.

[\[View full size image\]](#)



3.1.2.3. PDF for Two PJs

We have shown that the PDF for a single PJ does not depend on its initial phase condition if it is observed over many periods. However, in the case of two PJs, the relative phase relationship is important in determining the overall PDF function. Recall [equation 3.13](#), and expand it to cover two PJs. We get the following:

Equation 3.19

$$\Delta t(t) = A_1 \cos(\omega_1 t + \phi_1) + A_2 \cos(\omega_2 t + \phi_2)$$

Let us assume that the amplitude of those two PJs are the same—namely, $A_1 = A_2 = A$ —and use the formula of sum-to-product conversion for cosines. We get the following:

Equation 3.20

$$\Delta t(t) = 2A \left\{ \cos\left[\frac{(\omega_1 + \omega_2)t + (\phi_1 + \phi_2)}{2}\right] \cos\left[\frac{(\omega_1 - \omega_2)t + (\phi_1 - \phi_2)}{2}\right] \right\}$$

Let us further assume that the frequencies of these two PJs are the same—namely, $\omega_1 = \omega_2 = \omega$ —leaving only the phases being different. [Equation 3.20](#) then becomes

Equation 3.21

$$\Delta t(t) = 2A \cos\left(\frac{\phi_1 - \phi_2}{2}\right) \cos\left[\omega t + \frac{(\phi_1 + \phi_2)}{2}\right]$$

With [equation 3.21](#), we can study the PDF of two PJs and its dependency on their phase relationship.

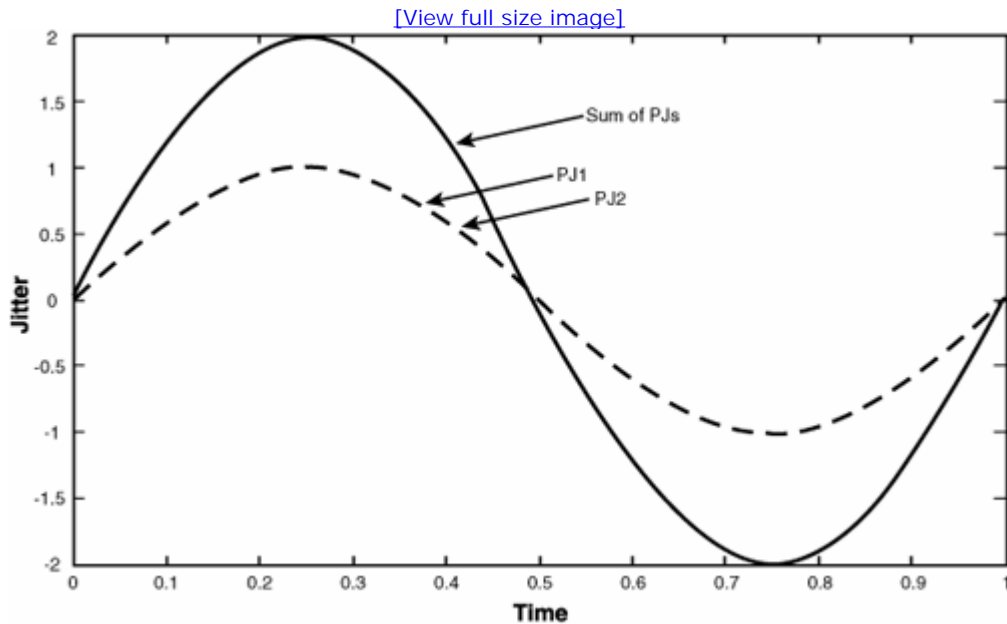
Case 1: $\phi_1 = \phi_2 = \phi$. In other words, they have the same phase or are in phase. [Equation 3.21](#) then becomes

Equation 3.22

$$\Delta t(t) = 2A \cos[\omega t + \phi]$$

This form is the same as the single PJ, but with twice as much of the amplitude. In other words, when two PJs with the same magnitude and frequency are added together, they form another PJ with twice the amplitude of the single PJ when their initial phases are the same. See [Figure 3.11](#).

Figure 3.11. The sum of two PJs with same frequency, same initial phase, and same peak amplitude. Note that the amplitude adds at each time sample and the sum of those two PJs has a peak magnitude that is twice that of each one.



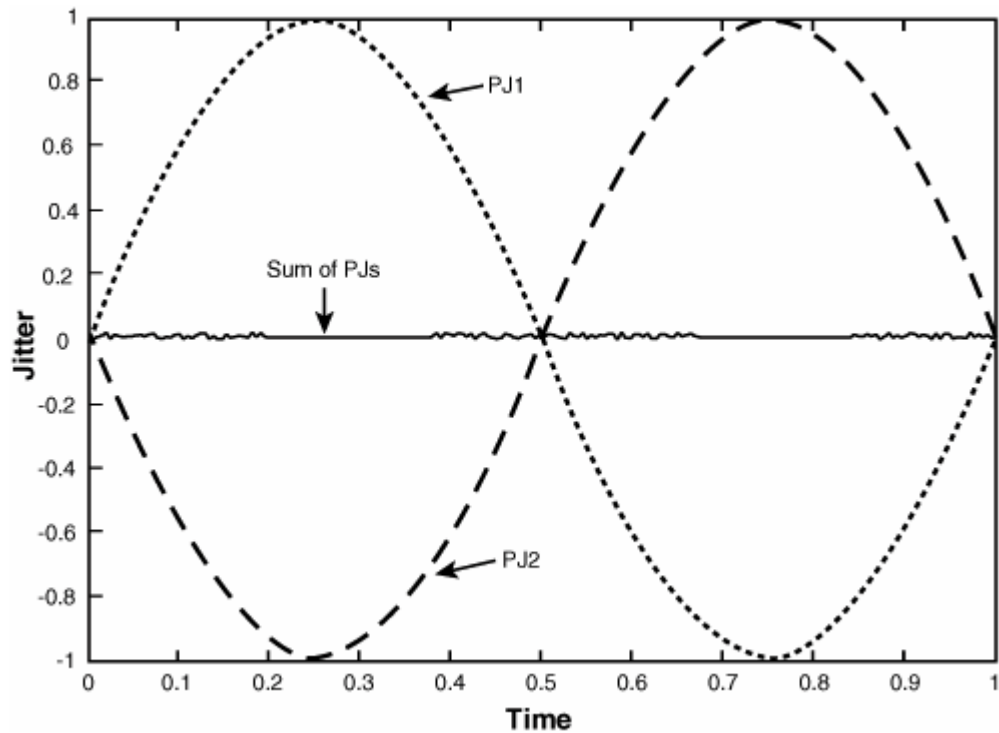
Case 2: $\phi_1 - \phi_2 = \pi$. In other words, they are in opposite phases. Equation 3.21 then becomes

Equation 3.23

$$\Delta t = 0$$

These two PJs are cancelled out. In other words, when two PJs with the same magnitude and frequency are added together, their sum is zero when their initial phases are opposite. See Figure 3.12.

Figure 3.12. The sum of two PJs with the same frequency and amplitude when their initial phases are opposite. Note the amplitude canceling each other at every sampling point with their sum equal to zero.

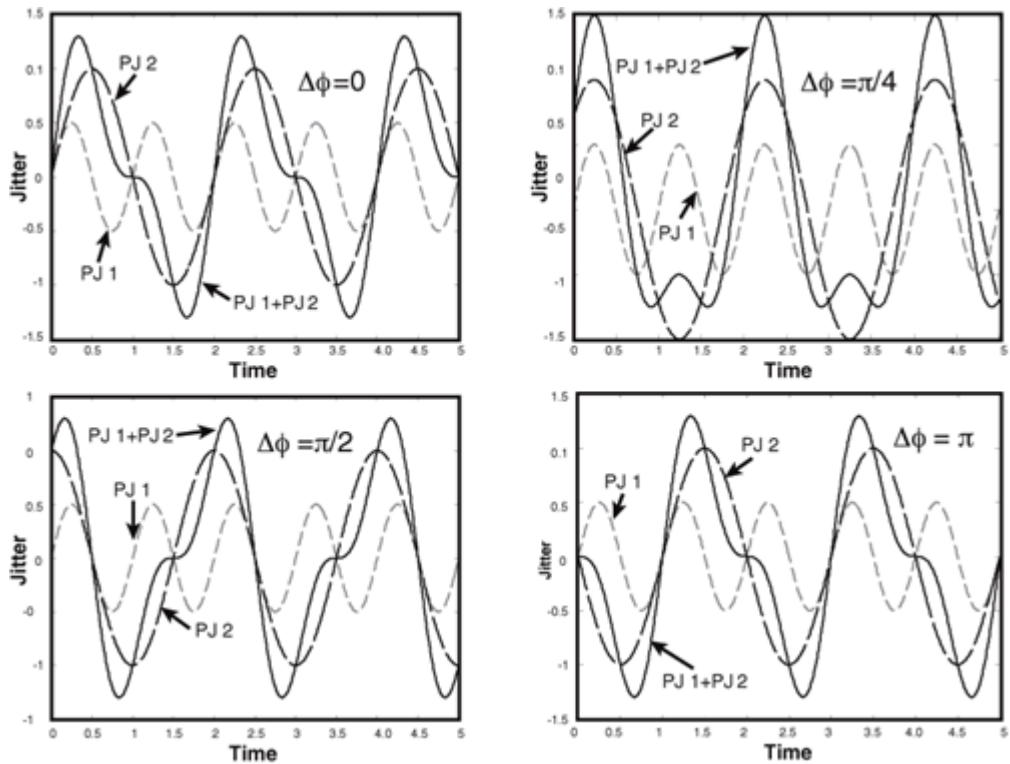


These two cases were developed by assuming that the frequencies of those two PJs are the same. When those two frequencies are different, we need to use [equation 3.20](#) to estimate the sum of the two PJs. The end results will depend on the frequency and phase of each PJ and can have many possible outcomes. In general, when two PJs are in phase—that is, their phase difference is small ($\phi_1 - \phi_2 \approx 0$)—the "adding" effect is dominant and the peak-to-peak of the summed function is $\Delta t(t)_{\text{pk-pk}} > 2(A_1 + A_2)$. When two PJs are out of phase—that is, their phase difference is large ($\phi_1 - \phi_2 \approx \pm\pi$)—the "subtracting" effect is dominant and the peak-to-peak of the summed function is $\Delta t(t)_{\text{pk-pk}} < 2 |A_1 - A_2|$. If the phase difference is between these two extremes of in-phase and out-of-phase, the outcome will have a peak-to-peak between those values of "in-phase" and "out-of-phase."

[Figure 3.13](#) shows numerical results for the general case of the sum of two PJs when they have different magnitude, frequency, and phase. The effects of the phase relationship effect are obvious. The sum of two PJs can have totally different shapes, depending on their phase relationships. The peak-to-peak values from the simulation are consistent with our extreme case discussion. [Figure 3.13](#) shows the importance of phase information in determining the resulting function from the sum of two PJs.

Figure 3.13. Simulation of the sum of two PJs with different frequency, magnitude, and a series of phase angles between them.

[\[View full size image\]](#)



For the sum of n PJs, similar results can be achieved as in the case of two PJs, but the possibilities of the form of the summed function are many times larger. The in-phase concept still holds, but it is hard to use the concept of out-of-phase for many PJs. When all the PJs are in phase—their phases are very close to each other—the peak-to-peak satisfies $\Delta t(t)_{\text{pk-pk}} > 2(A_1 + A_2 + \dots + A_N)$.

3.1.2.4. Spectrum for Two PJs

If we take the FT for equation 3.19, we get the following frequency-domain representation:

Equation 3.24

$$\Delta t(j\omega) = \frac{A_1}{\sqrt{2\pi}} \delta(\omega - \omega_1) e^{-j\phi_1} + \frac{A_2}{\sqrt{2\pi}} \delta(\omega - \omega_2) e^{-j\phi_2}$$

This is a complex spectrum and can be represented by two functions of magnitude and phase. We can further calculate those two parts explicitly and have the following two functions of magnitude:

Equation 3.25

$$|\Delta t(j\omega)| = \frac{A_1}{\sqrt{2\pi}} \delta(\omega - \omega_1) + \frac{A_2}{\sqrt{2\pi}} \delta(\omega - \omega_2)$$

and phase:

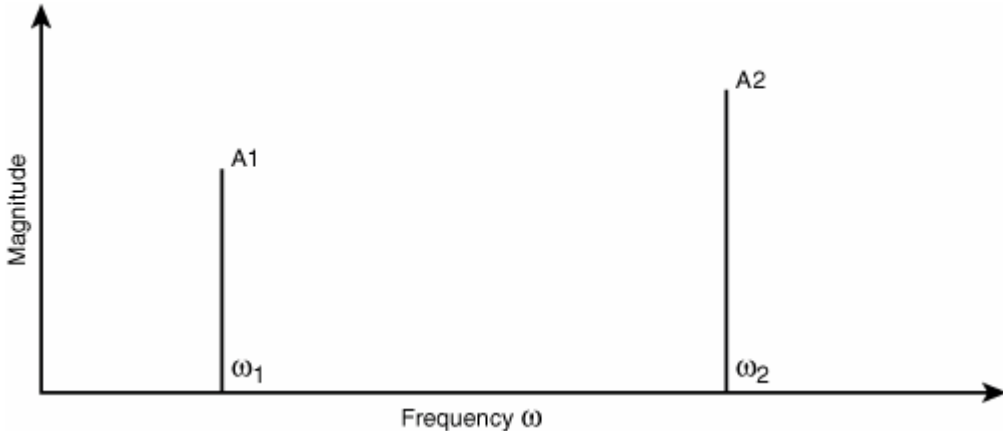
Equation 3.26

$$\text{Arg}(\Delta t(j\omega)) = \phi_1 + \phi_2$$

Clearly, the phase of each PJ affects the spectrum. To uniquely determine the time-domain function, both magnitude and phase responses of the spectrum are needed.

For illustration purposes, [Figure 3.14](#) shows the spectrum magnitude function for two PJs.

Figure 3.14. The spectrum magnitude function for the sum of two PJs.



3.1.2.5. PDF for Multiple ($n > 2$) PJs

For a general case of multiple PJs, the superposition rule still applies. The summation of all the PJs with different amplitude, frequency, and phase is given by

Equation 3.27

$$\Delta t(t) = \sum_{i=1}^N A_i \cos(\omega_i t + \phi_i)$$

The PDF can be estimated from the overall PJ time record of $\Delta t(t)$ through the following equation:

Equation 3.28

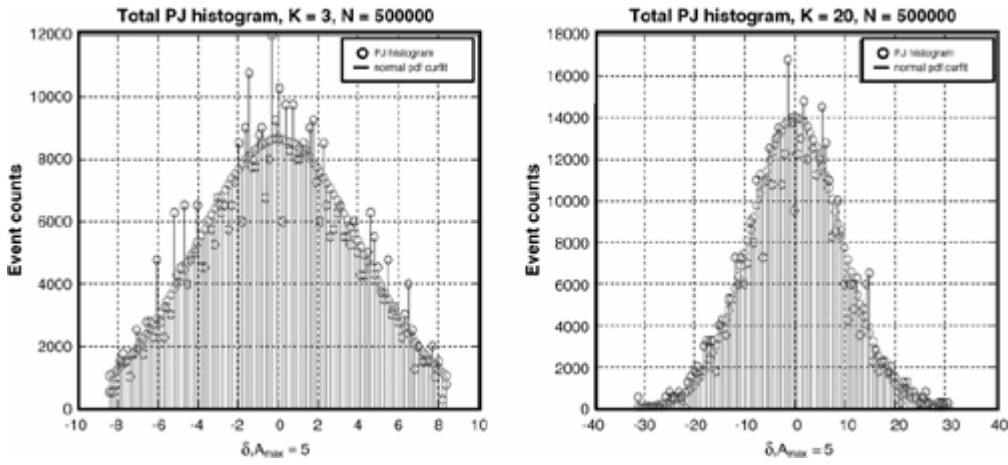
$$f_{PJ}(\Delta t) = \text{Hist}(\Delta t(t))$$

Hist is a histogram building function based on the $\Delta t(t)$ time record.

The overall PJ time record $\Delta t(t)$ is a multiple variable function, depending on each PJ amplitude, frequency, and phase, and the number of PJs. Therefore, it is hard to draw a general conclusion about the characteristics of the PDF for the overall PJ. However, we can do a Monte Carlo simulation to study the characteristics of f_{PJ} by assuming that all the PJs are independent, with their amplitude, frequency, and phase randomly distributed over the range of (A_{\min}, A_{\max}) , (f_{\min}, f_{\max}) , $(0, 2\pi)$, respectively. The simulation results are shown in [Figure 3.15](#).

Figure 3.15. The overall PJ PDF for three independent PJs (a) and 20 independent PJs overlaid with Gaussian distributions (b).

[\[View full size image\]](#)



It is clear that as the number of PJs increases, the agreement between the overall PJ PDF and the Gaussian distribution gets better within the PJ magnitude range. This is exactly the consequence of the "central-limiting theorem" discussed in [section 2.3.2](#) in [Chapter 2](#). Our simulation suggests that as long as the number of PJs is three or more, and they are independent, the overall PDF can be approximated by a truncated Gaussian distribution (as opposed to the conventional unbounded Gaussian) PDF, as discussed in the next section. The agreement between the overall PDF and the Gaussian gets better as the number of PJs increases.

3.1.2.6. Spectrum for Multiple PJs (> 2 PJs)

The spectrum estimation for multiple PJs is similar to that of two PJs. Again, the FT for [equation 3.27](#) results in

$$\text{Equation 3.29}$$

$$\Delta t(j\omega) = \sum_{i=1}^N \frac{A_i}{\sqrt{2\pi}} \delta(\omega - \omega_i) e^{-j\phi_i}$$

Its magnitude function is

$$\text{Equation 3.30}$$

$$|\Delta t(j\omega)| = \sum_{i=1}^N \frac{A_i}{\sqrt{2\pi}} \delta(\omega - \omega_i)$$

and its phase function is:

$$\text{Equation 3.31}$$

$$\text{Arg}(\Delta t(j\omega)) = \sum_{i=1}^N \delta(\omega - \omega_i) \phi_i$$

The magnitude spectrum response function of the multiple PJs is similar to [Figure 3.13](#), except that there will be many spectrum lines instead of two.

3.1.3. Bounded Uncorrelated Jitter (BUJ)

[Chapter 1](#) discussed the mechanisms for jitter caused by crosstalk. Because of the randomness of how crosstalk forms, BUJ is bounded,

as well as uncorrelated from a statistical distribution point of view. At the same time, BUJ can contain other bounded and uncorrelated jitter, such as electromagnetic interference (EMI). However, crosstalk is the dominant component of BUJ, and this section assumes that BUJ is crosstalk jitter. The similarity between BUJ and DDJ is that they are both bounded. The difference is that DDJ is correlated to its data pattern, and BUJ is not.

The comparison between BUJ and PJ can be very interesting. Both PJ and BUJ are bounded and uncorrelated, so they are similar from a statistical distribution point of view. However, from a frequency spectrum point of view, the difference can be large. For a single PJ, its spectrum is simply a spectral line. However, crosstalk jitter typically has a broad spectrum with many uncorrelated spectral lines. The difference between BUJ and many independent PJs can be very vague. In fact, BUJ can be modeled in terms of many independent PJs from a mathematical point of view. Because of those characteristics of BUJ, we can put PJ and crosstalk within the general category of BUJ. Along this line of thought, single-tone PJ should be called narrow-band BUJ (NB-BUJ), and crosstalk jitter should be called broadband BUJ (BB-BUJ).^[4]

3.1.3.1. PDF for BUJ

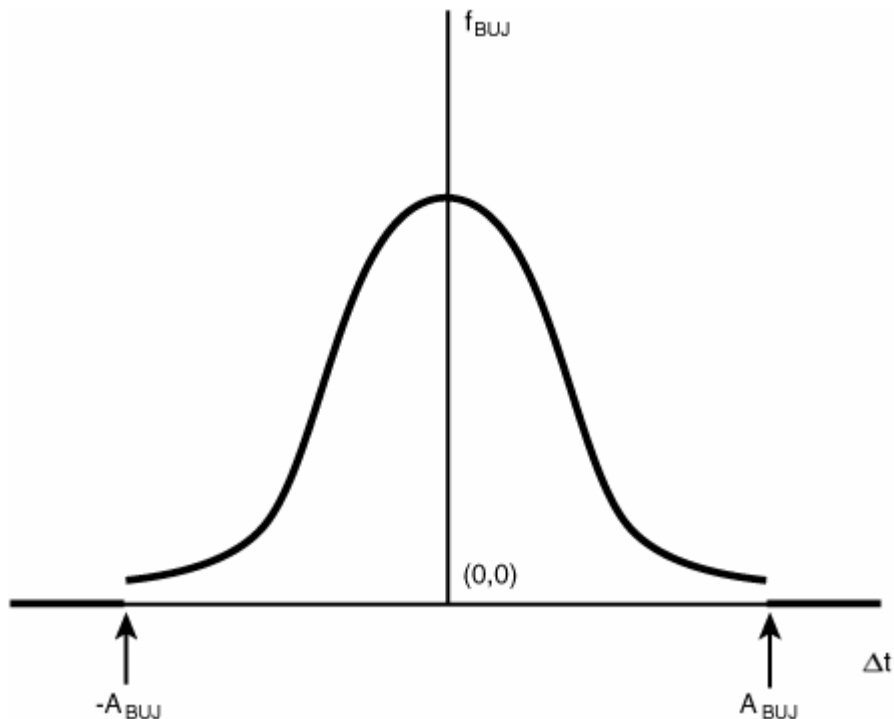
BUJ can be modeled by many independent PJs if it composed by many independent root sources. As suggested in [section 3.1.2.5](#), its time-domain PDF is a truncated Gaussian, as defined by the following equation:

Equation 3.32

$$f_{BUJ}(t) = \begin{cases} \frac{P_{BUJ}}{\sqrt{2\pi}\sigma_{BUJ}} e^{-\frac{t^2}{2\sigma_{BUJ}^2}} & \text{for } |t| \leq A_{BUJ} \\ 0 & \text{for } |t| > A_{BUJ} \end{cases}$$

A_{BUJ} is the peak value, σ_{BUJ} is the sigma value, and P_{BUJ} is the normalization probability for the BUJ PDF. The normalization probability P_{BUJ} is introduced to ensure that the integral of [equation 3.32](#) will be unit 1. Apparently, $P_{BUJ} > 1$. [Figure 3.16](#) graphically represents the BUJ PDF defined in [equation 3.32](#).

Figure 3.16. A BUJ PDF function represented as a truncated Gaussian.

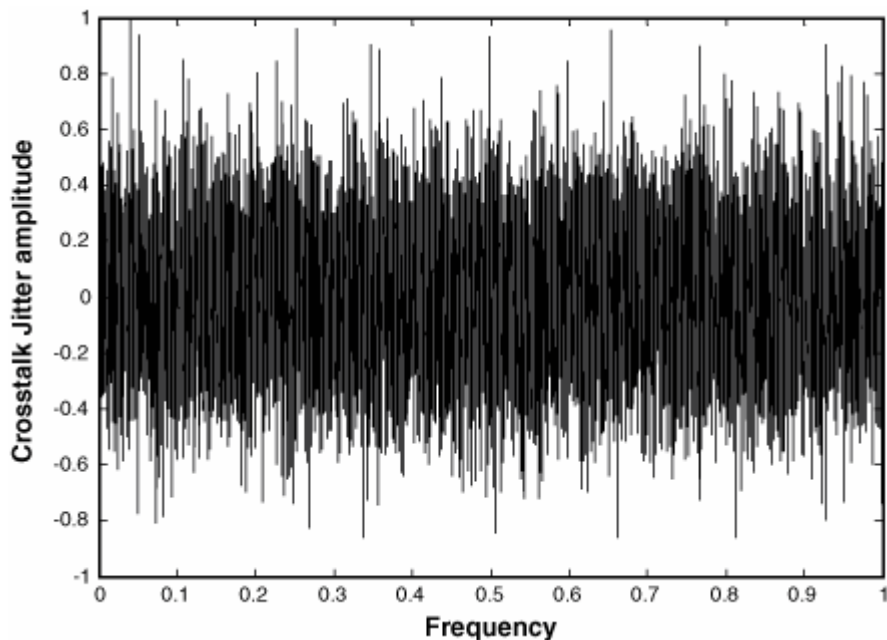


The major difference between the Gaussian and truncated Gaussian is at the tail parts of the PDF distribution. The truncated Gaussian has a zero probability when jitter reaches its peak value, and the Gaussian has a probability approaching zero only when the jitter reaches infinity. Experimental work on the BUJ PDF has been carried out, and the truncated Gaussian PDF has been verified.^[5]

3.1.3.2. Spectrum for BUJ

The spectrum of the BUJ can be modeled in a similar way as for the case of multiple PJ spectrums, because each crosstalk source can be treated as a single PJ at a given frequency. Of course, the spectrum of BUJ really depends on how many crosstalk sources it is composed of. As the number of independent crosstalk sources increases, the gap between each individual source in the frequency domain becomes smaller, and the spectrum looks like "finite" white noise. Figure 3.17 shows an example of the spectrum for BUJ when the number of crosstalk sources is large. The BUJ spectrum is characterized by bounded frequency range, randomness, and non-correlated with the signal's data pattern.

Figure 3.17. The spectrum of BUJ for a large number of crosstalk sources. It is similar to white noise spectrum but with finite frequency range.



When the number of BUJ sources is small, it is hard to describe its PDF with a closed-form distribution function. You must deal with BUJ on a case-by-case basis for both its statistical PDF and frequency-domain spectrum or PSD.

URL <http://access.proquest.safaribooksonline.com/9780132429610/ch03lev1sec1>

User name: CSU San Diego

Book: Jitter, Noise, and Signal Integrity at High-Speed

Section: Chapter 3. Source, Mechanism, and Math Model for Jitter and Noise

No part of any chapter or book may be reproduced or transmitted in any form by any means without the prior written permission for reprints and excerpts from the publisher of the book or chapter. Redistribution or other use that violates the fair use privilege under U.S. copyright laws (see 17 USC107) or that otherwise violates these Terms of Service is strictly prohibited. Violators will be prosecuted to the full extent of U.S. Federal and Massachusetts laws.

Information Theory Computer Science Mike Peng Li Prentice Hall Jitter, Noise, and Signal Integrity at High-Speed

3.2. Random Jitter (RJ)

Random jitter is caused by unbounded jitter sources, such as Gaussian white noise. Those types of jitter sources are usually corresponding noise processes of thermal noise, 1/f flicker noise, shot noise, and other high-order noise processes. As introduced in [section 1.2.2](#), a common noise-to-timing jitter conversion mechanism is the amplitude noise-to-phase jitter conversion through the slope of an edge transition. The statistical PDF for the random jitter is generally treated as Gaussian. However, a proof of such a PDF is generally based on a white jitter/noise model. The following sections discuss random jitter PDF, spectrum, and PSD for each type of the noise process.

3.2.1. Gaussian Jitter

The first type of random jitter is Gaussian jitter. In much literature, Gaussian jitter and random jitter are treated as the same jitter type. This treatment isn't precise, however, because in the presence of a nonwhite noise source, the corresponding PDF is not necessarily a Gaussian. Only when the PSD of the random jitter is predominantly white can its PDF be described by a Gaussian; this is an important point.

3.2.1.1. Gaussian Jitter PDF

The Gaussian jitter model is defined by [equation 3.33](#):

Equation 3.33

$$f_{GJ}(\Delta t) = \frac{1}{\sqrt{2\pi}\sigma} e^{-\frac{(\Delta t - \mu)^2}{2\sigma^2}}$$

This function is characterized as unbounded because its PDF is not zero unless the jitter Δt approaches infinity. Mathematically, we can show that the mean of this Gaussian form equals μ , and its standard deviation equals σ . Jitter and noise are physical quantities, and each has a corresponding physical unit or dimension. It will be easier to discuss the mathematical properties if we introduce another dimensionless variable of z as $z = (\Delta t - \mu)/\sigma$. Then we have the Gaussian PDF in terms of the normalized variable z :

Equation 3.34

$$f_{GJ}(\Delta t)d\Delta t = \phi(z)dz = \frac{1}{\sqrt{2\pi}} e^{-\frac{z^2}{2}} dz$$

$\phi(z)$ is called normal distribution function and was well studied. The integration of $\phi(z)$ is of particular interest, because it gives the CDF function and is defined as

Equation 3.35

$$\Phi(z) = \int_{-\infty}^z \phi(t) dt = \frac{1}{\sqrt{2\pi}} \int_{-\infty}^z e^{-\frac{t^2}{2}} dt = \frac{1}{2}(1 + \operatorname{erf}\left(\frac{z}{\sqrt{2}}\right))$$

where $\operatorname{erf}(\cdot)$ is an error function and is defined as

Equation 3.36

$$\operatorname{erf}(z) = \frac{2}{\sqrt{\pi}} \int_0^z e^{-t^2} dt$$

The numeric values of both normal distribution function and error function have been calculated and tabulated. An interesting application of the normal distribution is to estimate the probability when the deviation of the random jitter variable Δt is within a multiple of its σ value. For example, the probability of the random variable satisfying $|\Delta t - \mu| \leq \sigma$ can be estimated as

Equation 3.37

$$P(|\Delta t - \mu| \leq \sigma) = \Phi(1) - \Phi(-1) = 0.6826$$

A similar calculation for 2σ and 3σ yields results of

Equation 3.38

$$P(|\Delta t - \mu| \leq 2\sigma) = \Phi(2) - \Phi(-2) = 0.9545$$

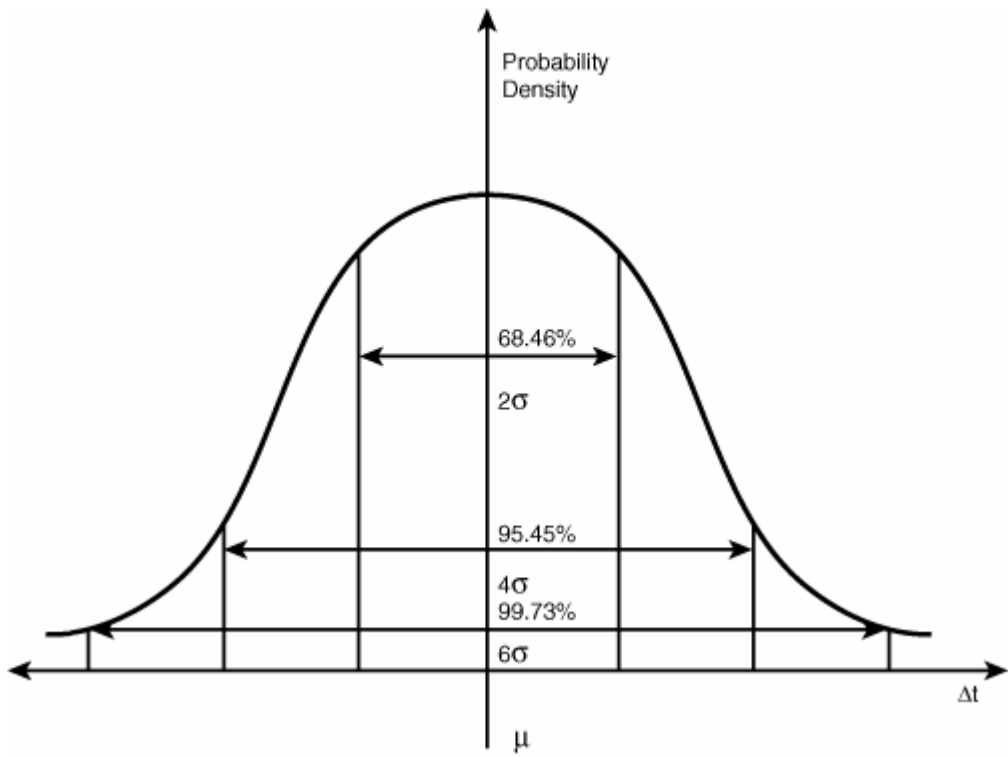
and

Equation 3.39

$$P(|\Delta t - \mu| \leq 3\sigma) = \Phi(3) - \Phi(-3) = 0.9973$$

These probability characteristics for a Gaussian distribution are shown in [Figure 3.18](#).

Figure 3.18. A Gaussian PDF with corresponding probability areas of 2σ , 4σ , and 6σ widths covering 68.46%, 95.45%, and 99.73% of the underneath area.

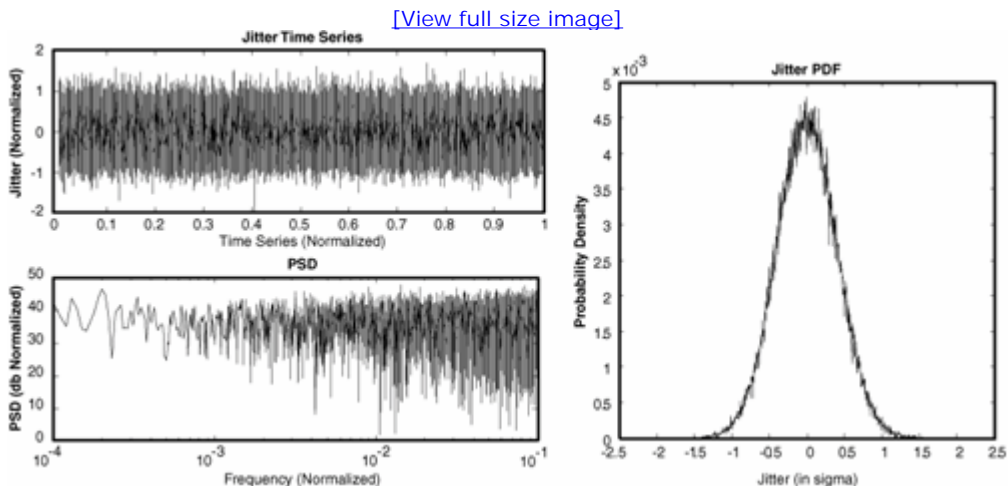


3.2.1.2. Gaussian Jitter PSD

It is well known that Gaussian jitter has a white PSD. This section does not pursue the analytical proof for this conclusion. Instead, we will conduct a numeric simulation to show the linkage between time-domain series, frequency-domain spectrum or PSD, and statistical-domain PDF for Gaussian jitter.

Assuming that $\Delta t_{GJ}(t)$ is the Gaussian jitter time record, this time record can be simulated by a random-number generator via Monte Carlo^{[6], [7]}, as shown in Figure 3.18. Its PSD can be estimated via the autocorrelation function and corresponding FT according to equation 2.112, introduced in section 2.2.4.2. The histogram can be obtained through the `Hist()` function. Gaussian jitter is commonly viewed via its statistical-domain PDF and frequency-domain PSD. Figure 3.19 gives three views from different domains to show the linkage for each representation.

Figure 3.19. Gaussian jitter time-domain record and frequency-domain PSD (a), as well as the statistical-domain PDF (b), for the same Gaussian jitter source with 10^6 samples.



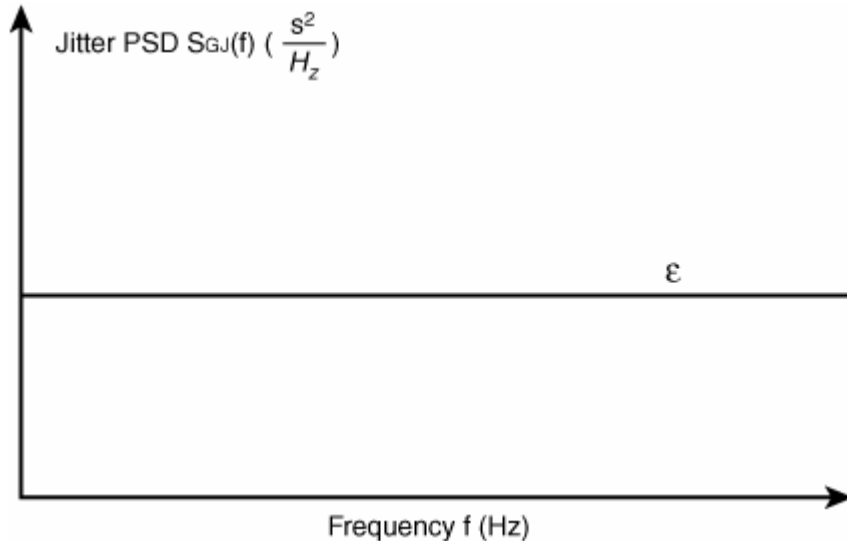
Analytically, the Gaussian PSD can be approximated by a white noise type of PSD of the following form:

Equation 3.40

$$S_{GJ}(f) = \varepsilon$$

It is worth pointing out that white PSD is a mathematical convenience rather than physical, because it is frequency-unlimited and gives rise to infinite energy. This contradicts any physical jitter or noise. [Figure 3.20](#) illustrates the PSD for a Gaussian jitter/noise source.

[Figure 3.20. Gaussian white jitter PSD.](#)



3.2.2. $f^{-\alpha}$ Higher-Order Jitter

This section focuses on the higher-order jitter processes with PSDs having a general form of $f^{-\alpha}$. As in the case of Gaussian jitter, we will discuss high-order jitter from the perspectives of statistical PDF and frequency-domain PSD.

3.2.2.1. $f^{-\alpha}$ Jitter PDF

$f^{-\alpha}$ is a general form for random jitter processes. For example, when $\alpha = 0$, it corresponds to white or Gaussian jitter. When $\alpha = 1$, it corresponds to flick jitter. When $\alpha = 2$, it corresponds to an integrated white. As the IC feature size continues to shrink to 90 nm or smaller, the higher-order power-law random jitter becomes increasingly important. However, the PDF of the high-order $f^{-\alpha}$ jitter is rarely addressed in the literature and is commonly mistreated the same as the Gaussian PDF. Because of this, we feel that $f^{-\alpha}$ random jitter PDF needs special attention.

We will start with the PDF of the f^{-2} random jitter, because its derivation is relatively straightforward. Let $\Delta t_G(t)$ be the Gaussian random jitter in the time domain. We denote its corresponding PSD as $S_G(f)$ and its Fourier spectrum as $\Delta t_G(f)$. Then we have

Equation 3.41

$$S_{GJ}(f) \sim (\Delta t_{GJ}(f))^2 \sim \varepsilon$$

Consider the time integral of the Gaussian random jitter of

Equation 3.42

$$\Delta t_{IG}(t) = \int_{-\infty}^t \Delta t_{GJ}(\tau) d\tau$$

Denoting the PSD and spectrum for the integrated Gaussian as $S_I(f)$ and $\Delta t_I(f)$ respectively gives us the following:

Equation 3.43

$$S_{IG}(f) \sim (\Delta t_{IG}(f))^2 \sim \frac{(\Delta t_{GJ}(f))^2}{f^2} \sim \frac{\epsilon}{f^2}$$

because

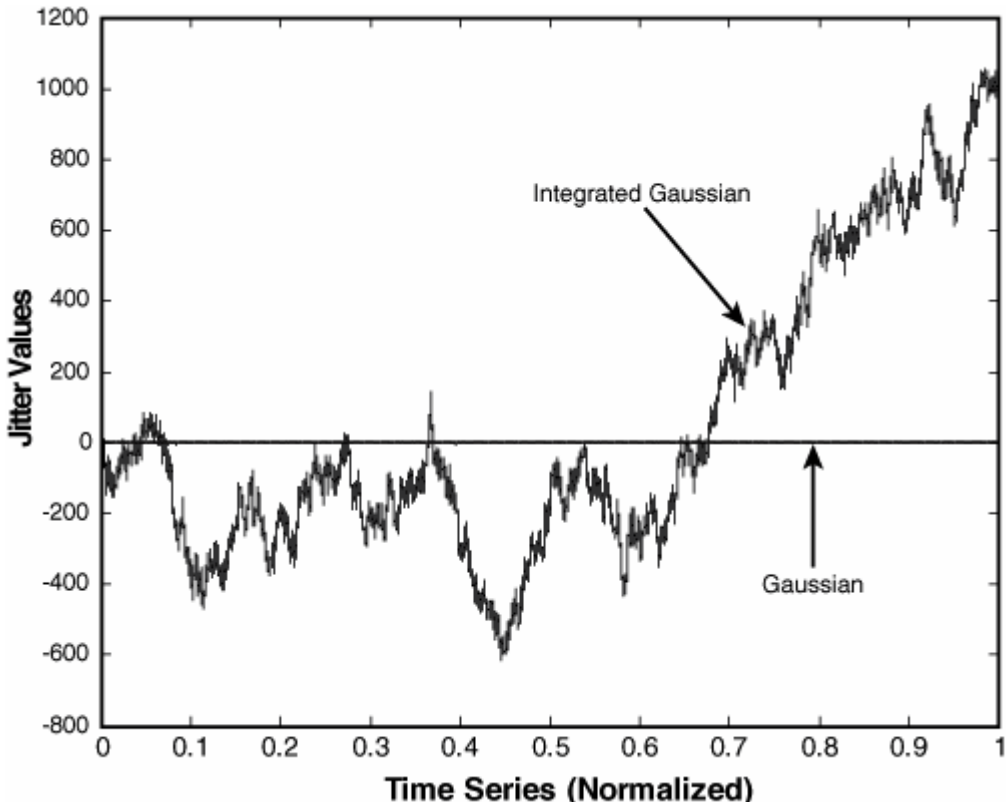
Equation 3.44

$$\Delta t_{IG}(f) = FT(\Delta t_{IG}(t)) = FT(\int \Delta t_{GJ}(t) dt) \sim \frac{\Delta t_{GJ}(f)}{f}$$

[Equations 3.43](#) and [3.44](#) suggest that the time-domain record function for the f^{-2} random jitter is an integrated Gaussian, justifying its name of integrated Gaussian jitter.

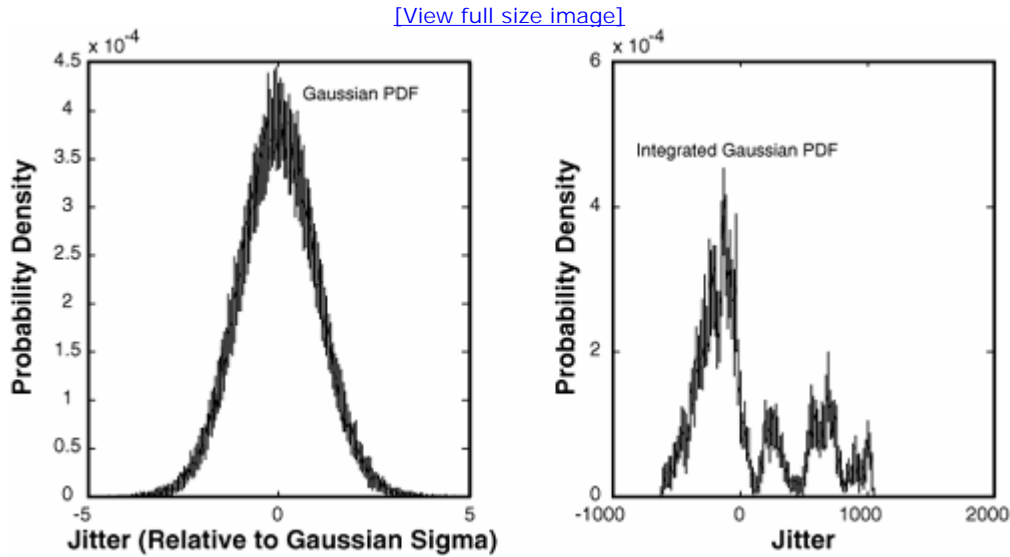
With [equation 3.44](#) as the theoretical guide, we will conduct a Monte Carlo simulation for the PDF for an f^{-2} random jitter process. First, the Gaussian random jitter time series $\Delta t_{GJ}(t_n)$ is generated via a Monte Carlo random-number generator with a Gaussian $\sigma = 1$, while 1 is a relative unit. We use 10^6 jitter samples in the simulation. The integrated Gaussian jitter time series $\Delta t_{IG}(t_n)$ can be obtained through [equation 3.42](#). The results for $\Delta t_{GJ}(t_n)$ and $\Delta t_{IG}(t_n)$ are shown in [Figure 3.21](#).

Figure 3.21. Monte Carlo-generated Gaussian and integrated Gaussian jitter time record. Jitter values are relative to a Gaussian $\sigma = 1$.



[Figure 3.21](#) suggests an unbounded "drunk walk" type of characteristic for the f^{-2} random jitter process. With the time record generated, we can establish the PDFs for both Gaussian and integrated Gaussian jitter processes. [Figure 3.22](#) shows the corresponding PDFs.

Figure 3.22. PDFs for Gaussian and integrated Gaussian derived from the jitter time records in Figure 3.21.



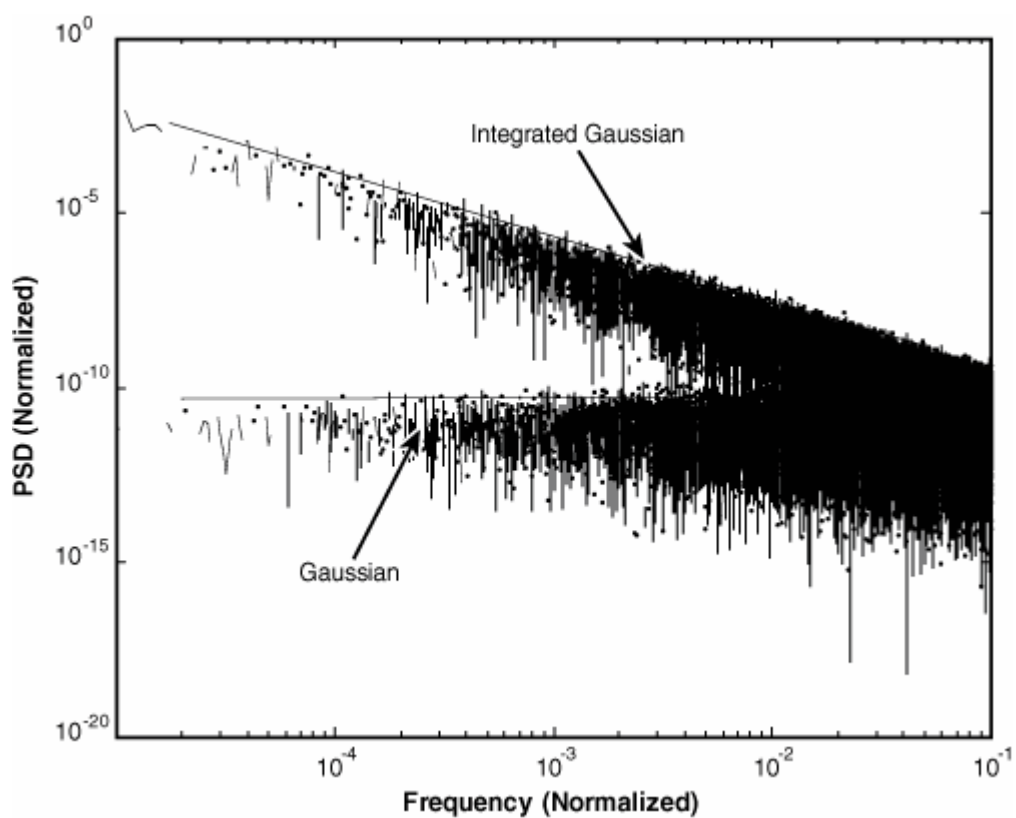
You can see that the PDF for the Gaussian jitter process obtained through random-number generation is indeed a Gaussian, as its name suggests. Further analytical Gaussian form comparison with this 10^6 sample Monte Carlo indicates that the agreement between them is at a 99.7% confidence level (3σ). However, the PDF of the integrated Gaussian PDF is by no means a Gaussian. If the Gaussian is the seed function to generate the integrated Gaussian, the jitter of the integrated Gaussian can be many times larger than the Gaussian itself.

Following the similar argument that the integration of a Gaussian time record yields an integrated Gaussian that has f^{-2} power-law PSD, if we make the integration of the integrated Gaussian time record again, we get another higher-order random-process time record, whose PDF is not a Gaussian for sure and whose PSD has an f^{-4} power-law PSD. Only the Gaussian process or a white PSD gives rise to a Gaussian PDF; other higher-order random processes do not give a Gaussian PDF. This fact has been overlooked in the past by most of the publications on this subject.

3.2.2.2. f^{-a} Jitter PSD

You already know that the PSD for a Gaussian has constant "white" spectrum density. The integrated Gaussian is shown in [equations 3.41](#) through [3.43](#) to have a power-law spectrum f^{-2} shape. To put this in perspective, we will show our Monte Carlo-generated PSDs for Gaussian and integrated Gaussian. The procedure is straightforward. We use the Gaussian jitter time record shown in [Figure 3.21](#) and take the FT to get the corresponding spectrum. Because we use a long record, we use the square of the spectrum to approximate the PSD. The PSD results are shown in [Figure 3.23](#).

Figure 3.23. PSDs for Gaussian and integrated Gaussian derived from the jitter time record in Figure 3.21. Note that the power-law PSD for the integrated Gaussian follows very closely an f^{-2} form—two orders of magnitude per decade.



A detailed analysis of the results shown in Figure 3.23 reveals that the mean or maximum of the PSDs follows approximately a constant and an f^{-2} power law well for Gaussian and integrated Gaussian, respectively.

It can be extrapolated from our integration demonstration that any higher-order random processes are the result of Gaussian white process integrals. However, the integral here is in a broad sense, because to generate an odd power index type of PSD such as f^{-1} , "half" integer integral must be invoked. It is clear that higher-order random processes do not have a Gaussian PDF, as we have shown in the case of f^{-2} type random processes.

URL <http://access.proquest.safaribooksonline.com/9780132429610/ch03lev1sec2>

User name: CSU San Diego

Book: Jitter, Noise, and Signal Integrity at High-Speed

Section: Chapter 3. Source, Mechanism, and Math Model for Jitter and Noise

No part of any chapter or book may be reproduced or transmitted in any form by any means without the prior written permission for reprints and excerpts from the publisher of the book or chapter. Redistribution or other use that violates the fair use privilege under U.S. copyright laws (see 17 USC107) or that otherwise violates these Terms of Service is strictly prohibited. Violators will be prosecuted to the full extent of U.S. Federal and Massachusetts laws.

Information Theory Computer Science Mike Peng Li Prentice Hall Jitter, Noise, and Signal Integrity at High-Speed

3.3. Overall Jitter PDF and PSD

This section discusses the relationship between the overall jitter PDF and component PDFs, as well as the overall PSD and individual component PSDs.

3.3.1. Overall Jitter PDF

We have discussed various jitter components and their related mathematical PDF models. A natural question is how those individual PDFs will relate to the overall total jitter PDFs that are commonly observable in practical measurement and verification exercises.

[Chapter 4](#), "Jitter, Noise, BER (JNB), and Interrelationships," has a detailed mathematical explanation and derivation. We will give just the final results here because it is logical to address this question here in an overview manner. Assuming that all the jitter components are independent, the overall jitter PDF is the convolution of each individual and independent jitter PDF. In the context of the jitter components introduced in this chapter, we have the following:

Equation 3.45

$$f_{TJ} = f_{DDJ} * f_{PJ} * f_{BUJ} * f_{RGJ} * f_{RHJ}$$

Knowing all the component PDFs, the overall total PDF is uniquely determined through convolution operations. Conversely, if one component PDF is unknown and rest of the PDFs are known, the overall total PDF can be uniquely determined through deconvolution. This topic is discussed further in [Chapter 5](#), "Jitter and Noise Separation and Analysis in the Statistical Domain."

3.3.2. Overall Jitter PSD

The overall jitter PSD and its relationship to the individual component PSDs follows the general energy conservation superimposition law. In other words, the sum of the component PSDs equals the overall total PSD, as given by the following equation:

Equation 3.46

$$S_{TJ} = S_{DDJ} + S_{PJ} + S_{BUJ} + S_{RGJ} + S_{RHJ}$$

Knowing all the component PSDs, the overall total PSD is uniquely determined through linear sum operations. Conversely, if one component PSD is unknown and rest of the PSDs are known, the overall total PSD can be uniquely determined through the linear subtraction operation.

URL <http://access.proquest.safaribooksonline.com/9780132429610/ch03lev1sec3>

User name: CSU San Diego

Book: Jitter, Noise, and Signal Integrity at High-Speed

Section: Chapter 3. Source, Mechanism, and Math Model for Jitter and Noise

No part of any chapter or book may be reproduced or transmitted in any form by any means without the prior written permission for reprints and excerpts from the publisher of the book or chapter. Redistribution or other use that violates the fair use privilege under U.S. copyright laws (see 17 USC107) or that otherwise violates these Terms of Service is strictly prohibited. Violators will be prosecuted to the full extent of U.S. Federal and Massachusetts laws.

Information Theory Computer Science Mike Peng Li Prentice Hall Jitter, Noise, and Signal Integrity at High-Speed

3.4. Summary

This chapter has discussed the cause mechanisms and corresponding mathematical models for individual and independent jitter components, in time, frequency, and statistical domains, and in terms of time series record, frequency PSD, and statistical PDF. This chapter then illustrated the relationship between the overall jitter PDF with its component PDFs through convolution. The overall jitter PSD equals the sum of all its component PSDs due to the nature of energy conservation law. Those PDF and PSD models for overall and component jitter are fundamentals and building blocks for jitter and noise analysis and separation. They are used extensively in the following chapters for jitter and noise separation and spectrum analysis.

URL <http://access.proquest.safaribooksonline.com/9780132429610/ch03lev1sec4>

User name: CSU San Diego

Book: Jitter, Noise, and Signal Integrity at High-Speed

Section: Chapter 3. Source, Mechanism, and Math Model for Jitter and Noise

No part of any chapter or book may be reproduced or transmitted in any form by any means without the prior written permission for reprints and excerpts from the publisher of the book or chapter. Redistribution or other use that violates the fair use privilege under U.S. copyright laws (see 17 USC107) or that otherwise violates these Terms of Service is strictly prohibited. Violators will be prosecuted to the full extent of U.S. Federal and Massachusetts laws.

Information Theory Computer Science Mike Peng Li Prentice Hall Jitter, Noise, and Signal Integrity at High-Speed

Endnotes

1. J. Buckwalter, B. Analui, and A. Hajimiri, "Predicting Data-Dependent Jitter," *IEEE Transactions on Circuits and Systems II, Analog Digital Signal Processing*, vol. 51, no. 9, pp. 450–457, 2004.
2. A. Sanders, M. Resso, and J. D'Ambrosia, "Channel Compliance Testing Utilizing Novel Statistical Eye Methodology," IEC, DesignCon, 2004.
3. V. Stojanovic and M. Horowitz, "Modeling and Analysis of High-Speed Links," IEEE, Customer Integrated Circuits Conference (CICC), 2003.
4. International Committee for Information Technology Standardization (INCITS), working draft of "Fibre Channel Methodologies for Jitter Specification-MJSQ," rev. 14.0, 2004.
5. A. Kuo, T. Farahmand, N. Ou, S. Tabatabaei, and A. Ivannov, "Jitter Model and Measurement Methods for High-Speed Interconnectors," IEEE International Test Conference (ITC), 2004.
6. R. Y. Rubinstein, *Simulation and the Monte Carlo Method*, John Wiley & Sons, Inc., 1981.
7. C. P. Robert and G. Casella, *Statistical Monte Carlo Method*, Springer, 2004.

URL <http://access.proquest.safaribooksonline.com/9780132429610/ch03lev1sec5>

User name: CSU San Diego

Book: Jitter, Noise, and Signal Integrity at High-Speed

No part of any chapter or book may be reproduced or transmitted in any form by any means without the prior written permission for reprints and excerpts from the publisher of the book or chapter. Redistribution or other use that violates the fair use privilege under U.S. copyright laws (see 17 USC107) or that otherwise violates these Terms of Service is strictly prohibited. Violators will be prosecuted to the full extent of U.S. Federal and Massachusetts laws.

Information Theory Computer Science Mike Peng Li Prentice Hall Jitter, Noise, and Signal Integrity at High-Speed

4. Jitter, Noise, BER (JNB), and Interrelationships

This chapter first discusses the total jitter PDF and its relationship to the PDFs of its components. Then it presents the similar relationship for the total noise PDF to the PDFs of its components. After that, this chapter discusses the two-dimensional joint PDF and BER CDF when both jitter and noise are considered.

URL <http://access.proquest.safaribooksonline.com/9780132429610/ch04>

User name: CSU San Diego

Book: Jitter, Noise, and Signal Integrity at High-Speed

Section: Chapter 4. Jitter, Noise, BER (JNB), and Interrelationships

No part of any chapter or book may be reproduced or transmitted in any form by any means without the prior written permission for reprints and excerpts from the publisher of the book or chapter. Redistribution or other use that violates the fair use privilege under U.S. copyright laws (see 17 USC107) or that otherwise violates these Terms of Service is strictly prohibited. Violators will be prosecuted to the full extent of U.S. Federal and Massachusetts laws.

Information Theory Computer Science Mike Peng Li Prentice Hall Jitter, Noise, and Signal Integrity at High-Speed

4.1. Eye Diagrams and BER Basics

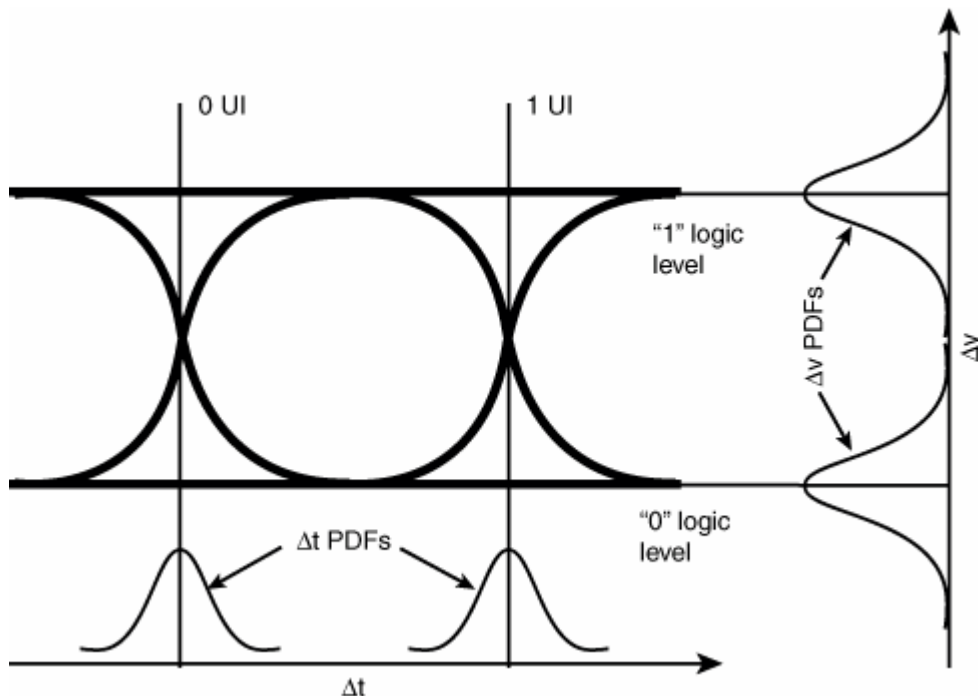
This subsection is a high-level introduction to BER, eye diagrams, and their interrelationships with timing jitter and amplitude noise.

A bit error for a serial data communication system can be caused by one of the following:

- Timing jitter that causes an edge transition to be either earlier or later referenced to an ideal timing location
- Amplitude noise that can cause a voltage high level to be below the reference threshold or a voltage low level to be above the reference threshold

One way to represent the effect of both timing jitter and amplitude noise is the eye diagram, in which many data voltage levels and edge transitions are superimposed over one UI range. An eye diagram gives an overall statistical qualitative view of the quality of the signal under test. [Figure 4.1](#) shows an eye diagram and its associated timing jitter and amplitude noise PDFs in one view.

Figure 4.1. An eye diagram and its associated timing jitter PDFs (horizontal) and amplitude noise PDFs (vertical) in one view.



Quantitative discussions of the interrelationships appear in the following sections.

URL <http://access.proquest.safaribooksonline.com/9780132429610/ch04lev1sec1>

User name: CSU San Diego

Book: Jitter, Noise, and Signal Integrity at High-Speed

Section: Chapter 4. Jitter, Noise, BER (JNB), and Interrelationships

No part of any chapter or book may be reproduced or transmitted in any form by any means without the prior written permission for reprints and excerpts from the publisher of the book or chapter. Redistribution or other use that violates the fair use privilege under U.S. copyright laws (see 17 USC107) or that otherwise violates these Terms of Service is strictly prohibited. Violators will be prosecuted to the full extent of U.S. Federal and Massachusetts laws.

Information Theory Computer Science Mike Peng Li Prentice Hall Jitter, Noise, and Signal Integrity at High-Speed

4.2. Jitter Total PDF and the Relationship to Its Component PDFs

This section discusses the detailed mathematical relationship between total jitter PDF and the PDFs of its components.

4.2.1. Overall Jitter PDF

As you saw in [Figure 1.11](#) in [Chapter 1](#), "Introduction," jitter can be classified as deterministic jitter (DJ) or random jitter (RJ) at the first layer of separation. It is reasonable to assume that DJ and RJ are independent, because they are caused by independent and different sources and mechanisms. Recall the theorem introduced in [Chapter 2](#), "Statistical Signal and Linear Theory for Jitter, Noise, and Signal Integrity." It says that the joint PDF sum of two independent variables is the convolution of their own PDFs (see [section 2.1.2.6](#) of [Chapter 2](#), [equation 2.36](#)). This gives us the following overall jitter PDF given PDFs of DJ and RJ:

Equation 4.1

$$f_{TJ} = f_{DJ} * f_{RJ}$$

Here the state variable is timing jitter Δt , and the PDF is for either the first zero-cross at 0 UI or the second zero-cross at 1 UI, as shown in [Figure 4.1](#). In the second-layer separation, DJ can be separated into components of DDJ, PJ, and BUJ, represented by the following equation:

Equation 4.2

$$f_{DJ} = f_{DDJ} * f_{PJ} * f_{BUJ}$$

Similarly, RJ can be separated into random Gaussian jitter (RGJ) and random higher-order jitter (RHJ), as represented by the following equation:

Equation 4.3

$$f_{RJ} = f_{RGJ} * f_{RHJ}$$

If we represent the overall jitter PDF in terms of its second-layer components, we have this equation:

Equation 4.4

$$f_{TJ} = f_{DJ} * f_{RJ} = f_{DDJ} * f_{PJ} * f_{BUJ} * f_{RGJ} * f_{RHJ}$$

[Equation 4.4](#) is the same as [equation 3.45](#), where we gave the final results without the derivation. [Equation 4.4](#) suggests that the overall jitter PDF equals the convolutions among all its jitter components' PDFs. It provides the math foundation to estimate the overall jitter PDF if all components' PDFs are known. Conversely, if the overall PDF and some of the component PDFs are known, some of the component PDFs can be estimated via the inverse operation of convolution, called deconvolution, which we denote as $*^{-1}$. If the total jitter PDF f_{TJ} is known, and any four of the five components' jitter PDF are also known, the fifth component PDF is uniquely determined via deconvolution. Using [Equation 4.1](#) as an example, if the total jitter and random jitter PDFs are known, the deterministic jitter PDF can be estimated as follows:

Equation 4.5

$$f_{DJ} = f_{TJ} *^{-1} f_{RJ}$$

A similar equation can be derived for the random jitter PDF if both deterministic and random jitter PDFs are known:

Equation 4.6

$$f_{RJ} = f_{TJ} *^{-1} f_{DJ}$$

4.2.2. Convolution for Jitter PDFs

It is helpful to demonstrate how to carry out the convolution for jitter PDFs to get the overall total jitter PDF. To conduct the convolution operation, jitter component PDFs of f_{DJ} and f_{RJ} need to be known for the first-layer separated jitter DJ and RJ.

This subsection assumes that RJ is a Gaussian or white, as defined by [equation 3.33](#), and ignores the higher-order random jitter effects. As discussed in [Chapter 2](#), DJ PDF has no fixed form due to the variety of possibilities of causing mechanisms for the DJ subcomponents. However, as discussed in [Chapter 3](#), "Source, Mechanism, and Math Model for Jitter and Noise," a DCD PDF is best approximated by a dual-Dirac delta model given by [equation 3.7](#). Furthermore, a single-frequency PJ PDF can also be approximated by a dual-Dirac delta model. Considering the fact that those practical DCD and PJ component PDFs are close to a dual-Dirac delta function, as well as for math simplification and illustration purposes, we will assume that the DJ PDF is a dual-Dirac delta function.

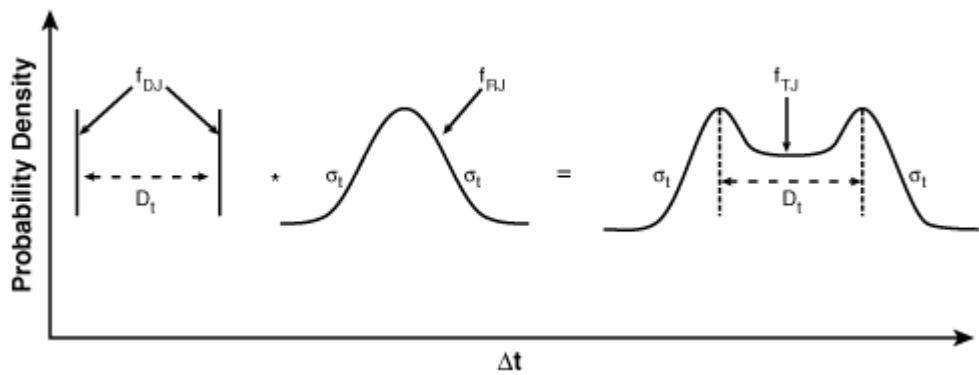
The convolution between a DJ dual-Dirac delta PDF and an RJ Gaussian PDF can be carried out analytically, using the property in which the convolution of an arbitrary function with a Dirac delta function equals the linearly shifted arbitrary function itself.^[1] This yields the following TJ PDF:

Equation 4.7

$$f_n(t) = \frac{1}{2\sqrt{2\pi}\sigma_t} \left[e^{-\frac{(t-\frac{D_t}{2})^2}{2\sigma_t^2}} + e^{-\frac{(t+\frac{D_t}{2})^2}{2\sigma_t^2}} \right]$$

D_t is the DJ PDF peak-to-peak value, and σ_t is the RJ sigma value. Graphically, this convolution operation can be represented as shown in [Figure 4.2](#).

Figure 4.2. TJ PDF determination from its DJ and RJ PDFs via a convolution operation.



Note that the TJ PDF is a bimodal distribution having even "twin peaks." The distance between those twin peaks is the same as the peak-to-peak value of the DJ PDF. In the tail region of the TJ PDF, its shape is the same as RJ Gaussian tails. Clearly, TJ PDF has some traceable characteristics of DJ and RJ PDF in this example. Chapter 5, "Jitter and Noise Separation and Analysis in Statistical Domain," has more information about the "inverse" problem of determining DJ PDF and RJ PDF by knowing TJ PDF.

4.2.3. Jitter PDF in the Context of an Eye Diagram

Figure 4.1 has two jitter PDFs: one for the 0 UI time location, and one for the 1 UI time location. Both correspond to the crossing point voltage. Due to how an eye diagram is constructed, the timing jitter PDF for 0 UI crossing and 1 UI crossing is the same. In this context, the overall jitter PDF is two identical PDFs, as defined by equation 4.7, separated by 1 UI time distance. The overall timing jitter PDF has this form:

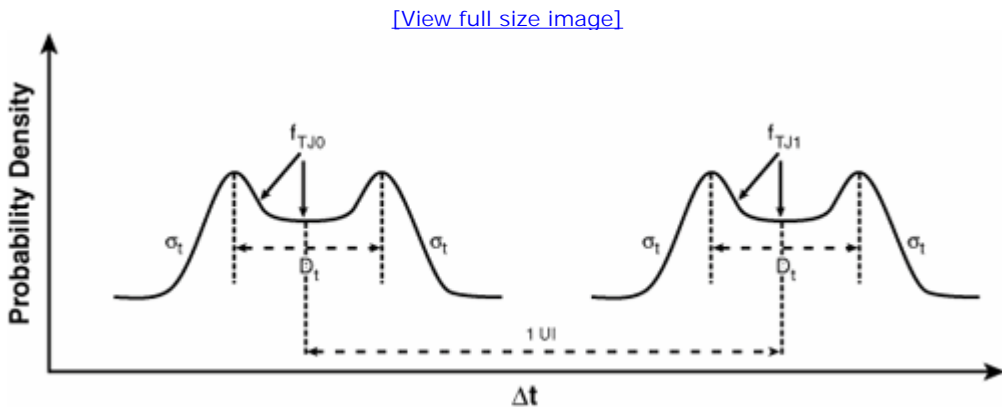
Equation 4.8

[View full size image]

$$f_n(t) = \frac{1}{4\sqrt{2\pi}\sigma_t} \left[e^{-\frac{(t-\frac{D_t}{2})^2}{2\sigma_t^2}} + e^{-\frac{(t+\frac{D_t}{2})^2}{2\sigma_t^2}} \right] \left[e^{-\frac{(t-UI-\frac{D_t}{2})^2}{2\sigma_t^2}} + e^{-\frac{(t-UI+\frac{D_t}{2})^2}{2\sigma_t^2}} \right]$$

Graphically, this TJ PDF in the context of an eye diagram looks like Figure 4.3.

Figure 4.3. TJ PDF that is composed of the identical TJ PDFs at the first 0 crossing and the second 0 crossing.



Clearly, the eye opening critically relies on the shape and characteristics of the TJ PDF and UI value.

URL <http://access.proquest.safaribooksonline.com/9780132429610/ch04lev1sec2>

User name: CSU San Diego

Book: Jitter, Noise, and Signal Integrity at High-Speed

Section: Chapter 4. Jitter, Noise, BER (JNB), and Interrelationships

No part of any chapter or book may be reproduced or transmitted in any form by any means without the prior written permission for reprints and excerpts from the publisher of the book or chapter. Redistribution or other use that violates the fair use privilege under U.S. copyright laws (see 17 USC107) or that otherwise violates these Terms of Service is strictly prohibited. Violators will be prosecuted to the full extent of U.S. Federal and Massachusetts laws.

Information Theory Computer Science Mike Peng Li Prentice Hall Jitter, Noise, and Signal Integrity at High-Speed

4.3. Noise Total PDF and the Relationship to Its Component PDFs

This section focuses on the amplitude noise PDF at a given sampling time t_s with $0 < t_s < 1 \text{ UI}$, as shown in [Figure 4.1](#). The amplitude noise has two PDFs: one for the logic 1 level, and another for the logic 0 level. We will focus first on one of them, and similar math will apply to the other.

4.3.1. Overall Amplitude Noise PDF

The same kind of component classification scheme for timing jitter apply well to amplitude noise analysis, as shown in [Figure 1.12](#) in [Chapter 1](#). The first-layer separation has deterministic noise (DN), and random noise (RN), of the total noise (TN). Like [equation 4.1](#), the total amplitude noise PDF is as follows:

Equation 4.9

$$f_{TN} = f_{DN} * f_{RN}$$

Here the state variable is amplitude noise Δv , the PDF is for either the logic 1 or high level or the logic 0 or low level. At the second-layer separation, DN can be separated into components of DDN, PN, and BUN, represented by the following equation:

Equation 4.10

$$f_{DN} = f_{DDN} * f_{PN} * f_{BUN}$$

Similarly, RN can be separated into random Gaussian noise (RGN) and random higher-order noise (RHN), as represented by the following equation:

Equation 4.11

$$f_{RN} = f_{RGN} * f_{RHN}$$

If we represent the overall noise PDF in terms of its second-layer components, we have this equation:

Equation 4.12

$$f_{TN} = f_{DN} * f_{RN} = f_{DDN} * f_{PN} * f_{BUN} * f_{RGN} * f_{RHN}$$

Equation 4.12 is similar to its counterpart, equation 4.4, for timing jitter. Component PDFs can be estimated if two of the three variables in the equation are known. If the total and random noise PDFs are known, the deterministic noise PDF can be estimated as follows:

Equation 4.13

$$f_{DN} = f_{TN} *^{-1} f_{RN}$$

A similar equation can be derived for the random noise PDF if both deterministic and random noise PDFs are known. We denote such an operation as follows:

Equation 4.14

$$f_{RN} = f_{TN} *^{-1} f_{DN}$$

4.3.2. Convolution for Noise PDFs

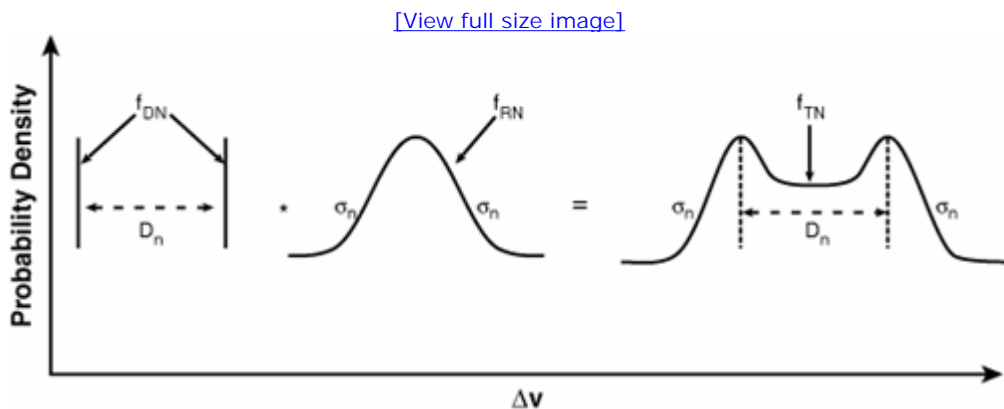
If we assume that the DN PDF is a dual-Dirac delta, and that RN is a Gaussian, the total noise PDF is the convolution between those DN and RN PDFs, yielding the following TN PDF:

Equation 4.15

$$f_n(v) = \frac{1}{2\sqrt{2\pi}\sigma_n} \left[e^{-\frac{(v-\frac{D_n}{2})^2}{2\sigma_n^2}} + e^{-\frac{(v+\frac{D_n}{2})^2}{2\sigma_n^2}} \right]$$

D_n is the DN PDF peak-to-peak value, and σ_n is the RN sigma value. The shape of the PDF defined by this equation is similar to that defined by equation 4.4 for the timing jitter, as shown in Figure 4.4.

Figure 4.4. TN PDF determination from its DN and RN PDFs via a convolution operation.



This TN PDF has characteristics similar to those of a TJ PDF, as we have discussed.

4.3.3. Noise PDF in the Context of an Eye Diagram

In the context of the eye diagram shown in [Figure 4.1](#), amplitude noise PDFs do not necessarily have the symmetry property for its logical 1 level and logical 0 level, unlike the PDFs for the timing jitter. This is especially true for fiber-optic communication, where the logical level is proportional to the optical power, resulting in a different noise level and distribution for logical high and low. Due to this broken symmetry, we have to introduce two different jitter PDFs for logical 1 and logical 0.

We will assume that DN PDF is a dual-Dirac delta function and that RN PDF is a Gaussian. Then, for the logical 1 level, the total noise amplitude PDF is as follows:

Equation 4.16

$$f_{n1}(v) = \frac{1}{2\sqrt{2\pi}\sigma_{n1}} \left[e^{-\frac{(v-\frac{D_{n1}}{2})^2}{2\sigma_{n1}^2}} + e^{-\frac{(v+\frac{D_{n1}}{2})^2}{2\sigma_{n1}^2}} \right]$$

D_{n1} is the DN PDF peak-to-peak, and σ_{n1} is the RN sigma value, for the logical 1.

Similarly, the noise PDF for the logical 0 may take the following form:

Equation 4.17

[\[View full size image\]](#)

$$f_{n0}(v) = \frac{1}{2\sqrt{2\pi}\sigma_{n0}} \left[e^{-\frac{(v-\frac{D_{n0}}{2})^2}{2\sigma_{n0}^2}} + e^{-\frac{(v+\frac{D_{n0}}{2})^2}{2\sigma_{n0}^2}} \right]$$

D_{n0} is the DN PDF peak-to-peak, and σ_{n0} is the RN sigma value, for the logical 0.

The overall noise PDF considering both logical 1 and 0 is as follows:

Equation 4.18

[\[View full size image\]](#)

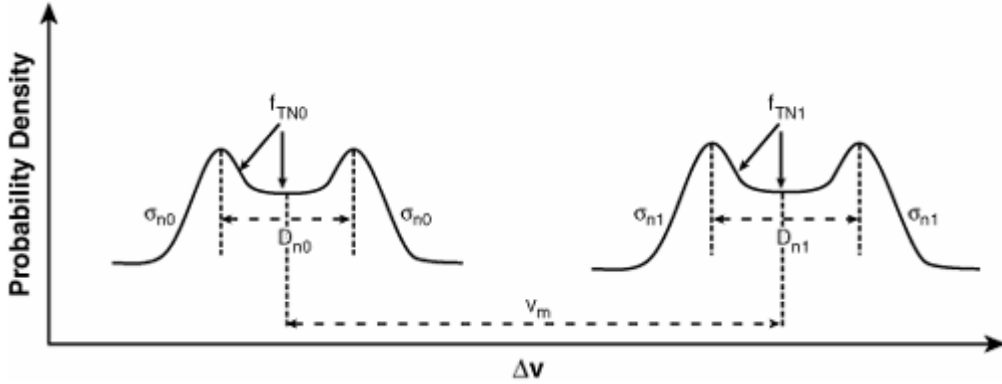
$$f_{\infty}(v) = \frac{1}{4\sqrt{2\pi}\sigma_{n1}} \left[e^{-\frac{(v-V_M-\frac{D_{n1}}{2})^2}{2\sigma_{n1}^2}} + e^{-\frac{(v-V_M+\frac{D_{n1}}{2})^2}{2\sigma_{n1}^2}} \right] + \frac{1}{4\sqrt{2\pi}\sigma_{n0}} \left[e^{-\frac{(v-\frac{D_{n0}}{2})^2}{2\sigma_{n0}^2}} + e^{-\frac{(v+\frac{D_{n0}}{2})^2}{2\sigma_{n0}^2}} \right]$$

V_M is the mean voltage difference between logical 1 and logical 0.

Graphically, this TN PDF in the context of an eye diagram looks like [Figure 4.5](#).

Figure 4.5. TN PDF that is composed of the two PDFs for logical 0 and logical 1.

[[View full size image](#)]



Clearly, the voltage eye opening critically relies on the shape and characteristics of the TN PDF and V_M value. Moreover, too much σ_{n1} and σ_{n0} can cause not only the voltage inner eye closure, but also a too-large outer eye, a manifestation of overdriving a device.

URL <http://access.proquest.safaribooksonline.com/9780132429610/ch04lev1sec3>

User name: CSU San Diego

Book: Jitter, Noise, and Signal Integrity at High-Speed

Section: Chapter 4. Jitter, Noise, BER (JNB), and Interrelationships

No part of any chapter or book may be reproduced or transmitted in any form by any means without the prior written permission for reprints and excerpts from the publisher of the book or chapter. Redistribution or other use that violates the fair use privilege under U.S. copyright laws (see 17 USC107) or that otherwise violates these Terms of Service is strictly prohibited. Violators will be prosecuted to the full extent of U.S. Federal and Massachusetts laws.

Information Theory Computer Science Mike Peng Li Prentice Hall Jitter, Noise, and Signal Integrity at High-Speed

4.4. The Joint PDF of Timing Jitter and Amplitude Noise

Sections 4.2 and 4.3 discussed timing jitter PDF and amplitude PDF separately, ignoring the potential correlation between timing jitter and amplitude noise PDFs. This section extends the discussion to cover the general case in which timing jitter and amplitude noise can be correlated.

4.4.1. Generic Two-Dimensional PDF

For serial data communication, a BER can be caused by either timing jitter or amplitude noise or both. So the timing jitter PDF at a given amplitude or voltage threshold, or the amplitude PDF at a given sampling time, is only part of the math description of the entire statistical problem. A complete description of the PDF for the BER is two-dimensional or two-variable problem and must be described with multiple variable statistical PDF. Furthermore, timing jitter and amplitude noise are not independent in general, particularly in the edge transition regions. We will describe the PDF for both timing jitter Δt and amplitude noise Δv as $f(\Delta v, \Delta t)$. One way to estimate $f(\Delta v, \Delta t)$ is through its conditional PDF and independent PDF relationship of the following:

Equation 4.19

$$f(\Delta v, \Delta t) = f_{\Delta v | \Delta t}(\Delta v | \Delta t) f_{\Delta t}(\Delta t) = f_{\Delta t | \Delta v}(\Delta t | \Delta v) f_{\Delta v}(\Delta v)$$

Equation 4.19 converts a two-dimensional PDF into a product of one conditional and one independent PDF. In the case where the jitter mechanism is due to the amplitude modulation via the edge rate, and if the slew rate of voltage with time is known, the joint PDF can be estimated with equation 4.19.

4.4.2. Two-Dimensional (2-D) Gaussian Distribution

One of the commonly encountered problems in practice is that when both timing jitter and amplitude noise are all random Gaussian, yet they are correlated, what is the joint distribution? It turns out that such a joint distribution, also called bivariate Gaussian distribution, is given by the following equation:[2]

Equation 4.20

[View full size image]

$$f_{GG}(\Delta v, \Delta t) = \frac{1}{2\pi\sigma_t\sigma_n\sqrt{1-\rho^2}} e^{-\frac{-1}{2(1-\rho^2)} \frac{(\Delta t - \mu_t)^2}{\sigma_t^2} - 2\rho \frac{(\Delta t - \mu_t)(\Delta v - \mu_n)}{\sigma_t\sigma_n} + \frac{(\Delta v - \mu_n)^2}{\sigma_n^2}}$$

μ_t and σ_t are mean and standard deviation for the timing jitter, μ_n and σ_n are mean and standard deviation for the amplitude noise, and ρ is the correlation coefficient between timing jitter and amplitude noise. As mentioned in Chapter 2, when $\rho = \pm 1$, timing jitter and

amplitude noise are linearly correlated. When $\rho=0$, they are not correlated and thus are independent.

The application of the 2-D Gaussian distribution of [equation 4.20](#) toward the problem of binary digital serial communication, particularly in the context of the so-called "eye" PDF contour, is not straightforward. The complication occurs because mean and standard deviation are unlikely to be constant, especially during the edge transitions.

URL <http://access.proquest.safaribooksonline.com/9780132429610/ch04lev1sec4>

User name: CSU San Diego

Book: Jitter, Noise, and Signal Integrity at High-Speed

Section: Chapter 4. Jitter, Noise, BER (JNB), and Interrelationships

No part of any chapter or book may be reproduced or transmitted in any form by any means without the prior written permission for reprints and excerpts from the publisher of the book or chapter. Redistribution or other use that violates the fair use privilege under U.S. copyright laws (see 17 USC107) or that otherwise violates these Terms of Service is strictly prohibited. Violators will be prosecuted to the full extent of U.S. Federal and Massachusetts laws.

Information Theory Computer Science Mike Peng Li Prentice Hall Jitter, Noise, and Signal Integrity at High-Speed

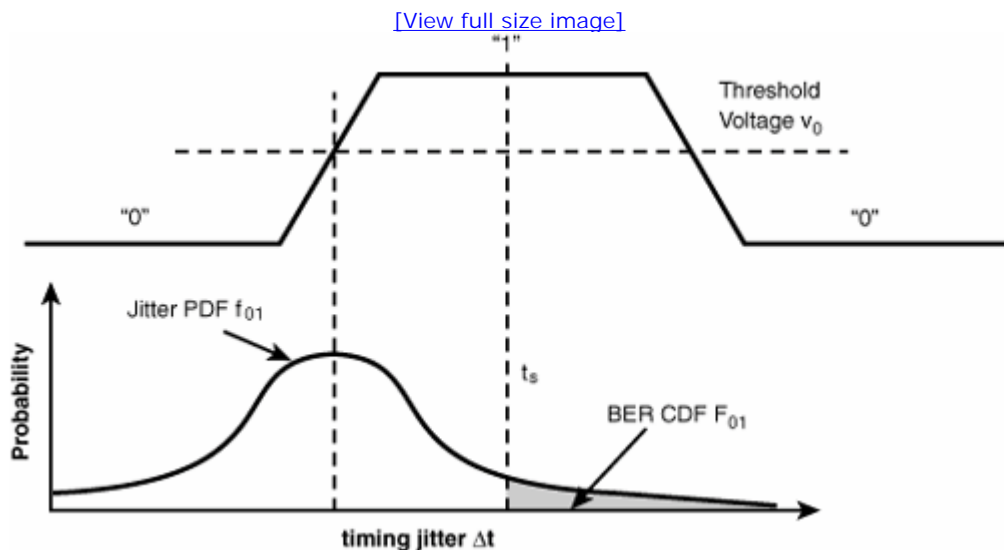
4.5. BER and Jitter/Noise Relationship

The mechanisms for either timing jitter or amplitude noise to cause a bit error rate are very similar, but not exactly the same. A bit error occurs when the relative timing relationship between the jitter value and the sampling time is out of the expected range. A similar conclusion is true for amplitude noise and bit error relationship when the relative levels between the amplitude noise and sampling voltage are out of the expected range. However, there is a difference. Timing jitter may cause a bit error only when there is an edge transition, while amplitude noise may cause a bit error at any time. In other words, amplitude noise is a constant function. We will first consider the timing jitter PDF and BER CDF relationship, and then the amplitude noise BER CDF relationship. After those two steps, we will discuss the BER CDF under the influence of both timing jitter and amplitude noise.

4.5.1. Timing Jitter and BER

The timing jitter PDF and BER CDF relationship can be easily illustrated by [Figure 4.6](#), a binary digital transmission system. It shows the logical 1 bit surrendered by 2 0 bits with 0-to-1 and 1-to-0 transitions. We will first study the BER CDF due to the 0-to-1 edge transition. As shown in the figure, the cause-and-consequence relationship for jitter and BER is closely related to the sampling timing location t_s . For the 0-to-1 transition jitter PDF, any edge transitions occurring on the right side of the sampling time t_s cause a bit error. The BER CDF function is all the edge transitions with their jitter values larger than sampling time t_s . Graphically, the BER CDF is the area with jitter larger than the sampling time t_s under the jitter PDF curve, as shown by the shaded area in the figure. Mathematically, this corresponds to the integration of 0-to-1 transition PDF from t_s to ∞ .

Figure 4.6. An illustrative relationship between digital 0 and 1 bits, jitter PDF, and BER CDF as a function of sampling time t_s .



The timing jitter PDF at a given voltage v_0 is denoted as $f_{01}(\Delta t)$. The probability or the transition density for 0-to-1 transition is P_{01} . The BER CDF due to the 0-to-1 edge transition jitter PDF is as follows:

Equation 4.21

$$F_{01}(t_s) = P_{01} \int_{t_s}^{\infty} f_{01}(\Delta t) d\Delta t$$

Clearly, this 0-to-1 edge transition corresponding to BER CDF is a nondecreasing function as the sampling time t_s moves toward the voltage-crossing time locations from the center of the bit UI.

By analogy, the BER CDF due to the logical 1-to-0 edge transition jitter PDF can be readily estimated. In this case, all the edge transitions happening earlier than the sampling time t_s cause a bit error, and the BER CDF is the integral of all these edge transitions. If we denote the PDF at a given voltage v_0 as $f_{10}(\Delta t)$ in this case, and the probability for 1-to-0 edge transition as P_{10} , BER CDF due to the 1-to-0 edge transition jitter PDF is as follows:

Equation 4.22

$$F_{10}(t_s) = P_{10} \int_{-\infty}^{t_s} f_{10}(\Delta t) d\Delta t$$

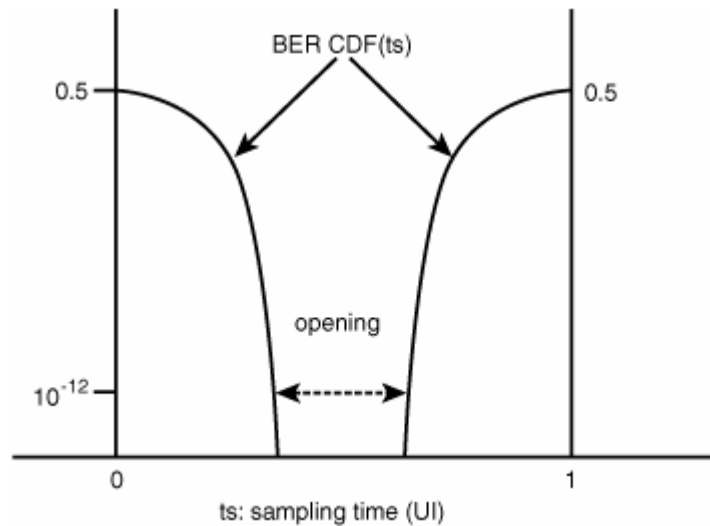
The overall BER CDF is made up of contributions from both 0-to-1 and 1-to-0 edge transitions. This is the summation of [equations 4.21](#) and [4.22](#), as given by the following equation:

Equation 4.23

$$F_{v0}(t_s) = P_{01} \int_{t_s}^{\infty} f_{01}(\Delta t) d\Delta t + P_{10} \int_{-\infty}^{t_s} f_{10}(\Delta t) d\Delta t$$

Because BER CDF is a nondecreasing function with sampling time t_s , its shape generally looks like [Figure 4.7](#).

Figure 4.7. Jitter-induced BER CDF as a function of sampling time.



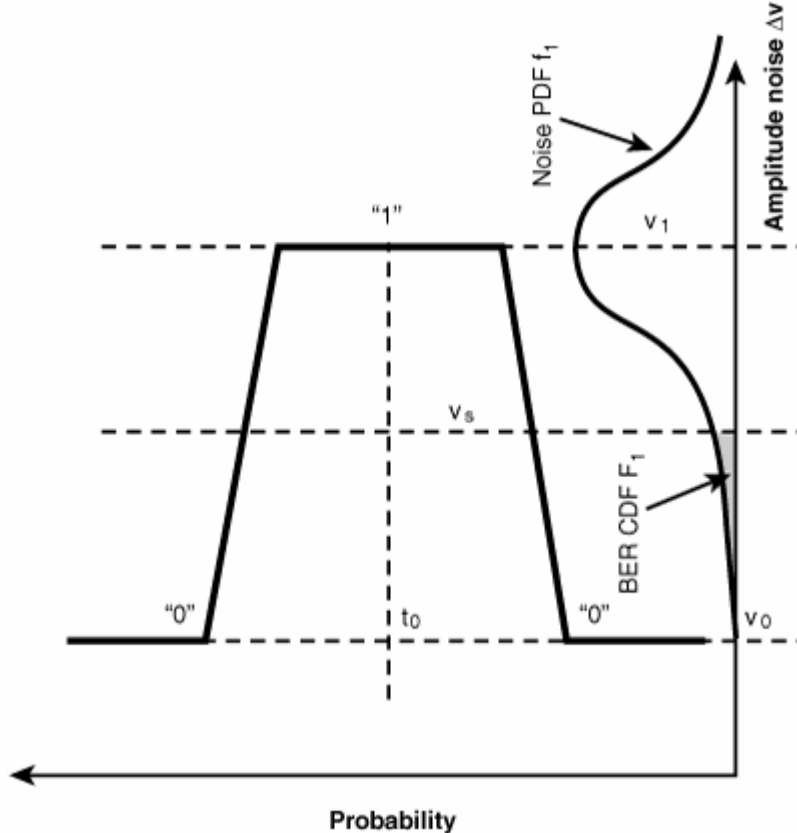
Because the shape of the BER CDF resembles a bathtub, it is sometimes called a BER bathtub curve.

4.5.2. Amplitude Noise and BER

Like timing jitter, the amplitude noise and BER relationship can be illustrated by Figure 4.8. It is similar to Figure 4.7, except that now we are dealing with the amplitude noise PDF. As shown in Figure 4.7, the cause and consequence relationship for amplitude noise and BER is closely related to the sampling voltage level v_s . For the logic 1 noise PDF, any logic 1 level occurring below the sampling logic level v_s causes a bit 1 to be detected as a bit 0, resulting in a bit error. The BER CDF due to the amplitude noise at a given sampling time threshold are all the logic 1 levels with their noise values being below sampling voltage v_s . Graphically, the BER CDF is the area with amplitude noise smaller than sampling voltage v_s under the amplitude noise PDF curve, as shown by the shaded area.

Mathematically, this corresponds to the integration of PDF from $-\infty$ to v_s .

Figure 4.8. The relationship between digital 0 and 1 bits, logic 1 amplitude noise PDF, and BER CDF as a function of sampling amplitude v_s .



The logic 1 amplitude noise PDF at a given time t_0 is denoted as $f_1(\Delta v)$. The probability for 1 bit transitions is P_1 . The BER CDF due to logic 1 level amplitude noise PDF is as follows:

Equation 4.24

$$F_1(v_s) = P_1 \int_{-\infty}^{v_s} f_1(\Delta v) d\Delta v$$

Amplitude noise PDF induced BER CDF is a nondecreasing function as the sampling voltage v_s moves toward the logic 1 or logic 0 mean values at a sampling time t_0 at the center of the bit data cell and along the amplitude or vertical axis.

By analogy, the BER CDF due to the logic 0 associated noise PDF can be estimated. In this case, all the 0 bits happening at levels above the sampling amplitude v_s cause a bit 0 to be identified as bit 1, causing a bit error, and the BER CDF is the integral of all these bits. If we denote the logic 0 associated noise PDF at a given time t_0 as $f_0(\Delta v)$ in this case, and the probability for a 0 bit is P_0 , the corresponding BER CDF is as follows:

Equation 4.25

$$F_0(v_s) = P_0 \int_{v_s}^{\infty} f_0(\Delta v) d\Delta v$$

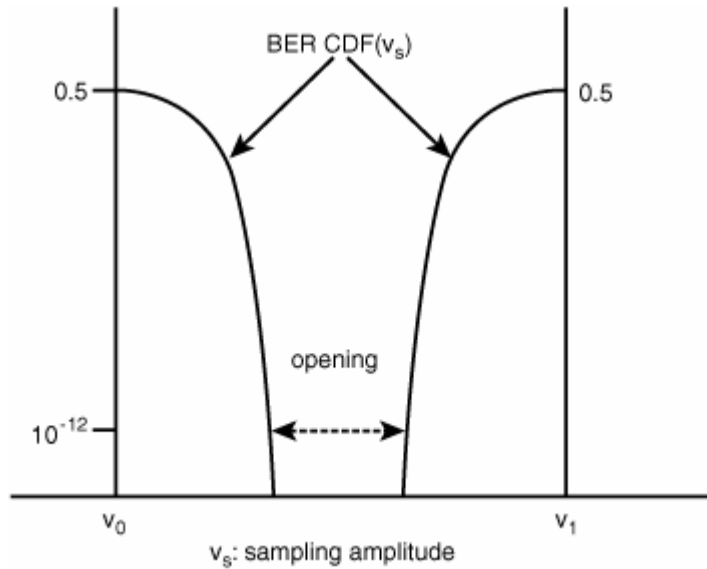
The overall BER CDF is made up of contributions of noise associated with both 0 and 1 bits. This is the summation of [equations 4.24](#) and [4.25](#), as given by the following equation:

Equation 4.26

$$F_{t0}(v_s) = P_0 \int_{v_s}^{\infty} f_0(\Delta v) d\Delta v + P_1 \int_{-\infty}^{v_s} f_1(\Delta v) d\Delta v$$

Just like timing jitter-induced BER CDF, amplitude noise-induced BER CDF is a nondecreasing function versus sampling voltage v_s . Its shape generally looks like [Figure 4.9](#).

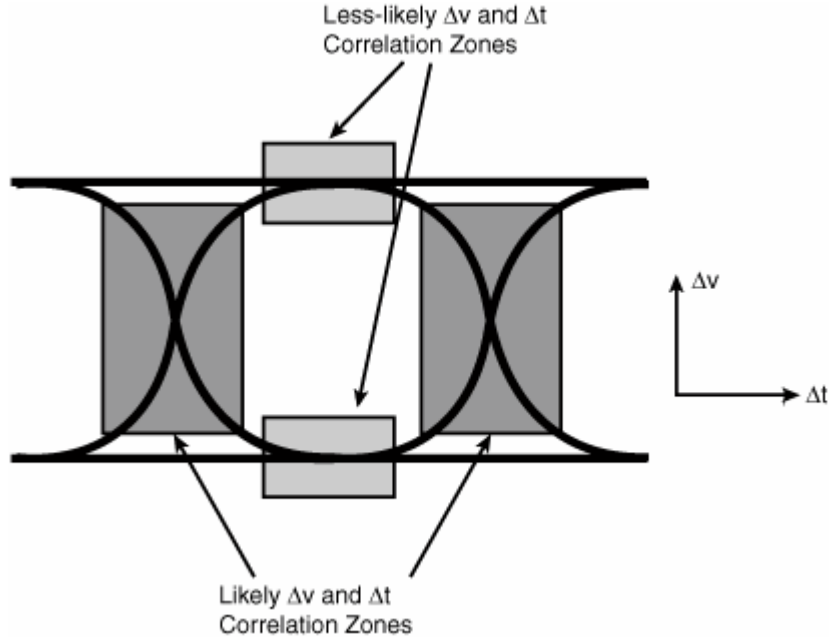
Figure 4.9. Jitter-induced BER CDF as a function of sampling amplitude.



4.5.3. BER Due to Both Jitter and Noise

In a practical communication system, BER can be caused by both timing jitter and amplitude noise, not just either one. Thus, to get an accurate and complete estimation of BER CDF, both timing jitter and amplitude noise need to be considered in a consistent and coherent manner. In other words, a complete BER CDF is, at least, a two-variable function. Furthermore, those two variables may not be independent, particularly within the time-amplitude zone of edge transitions. During the edge transition time window, amplitude noise and the timing jitter can be related, depending on the exact correlation. For example, a random amplitude noise can cause a random timing jitter through a "slew rate" perturbation effect during the edge transition period, as mentioned in [Chapter 1](#). In contrast, timing jitter in the clock causes only timing jitter of the data in a sequential logical system (a flip-flop); it does not cause amplitude noise for logical 1 or 0 amplitude levels at its bit center. At the bit center region, where edge transitions either have already settled down or have not yet started, and the amplitude noise is the dominant cause of the BER, the correlation between amplitude noise and jitter is weak or close to zero. [Figure 4.10](#) shows those different types of correlations at different zones of an eye diagram.

Figure 4.10. Graphical and qualitative showing for the timing jitter and amplitude noise correlation.



If we define a joint PDF for both amplitude noise Δv and timing jitter Δt as $f(\Delta t, \Delta v)$, Δv and Δt are related in general, while no correlation can be found in certain cases, as shown in [Figure 4.10](#). Combining [equations 4.23](#) and [4.26](#) and replacing the single variable timing jitter PDF and amplitude noise PDF with their joint two-variable PDF, the BER CDF as a function of sampling time t_s and voltage v_s is given by the following:

Equation 4.27

$$F_{BER}(t_s, v_s) = P_{01} \int_{t_s}^{\infty} f(\Delta t, \Delta v) \Big|_{v=v_s} d\Delta v + P_{10} \int_{-\infty}^{t_s} f(\Delta t, \Delta v) \Big|_{v=v_s} d\Delta v + \\ P_1 \int_{v_s}^{\infty} f(\Delta t, \Delta v) \Big|_{t=t_s} d\Delta t + P_0 \int_{-\infty}^{v_s} f(\Delta t, \Delta v) \Big|_{t=t_s} d\Delta t$$

Note that the 2-D BER function can, in fact, have more than two dimensions. For example, BER CDF is also pattern- or coding scheme-dependent. It closely depends on parameters such as transition density and probabilities of 1 and 0 bits of the pattern. To illustrate this fact, [Table 4.1](#) shows those parameters for some commonly used testing patterns for data communication.

Table 4.1. Examples of Testing Patterns and Corresponding Probabilities

Pattern	P ₀	P ₁	P ₀₁	P ₁₀
K25.5	50%	50%	26.3%	21.1%
K28.7	50%	50%	10.0%	5.0%
PRBS 2 ⁷ – 1	50%	50%	24.4%	25.2%
Extreme run-length pattern	90%	10%	10.0%	5.0%

[Table 4.1](#) demonstrates several key points:

- P₀₁ and P₁₀ can be different.
- P₀₁ and P₁₀ generally are smaller than 25%.
- P₀ and P₁ are not necessarily 50%.

This example reveals details of some of the pattern-related shortfalls with the traditional method that assumes a 50% transition density and 50% 1 or 0 bit occurrence probability.

[Equation 4.27](#) overcomes shortfalls in most of the BER analysis methods. It provides the most accurate method of determining BER when both timing jitter and amplitude noise present in a communication system.

To illustrate BER CDF in 2-D BER contour and three-dimensional (3-D) BER view, we assume that Δt and Δv are independent. [Figure 4.11](#) shows the eye contour with corresponding BER levels. The zone with a smaller BER contour level represents the optimal sampling zone for a receiver. Also, BER contour gives a quick view and estimation of the total jitter and total noise margin at a given BER level, such as 10⁻¹².

Figure 4.11. A two-dimensional contour diagram showing various BER "zones."

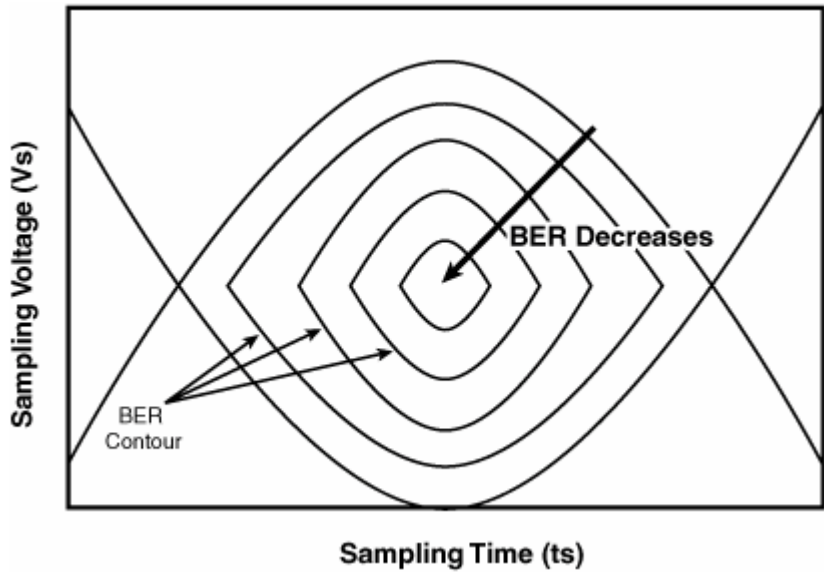
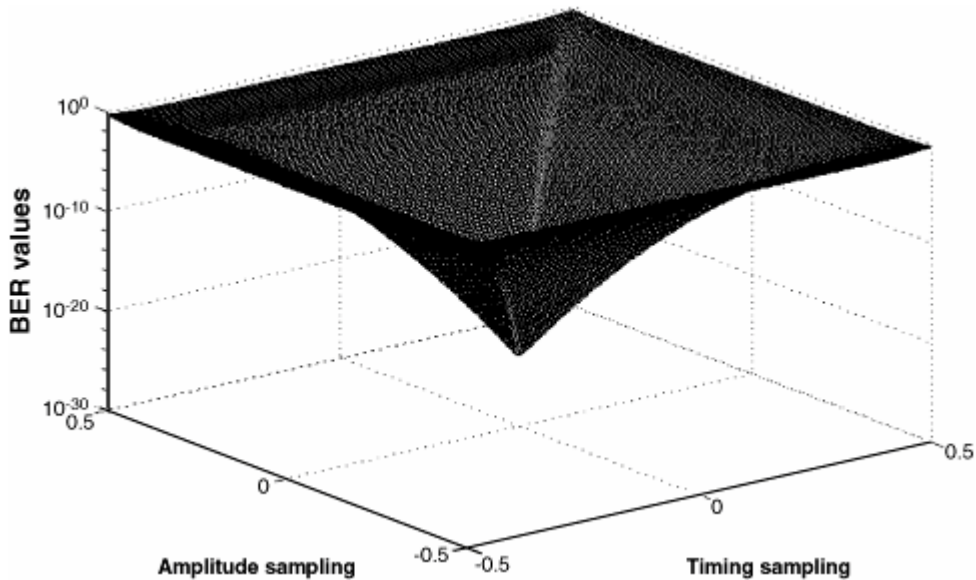


Figure 4.12 shows a 3-D BER function or "bathtub curve" surface plot. It contains significantly more information than the traditional "sliced" view of a timing jitter bathtub curve. Total timing jitter for a given voltage and BER level can be determined. Similarly, total amplitude noise for a given time and BER level can also be determined.

Figure 4.12. A three-dimensional surface plot of BER as a function of sampling timing and amplitude.



We have demonstrated the more-than-two-dimensional PDF function $f(\Delta t, \Delta v)$ and BER function $F_{BER}(t_s, v_s)$ in their higher-level variable dimensions of timing jitter/sampling time, amplitude noise/sampling amplitude, time, and implicit pattern characteristics. However, the n -dimensional nature of PDF and BER (or cumulative PDF) can also be looked at from other low-level dimensions:

- PDF/BER for a particular transition or transitions for a pattern, or a PDF/BER CDF for a pattern without a particular transition or transitions
- Data rate of the transmitting/receiving signals
- Transition density or maximum run length of the testing pattern
- Baseline wander, environmental variation/drifting

- Timing jitter/amplitude noise components of duty cycle distortion (DCD), intersymbol interference (ISI), data-dependent component, periodic component, deterministic component, thermal component, $1/f^n$ component, shot noise component, random component
- Reflection, crosstalk, ringing, ground bouncing, unwanted modulation, interference
- Chromatic dispersion (CD), polarization mode dispersion (PMD); wavelength shifting/broadening; nonlinear scatterings, four-wave mixing, chirp, crosstalk for fiber-optic communication

These extended examples suggest that PDF and BER functions are truly n -dimensional.^[3]

Multidimensional PDF and BER CDF is an increasingly important topic due to increasing data rates and associated eye diagram degradation. Much has been published on the detailed math treatment of this topic. For example, ^[4] present some high-level and rather abstract math on multidimensional eye diagram and BER CDF estimation, from the perspectives of link signaling modeling, with assumption for a link architecture, transmitter, medium, and receiver.

URL <http://access.proquest.safaribooksonline.com/9780132429610/ch04lev1sec5>

User name: CSU San Diego

Book: Jitter, Noise, and Signal Integrity at High-Speed

Section: Chapter 4. Jitter, Noise, BER (JNB), and Interrelationships

No part of any chapter or book may be reproduced or transmitted in any form by any means without the prior written permission for reprints and excerpts from the publisher of the book or chapter. Redistribution or other use that violates the fair use privilege under U.S. copyright laws (see 17 USC107) or that otherwise violates these Terms of Service is strictly prohibited. Violators will be prosecuted to the full extent of U.S. Federal and Massachusetts laws.

Information Theory Computer Science Mike Peng Li Prentice Hall Jitter, Noise, and Signal Integrity at High-Speed

4.6. Summary

This chapter started with a high-level introduction to the relationships between eye diagrams, BER, jitter, and noise. It then moved to timing jitter PDF and its relationship to the component jitter PDF such as DJ, and RJ at the first-layer separation, and DDJ, PJ, and BUJ at the second-layer separation for DJ, as well as Gaussian and higher-order Gaussian for random jitter. The key is using convolution to get the total jitter PDF from the component PDFs and deconvolution to get a PDF from the total PDF and some component PDF. This chapter extended a similar handling for amplitude noise total PDF to PDFs of its components. After that, this chapter introduced the joint PDF in multiple dimensions, including state variables of timing jitter and amplitude noise, as well as how to estimate the joint PDF from jitter and noise PDFs. It then moved on to the BER CDF due to timing jitter and its relationship with jitter PDF, followed by BER CDF due to amplitude noise and its relationship with noise PDF. Last, this chapter introduced BER CDF in multiple dimensions from its corresponding jitter and noise PDFs and their correlation. These fundamentals for PDF and BER CDF due to timing jitter and amplitude noise will be used extensively in the forthcoming chapters.

URL <http://access.proquest.safaribooksonline.com/9780132429610/ch04lev1sec6>

User name: CSU San Diego

Book: Jitter, Noise, and Signal Integrity at High-Speed

Section: Chapter 4. Jitter, Noise, BER (JNB), and Interrelationships

No part of any chapter or book may be reproduced or transmitted in any form by any means without the prior written permission for reprints and excerpts from the publisher of the book or chapter. Redistribution or other use that violates the fair use privilege under U.S. copyright laws (see 17 USC107) or that otherwise violates these Terms of Service is strictly prohibited. Violators will be prosecuted to the full extent of U.S. Federal and Massachusetts laws.

Information Theory Computer Science Mike Peng Li Prentice Hall Jitter, Noise, and Signal Integrity at High-Speed

Endnotes

1. A. V. Oppenheim, A. S. Willsky, and S. H. Nawab, *Signals & Systems*, Prentice Hall, 1996.
2. S. Kotz, N. Balakrishnan, and N. L. Johnson, "Continuous Multivariate Distributions," vol. 1, *Models and Applications*, John Wiley & Sons, Inc., 2000.
3. M. Li, J. Wilstrup, and J. Hamre, "N-dimensional determination of Bit-error rates," a pending U.S. patent application, filed in January 2004.
4. A. Sanders, M. Resso, and J. D'Ambrosia, "Channel Compliance Testing Utilizing Novel Statistical Eye Methodology," IEC, DesignCon, 2004.

URL <http://access.proquest.safaribooksonline.com/9780132429610/ch04lev1sec7>

User name: CSU San Diego

Book: Jitter, Noise, and Signal Integrity at High-Speed

No part of any chapter or book may be reproduced or transmitted in any form by any means without the prior written permission for reprints and excerpts from the publisher of the book or chapter. Redistribution or other use that violates the fair use privilege under U.S. copyright laws (see 17 USC107) or that otherwise violates these Terms of Service is strictly prohibited. Violators will be prosecuted to the full extent of U.S. Federal and Massachusetts laws.

Information Theory Computer Science Mike Peng Li Prentice Hall Jitter, Noise, and Signal Integrity at High-Speed

5. Jitter and Noise Separation and Analysis in the Statistical Domain

This chapter focuses on jitter separation methods in the statistical domain. First we discuss why jitter separation is necessary, as far as its value and benefits, in terms of understanding and practical application. Then we discuss jitter separation methods given jitter process observables of PDF and CDF. The well-known and widely used Tailfit method^[1] is covered in detail. Last, we discuss the dual-Dirac model DJ PDF and its accuracy.

URL <http://access.proquest.safaribooksonline.com/9780132429610/ch05>

User name: CSU San Diego

Book: Jitter, Noise, and Signal Integrity at High-Speed

Section: Chapter 5. Jitter and Noise Separation and Analysis in the Statistical Domain

No part of any chapter or book may be reproduced or transmitted in any form by any means without the prior written permission for reprints and excerpts from the publisher of the book or chapter. Redistribution or other use that violates the fair use privilege under U.S. copyright laws (see 17 USC107) or that otherwise violates these Terms of Service is strictly prohibited. Violators will be prosecuted to the full extent of U.S. Federal and Massachusetts laws.

Information Theory Computer Science Mike Peng Li Prentice Hall Jitter, Noise, and Signal Integrity at High-Speed

5.1. Rationale and Motivation for Jitter Separation

This section discusses the motivations and reasons for separating jitter into its various components. First we discuss the need for jitter separation, from the points of view of understanding, practical analysis, and testing. Then we discuss the needs from the diagnostic, characterization, and debug points of view.

5.1.1. Direct Observables for Practical Jitter Analysis and Test

Chapters 3 and 4 discussed jitter component models for DDJ, PJ, multiple PJs, and RJ. However, in real-world applications, what is encountered, in general, is the jitter process containing all the components. This is particularly true in the testing and measurement field. To understand the root causes of jitter, separating and identifying each jitter component is essential.

In time-domain measurements, jitter can be measured for a specific edge transition or over a time span of many edge transitions. In each case, many jitter samples can be collected for each edge transition so that statistical information can be gathered and analyzed. When the statistics of the jitter samples are collected for a single edge transition or a span of multiple edge transitions, the direct observables of PDF or histogram of the jitter can be obtained. However, the frequency implications for a single edge jitter PDF and the PDF for a span of multiple edges are different. When the statistical samples for a span of edge transitions are achieved, observables of jitter spectrum or PSD in the frequency domain are readily available. As a third example, observables of BER function or jitter CDF are measured, but it is difficult to get the jitter spectrum information from the jitter CDF, because it is the integral of PDF and is in a high-entropy state.

Those raw or direct jitter observables of PDF, CDF, or spectrum reveal some information, such as the overall peak-to-peak (pk-pk) or root-mean-square (rms). However, they do not offer clues or detailed information on different jitter processes involved or how much comes from DJ process or RJ process. As such, direct observables are not effective or useful for understanding jitter process and component quantification without further analysis or post-data processing.

5.1.2. Characterization, Diagnostics, and Debug Needs

Not only is jitter component information very useful for understanding the jitter process, but it also is critical for device characterization, diagnosis, and debugging. The jitter component and its time and/or frequency domain characteristics provide clues on what and how much of each jitter component the process has. For example, RJ is typically integrated circuit (IC) manufacturing process and edge rate or edge slope related. If a device fails in jitter testing because its RJ is too much, it might be due to slow edge rate or noisy manufacturing process technology. In another example, where DDJ is the dominant failure mechanism for a link channel medium, bandwidth for that channel medium may be limited, and channel equalization or compensation is needed to improve the DDJ performance. In the third example, where PJ is the dominant jitter failure mechanism, frequency and magnitude information of the PJ give clues on its origin and determine whether it is caused by switching power supply, or undesired crosstalk, or interference, or modulation. Thus, for characterization and debug purposes, time, frequency, and statistical domain information are all essential and important.

5.1.3. Overview of Jitter Separation in the Statistical Domain

Sections 5.1.1 and 5.1.2 discussed the motivation and rationale for separating jitter into its components from direct observables. The direct jitter observables are in three major domains: time, frequency, and statistical domain. Accordingly, jitter separation can be

conducted in those three domains. This chapter focuses jitter separation in the statistical domain, where observables of jitter PDF or BER CDF are given, and leaves the time and frequency domain jitter separations as topics for Chapter 6, "Jitter and Noise Separation and Analysis in the Time and Frequency Domains." Section 5.2 discusses PDF-based jitter separation, and section 5.3 discusses BER CDF-based jitter separation. Section 5.4 covers the accuracy of a simplified jitter model, where no curve fitting is involved, and its associated limitations.

URL <http://access.proquest.safaribooksonline.com/9780132429610/ch05lev1sec1>

User name: CSU San Diego

Book: Jitter, Noise, and Signal Integrity at High-Speed

Section: Chapter 5. Jitter and Noise Separation and Analysis in the Statistical Domain

No part of any chapter or book may be reproduced or transmitted in any form by any means without the prior written permission for reprints and excerpts from the publisher of the book or chapter. Redistribution or other use that violates the fair use privilege under U.S. copyright laws (see 17 USC107) or that otherwise violates these Terms of Service is strictly prohibited. Violators will be prosecuted to the full extent of U.S. Federal and Massachusetts laws.

Information Theory Computer Science Mike Peng Li Prentice Hall Jitter, Noise, and Signal Integrity at High-Speed

5.2. Jitter Separation Based on PDF

A commonly encountered direct jitter statistical observable is its PDF or histogram, which can be obtained by instruments such as time interval analyzer (TIA) or sampling scopes. As we have already pointed out, jitter PDF frequency response or contents can differ, depending on how the PDF is obtained. [Chapter 6](#) covers the frequency content or spectrum. This section assumes that the frequency content is governed by whatever sampling function the measurement or simulation is using, without getting into the details of whether it is a high-frequency jitter PDF or low-frequency jitter PDF.

5.2.1. Tailfit Method for PDF

Let us look at a jitter PDF (or histogram) for edge transitions. Such a jitter PDF reflects the mixture of DJ and RJ processes associated with the edge transitions. Here we assume that the timing reference used to obtain the jitter PDF is the ideal clock. This information has been available for many years, but, to our knowledge, no theory or method had been established to decompose the total jitter (TJ) PDF into DJ and RJ components until [\[1\]](#). The metrics that had been used to quantify jitter are simple and straightforward statistical pk-pk value and 1σ standard deviation, based on the entire PDF that has both DJ and RJ components. With the knowledge of jitter model introduced in [Chapter 4](#), "Jitter, Noise, BER (JNB), and Interrelationships," it is clear that the correct way to quantify jitter is to use the right metric for each jitter component. For example, use pk-pk value for DJ because it is bounded, and use 1σ standard deviation for RJ because it is unbounded and random. We assume that RJ is white and a Gaussian is a good model for it.

The following sections present a method/algorithm to decompose a total jitter PDF into DJ and RJ PDFs through the Tailfit method.

5.2.1.1. Theory for Total Jitter PDF and Its Relationship to DJ and RJ PDFs

An obvious consequence of DJ and RJ interaction through the convolution process is that the tail part of the PDF reflects the random jitter process. If the random jitter is due to the random motion of electrons or holes in a semiconductor, the random velocity of these particles in an equilibrium state is best described by a Gaussian distribution. This gives another justification for using the Gaussian model to describe the random jitter. Because multitemperature particle distribution is possible, a multiple-Gaussian distribution function may be needed to model certain random jitter processes. A single Gaussian jitter PDF is defined as follows:

Equation 5.1

$$f_{RJ}(\Delta t) = \frac{1}{\sqrt{2\pi}\sigma} e^{-\frac{-(\Delta t - \mu)^2}{2\sigma^2}}$$

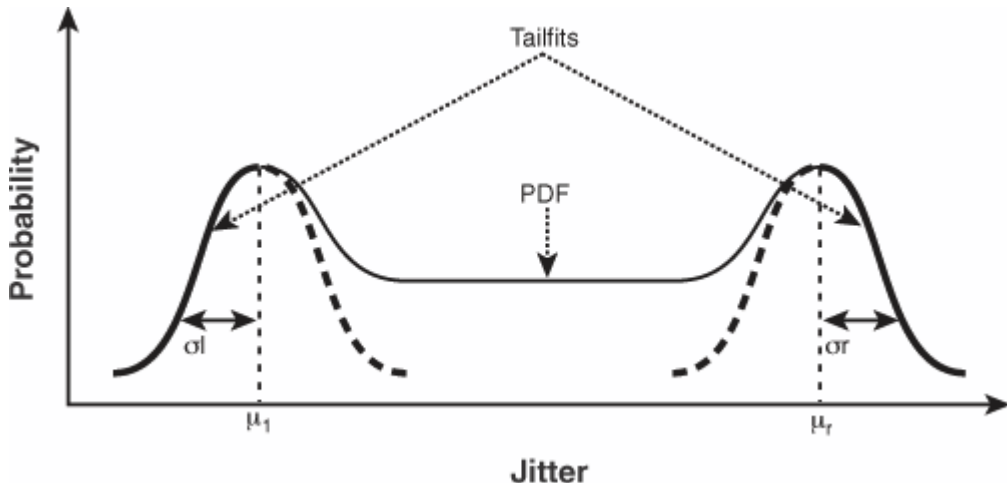
where Δt is the jitter and μ and σ are the Gaussian mean and standard deviation, respectively.

From an observational point of view, the measured or simulated total jitter histogram represents the scaled-up total jitter PDF. The tail part of the distribution should largely be determined by the random jitter process, which, in general, has a Gaussian type of distribution. The random jitter can be quantified by the 1σ (or rms) standard deviation of Gaussian distribution, and DJ can be quantified by the pk-

pk value.

In the absence of DJ, the total jitter PDF should be a Gaussian. Under this condition, only one maximum in the distribution corresponds to zero DJ. The rms of the PDF equals σ in this case. When both DJ and RJ processes play together, the resulting jitter PDF is broadened and is no longer a Gaussian as a whole. On the other hand, both ends of the distribution should still keep the Gaussian type of tails, because DJ PDF is bounded. These tail part distributions can be used to deduce the RJ distribution parameters. Because of the DJ, the mean of each tail is no longer at the same location, and multi-peaks can be present in the PDF. The time distance between far-left peak position and far-right peak position gives rise to the DJ pk-pk value. [Figure 5.1](#) shows such a broadened total jitter PDF in the presence of both DJ and RJ.

Figure 5.1. Total jitter PDF and Tailfits.



If there is no bias and statistical sampling noise or the asymmetry in rising and falling edges in the measurement, the two tails, which represent the random process, should be symmetrical. Because it is not possible to completely randomize measurements and reduce the sampling noise to zero, and because the rising and falling edges are different in a practical system, the σ values for the far-left and far-right Gaussian tails may not be the same. The total RJ σ value should be the average of these two, and DJ pk-pk is the distance between two peaks of far-left and far-right Gaussian tails:

Equation 5.2

$$DJ = \mu_r - \mu_l$$

and

Equation 5.3

$$\sigma_t = \frac{\sigma_r + \sigma_l}{2}$$

The average gives a typical value or mostly likely value for RJ. If a conservative RJ estimation is desired, the overall RJ should be the larger one among the left and right RJ rms—namely, $\sigma_t = \max(\sigma_r, \sigma_l)$.

5.2.1.2. Implementation Algorithm

Identifying the tail parts of the PDF, and then fitting them with the Gaussian function, are the key to DJ and RJ separation with a given measured/simulated jitter PDF or histogram. It is impossible to tell where the tail part of the PDF is without studying each individual data and its relationship with the neighboring data. The easiest way to identify a tail part is through the graphical display of the PDF and picking up the tail parts via visual inspection. The disadvantage of such an approach is that it lacks repeatability, and it cannot be adopted for automated testing. Therefore, the requirements for a search algorithm should be as follows:

- It can find the true tail part quickly, accurately, and repeatedly.

- It has to be automatic (no user intervention or visual inspection are required).

The fitting procedure should be able to deal with the statistical fluctuation and factor this into the fitting routines. The tail part has the lowest event counts, and statistical uncertainty can be high. A simple, straightforward, least-square fit algorithm would not work well, because the statistical error would propagate into the fitting parameters. This in turn gives rise to large errors in DJ and RJ estimation. A more advanced nonlinear fitting algorithm is needed to meet these requirements.

5.2.1.2.1. Tail PDF Identification

One of the key characteristics of a Gaussian tail is its monotonicity. That means that the left side of the tail monotonically increases, and the right side of the tail monotonically decreases. Due to the presence of DJ, monotonicity will break and this in turn will create local maximums near the left and right parts of the tail. Without DJ, only one maximum corresponds to the mean of the distribution.

A difficult issue that a tail-search algorithm faces is statistical fluctuation. In the presence of statistical fluctuations, the monotonicity of a real Gaussian distribution is no longer true, and using the raw fluctuated data to find the local maximum points for both left and right tails will be extremely difficult, if not impossible. The solution should be to first filter out the fluctuation noise and then use the smoothed PDF to locate the maximum points. There are two general ways to achieve this. One is through direct time domain averaging. Another is to use Fourier Transformation (FT) to get the spectrum, apply a low-pass filter, and do inverse FT (IFT). For time-domain averaging, you need to determine how many data points to use, because this determines the smooth level or, equivalently, the cutoff frequency of the low-pass filter. In the FT/IFT approach, you must determine the filter's bandwidth. The number of averaging points and filter bandwidth may need to be adjusted, depending on the fluctuation in noise frequency and amplitude. In other words, a rule-based artificial-intelligence algorithm must be used to enable the smoothing algorithm to deal with a wide range of fluctuation amplitudes and frequencies. This is an important requirement to guarantee that smoothing washes away only the unwanted fluctuation noise, not the true feature of the jitter histogram.

$$\bar{f}_{RJ}(\Delta t)$$

As soon as the smoothed measured PDF $\bar{f}_{RJ}(\Delta t)$ is obtained either through time domain averaging or time-frequency domain FT-low-pass filtering-IFT, the maximum locations can be found by calculating the first- and second-order derivatives of the jitter PDF. The only maximum points of interest are the first maximum from the far left and the first maximum from the far right.

5.2.1.2.2. Tailfitting

You should use a fitting algorithm that weights the data record based on the quality of the data. The bigger the error, the smaller the role it should play in minimizing the difference between the model expected value and the measured value. Thus, we need to use χ^2 as a gauge to determine how good the fit is. The fitting function is Gaussian, and the fitting algorithm is nonlinear, so it can handle both linear and nonlinear fitting functions. For details on χ^2 theory, refer to [2].

χ^2 fitting is an iterative process, in contrast to linear equation solving in the case of linear least-squared fitting. The final answer is obtained when the iteration converges. For this reason, initial values of the fitting parameters are needed. A primitive way to do this is to try different initial values and see whether they converge to the same final values. If the initial guessed values are far from the final actual values, they may either take longer to converge or get stuck at a local χ^2 minimum and never converge to the final global χ^2 minimum point. Calculations should be carried out to estimate the initial fitting parameters by using the tail parts of PDF so that the initial fitting parameters are close to the final converging values. This also makes the iteration converge rapidly and avoids stuck-in-local minimum (pivot). We would like to emphasize that the χ^2 method has proven to be very robust.

5.2.1.3. Monte Carlo Simulations

Another complication for a measured/simulated PDF is the sampling noise associated with it in practical application. The goal is to best determine the DJ and RJ PDF and associated parameters in the presence of the sampling noise. A good PDF-based jitter separation method should be immune to sampling noise. This section evaluates the χ^2 Tailfit method via Monte Carlo simulation to determine its accuracy in dealing with a "noisy" measured PDF.

5.2.1.3.1. PDF with Statistical Noise

We started with a known bimodal PDF, which is represented by two added Gaussian distributions superimposed with random noise. This makes the overall PDF close to that of a practical one. For example, in the presence of a PJ (approximated by a dual-Dirac), RJ (Gaussian), and sampling noise, the overall PDF is two separated Gaussians superimposed with sampling noise. Mathematically, such a PDF can be represented by the following equation:

Equation 5.4

$$f_{TJ}(\Delta t) = N_1 e^{-\frac{(\Delta t - \mu_l)^2}{2\sigma_l^2}} + N_r e^{-\frac{(\Delta t - \mu_r)^2}{2\sigma_r^2}} + N_n \text{ran}(\Delta t)$$

where N_1 and N_r are the peak values, μ_l and μ_r are means, and σ_l and σ_r are standard deviations for two Gaussian distributions. $\text{ran}(t)$ is a random-number-generating function based on the Monte Carlo method. It has a mean of 0 and a standard deviation of unity. N_n is the amplitude for the random number envelopes. For Monte Carlo-based random-number generation, refer to [3].

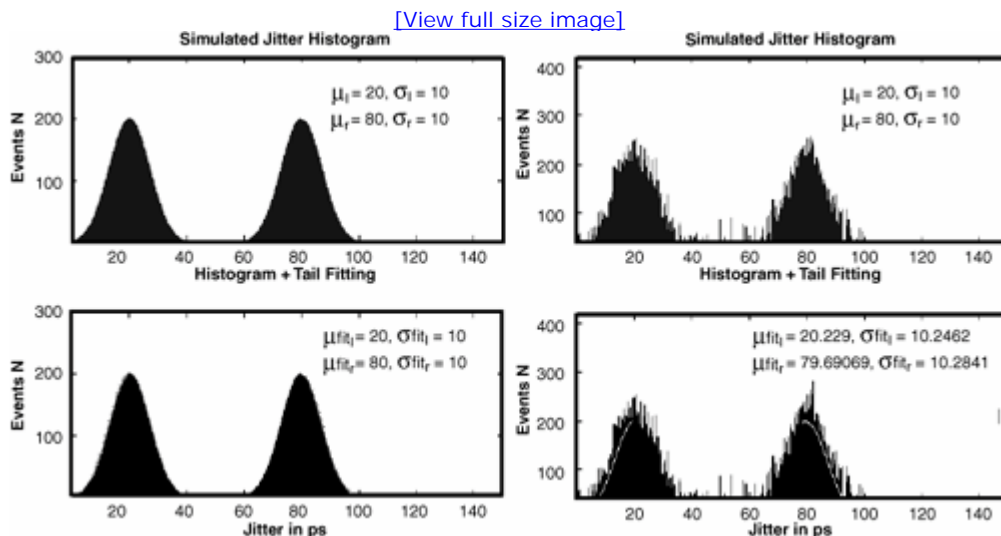
A good search and fitting algorithm should return the fitted parameters that are consistent with those predefined in the simulation. A critical test is as follows: Can an accurate fitting parameter be obtained in the presence of significant statistical fluctuations? In other words, N_n is a significant portion of N_1 or N_r . Otherwise, no accurate parameters can be obtained, because all the real-world measurements are subject to statistical fluctuation.

5.2.1.3.2. Fitting Results

There are two scenarios that we need to treat differently. The first is when two Gaussian distributions are well separated—that is, when $\mu_r - \mu_l > \sigma_l + \sigma_r$. Under such conditions, the two distributions are not mixed, and the tail parts up to the point of the first maximum are essentially uncontaminated. Therefore, we could use both left and right tail data from the lower value to the first maximums. This enhances the tail data usage, and the Gaussian model is better constrained. This can correspond to the case when $DJ \gg 2\sigma$ in the jitter analysis, as shown in Figure 5.2.

Figure 5.2. Two well-separated Gaussians: $N_n = 0$, with no statistical fluctuation (a), and $N_n = 30$, with significant statistical fluctuation (b). The lower panels show the overlay of the original PDF with the tailfit Gaussian.

Source: M. P. Li, J. Wilstrup, R. Jesson, and D. Petrich, "A New Method for Jitter Decomposition Through Its Distribution Tail Fitting," International Test Conference (ITC), 1999. (© 1999, IEEE)



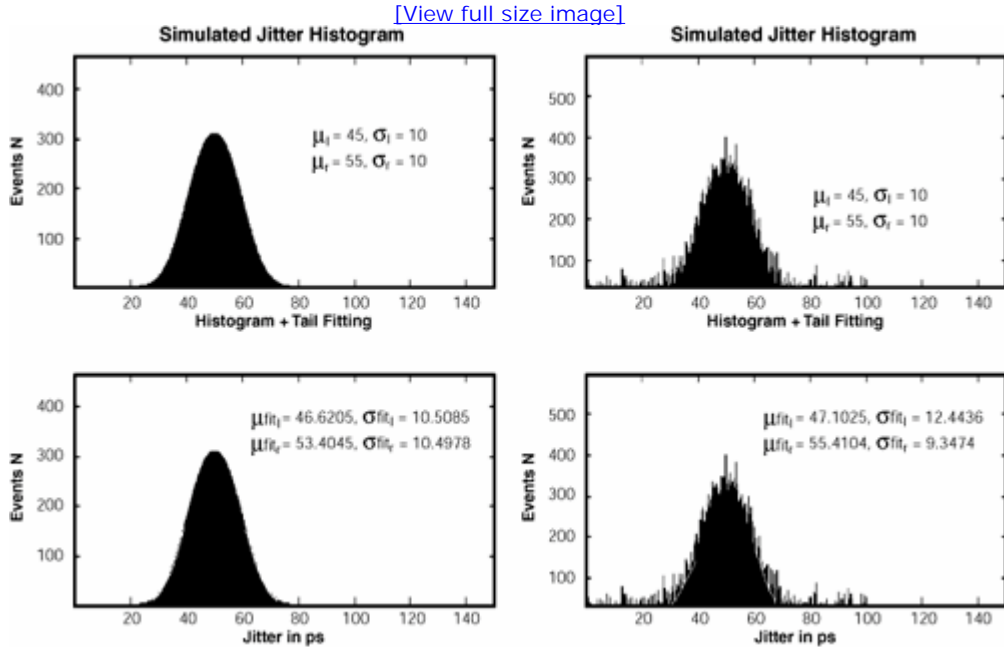
In both cases, the simulation results suggest that the fitted parameters are consistent with the predetermined parameters to within 2.8 %, even when the statistical fluctuation reaches 15% of the total PDF peak.

The second case is when two Gaussian distributions are not well separated—namely, $\mu_r - \mu_l < \sigma_l + \sigma_r$. Under such condition, the contamination of two distributions could extend to the tail parts. As a result, you should use only the lower parts of the tails for the fitting to minimize contamination. A conservative way is to use the tail part from the lowest event count to half of the N_1 or N_r . This can correspond to the case when $DJ < 2\sigma$ in the jitter analysis applications.

Figure 5.3 shows the results corresponding to two mixed Gaussian PDFs ($\mu_r - \mu_l < \sigma_l + \sigma_r$). In each case, nonfluctuated ($N_n = 0$) and fluctuated ($N_n \neq 0$) scenarios are considered. In both cases, the fitted parameters are consistent with the predetermined parameters to within 4%, even when the statistical fluctuation reaches 15% of the total PDF peak.

Figure 5.3. The same as **Figure 5.2**, but the two Gaussians are very close to each other. $N_n = 0$, with no statistical fluctuation (a), and $N_n = 30$, with significant statistical fluctuation (b). The lower panels show the overlay of the original PDF with the tailfit Gaussian.

Source: M. P. Li, J. Wilstrup, R. Jesson, and D. Petrich, "A New Method for Jitter Decomposition Through Its Distribution Tail Fitting," International Test Conference (ITC), 1999. (© 1999, IEEE)



5.2.2. DJ PDF Determination Through Deconvolution

The Tailfit method introduced in [section 5.2.1](#) determines the RJ PDF and DJ pk-pk value given the total jitter PDF. It also enables the extrapolation of jitter PDF from its higher-probability level to a lower-probability level. For example, if the total jitter PDF measured is at a probability level of 10^{-8} , and the RJ PDF is determined, the total jitter PDF can be extrapolated to 10^{-12} or smaller for BER and TJ estimation required for most serial data communications.

However, what Tailfit does not give is the DJ PDF function directly, yet it is very important to understand and determine the nature and causing mechanism for DJ process. Because of this, the next section introduces a deconvolution-based method for determining the DJ PDF.

5.2.2.1. Deconvolution Theory

We derived the relationship between the total jitter PDF and its DJ and RJ PDFs via [equation 4.1](#) of convolution by assuming that DJ and RJ are independent. This assumption can be justified, because DJ and RJ come from independent sources. In this section, we try to extract the DJ PDF from the TJ PDF, given that RJ PDF is known. A "blind" deconvolution is defined as a deconvolution process in which both DJ and RJ PDFs are unknown and are to be determined given the TJ PDF. Although from a pure theoretical standpoint a "blind" deconvolution may still be possible, the accuracy and uniqueness of a "blind" deconvolution is generally poor, and that is not what we are interested in here.

We will start with the multiple Dirac-delta model of [equation 3.9](#) and extend it as the general model for bounded DJ PDF. It is represented by the following:

Equation 5.5

$$f_{DJ}(\Delta t) = D(\Delta t) = \sum_{n=1}^N P(\Delta t_n) \delta(\Delta t - \Delta t_n)$$

Clearly, Δt_n represents the location of the n th delta pulse of the DJ PDF, and $P(\Delta t_n)$ represents the probability in this jitter location. Δt_1 and Δt_N represent the first (minimum) and last (maximum) time locations for the DJ PDF, respectively.

The TJ PDF is then given by the convolution between DJ PDF and RJ PDF, as defined by the following equation:

Equation 5.6

[\[View full size image\]](#)

$$f_{TJ}(\Delta t) = f_{DJ}(\Delta t) * f_{RJ}(\Delta t) = \int_{-\infty}^{\infty} f_{DJ}(\tau) * f_{RJ}(\Delta t - \tau) d\tau = \int_{-\infty}^{\infty} f_{RJ}(\tau) * f_{DJ}(\Delta t - \tau) d\tau$$

Given TJ PDF $f_{TJ}(\Delta t)$, the first step is to obtain the RJ PDF via Tailfit, as discussed in [section 5.2.1](#).

With a proper sampling scheme for both the TJ PDF and the RJ PDF, one of the approaches is to represent the convolution in a matrix form:

Equation 5.7

$$T = RD$$

where T, R, and D are matrixes representing TJ, RJ, and DJ PDFs, respectively.

Clearly, if there exists an inverse matrix R^{-1} , a true solution to [equation 5.7](#) can be obtained:

Equation 5.8

$$D = R^{-1}T$$

More generally, a pseudoinverse for R can be obtained. Assuming that the inverse of $(R'R)$ exists, R^+ is given as

Equation 5.9

$$R^+ = (R'R)^{-1} R'$$

where R' is the matrix transposition of R . Then the least-squares solution to [equation 5.8](#) can be written as

Equation 5.10

$$D^+ = R^+T$$

In other words, D^+ satisfies the following:

Equation 5.11

$$\min_d \|T - RD\|$$

For a detailed discussion of this matrix-based deconvolution, refer to [\[4\]](#).

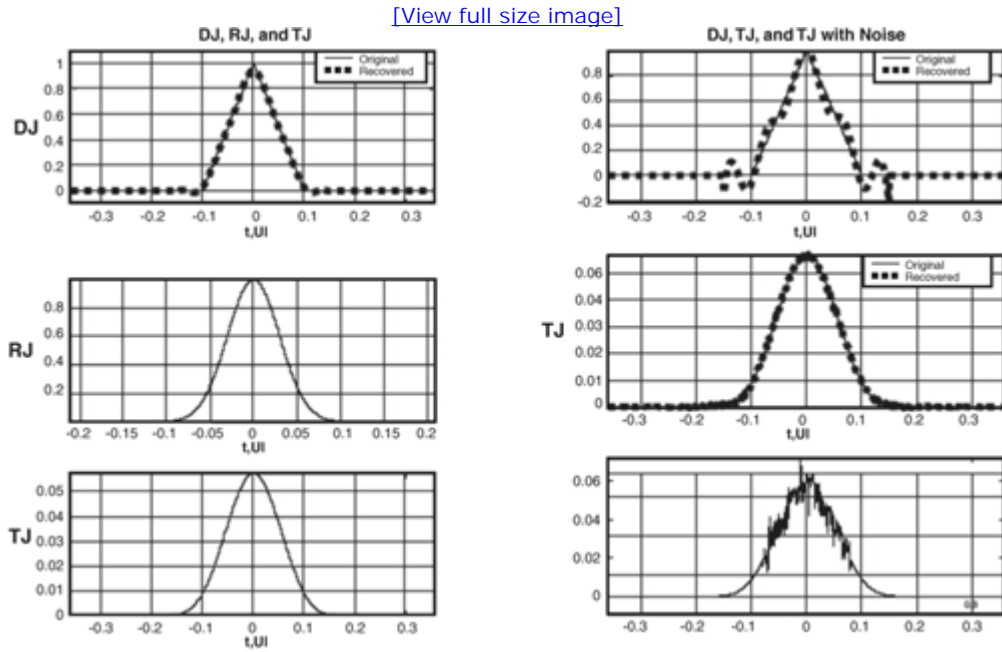
5.2.2.2. Deconvolution Simulations

Numerical studies are performed to demonstrate the deconvolution algorithm introduced in the preceding section. The simulation is set up as follows: First, in the forwarding problem, a hypothesized DJ PDF is convolved with a known single Gaussian RJ PDF. Thus, the test-case TJ PDF is obtained. Next, the RJ matrix R is constructed by using the known RJ PDF, and then the DJ PDF is estimated by using the matrix method introduced. Finally, the recovered or deconvolved DJ PDF is compared with the original hypothesized DJ PDF. In addition, the recovered TJ PDF is also compared with the assumed TJ PDF. We will study two distinct DJ PDFs, triangular and arbitrary shape, and present the simulation results accordingly.

5.2.2.2.1. Triangular DJ PDF

We will start with a triangular DJ PDF. To accommodate both theoretical and practical interests, two cases are considered: TJ PDF without statistical fluctuation, and TJ PDF with fluctuation. Figure 5.4 shows the results. In this figure, (a) is for "noiseless" deconvolution, and (b) is for "noisy" deconvolution. In both cases, the estimated DJ PDF is a dotted line. Note that in (b), DJ PDF is not plotted, because it is the same as in (a). Instead, "noisy" TJ PDF (lower panel), original TJ, and "recovered" TJ PDFs (middle panel) are shown.

Figure 5.4. DJ PDF estimation when the original DJ PDF is a triangular function.



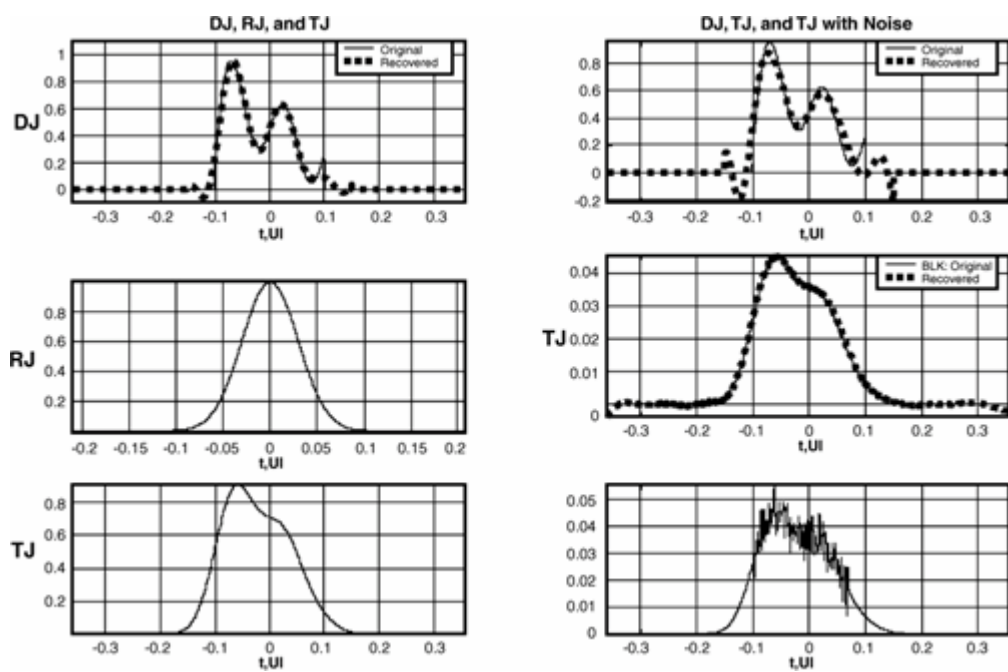
We conduct the simulation in the context of serial data communication. The DJ PDF pk-pk value used is 0.2 UI, and the RJ Gaussian has $\sigma = 0.33$ UI. In the "noiseless" case, no TJ PDF smooth is needed. We see that the estimated DJ PDF reconciles with the original DJ PDF well. In the "noisy" case, TJ PDF needs to be smoothed before the deconvolution algorithm can be used. The general shape of the original DJ PDF is reserved in the estimated DJ PDF. Even though extra small "ripples" are introduced due to the statistical fluctuation in the TJ PDF, we have found that "recovered" TJ PDF obtained through convolution between estimated DJ and the assumed RJ PDF still agrees with the original "noiseless" TJ PDF.

5.2.2.2.2. Arbitrary DJ PDF

Figure 5.5 shows simulation results for an arbitrary DJ PDF with the same pk-pk as the triangular DJ PDF from the preceding section. In this case, DJ PDF pk-pk and RJ PDF rms are kept unchanged. The agreement between the estimated and original DJ PDFs is even better for the arbitrary DJ PDF compared with that when the DJ PDF is triangular. This is because the arbitrary PDF we used does not have any "first-order" derivative discontinuity, although a triangular PDF does.

Figure 5.5. Similar to Figure 5.4, but for a rectangular DJ PDF.

[\[View full size image\]](#)



We have shown that for both triangular and arbitrary DJ PDFs, the matrix-based deconvolution method introduced in section 5.2.2 does a fairly good job of recovering the DJ PDF embedded in the TJ PDF, for both "ideal" and "practical" TJ PDFs. For a practical TJ PDF in which statistical fluctuation is present, a smooth process is needed to get a good DJ PDF recovery. The method can tolerate 10% statistical fluctuation while still recovering a nearly perfect DJ PDF.

URL <http://access.proquest.safaribooksonline.com/9780132429610/ch05lev1sec2>

User name: CSU San Diego

Book: Jitter, Noise, and Signal Integrity at High-Speed

Section: Chapter 5. Jitter and Noise Separation and Analysis in the Statistical Domain

No part of any chapter or book may be reproduced or transmitted in any form by any means without the prior written permission for reprints and excerpts from the publisher of the book or chapter. Redistribution or other use that violates the fair use privilege under U.S. copyright laws (see 17 USC107) or that otherwise violates these Terms of Service is strictly prohibited. Violators will be prosecuted to the full extent of U.S. Federal and Massachusetts laws.

Information Theory Computer Science Mike Peng Li Prentice Hall Jitter, Noise, and Signal Integrity at High-Speed

5.3. Jitter Separation Based on BER CDF

We have shown that the tailfit method can be applied to TJ PDF to estimate the RJ Gaussian PDF, as well as the DJ pk-pk value. DJ PDF, on the other hand, should be obtained through the deconvolution as soon as the RJ is obtained via tailfit. In fact, this method can be equally applied to the BER CDF function to estimate the RJ PDF and DJ pk-pk value, similar to the case when TJ PDF is given.

5.3.1. Tailfit Method for the BER CDF

Recall [equation 4.23](#) for the BER CDF:

Equation 5.12

[\[View full size image\]](#)

$$F_{BER}(t_s) = c_0 \left[\int_{t_s}^{\infty} f_{TJ}(\Delta t) d\Delta t + \int_{-\infty}^{t_s} f_{TJ}(\Delta t) d\Delta t \right] = F_{BER1}(t_s) + F_{BER2}(t_s)$$

where c_0 is the transition density of the data bit stream. Here we have assumed that the transition densities are the same for the first CDF branch F_{BER1} (the left branch) and the second CDF branch F_{BER2} (the right branch). Obviously, we have

Equation 5.13

[\[View full size image\]](#)

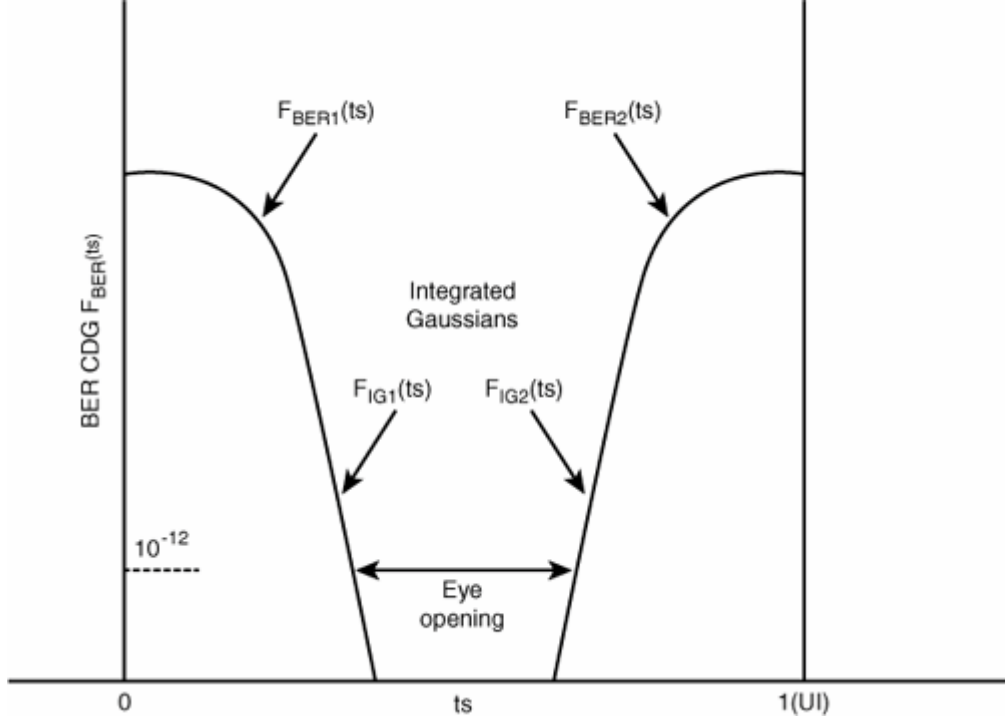
$$F_{BER1}(t_s) = c_0 \int_{t_s}^{\infty} f_{TJ}(\Delta t) d\Delta t, \quad F_{BER2}(t_s) = c_0 \int_{-\infty}^{t_s} f_{TJ}(\Delta t) d\Delta t$$

Because the tail part distributions of TJ PDF f_{TJ} are dominated by Gaussians, the tail parts of F_{BER1} and F_{BER2} are "integrated Gaussians," corresponding to Gaussian sigmas of σ_l and σ_r , respectively, as defined in [equation 5.4](#).

[Figure 5.6](#) shows the BER CDF function.

Figure 5.6. The BER CDF data base functions F_{BER1} and F_{BER2} , as well as the Tailfit "integrated Gaussian" models F_{IG1} and F_{IG2} . The eye opening at $BER = 10^{-12}$ is also shown.

[\[View full size image\]](#)



Now let us focus on developing the analytical math form for the integrated Gaussians. We will use the generic Gaussian model as shown in [equation 5.1](#) to derive the integrated Gaussian function. It is given by the following:

Equation 5.14

$$F_{IG}(t_s) = \int_{t_s}^{\infty} f_{RJ}(\Delta t) d\Delta t$$

Substituting the normalized Gaussian into this equation, we get the following:

Equation 5.15

$$F_{IG}(t_s) = \int_{t_s}^{\infty} \frac{1}{\sqrt{2\pi}\sigma} e^{-\frac{(\Delta t - \mu)^2}{2\sigma^2}} d\Delta t$$

[Equation 5.15](#) can be simplified by using a different integration variable such that the exponential is a single variable. Let $z = \frac{\Delta t - \mu}{\sqrt{2}\sigma}$. We obtain the following:

Equation 5.16

$$F_{IG}(t_s) = \frac{1}{\sqrt{\pi}} \int_{\frac{t_s - \mu}{\sqrt{2}\sigma}}^{\infty} e^{-z^2} dz$$

Using the definition of complementary error function, [equation 5.16](#) can be rewritten as follows:

Equation 5.17

$$F_{IG}(t_s) = \frac{1}{2} \operatorname{erfc}\left(\frac{t_s - \mu}{\sqrt{2}\sigma}\right) = \frac{1}{2} (1 - \operatorname{erf}\left(\frac{t_s - \mu}{\sqrt{2}\sigma}\right))$$

where the definition of an error function $\operatorname{erf}(x)$ and a complementary error function $\operatorname{erfc}(x)$ are given by

Equation 5.18

$$\operatorname{erf}(x) = \frac{1}{\sqrt{\pi}} \int_0^x e^{-u^2} du$$

and

Equation 5.19

$$\operatorname{erfc}(x) = \frac{1}{\sqrt{\pi}} \int_x^{\infty} e^{-u^2} du = 1 - \operatorname{erf}(x)$$

[Equation 5.17](#) gives the analytical form for an integrated Gaussian CDF $F_{IG}(t_s, \mu, \sigma)$. Clearly, it is valid only when $t_s \geq \mu$; otherwise, DJ contamination will occur, and the PDF function is no longer a Gaussian.

With the derived generic integrated Gaussian function in [equation 5.17](#), we can now derive the first and second such functions to be used to fit the first and second BER CDF branches at its tail parts to determine DJ and RJ parameters. The basic idea is the same as the PDF-based tailfit, but now the data or base function to be fitted is BER CDF, and the analytical model is an integrated Gaussian that can be expressed as either a complementary error function or an error function. To make the jitter PDF parameters be consistent with [section 3.1](#) of PDF-based Tailfit, we will write the integrated Gaussian functions for the first and second BER CDF branches shown in [Figure 5.6](#) as follows:

Equation 5.20

$$F_{IG1}(t_s) = \frac{1}{2} \operatorname{erfc}\left(\frac{t_s - \mu_r}{\sqrt{2}\sigma_r}\right) = \frac{1}{2} (1 - \operatorname{erf}\left(\frac{t_s - \mu_r}{\sqrt{2}\sigma_r}\right))$$

and

Equation 5.21

$$F_{IG2}(t_s) = \frac{1}{2} \operatorname{erfc}\left(\frac{T_0 - t_s - \mu_l}{\sqrt{2}\sigma_l}\right) = \frac{1}{2} [1 - \operatorname{erf}\left(\frac{T_0 - t_s - \mu_l}{\sqrt{2}\sigma l}\right)]$$

where T_0 is the UI measure of the data bit stream. These two equations are true only if the sampling time t_s is in the range where the BER CDF is dominated by Gaussian process or integrated Gaussian. This translates to two different constraints. For the first integrated Gaussian, we have

Equation 5.22

$$\mu_r \leq t_s \leq T_0$$

For the second integrated Gaussian, we have

Equation 5.23

$$0 \leq t_s \leq T_0 - \mu_l$$

Note that $\mu_l, \mu_r, \sigma_l, \sigma_r$ are all positive parameters and that we have changed the origin of the PDF to the center of its distribution so that the left mean is negative. As soon as they are determined through the fitting procedure such as χ^2 , both DJ pk-pk and RJ σ for the entire CDF can be estimated through [equations 5.2](#) and [5.3](#), similar to the case of PDF-based tailfit.

5.3.2. Tailfit Method for the "Transformed" BER CDF

You saw in [section 5.3.2](#) that DJ pk-pk and RJ rms can be determined via tailfit if the measured or simulated base distribution is the BER CDF. The major change is that the fitting model needs to be integrated Gaussian and that is basically a complementary error function $\operatorname{erfc}(x)$.

Mathematically, along the basic concept of Tailfit, there are unlimited ways to determine DJ pk-pk and RJ rms via transformation operations to both base data (jitter PDF or BER CDF) and base RJ model (Gaussian or integrated Gaussian). For example, a logarithmic operation can be applied to a measured jitter PDF. Accordingly, the same operation needs to be applied to the base model Gaussian to turn it into a quadratic function. In another example, a complementary inverse error function operation ($\operatorname{erfc}^{-1}(x)$) can be applied to base BER CDF. Accordingly, the same operation can be applied to the integrated Gaussian model to turn it into a linear function. Again, examples can be exhaustive. One common issue for those Tailfits based on "transformed data" and "transformed Gaussian model" is the numeric errors associated with the mathematic transform operations. Accuracy degradation due to the additional transformation operation cannot be overlooked for all those non-raw data-based Tailfit methods.

This section illustrates how the Tailfit-based method works in the context of transformed data and model by showing an example of inverse complementary error function ($\operatorname{erfc}^{-1}(x)$) transformation.[\[5\]](#) Recall [equation 5.20](#). Let us introduce β as the BER and be the same as F_{BER} . Then let us take the $\operatorname{erfc}^{-1}()$ operation for that equation in a general term without subscriptions. This results in the following:

Equation 5.24

$$\operatorname{erfc}^{-1}(2\beta(t_s)) = \operatorname{erfc}^{-1}(\operatorname{erfc}\left(\frac{t_s - \mu}{\sqrt{2}\sigma}\right)) = \left(\frac{t_s - \mu}{\sqrt{2}\sigma}\right)$$

$$Q = \frac{t_s - \mu}{\sigma}$$

Let us define Q . Here Q is often called the Q-factor. It has been used in optical communication to study optical power noise. Again, $\beta(t_s) = F_{BER}(t_s)$ is a general form for BER function, for both data and model, left and right branches. Then [equation 5.24](#) can be rewritten as follows:

Equation 5.25

$$Q(t_s) = \sqrt{2} \operatorname{erfc}^{-1}(2\beta(t_s))$$

[Equation 5.25](#) converts a BER function to a Q-function through an inverse complementary error function transformation. An alternative transformation using inverse error transformation ($\operatorname{erfc}^{-1}()$) is also possible due to the relationship between $\operatorname{erf}(x)$ and $\operatorname{erf}(x)$ functions.

If we substitute raw or base data BER functions of $F_{BER1}(t_s)$ and $F_{BER2}(t_s)$ in [equation 5.25](#), we get the following:

Equation 5.26

$$Q_1(t_s) = \sqrt{2} \operatorname{erfc}^{-1}(2F_{BER1}(t_s))$$

and

Equation 5.27

$$Q_2(t_s) = \sqrt{2} \operatorname{erfc}^{-1}(2F_{BER2}(t_s))$$

If we substitute the two integrated Gaussian BER CDF models of $F_{IG1}(t_s)$ and $F_{IG2}(t_s)$ defined in [equations 5.20](#) and [5.21](#) to [equation 5.25](#), we obtain the following:

Equation 5.28

$$Q_{M1}(t_s) = \sqrt{2} \operatorname{erfc}^{-1}(2F_{IG1}(t_s)) = \frac{t_s - \mu_r}{\sigma_r}$$

and

Equation 5.29

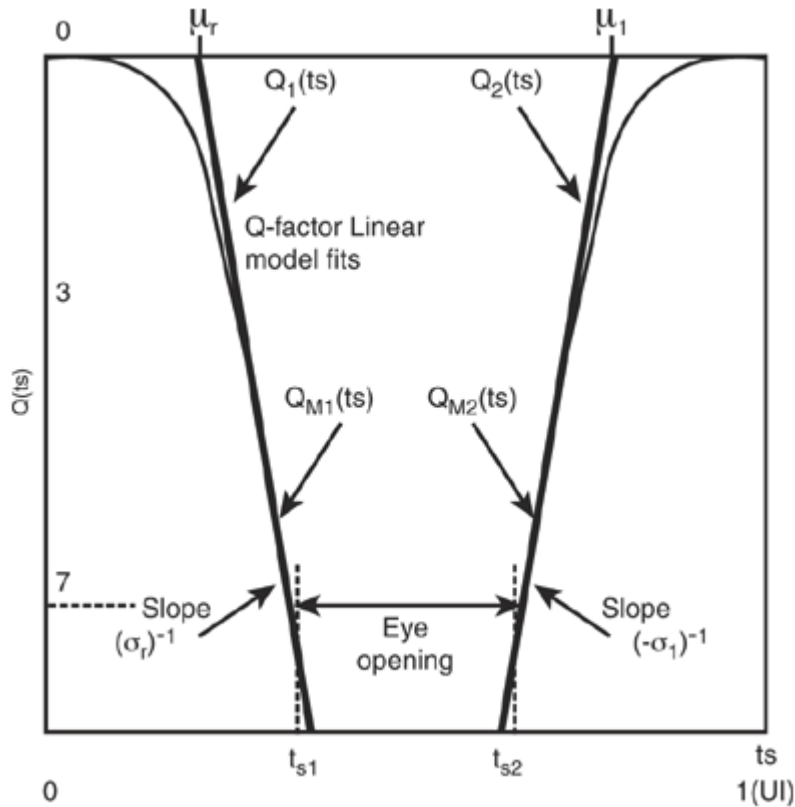
$$Q_{M2}(t_s) = \sqrt{2} \operatorname{erfc}^{-1}(2F_{IG2}(t_s)) = \frac{T_0 - t_s - \mu_l}{\sigma_l}$$

Through the inverse complementary error function transformation $\operatorname{erfc}^{-1}()$, we have converted the integrated Gaussian models in the BER space to linear models in the Q-space. Those two linear models are functions of Gaussian RJ and mean parameters, as well as sampling time.

The working mechanism of Tailfit in the Q-space is similar to that in the BER CDF space or PDF space. As soon as the measured or simulated $Q_1(t_s)$ and $Q_2(t_s)$ are obtained from the corresponding BER CDF functions $F_{IG1}(t_s)$ and $F_{IG2}(t_s)$, the Q-space linear models $Q_{M1}(t_s)$ and $Q_{M2}(t_s)$ are used to fit the tail parts of the $Q_1(t_s)$ and $Q_2(t_s)$ data. The best-fitted Gaussian parameters μ_l , μ_r , σ_l , σ_r are obtained. Consequently, both DJ pk-pk and RJ σ for the entire jitter process can be estimated through [equations 5.2](#) and [5.3](#), similar to the case of PDF or BER CDF-based tailfit.

[Figure 5.7](#) shows the Q-space tailfit.

Figure 5.7. The Q-space data functions and the best tailfit Q-factor linear models and associated Gaussian parameters. The eye opening at $Q = 7.0345$ (corresponding to $\text{BER} = 10^{-12}$) is also shown.



Again, Q-space Tailfit is just another implementation based on the transformed data and model. Given the fact that $\text{erfc}()$ and $\text{erfc}^{-1}()$ functions are not supported by library functions of common computer languages such as C and C++, the implementation of this method may not be handy or straightforward, and accuracy is subject to numeric errors.

5.3.3. DJ PDF Estimation from the BER CDF or Q-Factor

We have demonstrated a method to separate jitter into its DJ pk-pk and RJ rms values based on its BER CDF function via Tailfit with an integrated Gaussian model, or a Q-factor-based function with the linear model. The methods are quite similar to the Tailfit method based on a jitter PDF, except that the model used is a Gaussian. The parameters derived from those three related methods, with different base functions, can be consistent to some degree.

However, trying to find out the DJ PDF or CDF from the overall BER CDF or Q-factor function is not easy. CDF is a higher "entropy" state where DJ and RJ components are further contaminated, compared with the case of jitter PDF. Q-factor function is an even higher "entropy" state, and fine structures in DJ and RJ PDF are harder to dig out. A generic method of determining the DJ PDF or CDF from its jitter BER CDF or Q-function is beyond the scope of this book.

5.3.4. TJ Estimation from the BER CDF

TJ is commonly defined from the BER CDF. Refer to [Figure 5.6](#) where β is the BER, and T_{eye} is the eye opening. T_{eye} as a function of β and TJ at a given BER β is given by

Equation 5.30

$$TJ(\beta) = T_0 - T_{\text{eye}}(\beta)$$

This definition of TJ is always true, regardless of the shape of jitter PDF or BER CDF. Certainly it does not rely on the exact DJ and RJ values either. TJ can be obtained from either direct measurement or Gaussian model extrapolation from higher BER values to lower BER values. DJ and RJ parameters are determined from the Tailfit method, in the straight PDF space, or BER CDF space, or transformed space such as Q-space or logarithmic space.

However, it would be nice to derive a closed-form equation to estimate TJ if the tail Gaussian parameters are all determined. Refer to [Figure 5.7](#) for a given BER β or Q-factor $Q(\beta)$, the two corresponding sampling times are t_{s1} and t_{s2} for the left and right branches,

respectively. From [equations 5.28](#) and [5.29](#), those two sampling times can be represented as follows:

Equation 5.31

$$t_{s1} = Q\sigma_r + \mu_r$$

and

Equation 5.32

$$t_{s2} = T_0 - (Q\sigma_l + \mu_l)$$

Thus, the eye opening T_{eye} can be expressed as follows:

Equation 5.33

$$T_{eye} = t_{s2} - t_{s1}$$

Substituting [equations 5.31](#) and [5.32](#) into [equation 5.33](#), we obtain the following:

Equation 5.34

$$T_{eye} = T_0 - [(Q\sigma_l + \mu_l) + (Q\sigma_r + \mu_r)]$$

Substituting [equation 5.34](#) into [equation 5.30](#), we obtain the following:

Equation 5.35

$$TJ = Q(\sigma_l + \sigma_r) + (\mu_l + \mu_r)$$

Recall [equations 5.2](#) and [5.3](#) for the DJ and RJ definitions, and note that here the left Gaussian mean has a minus sign. We can rewrite [equation 5.35](#) in terms of DJ pk-pk and overall RJ σ_t as the following:

Equation 5.36

$$TJ(\beta) = DJ + 2Q(\beta)\sigma_t$$

[Equation 5.36](#) gives a closed-form TJ estimation using DJ and RJ values from Tailfit. Caution must be exercised when this equation is used for arbitrary jitter PDF where tail Gaussian is not well satisfied. In that case, [equation 5.36](#) should be used as a quick and rough estimation, rather than a precise TJ estimation.

The Q-factor as a function of BER β can be estimated according to [equation 5.25](#). [Table 5.1](#) gives Q values for the corresponding BER values. These Q-factor values can be plugged into [equation 5.36](#) to estimate TJ at a given BER when both DJ and RJ are determined through Tailfit.

Table 5.1. Q-Factor as a Function of BER β

BER β	10^{-6}	10^{-7}	10^{-8}	10^{-9}	10^{-10}	10^{-11}	10^{-12}	10^{-13}	10^{-14}
-------------	-----------	-----------	-----------	-----------	------------	------------	------------	------------	------------

Q(β)	4.753	5.199	5.612	5.998	6.361	6.706	7.035	7.349	7.651
--------------	-------	-------	-------	-------	-------	-------	-------	-------	-------

URL <http://access.proquest.safaribooksonline.com/9780132429610/ch05lev1sec3>

User name: CSU San Diego

Book: Jitter, Noise, and Signal Integrity at High-Speed

Section: Chapter 5. Jitter and Noise Separation and Analysis in the Statistical Domain

No part of any chapter or book may be reproduced or transmitted in any form by any means without the prior written permission for reprints and excerpts from the publisher of the book or chapter. Redistribution or other use that violates the fair use privilege under U.S. copyright laws (see 17 USC107) or that otherwise violates these Terms of Service is strictly prohibited. Violators will be prosecuted to the full extent of U.S. Federal and Massachusetts laws.

Information Theory Computer Science Mike Peng Li Prentice Hall Jitter, Noise, and Signal Integrity at High-Speed

5.4. Straightforward Dual-Dirac Jitter Separation Method

The straightforward dual-Dirac method assumes that DJ PDF is a dual-Dirac function and does not involve fitting the tail parts of the distribution function, from either PDF or CDF, to determine the DJ and RJ parameters.

Because many different DJ mechanisms exist, there is no unique mathematical model for DJ PDF or CDF. This creates challenges for modeling DJ PDF. DJ is bounded, and the simplest analytical model to describe a DJ PDF can be a dual-Dirac or double-delta. In particular, delta function makes the convolution easy to carry out. Any function convolves with a delta function equal to the function itself, as discussed in [Chapter 2](#), "Statistical Signal and Linear Theory for Jitter, Noise, and Signal Integrity." Due to the mathematical simplicity of the delta function, the dual-Dirac model has been used to represent DJ PDF in some literature.[\[6\]](#) The following few sections derive the TJ PDF by assuming a dual-Dirac model for DJ PDF and a Gaussian for the RJ PDF in an analytical way. Considering that the dual-Dirac function is not an exact model for most of the DJ PDFs, we will also discuss its accuracy so that we will know the limitations and shortfalls of this simplified model and apply guardbanding to the results appropriately when it is used in practical applications.

5.4.1. Total Jitter PDF

A dual-Dirac DJ PDF has the following form:

Equation 5.37

$$f_{DD}(\Delta t) = P_p \delta(\Delta t - D_p) + P_n \delta(\Delta t + D_n)$$

where $\delta(t)$ is the Dirac delta function, D_n is the jitter in the negative direction (earlier edge transitions), and D_p is the jitter in the positive direction (later edge transitions). P_p is the probability for the positive Dirac delta, and P_n is for the negative Dirac delta. Apparently, $P_p + P_n = 1$. The overall DJ pk-pk is $D = D_p + D_n$. Both D_p and D_n are positive values. When $D_p = D_n$, f_{DD} is a symmetrical function; otherwise, it is asymmetrical. The dual-Dirac gets its name from the fact that it has two Dirac delta functions.

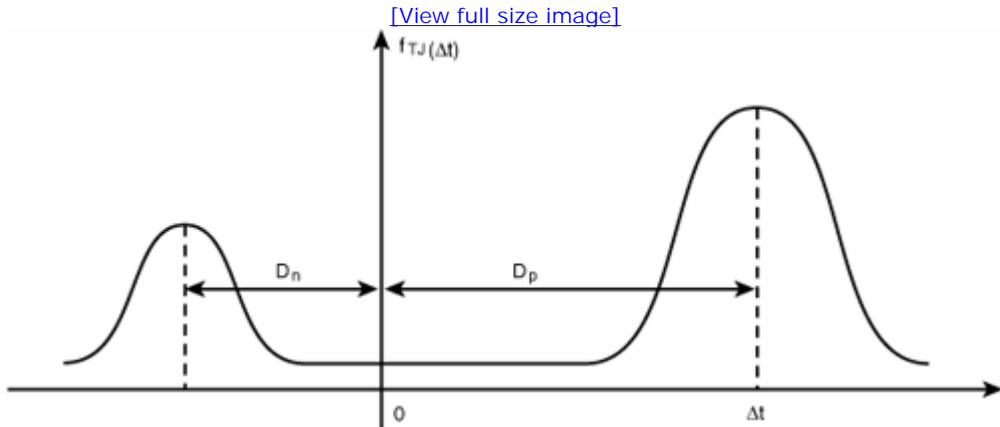
The RJ PDF is still a Gaussian, as defined in [equation 5.1](#). The TJ PDF is the convolution between DJ PDF and RJ PDF, as defined in [equation 5.6](#). Substituting [equations 5.1](#) and [5.37](#) into [equation 5.6](#), we obtain the TJ PDF of the following:

Equation 5.38

$$f_{TJ}(t) = \frac{1}{\sqrt{2\pi}\sigma} \left[P_p e^{-\frac{(t-D_p)^2}{2\sigma^2}} + P_n e^{-\frac{(t+D_n)^2}{2\sigma^2}} \right]$$

The shape of this TJ PDF is shown in [Figure 5.8](#).

Figure 5.8. A TJ PDF when its DJ PDF is a dual-Dirac and its RJ PDF is a Gaussian.



The TJ PDF shown in [Figure 5.8](#) is clearly a special type of jitter PDF. Many practical TJ PDFs do not fit into this type of "twin peak" characteristics. The major advantages of the dual-Dirac model are its mathematical simplicity and intuitive nature to illustrate the concept, rather than an accurate and comprehensive model for a general DJ PDF.

5.4.2. Overall BER CDF

With the analytical TJ PDF obtained in [equation 5.38](#), the BER CDF function can be estimated via [equation 5.12](#). Substituting [equation 5.38](#) into [equation 5.12](#), we obtain the BER CDF function as the following:

Equation 5.39

[View full size image](#)

$$f_{BER}(t_s) = \frac{C_0}{\sqrt{2\pi}\sigma} \int_{-\infty}^{t_s} \left[P_p e^{-\frac{(t-D_p)^2}{2\sigma^2}} + P_n e^{-\frac{(t+D_n)^2}{2\sigma^2}} \right] d_t + \dots$$

$$\frac{C_0}{\sqrt{2\pi}\sigma} \int_{-\infty}^{t_s} \left[P_p e^{-\frac{(t-T_0-D_p)^2}{2\sigma^2}} + P_n e^{-\frac{(t-T_0+D_n)^2}{2\sigma^2}} \right] d_t$$

Using the definition of the error function introduced in section 5.3.1, [equation 5.39](#) can be estimated by using these functions:

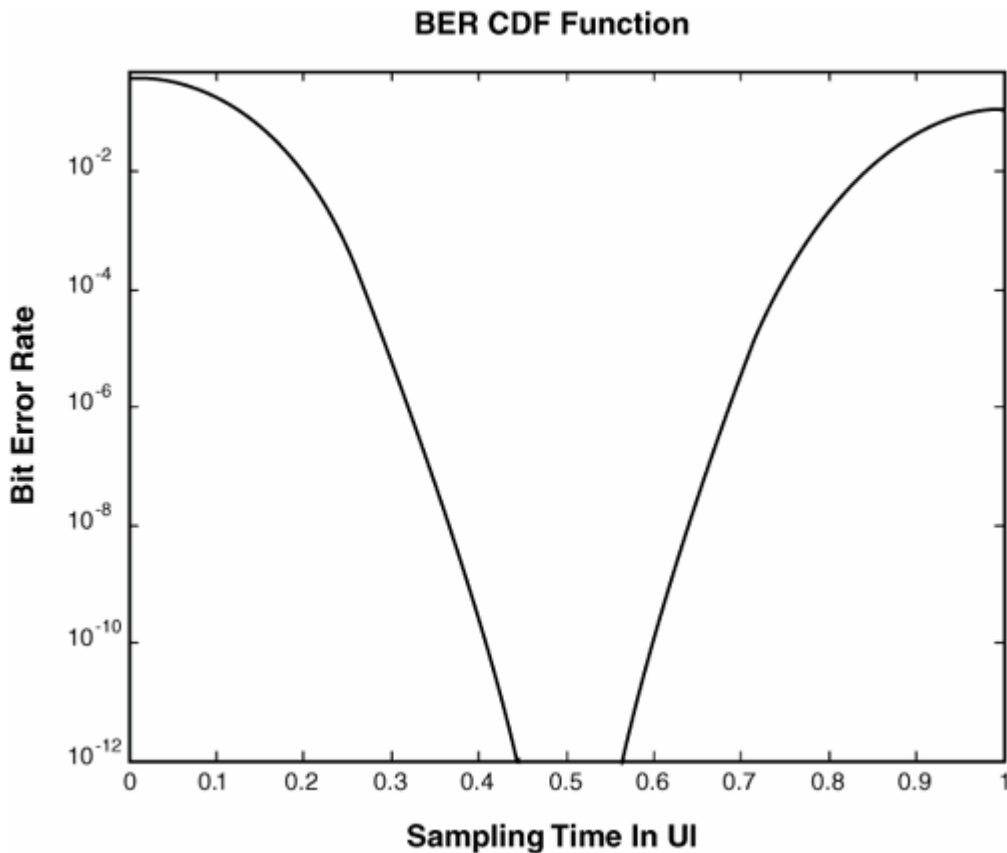
Equation 5.40

$$f_{BER}(t_s) = \frac{1}{2} C_0 \left\{ \left[P_p \operatorname{erfc}\left(\frac{t_s - D_p}{\sqrt{2}\sigma}\right) + P_n \operatorname{erfc}\left(\frac{t_s + D_n}{\sqrt{2}\sigma}\right) \right] + \dots \right. \\ \left. \left[P_p \operatorname{erfc}\left(\frac{T_0 - t_s + D_p}{\sqrt{2}\sigma}\right) + P_n \operatorname{erfc}\left(\frac{T_0 - t_s - D_n}{\sqrt{2}\sigma}\right) \right] \right\}$$

Clearly, the simple dual-Dirac DJ PDF model and the Gaussian RJ PDF model make the analytical solutions for both TJ PDF and BER CDF possible, enabling intuitive illustration and quick qualitative assessments. However, although dual-Dirac is useful, its limitations and accuracy must also be understood when it is used to solve practical problems.

[Figure 5.9](#) shows the BER CDF function using the analytical form of [equation 5.40](#). The simulation uses $C_0 = 50\%$ for the transition density and $P_n = 0.2$ and $P_p = 0.8$ for the left and right delta function probability for DJ PDF, respectively. DJ peak values are $D_n = 0.1$ UI and $D_p = 0.1$ UI, and RJ σ is 0.05 UI. The asymmetry of the DJ PDF is not easy to see in the BER CDF, but it is obvious in [Figure 5.8](#) of jitter PDF. Integration from jitter PDF to BER CDF tends to smooth or wash out the fine structures in PDF, making it hard to observe with BER CDF.

Figure 5.9. BER CDF simulation based on [equation 5.40](#), where DJ PDF is a dual-Dirac and RJ PDF is a Gaussian.



5.4.3. Accuracy for the Straight "Dual-Delta" DJ Model

As we mentioned, DJ can have any arbitrary PDF, depending on the exact root causes. Furthermore, the dual-Dirac model represents the "worst" DJ PDF as far as BER generation goes, because the edge transition always happens at the maximum jitter values for a dual-Dirac DJ PDF. The accuracy evaluation method used here has two steps. First, we consider the TJ estimation error when various DJ PDF functions are considered where DJ PDFs have the same pk-pk value. Second, we reverse the hypothesis and consider that if TJ at a certain BER such as 10^{-12} is the same for all different DJ PDFs, what will be an error due to the dual-Dirac DJ PDF assumption.

5.4.3.1. BER CDF Variation Error Given DJ PDFs

To study the DJ PDF variation and associated error, we consider three distinct DJ PDFs. The first is a dual-Dirac function. The second is a triangular function that is a "complementary" function to the dual-Dirac function. The third is a rectangular function representing a uniform distribution. The triangular PDF represents a "less damaging" scenario to the system because, most of the time, the edge transitions occur near the ideal timing (zero jitter) location. The occurrence rate decreases as the jitter gets bigger. The rectangular jitter PDF is between dual-Dirac and triangle in terms of its capability to cause a system BER. These qualitative predictions will become obvious when we present the simulation results next.

We start by illustrating PDFs for dual-Dirac, rectangular, and triangular in [Figure 5.10](#). The pk-pk value is chosen to be 0.2 UI, a typical DJ value allowed for the link budget (for example, the DJ budget is 0.2 UI in Fibre Channel 1 Gb/s jitter testing). All the DJ PDFs are assumed to be symmetrical. The random jitter PDF is a Gaussian having a form of [equation 5.1](#) with $\sigma = 0.05$ UI. The TJ PDFs are obtained via [equation 5.6](#) and are illustrated in [Figure 5.11](#). Note that an analytical TJ PDF for the dual-Dirac DJ has been given by [equation 5.38](#), with $D_p = D_n = 0.1$ UI, and $P_p = P_n = 0.5$.

Figure 5.10. DJ PDFs for dual-Dirac (solid line), rectangular (dotted line), and triangular (dash-dot). They all have the same pk-pk value of 0.2 UI with relative scaling.

Source: M. P. Li, J. Wilstrup, R. Jesson, and D. Petrich, "A New Method for Jitter Decomposition Through Its Distribution Tail Fitting," International Test Conference (ITC), 1999. (© 1999, IEEE)

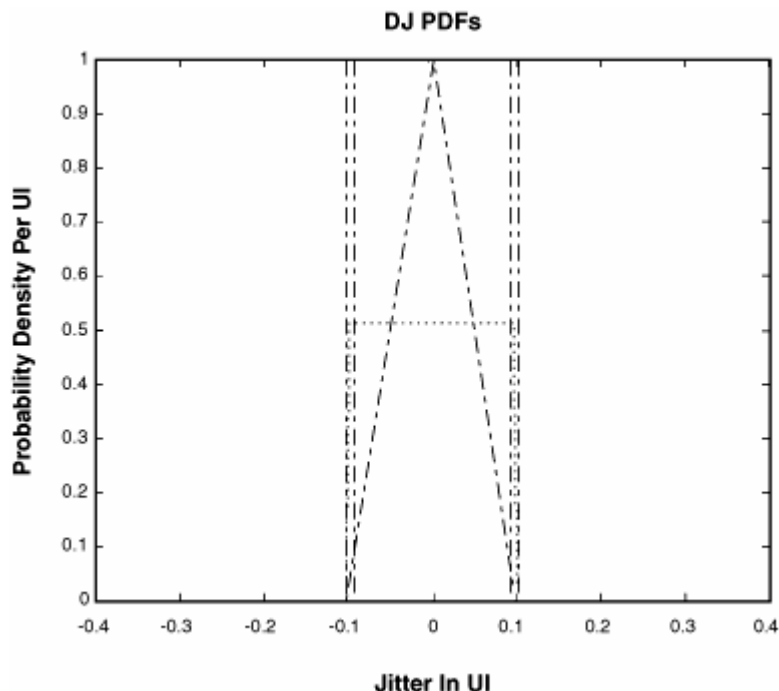
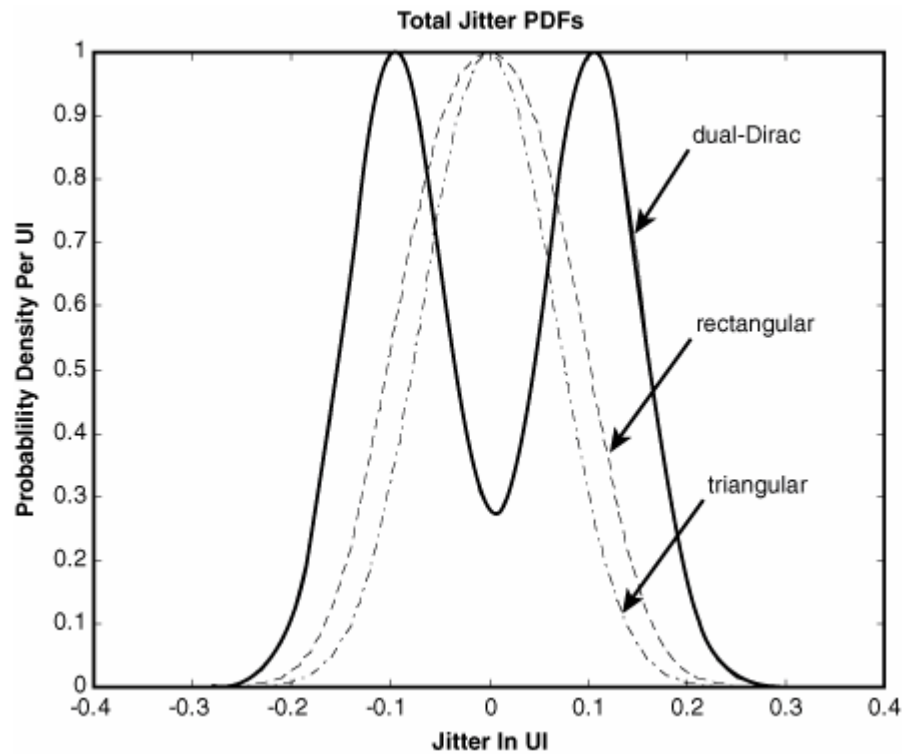


Figure 5.11. TJ PDFs corresponding to three distinct DJ PDFs and a simple RJ Gaussian.

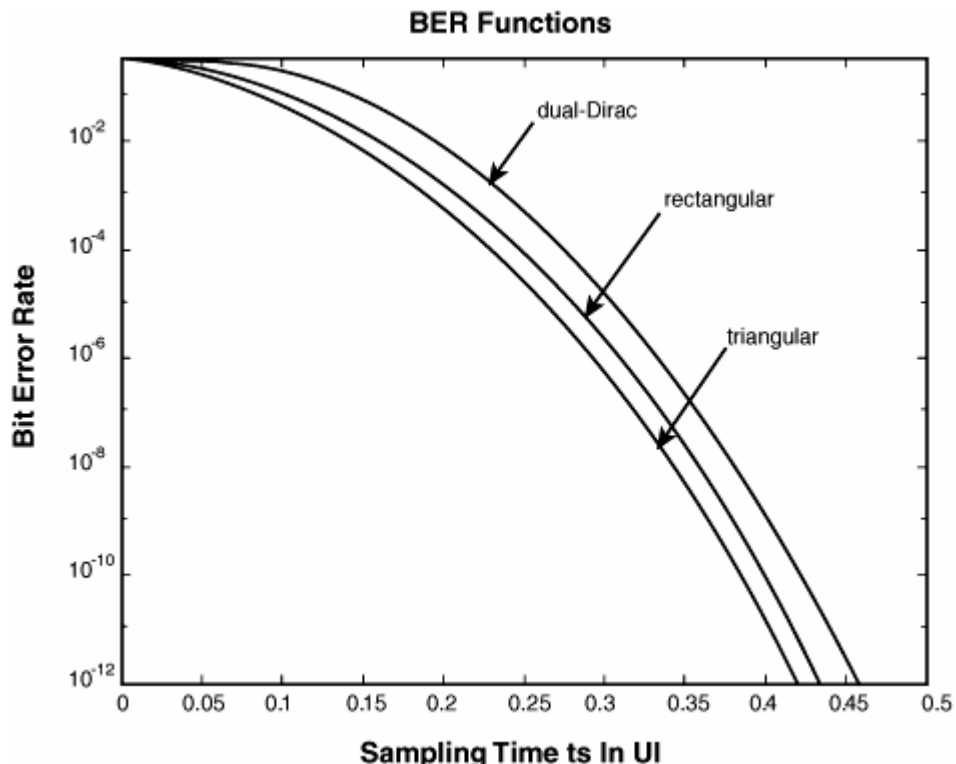
Source: M. P. Li, J. Wilstrup, R. Jesson, and D. Petrich, "A New Method for Jitter Decomposition Through Its Distribution Tail Fitting," International Test Conference (ITC), 1999. (© 1999, IEEE)



Knowing the TJ PDF, the BER CDF can be estimated according to equation 5.12. The results are shown in Figure 5.12. Here we also assume a 50% transition density. Note that for the dual-Dirac DJ PDF, the corresponding BER CDF is given by equation 5.40 analytically.

Figure 5.12. BER CDF estimation for three different DJ PDFs. Only the left side of the BER CDF is shown, and it is normalized so that at sampling time $t_s = 0$ UI, the BER CDF equals 0.5.

Source: M. P. Li, J. Wilstrup, R. Jesson, and D. Petrich, "A New Method for Jitter Decomposition Through Its Distribution Tail Fitting," International Test Conference (ITC), 1999. (© 1999, IEEE)



You can see that the dual-Dirac DJ PDF gives the highest TJ, while the triangular DJ PDF gives the lowest TJ, for a given BER value. In other words, for a given TJ value, the dual-Dirac DJ PDF gives the highest BER CDF, and the triangular DJ PDF gives the lowest BER CDF. [Table 5.2](#) lists the comparison results of TJ at BER = 10^{-12} .

Table 5.2. Comparison of TJ at BER = 10^{-12} ; Jitter Is in UI

DJ PDFs	DJ Pk-to-Pk	RJ σ	TJ at 10^{-12}	Diff	Diff%
Triangular	0.2	0.05	0.844	0	0
Rectangular	0.2	0.05	0.866	+0.022	2.6%
dual-Dirac	0.2	0.05	0.926	+0.082	9.7%

Source: M. P. Li, J. Wilstrup, R. Jesson, and D. Petrich, "A New Method for Jitter Decomposition Through Its Distribution Tail Fitting," International Test Conference (ITC), 1999. (© 1999, IEEE)

The TJ of the triangular PDF is used as the reference to estimate error. It is shown that the worst TJ difference is 0.082 UI, or 9.7%.

5.4.3.2. DJ Variation Error for a Given BER CDF Value

The purpose of the study in this section is to investigate how much variation there is in DJ pk-pk estimation when TJ at BER = 10^{-12} is given for these three different DJ PDFs. This is to emulate the case when DJ is estimated from the measured BER CDF function where the exact form of DJ PDF is unknown.

We have found that different BER CDF functions from different DJ PDFs can give rise to the same TJ value at a certain BER level. When the same TJ value is achieved, the DJ pk-pk values are significantly different for different forms of DJ PDF. The results are plotted in [Figure 5.13](#), and different DJ values are shown in [Table 5.3](#).

Figure 5.13. BER CDFs from different DJ PDFs give rise to the same TJ value at BER = 10^{-12} . A fixed RJ σ = 0.05 UI is used.

Source: M. P. Li, J. Wilstrup, R. Jesson, and D. Petrich, "A New Method for Jitter Decomposition Through Its Distribution Tail Fitting," International Test Conference (ITC), 1999. (© 1999, IEEE)

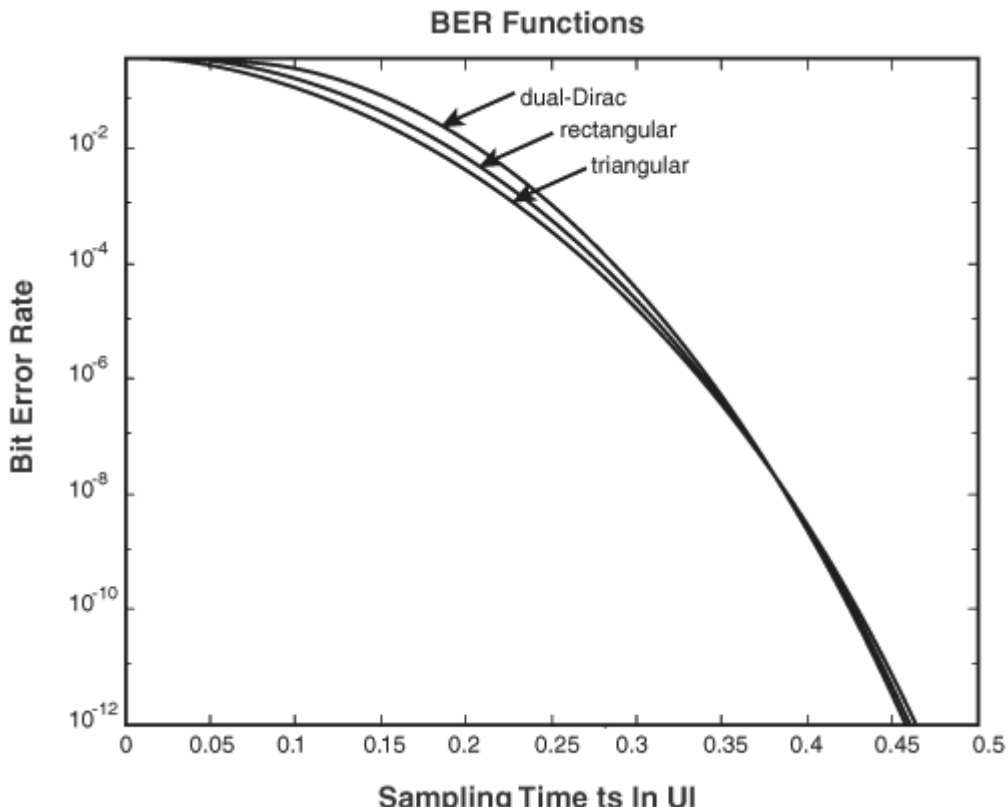


Table 5.3. The Same TJ Value from Different DJ PDFs

DJ PDFs	TJ at 10^{-12}	RJ σ	DJ Pk-Pk	DJ Diff	DJ Diff%
Triangular	0.926	0.05	0.31	0	0
Rectangular	0.929	0.05	0.27	-0.04	-12.9%
dual-Dirac	0.926	0.05	0.20	-0.11	-35.5%

Source: M. P. Li, J. Wilstrup, R. Jesson, and D. Petrich, "A New Method for Jitter Decomposition Through Its Distribution Tail Fitting," International Test Conference (ITC), 1999. (© 1999, IEEE)

Table 5.3 indicates that the differences in DJ pk-pk can be as high as 35%, or 0.11 UI, and they all give rise to the same (approximately) TJ at BER = 10^{-12} . This implies that DJ will be not well constrained if they were estimated from measured or simulated BER CDF with a straightforward dual-Dirac model (that is, without fitting). Moreover, the results in **Table 5.3** clearly show that a dual-Dirac PDF has the lowest DJ value, while the triangular DJ PDF has the highest DJ value when the same TJ at BER = 10^{-12} is achieved. This tells us that a dual-Dirac PDF can potentially overestimate the actual DJ pk-pk value if it is used to estimate the DJ based on a measured BER CDF. Although trying to cover all the DJ PDF scenarios can be time-consuming, you can intuitively see that this statement generally holds, especially when actual DJ PDF is not a dual-Dirac.

You have learned several very important facts and consequences when the dual-Dirac model is used for applications where DJ PDF is not a dual-Dirac without Tailfit:

- For the same DJ pk-pk value and the same RJ σ , the dual-Dirac method gives the highest TJ estimation among other common DJ PDFs.
- For the same RJ σ , to achieve the same TJ value at a certain BER level, DJ pk-pk values estimated from the dual-Dirac method will be the smallest among other common DJ PDFs.
- For a given BER CDF, the dual-Dirac method can overestimate actual RJ σ and underestimate DJ pk-pk value.
- The error in estimating DJ, RJ, and TJ varies, depending on the exact application. An error up to ~35% in DJ and RJ estimation is clear from a limited simulation, and up to 50% was observed from experiments.^[6]

These results strongly suggest that you must be careful when using the dual-Dirac DJ PDF model for practical jitter PDF and BER CDF analysis unless the DJ PDF is known to be a dual-Dirac.

URL <http://access.proquest.safaribooksonline.com/9780132429610/ch05lev1sec4>

User name: CSU San Diego

Book: Jitter, Noise, and Signal Integrity at High-Speed

Section: Chapter 5. Jitter and Noise Separation and Analysis in the Statistical Domain

No part of any chapter or book may be reproduced or transmitted in any form by any means without the prior written permission for reprints and excerpts from the publisher of the book or chapter. Redistribution or other use that violates the fair use privilege under U.S. copyright laws (see 17 USC107) or that otherwise violates these Terms of Service is strictly prohibited. Violators will be prosecuted to the full extent of U.S. Federal and Massachusetts laws.

Information Theory Computer Science Mike Peng Li Prentice Hall Jitter, Noise, and Signal Integrity at High-Speed

5.5. Summary

This chapter started by describing why jitter separation is needed, from the viewpoints of understanding the jitter process, as well as the practical values of having jitter components such as DJ and RJ. We then moved to the details of separating jitter into its components based on the jitter PDF in [section 5.2](#). The Tailfit method was introduced, covering theory, simulation, and experimental results. The key is that the tail parts of the PDF are dominated by the random jitter process, and it can best be modeled by a Gaussian distribution. The Tailfit method gives rise to the parameters defining the tail Gaussian distribution, including means and sigmas, and that in turn yield DJ pk-pk estimation and RJ sigma estimations. DJ PDF determination via deconvolution also was discussed in this section. [Section 5.3](#) introduced the Tailfit algorithm application and implementation BER CDF as the base function. Two scenarios were considered: the raw BER CDF-based, and the Q-space-based involving the transformation for both base data function and base model from BER CDF space to Q-space. In BER CDF space, Gaussian function becomes an integrated Gaussian, which is essentially a complementary error function, and in the Q-space, the Gaussian function becomes a linear function. The advantages and disadvantages of Tailfit in each space were also given. A quick and conditional accurate linear equation method for estimating TJ was derived under interesting DJ, RJ, and BER conditions. [Section 5.4](#) discussed the accuracy of using the dual-Dirac as the model for the DJ PDF as a straightforward application without involving the tailfit. The results suggest that the error can be significant and caution must be exercised when using dual-Dirac DJ PDF for an arbitrary DJ PDF.

URL <http://access.proquest.safaribooksonline.com/9780132429610/ch05lev1sec5>

User name: CSU San Diego

Book: Jitter, Noise, and Signal Integrity at High-Speed

Section: Chapter 5. Jitter and Noise Separation and Analysis in the Statistical Domain

No part of any chapter or book may be reproduced or transmitted in any form by any means without the prior written permission for reprints and excerpts from the publisher of the book or chapter. Redistribution or other use that violates the fair use privilege under U.S. copyright laws (see 17 USC107) or that otherwise violates these Terms of Service is strictly prohibited. Violators will be prosecuted to the full extent of U.S. Federal and Massachusetts laws.

Information Theory Computer Science Mike Peng Li Prentice Hall Jitter, Noise, and Signal Integrity at High-Speed

Endnotes

1. M. P. Li, J. Wilstrup, R. Jesson, and D. Petrich, "A New Method for Jitter Decomposition Through Its Distribution Tail Fitting," IEEE International Test Conference (ITC), 1999.
2. P. R. Bevington and D. K. Robinson, *Data Reduction and Error Analysis for the Physical Sciences*, McGraw-Hill, Inc., 1992.
3. Knuth, D. E., *Seminumerical Algorithm*, Second Edition, Addison-Wesley, 1981.
4. J. Sun, M. Li, and J. Wilstrup, "A Demonstration of Deterministic Jitter (DJ)," IEEE Instrumentation and Measurement Technology Conference (IMTC), 2002.
5. G. Arfken, *Mathematical Methods for Physicists*, Third Edition, Academic Press, Inc., 1985.
6. M. P. Li and J. Wilstrup, "On the Accuracy of Jitter Separation from Bit Error Rate Function," IEEE International Test Conference (ITC), 2002.

URL <http://access.proquest.safaribooksonline.com/9780132429610/ch05lev1sec6>

User name: CSU San Diego

Book: Jitter, Noise, and Signal Integrity at High-Speed

No part of any chapter or book may be reproduced or transmitted in any form by any means without the prior written permission for reprints and excerpts from the publisher of the book or chapter. Redistribution or other use that violates the fair use privilege under U.S. copyright laws (see 17 USC107) or that otherwise violates these Terms of Service is strictly prohibited. Violators will be prosecuted to the full extent of U.S. Federal and Massachusetts laws.

Information Theory Computer Science Mike Peng Li Prentice Hall Jitter, Noise, and Signal Integrity at High-Speed

6. Jitter and Noise Separation and Analysis in the Time and Frequency Domains

Chapter 5, "Jitter and Noise Separation and Analysis in the Statistical Domain," introduced jitter separation and analysis in statistical domains based on PDF or BER CDF functions. This chapter focuses on jitter separation in the time and frequency domains based on the jitter time record, frequency spectrum, or power spectrum. This chapter covers first-layer jitter components of DJ and RJ, and second- and third-layer jitter components such as DDJ, DCD, ISI, BUJ, and PJ. Various time and frequency domain separation methods are also compared.

URL <http://access.proquest.safaribooksonline.com/9780132429610/ch06>

User name: CSU San Diego

Book: Jitter, Noise, and Signal Integrity at High-Speed

Section: Chapter 6. Jitter and Noise Separation and Analysis in the Time and Frequency Domains

No part of any chapter or book may be reproduced or transmitted in any form by any means without the prior written permission for reprints and excerpts from the publisher of the book or chapter. Redistribution or other use that violates the fair use privilege under U.S. copyright laws (see 17 USC107) or that otherwise violates these Terms of Service is strictly prohibited. Violators will be prosecuted to the full extent of U.S. Federal and Massachusetts laws.

Information Theory Computer Science Mike Peng Li Prentice Hall Jitter, Noise, and Signal Integrity at High-Speed

6.1. Time and Frequency Domain Representations

Chapter 5 introduced jitter separation in the statistical domain based on jitter PDF or CDF. Because jitter is fundamentally a statistical signal process, it can also be handled in the time or frequency domain. This chapter focuses on the time-frequency domain jitter separation.

6.1.1. Jitter as a Function of Time

Chapter 1, "Introduction," mentioned that jitter is any time deviation Δt referenced to an ideal timing signal, such as an ideal bit clock, used in digital communication. Δt may contain all the jitter components. Furthermore, jitter can be measured or observed only when an edge transition exists. This means that jitter is also a function of sampling times—namely, $\Delta t(t_n)$. Because $\Delta t(t_n)$ can be measured m times for a given time location t_n , we will represent a generic jitter in the form of $\Delta t_m(t_n)$. Using this concept, we can represent the instant jitter in terms of its components of data-dependent jitter (DDJ), periodic jitter (PJ), bounded uncorrelated jitter (BUJ), and random jitter (RJ) using the following equation:

Equation 6.1

$$\Delta t_m(t_n) = \Delta t_{DDJ_m}(t_n) + \Delta t_{PJ_m}(t_n) + \Delta t_{BUJ_m}(t_n) + \Delta t_{RJ_m}(t_n)$$

Many mathematical operations can be applied to time-domain equation 6.1 to estimate jitter components of various kinds.

6.1.2. Jitter as a Function of Frequency

If a time-to-frequency domain operation or transfer is made to equation 6.1, the jitter frequency representation is obtained. The transformation operation can be a Fourier Transformation (FT), a Discrete Fourier Transformation (DFT), or a Laplace Transformation (LT), and so on. The frequency domain representation has a separate magnitude and phase part if a real frequency state variable is used. If a complex frequency s is used as the state variable, as in the case of LT, one representation is enough, because both magnitude and phase are contained in the complex s domain. For simplicity, we will use an FT operation and show only the magnitude part of the frequency domain representation. In the actual implementation of the time-frequency domain transformation, a fast operation such as a Fast Fourier Transformation (FFT) may be used.

6.1.2.1. Direct FT Spectrum

Performing an FT operation on both sides of equation 6.1, we get the following frequency domain representation for jitter and its components:

Equation 6.2

[\[View full size image\]](#)

$$FT[\Delta t_m(t_n)] = FT[\Delta t_{DDJ_m}(t_n)] + FT[\Delta t_{PJ_m}(t_n)] + FT[\Delta t_{BUJ_m}(t_n)] + FT[\Delta t_{RJ_m}(t_n)]$$

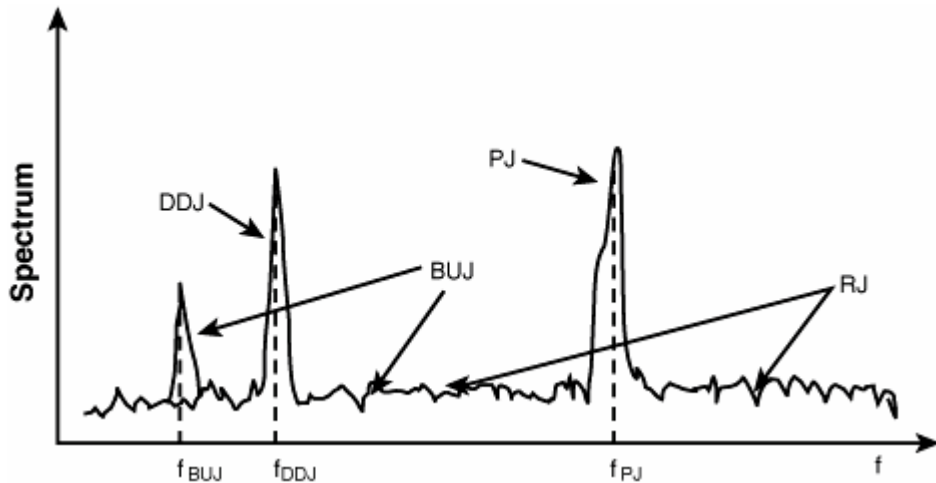
Each term in [equation 6.2](#) represents the spectrum (first order) of its corresponding jitter. We will use the uppercase to represent the jitter spectrum in the frequency domain. [Equation 6.2](#) can be rewritten as follows:

Equation 6.3

$$\Delta T_m(f_l) = \Delta T_{DDJ_m}(f_l) + \Delta T_{PJ_m}(f_l) + \Delta T_{BUJ_m}(f_l) + \Delta T_{RJ_m}(f_l)$$

where l is the subindex of the discrete frequency. Even though the features and characteristics of overall jitter are complicated, its components have certain and unique characteristics. For example, periodic jitter shows up as spikes or spectral lines in the frequency domain, making it easier to identify and quantify this jitter component compared with a time-domain analysis. In another example, where DDJ is associated with a repeating pattern, DDJ also shows up as spikes or spectral lines. Their frequency is integer multiples of the pattern frequency f_{patt} , where $f_{patt} = 1/(N_{patt} * UI)$ and N_{patt} is the length of the pattern in terms of UI. BUJ and RJ show up as broadband bounded background noise. [Figure 6.1](#) shows the jitter spectrum containing all jitter components.

Figure 6.1. Magnitude of jitter Fourier spectrum, with all the components present. The DDJ frequency satisfies $f_{DDJ} = n * f_{patt}$, where n is an integer and f_{patt} is the pattern length associated frequency.



Obviously, DDJ and PJ belong to the so-called "narrow-band" class. The major distinction between DDJ and PJ is that the DDJ frequency satisfies $f_{DDJ} = n * f_{patt}$, whereas a PJ does not satisfy this relationship in general. However, when $f_{DDJ} = f_{PJ}$, DDJ and PJ cannot be separated in this jitter spectrum-based separation method. There are two types of BUJ: "narrow-band" and high-magnitude, and "broadband" and low-magnitude. Obviously, "narrow-band" BUJ is indistinguishable from regular PJ unless its root cause is known beforehand. "Broadband" BUJ is indistinguishable from RJ in general, unless its magnitude and frequency range are known beforehand, or the RJ spectrum shape and magnitude are known beforehand.

To estimate jitter energy within certain frequency bands, PSD is needed, and that is different from the Fourier spectrum. In practice, you may use the Fourier spectrum to estimate the PSD over a time period T by considering the following:

Equation 6.4

$$S(f_l, T) = \frac{|\Delta T_m(f_l)|^2}{T}$$

However, it has been shown^[1] that [equation 6.4](#) cannot approach the true PSD $S(f)$, even when T approaches infinity. Thus, the Fourier spectrum does not provide a rational linkage to PSD for a given random process. Using [equation 6.4](#) to estimate PSD and subsequent jitter energy is an approximation; it does not stand on solid theoretical ground or warrant necessary accuracy.

6.1.2.2. Jitter PSD

For a random process, what is interesting is how its energy is distributed over the frequency, not the spectrum that is phase-dependent. Section 2.5.5 in [Chapter 2](#), "Statistical Signal and Linear Theory for Jitter, Noise, and Signal Integrity," established the math foundation for estimating the PSD for a random process under the condition of wide-sense stationary (WSS). We need to start with the estimation of autocorrelation function to calculate the PSD. Taking the autocorrelation function operation of [equation 6.1](#), we get the following:

Equation 6.5

[\[View full size image\]](#)

$$R_{\Delta t}(\tau_n) = R_{DDJ}(\tau_n) + R_{PJ}(\tau_n) + R_{BUJ}(\tau_n) + R_{RJ}(\tau_n) + \sum_{i,j} R_{ij-jj}(\tau_n)$$

where R_{ij-jj} are the cross-correlation functions between various jitter types. Because the sources of those different jitter types are distinctly different, it is not unreasonable to assume that they are independent or uncorrelated. The means for PJ, BUJ, and RJ are 0 by

$$\sum_{i,j} R_{ij-jj}(\tau) = 0$$

definition. Therefore, the cross-correlation functions are 0s—namely, . Because of this property, [equation 6.4](#) becomes

Equation 6.6

$$R_{\Delta t}(\tau_n) = R_{DDJ}(\tau_n) + R_{PJ}(\tau_n) + R_{BUJ}(\tau_n) + R_{RJ}(\tau_n)$$

Then, applying the FT to both sides of the equation, we get the following:

Equation 6.7

$$FT[R_{\Delta t}(\tau_n)] = FT[R_{DDJ}(\tau_n)] + FT[R_{PJ}(\tau_n)] + FT[R_{BUJ}(\tau_n)] + FT[R_{RJ}(\tau_n)]$$

Because an FT of the autocorrelation function gives rise to the PSD, [equation 6.6](#) yields the following:

Equation 6.8

$$S_{\Delta t}(f_l) = S_{DDJ}(f_l) + S_{PJ}(f_l) + S_{BUJ}(f_l) + S_{RJ}(f_l)$$

[Equation 6.8](#) suggests that the overall jitter PSD equals the sum of individual component jitter PSDs. Superimposition works in this case because those jitter components are all independent and uncorrelated, and all the cross-spectral density vanished.

URL <http://access.proquest.safaribooksonline.com/9780132429610/ch06lev1sec1>

User name: CSU San Diego

Book: Jitter, Noise, and Signal Integrity at High-Speed

Section: Chapter 6. Jitter and Noise Separation and Analysis in the Time and Frequency Domains

No part of any chapter or book may be reproduced or transmitted in any form by any means without the prior written permission for reprints and excerpts from the publisher of the book or chapter. Redistribution or other use that violates the fair use privilege under U.S. copyright laws (see 17 USC107) or that otherwise violates these Terms of Service is strictly prohibited. Violators will be prosecuted to the full extent of U.S. Federal and Massachusetts laws.

Information Theory Computer Science Mike Peng Li Prentice Hall Jitter, Noise, and Signal Integrity at High-Speed

6.2. DDJ Separation

This section discusses DDJ separation methods based on jitter time-domain record, frequency-domain spectrum, and PSD. In the end, we will discuss how to separate DDJ into its components of DCD and ISI.

6.2.1. Based on Jitter Time Function

By applying the average operation to [equation 6.1](#) over the number of measurements M for all the sampling times indexed by n, we get the following:

Equation 6.9

[\[View full size image\]](#)

$$\frac{1}{M} \sum_{m=1}^M \Delta t_m(t_n) = \frac{1}{M} \left[\sum_{m=1}^M \Delta t_{DDJ_m}(t_n) + \sum_{m=1}^M \Delta t_{PJ_m}(t_n) + \sum_{m=1}^M \Delta t_{BUJ_m}(t_n) + \sum_{m=1}^M \Delta t_{RJ_m}(t_n) \right]$$

The average of all PJ, BUJ, and RJ gives rise to 0 if the sample size and record are large enough, because they are uncorrelated to the data pattern. DDJ is static, and the average will not change its value. Therefore, [equation 6.9](#) becomes

Equation 6.10

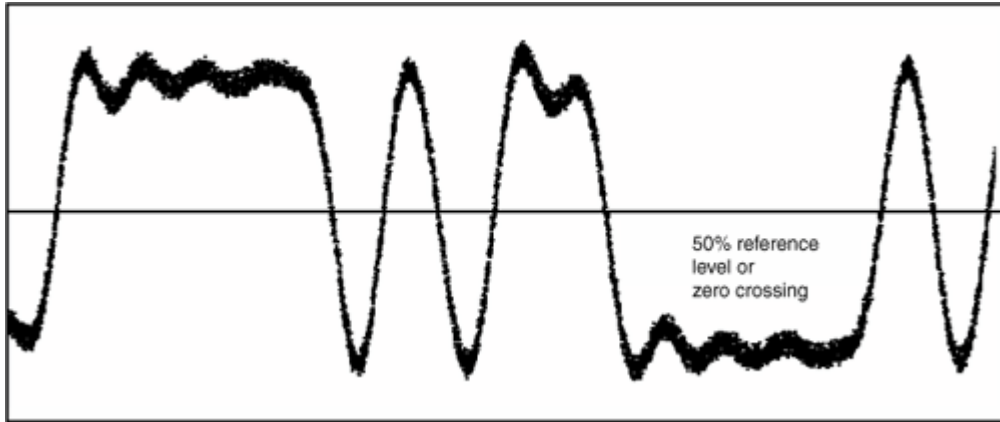
$$\frac{1}{M} \sum_{m=1}^M \Delta t_m(t_n) = \Delta t_{DDJ_m}(t_n)$$

[Equation 6.10](#) gives a quantitative way to estimate DDJ from the generic jitter Δt time record in the time domain. In the context of data communication, the jitter test or estimation is generally performed using a certain repeating test pattern with a fixed number of transitions.

To put [equations 6.9](#) and [6.10](#) into perspective, [Figure 6.2](#) shows a digital waveform (a 20-bit long K28.5 pattern commonly used in high-speed testing) that has jitter components of DDJ, PJ, and RJ. DDJ is due to the limited bandwidth of the medium where the high-speed signal passes through. PJ and RJ are due to the amplitude modulation of both periodic and random noises to the signal.

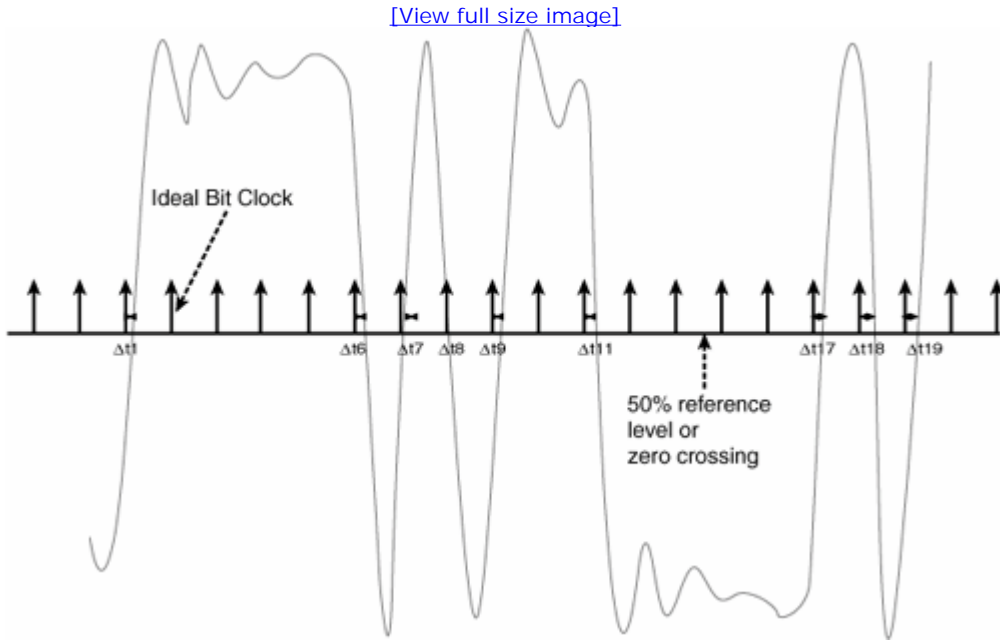
Figure 6.2. A digital waveform with DDJ, PJ, and RJ at its 50% reference level.

[\[View full size image\]](#)



Performing the averaging for the waveform shown in Figure 6.2, we obtain the waveform shown in Figure 6.3, where pattern uncorrelated jitter PJ and RJ both average out. Therefore, the edge transition deviation relative to the ideal bit clock gives rise to DDJ estimation.

Figure 6.3. The averaged waveform of Figure 6.2. Note that PJ and RJ are averaged out so that edge transition deviation relative to the ideal clock is DDJ only.



The DDJ PDF can be built based on the DDJ time record given by equation 6.10 through the histogram binning:

Equation 6.11

$$f_{DDJ}(\Delta t) = \text{Hist}(\Delta t_{DDJ_m}(t_n))$$

where Hist represents the histogram binning function.

Time-domain DDJ was first developed by [2].

6.2.2. Based on Fourier Spectrum or PSD

DDJ can be estimated in the frequency domain via Fourier spectrum or PSD. The criteria are that DDJ magnitude in the frequency

domain needs to be a few sigmas above the background RJ and BUJ spectrum, and DDJ frequency needs to be integer multiples of the pattern repeating frequency. In other words, when the following conditions are satisfied, a DDJ is identified. For Fourier spectrum-based identification, the criteria are as follows:

Equation 6.12

$$\Delta T(f_l) \geq N\sigma_{FS} \quad \text{and} \quad f_l = n * f_{patt}$$

where σ_{FS} is the background rms for the Fourier spectrum and N is the threshold level. Typically N satisfies that $N \geq 3$. When $N = 3$, a 99.97% statistical confidence level is warranted (see [section 3.2.1.1](#)). Fourier spectrum-based DDJ separation can also be found in [\[3\]](#).

For a PSD-based identification, the criteria are as follows:

Equation 6.13

$$S_{\Delta t}(f_l) \geq N\sigma_{PSD} \quad \text{and} \quad f_l = n * f_{patt}$$

where σ_{PSD} is the rms for the PSD, and the N threshold level is similar to the case of Fourier spectrum-based DDJ separation.

The number of DDJ spikes is determined by the pattern length, transition density, run length, and so on. If $\Delta t_{DDJ}(f_l)$ is the peak value of DDJ at frequency f_l , the DDJ PDF will be

Equation 6.14

$$f_{DDJ}(\Delta t) = Hist(\Delta t_{DDJ}(f_l))$$

This is very similar to [equation 6.11](#), in which DDJ is determined through time-domain average.

6.2.3. DCD and ISI Separation from DDJ

Before we get into DCD and ISI separation from DDJ, let us first review their definitions.

DCD is duty cycle distortion. DCD can be caused by variations in the reference voltage level used to determine the pulse width. It also can be caused by different propagation delays for positive and negative data transitions.

ISI is intersymbol interference. ISI is caused by a data path propagation delay that is a function of past data history and occurs in all finite bandwidth data paths.

DDJ is composed of both DCD and ISI.

Let us assume that the PDFs for DDJ rising and falling edges are f_{DDJ_r} and f_{DDJ_f} respectively. We have the following relationship:

Equation 6.15

$$f_{DDJ}(\Delta t) = f_{DDJ_r}(\Delta t) + f_{DDJ_f}(\Delta t)$$

We define the maximum PDF corresponding jitter location as Δt_{max_r} and Δt_{max_f} for rising and falling edges, respectively. The ISI PDF is the DDJ PDF when Δt_{max_r} and Δt_{max_f} are identical because, by definition, if there is no DCD, rising- and falling-edge PDFs should be lined up. This can be achieved by the following math operation:

Equation 6.16

[\[View full size image\]](#)

$$f_{ISI}(\Delta t) = \frac{1}{2} [f_{DDJ_r}(\Delta t - \frac{\Delta t_{max_f} - \Delta t_{max_r}}{2}) + f_{DDJ_f}(\Delta t + \frac{\Delta t_{max_f} - \Delta t_{max_r}}{2})]$$

when $\Delta t_{max_f} \geq \Delta t_{max_r}$. and

Equation 6.17

[\[View full size image\]](#)

$$f_{ISI}(\Delta t) = \frac{1}{2} [f_{DDJ_f}(\Delta t - \frac{\Delta t_{max_r} - \Delta t_{max_l}}{2}) + f_{DDJ_r}(\Delta t + \frac{\Delta t_{max_r} - \Delta t_{max_l}}{2})]$$

when $\Delta t_{max_r} \geq \Delta t_{max_l}$.

Because DDJ is composed of DCD and ISI, and their PDFs are linked through the convolution process, DCD PDF can be obtained through the following deconvolution process:

Equation 6.18

$$f_{DCD}(\Delta t) = f_{DDJ}(\Delta t)^{*^{-1}} f_{ISI}(\Delta t)$$

where $*^{-1}$ denotes the deconvolution operation.

In the case when both rising- and falling-edge DDJ PDFs are symmetrical, with only one peak, DCD PDF is simply a dual-Dirac delta function represented by the following:

Equation 6.19

$$f_{DCD}(\Delta t) = \frac{1}{2} [\delta(\Delta t - \Delta t_{max_f}) + \delta(\Delta t + \Delta t_{max_r})]$$

and its pk-pk value in this case is $\Delta t_{max_f} - \Delta t_{max_r}$ for $\Delta t_{max_f} \geq \Delta t_{max_r}$.

In the case when $\Delta t_{max_f} \leq \Delta t_{max_r}$, we have

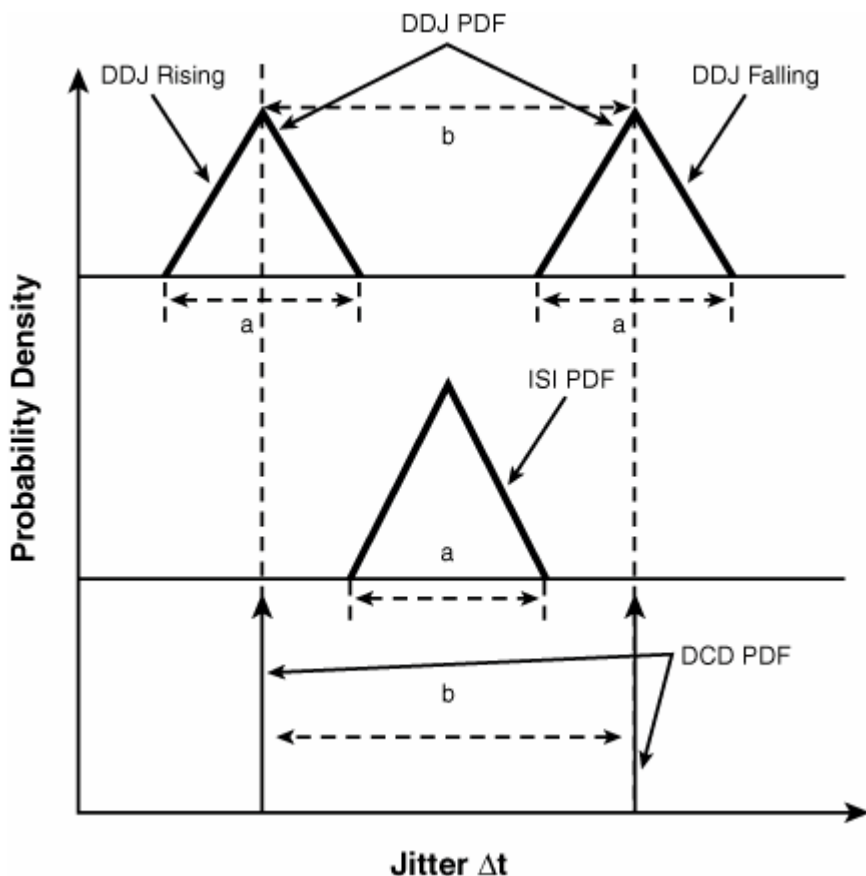
Equation 6.20

$$f_{DCD}(\Delta t) = \frac{1}{2} [\delta(\Delta t - \Delta t_{max_r}) + \delta(\Delta t + \Delta t_{max_f})]$$

with a pk-pk value of $\Delta t_{max_r} - \Delta t_{max_f}$.

Figure 6.4 shows the relationship between DDJ, DCD, and ISI in a single graph. For simplicity, the rising-edge PDF and falling-edge PDF are identical and have only single peaks. We consider the case of $\Delta t_{max_f} \geq \Delta t_{max_r}$. According to [equation 6.16](#), ISI PDF is the superimposition of the rising- and falling-edge PDFs when their peaks are aligned. Because rising- and falling-edge PDFs are identical and have a pk-pk value of a, the ISI PDF derived from [equation 6.16](#) also has the same PDF with the same pk-pk value a. With DDJ and ISI PDFs, DCD PDF can be estimated via [equation 6.18](#) of deconvolution, yielding a dual-Dirac PDF for DCD.

Figure 6.4. PDFs for a DDJ and its components of ISI and DCD. DDJ rising- and falling-edge PDFs are single-peaked and symmetrical.



URL <http://access.proquest.safaribooksonline.com/9780132429610/ch06lev1sec2>

User name: CSU San Diego

Book: Jitter, Noise, and Signal Integrity at High-Speed

Section: Chapter 6. Jitter and Noise Separation and Analysis in the Time and Frequency Domains

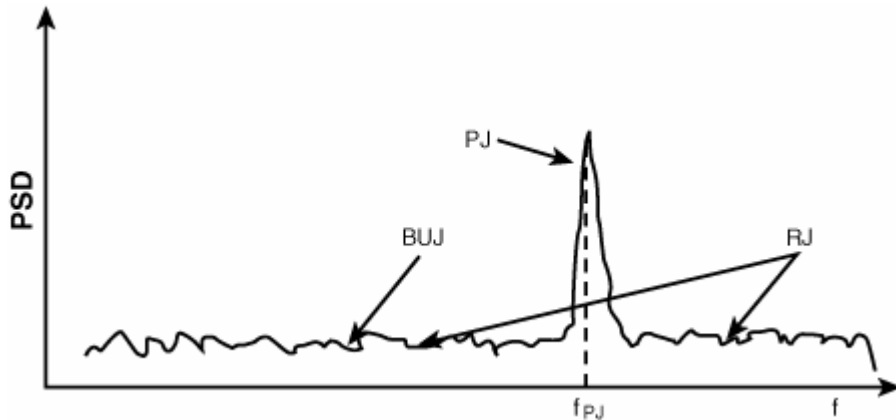
No part of any chapter or book may be reproduced or transmitted in any form by any means without the prior written permission for reprints and excerpts from the publisher of the book or chapter. Redistribution or other use that violates the fair use privilege under U.S. copyright laws (see 17 USC107) or that otherwise violates these Terms of Service is strictly prohibited. Violators will be prosecuted to the full extent of U.S. Federal and Massachusetts laws.

Information Theory Computer Science Mike Peng Li Prentice Hall Jitter, Noise, and Signal Integrity at High-Speed

6.3. PJ, RJ, and BUJ Separation

PJ and RJ separation in the frequency domain will be discussed under the assumption that DDJ spikes have been removed from either the Fourier spectrum or PSD functions, as discussed in the preceding section. [Figure 6.5](#) shows a PSD function without any DDJ spikes.

Figure 6.5. This PSD function contains PJ, RJ, and BUJ. DDJ spikes have been removed.



6.3.1. Based on the Fourier Spectrum

The Fourier spectrum in this case contains PJ, BUJ, and RJ. PJ appears as spikes or spectral lines. The PJ identification is based solely on its magnitude relative to the neighboring RJ and BUJ background. Any spectral lines that satisfy the following condition:

Equation 6.21

$$\Delta T(f_l) \geq N\sigma_{FS}$$

are identified as a PJ. The definitions of N and σ_{FS} are similar to those defined in [equation 6.12](#). Many PJs may be identified. To get the overall PJ PDF from many individual PJs, PJ phase information is needed. PJs follow the superimposition rule, so the overall PDF can be established through the following relation:

Equation 6.22

$$f_{PJ}(\Delta t) = \text{Hist}[\sum_{l=1}^L \Delta t_{PJ_l} \sin(2\pi f_l t_n + \phi_l)], n = 1, 2, \dots, N$$

where Δt_{PJ_l} , f_l , and ϕ_l are the peak value, frequency, and phase, respectively, for an individual l th PJ, and the summation is done over all the L PJs, with sampling times of t_1 to t_N .

When the PJs are identified and estimated, they can all be removed from the spectrum. However, Fourier spectrum is not PSD. Approximated conversion of Fourier spectrum to PSD must be done through [equation 6.4](#) and will not result in an accurate RJ estimation, as discussed in section 6.1.3.1. The RJ rms can be estimated via the following equation over an interested frequency range between f_L and f_H :

Equation 6.23

$$\sigma_{RJ} = \int_{f_L}^{f_H} S(f, T) df$$

As soon as the RJ rms value is determined, its PDF is a Gaussian with the same rms or sigma value, assuming that the PSD is white.

Broadband BUJ is hard to separate from the RJ in the Fourier spectrum domain in general. As such, the RJ estimation may be inflated due to the presence of broadband BUJ in the Fourier spectrum.

One exception is that BUJ presence is under a controlled experiment or operation. For example, if the BUJ is caused by crosstalk from neighboring channels, BUJ can be estimated through two measurements. One uses the neighboring channel in quiescent mode and measures the PSD of RJ. Another method uses the neighboring channels in active mode and measures the PSD of RJ and BUJ. Because PSD follows the superimposition, the BUJ PSD can be estimated by taking the difference of the two PSDs measured. The result is the BUJ PSD estimation.

6.3.2. Based on PSD

There are similarities and differences between Fourier spectrum and PSD-based jitter separation. The PJ identification is similar to using the Fourier spectrum. Any spectral lines that satisfy the following condition:

Equation 6.24

$$S_{\Delta t}(f_l) \geq N\sigma_{PSD}$$

are identified as a PJ. The definitions of N and σ_{PSD} are similar to those defined in [equation 6.13](#). Many PJs might be identified. However, no phase information is available in the PSD, because power is a scalar, not a vector. To get the overall PJ PDF from many individual PJs, the PJ phase information needs to be assumed, unlike the case of Fourier spectrum-based PJ separation. If there are many independent PJs, it may not be a bad idea to assume that their phases are randomly distributed, as shown in [section 3.1.2](#). Under this assumption, the overall PJ PDF can be established through the following relation:

Equation 6.25

$$f_{PJ}(\Delta t) = \text{Hist}[\sum_{l=1}^L \Delta t_{PJ_l} \sin(2\pi f_l t_n + \phi_l)], n = 1, 2, \dots, N$$

where Δt_{PJ_l} , f_l , and ϕ_l have the same meanings as in [equation 6.20](#), except here the phases ϕ_l are assumed to be randomly and uniformly distributed, rather than determined, as in the case of Fourier spectrum-based separation.

The RJ PSD is obtained by removing all the PJs identified. The RJ rms can be estimated via the following equation over an interested frequency range between f_L and f_H :

Equation 6.26

$$\sigma_{RJ} = \sqrt{\int_{f_L}^{f_H} S_{\Delta t}(f) df}$$

This is the only accurate and correct way to estimate RJ rms over a certain frequency band. As soon as the RJ rms value is determined, its PDF is a Gaussian with the same rms or sigma value if the PSD is a Gaussian.

As we have mentioned, broadband BUJ is hard to separate from the RJ in the PSD domain too. Therefore, the RJ estimation can be inflated because of the presence of broadband BUJ in the PSD.

As mentioned in [section 6.3.1](#), broadband BUJ can be determined with two PSD measurements and by estimating the difference residual if its presence can be controlled.

6.3.3. Based on Time-Domain Variance Function

PJ and RJ can be separated in the time domain given that jitter time record is available. We will start with the simplest model for PJ and RJ (DDJ has been separated at this stage), taking the sum of several sinusoidal signals (PJs) and the additive Gaussian white noise (RJ):

Equation 6.27

$$\Delta t(t) = \Delta t_{PJ}(t) + \Delta t_{RJ}(t) = \sum_{l=1}^L \Delta t_{PJ_l} \sin(2\pi f_l t + \phi_l) + \Delta t_{RJ}(t)$$

where Δt_{PJ_l} , f_l , and ϕ_l are the amplitude, frequency, and initial phase of the PJs, respectively. $\Delta t(t)$ denotes the jitter signal, and $\Delta t_{RJ}(t)$ is the zero mean Gaussian white noise with a variance of σ_{RJ}^2 .

The goal here is to accurately estimate the number of PJs (L), their amplitudes and frequencies ($\Delta t_{PJ_l}, f_l$), and the RJ variance (σ_{RJ}^2).

The mean, variance, and autocorrelation function for $\Delta t(t)$ can be written as follows:

Equation 6.28

$$\left\{ \begin{array}{l} \mu_t = \lim_{T \rightarrow \infty} \frac{1}{T} \int_0^T \Delta t(t) dt = 0 \\ \sigma_0^2 = \lim_{T \rightarrow \infty} \frac{1}{T} \int_0^T (\Delta t(t) - \mu_t)^2 dt = \sum_{l=1}^L \frac{\Delta t_{PJ_l}^2}{2} + \sigma_{RJ}^2 \\ R_t(\tau) = \sum_{l=1}^L \frac{\Delta t_{PJ_l}^2}{2} \cos(2\pi f_l \tau) + \sigma_{RJ}^2 \delta(\tau) \end{array} \right.$$

where δ represents the Dirac delta function and τ is the time lag for the autocorrelation. In this case, the mean and variance are constant, and the autocorrelation is a function of only the time lag. In other words, all of them are independent of the time translation.

From the theoretical expression of the autocorrelation $R_{\Delta t}(\tau)$ in [equation 6.28](#), jitter variance (RJ variance) σ_n^2 can easily be estimated by averaging the integral of the autocorrelation function.

There are a few ways to solve [equation 6.28](#) to find the solutions for PJ and RJ parameters. Two methods are worth mentioning because they are commonly used in mainstream digital signal processing. The first method converts the [equation 6.28](#) into a matrix format and solves it with eigenvalue and eigen function. (Refer to [\[4\]](#) for more details.) The second method solves [equation 6.28](#) through iterative optimization. We will discuss this method in depth here because it is relatively intuitive.

The variance record of the overall PJ and RJ relates to its autocorrelation function through

Equation 6.29

$$\sigma_{\Delta t}^2(\tau) = 2[\sigma_0^2 - R_{\Delta t}(\tau)]$$

where σ_0^2 is a constant representing the overall energy of the random process. σ_0^2 is given by the second part of the [equation 6.28](#) equation sets. If we rewrite the variance record of [equation 6.29](#) in a discrete form as

Equation 6.30

$$\sigma_{\Delta t}^2[k] = \sum_{l=1}^L \Delta t_{PJ_l}^2 (1 - \cos(2\pi f_l k)) + 2\sigma_{RJ}^2 (1 - \delta[k])$$

the optimizer approach is fairly intuitive. Consider [equation 6.30](#). We will "peel off" the sinusoids one by one. This is an uninvariant search process, assuming that the parameters are not interacting. In our case, let us define a cost function or gauge function:

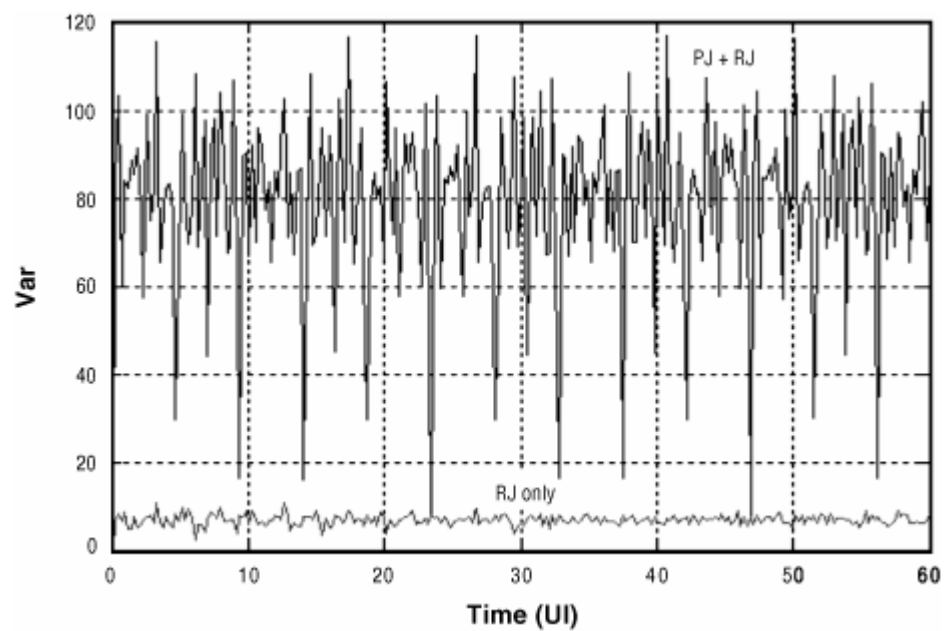
Equation 6.31

$$E = \sum_{k=0}^N (\sigma_{\Delta t}^2[k] - \Delta t_{PJ_e}^2 [1 - \cos(2\pi f_e k)])^2$$

By fixing arbitrary initial amplitude, we first sweep through a frequency range to find an f_e that minimizes E . Then we search through an amplitude range to find a Δt_{PJ_e} that minimizes E . With both amplitude and frequency known, we can remove one sinusoidal from the variance record. We can repeat this process until all the sinusoids are removed. The remainder then is pure noise.

[Figure 6.6](#) shows an example of PJ and RJ separation based on time-domain variance function through the optimization method. This example has seven PJs and one RJ in the variance function. All seven PJs are separated in sequence, with both magnitude and frequency uniquely determined. The final residue in the variance function represents the RJ components. The determined PJs and RJ are very close to the expected values.

Figure 6.6. Time-domain PJ and RJ separation through the optimization method. The PJ+RJ variance function is shown at the top, and the separated RJ variance function is shown at the bottom.



URL <http://access.proquest.safaribooksonline.com/9780132429610/ch06lev1sec3>

User name: CSU San Diego

Book: Jitter, Noise, and Signal Integrity at High-Speed

Section: Chapter 6. Jitter and Noise Separation and Analysis in the Time and Frequency Domains

No part of any chapter or book may be reproduced or transmitted in any form by any means without the prior written permission for reprints and excerpts from the publisher of the book or chapter. Redistribution or other use that violates the fair use privilege under U.S. copyright laws (see 17 USC107) or that otherwise violates these Terms of Service is strictly prohibited. Violators will be prosecuted to the full extent of U.S. Federal and Massachusetts laws.

Information Theory Computer Science Mike Peng Li Prentice Hall Jitter, Noise, and Signal Integrity at High-Speed

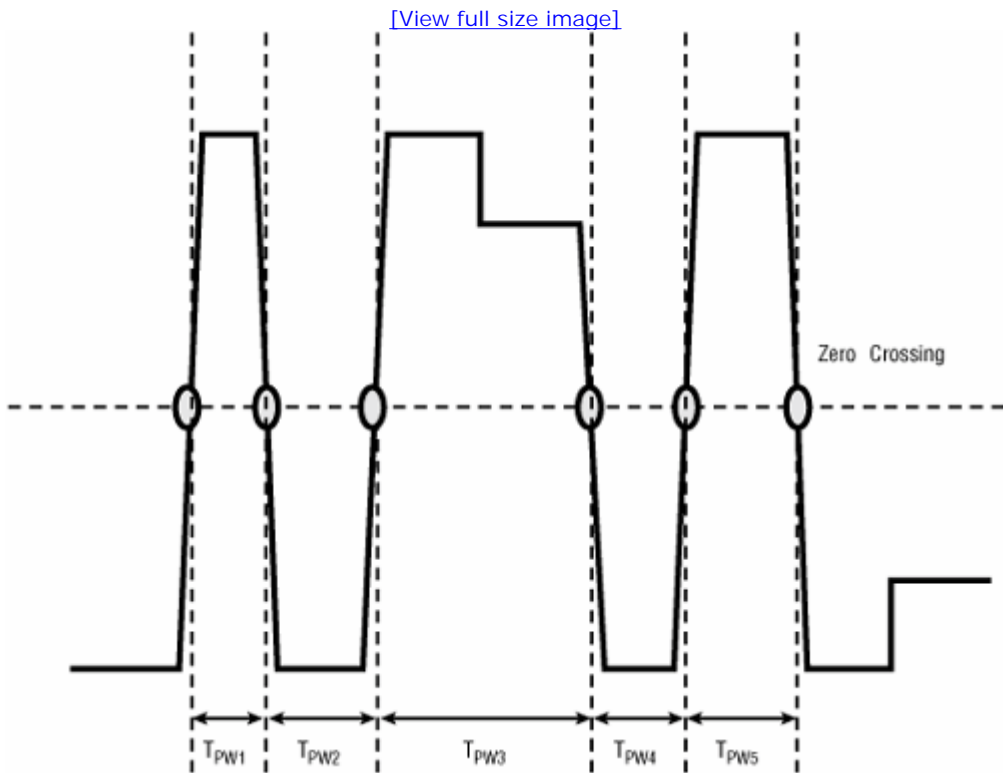
6.4. Pulse Width Shrinkage (PWS)

We will first discuss the pulse width shrinkage (PWS) definition and mathematical representation. Then we will discuss its relation to the DDJ.

6.4.1. PWS Definition

Channel crosstalk and jitter amplification critically depend on the PWS of the transmitter signal launched into the channel in recent high-speed channel simulations.^[5] The definition of a wide-sense pulse width (PW) is shown in Figure 6.7.

Figure 6.7. A generic pulse width (PW) definition.



PW is defined as the time distance between two consecutive edge transitions. PWS is defined as the time difference between the actual

PW and the ideal PW. Note that the PW can be several UIs long.

Assuming that the ideal UI for the waveform is T_0 , and that the actual PW is T_{PW_n} , the PWS is given by the following equation:

Equation 6.32

$$\Delta t_{PWS_n} = T_{PW_n} - M_n T_0$$

where M_n is the run length of the n th pulse. Clearly, the upper limit of M_n is the maximum run length of the data pattern. The sign for PWS should be negative—namely, $\Delta t_{PWS_n} < 0$.

Referring to [Figure 6.3](#) for the ideal bit clock definition, we can rewrite [equation 6.32](#) as follows:

Equation 6.33

[\[View full size image\]](#)

$$\Delta t_{PWS_n} = (t_{n+N_n} - t_n) - M_n T_0 = [t_{n+N_n} - (n + M_n)T_0] - [t_n - nT_0]$$

$$[t_{n+N_n} - (n + M_n)T_0] \text{ and } [t_n - nT_0]$$

Note that $[t_{n+N_n} - (n + M_n)T_0]$ and $[t_n - nT_0]$ give rise to the instantaneous jitter definition for the $(n + M_n)$ th and n th edge transitions, respectively. Therefore, [equation 6.33](#) becomes

Equation 6.34

$$\Delta t_{PWS_n} = \Delta t_{n+N_n} - \Delta t_n$$

[Equation 6.34](#) suggests that PWS jitter is the difference between the consecutive edge transition corresponding jitters. The difference is over the run length of a particular pulse— $M_n * T_0$. Because a difference function implies a high-pass filter function (as discussed in detail in [Chapter 7](#), "Clock Jitter"), PWS jitter has less low-frequency content compared to the instantaneous edge transition jitter. The relationship revealed by [equation 6.34](#) not only gives us insights into the relationship between PWS and instantaneous edge transition jitter, but it also gives us a quantitative way to estimate it if either one is known.

6.4.2. Averaged PWS and DDJ

If the waveform shown in [Figure 6.6](#) is an averaged waveform similar to that shown in [Figure 6.3](#), any pattern uncorrelated jitter such as PJ, RJ, or BUJ is removed, and what is left is the DDJ only. Using [equation 6.34](#), we have the following relationship between PWS and DDJ under the averaged waveform condition:

Equation 6.35

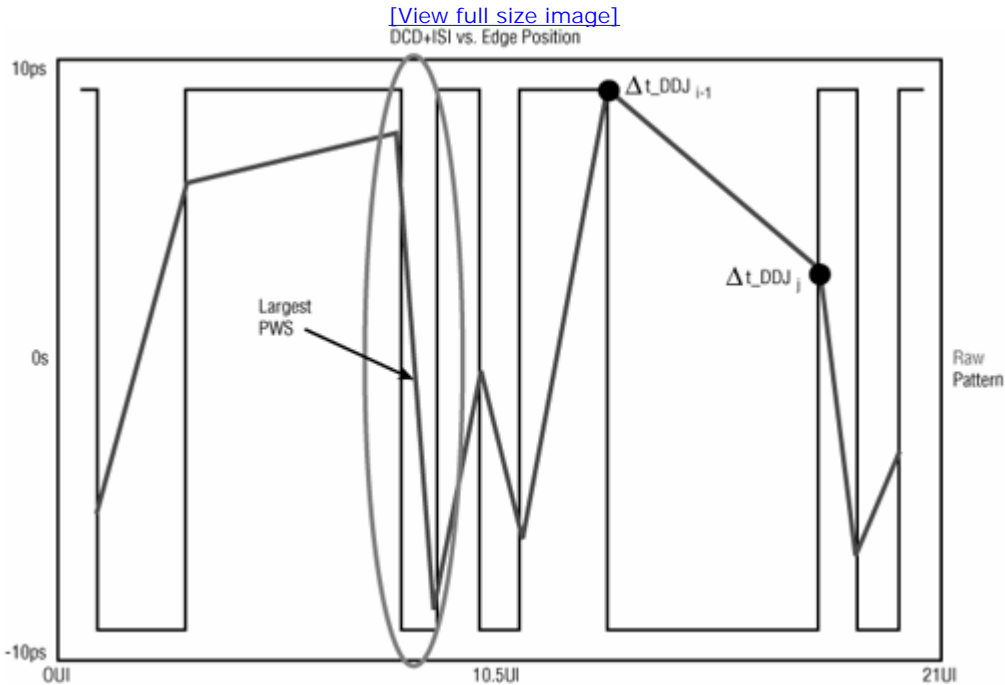
$$\overline{\Delta t}_{PWS_n} = \Delta t_{DDJ_n+N_n} - \Delta t_{DDJ_n}$$

[Equation 6.35](#) indicates that the averaged PWS is related to DDJ through the difference function. This relationship can be used to estimate the averaged PWS if DDJ's time records for each edge transition are known.

6.4.3. PWS Estimation

We will show a method that uses [equation \(6.35\)](#) to estimate PWS based on the DDJ time record that can be obtained by a time interval analyzer (TIA) or a sampling oscilloscope (SO). [Figure 6.8](#) shows an example of PWS estimation with DDJ versus time span measurement data.

Figure 6.8. A PWS estimation method illustration.



In this figure, the "+" DDJ means that the edge transition happens later than the ideal (jitter free) timing, and "-" DDJ means that the edge transition happens earlier than the ideal (jitter free) timing. Whether a PWS is positive or negative will depend on the polarity and magnitude for Δt_{DDJ_n} and $\Delta t_{DDJ_n+M_r}$. Although it is hard to rule out the other cases, worst case PWS will happen when Δt_{DDJ_n} is positive and $\Delta t_{DDJ_n+M_r}$ is negative for most times. This corresponds to PWS determined by edge transition 8 and 9 as shown in this figure and is valued at -16.8 ps in this example.

URL <http://access.proquest.safaribooksonline.com/9780132429610/ch06lev1sec4>

User name: CSU San Diego

Book: Jitter, Noise, and Signal Integrity at High-Speed

Section: Chapter 6. Jitter and Noise Separation and Analysis in the Time and Frequency Domains

No part of any chapter or book may be reproduced or transmitted in any form by any means without the prior written permission for reprints and excerpts from the publisher of the book or chapter. Redistribution or other use that violates the fair use privilege under U.S. copyright laws (see 17 USC107) or that otherwise violates these Terms of Service is strictly prohibited. Violators will be prosecuted to the full extent of U.S. Federal and Massachusetts laws.

Information Theory Computer Science Mike Peng Li Prentice Hall Jitter, Noise, and Signal Integrity at High-Speed

6.5. Comparison of Various Time and Frequency Domain Jitter Separation Methods

This chapter has introduced four time and/or frequency domain-based jitter separation methods. Each method has its unique characteristics, advantages, limitations, and performance. [Table 6.1](#) reviews these in terms of their capabilities in determining jitter components of DDJ, DCD, ISI, PJ, RJ, and BUJ and associated accuracy.

Table 6.1. Comparison of the Capability and Performance of Different Jitter Separation Methods

	DDJ	DCD	ISI	PJ	RJ	BUJ
1. Time-domain averaging	Yes: Give the <i>most accurate DDJ estimation.</i>	Yes, if rising and falling edges are distinctive.	Yes, if rising and falling edges are distinctive.	No	No	No
2. Frequency-domain Fourier spectrum (FS)	Yes, but may contain PJ if its frequency meets certain conditions.	Yes, if rising and falling edges are distinctive.	Yes, if rising and falling edges are distinctive.	Yes: Magnitude, frequency, and phase are possible, but PJ may be misidentified as DDJ. FFT and interpolation are needed.	Yes: Not accurate, because exact PSD is not possible from FS. FFT and interpolation are needed.	Maybe: Broadband BUJ is difficult to separate from RJ in FS in general, unless it can be controlled.
3. Frequency-domain power spectrum density (PSD)	Yes, if method 1 is used.	Yes, if rising and falling edges are distinctive.	Yes, if rising and falling edges are distinctive.	Yes: Only magnitude and frequency, not phase, are possible. FFT and interpolation are needed.	Yes: <i>Most accurate RJ estimation.</i> FFT and interpolation are needed.	Maybe: Broadband BUJ is difficult to separate from RJ in FS in general, unless it can be controlled.
4. Time-domain variance function	No	No	No	Yes: FFT and interpolation are not needed, only magnitude and frequency, no phase.	Yes: FFT and interpolation are not needed.	Maybe: Broadband BUJ is difficult to separate from RJ in FS in general, unless it can be controlled.

You can see from [Table 6.1](#) that no single method can separate all the jitter components with good performance accuracy. An optimized combination of some of those methods will give rise to a hybrid method that has overall better capability and performance than individual methods for separating all the jitter components. In any case, time or frequency domain-based methods all suffer from their inability to determine broadband BUJ when all the jitter components are present unless broadband BUJ can be controlled in the estimation procedure. The best chance to resolve broadband BUJ still is to rely on the statistical domain approach introduced in [Chapter 5](#) for a single measurement where broadband BUJ cannot be controlled and there is no knowledge prior to the measurement.

URL <http://access.proquest.safaribooksonline.com/9780132429610/ch06lev1sec5>

User name: CSU San Diego

Book: Jitter, Noise, and Signal Integrity at High-Speed

Section: Chapter 6. Jitter and Noise Separation and Analysis in the Time and Frequency Domains

No part of any chapter or book may be reproduced or transmitted in any form by any means without the prior written permission for reprints and excerpts from the publisher of the book or chapter. Redistribution or other use that violates the fair use privilege under U.S. copyright laws (see 17 USC107) or that otherwise violates these Terms of Service is strictly prohibited. Violators will be prosecuted to the full extent of U.S. Federal and Massachusetts laws.

Information Theory Computer Science Mike Peng Li Prentice Hall Jitter, Noise, and Signal Integrity at High-Speed

6.6. Summary

This chapter started by discussing jitter representations in the time and frequency domains. In the frequency domain, commonly used functions are jitter FS and PSD functions. FS is obtained through Fourier Transformation of the jitter time function, and PSD is obtained through the jitter time-domain autocorrelation function. Approximated jitter PSD can also be obtained through time average of the squared jitter FS. This chapter then discussed DDJ separation in the time and frequency domains. In the time domain, DDJ can be estimated by averaging the waveform and associated zero-crossing time deviations. In the frequency domain, DDJ is spectral lines with frequencies being the integer multiples of the pattern repeating frequency, from either FS or PSD function. [Section 6.3](#) introduced PJ, RJ, and BUJ separation in the frequency domain based on either jitter FS or PSD. PJ detection through techniques such as "sliding window" was discussed, along with broadband BUJ separation via two measurements when BUJ can be switched on and off in two measurements. Time-domain PJ and RJ separation also were introduced in this section. [Section 6.4](#) described the new jitter parameter of PWS and its relationship with instantaneous edge transition jitter referenced to ideal timing. We showed the "difference function" between the PWS and instantaneous jitter. When this relationship is used for an averaged waveform, the averaged PWS equals the DDJ difference function. A PWS estimation method based on the DDJ time record is presented. [Section 6.5](#) compared the advantages and limitations of each jitter separation method. It also described how to create a hybrid method from each of the methods that will not suffer from shortfalls.

URL <http://access.proquest.safaribooksonline.com/9780132429610/ch06lev1sec6>

User name: CSU San Diego

Book: Jitter, Noise, and Signal Integrity at High-Speed

Section: Chapter 6. Jitter and Noise Separation and Analysis in the Time and Frequency Domains

No part of any chapter or book may be reproduced or transmitted in any form by any means without the prior written permission for reprints and excerpts from the publisher of the book or chapter. Redistribution or other use that violates the fair use privilege under U.S. copyright laws (see 17 USC107) or that otherwise violates these Terms of Service is strictly prohibited. Violators will be prosecuted to the full extent of U.S. Federal and Massachusetts laws.

Information Theory Computer Science Mike Peng Li Prentice Hall Jitter, Noise, and Signal Integrity at High-Speed

Endnotes

1. W. B. Davenport and W. L. Root, *An Introduction to the Theory of Random Signals and Noise*, IEEE Press, 1987.
2. J. Wilstrup, "A Method of Serial Data Jitter Analysis Using One-Shot Time Interval Measurements," IEEE International Test Conference (ITC), 1998.
3. B. Ward, K. Tan, and M. Guenther, "Apparatus and Method for Spectrum Analysis-Based Serial Data Jitter Measurement," U.S. patent number 6,832,172, 2004.
4. L. Scharf, *Statistical Signal Processing: Detection, Estimation, and Time Series Analysis*, Prentice Hall, 1990.
5. Information Technology Industry Council and the American National Standards Institute, Inc. (ANSI), "Fiber Channel Physical Interfaces (FC-PI-4) Rev 1.00," 2006.

URL <http://access.proquest.safaribooksonline.com/9780132429610/ch06lev1sec7>

User name: CSU San Diego

Book: Jitter, Noise, and Signal Integrity at High-Speed

No part of any chapter or book may be reproduced or transmitted in any form by any means without the prior written permission for reprints and excerpts from the publisher of the book or chapter. Redistribution or other use that violates the fair use privilege under U.S. copyright laws (see 17 USC107) or that otherwise violates these Terms of Service is strictly prohibited. Violators will be prosecuted to the full extent of U.S. Federal and Massachusetts laws.

Information Theory Computer Science Mike Peng Li Prentice Hall Jitter, Noise, and Signal Integrity at High-Speed

7. Clock Jitter

This chapter first discusses data jitter and clock jitter definitions and their roles in synchronized computer systems and asynchronous communication systems. Then it discusses the definitions of various kinds of jitter, such as phase jitter, period jitter, and cycle-to-cycle jitter, as well as their interrelationships using the uniform nature of a clock signal waveform. Last, this chapter covers clock jitter and its relationship with phase noise, including the conversion from phase jitter to phase noise and vice versa.

URL <http://access.proquest.safaribooksonline.com/9780132429610/ch07>

User name: CSU San Diego

Book: Jitter, Noise, and Signal Integrity at High-Speed

Section: Chapter 7. Clock Jitter

No part of any chapter or book may be reproduced or transmitted in any form by any means without the prior written permission for reprints and excerpts from the publisher of the book or chapter. Redistribution or other use that violates the fair use privilege under U.S. copyright laws (see 17 USC107) or that otherwise violates these Terms of Service is strictly prohibited. Violators will be prosecuted to the full extent of U.S. Federal and Massachusetts laws.

Information Theory Computer Science Mike Peng Li Prentice Hall Jitter, Noise, and Signal Integrity at High-Speed

7.1. Clock Jitter

Clock is widely used in modern electronics, from computers, to communications, to consumer electronics. In a computer system, clock is used to provide timing or synchronization for the system. In a communication system, clock is used to specify when a data switch or bit transaction should be transmitted and received. In a synchronized system, a central global clock is distributed to its subsystems. In a communication system, particularly an asynchronous system, a clock can be either recovered or forwarded. Clearly, timing accuracy degradation in a clock affects the performance of the system it resides in. This chapter focuses on the single most important degrader of clock performance: clock jitter.

We start with clock jitter definition and then move to its impact on synchronized and asynchronous systems in a quantitative manner.

7.1.1. Clock Jitter Definition

From a signal or waveform point of view, clock signal or waveform is a special case of a data signal or waveform because the clock signal has a uniform transition distribution and repeats at its minimum period. Assuming that the clock signal over one period is represented by $f(t)$, we have

Equation 7.1

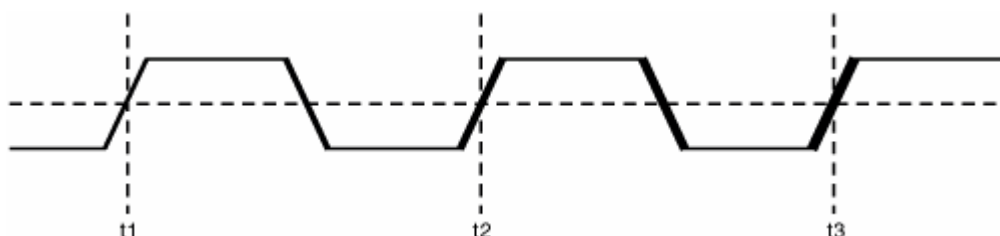
$$f(t) = f(t \pm nT)$$

where T is the period of the clock signal and n is an integer.

Because clock signal is a special form of the general data signal, most of definitions of data jitter apply to clock jitter, such as DJ and RJ. However, some of the subcomponents of DJ for a data signal do not apply to clock jitter. The ISI does not apply to a clock signal because there is no uneven transition for a clock signal or waveform. The rest of the jitter components that were introduced for a data signal in the previous chapters still apply to a clock signal.

The unique characteristic of uniform edge transition for a clock signal determines its jitter root-cause mechanisms, as well as its measurement metrics. [Figure 7.1](#) shows clock jitter in reference to its ideal edge transitions.

Figure 7.1. A jittery clock signal with its reference voltage/power crossing times shown.



For a clock signal, an edge transition is expected to occur at every period. It permits a uniform sampling for the clock jitter record, facilitating a direct Fourier Transformation (FT) or Fast Fourier Transformation (FFT)^[1] for jitter spectrum analysis. There's no need to "fill" the holes because of nonuniform sampling, as in the case of data pattern signal, where edge transitions do not occur evenly.

In general, the jitter analysis method developed for a data signal can be applied to clock signal analysis equally well because it is a special case. But the opposite is not necessarily true. For example, FFT can be applied to clock jitter directly but cannot be applied to data jitter unless missing data holes have been filled (see Chapter 6, "Jitter and Noise Separation and Analysis in the Time and Frequency Domains"). Clock jitter analysis is subject to fewer sampling constraints compared to data signal jitter; therefore, more direct and versatile methods are possible for clock jitter analysis. In another example, clock jitter can be measured and analyzed by time-domain instruments such as time interval analyzer (TIA) or sampling oscilloscope (OS), and frequency-domain measurement instruments such as spectrum analyzer (SA).^[2] However, in practice, data jitter has been measured and analyzed mostly by time-domain instruments, not frequency-domain instruments such as SA, largely due to the difficulty of separating various jitter components with the SA data.^[3]

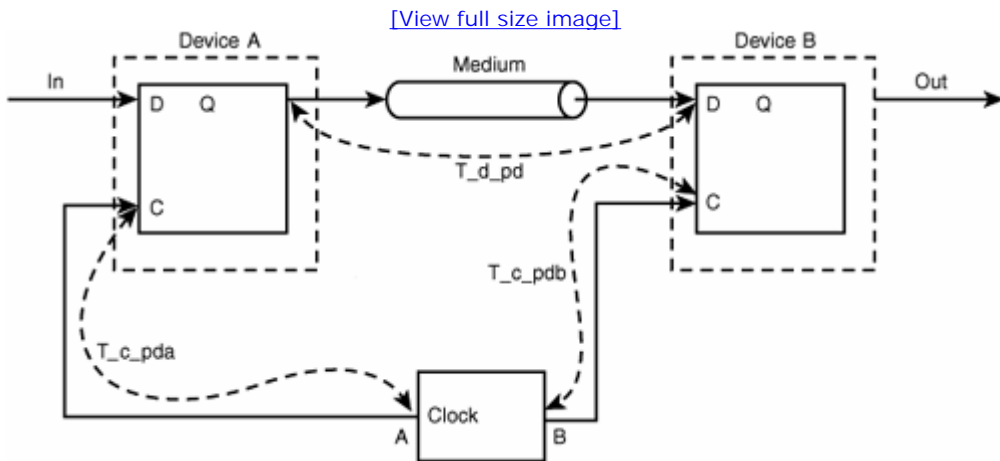
7.1.2. Impacts of Clock Jitter

When a clock experiences jitter, it affects the performance of the device or system that uses it. We will discuss the impact of clock jitter on two distinct link systems: synchronized and asynchronous.

7.1.2.1. Synchronized System

A synchronized system is commonly used in computer applications. Figure 7.2 shows a typical synchronized link system in which a global clock is used to update and determine the logical bits for driver, sampler, or register.^{[4] [5]} If the clock has jitter, it degrades the systems' functionality and performance.

Figure 7.2. A synchronized system in which a global clock is used for both driving (device A) and receiving (device B) devices. Propagation delays (PD) from clock to data latch inputs (T_{c_pda} , T_{c_pdb}) and data drive (device A) output to data receiver (device B) input (T_{d_pd}) are also shown.



In this synchronized system, the initial clock pulse causes the driving device A to latch the data from the input and launch it into the transmission medium. The second clock causes device B to latch the incoming data. The time available for sending and receiving a data bit is one clock period T_0 . Figure 7.3 shows the relationships between those critical timing parameters.

Figure 7.3. The relative relationships between the various timing parameters shown in Figure 7.2. Here T_{su} is the setup time, T_{su_mg} is the setup time margin, T_{hd} is the hold time, T_{hd_mg} is the hold time margin, and T_0 is the clock period.

[View full size image]

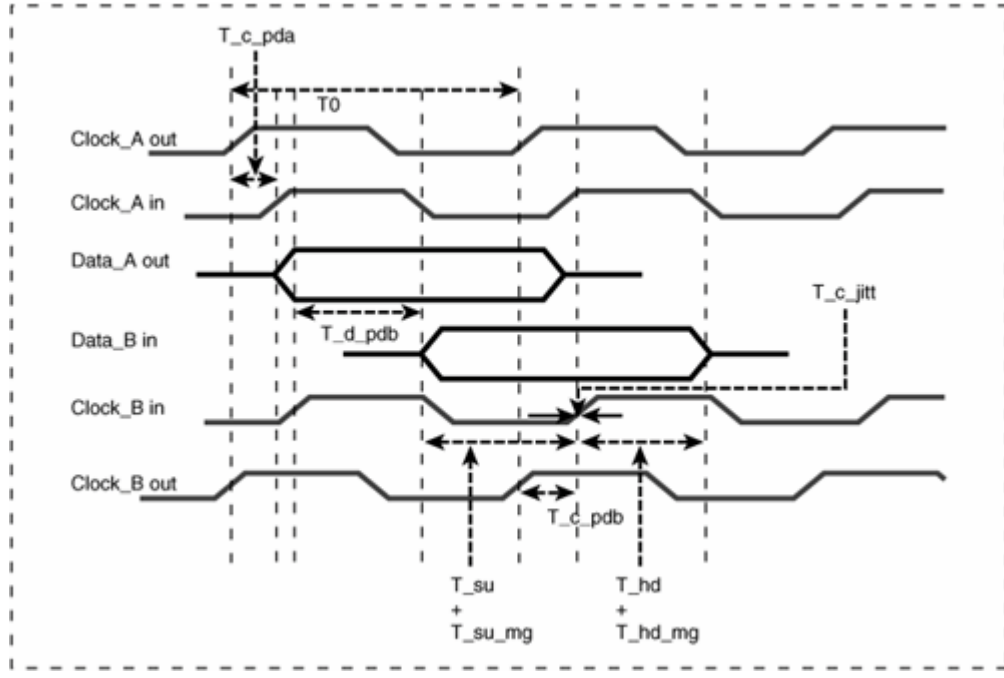


Figure 7.3 suggests the following relationships for these timing parameters:

Equation 7.2

$$T_0 + T_{c_pdb} + T_{c_jitt} - T_{su_mg} - T_{su} - T_{d_pd} - T_{c_pda} = 0$$

Equation 7.3

$$T_{c_pda} + T_{d_pd} - T_{c_jitt} - T_{hd_mg} - T_{hd} - T_{c_pdb} = 0$$

These two equations can be rewritten in a different format:

Equation 7.4

$$T_{su_mg} = T_0 + T_{c_jitt} - (T_{c_pda} - T_{c_pdb}) - T_{su} - T_{d_pd}$$

Equation 7.5

$$T_{hd_mg} = T_{d_pd} - T_{c_jitt} - T_{hd} + (T_{c_pda} - T_{c_pdb})$$

Let us define $T_{c_skew} = T_{c_pda} - T_{c_pdb}$. The minimum conditions are that both setup time and hold time margin should be larger than 0. This leads to the following inequalities for setup and hold time conditions:

Equation 7.6

$$T_0 \geq -T_{c_jitt} + T_{c_skew} + T_{d_pd} + T_{su}$$

Equation 7.7

$$T_{hd} \leq T_{d_pd} + T_{c_skew} - T_{c_jitt}$$

Equations 7.6 and 7.7 give the quantitative descriptions of how clock jitter and clock skew affect the performance of the synchronized system in which a common or global clock for both driver and receiver is used.

In the absence of clock jitter ($T_{c_jitt} = 0$), if $T_{c_skew} > 0$, the minimum clock period increases, degrading system performance. Under this condition, the maximum hold time also increases, making the hold time condition easy to meet. On the other hand, if $T_{c_skew} < 0$, the minimum clock period decreases, improving system performance. Under such conditions, the maximum hold time decreases, making the hold time condition harder to meet (a race condition).

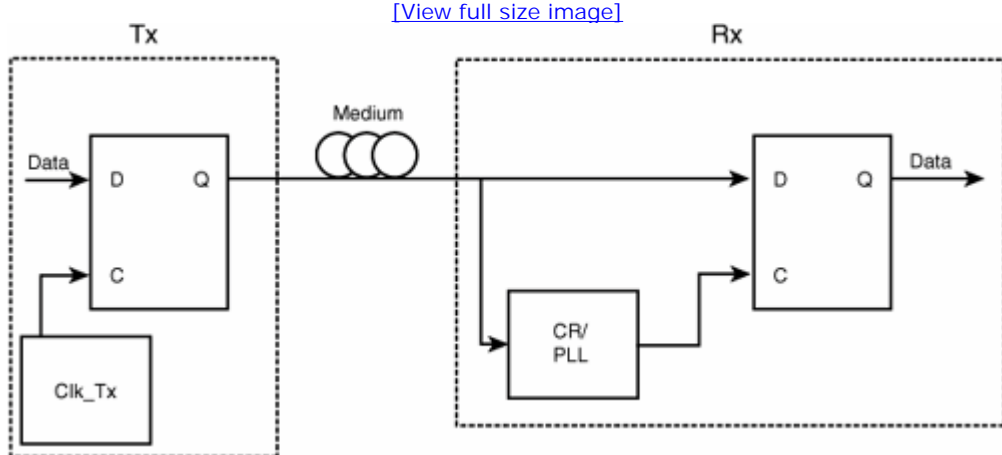
In the absence of skew ($T_{c_skew} = 0$), if $T_{c_jitt} > 0$ (longer cycle), the minimum clock period increases, degrading system performance. Meanwhile, under this same condition, the maximum hold time decreases, making the hold time condition hard to meet. So positive jitter over one clock period makes both clock period and hold time hard to meet. If $T_{c_jitt} < 0$ (a shorter cycle), the minimum clock period decreases, improving system performance. Under this condition, the maximum hold time increases, making the hold time condition easier to meet and eliminating race conditions. You can see that a longer cycle does more harm to system performance.

When both skew and jitter are present, system performance can be any of the four scenarios just discussed. If skew is the dominant effect, the discussions of skew impact continue to hold. Similarly, if jitter is dominant over skew, the discussions of jitter impact continue to hold. When jitter and skew are comparable, quantitative numbers for both jitter and skew are needed to assess the net effect on system performance.

7.1.2.2. Asynchronized System

We have discussed both skew and jitter effects on system performance for a synchronized system. Using link I/O as an example, the skew for a synchronized system becomes hard to manage when the data rate increases, typically above 1 Gb/s. At multiple Gb/s data rates, an asynchronized system is commonly used, as shown in Figure 7.4.

Figure 7.4. A block diagram of an asynchronized link system. Note that there is no global clock, as in the case of the synchronized system shown in Figure 7.2.



Unlike a synchronized system, this asynchronized link system does not send clock with data to the receiver. Instead, only data bit stream is sent. The clock is embedded in the data signal and gets recovered at the receiver through a unit called clock recovery (CR). Obviously, this asynchronized link system has no clock skew, because clock at the receiver is not distributed or sent, but rather is recovered. Phase-locked loop (PLL) is typically used to recover the clock from the incoming data stream.

Let us assume that the jitter for the transmitter clock and recovered clock are composed of DJs and RJs. Further assume that the DJ and RJ for the transmitter clock after the high-pass filter of the clock recovery jitter transfer function^[6] (see Chapters 9, 10, and 11) are DJ_{clk_tx} for its pk-pk and σ_{clk_tx} for its Gaussian sigma or rms, respectively. Similarly, for the recovered clock, we assume that its DJ pk-pk and RJ Gaussian sigma are DJ_{clk_rx} and σ_{clk_rx} , respectively. Let us also assume that the jitter from the transmitter clock and jitter from the recovered clock are independent. Then the worst-case jitter at the receiver eye closure due to clock jitter is as follows:

Equation 7.8

$$DJ_{clk_tot} = DJ_{clk_tx} + DJ_{clk_rx}$$

Equation 7.9

$$\sigma_{clk_tot}^2 = \sigma_{clk_tx}^2 + \sigma_{clk_rx}^2$$

The jitter from the transmitter clock and recovered clock both impact the receiver eye closure according to [equations 7.8](#) and [7.9](#). They both need to be minimized to achieve good overall system performance. Low-frequency jitter from the transmitter clock can be tracked or attenuated by the clock recovery function if it has a high-enough corner frequency. A low phase noise oscillator within a PLL clock recovery also provides smaller RJ generations. These are two obvious design guides for reducing jitter from both the transmitter clock and receiver recovered clock if cost is not a constraint.

URL <http://access.proquest.safaribooksonline.com/9780132429610/ch07lev1sec1>

User name: CSU San Diego

Book: Jitter, Noise, and Signal Integrity at High-Speed

Section: Chapter 7. Clock Jitter

No part of any chapter or book may be reproduced or transmitted in any form by any means without the prior written permission for reprints and excerpts from the publisher of the book or chapter. Redistribution or other use that violates the fair use privilege under U.S. copyright laws (see 17 USC107) or that otherwise violates these Terms of Service is strictly prohibited. Violators will be prosecuted to the full extent of U.S. Federal and Massachusetts laws.

Information Theory Computer Science Mike Peng Li Prentice Hall Jitter, Noise, and Signal Integrity at High-Speed

7.2. Definitions of and Math Model for Various Jitter Types

Conventionally, jitter is defined as any deviation of the edge transition timing from the ideal timing. This is a good metric for most asynchronous systems, in which a PLL or phase interpolator (PI) is used to generate or recover a clock signal. However, in many synchronous systems, the digital circuits don't use clock edge timings directly. Rather, what matters is period or the period variation from one cycle to another. For example, in the global clock system, period variations (or changes) are important because longer period can cause hold time violation, resulting in logical failure. In another example, cycle-to-cycle jitter is a good performance indicator for multiplication PLLs because it can capture the timing disturbance caused by the dividing circuits. This section first gives the definitions and mathematical representations for each type of jitter and points out their appropriate applications. Then it discusses their interrelationships.

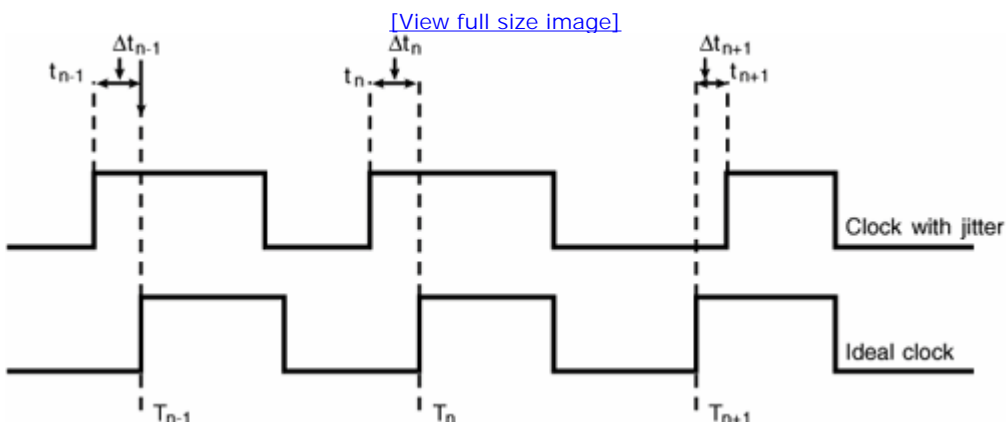
7.2.1. Phase Jitter

The basic phase jitter (also called accumulated jitter) concept is illustrated in Figure 7.5. It shows two waveforms: the ideal clock with zero jitter and the clock with jitter. The phase jitter is then defined as the actual edge transition timing deviation from the corresponding ideal clock timing. Mathematically, this means that phase jitter Δt_n is defined by the following equation:

Equation 7.10

$$\Delta t_n = t_n - T_n$$

Figure 7.5. Phase jitter definition using waveforms of jittery clock and ideal clock.



where t_n and T_n are timings for the nth edge transitions for jittery clock and ideal clock, respectively. If T_0 is the ideal clock period, we

have the following:

Equation 7.11

$$T_n - T_{n-1} = T_{n+1} - T_n = T_0$$

and

Equation 7.12

$$T_n = nT_0$$

In frequency-domain analysis, timing jitter is commonly quantified as phase change in radians, such as phase noise analysis. Because one complete cycle in time is equivalent to 2π in phase, phase jitter can be represented in terms of phase unit, such as radians. The relationship between phase jitter in radians and a time unit such as seconds is given by the following:

Equation 7.13

$$\phi_n = \frac{t_n}{T_0} 2\pi$$

Clearly, phase jitter captures the instance timing deviation from the ideal for each edge transition. Here the reference is fixed and uniform. Jitter measured with phase jitter is absolute and accumulates over time.

7.2.2. Period Jitter

Period jitter is defined as the period deviation from the ideal period. Mathematically, the nth period is given by $(t_n - t_{n-1})$. Therefore, period jitter is defined as

Equation 7.14

$$\Delta t_{pn} = (t_n - t_{n-1}) - T_0$$

According to [equation 7.11](#), $T_0 = T_n - T_{n-1}$. Substituting this in [equation 7.14](#), we obtain

Equation 7.15

$$\Delta t_{pn} = (t_n - t_{n-1}) - (T_n - T_{n-1}) = (t_n - T_n) - (t_{n-1} - T_{n-1}) = \Delta t_n - \Delta t_{n-1}$$

We can also represent the period jitter in terms of phase unit of radians as the following:

Equation 7.16

$$\phi'_n = \Phi_n - \Phi_{n-1}$$

where $\Phi'_n = 2\pi(\Delta t_{pn} / T_0)$. [Equations 7.15](#) and [7.16](#) suggest that period jitter is in fact the difference in consecutive phase jitter, or a difference function of phase jitter. Thus, period jitter and phase jitter are not independent. Rather, they are different but

related mathematical measures or representations of the same jitter process. Knowing one of them, you can derive another based on their difference function relationship.

7.2.3. Cycle-to-Cycle Jitter

Cycle-to-cycle jitter is defined as the period deviation of two consecutive periods. Mathematically, the n th period is given by $(t_n - t_{n-1})$, and the $(n - 1)$ th period is given by $(t_{n-1} - t_{n-2})$. Therefore, cycle-to-cycle jitter is defined as follows:

Equation 7.17

$$\Delta t_{cn} = (t_n - t_{n-1}) - (t_{n-1} - t_{n-2}) = t_n + t_{n-2}$$

Using the definition of period jitter in [equation 7.15](#), we know that the difference between two consecutive period jitters is

Equation 7.18

$$\Delta t_{pn} - \Delta t_{pn-1} = (t_n - t_{n-1} - T_0) - (t_{n-1} - t_{n-2} - T_0) = t_n + t_{n-2}$$

Comparing [equation 7.17](#) to [equation 7.18](#) leads to the relationship between cycle-to-cycle jitter and period jitter:

Equation 7.19

$$\Delta t_{cn} = \Delta t_{pn} - \Delta t_{pn-1}$$

To represent cycle-to-cycle jitter in terms of phase jitter, substituting period jitter in terms of phase jitter of [equation 7.15](#) to [equation 7.19](#), we obtain

Equation 7.20

$$\Delta t_{cn} = \Delta t_{pn} - \Delta t_{pn-1} = (\Delta t_n - \Delta t_{n-1}) - (\Delta t_{n-1} - \Delta t_{n-2})$$

[Equation 7.20](#) is very important because it gives the interrelationship between cycle-to-cycle jitter, period jitter, and phase jitter. It says that cycle-to-cycle jitter is the first difference of period jitter and the second difference of the phase jitter.

We can also represent cycle-to-cycle jitter in terms of phase unit of radians:

Equation 7.21

$$\Phi_n = \Phi_n - \Phi_{n-1} = (\Phi_n - \Phi_{n-1}) - (\Phi_{n-1} - \Phi_{n-2})$$

where $\Phi_n' = 2\pi(\Delta t_{pn} / T_0)$. [Equations 7.20](#) and [7.21](#) say that cycle-to-cycle jitter, period jitter, and phase jitter are related through the first and second difference functions. If you know the phase jitter, the period jitter and cycle-to-cycle jitter can be uniquely estimated. Conversely, if you know the cycle-to-cycle jitter, the period jitter and phase jitter can be estimated through the first and second summing or integration functions. If period jitter is given, the first difference gives rise to cycle-to-cycle jitter, and the first integration gives rise to phase jitter. It is worth pointing out that the integration function may introduce a constant, so an initial condition is needed to ensure a unique determination.

Phase jitter, period jitter, and cycle-to-cycle jitter relationships are similar to position, speed, and acceleration relationships in Newtonian mechanics. Mathematically, you may define the third difference jitter or cycle-to-cycle jitter difference, and so forth. However, those jitter definitions with higher-order difference functions have not found much practical use yet.

Clearly, the simple math model established here provides useful insights into the difference jitter definition and interrelationship. If you know one of them, others can be estimated. For more information on phase, period, and cycle-to-cycle jitter, refer to [7] and [8].

7.2.4. Interrelationships

It is useful to show the interrelationships between phase jitter, period jitter, and cycle-to-cycle jitter with some practical examples to give you further insights. We will demonstrate their relationship in both time and frequency domains.

7.2.4.1. Time Domain

A simple example to demonstrate the phase, period, and cycle-to-cycle jitter relationship starts with a phase jitter that is a sinusoidal of the following:

Equation 7.22

$$\Delta t_n = \sin\left(\frac{2\pi}{T_m} t_n\right) = \sin(2\pi f_m t_n) = \sin(\omega_m t_n)$$

We assume that this sinusoidal jitter has a zero initial phase and a unit-normalized magnitude. In addition, we define T_m as the period, with a corresponding frequency f_m and an angular frequency ω_m . Obviously we have $f_m = 1/T_m$, $\omega_m = 2\pi f_m = 2\pi/T_m$. This sinusoidal is sampled at the carrier clock period of T_0 . Using the definition of sinusoidal jitter in [equation 7.22](#) and the phase jitter to period jitter relationship in [equation 7.15](#), we have the following:

Equation 7.23

$$\Delta t_{pn} = 2\sin\left(\omega_m \frac{T_0}{2}\right) \cos\left[\omega_m(t_n - \frac{1}{2}T_0)\right]$$

Comparing [equations 7.22](#) and [7.23](#) suggests the following peak magnitude relationship between phase jitter and period jitter:

Equation 7.24

$$\frac{(\Delta t_{pn})_{pk}}{(\Delta t_n)_{pk}} = 2 \left| \sin\left(\omega_m \frac{T_0}{2}\right) \right|$$

The peak magnitude ratio between period jitter and phase jitter follows a sinusoidal having the same frequency as the sinusoidal phase jitter. When the period of the sinusoidal jitter T_m is much larger than the carrier clock period of T_0 —namely, low-frequency

modulation—we have $T_m \gg T_0$ and $\omega_m T_0 \ll 1$. [Equation 7.24](#) then can be simplified by using an approximation of $\sin(x) \approx x$ when $x \ll 1$ as

Equation 7.25

$$\frac{(\Delta t_{pn})_{pk}}{(\Delta t_n)_{pk}} \approx \omega_m T_0 \propto \omega_m$$

[Equation 7.25](#) implies that the peak ratio between period jitter and phase jitter is proportional to the sinusoidal jitter frequency when it is much smaller than the clock frequency or the sampling frequency. Apparently, [equation 7.25](#) implies a first-order high-pass functional for the period jitter peak magnitude.

Similarly, using the definition of sinusoidal jitter in [equation 7.22](#) and the phase jitter to cycle-to-cycle jitter relationship in [equation 7.20](#), we have

Equation 7.26

$$t_{cn} = -4 \left[\sin\left(\omega_m \frac{T_0}{2}\right) \right]^2 \sin(\omega_m t_{n-1})$$

Comparing [equations 7.22](#) and [7.26](#) suggests the following peak magnitude relationship between phase jitter and cycle-to-cycle jitter:

Equation 7.27

$$\frac{(t_{cn})_{pk}}{(t_n)_{pk}} = 4 \left[\sin\left(\omega_m \frac{T_0}{2}\right) \right]^2$$

The peak ratio between cycle-to-cycle jitter and phase jitter follows a square of sinusoidal having the same frequency of the sinusoidal phase jitter. In analogy to period jitter analysis, when the period of the sinusoidal jitter T_m is much larger than the carrier clock period of T_0 , we have $T_m \gg T_0$ and $\omega_m T_0$. [Equation 7.27](#) then can be simplified by using $\sin(x) \approx x$ when $x \ll 1$ as

Equation 7.28

$$\frac{(t_{pn})_{pk}}{(t_n)_{pk}} \approx (\omega_m T_0)^2 \propto \omega_m^2$$

[Equation 7.28](#) implies that the peak ratio between cycle-to-cycle jitter and phase jitter is proportional to the sinusoidal jitter frequency square when it is much smaller than the clock frequency or the sampling frequency—namely, low-frequency modulation. Apparently, [equation 7.28](#) implies a second-order high-pass function for the cycle-to-cycle jitter peak magnitude.

[Figure 7.6](#) shows a numerical simulation of phase jitter, period jitter, and cycle-to-cycle jitter.

Figure 7.6. Phase jitter, period jitter, and cycle-to-cycle jitter demonstration in the time domain when phase jitter is a sinusoidal. In this example, the sinusoidal period is 25 times the carrier or sampling clock— $T_m = 25 T_0$.

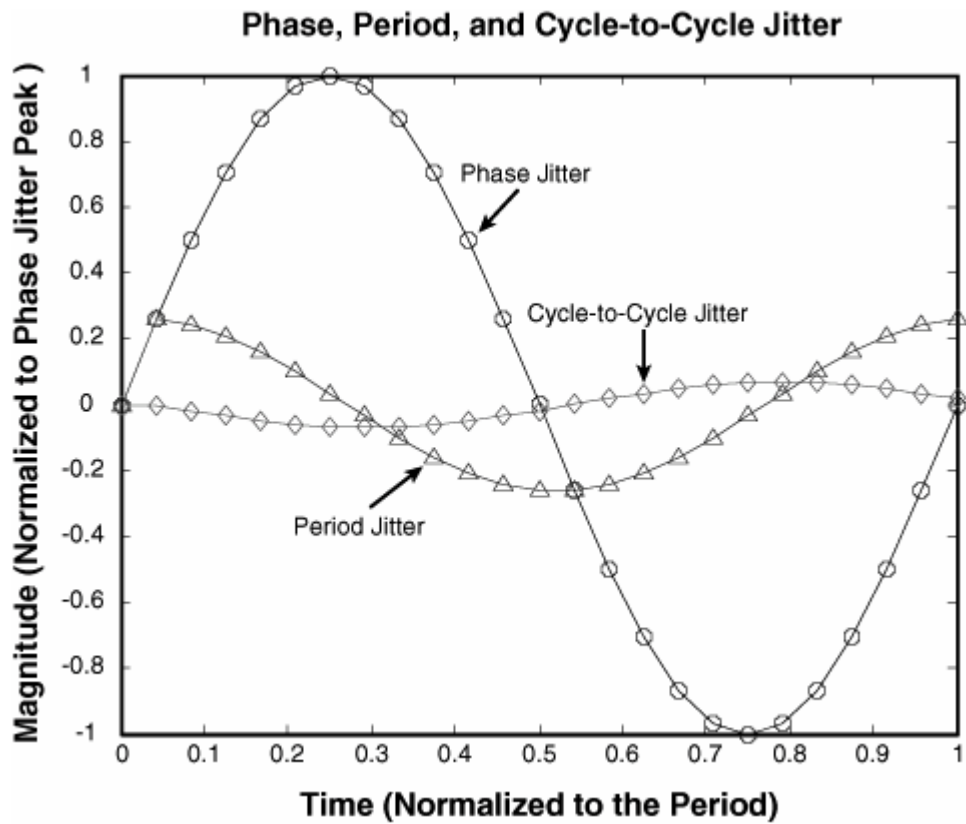


Figure 7.6 shows a few interesting points for this particular example. From phase jitter, to period jitter, to cycle-to-cycle jitter, we see that the jitter peak magnitude gets smaller and that the phase changes by π radians from phase jitter to period jitter and from period jitter to cycle-to-cycle. This is due to the first and second difference function from phase jitter to period jitter and from phase jitter to cycle-to-cycle jitter, respectively. They are also well expected from [equation 7.24](#) for a peak ratio of period jitter to phase jitter and from [equation 7.27](#) for a peak ratio of cycle-to-cycle jitter to phase jitter. In general, the higher-order the difference function is, the smaller the magnitude is.

It is important to note that a smaller jitter given by cycle-to-cycle does not necessarily mean that the system is good. The jitter magnitude is closely related to the jitter definition, so you need to clearly understand what jitter type should be used and how to interpret its meaning correctly.

7.2.4.2. Frequency Domain

Phase jitter, period jitter, and cycle-to-cycle jitter interrelationships can also be studied in the frequency domain. In fact, we touched on this issue a bit when deriving [equations 7.25](#) and [7.28](#), which implied the spectral relationship between those three jitter types in the sinusoidal phase jitter example.

We will use the notation of jitter in radians in [equations 7.16](#) and [7.21](#) to study the frequency-domain relationship. We start with [equation 7.16](#) and rewrite it as follows:

Equation 7.29

$$\phi_n(t) = \Phi_n(t) - \Phi_{n-1}(t) = T_0 \frac{\Phi_n(t) - \Phi_{n-1}(t)}{t_n - t_{n-1}}$$

Using the derivative notation, we can rewrite the equation as the following as an approximation:

Equation 7.30

$$\phi_n(t) \approx T_0 \frac{d\Phi_n(t)}{dt_n}$$

Let us denote the spectrum for phase, period, and cycle-to-cycle jitter as $\phi_n(f) = FT(\Phi_n(t))$; $\phi_n(f) = FT(\phi_n(t))$ and $\phi_n(f) = FT(\phi_n(t))$, where FT represents the Fourier Transformation.^[1] Taking the FT for [equation 7.30](#) gives us

Equation 7.31

$$FT(\phi_n(t)) \approx FT(T_0 \frac{d\Phi_n(t)}{dt_n}) = T_0 FT(\frac{d(\Phi_n(t))}{dt_n})$$

$$FT(\frac{d(\Phi_n(t))}{dt_n}) = (j2\pi f)FT(\Phi_n(t)) = (j2\pi f)\Phi_n(f)$$

, where $j = \sqrt{-1}$ is the imaginary unit.

Therefore, [equation 7.31](#) can be rewritten as follows:

Equation 7.32

$$|\phi_n(f)| \approx |T_0(j2\pi f)\Phi_n(f)| \propto f |\Phi_n(f)|$$

[Equation 7.32](#) implies that the spectrum magnitude for the period jitter is proportional to the spectrum magnitude for the phase jitter after a first-order high-pass function. In other words, low-frequency jitter contents are filtered out in the period jitter spectrum in comparison with the phase jitter spectrum. This result also agrees with [equation 7.25](#) for the sinusoidal phase jitter sample study.

Similarly, using the time-domain relationship of [equation 7.21](#), the spectrum magnitude relationship between period jitter and cycle-to-cycle jitter is

Equation 7.33

$$|\phi_n(f)| \approx |T_0(j2\pi f)\Phi'_n(f)| \propto f |\Phi'_n(f)|$$

and the spectrum magnitude relationship between phase jitter and cycle-to-cycle jitter is

Equation 7.34

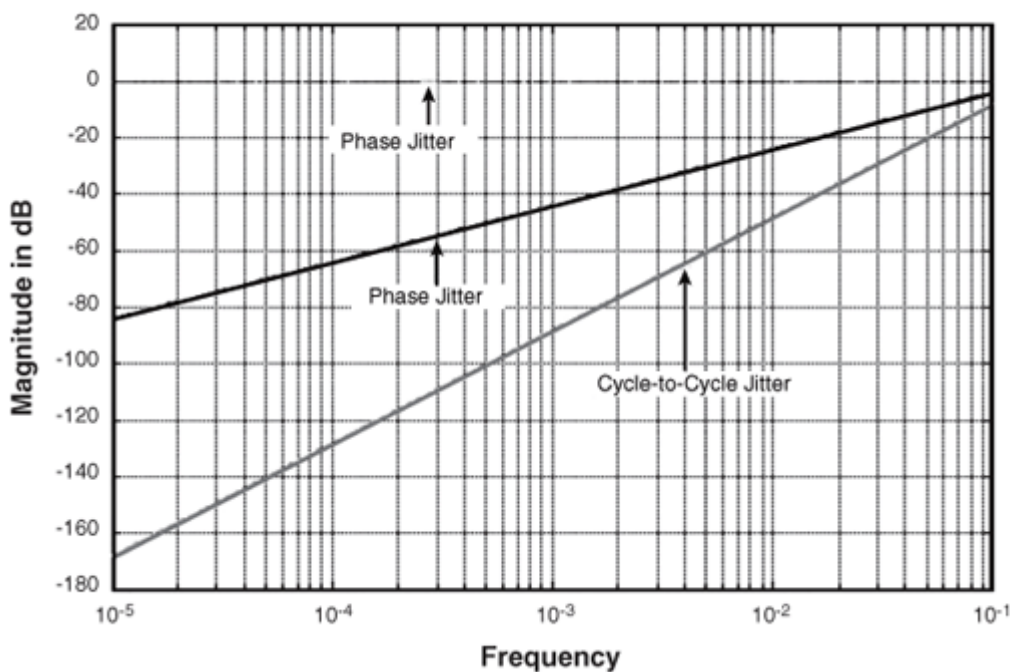
$$|\phi_n(f)| \approx [T_0(j2\pi f)]^2 |\Phi_n(f)| \propto f^2 |\Phi_n(f)|$$

[Equation 7.34](#) implies that the cycle-to-cycle jitter spectrum magnitude is proportional to the phase jitter spectrum after a second-order high-pass function. Low frequency jitter spectrum gets attenuated even more for the cycle-to-cycle compared to period jitter spectrum. This result is consistent with the conclusion of [equation 7.28](#) for the sinusoidal phase jitter study.

Assuming that the phase jitter spectrum is a constant (white spectrum, as discussed in [Chapter 4](#), "Jitter, Noise, BER (JNB), and Interrelationships"), the corresponding period jitter and cycle-to-cycle jitter spectra can be estimated according to [equations 7.32](#) and [7.34](#). [Figure 7.7](#) shows the results.

Figure 7.7. The spectra relationship between phase jitter, period jitter, and cycle-to-cycle jitter assuming that the phase jitter spectrum is a constant or "white."

[\[View full size image\]](#)
Various Jitter Measurement Spectrum



From the frequency-domain spectrum relationship, you can see that, in general, the jitter magnitude decreases from phase jitter, to period jitter, to cycle-to-cycle jitter due to the first- and second-order high-pass functions associated with them that attenuate the low-frequency contents in the phase jitter spectrum. Again, you need to understand the application and use the right jitter definition as the performance metric.

URL <http://access.proquest.safaribooksonline.com/9780132429610/ch07lev1sec2>

User name: CSU San Diego

Book: Jitter, Noise, and Signal Integrity at High-Speed

Section: Chapter 7. Clock Jitter

No part of any chapter or book may be reproduced or transmitted in any form by any means without the prior written permission for reprints and excerpts from the publisher of the book or chapter. Redistribution or other use that violates the fair use privilege under U.S. copyright laws (see 17 USC107) or that otherwise violates these Terms of Service is strictly prohibited. Violators will be prosecuted to the full extent of U.S. Federal and Massachusetts laws.

Information Theory Computer Science Mike Peng Li Prentice Hall Jitter, Noise, and Signal Integrity at High-Speed

7.3. Clock Jitter Versus Phase Noise

We have discussed different jitter types for a clock signal in the time and frequency domains. This section discusses another important topic of frequency-domain phase noise used widely in radio frequency (RF) design and testing. We will first define phase noise, and then we will discuss the interrelationship between phase noise and phase jitter and the conversion method from one metric to another.

7.3.1. Phase Noise

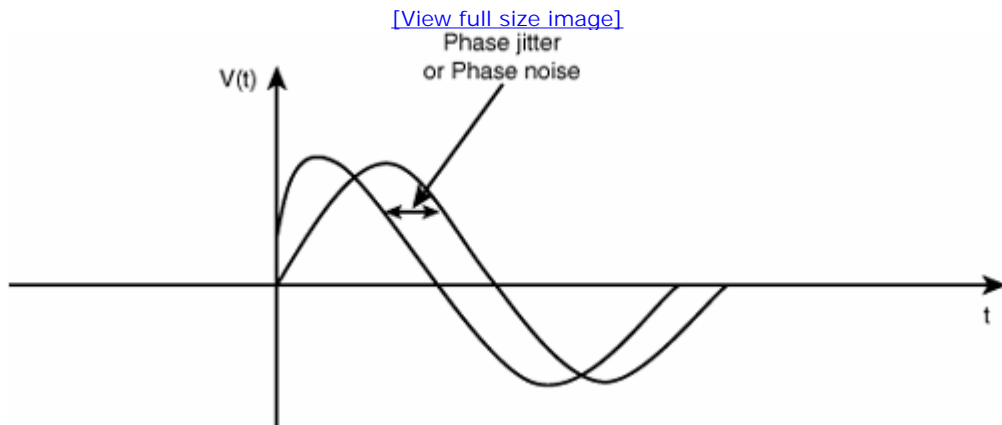
Phase noise can best be illustrated by a periodic signal or waveform, such as a sinusoidal waveform generated by an oscillator. A general periodic signal or waveform can be expressed as follows:

Equation 7.35

$$V(t) = V_0 f(2\pi f_0 t + \Phi_0(t))$$

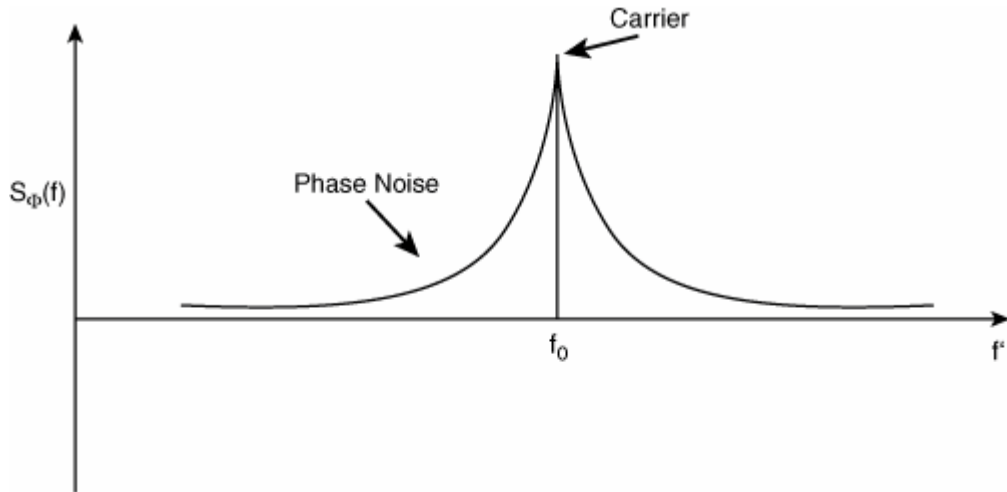
where $V(t)$ is the amplitude at a given time t , V_0 is the maximum amplitude, f_0 is the frequency of the carrier, and $\Phi_0(t)$ is the phase. If the phase varies, the waveform $V(t)$ shifts back and forth along the time axis, and this creates timing jitter or, more specifically, phase jitter (as defined in [section 7.2.1](#)), with a fixed time reference. Therefore, phase noise and phase jitter are two different representations or manifestations of the same noise mechanism, as shown in [Figure 7.8](#).

Figure 7.8. Phase noise or phase jitter in the time domain.



Traditionally, phase noise is studied in the frequency domain. Phase noise appears as sidebands centered around the carrier frequency. [Figure 7.9](#) shows the phase noise in the frequency domain.

Figure 7.9. The spectrum of a sinusoidal wave with "additive" phase noise. Phase noise appears as sidebands offset from the carrier frequency f_0 .



The phase noise frequency normally is specified at a particular frequency measured from the carrier, such as $f = f - f_0$, where f is the frequency referenced to zero or absolute frequency and f_0 is the carrier frequency. Phase noise magnitude normally is specified relative to the carrier's power on a per-hertz basis:

Equation 7.36

$$L(f) = \frac{P_n(f)}{P_0 \Delta f}$$

where $P_n(f)$ is the phase noise power (in watts) at the offset frequency f , P_0 is the carrier's power (also in watts) ($f = 0$), and Δf (in hertz) is the phase noise bandwidth. As $\Delta f > 0$, [equation 7.36](#) gives the definition for a phase noise power spectrum density (PSD) $S_\phi(f)$. Because $L(f)$ is a single-sideband PSD, it is half of the phase noise PSD $S_\phi(f)$:

Equation 7.37

$$L(f) \approx \frac{1}{2} S_\phi(f)$$

where the approximation is because phase noise is defined in an average sense, and PSD is defined "per point" (phase noise power over an indefinitely small frequency range). $L(f)$ and $S_\phi(f)$ defined in [equations 7.36](#) and [7.37](#) have a physical unit of $\text{rad}^{[2]}/\text{Hz}$.

Phase noise is often defined in its decibel unit by taking the logarithmic of [equation 7.38](#):

Equation 7.38

$$L(f) = 10 \log_{10} \left(\frac{P_n(f)}{P_0 f} \right)$$

The phase noise is defined in units of dBc/Hz . If you know the phase noise PSD $S_\phi(f)$, to get dBc/Hz , you must use the following equation:

Equation 7.39

$$L(f) = 10 \log_{10} \left(\frac{S_\Phi(f)}{2} \right)$$

Equations 7.38 and 7.39 give the formulas for calculating the phase noise in dBc/Hz when phase noise power or PSD are given, respectively. For more information on phase noise and jitter relationship, particularly oscillator phase noise, refer to [9], [10], and [11]. Here, our focus is on the relationship between phase noise and phase jitter.

7.3.2. Phase Jitter to Phase Noise Conversion

Obviously, phase jitter and phase noise are two different metrics or manifestations for the same jitter or noise process. Therefore, they are related to each other. Because phase jitter generally is measured in the time domain by instruments such as an SO or TIA, and phase noise generally is measured by frequency-domain instruments such as an SA, they are not always discussed in the same context. Phase jitter to phase noise conversion is a relatively new topic because of the wide use of high-speed data communication technologies. This section gives the math theory for the conversions from phase jitter to phase noise.

Suppose that the phase jitter is given and we denote it as $\Phi(t)$. Its corresponding autocorrelation function (see section 2.5.3 in Chapter 2, "Statistical Signal and Linear Theory for Jitter, Noise, and Signal Integrity") is as follows:

Equation 7.40

$$R_\Phi(\tau) = \lim_{T \rightarrow \infty} \left[\frac{1}{2T} \int_{-T}^{+T} \Phi(t)\Phi(t+\tau)dt \right]$$

where T is the time average period. Then the phase jitter PSD (see section 2.5.4 in Chapter 2) $S_\Phi(f)$ can be estimated by the following:

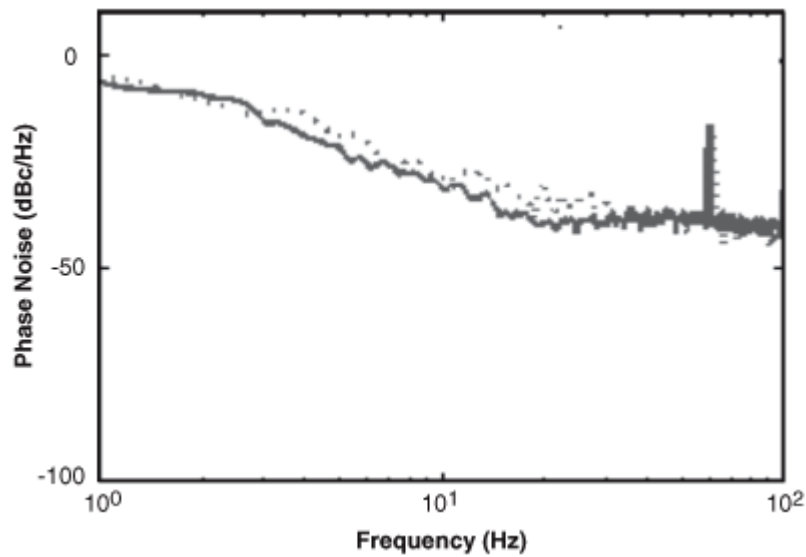
Equation 7.41

$$S_\Phi(\omega) = \int_{-\infty}^{\infty} R_\Phi(\tau) e^{-j\omega\tau} d\tau$$

After the phase jitter PSD is obtained, the phase noise PSD in rad²/Hz or dBc/Hz can be estimated by using equations 7.37 and 7.39, respectively.

It will be interesting to see how well the phase noise estimated through using a frequency-domain SA agrees with that estimated by a time-domain instrument such as a TIA. The results shown in Figure 7.10 indicate good agreement.

Figure 7.10. Phase noise measurement in dBc/Hz. The solid is measured from an SA—a frequency-domain instrument—and the dashed line is from a TIA—a time-domain instrument.

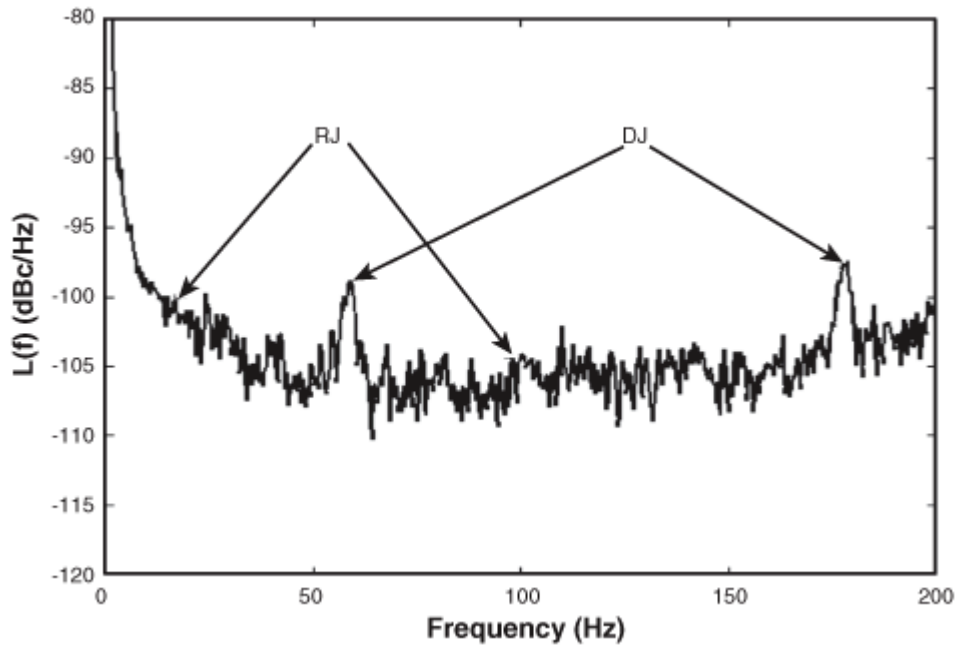


7.3.3. Phase Noise to Phase Jitter Conversion

As jitter or phase jitter become a dominant metric in quantifying the performance of a communication link, there is a need to convert the phase noise measured in the frequency domain to phase jitter for devices' PLLs, clocks, or oscillators used in the link.

From the phase noise PSD $L(f)$, random jitter (RJ) can be identified as the background envelope, and deterministic jitter (DJ) can be identified as spectral lines above the RJ floor (see Figure 7.11). Here DJ may include DCD, PJ, and BUJ. No ISI is associated with a clock signal as we had discussed earlier. Because the phase information affects the overall DJ PDF and pk-pk value, and the phase noise PSD $L(f)$ does not have the phase information. Therefore, it is not possible to determine the overall DJ (considering all the spectral lines above the RJ background) PDF and pk-pk completely and accurately based on the DJ part of $L(f)$. However, we can still establish a useful upper limit for the DJ peak (or pk-pk) value given $L(f)$. RJ rms estimation is relatively straightforward compared to DJ PDF and pk-pk determination.

Figure 7.11. RJ and DJ signatures on a measured phase noise PSD $L(f)$.



If the phase noise PSD $L(f)$ is in rad^2/Hz , as defined by equation 7.36, the DJ PSD composed of spectral lines above the RJ continuous spectral floor is given by the following:

Equation 7.42

$$S_{\Phi_{DJ}}(f) = 2 \left[\sum_{i=1}^N L_{DJ_i} \delta(f - f_i) \right]$$

where L_{DJ_i} represents the DJ spectral line magnitudes at frequency f_i in the $L(f)$ domain and $i = 1, 2, \dots, N$. $\delta(f - f_i)$ is a Dirac delta function at frequency f_i . Similarly, the RJ PSD with DJ spectral lines removed is given by the following:

Equation 7.43

$$S_{\Phi_{RJ}}(f) = 2L(f) - S_{\Phi_{DJ}}(f) = 2 \left[L(f) - \sum_{i=1}^N L_{DJ_i} \delta(f - f_i) \right]$$

Denote the DJ pk value as Φ_{DJ_pk} and the RJ rms or sigma value as Φ_{RJ_rms} . Then they can be readily estimated as

Equation 7.44

$$\Phi_{DJ_pk} \leq \sqrt{2 \sum_{i=1}^N L_{DJ_i}}$$

and

Equation 7.45

$$\Phi_{RJ_rms} = \sqrt{\int_{f_l}^{f_h} S_{\Phi_{RJ}}(f) df}$$

where f_l and f_h are the lower and higher frequency limits for the RJ frequency band. Obviously, [equation 7.44](#) does not give an exact DJ peak value solution. Instead, it gives an upper limit or worst-case DJ peak that is also very useful.

However, if the phase noise PSD $L(f)$ is in dBc/Hz, as defined by [equation 7.39](#), phase jitter PSD in rad²/Hz can be represented in terms of $L(f)$ as follows:

Equation 7.46

$$S_{\Phi}(f) = 2 \cdot 10^{\frac{L(f)}{10}}$$

$$\Phi^2$$

Let us denote the DJ spectral line magnitudes in the S_{Φ} domain as DJ_i at frequency f_i , and $i = 1, 2, \dots, N$. We have the following:

Equation 7.47

$$S_{\Phi_{DJ}}(f) = \sum_{i=1}^N \Phi_{DJ_i}^2 \delta(f - f_i)$$

Note that $\Phi_{DJ_i} > 0$. Similarly, the RJ PSD with DJ power spectral lines removed is given by

Equation 7.48

$$S_{\Phi_{RJ}}(f) = S_{\Phi}(f) - S_{\Phi_{DJ}}(f) = S_{\Phi}(f) - \sum_{i=1}^N \Phi_{DJ_i}^2 \delta(f - f_i)$$

As soon as the DJ PSD and RJ PSD are determined, DJ peak Φ_{DJ_pk} upper limit can be estimated as

Equation 7.49

$$\Phi_{DJ_pk} \leq \sum_{i=1}^N \Phi_{DJ_i}$$

and the RJ rms value Φ_{RJ_rms} can be estimated the same way as [equation 7.45](#).

Thus, we have established a complete set of equations to estimate DJ peak value (or pk-pk, assuming that pk-pk = 2pk) upper limits and RJ rms over certain frequency bands from the phase noise PSD measured in either rad²/Hz or dBc/Hz.

Note that most of the phase noise to jitter conversion techniques existing in the literature (such as [12] and [13], to name a couple) do not convert phase noise to DJ pk-pk and RJ rms parameters that are widely used in quantifying time-domain jitter in today's high-speed device characterization and testing. Most of those techniques do not separate DJ from RJ in the phase noise PSD and only give a mixed and broadband rms value that has some serious limitations in the application. The new technique introduced in this section addresses this new emerging need with better comprehension, accuracy, and math rigor.

URL <http://access.proquest.safaribooksonline.com/9780132429610/ch07lev1sec3>

User name: CSU San Diego

Book: Jitter, Noise, and Signal Integrity at High-Speed

Section: Chapter 7. Clock Jitter

No part of any chapter or book may be reproduced or transmitted in any form by any means without the prior written permission for reprints and excerpts from the publisher of the book or chapter. Redistribution or other use that violates the fair use privilege under U.S. copyright laws (see 17 USC107) or that otherwise violates these Terms of Service is strictly prohibited. Violators will be prosecuted to the full extent of U.S. Federal and Massachusetts laws.

Information Theory Computer Science Mike Peng Li Prentice Hall Jitter, Noise, and Signal Integrity at High-Speed

7.4. Summary

This chapter focused on clock jitter to address the special and important roles it plays in synchronized and asynchronous link systems. We started with the reasons and rationales for why we single out clock jitter. Then we discussed the definition of jitter along the same lines as the data jitter definition introduced in previous chapters. The impacts of clock jitter on two distinct systems of synchronized and asynchronous systems were discussed, along with their performance relationships to clock jitter and clock skew. [Section 7.2](#) focused on different types of jitter and metrics for a clock signal due to its even and uniform edge transition property. Phase jitter, period jitter, and cycle-to-cycle jitter were introduced, along with their interrelationships in the time and frequency domains. We pointed out that those different jitter types are different manifestations of the same jitter mechanism and are uniquely related. If you know one of them, you can determine the other with appropriate conditioning. With the introduction of phase jitter, we discussed the important topic of the interrelationship between phase jitter and phase noise in [section 7.3](#). The mathematical representations of phase jitter and phase noise were derived. Detailed procedures and math mapping equations for phase jitter to phase noise conversion, as well as phase noise to phase jitter conversion, were given for both deterministic and random components in the respective phase noise and jitter domains. This information can be very useful given the recent trend that clock performance is specified in terms of phase jitter and/or phase noise. The interchange between them becomes common and necessary.

URL <http://access.proquest.safaribooksonline.com/9780132429610/ch07lev1sec4>

User name: CSU San Diego

Book: Jitter, Noise, and Signal Integrity at High-Speed

Section: Chapter 7. Clock Jitter

No part of any chapter or book may be reproduced or transmitted in any form by any means without the prior written permission for reprints and excerpts from the publisher of the book or chapter. Redistribution or other use that violates the fair use privilege under U.S. copyright laws (see 17 USC107) or that otherwise violates these Terms of Service is strictly prohibited. Violators will be prosecuted to the full extent of U.S. Federal and Massachusetts laws.

Information Theory Computer Science Mike Peng Li Prentice Hall Jitter, Noise, and Signal Integrity at High-Speed

Endnotes

1. A. V. Oppenheim, A. S. Willsky, and S. H. Nawab, *Signals & Systems*, Prentice Hall, 1996.
2. D. Derickson, *Fiber Optic Test and Measurement*, Prentice Hall, 1998.
3. National Committee for Information Technology Standardization (NCITS), working draft for "Fibre Channel—Methodologies for Jitter Specification-MJSQ," Rev 14, 2005.
4. J. M. Rabaey, *Digital Integrated Circuits: A Design Perspective*, Englewood Cliffs, NJ: Prentice Hall, 1996.
5. W. J. Dally and J. W. Poulton, *Digital Systems Engineering*, Cambridge University Press, 1998.
6. M. Li and J. Wilstrup, "Paradigm Shift for Jitter and Noise in Design and Test > 1 Gb/s Communication Systems," IEEE International Conference on Computer Design (ICCD), 2003.
7. M. Li, A. Martwick, G. Talbot, and J. Wilstrup, "Transfer Functions for the Reference Clock Jitter in a Serial Link: Theory and Applications," IEEE International Test Conference (ITC), 2004.
8. PCI Express Jitter white paper (I), 2004:
http://www.pcisig.com/specifications/pcieexpress/technical_library.
9. B. Razavi, "A Study of Phase Noise in CMOS Oscillators," IEEE J. Solid-State Circuits, vol. 31, pp. 331–343, Mar. 1996.
10. J. A. McNeill, "Jitter in Ring Oscillators," IEEE J. Solid-State Circuits, vol. 32, pp. 870–879, June 1997.
11. T. H. Lee and A. Hajimiri, "Oscillator Phase Noise: A Tutorial," IEEE J. Solid-State Circuits, vol. 35, pp. 326–336, Mar. 2000.
12. Rutman, J., "Characterization of Phase and Frequency Instabilities in Precision Frequency Sources: Fifteen Years of Progress," Proceedings of the IEEE, vol. 66, no. 9, Sept. 1978.
13. Boris Drakhlis, "Calculate Oscillator Jitter by Using Phase-Noise Analysis," Microwaves & RF, pp. 82–90, Jan. 2001.

URL <http://access.proquest.safaribooksonline.com/9780132429610/ch07lev1sec5>

User name: CSU San Diego

Book: Jitter, Noise, and Signal Integrity at High-Speed

No part of any chapter or book may be reproduced or transmitted in any form by any means without the prior written permission for reprints and excerpts from the publisher of the book or chapter. Redistribution or other use that violates the fair use privilege under U.S. copyright laws (see 17 USC107) or that otherwise violates these Terms of Service is strictly prohibited. Violators will be prosecuted to the full extent of U.S. Federal and Massachusetts laws.

Information Theory Computer Science Mike Peng Li Prentice Hall Jitter, Noise, and Signal Integrity at High-Speed

8. PLL Jitter and Transfer Function Analysis

Chapter 7, "Clock Jitter," was dedicated to clock jitter. A commonly used clock generation subsystem is phase-locked loop (PLL), which has many unique and important technical aspects and deserves special attention. As such, this chapter focuses on jitter for PLL and its relationship to the PLL characteristics. We start with PLL basics and then move to the generic quantitative study of functional, parametric, jitter, and noise analysis. Last, we focus on practical and specific analysis for second-order and third-order PLLs, covering quantitative details of transfer functions, dynamic parameters, jitter, and noise.

URL <http://access.proquest.safaribooksonline.com/9780132429610/ch08>

User name: CSU San Diego

Book: Jitter, Noise, and Signal Integrity at High-Speed

Section: Chapter 8. PLL Jitter and Transfer Function Analysis

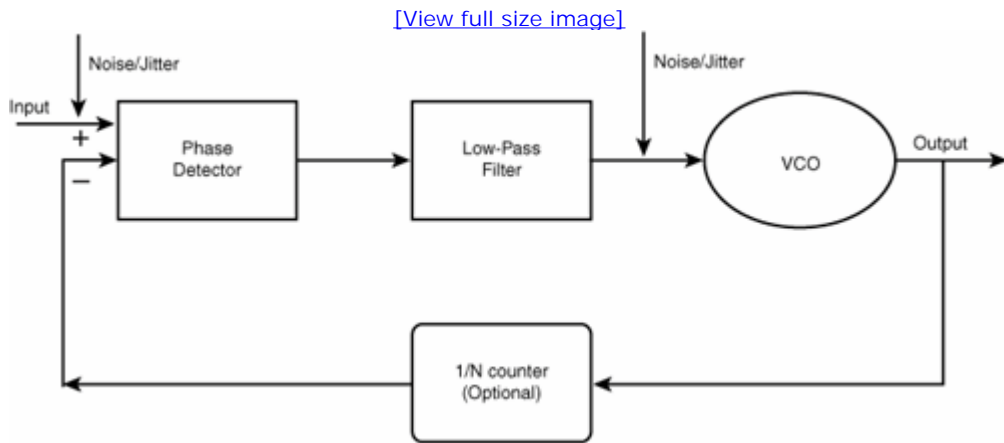
No part of any chapter or book may be reproduced or transmitted in any form by any means without the prior written permission for reprints and excerpts from the publisher of the book or chapter. Redistribution or other use that violates the fair use privilege under U.S. copyright laws (see 17 USC107) or that otherwise violates these Terms of Service is strictly prohibited. Violators will be prosecuted to the full extent of U.S. Federal and Massachusetts laws.

Information Theory Computer Science Mike Peng Li Prentice Hall Jitter, Noise, and Signal Integrity at High-Speed

8.1. PLL Introduction

PLLs are widely used in modern data communication, telecommunication, and computer systems. The PLL itself is a complicated electrical feedback system. Its purpose is to provide clean and stable clock output that will be used by the other parts of the system. A PLL is generally composed of four basic components: phase detector (PD), low-pass filter (LPF), voltage-control oscillator (VCO), and divider/multiplier. [Figure 8.1](#) is a diagram of a PLL system.

Figure 8.1. A PLL block diagram. The noise can be within and/or outside the loop.



Phase noise or jitter is the key metric for evaluating the performance of a PLL system. It can come from within or outside the PLL. The major jitter or noise source outside the PLL comes from the reference clock input. The major noise source within PLL comes from the VCO, which typically has a 1/f PSD shape. For relevant reviews of PLLs and related noise basics and tutorials, refer to [\[1\]](#), [\[2\]](#), and [\[3\]](#).

In addition to clock generation with either multiplied or divided frequency output, PLLs are widely used in modern serial communications to recover the clock from the data bit stream, as discussed in [Chapters 1](#), "Introduction," and [7](#). The recovered clock must have as little noise and jitter as possible; otherwise, the receiver performance will be degraded, and the system's BER will increase.

A PLL is described and quantified in terms of its transfer function, which can be represented in either the time domain or frequency domain. (See [Chapter 2](#), "Statistical Signal and Linear Theory for Jitter, Noise, and Signal Integrity," for more on transfer functions.) The frequency-domain response function in general is an n th-order fractional function that has zeros/poles. The PLL output is the interaction of input signal, jitter and noise processes, and the transfer function. At the design stage, input signal form, jitter and noise temporal and spectral form, and the transfer function can be assumed or determined. Simulating the output signal in both the time and frequency domains is a standard forward problem. However, at the prototype integrated circuit (IC) stage, the situation is quite different and more difficult. What can be accessed in most cases are the PLL's input and/or output signals. On the other hand, it is very important to measure the PLL transfer function and noise processes so that design specifications and simulation assumptions can be checked and verified and potential design flaws and noise sources can be identified and then fixed or improved.

URL <http://access.proquest.safaribooksonline.com/9780132429610/ch08lev1sec1>

User name: CSU San Diego

Book: Jitter, Noise, and Signal Integrity at High-Speed

Section: Chapter 8. PLL Jitter and Transfer Function Analysis

No part of any chapter or book may be reproduced or transmitted in any form by any means without the prior written permission for reprints and excerpts from the publisher of the book or chapter. Redistribution or other use that violates the fair use privilege under U.S. copyright laws (see 17 USC107) or that otherwise violates these Terms of Service is strictly prohibited. Violators will be prosecuted to the full extent of U.S. Federal and Massachusetts laws.

Information Theory Computer Science Mike Peng Li Prentice Hall Jitter, Noise, and Signal Integrity at High-Speed

8.2. PLL Time and Frequency Domain Behavior

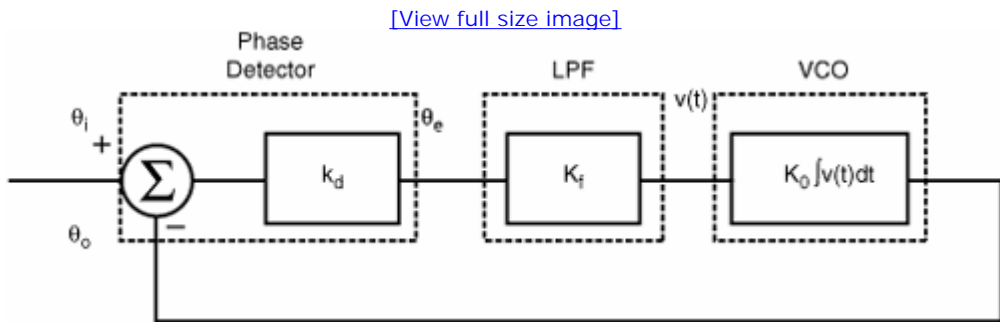
As we have mentioned, a PLL is essentially a complicated feedback system. Therefore, system-level modeling is needed to understand the physical processes. Although a PLL is traditionally studied and modeled in the frequency domain, time-domain modeling can offer some unique information that the frequency domain generally cannot for most practical applications. For example, phase information of a signal is available in the time domain if it is measured by either a sampling or digitizing oscilloscope. It is not available in frequency domain if it is measured by a spectrum analyzer. However, PLL time-domain system impulse response is hard to deal with mathematically, particularly if it is a second-order or higher PLL. Therefore, to get a complete description, both time and frequency domain analyses are needed.

This section discusses PLL system analysis in both the time and frequency domains, as well as the transformation from one to the other.

8.2.1. Time-Domain Modeling and Analysis

Figure 8.2 is a simplified diagram for a time-domain PLL block diagram.

Figure 8.2. Time-domain modeling of a PLL.



In this example, the LPF is simplified by a constant gain factor of K_f . The equation determines the phase error (θ_e) and input phase relationship (θ_i) given the following:^[1], ^[2], ^[3]

Equation 8.1

$$\theta_e(t) = K_d(\theta_i - K_0 K_f \int \theta_e dt)$$

An integral equation generally is hard to solve, so we take the derivative of equation 8.1 and obtain equation 8.2:

Equation 8.2

$$\dot{\theta}_e(t) + K_d K_f K_0 \theta_e = K_d \dot{\theta}_i$$

As soon as θ_e is solved, the PLL output θ_o is readily obtained by the relationship of $\theta_o = \theta_i - \theta_e$.

Equation 8.2 has a general solution of

Equation 8.3

$$\theta_e = e^{-Kt} \left(\int e^{Kt} \theta_i(t) dt + c \right)$$

where $K = K_d K_f K_0$ is the overall loop gain. You can see that θ_e has an exponential decay envelope indicating that the phase error decreases as time increases. However, whether θ_e decays to 0 or a constant phase error depends on the input phase error. If θ_i = constant, it can be shown that as $t \rightarrow \infty$, $\theta_e \rightarrow 0$. In other words, a PLL locks to its frequency with a zero phase error. If the phase increases with time linearly ($\theta_i = \omega t$), it can be shown that as $t \rightarrow \infty$, $\theta_e \rightarrow \text{constant}$. In other words, a PLL can lock to its frequency, but with nonzero error.

The time-domain PLL study indicates a couple points:

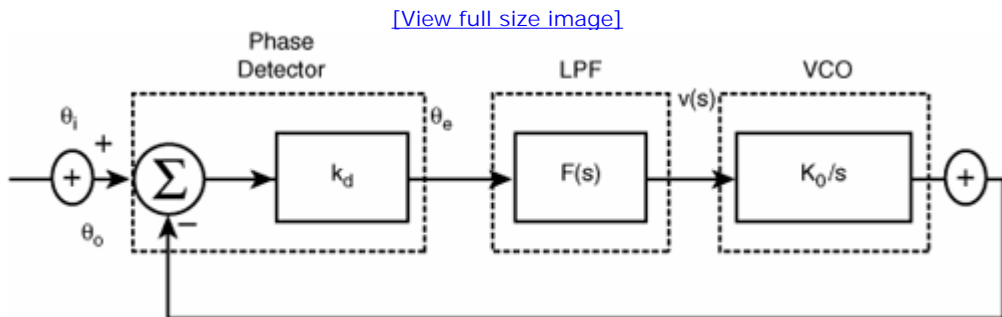
- When the PLL is a first-order system (that is, LPF has a constant gain), it can be modeled by a closed-form solution.
- It is not straightforward to model the jitter/noise process and its interrelationship with loop components in the time domain.

The next section explores frequency-domain analysis and how it plays out.

8.2.2. Frequency-Domain Modeling and Analysis

A PLL can also be modeled in a complex frequency domain (s-domain or Laplace domain) with the linear system assumption. A linear system assumption is a good approximation for PLLs. Figure 8.3 shows a mathematical model for a PLL in the s-domain.

Figure 8.3. A complex s-domain PLL model. Note that the gain and s-domain transfer functions for the loop components are all shown.



Due to the interrelationship that an integral in the time domain is equivalent to $1/s$ in the s-domain (see section 2.5 in Chapter 2), the VCO transfer function becomes K_0/s . The LPF is represented by a general function of the form $F(s)$. Because this is a linear feedback system, the overall transfer function can be obtained through multiplication and division operations of the transfer functions for individual components in the system. This greatly simplifies the mathematical difficulties. The PLL system transfer function is given by

Equation 8.4

$$H_o = \frac{\theta_0(s)}{\theta_i(s)} = \frac{K_d K_o F(s)}{s + K_d K_o F(s)}$$

and the error transfer function is

Equation 8.5

$$H_e(s) = \frac{\theta_e(s)}{\theta_i(s)} = \frac{K_d s}{s + K_d K_o F(s)} = 1 - H_0(s)$$

From [equations 8.4](#) and [8.5](#), you can see that as soon as the transfer function is given, the output signal θ_o is readily obtained for a given input signal θ_i in the s-domain. The time-domain response can then be solved through the inverse Laplace transformation.

[Equation 8.5](#) suggests a complementary relationship ($H_e(s) + H_0(s) = 1$) between the system transfer function $H_0(s)$ and the error transfer function $H_e(s)$. This means that if $H_0(s)$ is a low-pass function, a general case for practical PLLs, $H_e(s)$ should be a high-pass function. The exact form of $H_0(s)$ and $H_e(s)$ depends on the exact LPF transfer function $F(s)$. We will discuss the specific $F(s)$ for second- and third-order PLLs in later sections.

URL <http://access.proquest.safaribooksonline.com/9780132429610/ch08lev1sec2>

User name: CSU San Diego

Book: Jitter, Noise, and Signal Integrity at High-Speed

Section: Chapter 8. PLL Jitter and Transfer Function Analysis

No part of any chapter or book may be reproduced or transmitted in any form by any means without the prior written permission for reprints and excerpts from the publisher of the book or chapter. Redistribution or other use that violates the fair use privilege under U.S. copyright laws (see 17 USC107) or that otherwise violates these Terms of Service is strictly prohibited. Violators will be prosecuted to the full extent of U.S. Federal and Massachusetts laws.

Information Theory Computer Science Mike Peng Li Prentice Hall Jitter, Noise, and Signal Integrity at High-Speed

8.3. PLL Functional and Parametric Analysis

This section discusses functional and parametric analysis for a PLL. Functional analysis focuses on different representations derived from the transfer functions to highlight different PLL characteristics. Parametric analysis focuses on parameters associated with PLL dynamic tracking and acquisition processes, as well as noise bandwidth.

8.3.1. Functional Analysis

With the PLL s-domain transfer function, a few interesting and important functional analyses can be carried out. These include magnitude and phase, impulse or step response, Bode plots, and pole zero locations. They provide useful insights into PLL characteristics.

8.3.1.1. Phase and Magnitude Responses

The PLL s-domain transfer function can be rewritten as a product of magnitude and phase functions of the following:

Equation 8.6

$$H_o(s) = H_o(\omega)e^{j\phi(\omega)}$$

where $H_0(\omega)$ is the magnitude frequency response and $\phi(\omega)$ is the phase frequency response. They relate to the s-domain transfer function with $s = j\omega$ as

Equation 8.7

$$H_o(\omega) = |H_0(j\omega)| = \left| \frac{K_d K_o F(j\omega)}{j\omega + K_d K_o F(j\omega)} \right|$$

and

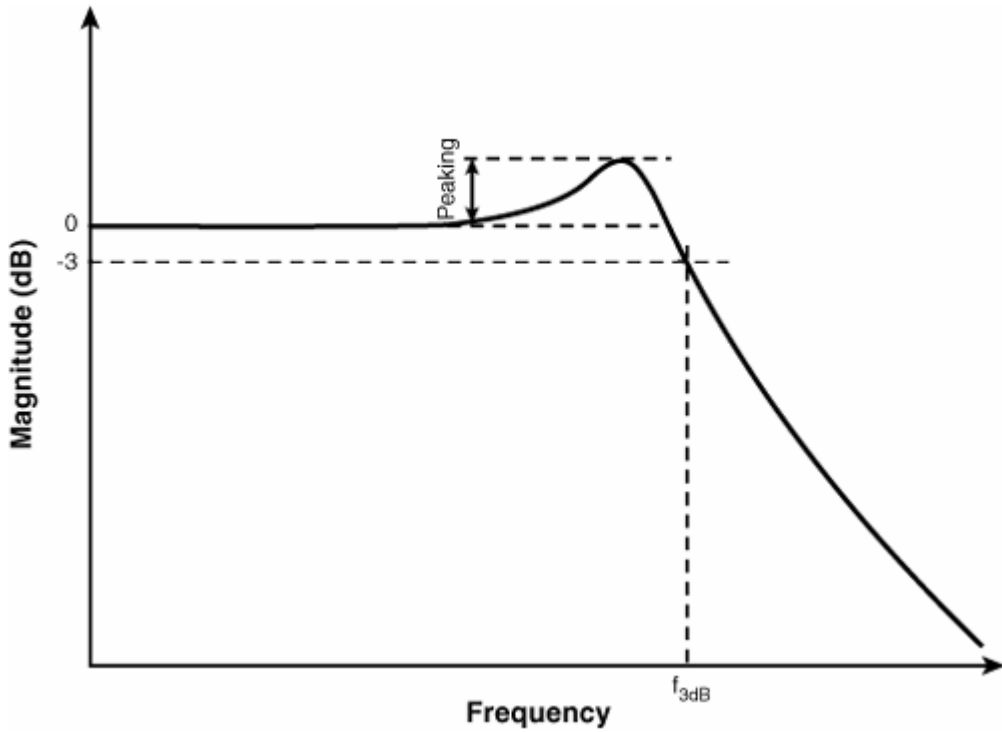
Equation 8.8

$$\phi(\omega) = \text{Arg}(H_0(j\omega)) = \text{Arg} \left[\frac{K_d K_o F(j\omega)}{j\omega + K_d K_o F(j\omega)} \right]$$

where $||$ is the magnitude operation and Arg is the phase angle operation for a complex function. We would like to point out that both are important for a linear system. One cannot replace the other, and both need to be studied for linear system analyses (see [section 2.5](#)). For example, peaking effect and 3 dB frequency can be studied with magnitude frequency response, and phase linearity and group delay can be studied with phase frequency response function.

Because $F(s)$ is a LPF, the magnitude function is a low-pass function in general, according to [equation 8.7](#). [Figure 8.4](#) shows the general PLL magnitude response function.

Figure 8.4. The PLL transfer function magnitude response, along with the definition of peaking and 3 dB bandwidth.



Two important parameters associated with a PLL magnitude response function are illustrated: its peaking and its 3 dB frequency. A large peaking causes the PLL to be unstable, and a larger 3 dB frequency implies a faster PLL tracking capability. If the PLL is used as a clock recovery unit in a receiver, larger peaking causes the jitter amplification, a scenario that increases the chance of receiver bit error.

8.3.1.2. PLL Impulse/Step Response

We have shown that a PLL system can be studied in a complex s-domain in terms of its transfer function. Due to the linear system property, the time-domain impulse or step response can also be studied given the complex s-domain transfer function. Assuming that $h(t)$ is the impulse response and $u(t)$ is the step response of the PLL, $H_0(s)$, $h(t)$, and $u(t)$ can be related through the Laplace transformation (see [section 2.5](#)). Specifically, we have

Equation 8.9

$$h(t) = \int_{c-j\infty}^{c+j\infty} H_0(s)e^{st} ds$$

and

Equation 8.10

$$u(t) = \int_0^t h(\tau) d\tau = \int_{c-j\omega}^{c+j\omega} \frac{H_0(s)}{s} e^{st} ds$$

With the impulse response, you can predict the output through convolution given the input in the time domain. Suppose that $\theta_i(t)$ is the input for the PLL. The output $\theta_o(t)$ is given by

Equation 8.11

$$\theta_o(t) = \int_{-\infty}^{\infty} \theta_i(\tau) h(t - \tau) d\tau$$

8.3.1.3. Bode Plots

PLL is a feedback system, and stability analysis is an important aspect. The transfer function of [equation 8.4](#) can be rewritten as

Equation 8.12

$$H_o(s) = \frac{\theta_0(s)}{\theta_i(s)} = \frac{K_d K_o \frac{F(s)}{s}}{1 + K_d K_o \frac{F(s)}{s}}$$

$$1 + K_d K_o \frac{F(s)}{s} = 0, H_o(s)$$

The PLL is unstable if the singularity condition (or Barkhausen condition) is satisfied. In other words, if $\rightarrow \infty$. The singularity condition is a complex equation; it implies that both magnitude and phase need to satisfy

Equation 8.13

$$|K_d K_o \frac{F(s)}{s}| = 1$$

and

Equation 8.14

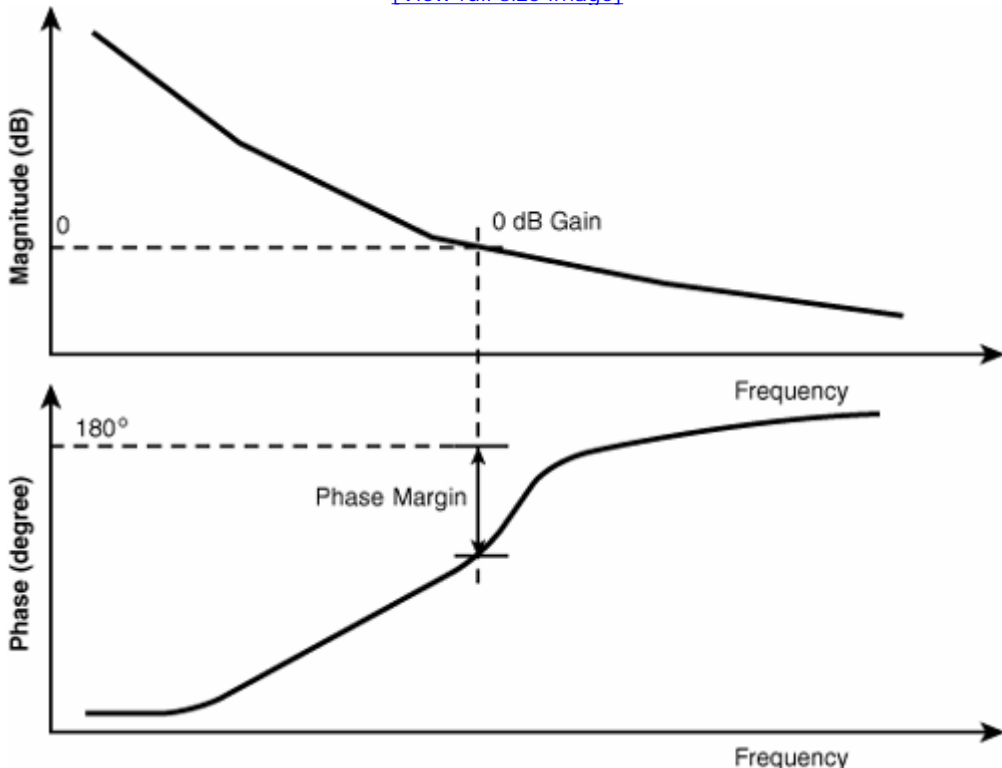
$$\text{Arg} \left[K_d K_o \frac{F(s)}{s} \right] = 180^\circ$$

$$G(s) = K_d K_o \frac{F(s)}{s}$$

Note that $s = j\omega$. Defining $G(s)$ is the open-loop gain function for the PLL. [Equations 8.13](#) and [8.14](#) imply that the open-loop gain determines the stability. The magnitude and phase frequency function plots are called Bode plots. The singularity conditions of [equations 8.13](#) and [8.14](#) suggest that to achieve a stable PLL, the open-loop gain magnitude should be less than 1 when its phase is at 180° , or its phase should be less than 180° when the open-loop gain magnitude is at 1, as shown in [Figure 8.4](#). Note that the phase margin is also shown in [Figure 8.5](#).

Figure 8.5. Bode plot illustration. Open-loop magnitude and phase responses, 0 dB or unit gain, and phase margin are all shown.

[\[View full size image\]](#)



8.3.1.4. Poles and Zeros

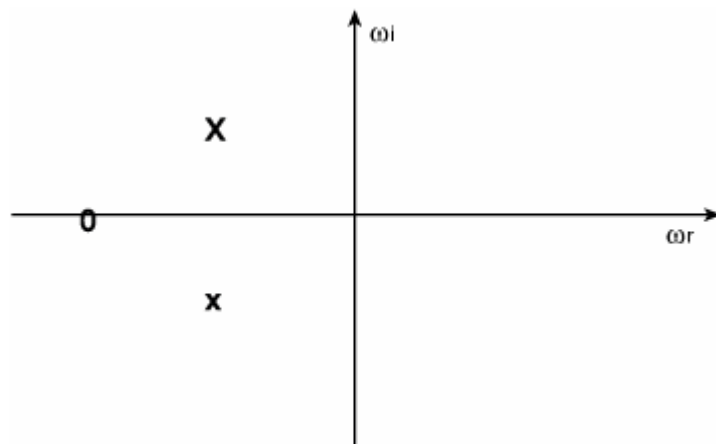
Pole and zero analysis is very useful for a linear system and is complementary to other functional analysis methods. By studying the number of poles and zeros and their locations on the complex frequency domain, system instability, ringing, and decaying characteristics can be determined very quickly.

Poles are complex frequencies at which the system transfer function $H_o(s)$ goes to infinite. These are the solutions when the denominator polynomial of the transfer function $H_o(s)$ equals zero. Zeros are complex frequencies at which the system transfer function $H_o(s)$ goes to zero. These are the solutions for the equation when the numerator polynomial of the transfer function $H_o(s)$ equals zero.

Zeros locate at frequencies when a transmission zero can occur. Poles offer quick diagnostics for PLL stability. In general, poles close to the imaginary axis generate ringing or oscillation features in the time domain. Poles located close to the real axis produce exponential decay in the time domain, or phase delay in the frequency domain. Poles located on the right side of the imaginary axis make the system unstable. For a stable PLL, all poles must be located on the left side of the imaginary axis of the s-plane.

Figure 8.6 shows a pole and zero plot for a second-order PLL system (two poles, one zero).

Figure 8.6. A pole and zero location plot for a two-pole, one-zero PLL. Poles are denoted as X, and zero is denoted as 0.

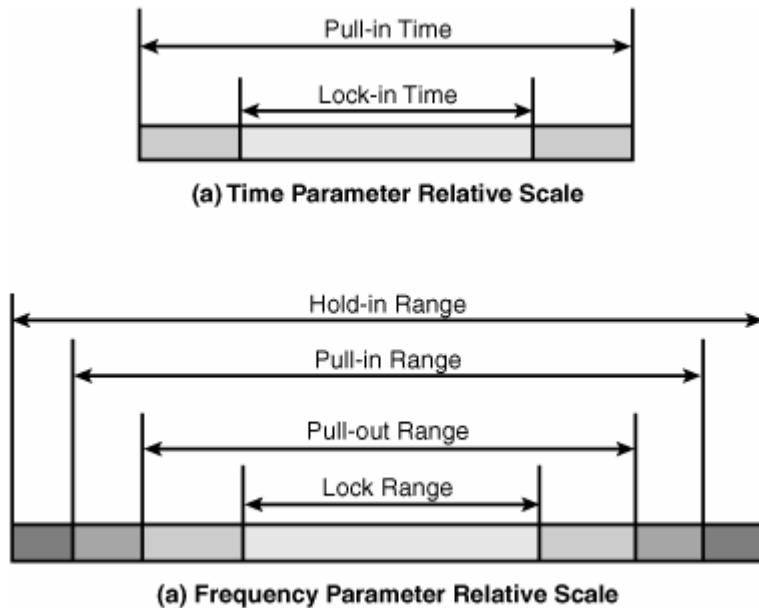


8.3.2. Parametric Analysis

So far we have assumed that a PLL is a linear system and is under the locked condition. However, when the PLL is under an unlocked condition, the PLL system becomes nonlinear. Of course, a nonlinear treatment for an unlocked PLL is needed if comprehensive modeling and analysis are required. When a PLL is not in a locked state, common questions include the following: What is the condition for a PLL to get locked? What is the condition for a PLL to lose the lock? How long does it take for a PLL to get locked? These questions can be studied and answered without going into the details of solving a general nonlinear system equation.

A few key parameters are critical to understanding and quantifying the locking (acquisition) and unlocking (tracking) processes. They are lock-in time, lock range, pull-in time, pull-in range, and hold range for acquisition, and pull-out range for tracking. Lock-in time is defined as the time for a PLL to lock on to the input reference signal frequency within one frequency beat-note period (between the PLL output and the input reference signal). It is a fast locking process. Lock-in range is the frequency range within which the PLL locks to the reference frequency in one beat-note period. Pull-in time is the time for a PLL to remain locked on the reference frequency but within a time frame of longer than several beat-note periods. It is the metric for a slow locking process. Pull-in range is the frequency range that is larger than the lock-in range but that still permits a PLL to lock on to the input reference signal frequency within a time frame of several frequency beat notes. As a matter of fact, the locking process corresponds to a time frame of within one frequency beat-note period, and the pull-in process corresponds to a time frame of several beat-note periods. It is apparent that lock-in time and lock-in range are smaller than pull-in time and pull-in range, respectively. Hold range has more theoretical interest than practical interest. It is defined as the frequency range for an input reference beyond which a PLL never locks in. Hold range is larger than both pull-in and locking range. When the frequency offset of the reference signal is less than the holding range but larger than the pull-in range, the PLL is called conditionally stable. Pull-out range is the maximum abrupt frequency change that can be applied to the PLL input reference signal while a lock-in state can still be achieved. If a sudden frequency deviation exceeds the pull-out range, the PLL unlocks. [Figure 8.7](#) gives relative scale for all those times associated with PLL acquisition and tracking processes.

Figure 8.7. Relative scales for PLL acquisition and tracking times and frequencies.



Another aspect of the PLL is the jitter and/or noise. When significant jitter and/or noise are present on the input reference signal, the PLL lock-in and pull-in processes are affected. The question becomes how big the jitter, the signal-to-noise-ratio (SNR), and the noise bandwidth need to be such that lock-in and pull-in processes will not be bothered by the presence of noise. It is intuitive that smaller jitter, higher SNR, and smaller noise bandwidth give better noise performance.

Quantitative discussions about those time and noise parameters for second- and third-order PLLs appear in the next sections, when the exact PLL transfer functions are given. This section serves as a general introduction to and overview of those parameters.

User name: CSU San Diego

Book: Jitter, Noise, and Signal Integrity at High-Speed

Section: Chapter 8. PLL Jitter and Transfer Function Analysis

No part of any chapter or book may be reproduced or transmitted in any form by any means without the prior written permission for reprints and excerpts from the publisher of the book or chapter. Redistribution or other use that violates the fair use privilege under U.S. copyright laws (see 17 USC107) or that otherwise violates these Terms of Service is strictly prohibited. Violators will be prosecuted to the full extent of U.S. Federal and Massachusetts laws.

Information Theory Computer Science Mike Peng Li Prentice Hall Jitter, Noise, and Signal Integrity at High-Speed

8.4. PLL Jitter and Noise Analysis

Three aspects are essential for PLL:

- The overall loop transfer function that is determined by its subsystem characteristics
- The noise process and its origin and spectrum shape
- The interrelationship and interaction between the loop-transfer function and noise process, and how they affect PLL's overall performance

Theoretically, you can address these aspects from the time domain, the frequency domain, or both. However, it is much easier to estimate phase noise at the PLL in terms of each noise source associated with the PLL elements in the complex s-domain due to the linear operation in such a domain.

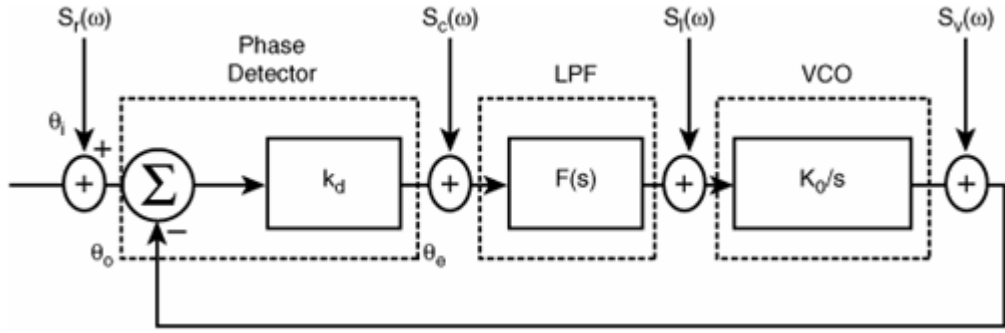
8.4.1. Phase Jitter Power Spectrum Density (PSD)

Traditionally, a PLL noise process is quantified by the overall noise power and noise bandwidth. The major shortfall of this approach is that it does not give the dynamic aspect of the PLL behavior. Given the importance of jitter as a metric for PLL performance, it is hard to separate jitter from noise, especially for PLL where the relevant noise is phase noise and the relevant jitter is phase jitter. The question of how the PLL noise or jitter changes as a function of time or frequency is not addressed by noise bandwidth and noise power. A more comprehensive method is needed to address the dynamic aspect of the PLL noise or jitter behavior. If we assume that the noise contribution in a PLL is additive, and if we know which component the noise or jitter is associated with, the PLL noise or jitter PSD can be estimated, as demonstrated in this section. Because phase jitter and phase noise are related by the carrier frequency (see [section 7.3](#) in [Chapter 7](#)), phase jitter is readily obtainable if phase noise is determined.

PLL noise or jitter can potentially come from each element, as shown in [Figure 8.8](#). The PSD for the phase noise or jitter associated with the reference input is denoted as $S_r(\omega)$. It is commonly caused by the oscillator thermal or 1/f noise in the reference signal generator. $S_c(\omega)$ is the charge-pump phase noise or jitter PSD and is commonly caused by thermal noise within the charge pump. A charge pump is used to enable simple loop filter implementation. $S_l(\omega)$ is the phase noise or jitter PSD associated with the LPF and is commonly in the active LPF. $S_v(\omega)$ is the phase noise or jitter PSD associated with the VCO, and its spectrum is mostly dominated by the 1/f noise. Note that phase noise and jitter PSDs are the same PSD physically, but with different and related units.

Figure 8.8. PLL elements, associated transfer function, and phase noise source.

[\[View full size image\]](#)



Using the general input-output relationship between PSD and transfer function between the input-output pair, we can derive the relationship between the PLL output PSD with each individual input PSD, because all the individual phase noise or jitter can be considered additive and independent. For the reference phase noise or jitter input, we have

Equation 8.15

$$S_{or}(\omega) = S_r(\omega) \left| \frac{K_d K_o F(s)}{s + K_d K_o F(s)} \right|_{s=j\omega}^2$$

For the charge pump phase noise or jitter input, we have

Equation 8.16

$$S_{oc}(\omega) = S_c(\omega) \left| \frac{K_o F(s)}{s + K_d K_o F(s)} \right|_{s=j\omega}^2$$

For the LPF noise or jitter input, we have

Equation 8.17

$$S_{ol}(\omega) = S_l(\omega) \left| \frac{K_o}{s + K_d K_o F(s)} \right|_{s=j\omega}^2$$

For the VCO phase noise or jitter input, we have

Equation 8.18

$$S_{ov}(\omega) = S_v(\omega) \left| \frac{s}{s + K_d K_o F(s)} \right|_{s=j\omega}^2$$

The overall PSD at the PLL output is the sum of all the PSDs at the output location due to the individual noise or jitter source because of the superimposition property for the PSD. Thus, we have

Equation 8.19

[\[View full size image\]](#)

$$S_o(\omega) = S_{or}(\omega) + S_{oc}(\omega) + S_{oi}(\omega) + S_{ov}(\omega) \\ = \left[S_r(\omega) \left| \frac{K_d K_o F(s)}{s + K_d K_o F(s)} \right|^2 + S_c(\omega) \left| \frac{K_o F(s)}{s + K_d K_o F(s)} \right|^2 + S_i(\omega) \left| \frac{K_o}{s + K_d K_o F(s)} \right|^2 + S_v(\omega) \left| \frac{s}{s + K_d K_o F(s)} \right|^2 \right]_{s=j\omega}$$

Recall the open-loop gain for a PLL:[\[1\]](#), [\[2\]](#), [\[3\]](#)

Equation 8.20

$$G_{OL}(s) = \frac{K_d K_o F(s)}{s}$$

Then [equation 8.19](#) can be generalized to the following form for N individual noise/jitter input:

Equation 8.21

$$S_o(\omega) = \sum_{i=1}^N S_i(\omega) \left| \frac{G_{FG_i}(s)}{1 + G_{OL}(s)} \right|_{s=j\omega}^2$$

where $S_i(\omega)$ is the individual phase noise or jitter input PSD and $G_{FG_i}(s)$ is the forward gain function starting from the phase noise or jitter injection point.

[Equation 8.19](#) can have several implications. First, it provides an analytical relationship between PLL output phase noise or jitter PSD and individual PSD within and outside the PLL, through various well-defined transfer functions. This implication is more relevant to the modeling and simulation applications of [equation 8.19](#) where individual phase noise or jitter and transfer function can be assumed. Second, it allows the determination of PLL internal or external phase noise or jitter PSD and transfer function parameters if the output phase noise or jitter PSD and forms of both transfer function and internal noise PSD are known. This implication is more relevant to PLL individual phase noise or jitter and transfer function characterization or measurement given that the PLL phase noise or jitter is measured or known. We will discuss the application modes of [equation 8.19](#) in [sections 8.5](#) and [8.6](#) in more detail. Even though four or more individual phase noise or jitter sources can be associated with a PLL, there are only two dominant ones for most practical PLLs: one source from the reference signal such as the reference clock, and another from the VCO.

8.4.2. Variance and PSD

The preceding section discussed PLL jitter or noise analysis in the complex frequency domain in terms of PSD. This section discusses its counterpart in the time domain—specifically, the autocorrelation function and how it and PSD are related for a PLL.

In the absence of deterministic jitter or noise, the variance function describes rms change as a function of time. Recall [equation 6.29](#) for the relationship between the variance function and the autocorrelation function in the time domain:

Equation 8.22

$$\sigma_t^2(t) = 2(\sigma_0^2 - R_{tt}(\Delta t_n(t), \Delta t_0))$$

where σ_t^2 is the variance at time t , σ_0^2 is the total variance of the underlying jitter or noise process, and R_{tt} is the autocorrelation function between jitter or noise $\Delta t_n(t)$ and Δt_0 . It is well known that the autocorrelation function R_{tt} relates to the PSD $S(f)$ through Fourier Transformation (that is, the Wiener-Khinchine theorem; see [section 2.4.4.2](#)):

Equation 8.23

$$R_{tt}(\Delta t_n(t), \Delta t_0) = \mathcal{F}^{-1}(S(\omega))$$

where \mathfrak{I}^{-1} denotes the inverse Fourier Transformation. Substituting [equation 8.23](#) into [equation 8.22](#), we obtain the equation that relates variance time series with the frequency-domain PSD of the jitter or noise process:

Equation 8.24

$$\sigma_j^2(t) = 2(\sigma_0^2 - \mathfrak{I}^{-1}(S(\omega)))$$

[Equation 8.24](#) lays a theoretical foundation to link the phase jitter or noise process measurable in the time domain to that in the frequency domain.

One application of [equations 8.23](#) and [8.24](#) is to estimate the time-domain autocorrelation function or variance function from the PSD $S_0(\omega)$ at the PLL output, as discussed in [section 8.4.1](#).

Recall [equation 2.113](#). At $t = 0$, we have

Equation 8.25

$$R_n(0) = \frac{1}{2\pi} \int_{-\infty}^{\infty} S_x(\omega) d\omega = \sigma_0^2$$

This tells us that the autocorrelation function at time zero or delay zero gives the estimation of the total power for the phase noise or jitter.

The following section uses [equations 8.22](#) through [8.25](#) extensively to study the phase jitter or noise characteristics of second- and third-order PLLs.

URL <http://access.proquest.safaribooksonline.com/9780132429610/ch08lev1sec4>

User name: CSU San Diego

Book: Jitter, Noise, and Signal Integrity at High-Speed

Section: Chapter 8. PLL Jitter and Transfer Function Analysis

No part of any chapter or book may be reproduced or transmitted in any form by any means without the prior written permission for reprints and excerpts from the publisher of the book or chapter. Redistribution or other use that violates the fair use privilege under U.S. copyright laws (see 17 USC107) or that otherwise violates these Terms of Service is strictly prohibited. Violators will be prosecuted to the full extent of U.S. Federal and Massachusetts laws.

Information Theory Computer Science Mike Peng Li Prentice Hall Jitter, Noise, and Signal Integrity at High-Speed

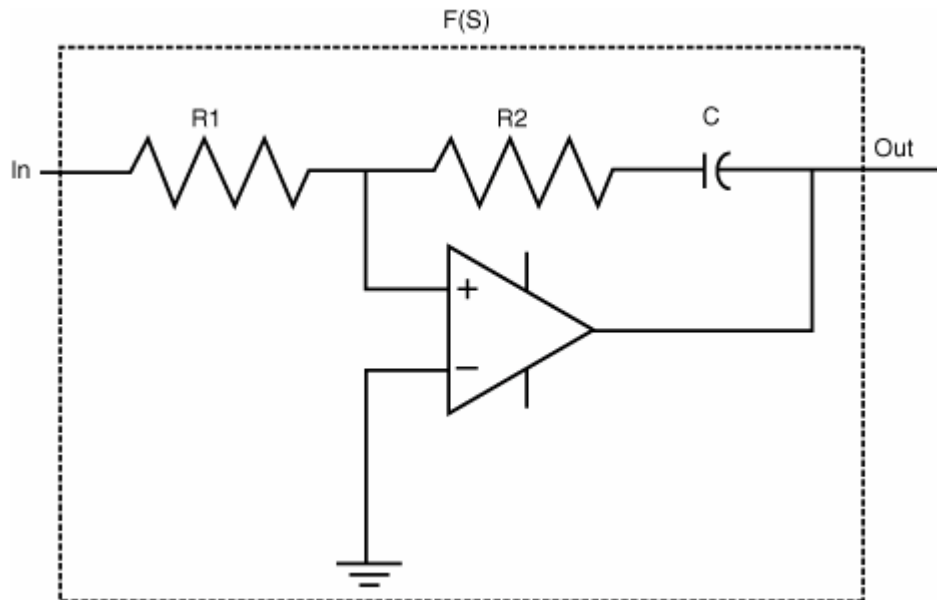
8.5. A Second-Order PLL Analysis

This section focuses on second-order PLL analysis. We will first derive its transfer function. Then we will discuss how to determine and analyze its jitter or noise, as well as the transfer function for types of PLLs with the variance method introduced in [section 8.4](#). Some experimental results are shown at the end of the section.

8.5.1. System Transfer Function

The commonly implemented PLLs are second-order because they can track both frequency and phase changes. The order of the PLL is determined by the LPF of the PLL. A second-order PLL can be achieved with the first-order active proportional-integrating (PI) filter, shown in [Figure 8.9](#).

Figure 8.9. An active proportional-integrating circuit for a second-order PLL.



The transfer function for such a LPF can be found as:

Equation 8.26

$$F(s) = \frac{1+sR_2C}{sR_1C} = \frac{1+s\tau_2}{s\tau_1}$$

where τ_1 and τ_2 are RC time constants for resistors R_1 and R_2 . Substituting [equation 8.26](#) into [8.4](#), we find that the overall PLL transfer function is

Equation 8.27

$$H_2 = \frac{\frac{K_d K_0}{\tau_1} \tau_2 s + \frac{K_d K_0}{\tau_1}}{s^2 + \frac{K_d K_0}{\tau_1} \tau_2 s + \frac{K_d K_0}{\tau_1}}$$

For easy mathematical handling and comparison to [equation 8.27](#), it would be beneficial to rewrite [equation 8.27](#) in a standard second-order dynamic damping system in terms of natural frequency and damping factor:

Equation 8.28

$$H_2(s) = \frac{2\zeta\omega_n s + \omega_n^2}{s^2 + 2\zeta\omega_n s + \omega_n^2}$$

$$\omega_n = \sqrt{\frac{K_d K_0}{\tau_1}} \quad \zeta = \frac{\tau_2}{2} \sqrt{\frac{K_d K_0}{\tau_1}} = \frac{\omega_n \tau_2}{2}$$

with natural frequency ω_n and damping factor ζ . Damping factor and natural frequency are system parameters, and gain and RC time constant are circuit parameters. They are interchangeable according to their definition relationships.

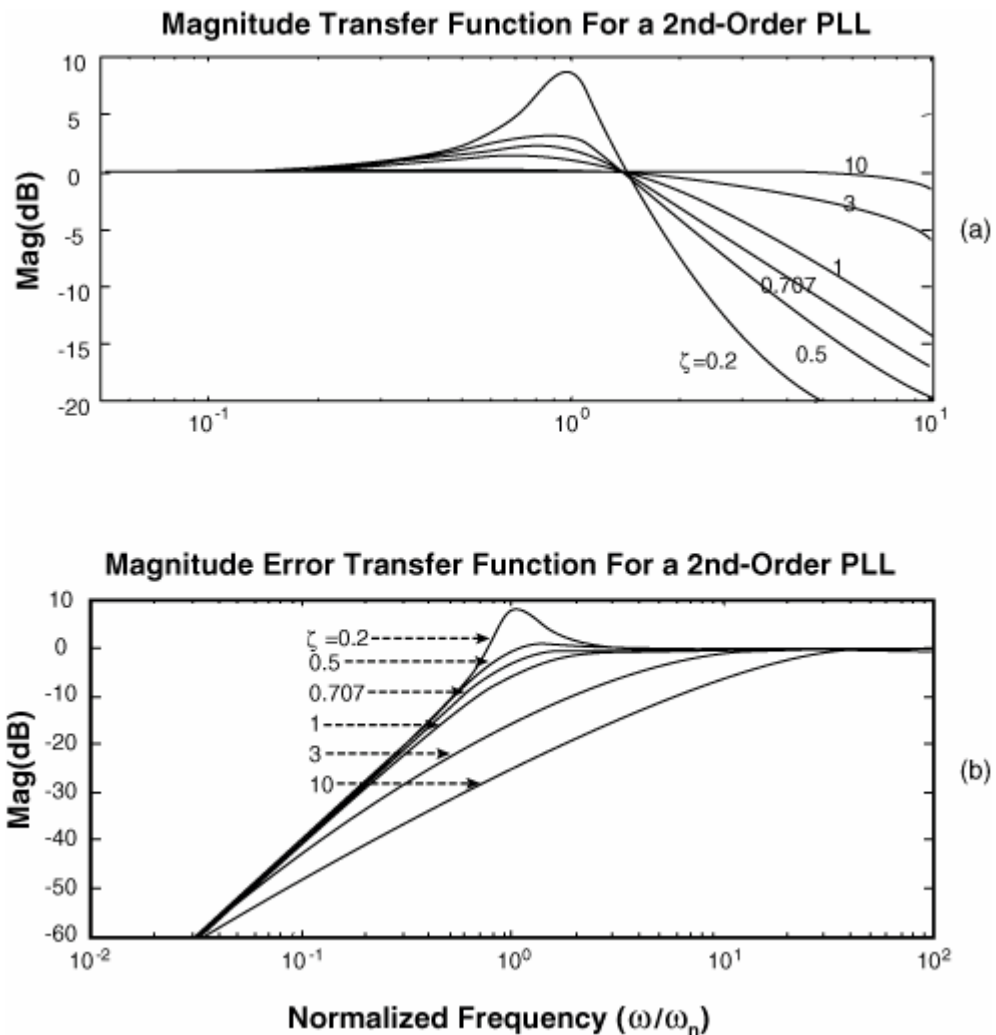
Although we have derived the standard second-order PLL transfer function of [equation 8.28](#) with an active PI LPF implemented, other first-order LPF implementations are also possible. Under the high-gain condition—namely, $K_d K_0 \gg 1$ —all the first-order LPF implementation converges to the form of [equation 8.28](#). Because most PLLs operate under the high-gain condition, [equation 8.28](#) has become the standard form for a second-order PLL.

The characteristics of the second-order PLL are shown in [Figure 8.10](#) as a function of its damping factor for both the system transfer function and error transfer function. The error transfer function is of particular interest because it is a jitter transfer function for the receiver in a serial link where a PLL is used as the clock recovery circuit. ([Chapter 9](#), "Jitter and Signal Integrity Mechanisms for High-Speed Links," contains a more detailed discussion.) Apparently, the system transfer function has a low pass, with a -20 dB/decade decay rate for $\omega > \omega_n$. This means that high-frequency input phase is attenuated by the PLL. On the other hand, the error transfer function is a high pass with a 40 dB/decade slope for $\omega < \omega_n$. This means that low-frequency phase error is attenuated by the PLL. The transfer function has three distinctive behaviors. For $\zeta < 1$, it is called an underdamped PLL, and peaking can occur. For $\zeta > 1$, it is called an overdamped PLL. For $\zeta = 1$, it is called a critically damped PLL. The optimal PLL transfer function has a flat gain at $\omega < \omega_n$.

$$\zeta = \frac{1}{\sqrt{2}} \approx 0.707$$

A $\zeta = \frac{1}{\sqrt{2}}$ gives a close-to-flat transfer function response. Under such a condition, PLL transfer function is the same as a second-order Butterworth low-pass filter.

Figure 8.10. System (a) and error (b) transfer functions and their dependencies on the damping factor.



3 dB frequency and peaking are the common observables for PLL magnitude transfer function $|H_o(s)|$. The 3 dB frequency for a second-order PLL can be estimated in terms of damping factor ζ and natural frequency ω_n as follows:

Equation 8.29

$$\omega_{3dB} = \sqrt{1 + 2\zeta^2 + \sqrt{(1 + 2\zeta^2)^2 + 1}} \quad \omega_n$$

The peaking estimation for a second-order PLL is typically done through the numeric method because the close-form solution is complex. Conceptually, we should be able to express the PLL transfer function in terms of its peaking and 3 dB pair

$(|\Delta H_o(s)|_{PK}, \omega_{3dB})$ as well. Theoretically, a mapping relationship exists between peaking and 3 dB pair of $(|\Delta H_o(s)|_{PK}, \omega_{3dB})$ and damping factor and natural frequency pair of (ζ, ω_n) . However, due to the complexity of the close-form relationship, the mapping normally is done using numeric approaches.

8.5.2. Characteristic Parameters

A second-order PLL transfer function is uniquely determined by the damping factor ζ and natural frequency ω_n . With those two key parameters, other PLL parameters related to PLL tracking, acquisition, and noise bandwidth can be derived in terms of those two parameters.

The PLL jitter or noise bandwidth can be better derived from the phase noise relationship between PLL output and input. The total rms value for the PLL phase jitter or noise at its output can be estimated by the following:

Equation 8.30

$$\sigma_o^2 = \int_0^\infty S_o(\omega) d\omega = \int_0^\infty S_r(\omega) |H_0(j\omega)|^2 d\omega$$

Here we use the PSD and transfer function relationships introduced in [section 8.4](#) and assume that jitter or noise is introduced only at the PLL reference input. Let us further assume that the jitter or noise PSD at the reference input is a constant—namely, $S_r(\omega) = \Phi_0$. An example of this type of PSD is thermal or white jitter or noise. Then [equation 8.30](#) can be simplified as follows:

Equation 8.31

$$\sigma_o^2 = \Phi_0 \int_0^\infty |H_0(j\omega)|^2 d\omega$$

The integral part within [equation 8.31](#) has a dimension of angular frequency. If we define the jitter or noise bandwidth as

Equation 8.32

$$\omega_{NB} = \int_0^\infty |H_0(j\omega)|^2 d\omega$$

substituting this definition into [equation 8.31](#), we obtain the following:

Equation 8.33

$$\sigma_o^2 = \Phi_0 \omega_{NB}$$

[Equation 8.33](#) is a quick way to estimate the PLL output jitter or noise rms given the PSD and the bandwidth for jitter or noise. Using the transfer function H_2 defined in [equation 8.28](#), the jitter or noise bandwidth for a second-order PLL can be estimated as follows:

Equation 8.34

$$\omega_{NB2} = \frac{\omega_n}{2} \left(\zeta + \frac{1}{4\zeta} \right)$$

Other parameters for tracking and acquisition processes can also be estimated in terms of ζ and ω_n , such as lock-in time, lock-in range, pull-in time, and pull-in range. Refer to [\[1\]](#), [\[2\]](#), and [\[3\]](#) for detailed derivations. Here we give only the formulas for estimating those parameters in terms of ζ and ω_n . [Table 8.1](#) lists the results, assuming that the PLL LPF is an active PI filter.

Table 8.1. Second-Order PLL Parameters

Acquisition	Lock-in time	$\frac{2\pi}{\omega_n}$
	Lock-in range	$2\zeta \omega_n$
	Pull-in time	$\frac{\pi^2}{16} \frac{\Delta\omega_0^2}{\zeta \omega_n^3}$

	Pull-in range	∞
	Hold range	∞
Tracking	Pull-out range	$1.8(\zeta+1)\omega_n$
Noise	Noise bandwidth	$\frac{\omega_n}{2}(\zeta + \frac{1}{4\zeta})$

Clearly, ζ and ω_n are the key. As soon as they are known, the rest of the parameters can be calculated based on the formulas in [Table 8.1](#).

8.5.3. Jitter and Transfer Function Analysis

This section addresses PLL jitter or noise and transfer function measurement and analysis. A novel PLL transfer function determination method is discussed first, followed by experiment results.[\[6\]](#), [\[7\]](#)

8.5.3.1. Time-Domain Variance Function-Based Methodology

This section focuses on PLL jitter and transfer function analysis. The jitter output of a PLL is rather straightforward and falls into the clock jitter measurement and analysis general category introduced in [Chapter 7](#). Time-domain variance function measurement is of particular interest, because it provides the linkage to the PLL jitter PSD that links to the PLL transfer function. What we try to establish is a method to determine the PLL transfer function by measuring and analyzing PLL output jitter variance function.

Recall [equation 8.24](#) for a general variance function. PLL jitter or noise typically has two sources.[\[2\]](#) One is the jitter or noise associated with the reference clock at the PLL input denoted by its PSD of $S_r(\omega)$, and another is the jitter or noise associated with the VCO denoted by its PSD.

When the reference clock noise/jitter is dominant, its variance function can be estimated using [equations 8.19](#), [8.24](#), and [8.28](#):

Equation 8.35

$$\sigma_{rl}^2(t) = 2 \left(\sigma_0^2 - \Im^{-1} \left(S_r(\omega) \left| \frac{2\zeta\omega_n s + \omega_n^2}{s^2 + 2\zeta\omega_n s + \omega_n^2} \right|^2 \right) \right)$$

Similarly, when the VCO jitter or noise is dominant, its variance function can be estimated as follows:

Equation 8.36

$$\sigma_{vl}^2(t) = 2 \left(\sigma_0^2 - \Im^{-1} \left(S_v(\omega) \left| \frac{s^2}{s^2 + 2\zeta\omega_n s + \omega_n^2} \right|^2 \right) \right)$$

When both the reference clock and VCO jitter or noise are dominant, its variance function can be estimated as follows:

Equation 8.37

[\[View full size image\]](#)

$$\sigma_{rl}^2(t) = 2 \left(\sigma_0^2 - \Im^{-1} \left(S_r(\omega) \left| \frac{2\zeta\omega_n s + \omega_n^2}{s^2 + 2\zeta\omega_n s + \omega_n^2} \right|^2 + S_v(\omega) \left| \frac{s^2}{s^2 + 2\zeta\omega_n s + \omega_n^2} \right|^2 \right) \right)$$

Given the measured or assumed jitter $\sigma_{mea}^2(t)$, ζ and ω_n can be estimated through optimization with a goal of minimizing the difference between $\sigma_t^2(t)$ and $\sigma_{mea}^2(t)$:

Equation 8.38

$$\text{Min} \left(\int |\sigma_t(t) - \sigma_{mea}(t)| dt \right) \rightarrow 0$$

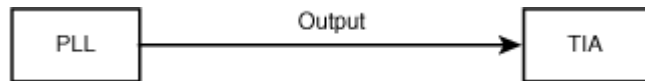
where $\sigma_t^2(t)$ can take the form of [equation 8.35](#) or [8.37](#), depending on the circumstances. There are many optimization methods, including commonly used least-squared, χ^2 , and maxima likelihood.^[4]

After ζ and ω_n are determined, the PLL transfer function is known. Other functional analyses such as error transfer function, Bode plots, and pole/zero locations are readily calculated following the discussions in [section 8.3.1](#). Similarly, PLL tracking, acquisition, and noise bandwidth parameters can be estimated according to [Table 8.1](#).

8.5.3.2. Experimental Results

The variance function-based PLL analysis only needs to measure the PLL output. [Figure 8.11](#) shows the setup for the measurement. It is very straightforward, and there is no need for a modulation signal generator as the stimulus at the PLL input. Here we show a time interval analyzer (TIA) as the measurement equipment because it is well suited for variance function measurement due to its precision timing and high throughput.

Figure 8.11. PLL measurements using the variance method with a TIA system.



The device under test (DUT) in the following example is a 150 MHz clock recovery PLL. It has three distinct designs: underdamped, overdamped, and moderately damped. In each scenario, both functional and parametric analyzing results are presented.

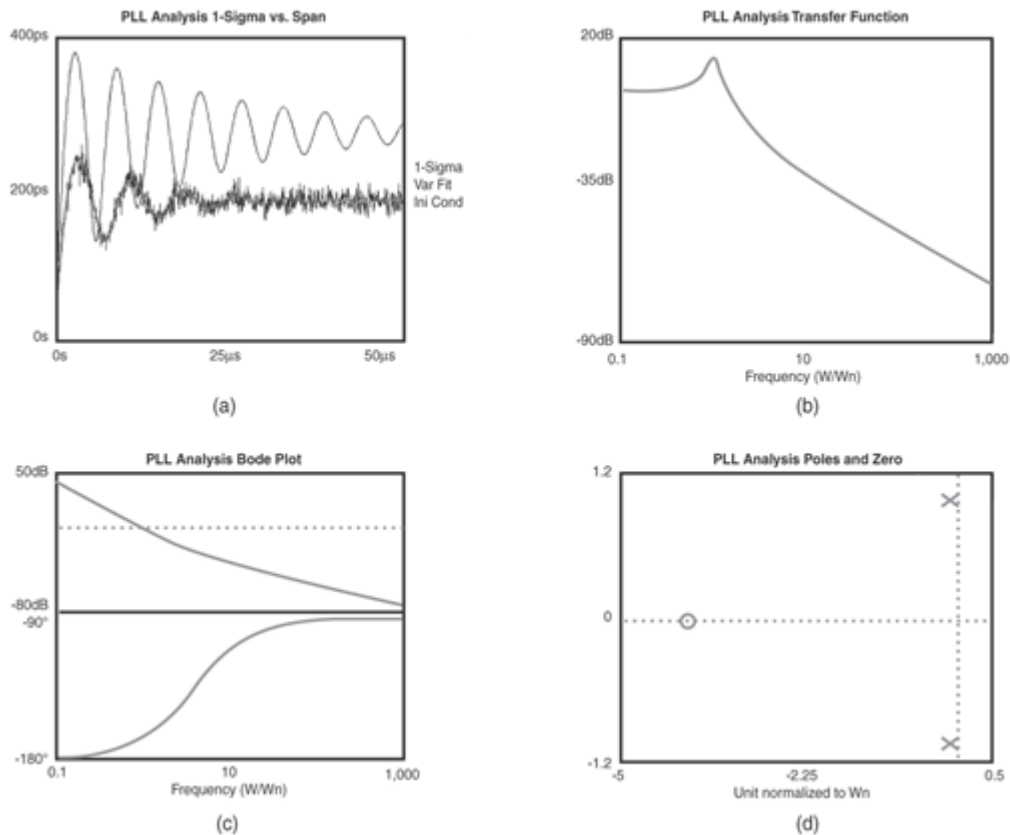
8.5.3.2.1. An Underdamped PLL

In this case, the PLL is operated under the $\zeta < 1$ condition. Also, it is assumed that the PLL is dominated by the thermal noise ($S_r(\omega) = N_0 = \text{constant}$) from the reference clock and that the variance function model takes the form of [equation 8.35](#). The variance function is first measured with a TIA (such as SIA 4000). Then the variance model defined by [equation 8.35](#) is used to fit the variance record. The best fitted parameters ζ , ω_n , and N_0 are obtained through the χ^2 fit method^[5] that gives the best immunity to statistical noise and fluctuation in the measurement variance record.

[Figure 8.12](#) shows four different functional analyses for this PLL. The decay oscillating characteristic is obvious in (a), suggesting that this is an underdamped PLL. Its magnitude transfer function (b) shows ~ 15 dB peaking. Its Bode plots (c) suggest that it has only a few degrees of stability margin. Its poles are located very close to the imaginary axis, suggesting a marginally stable PLL.

Figure 8.12. Functional analyses for an underdamped PLL. (a) Measured variance record, with an initial estimated variance function and the optimized variance record; (b) measured transfer function magnitude frequency response; (c) measured Bode plots, in which the upper panel is for the magnitude frequency response, and the lower panel is for the phase frequency response; (d) measured pole and zero locations.

[\[View full size image\]](#)



The exact parameters for the transfer function, thermal noise magnitude, noise bandwidth, tracking, and acquisition are listed in [Table 8.2](#).

Table 8.2. Parametric Analyses for an Underdamped PLL

Damping factor : ζ	0.124811
Natural frequency: ω_n	135.384105 kHz
PSD of noise : N_0	-83.003435 dBc/Hz
Lock range	33.794923 kHz
Lock-in time	7.386391 μs
Pull-in time	4.54924 ms
Pull-out range	274.106821 kHz
Noise bandwidth	144.037557 kHz

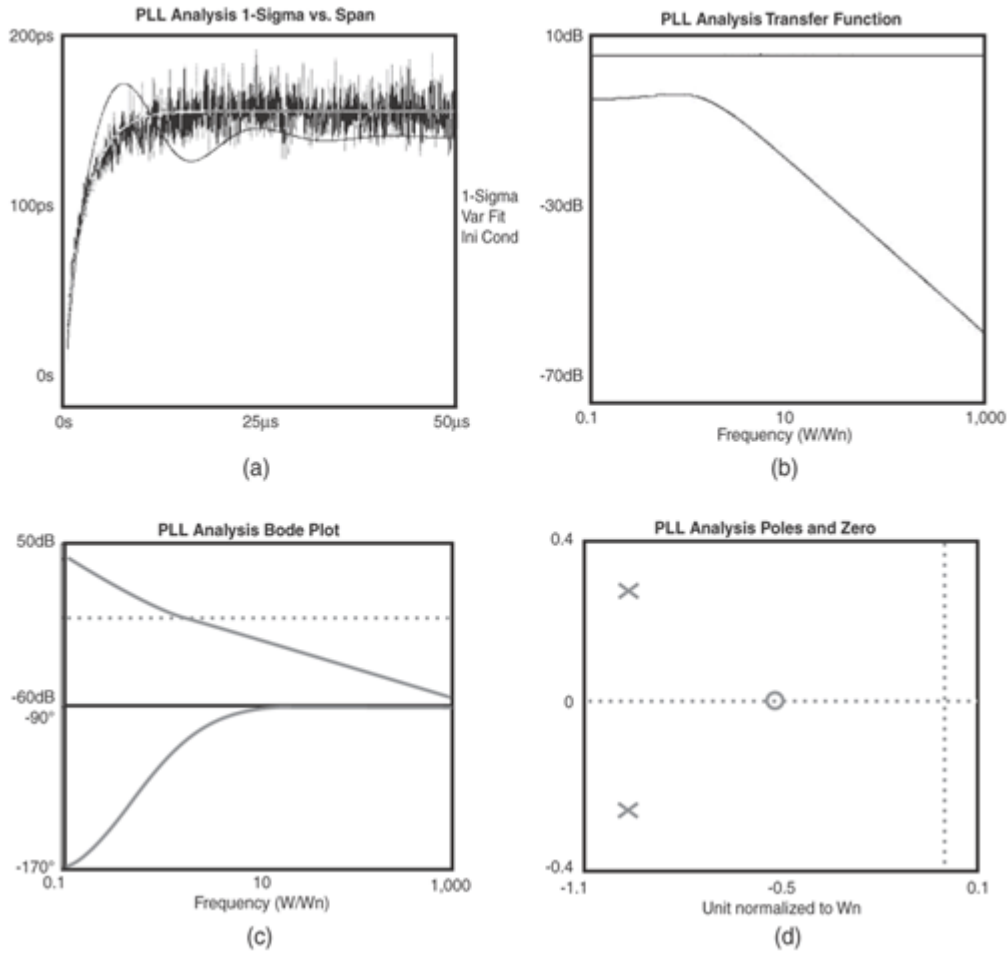
The quantitative numbers of damping factor and natural frequency give the expected damping and oscillating behavior for the variance function, and the peaking for the transfer function. Thus, self-consistent results are obtained.

8.5.3.2.2. An Overdamped PLL

In this case, PLL is overdamped, and we should expect no oscillation in the variance function and no peaking in the transfer function. [Figure 8.13](#) shows the results in a format similar to that for an undersampled PLL.

Figure 8.13. The same as Figure 8.12, but for an overdamped PLL.

[\[View full size image\]](#)



The PLL Bode plots indicate that it has a safe $\sim 90^\circ$ of stability margin, larger than that of an underdamped PLL. Its poles are located very far from the imaginary axis, suggesting a very stable PLL.

Table 8.3 lists key PLL parameters.

Table 8.3. Parametric Analyses for an Overdamped PLL

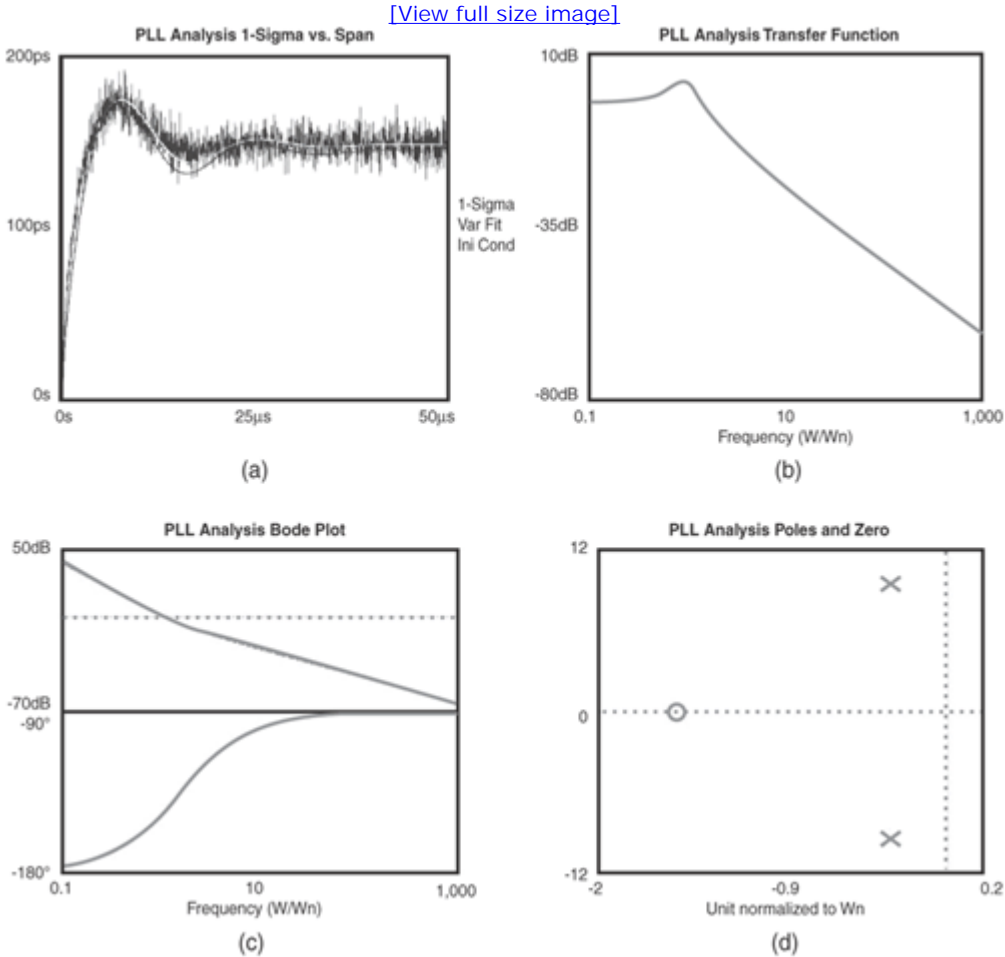
Damping factor	0.96456
Natural frequency	67.439788 kHz
PSD of noise	-78.907076d dBc/Hz
Lock range	130.099482 kHz
Lock-in time	14.828042 μs
Pull-in time	4.68902 ms
Pull-out range	238.481151 kHz
Noise bandwidth	41.264577 kHz

In comparison with Table 8.2, we notice that the damping factor is now close to unity. However, the natural frequency has dropped by roughly half. Due to the increase in damping factor and the decrease in natural frequency, the lock range, lock-in time, and pull-in time all increase, and the noise bandwidth gets smaller due to the dominant effect of the decrease in natural frequency.

8.5.3.2.3. A Moderately Damped PLL

The PLL under test does not have the fine resolution to be programmed as a critically damped or optimized PLL—namely, $\zeta = 0.707$. Figure 8.14 shows the best that we can achieve.

Figure 8.14. The same as Figure 8.12, but for a moderately damped PLL.



Its peaking in magnitude frequency response, phase margin in Bode plots, and pole and zero locations are between overdamped and underdamped PLLs.

The key parameters are listed in Table 8.4.

Table 8.4. Parametric Analyses for a Moderately Damped PLL

Damping factor	0.322121
Natural frequency	59.410615 kHz
PSD of noise	-78.465001 dBc/Hz
Lock range	38.274839 kHz
Lock-in time	16.832009 μs
Pull-in time	20.5467 ms
Pull-out range	141.386462 kHz
Noise bandwidth	32.623158 kHz

In comparison with Tables 8.2 and 8.3, we notice that the damping factor for this PLL is between overdamped and underdamped PLLs. It has the best (smallest) noise bandwidth among these three distinct PLLs. Its lock-in and pull-in characteristics are not as good as the underdamped PLL, but it is comparable to the overdamped PLL. It seems that moderately damped and overdamped PLL has comparable overall performance. They are both better than the underdamped PLL.

Correlation studies are also done for the same PLL with other methods and simulation results. The agreements are good and typically

are within 10% with assumptions about dominant thermal noise in the reference input and a second-order PLL.

URL <http://access.proquest.safaribooksonline.com/9780132429610/ch08lev1sec5>

User name: CSU San Diego

Book: Jitter, Noise, and Signal Integrity at High-Speed

Section: Chapter 8. PLL Jitter and Transfer Function Analysis

No part of any chapter or book may be reproduced or transmitted in any form by any means without the prior written permission for reprints and excerpts from the publisher of the book or chapter. Redistribution or other use that violates the fair use privilege under U.S. copyright laws (see 17 USC107) or that otherwise violates these Terms of Service is strictly prohibited. Violators will be prosecuted to the full extent of U.S. Federal and Massachusetts laws.

Information Theory Computer Science Mike Peng Li Prentice Hall Jitter, Noise, and Signal Integrity at High-Speed

8.6. A Third-Order PLL Analysis

Third-order PLL has been getting more attention in high-speed link component usage in recent years as data rates increase to multiple Gbps. One of the major advantages of a third-order PLL is that it can track frequency acceleration, whereas a second-order PLL can track only the frequency change (or phase acceleration). Furthermore, a third-order PLL can suppress more high-frequency harmonics above its 3 dB frequency for a feed-through clock than that of a second-order PLL. This section presents a third-order PLL study in a format similar to that for a second-order PLL. However, the method of determining the jitter transfer function for a third-order PLL is in the frequency domain and is more generic, yet still is backward-scalable to a second-order PLL,^[8] as discussed extensively in [section 8.5](#).

8.6.1. System Transfer Function

The steady state of the phase error after any transients have died away can be evaluated using the final value theorem of a Laplace transformation (L-transform), which states

Equation 8.39

$$\lim_{t \rightarrow \infty} y(t) = \lim_{s \rightarrow 0} sY(s)$$

where $y(t)$ and $Y(s)$ are the system output in the time and complex frequency domains, respectively. In other words, the steady-state value of a function in the time domain can be determined by inspecting its transform in the complex frequency domain. Applying the final value theorem of the PLL phase error given by [equation 8.5](#) yields the following:

Equation 8.40

$$\lim_{t \rightarrow \infty} \theta_e(t) = \lim_{s \rightarrow 0} \frac{s^2 \theta_i(s)}{s + K_0 K_d F(s)}$$

To achieve zero phase error in the steady state in [equation 8.40](#), the filter function $F(s)$ has to take the form of $F(s) = Y(s)/s^2$, where $Y(0) \neq 0$. Furthermore, the constraint of $\lim_{s \rightarrow \infty} F(s) < +\infty$ requires that the order of $Y(s)$ cannot exceed 2, which is the order of the denominator of $F(s)$. Let

Equation 8.41

$$Y(s) = s^2 + a_2 s + a_3$$

where a_2 and a_3 are constants and $a_3 \neq 0$. Then the loop filter transfer function $F(s)$ of a typical third-order PLL is given as

Equation 8.42

$$F(s) = \frac{s^2 + a_2 s + a_3}{s^2}$$

and the closed-loop PLL transfer function according to equation 8.4 is given as

Equation 8.43

$$H_3(s) = \frac{K(s^2 + a_2 s + a_3)}{s^3 + K(s^2 + a_2 s + a_3)}$$

where $K = K_0 K_d$ is the loop gain. According to equation 8.43, the loop filter transfer function of the third-order PLL contains two cascaded ideal integrators and can eliminate the steady-state acceleration error corresponding to the input phase change of acceleration ($\theta_i(t) = \frac{1}{2} \Delta \omega t^2 u(t)$), phase change of speed ($\theta_i(t) = \Delta \omega t u(t)$), and phase change itself ($\theta_i(t) = \Delta \theta_0 u(t)$).

Following the procedure just shown, the closed-loop transfer function of a general n th-order PLL can also be obtained as follows:

Equation 8.44

$$H_n(s) = \frac{K(s^{n-1} + a_2 s^{n-2} + \dots + a_n)}{s^n + K(s^{n-1} + a_2 s^{n-2} + \dots + a_n)}$$

Third-order PLL transfer function examples are shown in Figure 8.15. Notice that the "negative" peaking predicted by a third-order PLL model cannot be created by a second-order. Later we will show an example with such "negative" peaking from a real-world third-order PLL. This is a new signature for a third-order PLL.

Figure 8.15. Third-order PLL transfer functions. The upper panel shows conventional peaking (positive); the lower panel shows new "negative" peaking that is not possible from a second-order PLL.

Source: J. Ma, M. Li, and M. Marlett, "A New Measurement and Analysis Method for a Third-Order Phase Locked Loop (PLL) Transfer Function," International Test Conference, 2005. (© 2005 IEEE)

[\[View full size image\]](#)

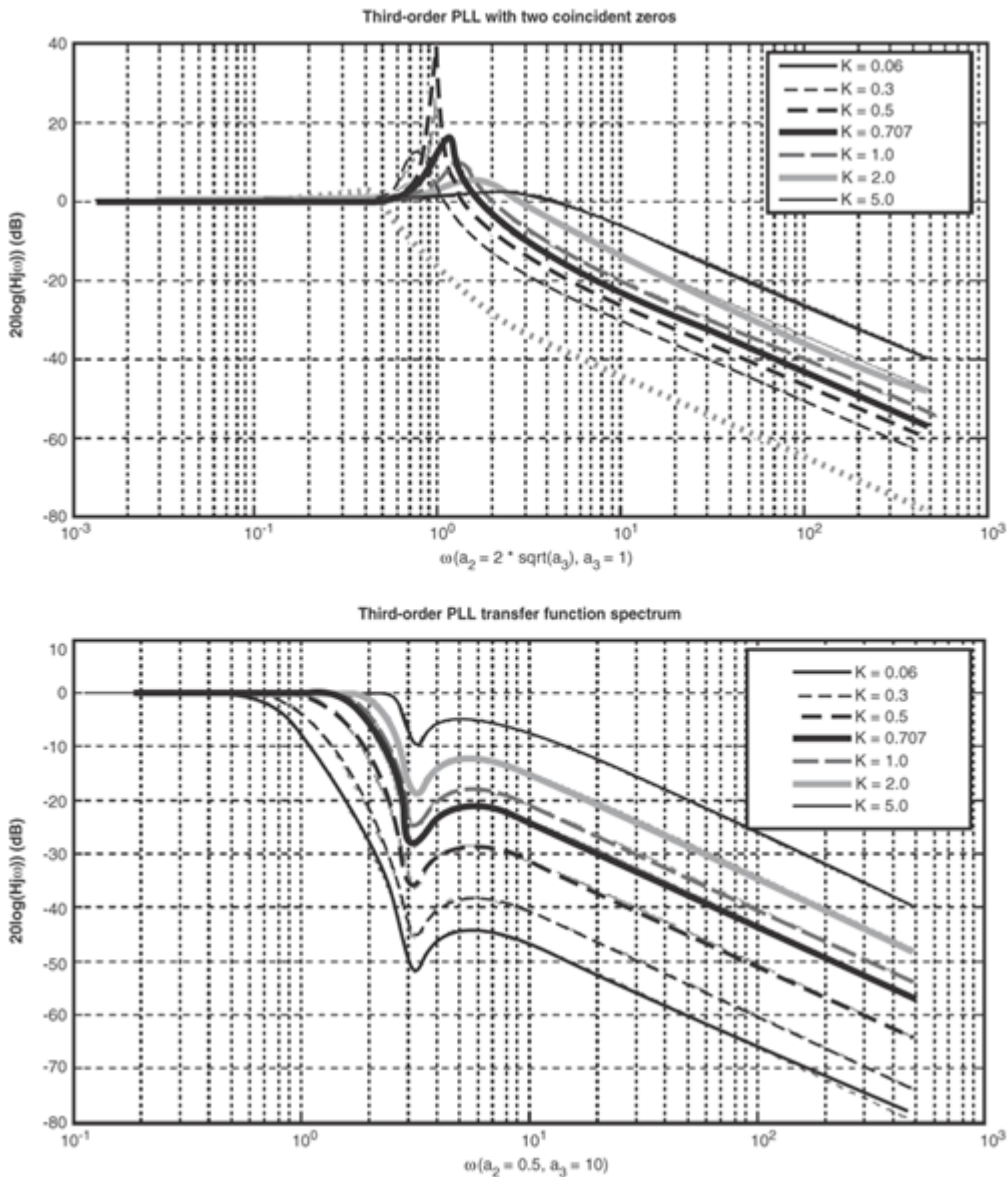


Figure 8.15 shows typical third-order PLL transfer functions with different loop gain K values. The top panel (a) shows the conventional peaking (positive) with $a_2 = 2$ and $a_3 = 1$ for various loop-gain K values. The bottom panel (b) shows the transfer functions with $a_2 = 0.5$ and $a_3 = 10$ for various K values. However, (b) exhibits local minimum or "negative peaking" in the transition band, which could never be observed in second-order PLLs. Frequency contents can be significantly attenuated at the "negative peaking" frequency and this is a new feature for a third-order PLL. A useful application for "negative peaking" is in suppressing periodic jitter at the peaking frequency if a clock recovery is designed to have this characteristic.

8.6.2. Characteristic Parameters

A third-order PLL transfer function is uniquely determined by the loop gain K and parameters a_2 and a_3 . With these three parameters, other PLL parameters related to PLL tracking, acquisition, and noise bandwidth can be derived, similar to the case for a second-order PLL.

Recall the jitter or noise bandwidth for a generic PLL of equation 8.32. The jitter or noise bandwidth for a third-order PLL is given by

$$\text{Equation 8.45}$$

$$\omega_{NB3} = \int_0^{\infty} |H_3(j\omega)|^2 d\omega = \frac{1}{4} K \frac{a_2 K - a_2^2 - a_3}{a_2 K - a_3}$$

Other parameters for tracking and acquisition processes can also be estimated in terms of K , a_2 , a_3 , and DC loop gain $K_{DC} = K_d K_o F(0)$. Refer to [1] and [8] for detailed derivations. Here we give only the formulas for estimating those parameters in terms of K , a_2 , a_3 , and K_{DC} . [Table 8.5](#) shows the results.

Table 8.5. Third-Order PLL Parameters

Acquisition	Lock-in time	$\frac{2\pi}{\sqrt{K a_2}}$
	Lock-in range	K
	Pull-in time	$\sqrt{\frac{\pi}{a_3}} \frac{\Delta\omega_0}{K}$ when $\Delta\omega_0 \gg K$
	Pull-in range	$\sqrt{2 K K_{DC}}$ when $K_{DC} \gg K$
	Hold range	K_{DC}
Tracking	Pull-out range	$1.8(\frac{K}{2} + \sqrt{K a_2})$
Noise	Noise bandwidth	$\frac{K}{4} \frac{a_2 K - a_2^2 - a_3}{a_2 K - a_3}$

Source: J. Ma, M. Li, and M. Marlett, "A New Measurement and Analysis Method for a Third-Order Phase Locked Loop (PLL) Transfer Function," International Test Conference, 2005. (© 2005 IEEE)

Similar to the case for a second-order PLL, as soon as K , a_2 , and a_3 are known, the rest of the parameters are ready to be calculated based on the formulas in [Table 8.5](#).

8.6.3. Jitter and Transfer Function Analysis

For second-order PLL, jitter/noise and transfer function analysis was done in the time domain by matching the model variance function with that of the measured variance function, according to [equation 8.24](#). For a third-order PLL, we realize that the math is too complicated to conduct an inverse FFT for a third-order PLL to obtain a close-form solution. Because the variance function and PSD are dual pairs and are related through [equation 8.24](#), we will explore frequency-domain PSD matching to determine the best model parameters for a third-order PLL to simplify the math and make the method scalable. We will use the PSD frequency-domain close-form models given and discussed in [section 8.4.1](#) for various jitter or noise sources and injection points.

8.6.3.1. Frequency-Domain PSD-Based Methodology

As with a second-order PLL, we will consider two important and commonly encountered jitter or noise sources. One is associated with the reference clock at the PLL input denoted by its PSD $S_r(\omega)$, and the other is associated with the VCO denoted by its PSD $S_v(\omega)$.

Substituting third-order PLL transfer function [equation 8.43](#) to the PLL PSD output general formula of [equation 8.19](#), we can derive the PSD for the third-order PLL. When the reference clock jitter or noise is dominant, the PSD at the output can be estimated as follows:

Equation 8.46

$$S_{\text{ref}}(\omega) = \left(S_r(\omega) \left| \frac{K(s^2 + a_2 s + a_3)}{s^3 + K(s^2 + a_2 s + a_3)} \right|^2 \right)$$

When the VCO jitter or noise is dominant, its PSD at the output can be estimated as follows:

Equation 8.47

$$S_{\text{v}}(\omega) = \left(S_v(\omega) \left| \frac{s^3}{s^3 + K(s^2 + a_2 s + a_3)} \right|^2 \right)$$

When both reference clock and VCO jitter or noise are dominant, its PSD can be estimated as follows:

Equation 8.48

$$S_{\text{all}}(\omega) = \left(S_r(\omega) \left| \frac{K(s^2 + a_2 s + a_3)}{s^3 + K(s^2 + a_2 s + a_3)} \right|^2 \right) + \left(S_v(\omega) \left| \frac{s^3}{s^3 + K(s^2 + a_2 s + a_3)} \right|^2 \right)$$

Given the measured or simulated jitter $S_{0_mea}(\omega)$, the K , a_2 , and a_3 parameters can be estimated through optimization with a goal of minimizing the difference between $S_0(\omega)$ and $S_{0_mea}(\omega)$:

Equation 8.49

$$\text{Min} \left(\int (S_o(\omega) - S_{o_mea}(\omega))^2 d\omega \right) \rightarrow 0$$

where $S_0(\omega)$ can take the form of [equation 8.46](#) or [8.48](#), depending on the circumstances. As is the case for the second-order PLL, we use the $\chi^{[2]}$ minimization method.

If the measured or simulated data is the time domain $\sigma_{mea}^2(t)$, it can be converted to the frequency domain $S_{0_mea}(\omega)$ through a different form of [equation 8.24](#):

Equation 8.50

$$S_{0_mea}(\omega) = \Im \left(\sigma_0^2 - \frac{1}{2} \sigma_{mea}^2(t) \right)$$

where \Im stands for Fourier Transformation. Having obtained parameters of K , a_2 , and a_3 , the third-order PLL transfer functions and acquisition and tracking parameters can also be determined.

From the preceding analysis procedure, you can see that the frequency-domain PSD-based analysis method is scalable in terms of PLL order and is backward-compatible to a second-order. The math is relatively easier compared with the time-domain variance-based method, as far as the close-form model is concerned.

8.6.3.2. Experimental Results

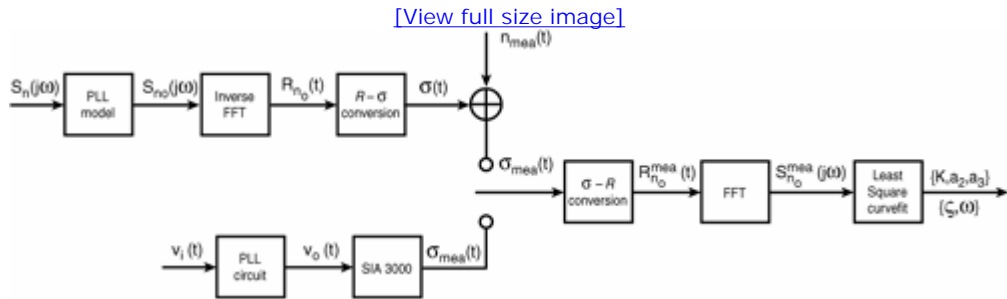
We will show experimental results to verify the validity and accuracy of third-order PLL jitter/noise and transfer function analysis based on the PSD in the frequency domain. We will present two levels of verification. One is simulation-based, where PLL PSD at the output is generated by a simulation program. The other is actually device-based, where the PLL PSD is measured from a real third-order PLL. The simulation is less constrained compared with an actual PLL device in terms of test coverage and control flexibility.

8.6.3.2.1. Simulation and Verification

A simulation model and flowchart is shown in [Figure 8.16](#). The jitter variance record of the PLL output phase jitter can come from two sources. The upper-left branch of [Figure 8.16](#) is a computer-generated measurement source with measurement noise $n_{\text{mea}}(t)$ added to the $\sigma(t)$ to obtain a simulated 1-sigma jitter variance record $\sigma_{\text{mea}}(t)$, assuming a third-order PLL. The lower-left branch is a direct measurement using a TIA from a real third-order PLL circuit.

Figure 8.16. Third- or higher-order PLL simulation/verification model and flowchart.

Source: J. Ma, M. Li, and M. Marlett, "A New Measurement and Analysis Method for a Third-Order Phase Locked Loop (PLL) Transfer Function," International Test Conference, 2005. (© 2005 IEEE)



Part (a) of [Figure 8.17](#) shows the simulation model generated jitter variance record results of a third-order PLL with closed-loop transfer function given as

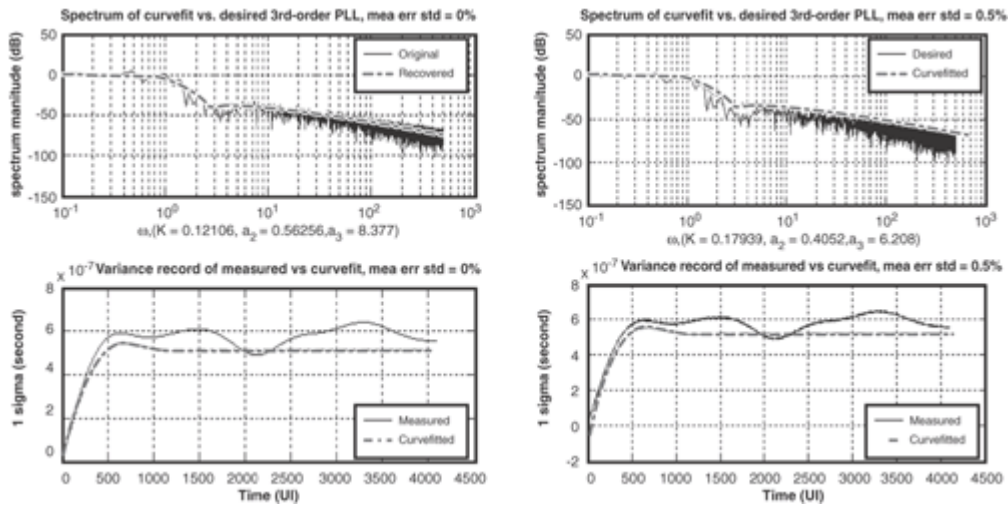
Equation 8.51

$$H_3(s) = \frac{0.1(s^2 + 0.5s + 10)}{s^3 + 0.1(s^2 + 0.5s + 10)}$$

Figure 8.17. Top (a): desired versus curve-fitted third-order PLL system transfer function; bottom (a): simulated versus curve-fitted 1-sigma jitter variance record, 0% sampling noise; top (b): desired versus curve-fitted third-order system transfer function; bottom (b): measured versus curve-fitted 1-sigma jitter variance record, 0.5% noise.

Source: J. Ma, M. Li, and M. Marlett, "A New Measurement and Analysis Method for a Third-Order Phase Locked Loop (PLL) Transfer Function," International Test Conference, 2005. (© 2005 IEEE)

[\[View full size image\]](#)



This corresponds to the upper-left branch of Figure 8.16 for computer-generated variance record. The PLL input phase noise jitter is assumed to be white, and its model is described by equation 8.46. The simulated PSD of the third-order PLL at its output is shown at the top of Figure 8.17, (a) and (b). The curve-fitted third-order PLL PSDs are overlaid. You can see a local minimum or "negative peaking" in the transition band of the PSD, which is unique to a third-order PLL. Note that because the reference clock jitter PSD is thermal, the shape of the PSD tracks the shape of the system transfer function. The simulated 1-sigma jitter variance record and the curve-fitted variance record are shown at the bottom of Figure 8.17, (a) and (b). No fluctuation noise is added in Figure 8.17 (a). The discrepancy between the simulated and curve-fitted 1-sigma variance record occurs because the simulated variance record is obtained from the PSD of the PLL output jitter, whereas the curve-fitted variance is obtained from the curve-fitted PSD. The curve-fitted parameters, which are ($K = 0.121$, $a_2 = 0.563$, $a_3 = 8.377$), match well with the desired parameters, which are ($K = 0.100$, $a_2 = 0.500$, $a_3 = 10.000$).

In Figure 8.17 (b), about 0.5 % pk-pk Gaussian noise is added to the simulated jitter variance record. The effect can be seen in the bottom part of Figure 8.17 (b). The curve-fitted parameters, which are ($K = 0.179$, $a_2 = 0.405$, $a_3 = 6.208$), still match the original desired parameters. Namely, the χ^2 curve-fitting optimization procedure is immune to the sampling noise that is intrinsic to any measurements.

8.6.3.2.2. Experimental Measurements and Verification

In this section, lab-measured phase jitter data is taken and fed into the simulation model shown in the bottom branch of Figure 8.16. The PLL circuit is chosen from a commercial PLL chip with reconfigurable parameters to set the PLL to behave as either second-order or third-order transfer function characteristics. Again, a second-order PLL is characterized by ζ and ω_n , and third-order PLL is characterized by K , a_2 , a_3 .

The PLL parameters derived from the best fittings are summarized in Table 8.6. Four cases are shown in the table—A, B, C, and D. The first two cases, A and B, correspond to the second-order-type PLL transfer functions. Cases C and D correspond to the third-order-type PLL transfer functions. To verify and demonstrate the correctness of the frequency-domain PSD-based method, for each case, both second-order and third-order model curve fittings are applied. The results are compared and shown in Figures 8.18 through 8.21. Part (a) of the figures shows the model curve fitting results using the second-order model. Part (b) shows the model curve fitting result using the third-order model. In each figure, the top subplot shows the measured PSD (solid line) versus the curve-fitted PSD (dashed line), and the bottom subplot shows the measured 1-sigma jitter variance record (solid line) versus the curve-fitted 1-sigma jitter variance record (dashed line).

Table 8.6. PLL Parameters Derived from Lab Measurements

	Second Order		Third Order		
$F_c = 4$ MHz	ζ	ω_n (rad)	K	a_2 (rad)	a_3 (rad)
A	0.46	0.0108	0.02	0.0052	0.0353
B	0.36	0.0143	0.01	0.0175	0.0524
C	0.84	0.0654	0.07	0.0079	0.7886
D	1.00	0.0738	0.10	0.0094	0.1807

Source: J. Ma, M. Li, and M. Marlett, "A New Measurement and Analysis Method for a Third-Order Phase Locked Loop (PLL) Transfer Function," International Test Conference, 2005. (© 2005 IEEE)

Figure 8.18. (a): Case A, second-order curve-fitting result; (b): Case A, third-order curve-fitting result.

Source: J. Ma, M. Li, and M. Marlett, "A New Measurement and Analysis Method for a Third-Order Phase Locked Loop (PLL) Transfer Function," International Test Conference, 2005. (© 2005 IEEE)

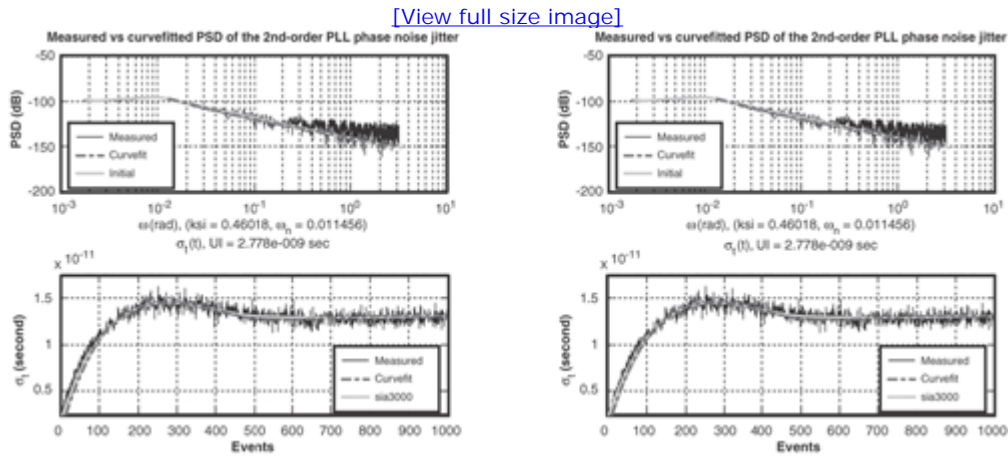


Figure 8.19. (a): Case B, second-order curve-fitting result; (b): Case B, third-order curve-fitting result.

Source: J. Ma, M. Li, and M. Marlett, "A New Measurement and Analysis Method for a Third-Order Phase Locked Loop (PLL) Transfer Function," International Test Conference, 2005. (© 2005 IEEE)

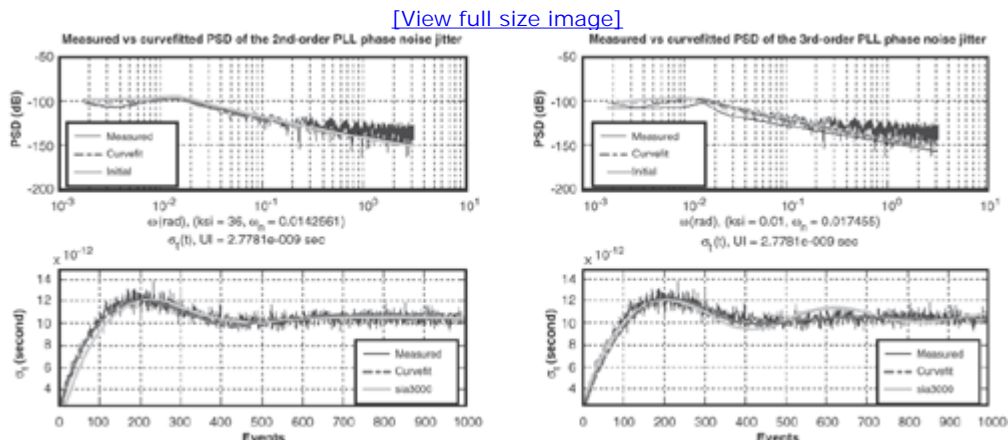


Figure 8.20. (a): Case C, second-order curve-fitting result; (b): Case C, third-order curve-fitting result.

Source: J. Ma, M. Li, and M. Marlett, "A New Measurement and Analysis Method for a Third-Order Phase Locked Loop (PLL) Transfer Function," International Test Conference, 2005. (© 2005 IEEE)

[View full size image]

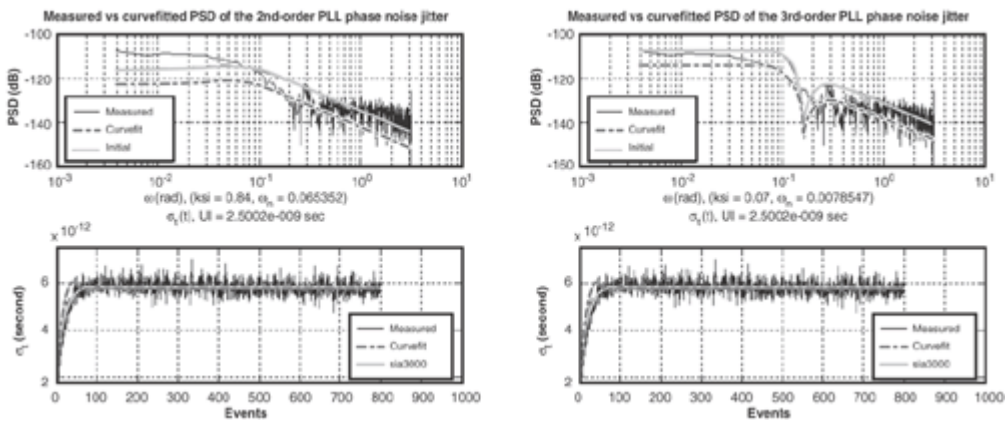
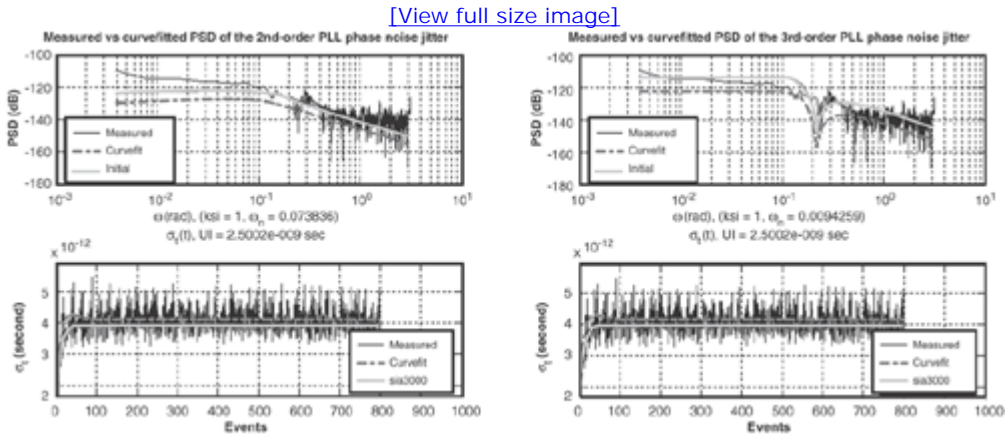


Figure 8.21. (a): Case D, second-order curve-fitting result; (b): Case D, third-order curve-fitting result.

Source: J. Ma, M. Li, and M. Marlett, "A New Measurement and Analysis Method for a Third-Order Phase Locked Loop (PLL) Transfer Function," International Test Conference, 2005. (© 2005 IEEE)



You can see that in Figures 8.18 and 8.19, part (a) fits well with the measured data. This means that the chip is configured to behave as a second-order characteristic, as shown in the first two rows of Table 8.6. In Figures 8.20 and 8.21, part (b) fits well with the measured data. This means that the chip is configured to behave as a third-order characteristic, as shown in the last two rows of Table 8.6.

In Figure 8.20, part (b), and Figure 8.21, part (b), the third-order PLL transfer function exhibits a local minimum or a dip in its transition band, which can never happen for the second-order case. Therefore, only PLL with transfer function models of third-order and above can capture such an important signature and curve-fit this type of measured PSD spectrum. The curve-fitting-obtained PLL transfer functions are also cross-verified by the PLL circuit design simulation results. The comparison shows a good match between the model curve-fitted transfer function behavior and the desired transfer function behavior.

URL <http://access.proquest.safaribooksonline.com/9780132429610/ch08lev1sec6>

User name: CSU San Diego

Book: Jitter, Noise, and Signal Integrity at High-Speed

Section: Chapter 8. PLL Jitter and Transfer Function Analysis

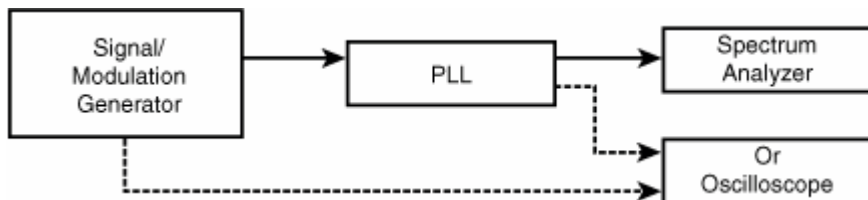
No part of any chapter or book may be reproduced or transmitted in any form by any means without the prior written permission for reprints and excerpts from the publisher of the book or chapter. Redistribution or other use that violates the fair use privilege under U.S. copyright laws (see 17 USC107) or that otherwise violates these Terms of Service is strictly prohibited. Violators will be prosecuted to the full extent of U.S. Federal and Massachusetts laws.

Information Theory Computer Science Mike Peng Li Prentice Hall Jitter, Noise, and Signal Integrity at High-Speed

8.7. Comparison with the Conventional PLL Analysis Methods

The PLL jitter and transfer function analysis methods introduced in [sections 8.5](#) and [8.6](#) do not require the use of a stimulus. As such, they are not subject to those limitations imposed to conventional PLL measurement method where the stimulus is needed. [Figure 8.22](#) is a typical PLL measurement setup requiring a stimulus source.

Figure 8.22. A typical PLL transfer function measurement experimental setup requiring a stimulus.



The working mechanism for this conventional method is basically straightforward. A sinusoidal $A_i(t) = A_i \sin(2\pi ft)$ is introduced at the PLL reference clock input through phase modulation. Its magnitude at the PLL output A_o is measured by a spectrum analyzer or a sampling oscilloscope through phase demodulation. According to the definition, the ratio between the output magnitude and the input magnitude for the sinusoidal gives rise to the PLL system transfer function magnitude:

Equation 8.52

$$\frac{A_o(f)}{A_i(f)} = |H_o(j2\pi f)|$$

Note that [equation 8.52](#) gives rise to the generic PLL transfer function magnitude and does not provide the PLL parameters directly. If the PLL parameters are sorted for, such as ζ and ω_n for a second-order PLL, and K, a_2, a_3 for a third-order PLL, procedures similar to those described in [sections 8.5](#) and [8.6](#) are needed.

Advantages of the stimulus-based method are that it is direct and you do not need to make assumptions about the PLL under test. Its major limitations may include the following:

- It requires a stimulus source that has certain constraints, such as maximum modulation frequency, and that adds cost to the test.
- For some embedded PLLs where reference clock input is inaccessible, this method cannot be used.
- Frequency sweeping can be time-consuming.

Advantages of the non-stimulus-based method include the following:

- It does not need a stimulus source (which results in cost savings).
- It can measure embedded PLL because it does not need to access the PLL input.
- It can measure PLL transfer function up to Nyquist.
- It can be very fast with a fast TIA (< 1 s test time).

Its limitations may include the following:

- It needs to make assumptions about the PLL order and noise characteristics.
- When many variables are derived from the curve-fitting procedures, the sensitivity and accuracy of estimated PLL parameters may not be perfect.

Which method should be used for testing PLL depend on the application, testing circumstances, and requirements.

URL <http://access.proquest.safaribooksonline.com/9780132429610/ch08lev1sec7>

User name: CSU San Diego

Book: Jitter, Noise, and Signal Integrity at High-Speed

Section: Chapter 8. PLL Jitter and Transfer Function Analysis

No part of any chapter or book may be reproduced or transmitted in any form by any means without the prior written permission for reprints and excerpts from the publisher of the book or chapter. Redistribution or other use that violates the fair use privilege under U.S. copyright laws (see 17 USC107) or that otherwise violates these Terms of Service is strictly prohibited. Violators will be prosecuted to the full extent of U.S. Federal and Massachusetts laws.

Information Theory Computer Science Mike Peng Li Prentice Hall Jitter, Noise, and Signal Integrity at High-Speed

8.8. Summary

We started the chapter with an introduction to PLL. Its system block diagram and system elements, as well as the working mechanism, were covered.

Section 8.2 introduced PLL system analysis in the time domain through the differential equation approach, as well as complex frequency-domain (or s-domain) analysis through transfer functions. Two important transfer functions were introduced for a PLL: system transfer function, which defines the output and input phase relationship, and the error transfer function, which defines the phase error to input phase relationship. Transfer function in the s-domain and impulse response in the time domain are related via Laplace transformation.

Section 8.3 discussed two types of analysis for PLLs. One is functional, including time-domain impulse or step response, frequency-domain transfer function, forward gain function, Bode plots, and poles and zeros location analyses. Another is parametric analysis, including parameters associated with PLL dynamic acquisition, tracking, and jitter and noise parameters such as lock, pull, hold times and ranges, and jitter or noise bandwidth.

After the basics of PLL system and dynamic behavior knowledge had been covered, section 8.4 discussed PLL jitter and noise analysis. The mathematical tools we adopted to handle jitter and noise are variance function in the time domain and PSD in the frequency domain. The estimation of PSD at the PLL output as a function of individual PSD associated with different PLL elements becomes a linear operation, simplifying the mathematics significantly. The dual counterpart of PSD in the time domain is the autocorrelation function, which is related to variance function in a linear manner. The transformation between frequency-domain PSD, time-domain autocorrelation function, and variance function also were discussed.

Section 8.5 applied what you learned in sections 8.1 through 8.4 in analyzing a concrete and commonly used PLL: a second-order PLL. We started with detailed second-order PLL transfer function, which is characterized by two parameters: damping factor ζ , and natural frequency ω_n . Its transfer function has two poles and one zero. Parameters of acquisition and tracking were given in terms of those two parameters. Then we introduced a novel second-order PLL transfer function determination method based on measured or simulated variance function. Measurement and verification for a real second-order PLL device were carried out. PLL functional and parametric results were presented. They were proven to be self-consistent and correlated with circuit simulation and other alternative measurement.

Section 8.6 focused on the detailed and concrete analysis of third-order PLLs in analogy to section 8.5 for a second-order PLL. For a third-order PLL, its transfer function is determined by three parameters of K , a_2 , a_3 , and it has three poles and two zeros. We used the frequency-domain PSD-based method to avoid complex close-form math of variance function for a third-order PLL transfer function. Laboratory measurements based on a real-world third-order PLL and computer simulation were carried out to verify the validity and accuracy of the novel method for transfer function determination. Good agreement with the circuit simulation and other measurement were achieved. The method for the third-order PLL analysis is extendable to an n th-order PLL.

Section 8.7 compared the new nonstimulus variance function/PSD-based PLL transfer function determination method to the conventional stimulus-based method. We discussed the advantages and limitations of each method. We pointed out that test circumstances and test requirements drive the selection of each method to be used.

User name: CSU San Diego

Book: Jitter, Noise, and Signal Integrity at High-Speed

Section: Chapter 8. PLL Jitter and Transfer Function Analysis

No part of any chapter or book may be reproduced or transmitted in any form by any means without the prior written permission for reprints and excerpts from the publisher of the book or chapter. Redistribution or other use that violates the fair use privilege under U.S. copyright laws (see 17 USC107) or that otherwise violates these Terms of Service is strictly prohibited. Violators will be prosecuted to the full extent of U.S. Federal and Massachusetts laws.

Information Theory Computer Science Mike Peng Li Prentice Hall Jitter, Noise, and Signal Integrity at High-Speed

Endnotes

1. F. M. Gardner, *Phaselock Techniques*, Second Edition, John Wiley & Sons, 1979.
2. D. R. Stephens, *Phase-Locked Loops for Wireless Communications: Digital and Analog Implementation*, Kluwer Academic Publishers, 1998.
3. R. E. Best, *Phase-Locked Loops, Design, Simulation, and Applications*, Fourth Edition, McGraw Hill, 1999.
4. A. Demir and A. Sangiovanni-Vincentelli, *Analysis and Simulation of Noise in Nonlinear Electronic Circuits and Systems*, Kluwer Academic Publishers, 1998.
5. P. R. Bevington and D. K. Robinson, *Data Reduction and Error Analysis for the Physical Sciences*, McGraw-Hill, Inc., 1992.
6. M. Li and J. Wilstrup, "A New Method for Analyzing PLL," IEC DesignCon, 2002.
7. M. Li and J. Wilstrup, "Applications of the New Variance Based PLL Measurement and Analysis Method," IEC DesignCon, 2003.
8. J. Ma, M. Li, and M. Marlett, "A New Measurement and Analysis Method for a Third-Order Phase Locked Loop (PLL) Transfer Function," IEEE International Test Conference (ITC), 2005.

URL <http://access.proquest.safaribooksonline.com/9780132429610/ch08lev1sec9>

User name: CSU San Diego

Book: Jitter, Noise, and Signal Integrity at High-Speed

No part of any chapter or book may be reproduced or transmitted in any form by any means without the prior written permission for reprints and excerpts from the publisher of the book or chapter. Redistribution or other use that violates the fair use privilege under U.S. copyright laws (see 17 USC107) or that otherwise violates these Terms of Service is strictly prohibited. Violators will be prosecuted to the full extent of U.S. Federal and Massachusetts laws.

Information Theory Computer Science Mike Peng Li Prentice Hall Jitter, Noise, and Signal Integrity at High-Speed

9. Jitter and Signal Integrity Mechanisms for High-Speed Links

This chapter focuses on jitter, noise, and signal integrity generation and interaction mechanisms within the context of high-speed link systems. It is important to know where jitter, noise, and signal integrity come from to develop a good design method to eliminate or mitigate the degradations caused by them, or to develop a verification or test method that can measure them accurately with good coverage. This chapter starts by introducing leading-edge high-speed link architectures and operation mechanisms. Next, we get into the details of link subsystem architectures, operating mechanisms, and jitter, noise, and signal integrity generation mechanisms for transmitter, receiver, channel or medium, and reference clock. Finally, we discuss the link jitter budget and the latest statistics-based method in addition to the conventional linear method.

URL <http://access.proquest.safaribooksonline.com/9780132429610/ch09>

User name: CSU San Diego

Book: Jitter, Noise, and Signal Integrity at High-Speed

Section: Chapter 9. Jitter and Signal Integrity Mechanisms for High-Speed Links

No part of any chapter or book may be reproduced or transmitted in any form by any means without the prior written permission for reprints and excerpts from the publisher of the book or chapter. Redistribution or other use that violates the fair use privilege under U.S. copyright laws (see 17 USC107) or that otherwise violates these Terms of Service is strictly prohibited. Violators will be prosecuted to the full extent of U.S. Federal and Massachusetts laws.

Information Theory Computer Science Mike Peng Li Prentice Hall Jitter, Noise, and Signal Integrity at High-Speed

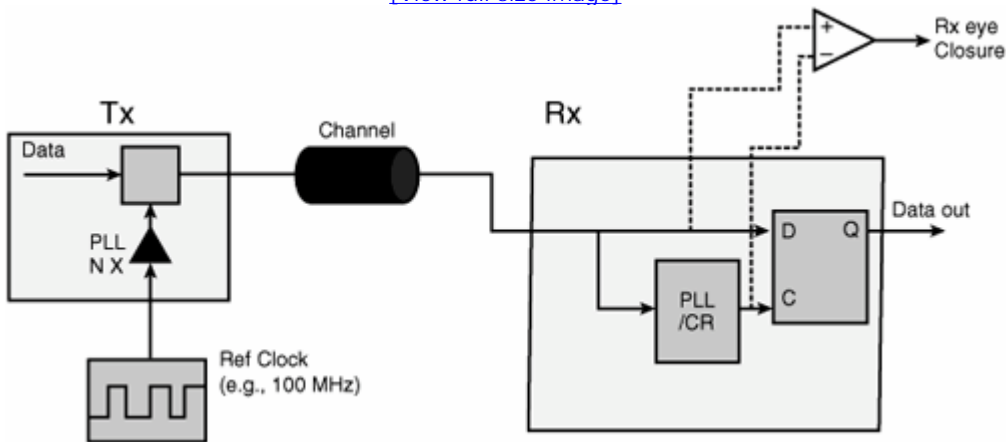
9.1. Link System Architecture and Components

As mentioned in [Chapter 1](#), "Introduction," any communication link is composed of three fundamental components: transmitter (Tx), medium or channel, and receiver (Rx). This is true of both wired and wireless communication link systems.

At multiple Gbps data rates, the clock recovery architecture or topology (see [Figure 9.1](#)) has evolved as the dominant one for wired link systems with a transmission distance of greater than 10 meters. Most of them use optical fiber as the medium or channel. [Figure 9.1](#) is a more detailed version of [Figure 1.14](#) for a link architecture diagram. Those types of link systems are network application-oriented, including Fibre Channel (FC), Gigabit Ethernet (GBE), Synchronous Optical Network (SONET), and Optical Internetworking Forum (OIF).

Figure 9.1. A serial link architecture/topology in which the clock recovery in its receiver is driven by the receiving data bit stream.

[\[View full size image\]](#)



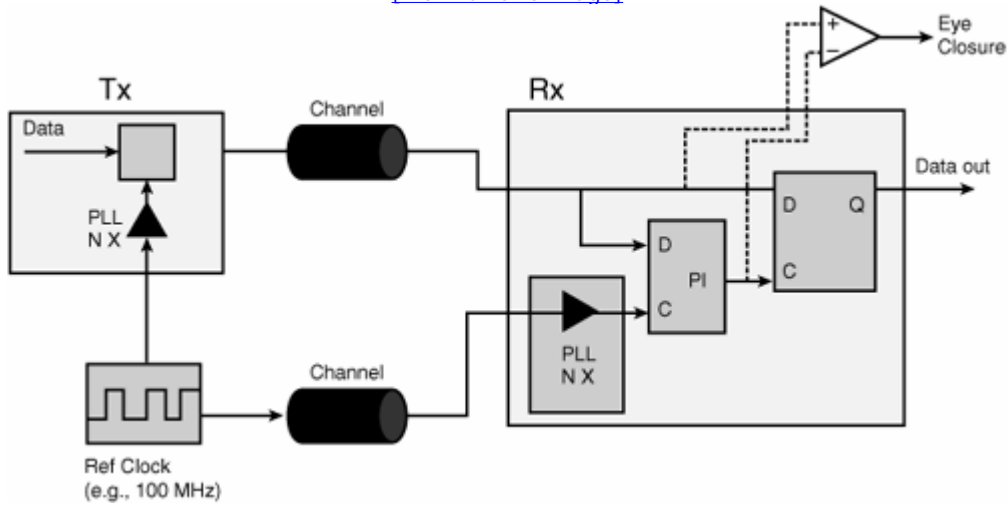
In this data-driven architecture, data is launched to a channel that is composed of either copper cable or optical fiber cable. The timing and clock function at the Tx typically are provided by a multiplication clock PLL that takes a base clock, typically in the 100 MHz range, and generates an in-rate multiple GHz clock. On the receiver side, the bit clock is recovered by a clock recovery (CR) unit that is commonly implemented by a PLL with its input from the incoming data bit stream. The receiver data is retimed or resampled using the recovered clock.

However, for multiple Gbps links with a distance of less than 10 meters or so, new link architectures such as common clock architecture have been developed in recent years in addition to conventional clock and data recovery architecture (as shown in [Figure 9.1](#)). The common clock architecture is widely used for computer and backplane multiple Gbps data transmission applications. For example, most link architectures implemented in computer input/output (I/O), such as PCI Express and fully buffered dual inline memory module (FB DIMM), use common clock architecture.

Figure 9.2 shows the common clock link architecture.

Figure 9.2. A serial link common clock architecture/topology in which the same clock is sent to both transmitter and receiver. In this architecture, the receiver bit clock or sampling clock is recovered from the received data and multiplied clock.

[View full size image]



In the common clock architecture, a low-frequency base reference clock is sent to both Tx and Rx. On the Tx side, the multiplication PLL converts the reference clock to an in-rate and much higher frequency clock to provide the timing function for the Tx to drive the data bits. On the receiver side, the reference clock is first fed to an Rx multiplication PLL and then is converted to an in-rate clock. The bit clock is then generated by a digital clock recovery unit such as a phase interpolator (PI). It takes both in-rate clock and data as inputs and generates a bit clock that is phase-aligned (to a certain degree or limit, of course) with the incoming data. The data is then retimed/sampled with the recovered bit clock.

Clearly, there is a new variant for the common clock architecture—the reference clock—because it affects the performance of both Tx and Rx. The reference clock itself becomes an important element in the link timing closure consideration. Thus, there are four components to consider for common clock link architecture/topology.

The following sections discuss subsystem architecture/topology, as well as associated performance, for the four link elements of transmitter, receiver, channel or medium, and reference clock.

URL <http://access.proquest.safaribooksonline.com/9780132429610/ch09lev1sec1>

User name: CSU San Diego

Book: Jitter, Noise, and Signal Integrity at High-Speed

Section: Chapter 9. Jitter and Signal Integrity Mechanisms for High-Speed Links

No part of any chapter or book may be reproduced or transmitted in any form by any means without the prior written permission for reprints and excerpts from the publisher of the book or chapter. Redistribution or other use that violates the fair use privilege under U.S. copyright laws (see 17 USC107) or that otherwise violates these Terms of Service is strictly prohibited. Violators will be prosecuted to the full extent of U.S. Federal and Massachusetts laws.

Information Theory Computer Science Mike Peng Li Prentice Hall Jitter, Noise, and Signal Integrity at High-Speed

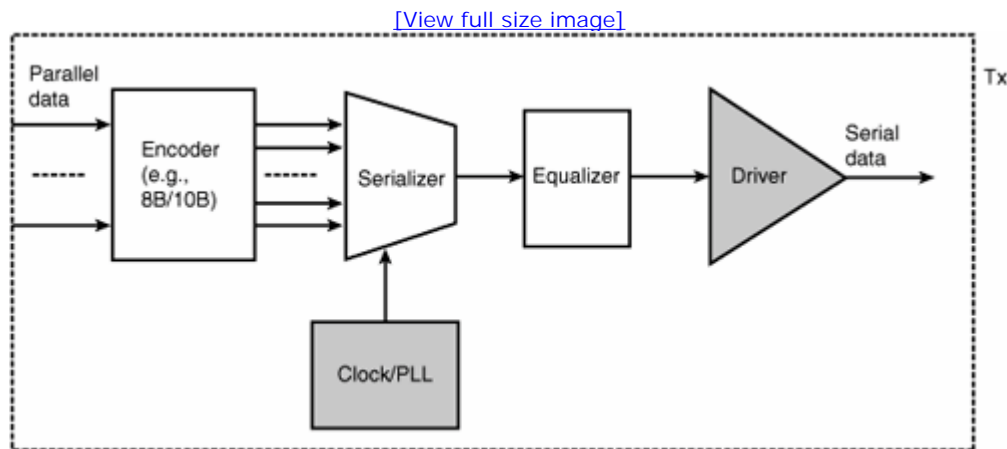
9.2. Transmitter

We will discuss transmitter from two perspectives: the Tx subsystem architecture and operation mechanism, and its performance-limiting factors and analysis.

9.2.1. Transmitter Subsystem Architecture

A multiple Gbps transmitter typically is composed of a data encoder, serializer, clock generator/PLL equalizer, and voltage driver. A typical transmitter subsystem looks like [Figure 9.3.^{\[1\]}](#)

Figure 9.3. A typical serial link transmitter subsystem. The shaded elements of driver and clock/PLL are critical to transmitter jitter and noise performance.



The input data often comes in a parallel bus topology. An encoder typically converts M data bits to N-bit code. In data communication, the 8b/10b coding scheme is commonly used for the benefits of direct current (DC) balancing and error minimization. With 8b/10b encoding, 8-bit data is converted to 10-bit codes. Clearly, 2 additional bits are sent after 8b/10b encoding, increasing the transmitter system's overhead. The parallel bit stream after the encoder is converted to serial through a serializer or multiplexer. A local system clock commonly generated by a PLL provides clock timing function to the serializer. A transmitter equalizer is used to compensate for the channel effect to minimize the data-dependent jitter (DDJ) and data-dependent noise (DDN) resulting from the band-limited lossy channel. The commonly used transmitter equalizer is the feed-forward equalization (FFE).^{[2], [3]} This is basically a linear finite impulsive response (FIR) filter implementation with predetermined tap coefficients. Two types of FFE are commonly implemented. Pre-emphasize increases the high-frequency content intensity relative to the low-frequency one. De-emphasize decreases the low-frequency content intensity relative to the high-frequency one. Both of them serve the goal of reducing the degradation of the waveform or eye diagram at the receiver input after the signal going through the lossy channel. In other words, the effective bandwidth of the lossy channel increases with pre-emphasize or de-emphasize compensation compared to that without either compensation. In the final stage, the driver drives the required differential signal or single-ended voltage via either current source or voltage sources for each data bit at

the given time provided by the transmitter system clock.

9.2.2. Performance Determining Factors

The encoder, serializer, and FFE equalization are digital elements. As such, they contribute little or near-zero random jitter. The serializer may contribute some deterministic jitter due to skew and quantization error.

The major jitter contributor for the transmitter comes from the system clock that is commonly generated by a PLL. As we have mentioned, the input to the PLL is commonly a substrate reference clock. The PLL multiplies the substrate reference clock to an in-rate clock at multiple GHz to provide the timing function for the transmitter. Both PJ and RJ are possible for the PLL. However, for a well-designed PLL, RJ should be the only limiting jitter. PLL jitter performance was discussed extensively in [Chapter 8](#), "PLL Jitter and Transfer Function Analysis."

The major noise contributor is the driver due to its analog circuits, in either current-mode or voltage-mode driving. For optical, a laser driver is used. The voltage noise, impedance/return loss, termination, and rise/fall time affect the jitter and noise performance for the transmitter output. Improper source impedance/termination can result in reflection, degrading the output waveform and causing both timing jitter and voltage distortion. A too-fast or too-slow rise/fall time produces ISI, causing both DDJ and DDN for the output. Last, power-supply noise can be coupled with driver signal or voltage reference signal, causing voltage noise in its output. Voltage noise can potentially be converted to timing jitter via finite slew rate for each edge transition.

URL <http://access.proquest.safaribooksonline.com/9780132429610/ch09lev1sec2>

User name: CSU San Diego

Book: Jitter, Noise, and Signal Integrity at High-Speed

Section: Chapter 9. Jitter and Signal Integrity Mechanisms for High-Speed Links

No part of any chapter or book may be reproduced or transmitted in any form by any means without the prior written permission for reprints and excerpts from the publisher of the book or chapter. Redistribution or other use that violates the fair use privilege under U.S. copyright laws (see 17 USC107) or that otherwise violates these Terms of Service is strictly prohibited. Violators will be prosecuted to the full extent of U.S. Federal and Massachusetts laws.

Information Theory Computer Science Mike Peng Li Prentice Hall Jitter, Noise, and Signal Integrity at High-Speed

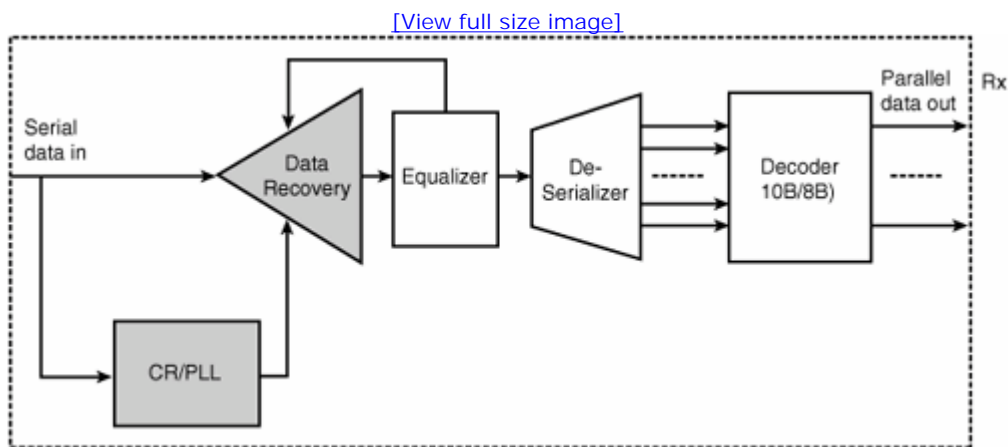
9.3. Receiver

Similar to Tx, we will discuss Rx from two perspectives: the Rx subsystem architecture and operation mechanism, and its performance-limiting factors and analysis.

9.3.1. Receiver Subsystem Architecture

The signal processing flow of the multiple Gbps serial receiver architecture is almost the inverse function of the transmitter signal processing flow, as far as the encoder/decoder, serializer/deserializer are concerned. A typical serial receiver is composed of a data voltage sampler, clock recovery, equalizer, deserializer, and decoder. A typical receiver subsystem looks like Figure 9.4.^[1]

Figure 9.4. A typical serial link receiver subsystem. The shaded elements of data recovery and clock/PLL are critical to receiver jitter and noise performance.



The incoming data bit stream from the medium or channel is split into two paths. One goes to the data recovery unit, which samples and detects the voltage level of the incoming bit at the time defined by the bit clock. Another goes to the clock recovery, which generates the bit clock used in the data recovery and that is often implemented by a PLL, as we have mentioned many times in previous chapters. Obviously, the voltage sensitivity and resolution of the data recovery and the phase accuracy or phase jitter of the clock recovery critically affect the performance of the clock and data recovery (CDR). A receiver equalization is commonly used in multiple Gbps receiver design due to the lossy channel. Most of the receiver equalization implementations use decision feedback equalization (DFE). This forms a feedback system with the data recovery and corrects the channel distortion effects of the next bits based on the current and past bits' information.^{[4], [5]} After the serial data is correctly sampled at the appropriate time and voltage, the recovered data bit stream is deserialized to a low-speed parallel bit stream in the coded data format. Then the coded data is decoded to raw data (10b/8b decoding) information in parallel data bus format.

9.3.2. Receiver Performance Determining Factors

As in the case of a transmitter, the deserializer, decoder, and DFE are digital elements. As such, they contribute little or zero random jitter. The serializer may contribute some deterministic jitter or channel to channel skew.

Because the bit clock is generated by the clock recovery unit, its phase jitter and frequency response affect the receiver's data recovery performance. The input to the clock recovery is the data bit stream from the transmitter after passing through the lossy channel, and the clock recovery is expected to recover the bit clock from the incoming data. At the same time, it also tracks jitter associated with the data bit stream. An ideal clock recovery should generate zero jitter, yet still be able to operate under incoming data with a significant amount of jitter and noise. When the clock recovery is implemented with a PLL, it can operate under a significant amount of low-frequency jitter because the PLL can track it. Meanwhile, the PLL is the major source of RJ for the receiver. A receiver clock recovery PLL needs to operate under data input that does not have an edge transition at every UI. This is different from the transmitter PLL operation. Keeping low jitter for the PLL output when there is no edge transition (or phase information) at its input is a nontrivial task. In general, maintaining small jitter generation and good jitter tracking are the two most important goals for the receiver clock recovery/PLL design. High-frequency jitter cannot be tracked by the PLL and needs to be factored into the receiver jitter budget consideration. As mentioned in [Chapter 8](#), second- and third-order PLLs are commonly used in receiver clock recovery.

Data recovery is the major noise contributor for the receiver. The data recovery unit typically is composed of an amplifier and a sampling flop or comparator. The resolution, sensitivity, and noise for the reference voltage thereby play important roles in determining the data recovery performance in addition to the phase jitter on the recovered clock. The receiver's impedance/return loss also plays an important role in receiver ISI generation, manifested in DDJ or DDN for the receiver due to reflection. As with the transmitter, power-supply noise can be coupled with the reference signal, causing bit errors in the data recovery.

URL <http://access.proquest.safaribooksonline.com/9780132429610/ch09lev1sec3>

User name: CSU San Diego

Book: Jitter, Noise, and Signal Integrity at High-Speed

Section: Chapter 9. Jitter and Signal Integrity Mechanisms for High-Speed Links

No part of any chapter or book may be reproduced or transmitted in any form by any means without the prior written permission for reprints and excerpts from the publisher of the book or chapter. Redistribution or other use that violates the fair use privilege under U.S. copyright laws (see 17 USC107) or that otherwise violates these Terms of Service is strictly prohibited. Violators will be prosecuted to the full extent of U.S. Federal and Massachusetts laws.

Information Theory Computer Science Mike Peng Li Prentice Hall Jitter, Noise, and Signal Integrity at High-Speed

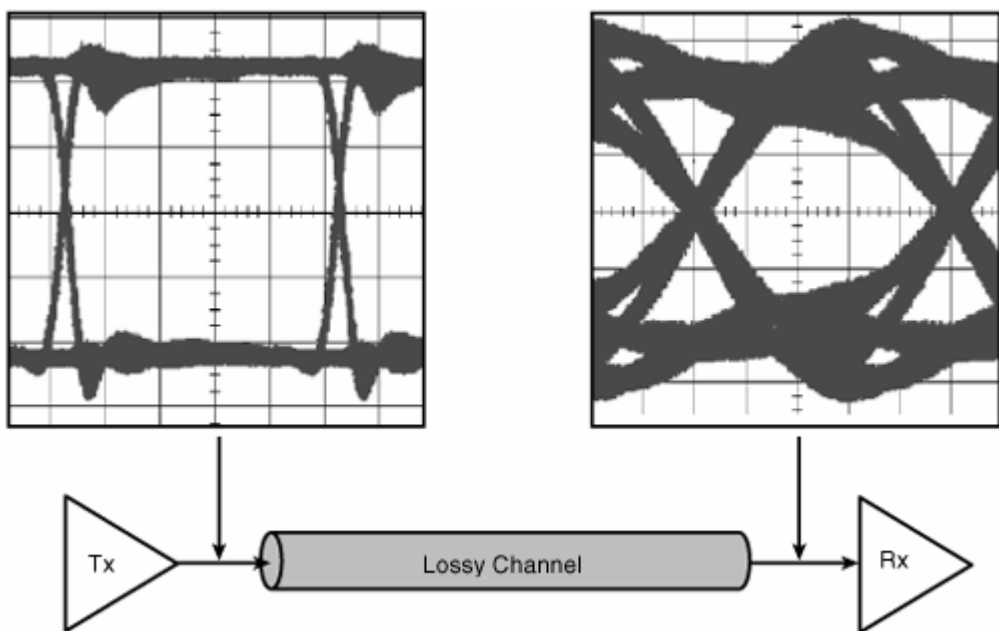
9.4. Channel or Medium

We will discuss channel from two viewpoints: the channel's intrinsic or physical properties and their associated signal integrity consequences, and "interaction"-related impairments such as crosstalk and reflection-induced signal integrity issues. Both copper and optical channels are covered.

9.4.1. Channel Material and Characteristics

The effect of bandwidth-limited channel on signal integrity and jitter at multiple Gbps data rates is shown in [Figure 9.5](#).

Figure 9.5. The effect that a lossy channel has on the signal quality in terms of eye diagrams at the channel input and output.
Notice the degradation of the eye diagram and the reduced eye opening after the lossy channel.



After propagating through the lossy channel, the clean and open eye diagram at the Tx output becomes smeared with a much reduced eye opening at the Rx input. A smaller eye opening manifests the ISI effect due to the lossy channel, suggesting increased DDJ and DDN at the Rx input. Signal or eye diagram degradation is common for any lossy or bandwidth-limited channels, including both copper and fiber-optic channel materials.

For short-distance (< 10 m) multiple Gbps links, such as those used for computer systems, the link channel material is commonly copper cables. For long-distance (> 10 m) multiple Gbps links, optical fiber cables are commonly used, because the loss for the copper

cable is too significant over this long distance. Both copper and optical fiber can cause signal quality distortion, DDJ, and DDN. However, the physical causing mechanisms are not the same. The next sections discuss their respective causing mechanisms accordingly.

9.4.1.1. Copper-Based Channels

Copper-based cables, in the form of coaxial, twisted pair, microstrip, or stripline, can be modeled as lumped LRC or series LRC circuits. For most low-frequency applications, the dependency of resistance, inductance, or capacitance on the frequency can be ignored because it is small. At multiple GHz frequencies, the frequency dependences of those parameters become significant and distort the signal quality. The two most significant loss mechanisms at a GHz frequency are the loss caused by skin effect and dielectric loss, as discussed in the next sections.

9.4.1.1.1. Skin Effect

Skin effect is the physical property for a waveguide conductor. Its physics are governed by the Maxwell equations. Skin effect is discussed in most electromagnetic books (such as [6]). When a signal or electromagnetic wave propagates along a copper cable, the current distribution can be estimated based on the Maxwell equations, and the solution is unique if the initial and boundary conditions are given. The boundary condition depends on the specific form factor or geometry of the copper cable. It turns out that the current density distribution over the cross section of the conductor follows the exponential decay of the following:

Equation 9.1

$$J(d) = J_0 e^{-\frac{d}{\delta}}$$

$J(d)$ is the current density distribution over the distance d estimated from the surface of the conductor. J_0 is the current density at the surface. δ is the constant called *skin depth* that defines the distance at which the current density has decayed to 1/e of the surface density J_0 . Skin depth is similar to the RC time constant in terms of its math meaning. The skin depth is given by

Equation 9.2

$$\delta = (\pi \mu \sigma f)^{-1/2}$$

where σ is the conductivity, μ is the cable's magnetic permeability, and f is the frequency of the current or signal waveform. As the frequency increases, the skin depth decreases, causing the current to distribute along a small area near the surface of the conductor. This nonuniform current distribution effectively increases the conductor's resistance, resulting in more Ohmic heat energy consumption. As a result, the waveform's intensity or voltage level is attenuated at the output end of the conductor. The exact attenuation is given by the following:

Equation 9.3

$$\frac{V_o}{V_i} = e^{-\alpha_s \sqrt{f}}$$

where the coefficient α_s depends on the skin depth and the conductor geometry and is proportional to the length of the channel medium.

[7] Equation 9.3 suggests that the voltage attenuation in dB is proportional to the length and \sqrt{f} . For a typical FR-4 strip line cable, the skin effect loss at 1 GHz can be ~ 5 dB per meter, while at 10 GHz, it can reach as high as -18 dB per meter. Clearly, skin effect is a major challenge for copper-based cable at multiple GHz frequencies.

9.4.1.1.2. Dielectric Loss

When an electrical waveform propagates through a conductor, the electric and magnetic fields associated with the waveform interact with the molecular dipole and make the dipole electrical field aligned with the opposite direction. Physically, the changing of the electromagnetic field associated with the waveform does work to the molecular dipole of the conductor medium. As such, the voltage amplitude associated with the waveform is attenuated, and the lost energy of the electromagnetic wave goes to the dipoles' potential energy. This effect is called dielectric loss.[6],[7]

In general, the dielectric constant ϵ is a complex number $\epsilon = \epsilon_r + j\epsilon_i$. The common parameter used to quantify dielectric loss is *loss tangent*—the ratio of the imaginary part to the real part of the dielectric parameter. Mathematically, the ratio of imaginary part to real part gives the definition of tangent; this is how the loss tangent got its name. The ratio of ϵ_i / ϵ_r can also be represented with conductivity and frequency as follows:

Equation 9.4

$$\tan \delta_D = \frac{\epsilon_i}{\epsilon_r} = \frac{\sigma}{2\pi f |\epsilon|}$$

Similar to skin effect loss, dielectric loss can be estimated as follows:

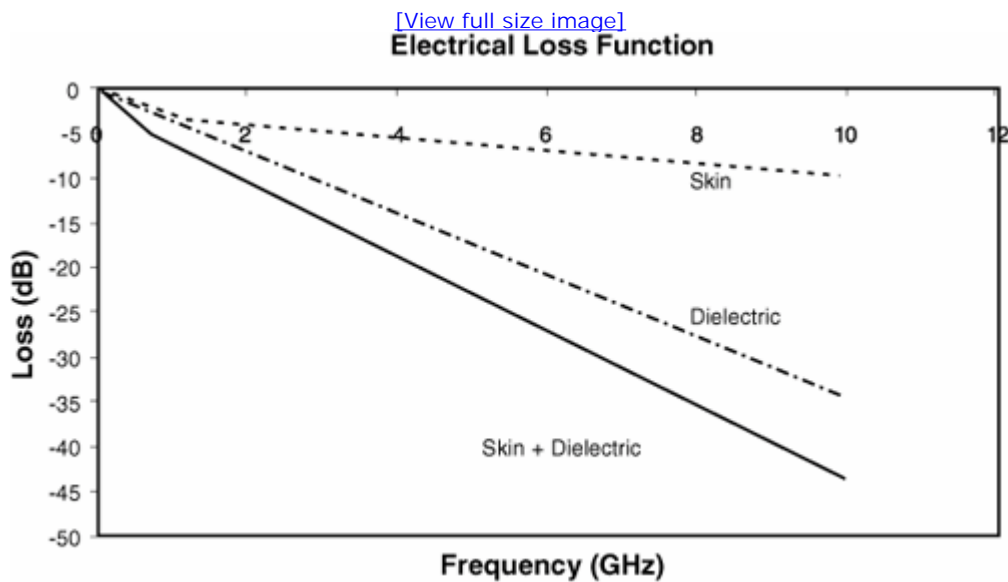
Equation 9.5

$$\frac{V_o}{V_i} = e^{-\alpha_D f}$$

where α_D is attenuation coefficient, and $\alpha_D = (\pi \sqrt{\epsilon_r} \tan \delta_D l) / c$, where ϵ_r is the relative permittivity, c is the speed of light in a vacuum, and l is the length of the medium. Obviously, the voltage attenuation in dB due to dielectric loss is proportional to length, loss tangent, and frequency. For a typical FR-4 strip line cable, we have $\epsilon_r = 4.4$ and $\tan \delta_D = 0.018$. Therefore, the dielectric loss at 1 GHz is ~ -3 dB per meter. At 10 GHz, it can be as high as -34 dB per meter. Clearly, the dielectric loss is dominant over the skin effect loss at 10 GHz due to the linear relationship between the loss rate and frequency for the dielectric loss. That is faster than the \sqrt{f} relationship for the skin effect loss.

If we consider both skin effect and dielectric for an FR-4 strip line cable with a 1-meter length, Figure 9.6 shows the three different loss curves.

Figure 9.6. Loss due to skin effect (dashed line), dielectric loss (dot-dashed line), and the sum of both (solid line), as a function of frequency, for a typical 1-meter FR-4 strip line cable.



At $f > 1$ GHz, dielectric loss is dominant over skin loss. At 10 GHz, skin effect loss reaches ~ -9.3 dB, and dielectric loss reaches ~ -34.7 dB, with a total of -43.7 dB—very significant.

9.4.1.2. Optical Fiber-Based Channels

Copper-based cable can exhibit significant loss at GHz due to skin effect loss and dielectric loss. In contrast, loss due to optical fiber when a light waveform propagates through it is significantly smaller. At an 850 nm wavelength, the loss due to material absorption is about 3 dB/km. At 1300 nm, the loss drops to 1 dB/km. At 1550 nm, it is about 0.2 dB/km. Those loss figures are significantly smaller than copper cable when the signal is electrical.^[8] It is not surprising that optical links with optical fiber, transmitter, and receiver at the front end are the only implementation form for > 10 Gbps data rates and with a link distance of greater than 10 m.

Even though optical fiber offers tremendous loss advantages over copper cable, it faces other challenges that degrade the signal quality and eye diagram at the receiver input. Chromatic dispersion (CD) and polarization mode dispersion (PMD) are the two dominant mechanisms for signal integrity for optical fiber.

9.4.1.2.1. Chromatic Dispersion

For optical fiber, both its material and waveguide properties are critical to the light wave's propagation velocity. On the material side, the fiber's refraction index is a function of the wavelength, meaning that different wavelengths of the light will travel at different speeds, resulting in arrival time spreading and waveform smearing at the fiber output. On the waveguide side, shorter-wavelength light is confined around the center of the fiber. Longer-wavelength light is distributed in the outer layers of the fiber, which have a different refraction index. As a result, light with different wavelengths travels at different speeds, causing arrival time spreading and waveform smearing similar to the material dispersion. For a single-mode fiber, the dominant dispersion effect is the material dispersion. Because all the practical laser sources used in optical communication are light-emitting diodes (LEDs) or laser diodes (LDs), they all have finite-wavelength spectral width. Thus, chromatic dispersion effect is always present. The time spread Δt caused by the dispersion can be expressed as follows:

Equation 9.6

$$\Delta t = D_{CD} L \Delta \lambda$$

where D_{CD} is the chromatic dispersion coefficient, L is the length of the fiber, and the $\Delta \lambda$ is the spectral width of the light source. For a typical single-mode fiber, D_{CD} is a function of wavelength, with a value of ~ 10 ps/(nm•km) at 1200 nm to ~ 20 ps/(nm•km) at 1600 nm. Obviously, larger spectral width, longer distance, and larger dispersion coefficient will make the time dispersion worse. As mentioned in Chapter 1, time dispersion is a type of ISI for optical fiber.

9.4.1.2.2. Polarization Mode Dispersion

A symmetrical, uniform, homogeneous optical fiber has two orthogonally polarized wave electromagnetic (EM) wave modes. However, with realistic optical fiber, geometric and mechanical asymmetry (birefringence) and inhomogeneity will cause two orthogonally polarized EM wave modes to travel at different speeds, resulting in different arrival times and pulse spreading at the other end of the fiber. Spreading caused by polarization is called polarization mode dispersion (PMD). The two orthogonally polarized EM wave modes are usually coupled in a random manner and generally are characterized by the root-mean-square (rms) value of a Gaussian distribution. The rms for the time spread due to PMD can be expressed as follows:

Equation 9.7

$$\sigma_{\Delta t} = D_{PMD} \sqrt{L}$$

where D_{PMD} is the PMD coefficient, commonly in units of $\text{ps}/\sqrt{\text{km}}$, and L is the fiber's length. For a single-mode fiber, D_{PMD} typically is in the range of 0.1 – 1 $\text{ps}/\sqrt{\text{km}}$. PMD starts to become a major limiting factor at a data rate of 10 Gbps or above for a long-haul (greater than 1 km in distance) optical connection.

9.4.2. Other Impairments for the Channel

So far, we have discussed high-frequency, high-data-rate-related limiting factors caused by channel materials, or intrinsic consequences. Other limiting factors affect the signal quality at the channel's output. We will focus on two major factors:

- Crosstalk when multiple channels are implemented over the channel medium
- Reflection at the interfaces between the transmitter/channel and channel/receiver due to the discontinuity between them

From a waveguide point of view, those limiting factors can occur for both copper-based channels and optical-fiber channels. We will

discuss crosstalk first, followed by reflection.

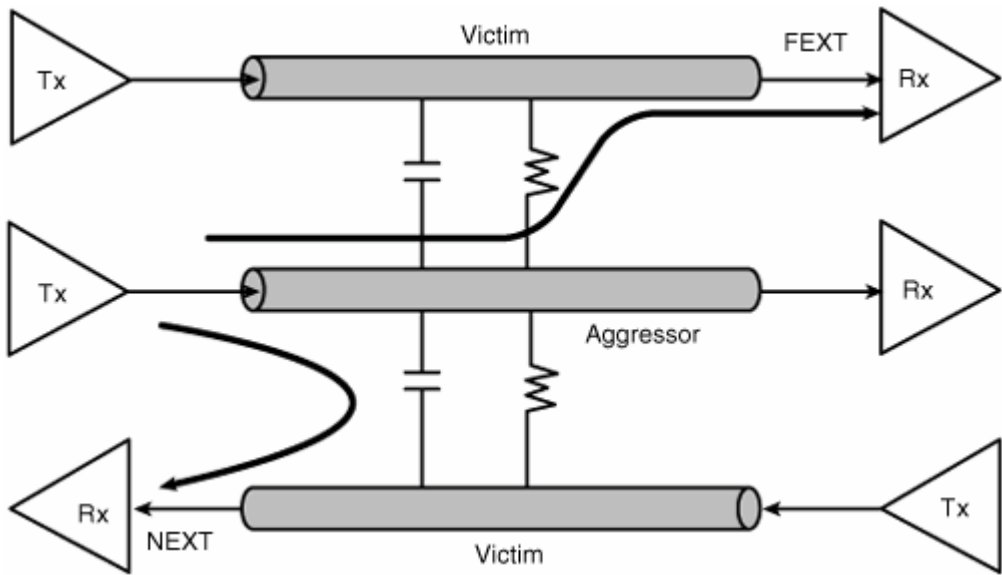
9.4.2.1. Crosstalk

Because both copper and fiber channels exist, we will discuss crosstalk associated with each type of channel material.

9.4.2.1.1. Electrical Crosstalk

As mentioned in [Chapter 1](#), crosstalk is caused by the capacitive and inductive coupling between channels carrying electrical signals. High-speed electrical channels have two types of crosstalk. They have different forming mechanisms and characteristics due to different channel topologies. One is far-end crosstalk (FEXT), which is crosstalk stimulated by the aggressor transmitter and observed by the receiver at the other end (the far end) of the link. The other is near-end crosstalk (NEXT), which is stimulated by the aggressor transmitter and observed by the receiver at the same end or near end of the link.[\[9\]](#), [\[10\]](#) The FEXT and NEXT forming mechanisms are shown in [Figure 9.7](#).

Figure 9.7. Two types of crosstalk mechanisms: far-end crosstalk (FEXT) and near-end crosstalk (NEXT).

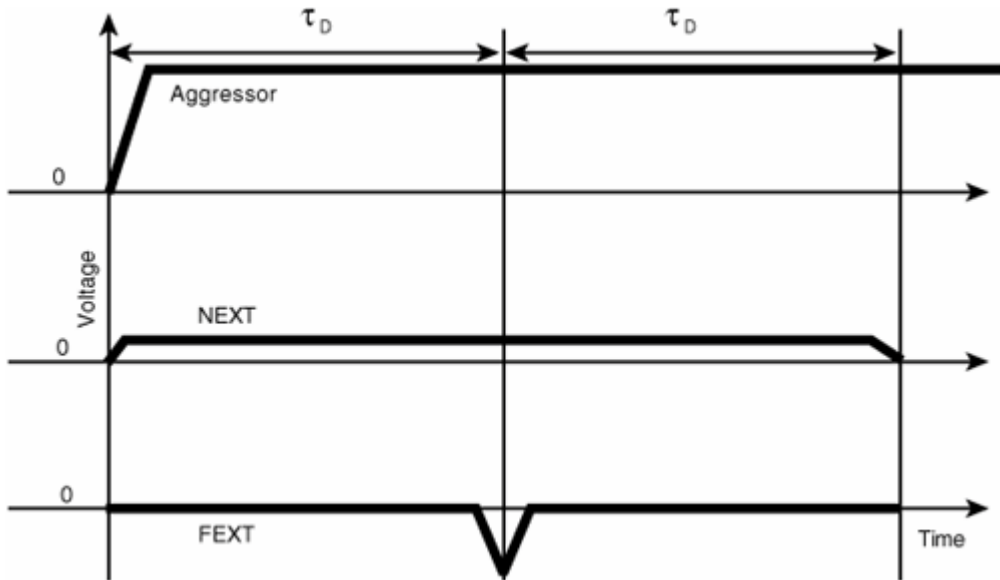


For FR-4-based backplane strip line channels, inductive coupling is dominant over capacitive coupling. When the current is excited at an adjacent victim line by a signal pulse from an aggressor transmitter due to capacitive coupling, it flows to both the far end and near end. On the other hand, the current generated at an adjacent victim line due to inductive coupling flows only from the far end to the near end, opposite the current flow of the aggressor or drive line due to Lenz's law. Therefore, for FEXT, capacitive current and inductive current subtract from each other, and for NEXT, capacitive current and inductive current add to each other. Because inductive is dominant over capacitive, the voltage pulse polarities for NEXT and FEXT are opposite.

When both aggressor and victim lines are terminated, NEXT starts with the aggressor pulse and ends at the arrival time of the reflected pulse. Therefore, its duration is twice that of the channel propagation time τ_D . Because it takes τ_D time for the pulse to travel from the near end to the far end, and the capacitive and inductive current subtract from each other, FEXT starts at $t = \tau_D$ and lasts for the period or edge transition (the rise time/fall time), during which the current changes with time. So the NEXT and FEXT temporal profile looks like [Figure 9.8](#).

Figure 9.8. The NEXT and FEXT temporal profile when both aggressor and victim channels are terminated.

[\[View full size image\]](#)



Both NEXT and FEXT depend on the capacitive and inductive couplings and are proportionally inverse to the channel spacing. Therefore, by increasing the channel spacing, NEXT and FEXT can be reduced. Also, the NEXT duration is proportional to the channel's length, so shortening the channel length decreases NEXT. Because FEXT is proportional to the current change rate, it is proportionally inverse to the rise/fall time. So by increasing the signal's rise/fall time, FEXT can be reduced. These are obvious ways to reduce NEXT and FEXT based on their forming mechanisms. Other NEXT and FEXT reduction solutions are possible by adding circuits to Tx or Rx.

9.4.2.1.2. Optical Crosstalk

Crosstalk is less an issue for a single-wavelength carrier optical data transmission. But it can be a serious issue for a wavelength division multiplexing (WDM) system, in which each channel uses a different carrier wavelength and is optically modulated with the digital bit stream. Multiple channel data bits are transformed over the same optical-fiber medium. WDM technology enables a significant increase in data transmission capacity over the same fiber medium, but it also introduces crosstalk.^[9] [11]

Optical crosstalk is the interference between simultaneously propagating signals. Crosstalk causes power transfer/amplitude fluctuation between channels. The two main types of optical crosstalk are linear and nonlinear.

Linear crosstalk is composed of out-of-band crosstalk, which typically is associated with the optical filter and demultiplexer, and in-band crosstalk, which is associated with the wavelength router. Out-of-band crosstalk is incoherent (to the carrier), and in-band crosstalk is coherent. Therefore, in-band crosstalk is more severe than out-of-band crosstalk.

Nonlinear optical crosstalk is caused by stimulated Raman scattering (SRS), stimulated Brillouin scattering (SBS), cross-phase modulation (XPM), and four-wave mixing (FWM). Nonlinear SRS and SBS are examples of fiber acting as an amplifier for longer wavelengths when the differences between longer wavelengths and short wavelengths fall within a certain range. The probability of SRS occurring is much higher than that for SBS because the gain bandwidth for SRS is ~5 THz, whereas the gain bandwidth for SBS is only ~0.05 GHz. XPM is caused by the intensity-dependent phase shift that originates from the refraction index dependence on the signal intensity. XPM can convert intensity noise to phase noise and, in turn, phase jitter for a digital system. When a WDM system has more than three channels, FWM will occur at a frequency value equal to a superposition of the original three. A WDM system with many channels has many FWM possibilities. FWM can cause both in-band and out-of-band crosstalk.

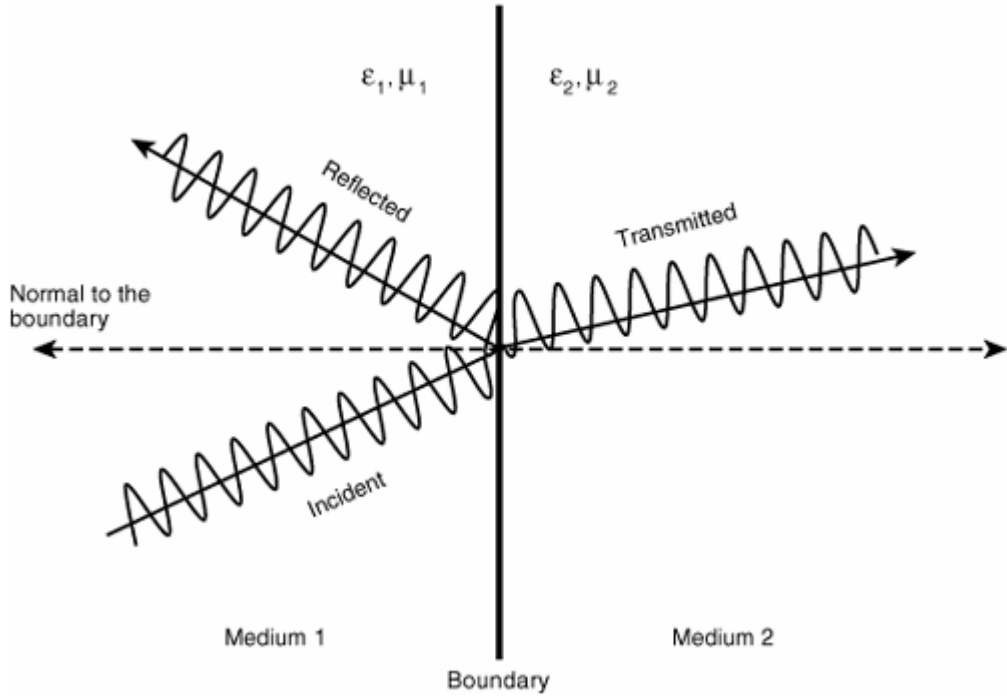
9.4.2.2. Reflection

When the terminology of reflection is used, we have implicitly adopted the wave concept. Both electrical and light waves can be viewed as electromagnetic waves. They can be treated within the framework of Maxwell equations and be related to boundary conditions for electrical and magnetic fields. By taking this approach, reflections for copper and fiber channels can be treated under the same theory framework and bear the simplicity and synergy.

According to the Maxwell theory, when an electromagnetic wave hits the boundary formed by two different media, some of the waves penetrate to the second medium, and others are reflected to the first medium, as shown in Figure 9.9.

Figure 9.9. Incident, reflected, and transmitted waves at the boundary of two different media.

[\[View full size image\]](#)



In general, the intensity of the reflected wave and transmitted wave depend on the medium parameters of electrical permittivity (ϵ) and magnetic permeability (μ), as well as angles of reflection and transmission. When the incident angle is zero or is perpendicular to the boundary (a scenario for most copper and fiber channel reflections), the reflection and transmission coefficients are given by the following:^[6]

Equation 9.8

$$\rho_r = \frac{V_r}{V_i} = \frac{\sqrt{\epsilon_2 \mu_2} - \sqrt{\epsilon_1 \mu_1}}{\sqrt{\epsilon_2 \mu_2} + \sqrt{\epsilon_1 \mu_1}}$$

and the transmission coefficient is

Equation 9.9

$$\rho_t = \frac{V_t}{V_i} = \frac{2\sqrt{\epsilon_2 \mu_2 \epsilon_1 \mu_1}}{\sqrt{\epsilon_2 \mu_2} + \sqrt{\epsilon_1 \mu_1}}$$

Energy conservation warrants the following:

Equation 9.10

$$\rho_r^2 + \rho_t^2 = 1$$

Equations 9.8 through 9.10 will be used for electrical and optical reflection in different forms.

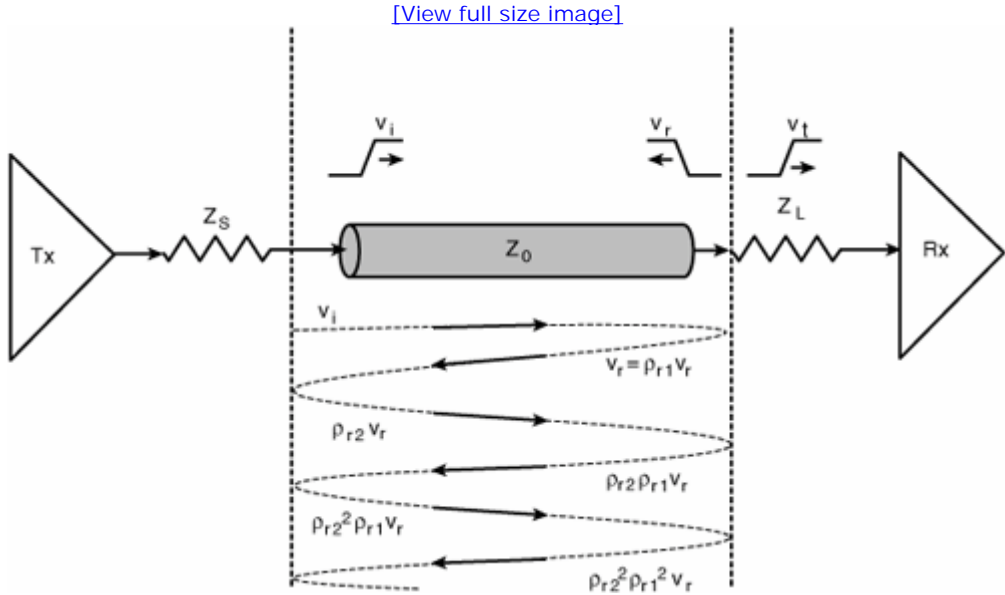
9.4.2.2.1. Electrical Reflection

In an electrical transmission system, the transmission line electrical property typically is characterized in terms of its impedance Z ,

which is related to electrical permittivity and magnetic permeability as $Z = \sqrt{\mu/\epsilon}$. Note that ϵ and μ are complex numbers in general.

Consider the reflection for the link system, as shown in Figure 9.10.

Figure 9.10. The reflection for a link system. Multiple reflections are shown.



Because electrical impedance is proportional to $1/\sqrt{\epsilon}$, and magnetic permeability for source, transmission line, and load are the same, we can express equation 9.8 in terms of impedances of the following:

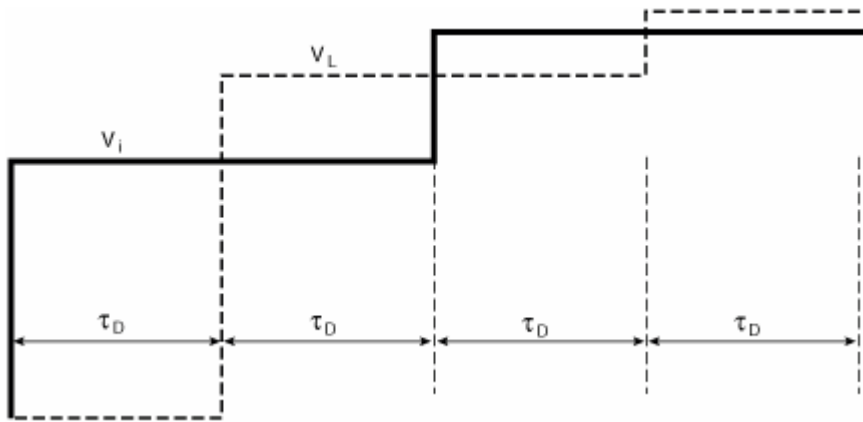
Equation 9.11

$$\rho_r = \frac{V_r}{V_i} = \frac{\sqrt{\frac{1}{\epsilon_1}} - \sqrt{\frac{1}{\epsilon_2}}}{\sqrt{\frac{1}{\epsilon_1}} + \sqrt{\frac{1}{\epsilon_2}}} = \frac{Z_0 - Z_L}{Z_0 + Z_L}$$

For the link system shown in Figure 9.10, the initial wave V_i is launched to the transmission line. At the other end of the transmission line, reflection occurs because of the mismatched impedances between the transmission line and receiver load. The reflected wave V_r gets bounced back at the boundary between source impedance and transmission line due to their mismatches. The reflection can happen many times with decreasing magnitude. The reflected wave becomes superimposed on the initial wave, degrading the waveform before it reaches the receiver.

We will consider an example in which both source and load impedance are half of the transmission line impedance and the initial step duration is much longer than the propagation delay τ_D of the transmission line. Ignoring the loss of the transmission line, we have the initial waveform and the waveform at the load/receiver shown in Figure 9.11, which is based on equation 9.11.

Figure 9.11. The initial waveform at Tx (V_i) and Rx (V_L) when multiple reflections are considered.



Obviously, the time and voltage deviations caused by reflection occur at a frequency of every $(1/2\tau_D)$. The resulting jitter and noise are deterministic in nature because they are bounded. Reflection-induced jitter and noise fall into the DDJ or DDN category in general. Because reflection is caused by the impedance mismatch, any effort to minimize or remove the mismatch will reduce the effects of reflection. Termination at the source and load are the common means of mitigating reflection.

9.4.2.2. Optical Reflection

For an optical link, reflections similar to Figure 9.10 can happen because of discontinuities in optical material properties between Tx, optical-fiber cable, and Rx. An optical medium typically is characterized by its refraction index n . The refraction index n is related to electrical permittivity and magnetic permeability through $n = c\sqrt{\epsilon\mu}$. In optical communication, the signal is represented by its power that is proportional to the electrical field or voltage square. Therefore, the appropriate ratio should be the reflectance R that is the square of the reflection coefficient, as defined by equation 9.8. If we consider the reflection between the boundary of fiber cable and receiver, the reflectance can be expressed in terms of refraction index n :

Equation 9.12

$$R = \rho_r^2 = \frac{I_r}{I_i} = \left(\frac{n_L - n_0}{n_L + n_0} \right)^2$$

where R is the reflectance, I_r and I_i are the intensity of reflected and incident waves, and n_L and n_0 are the refraction index for the optical receiver and optical fiber, respectively.

The effect of reflection on the signal in an optical link is similar to that shown in Figures 9.10 and 9.11. However, its impact on the optical transmitter can be more severe, because the reflected wave can cause instability within a transmitter laser cavity.^[12] The laser instability introduces both timing jitter and intensity noise for the initial wave, making the signal integrity at the optical transmitter output and receiver input worse. It is uncommon to find a counterpart for optical laser instability caused by the optical reflection in the electrical domain. In addition to matching the refraction index at the channel or medium boundary, an optical isolator, which can stop reflected waves, is commonly used in optical links to mitigate optical reflections. Most of the isolators were developed based on polarization in that the forward wave and reflected wave have different polarization state, and a polarization filter can be used to filter out the unwanted reflected waves.

User name: CSU San Diego

Book: Jitter, Noise, and Signal Integrity at High-Speed

Section: Chapter 9. Jitter and Signal Integrity Mechanisms for High-Speed Links

No part of any chapter or book may be reproduced or transmitted in any form by any means without the prior written permission for reprints and excerpts from the publisher of the book or chapter. Redistribution or other use that violates the fair use privilege under U.S. copyright laws (see 17 USC107) or that otherwise violates these Terms of Service is strictly prohibited. Violators will be prosecuted to the full extent of U.S. Federal and Massachusetts laws.

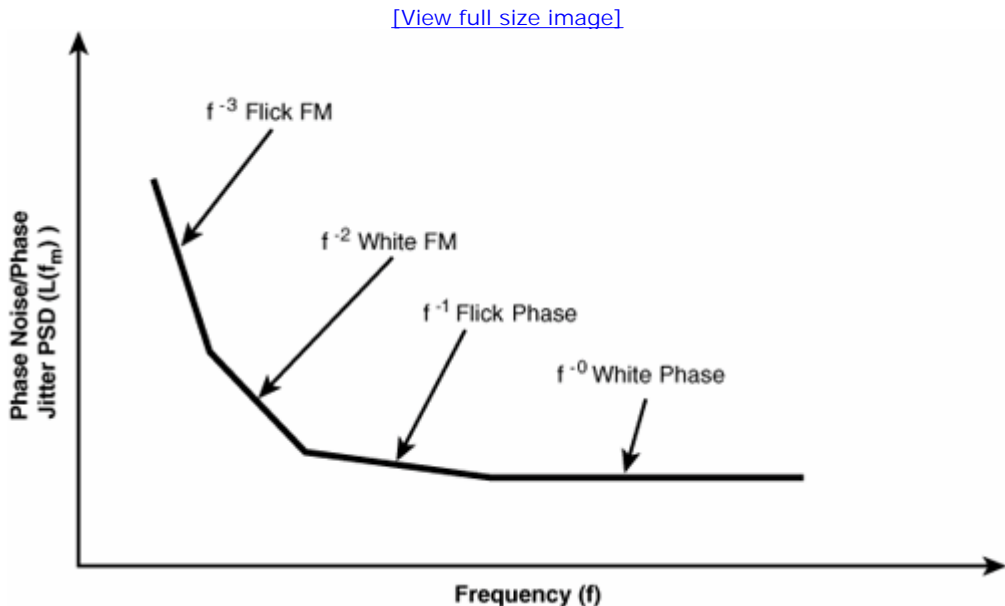
Information Theory Computer Science Mike Peng Li Prentice Hall Jitter, Noise, and Signal Integrity at High-Speed

9.5. Reference Clock

The reference clock in the high-speed communication typically is generated by a reference crystal oscillator and a PLL. A crystal oscillator is responsible for generating a low-frequency clock in a 10 MHz range or so, and the PLL is responsible for multiplying the low-frequency clock to a higher-frequency clock. Cascaded PLL may be used to provide a wide range of clock output frequencies, from 100 MHz to several GHz. For example, in PCI Express, it is commonly found that a 100 MHz reference clock is first generated with a reference crystal in the frequency range of 10–20 MHz, and then it is multiplied by PLL or PLLs reach 100 MHz.

Due to the generation mechanism, the jitter performance of a reference clock depends on the jitter performance of the reference crystal oscillator and PLL (as covered extensively in [Chapter 8](#)). Crystal oscillator performance is traditionally measured by its phase noise. Phase noise to phase jitter conversion is covered in [Chapter 7](#), "Clock Jitter." The crystal's phase noise or phase jitter spectral shape is composed of white or thermal at higher frequencies and 1/f or higher-order power-law spectra at low frequencies close to the carrier. A typical phase noise power spectrum density (PSD) looks like [Figure 9.12](#).^[13]

Figure 9.12. Phase jitter or phase noise PSD for a crystal oscillator.



Higher-order power-law phase noise at low frequencies is the cause of the low-frequency phase jitter in the time domain or long-term frequency instability for the crystal oscillator. Therefore, maintaining the low-frequency phase noise or jitter below a certain level is an important metric for design and verification of the crystal oscillator or reference clock.

To reduce the electromagnetic interference (EMI) effect caused by the reference clock, a spread-spectrum clock (SSC) method is used

for most computer applications. SSC redistributes the energy spectrum so that spectral line magnitude at a given frequency is below a certain threshold. Consequently, the radiation of EMI due to periodic clock voltage level switch at its carrier frequency is reduced. Note that SSC does not reduce the clock's total energy. Rather, it redistributes its energy evenly in the vicinity of the carrier frequency. Frequency dither is commonly used to achieve SSC. There are three basic SSC types:

- Down spreading, in which the clock spectrum is spread to frequencies lower than the original one
- Center spreading, in which the clock spectrum is spread in both directions, below and above the original one
- Up spreading, in which the clock spectrum is spread to frequencies above the original one

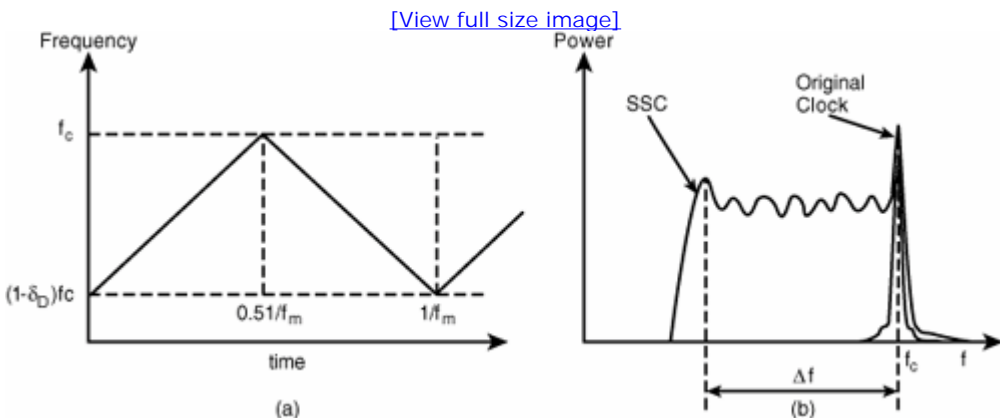
Most of the SSCs in synchronized digital computer systems use the down-spreading method to meet the maximum frequency or minimum period requirement for those systems. A key parameter of SSC called spreading rate is defined as

Equation 9.13

$$\delta_D = -\frac{\Delta f}{f_c}$$

where Δf is the spreading frequency range and f_c is the original frequency without spreading. If the spreading range repeats at a frequency of f_m with a triangular modulation profile, a down-spreading SSC in the time and frequency domains may look like Figure 9.13.

Figure 9.13. A down-spreading SSC frequency profile in the time domain (a) and frequency domain (b). The frequency-domain graph shows the original or nominal frequency spectra.



Both PCI Express and SATA require a spreading rate of 0–5,000 PPM or 0%–0.5% for SSC and a modulation frequency in the range of 30–33 KHz. The SSC phase jitter can be estimated as follows:

Equation 9.14

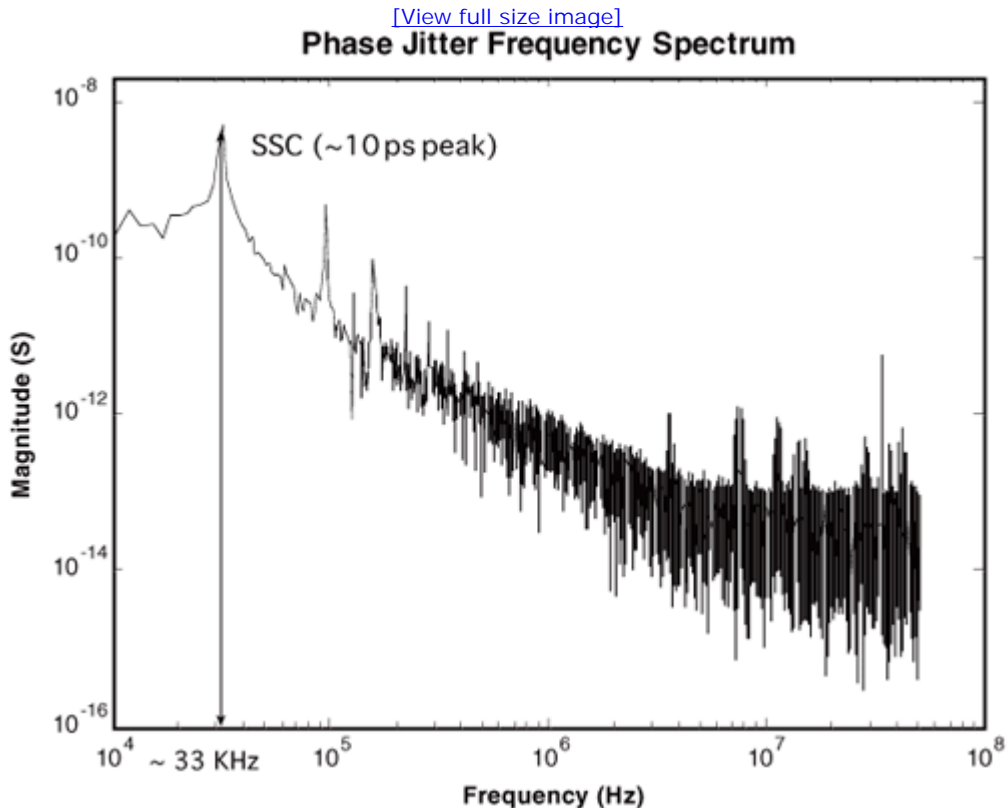
$$\Delta t = \frac{\phi}{\omega} = \frac{2\pi f_c (1-\delta_D) T_c}{2\pi f_c} = (1-\delta_D) T_c$$

For a –5,000 PPM SSC frequency down-spreading, the corresponding phase jitter peak at the fundamental modulation is $0.995T_c$, where T_c is the original or nominal period for the reference clock. For example, for the 10 MHz reference clock, the SSC phase jitter peak is 9.95 ns.

Figure 9.14 shows the phase jitter spectrum for a 100 MHz reference clock used in PCI Express. It shows the 1/f type of random phase noise at frequencies below ~10 MHz and white random noise above ~10 MHz. Superimposed on the random noise background is a 33

KHz SSC with a magnitude of ~10 ns. Many of its harmonics up to 14 times fundamental can also be seen.

Figure 9.14. The phase jitter spectrum for a 100 MHz reference clock used for PCI Express. The SSC modulation frequency is at 33 KHz, with a modulation magnitude of ~10 ns.



In the frequency range of 1 MHz to 1 GHz, the phase jitter random spectrum can be as high as a few ps. Thus, the link architecture must cope with the reference clock phase jitter spectrum to achieve the overall 10^{-12} BER goal. The next section discusses how PI-based common clock "differential signaling" helps reduce the phase jitter contribution from the reference clock.

URL <http://access.proquest.safaribooksonline.com/9780132429610/ch09lev1sec5>

User name: CSU San Diego

Book: Jitter, Noise, and Signal Integrity at High-Speed

Section: Chapter 9. Jitter and Signal Integrity Mechanisms for High-Speed Links

No part of any chapter or book may be reproduced or transmitted in any form by any means without the prior written permission for reprints and excerpts from the publisher of the book or chapter. Redistribution or other use that violates the fair use privilege under U.S. copyright laws (see 17 USC107) or that otherwise violates these Terms of Service is strictly prohibited. Violators will be prosecuted to the full extent of U.S. Federal and Massachusetts laws.

Information Theory Computer Science Mike Peng Li Prentice Hall Jitter, Noise, and Signal Integrity at High-Speed

9.6. Overall Link Jitter Budget

Modern link systems allow the system integrator to build a working system with components from different manufacturers. To achieve this goal, a specification for each component is needed to ensure interoperability and performance goals such as 10^{-12} BER. In making the component specification, the overall link system architecture and subsystem architecture for other components need to be assumed or specified. For example, the specification for transmitter cannot be made unless the subsystem architectures and performance metrics for receiver, medium, and reference clock are known or assumed, for the link shown in [Figure 9.2](#).

The total available jitter budget for a link is 1 UI, and that is shared by all the link subsystems or components. The allocation of the exact jitter budget for the subsystem is derived with the considerations of link architecture and technology capabilities of the subsystems. If jitter components of DJ and RJ are not known, the link jitter budget typically is done through a linear sum (LS) of TJs from each subsystem and making sure that the net result is less than 1 UI:

Equation 9.15

$$TJ_{sys} = TJ_{Tx} + TJ_{Ch} + TJ_{clk} + TJ_{Rx} \leq 1UI$$

Here TJ is the total jitter at $BER = 10^{-12}$. Obviously, the independence between the subsystems' jitter is assumed in this approach. For example, [\[14\]](#) uses this approach for its jitter budgeting.

It turns out that this method of TJ summing is overly conservative and leaves some jitter budget unused. It fails some subsystems that in fact do not cause interoperability problems in actual systems. The underlying reason for being conservative is that the RJs of each independent interact through root-sum-square (RSS) and do not sum linearly in the real world.

To overcome the shortfalls of the LS-based jitter budgeting method, the RJ RSS method was developed.[\[16\]](#) In the RSS jitter budget method, dual-Dirac DJ and Gaussian RJ (as discussed in [Chapter 5](#), "Jitter and Noise Separation and Analysis in the Statistical Domain") are used for all the link subsystems, and the independence among them is also assumed. Due to the DJ dual-Dirac PDF, the overall DJ for the link is the superimposition of the DJs from all the subsystems:

Equation 9.16

$$DJ_{sys} = DJ_{Tx} + DJ_{Ch} + DJ_{clk} + DJ_{Rx}$$

The RJ σ s for all the subsystems is "summed" through RSS to give rise to the overall σ for the link through the following:

Equation 9.17

$$\sigma_{sys} = \sqrt{\sigma_{Tx}^2 + \sigma_{Clk}^2 + \sigma_{Ch}^2 + \sigma_{Rx}^2}$$

For a passive channel, RJ σ_{Ch} is 0. Recalling equation 5.36 for the TJ calculation given a dual-Dirac DJ PDF and a Gaussian RJ PDF, we have the following:

Equation 9.18

$$TJ_{sys}(\beta) = DJ_{sys} + 2Q(\beta)\sigma_{sys}$$

For BER or $\beta = 10^{-12}$, Table 5.1 gives $Q(\beta) = 7.035$, so equation 9.18 becomes

Equation 9.19

$$TJ_{sys}(10^{-12}) = DJ_{sys} + 14.07\sigma_{sys}$$

Equation 9.19 gives the TJ or eye closure estimation for the link given its subsystem DJs and RJs. This provides a mathematical linkage from subsystem jitter performance to overall link jitter performance. It is the foundation of the RSS-based link jitter budget method.

Table 9.1 compares the jitter budget for the LS-based method (PCI Express 1.0a) and RSS method (PCI Express 1.1).^{[15], [16]}

Table 9.1. Linear and RSS Methods for Total System Jitter Budgeting

Subsystem Component	Minimum RJ σ (ps)	Maximum DJ (ps) Pk-Pk	TJ (ps) at BER 10^{-12}
Tx	2.8	60.6	100
Reference Clock	4.7	41.9	108
Channel	0	90	90
Rx	2.8	120.6	160
Linear Sum (LS) TJ			458
Root-Sum-Square (RSS) TJ			399.13
TJ Delta			58.87 (14.7%)

In this table, we see that the TJ difference between the LS-based method and RSS-based method is 58.87 ps, or 14.7% of 1 UI in this example. In other words, for the LS-based method, the overall system TJ is 58.87 ps shorter than the total available jitter budget of 1 UI or 400 ps, and the system will fail. On the other hand, the RSS method gives the system TJ that fits exactly within 1 UI or 400 ps available budget. If the LS-based method is used, the TJ for all or some of the subsystems must be reduced so that the total system TJ is within 1 UI to pass. Reducing jitter for a link subsystem typically involves redesigning the subsystem circuits and using more expensive and accurate components. Both of these methods are costly. On the other hand, one can make the total system TJ be within the 1 UI limit without redesigning or using better and more expensive components—a very neat and cost-effective approach. Obviously, DJ or RJ and TJ for the link subsystem need to be specified and verified for the RSS-based jitter budget method. For the LS-based method, only TJ for the link component needs to be specified and verified.

User name: CSU San Diego

Book: Jitter, Noise, and Signal Integrity at High-Speed

Section: Chapter 9. Jitter and Signal Integrity Mechanisms for High-Speed Links

No part of any chapter or book may be reproduced or transmitted in any form by any means without the prior written permission for reprints and excerpts from the publisher of the book or chapter. Redistribution or other use that violates the fair use privilege under U.S. copyright laws (see 17 USC107) or that otherwise violates these Terms of Service is strictly prohibited. Violators will be prosecuted to the full extent of U.S. Federal and Massachusetts laws.

Information Theory Computer Science Mike Peng Li Prentice Hall Jitter, Noise, and Signal Integrity at High-Speed

9.7. Summary

This chapter started by introducing two major link architectures for multiple Gbps link systems. One uses the data-driven clock recovery receiver, in which no reference clock is needed and the receiver needs to recover both frequency and phase to generate the bit clock. PLL clock recovery is commonly used in this data-driven architecture. Another is the common clock architecture in that a low-frequency 100 MHz reference clock is sent to both transmitter and receiver. The receiver uses a digital phase interpolator (PI) to recover the clock phase. The frequency is recovered by a multiplication PLL in the receiver, taking the 100 MHz reference clock as the input.

We preceded to the subsystem architecture, operation mechanisms, and jitter and noise performance for the link subsystems of transmitter, receiver, channel, and reference clock.

For transmitter, we pointed out that the key jitter contributor is the substrate reference clock and multiplication PLL, and the key noise contributor is the voltage driver, operating with a current mode or a voltage mode. For receiver, we pointed out that the major jitter contributor is the clock recovery (CR) circuit, and the major noise contributor is the data recovery, which may include an amplifier, data sampler, or comparator.

We discussed the channel or medium properties and associated jitter and signal integrity performance. We went a bit in depth because these channel properties are physics-based and therefore more transparent and less design-specific. Both electrical copper and optical fiber-based channels were discussed. For a copper-based channel, frequency-dependent losses due to skin effect and dielectric or loss tangent were covered. For an optical fiber channel, chromatic dispersion (CD) and polarization mode dispersion (PMD) were discussed. Signal impairments due to the interactions between channels and other link subsystems were also discussed, including crosstalk and reflection. For electrical copper, crosstalk is caused by interference between channels. Both near-end crosstalk (NEXT) and far-end crosstalk (FEXT) were covered. For optical fiber, both linear crosstalk (such as that caused by wavelength filter leakage) and nonlinear crosstalk (such as that caused by scattering and four-wave mixing (FWM)) were covered. We discussed reflection from a unified and generic Maxwellian theorem and equations. We treated electrical reflection as a special form caused by electrical impedance discontinuity, and optical reflection due to refraction index discontinuity. The basic physics for the jitter and signal integrity-forming mechanism can be equally applied to devices or integrated circuits, as well as on-chip interconnects.

We then discussed the reference clock generation method and associated jitter performance. We emphasized the importance of the phase noise or phase jitter spectrum for the reference oscillator to reference clock jitter performance. Spread-spectrum clocking (SSC) was discussed in detail, along with SSC phase jitter and its linkage to the spreading rate.

Having discussed jitter and signal integrity for all the link subsystems, we discussed the link jitter budget for the entire system by considering the common clock architecture in the end. Both linear sum (LS) and root-sum-square (RSS) methods were discussed. We showed with a real-world example that, for the same BER target, the RSS method allows more subsystem jitter budget compared to the LS method. RSS requires knowledge of the jitter component of DJ and RJ for each link subsystem, whereas the LS method does not. The RSS method is very attractive for link jitter budgeting because it can give additional jitter budget for the link subsystem for "free," compared with that of the LS method.

URL <http://access.proquest.safaribooksonline.com/9780132429610/ch09lev1sec7>

User name: CSU San Diego

Book: Jitter, Noise, and Signal Integrity at High-Speed

Section: Chapter 9. Jitter and Signal Integrity Mechanisms for High-Speed Links

No part of any chapter or book may be reproduced or transmitted in any form by any means without the prior written permission for reprints and excerpts from the publisher of the book or chapter. Redistribution or other use that violates the fair use privilege under U.S. copyright laws (see 17 USC107) or that otherwise violates these Terms of Service is strictly prohibited. Violators will be prosecuted to the full extent of U.S. Federal and Massachusetts laws.

Information Theory Computer Science Mike Peng Li Prentice Hall Jitter, Noise, and Signal Integrity at High-Speed

Endnotes

1. "Fibre Channel Physical Interfaces (FC-PI-4)," a working draft of Secretariat International Committee for Information Technology Standardization (INCITS), Rev 3.0, Oct. 2006.
2. R. Gu, J. Tran, H. C. Lin, A. L. Yee, and M. Izzard, "A 0.5-3.5 Gbps low power low jitter serial data CMOS transceiver," in IEEE Int. Solid State Circuit Conference (ISSCC), Dig. Tech. Papers, San Francisco, CA, pp. 352–353, 1999.
3. J. T. Stonik, G. Y. Wei, J. L. Sonntag, and D. K. Weinlader, "An adaptive PAM-4.5 Gbps backplane transceiver in 0.25 μ m CMOS," IEEE J. Solid State Circuits, vol. 38, no. 3, pp. 436–443, Mar. 2003.
4. V. Stojanovic and M. Horowitz, "Model and analysis of high-speed serial links," Proc. IEEE Conf. Customer Integrated Circuits, pp. 589–594, Sept. 2003.
5. Payne et al., "A 6.25-Gb/s binary transceiver in 0.13- μ m CMOS for serial data transmission across high loss legacy backplane channels," IEEE J. Solid State Circuits, vol. 40, no. 12, pp. 2646–2657, Dec. 2005.
6. J. D. Jackson, *Classical Electrodynamics*, John Wiley & Sons, Inc., 1975.
7. C. Nguyen, *Analysis Methods for RF, Microwave, and Millimeter Wave Planar Transmission Line Structures*, John Wiley, New York.
8. G. P. Agrawal, *Fiber-Optic Communication Systems*, Second Edition, John Wiley & Sons, Inc., 1997.
9. W. J. Dally and J. W. Poulton, *Digital Systems Engineering*, Cambridge University Press, 1998.
10. H. Johnson and M. Graham, *High-Speed Digital Design*, Prentice Hall PTR, 1993.
11. S. V. Kartalopoulos, *Introduction to DWDM Technology*, SPIE Press/IEEE Press, 2000.
12. M. Shikada, S. Takano, S. Fujita, I. Mito, and Minemura, "Evaluation of power penalties caused by feedback noise of distributed feedback laser diodes," J. of Lightwave Technology, vol. 6, pp. 655–659, 1988.
13. T. E. Parker, "Characteristics and phase noise in a stable oscillator," Proc. of 41st Annual Symp. Freq. Control, 1987.
14. PCI-SIG, "PCI Express Base Specification, Rev. 1.0a," <http://www.pcisig.com/specifications/pciexpress/base>, 2003.
15. PCI-SIG, "PCI Express Base Specification, Rev. 1.1," <http://www.pcisig.com/specifications/pciexpress/base>, 2004.
16. PCI-SIG, "Jitter and BER white paper (II)," http://www.pcisig.com/specifications/pciexpress/technical_library, 2005.

URL <http://access.proquest.safaribooksonline.com/9780132429610/ch09lev1sec8>

User name: CSU San Diego

Book: Jitter, Noise, and Signal Integrity at High-Speed

No part of any chapter or book may be reproduced or transmitted in any form by any means without the prior written permission for reprints and excerpts from the publisher of the book or chapter. Redistribution or other use that violates the fair use privilege under U.S. copyright laws (see 17 USC107) or that otherwise violates these Terms of Service is strictly prohibited. Violators will be prosecuted to the full extent of U.S. Federal and Massachusetts laws.

Information Theory Computer Science Mike Peng Li Prentice Hall Jitter, Noise, and Signal Integrity at High-Speed

10. Modeling and Analysis for Jitter and Signaling Integrity for High-Speed Links

This chapter focuses on the mathematical modeling and analysis aspects for the jitter and signal integrity of a link system, including its subsystems of transmitter (Tx), channel, and receiver (Rx). Furthermore, components within transmitter, channel, and receiver are also discussed and modeled, along with the signaling, jitter, and noise properties.

URL <http://access.proquest.safaribooksonline.com/9780132429610/ch10>

User name: CSU San Diego

Book: Jitter, Noise, and Signal Integrity at High-Speed

Section: Chapter 10. Modeling and Analysis for Jitter and Signaling Integrity for High-Speed Links

No part of any chapter or book may be reproduced or transmitted in any form by any means without the prior written permission for reprints and excerpts from the publisher of the book or chapter. Redistribution or other use that violates the fair use privilege under U.S. copyright laws (see 17 USC107) or that otherwise violates these Terms of Service is strictly prohibited. Violators will be prosecuted to the full extent of U.S. Federal and Massachusetts laws.

Information Theory Computer Science Mike Peng Li Prentice Hall Jitter, Noise, and Signal Integrity at High-Speed

10.1. A Linear Time-Invariant (LTI) Approach

We will use LTI theory as the basis for jitter and signaling modeling for link subsystems of transmitter, channel or medium, and receiver. LTI theory and basics were discussed extensively in [Chapter 2](#), "Statistical Signal and Linear Theory for Jitter, Noise, and Signal Integrity." Here we will focus on its application in jitter and signaling quantification in a high-speed link.

There are essentially unlimited implementations for circuit or transistor-level details for a link subsystem or component. Therefore, we will focus on system or subsystem behavior modeling for the link to maintain the generality of our more physics-based model. We will start with the transmitter, and then cover the channel, and finally the receiver.

URL <http://access.proquest.safaribooksonline.com/9780132429610/ch10lev1sec1>

User name: CSU San Diego

Book: Jitter, Noise, and Signal Integrity at High-Speed

Section: Chapter 10. Modeling and Analysis for Jitter and Signaling Integrity for High-Speed Links

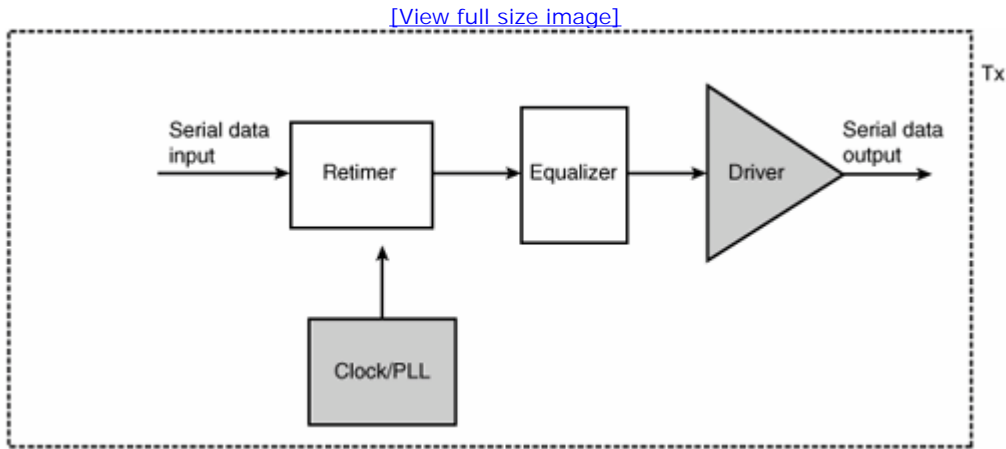
No part of any chapter or book may be reproduced or transmitted in any form by any means without the prior written permission for reprints and excerpts from the publisher of the book or chapter. Redistribution or other use that violates the fair use privilege under U.S. copyright laws (see 17 USC107) or that otherwise violates these Terms of Service is strictly prohibited. Violators will be prosecuted to the full extent of U.S. Federal and Massachusetts laws.

Information Theory Computer Science Mike Peng Li Prentice Hall Jitter, Noise, and Signal Integrity at High-Speed

10.2. Transmitter Modeling and Analysis

A generic transmitter subsystem block diagram is shown in [Figure 9.3 of Chapter 9](#), "Jitter and Signal Integrity Mechanisms for High-Speed Links." The purpose of this chapter is to model and analyze the jitter and signaling for the transmitter. As such, we will focus on the noise-sensitive component of the voltage driver and the jitter-sensitive component of the clock generator. [Figure 10.1](#) shows a simplified block diagram for a transmitter.

[Figure 10.1. A simplified block diagram for a transmitter.](#)

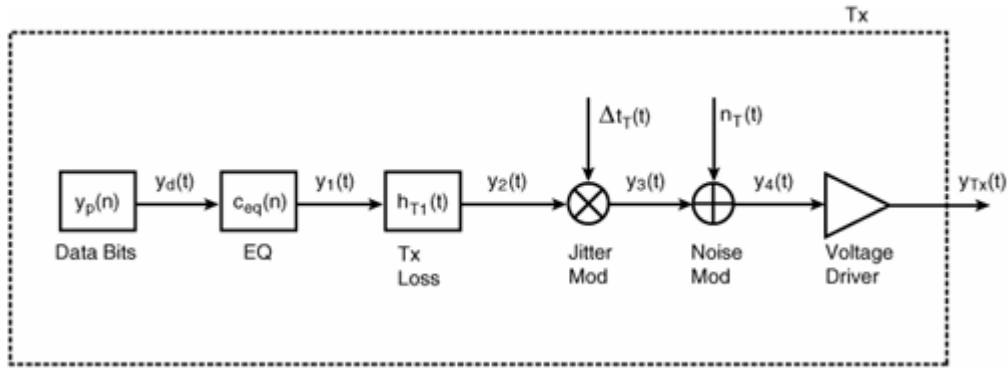


In this simplified transmitter subsystem block diagram, the coded serial data is retimed with the timing function provided by a clock or PLL. A transmitter equalizer is also included to reflect the necessity of equalization in multiple Gbps links. In the end, the retimed and equalized signal is fed to a voltage driver to generate a required voltage level for the transmitter output.

The starting point for the Tx signaling is the raw digital data pattern without any distortion; we denote it as $y_p(n)$. We also assume a linear digital equalization with coefficient series of $\{c_m\}$. The driver's finite rise and fall time driving capability is characterized by its loss function, denoted as $h_{Tl}(t)$. The loss function reflects the on-chip interconnect and package effects. The amplitude noise generated by the driver is denoted as $n_T(t)$, and the timing jitter generated by the clock and the PLL of the transmitter is denoted as $\Delta t_T(t)$. The signal output is defined at the transmitter's output pin. [Figure 10.2](#) shows the transmitter subsystem model block diagram we plan to use.

[Figure 10.2. A transmitter behavior model block diagram.](#)

[View full size image]



In this "mixed-signal" behavior model, the signal is purely digital bits before the loss function. After the loss function, the digital signal is converted into an analog signal with finite rise and fall times. Jitter is introduced through phase modulation that moves the digital timing around the ideal. The analog signal interacts with the on-chip loss term through convolution. The on-chip loss manifests interconnect, parasitic, and packaging effects. The amplitude noise is introduced through amplitude modulation, reflecting the driver noise generation.

10.2.1. Transmitter Digital Data Bits

Mathematically, the digital pulse train $y_d(t)$ as a function of digital bit sequence $y_p(n)$ can be expressed as follows:

Equation 10.1

$$y_d(t) = \sum_k [y_p(kT_0) - y_p((k-1)T_0)]u(t - kT_0)$$

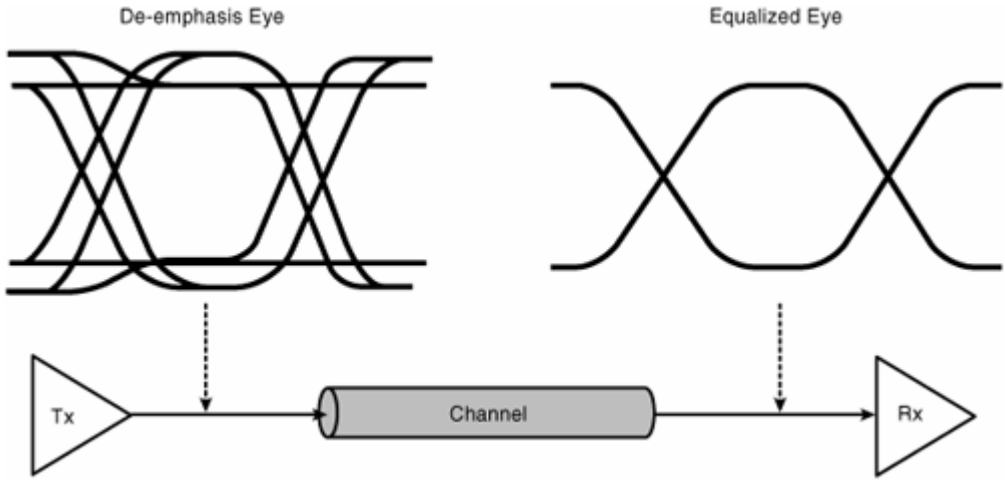
where $u(t)$ is a unit step function with a definition of $u(t) = 1$ if $t \geq 0$ and $u(t) = 0$ if $t < 0$.

10.2.2. Transmitter Equalization

Equalization has become mandatory for multiple Gbps communication links, particularly for copper-based channel media. The two basic types of equalization for a transmitter are pre-emphasis and de-emphasis.^{[1], [2], [3]} As we have mentioned in Chapter 9, pre-emphasis increases (positive compensation) the spectrum energy at high frequencies so that the increased spectral content is attenuated by the lossy channel. This results in an undistorted signal spectrum at the receiver input even after the lossy channel. In contrast, de-emphasis decreases the spectrum energy at low frequencies so that after attenuation due to the lossy channel, undistorted but level reduced signal spectrum content is achieved at the receiver input. Figure 10.3 shows the pre-emphasis transmitter signal eye diagram at the channel input and the well-equalized signal eye diagram at the channel output.

Figure 10.3. Transmitter de-emphasis equalization associated eye diagrams.

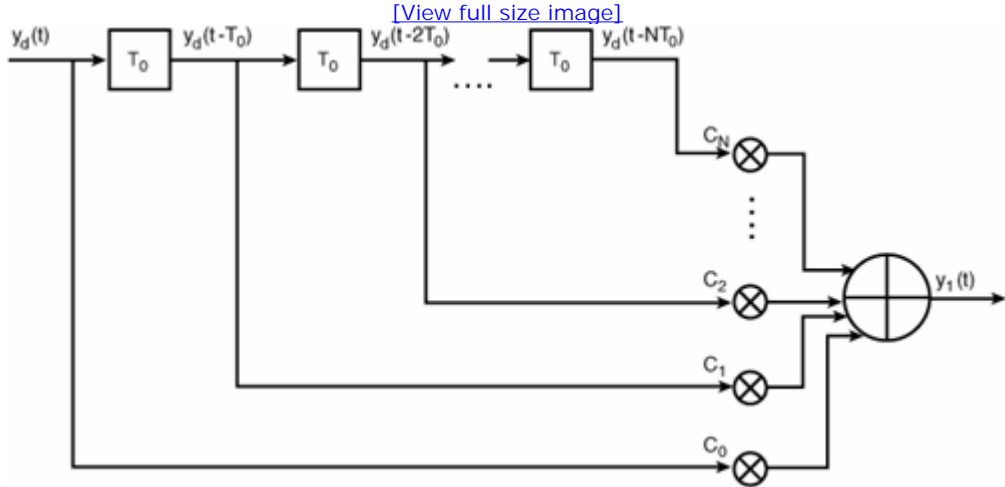
[\[View full size image\]](#)



In this example, the amplitudes for all the bits of consecutive 1s or 0s are reduced except for the first one. This de-emphasis example has only four types of edge transitions: full swing 1 to full swing 0, full swing 0 to full swing 1, de-emphasis 1 to full swing 0, and de-emphasis 0 to full swing 1. Because of the de-emphasis, an open data eye is obtained even after the lossy channel. Because the equalization uses de-emphasis, the amplitude of the data eye at the receiver gets reduced. A similar open data eye at the receiver can also be achieved with pre-emphasis equalization, but the data eye amplitude at the receiver is not reduced in this case.

Transmitter linear equalization such as pre-emphasis or de-emphasis typically is implemented by a digital finite impulse response (FIR) filter. Figure 10.4 illustrates a FIR implementation for a Tx equalization.

Figure 10.4. A Tx equalization implementation using an N-tap FIR filter.



The relationship between the Tx FIR equalization output and input, as well as the filter coefficients (also called taps), are given by the following equation:

Equation 10.2

$$\begin{aligned}
 y_1(t) &= c_0 y_d(t) + c_1 y_d(t - T_0) + c_2 y_d(t - 2T_0) + \dots + c_N y_d(t - NT_0) \\
 &= \sum_{i=0}^N c_i y_d(t - iT_0)
 \end{aligned}$$

The determination of the FIR coefficients or tap coefficients typically is based on channel lossy and crosstalk characteristics, such as S-parameters, impulse response, or step response, as discussed in the next section.

Equalization with a digital FIR type of filter is easy to verify because the observability at the Tx output is an on-issue, and the Tx output pin is accessible for most times. Controllability and flexibility for a FIR filter generally are good, with relatively simple implementation circuits. However, Tx equalization needs loopback mode for the receiver to send a signal back to the transmitter for dynamic and fine-tuned equalization.

10.2.3. Transmitter Jitter Phase Modulation

As mentioned in [Chapter 9](#), the transmitter's major jitter source comes from the clock generator that is commonly implemented with a PLL. The PLL's phase jitter causes the phase jitter for the data bit signal generated by the transmitter. Given the phase jitter time function, its impact on the phase jitter of the data bit signal can be modeled as the phase modulation. Assuming a generic phase jitter time function $\Delta t(t)$, its effect on the data bit signal timing and waveform can be expressed by the following equation:

Equation 10.3

$$y_2(t) = y_1(t + \Delta t_T(t))$$

The phase jitter or modulation "perturbation" to the data bit signal causes the data edge transition times to move around the ideal time locations. The resulting time deviations formulate the phase jitter for the data bit signal.

10.2.4. Transmitter Noise Amplitude Modulation

As we mentioned [Chapter 9](#), the key amplitude noise source for the transmitter comes from the driver that generates the digital bits at a certain voltage level. We will treat noise as digital amplitude noise. This amplitude noise $n_D(t)$ interacts with the digital waveform through the amplitude modulation or amplitude perturbation. This amplitude modulation can be expressed by the following:

Equation 10.4

$$y_3(t) = y_2(t) + n_D(t)$$

10.2.5. Transmitter Loss

The channel connecting the transmitter and receiver has been discussed extensively, but the on-chip subsystem interconnect channels are not well explored in much of the high-speed signaling modeling literature.[\[4\]](#), [\[5\]](#), [\[6\]](#) Interestingly, the fundamental physics of on-chip channel signaling and link system signaling are not much different. The LTI channel model has proven to be a good model for the linear passive channel. Thus, we will adopt the LTI channel model method for on-chip subsystem channel analysis. The loss characteristics will be expressed in terms of the impulse response in the time domain to match the rest of the time domain models for other transmitter subsystems. Introducing the on-chip loss term also allows us to include the package loss effect and gives us more flexibility to do accurate modeling. We express the impulse response of the on-chip loss as $h_{TL}(t)$. Its output is

Equation 10.5

$$y_4(t) = y_3(t) * h_{TL}(t)$$

where $*$ represents the convolution operation.

10.2.6. Transmitter Driver

This last stage of our transmitter model introduces the electrical voltage driver or optical driver subsystem. Its functionality is to generate the waveform at a certain voltage level or optical power, and it is essentially an ideal digital-to-analog converter (DAC). The digital signal waveform becomes a physical waveform. We represent the final transmitter output as follows:

Equation 10.6

$$y_{TX}(t) = Ay_4(t)$$

where A represents the intended voltage or power level.

Finally, we have developed an "end-to-end" model for the transmitter signal waveform at its output in terms of characteristic properties of its accumulated subsystems along the signal-generation sequence chain. So far we have assumed that the medium's electrical (impedance) or optical (refraction index) property has no discontinuity between transmitter and channel; thus, there is no reflection. However, if the medium's discontinuity is considered, [equation 10.6](#) needs to be uttered. Because a behavior model is not suited for detailed reflection physics that depends on the channel's electrical or optical properties, we will give only a high-level discussion of reflection when it is considered.

Assume that the reflection coefficient at the boundary between the transmitter and channel is $\rho_{rt}(s)$ and is frequency-dependent. We denote its inverse Laplace transformation as $\rho_{rt}(t)$. Then the signal at the output of the transmitter will be

Equation 10.7

$$y_{tx}(t) = A [y_4(t) + \rho_{rt}(t) * y_4(t)]$$

when reflection is considered. If no reflection exists—namely, $\rho_{rt}(t) = 0$ —[equation 10.7](#) returns to [equation 10.6](#).

The relationship for the transmitter signal is in a cascading form. We will not give a single equation for the transmitter output waveform in terms of all its subsystem parameters and characteristic functions, because it would be too long and complex, but the information and math basics are all there to enable such a deviation.

As soon as the waveform or amplitude versus time function is obtained for the transmitter output, the corresponding eye diagram can be built accordingly because it is just overlays of waveform on a per-UI basis. Associated jitter, including its components of DJ, RJ, and TJ, and noise, including its components of DN, RN, and TN, can be obtained using the methods described in [Chapters 4, 5, and 6](#).

URL <http://access.proquest.safaribooksonline.com/9780132429610/ch10lev1sec2>

User name: CSU San Diego

Book: Jitter, Noise, and Signal Integrity at High-Speed

Section: Chapter 10. Modeling and Analysis for Jitter and Signaling Integrity for High-Speed Links

No part of any chapter or book may be reproduced or transmitted in any form by any means without the prior written permission for reprints and excerpts from the publisher of the book or chapter. Redistribution or other use that violates the fair use privilege under U.S. copyright laws (see 17 USC107) or that otherwise violates these Terms of Service is strictly prohibited. Violators will be prosecuted to the full extent of U.S. Federal and Massachusetts laws.

Information Theory Computer Science Mike Peng Li Prentice Hall Jitter, Noise, and Signal Integrity at High-Speed

10.3. Channel Modeling and Analysis

This section starts with basic channel modeling by applying LTI theory. Then we discuss various channel characterization methods to obtain transfer functions in different forms of time or frequency domains. Finally, we discuss a generic, pole/zero-based channel modeling method.

10.3.1. Channel LTI Modeling

As mentioned in [Chapter 9](#), the two commonly used channel media for high-speed multiple Gbps links are copper-based and fiber-optic-based. Copper-based cable is commonly used in short-distance links (less than 10 m), such as motherboard and backplane applications, and optical fiber is commonly used in long-distance links (greater than 10 m), such as data center to storage network applications.

Both copper and fiber-optic channels are passive, and an LTI can be used to quantify their behavior. The channel characteristics can be represented by the channel transfer function that can have different forms. In the time domain, its characteristic is represented by its impulse response function $h_{ch}(t)$. Because the integration of the impulse response gives rise to the step response, this channel characteristic can also be represented by its step response $u_{ch}(t)$. In the frequency domain, channel characteristic can be represented by its transfer function $H_{ch}(s)$, where s is the complex frequency.

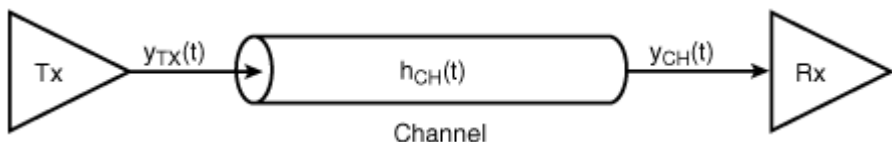
The preceding section derived the transmitter output $y_{TX}(t)$ waveform in terms of its subsystem characteristics. $y_{TX}(t)$ is input for the channel modeling. [Figure 10.5](#) shows the channel input $y_{TX}(t)$, impulse response $h_{CH}(t)$, and output $y_{CH}(t)$ topology. Their relationship is given by the following equation:

Equation 10.8

$$y_{CH}(t) = h_{CH}(t) * y_{TX}(t)$$

The convolution (*) between the input signal and channel impulse response function gives rise to the output signal.

Figure 10.5. Channel input, impulse response, and output topology.



In practice, particularly for digital signals, it is much easier and more convenient to generate a step response rather than an impulse response. In that case, [equation 10.8](#) can be rewritten as

Equation 10.9

$$y_{CH}(t) = \frac{dw_{CH}(t)}{dt} * y_{TX}(t)$$

where $w_{CH}(t)$ is the unit step response. As introduced in [Chapter 2](#), convolution in the time domain becomes multiplication in the complex frequency domain (or s-domain). If a Laplace transformation is applied to [equation 10.8](#), its complex frequency-domain relation becomes

Equation 10.10

$$Y_{CH}(s) = H_{CH}(s)Y_{TX}(s)$$

where $Y_{TX}(s)$, $H_{CH}(s)$, and $Y_{CH}(s)$ are the Laplace-transformed functions of $y_{TX}(t)$, $h_{CH}(t)$, and $y_{CH}(t)$, respectively. $H_{CH}(s)$ is also called the channel transfer function.

Similarly, when a Laplace transformation is applied to [equation 10.9](#), it becomes

Equation 10.11

$$Y_{CH}(s) = sW_{CH}(s)Y_{TX}(s)$$

where $W_{CH}(s)$ is the Laplace-transformed function for step response $w_{CH}(t)$.

In practice, it is common to start with [equation 10.8](#) in the time domain and then apply a Laplace transformation to obtain the channel output $Y_{CH}(s)$ in the complex s-domain. In the end, the time-domain function $y_{CH}(t)$ can be obtained by applying an inverse Laplace transformation to $Y_{CH}(s)$. For a channel that is composed of several cables of different lengths connected in serial by connectors, frequency domain calculation allows simple multiplication cascading compared to the time-domain convolution, which is computation-intensive.

10.3.2. Channel Transfer Functions

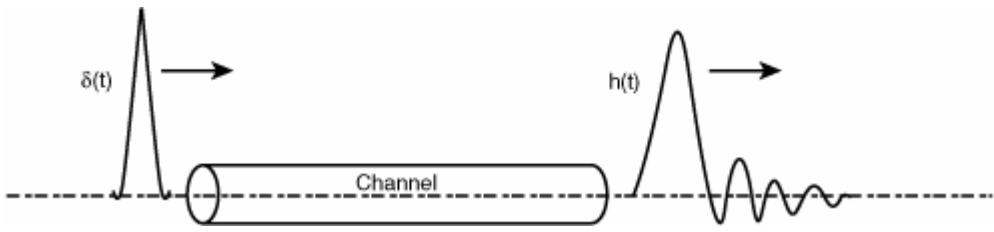
Channel transfer functions play a critical role in estimating or predicting the channel signal output given the signal input. There are two ways to determine the channel transfer function: based on the channel's circuit model, or based on the experimental characterizations. The circuit model needs assumptions on the channel implementation that can be application-specific. Because our intent is to develop a behavior model for the link, we will discuss only the methods that give rise to generic transfer functions, without knowing the details of the channel circuit property.

We will discuss three commonly used methods for channel transfer function determination and characterization. Two of them are time-domain methods, and the third is the frequency-domain method; they are all related. Knowing one of them, you can derive the other two through appropriate mathematical transformation.

10.3.2.1. Channel Impulse Response

The first method is to send a super-narrow pulse to the lossy dispersive channel and measure the response—the impulse response at the end of the channel. Theoretically, this super-narrow or indefinitely narrow pulse is called a Dirac impulse function, as defined in [Chapter 2](#). In optical communication, a narrow laser pulse with its width down to ~30 fs has been achieved with today's technology.^[7] Obviously, the narrower the pulse width, the more accurate the impulse is. [Figure 10.6](#) shows a typical response of the lossy channel to the ideal Dirac pulse.

Figure 10.6. Lossy channel response to a Dirac input impulse.



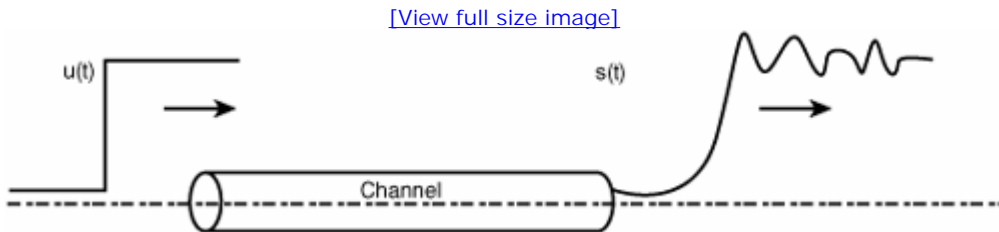
As soon as the impulse response is obtained, the corresponding transfer function $H_{CH}(s)$ can be obtained via its Laplace transformation.

Note that if the channel impulse response is obtained when the channel is coupled with active neighboring channels, the crosstalk effect is also captured in the impulse response. Thus, channel impulse can capture both lossy and crosstalk effects that are critical to the signal quality at the channel output.

10.3.2.2. Channel Unit Step Response

The second method to determine the impulse response is to send an ideal step signal to the lossy channel and observe the response—the step response. This is more practical for a copper-based channel, because it is basically straightforward to generate a step signal with a digital circuit. Ideally, a step signal with zero rise or fall time is needed to obtain the ideal step response. In practice, a step signal generated by a circuit always has a finite rise/fall time. A typical 40 GHz signal generator can generate a step signal with a rise/fall time on the order of a few ps. [Figure 10.7](#) shows the step response to unit signal input for a lossy channel.

[Figure 10.7. Lossy channel response to an ideal unit step signal input.](#)



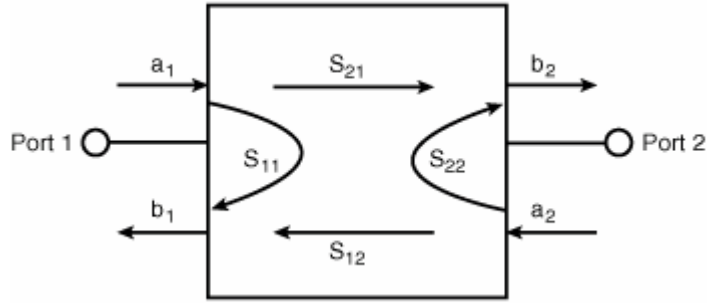
After the unit step response is obtained, the impulse response can be obtained by taking the time derivative— $h_{CH}(t) = dw_{CH}(t) / dt$. The transfer function $H_{CH}(s)$ can be obtained via its Laplace transformation, just as in the case of the Dirac pulse method. Alternatively, the transfer function $H_{CH}(s)$ can be obtained directly through $H_{CH}(s) = sW_{CH}(s)$, where $W_{CH}(s)$ is the Laplace transformation of the unit step response function $w_{CH}(t)$.

10.3.2.3. Channel S-Parameters

S-parameter stands for scattering parameter.^[8] It is widely used in microwave engineering to characterize a two-port system for the relationships between the transmitted wave and reflected wave to the incident or input wave.^[9] Typically, the relationship is quantified by the frequency-dependent transmission coefficient and reflection coefficient. In fact, transfer function is the frequency-dependent transmission coefficient. The channel transfer function discussed in the preceding two sections is related to one of the S-parameters. To incorporate the reflection effect in link modeling, a reflection coefficient is essential. This section gives an overview of the S-parameters and their relationship to the transfer function.

For a two-port system, incident waves move toward each port, reflected waves move away from each port, and transmitted waves move from one port to the other, as shown in [Figure 10.8](#).

[Figure 10.8. A two-port system and associated S-parameters.](#)



In Figure 10.8, a_1 and b_1 are the amplitudes of the incident and reflected waves at port 1, respectively. a_2 and b_2 are the amplitudes of the incident and reflected waves at port 2, respectively. The relationship between reflected waves to incident waves at each port can be expressed by the following matrix relationship:

Equation 10.12

$$\begin{pmatrix} b_1 \\ b_2 \end{pmatrix} = \begin{pmatrix} S_{11} & S_{12} \\ S_{21} & S_{22} \end{pmatrix} \begin{pmatrix} a_1 \\ a_2 \end{pmatrix}$$

In the absence of the incident wave at port 2, a common scenario for the high-speed link because it is usually unidirectional during data transmission, we have $b_1 = S_{11}a_1$ and $b_2 = S_{21}a_1$. Thus, we can derive an S-parameter for port 1 in terms of amplitude ratios of $S_{11} = b_1/a_1$ and $S_{21} = b_2/a_1$. Similarly, in the absence of the incident wave at port 1, we have $b_2 = S_{22}a_2$ and $b_1 = S_{12}a_2$. Thus, we can derive the S-parameter for port 2 in terms of amplitude ratios of $S_{22} = b_2/a_2$ and $S_{12} = b_1/a_2$. The following four sets of equations summarize the discussion. They give all four S-parameters in terms of amplitude ratios between reflected wave and incident wave, and between transmitted wave and incident wave.

Equation 10.13

$$\begin{aligned} S_{11} &= \frac{b_1}{a_1} \Big|_{a_2=0}, & S_{21} &= \frac{b_2}{a_1} \Big|_{a_2=0} \\ S_{22} &= \frac{b_2}{a_2} \Big|_{a_1=0}, & S_{12} &= \frac{b_1}{a_2} \Big|_{a_1=0} \end{aligned}$$

Physically, S_{11} is the reflection coefficient, and S_{21} is the transmission coefficient for port 1. Similarly, S_{22} is the reflection coefficient, and S_{12} is the transmission coefficient for port 2. They are frequency-dependent in general.

Similar to impulse response function determination, if S_{21} or S_{12} is obtained when the channel is coupled with the active neighboring channels, the crosstalk effect is also captured. Thus, channel S-parameters can capture both lossy and crosstalk effects of the channel.

10.3.2.4. S-Parameters, Transfer Function, and Reflection Coefficient

We have introduced a channel transfer function that is derived from its time-domain impulse response or step response via Laplace transformation. Because the transfer function $H_{CH}(s)$ is the ratio of output signal to input signal in the frequency domain, the transfer function and the S_{21} parameter represent the same physical value, with different names. Therefore, we have

Equation 10.14

$$S_{21}(s) = H_{CH}(s)$$

As soon as the transfer function is obtained, the time-domain impulse response is readily available via inverse Laplace transformation.

[Section 10.2](#) introduced the reflection coefficient $\rho_{rt}(s)$ for transmitter output signal modeling. This frequency-domain reflection coefficient is in fact an S_{11} or S_{22} parameter, depending on which port is considered. Engineers like to use dB as the unit. When the reflection or transmission S-parameter is represented in dBs, a different name is given. For example, $20\log S_{11}$ (or $20\log S_{22}$) is called return loss (RL), and $20\log S_{21}$ (or $20\log S_{12}$) is called insertion loss (IL).

The S-parameter direct measurement is in the frequency domain with instruments such as a vector network analyzer (VNA). It measures the four S-parameters in the complex frequency domain by frequency sweeping the sinusoidal wave used as the stimulus. Both magnitude and phase are included in the S-parameters. S-parameters can also be measured with time-domain methods. The time domain reflectometry (TDR) method uses a well-controlled step signal as the stimulus and measures the reflected wave. The time domain transmission (TDT) method measures the transmitted wave.

TDT essentially measures the step response $w_{CH}(t)$ introduced in [section 10.3.1](#). By applying the Laplace transformation, you can obtain its complex s-domain response $W_{CH}(s)$. According to [equation 10.11](#), transfer functions $H_{CH}(s)$ and $W_{CH}(s)$ are related through $H_{CH}(s) = sW_{CH}(s)$. Because $S_{21}(s) = H(s)$ according to [equation 10.14](#), we have $S_{21}(s) = sW_{CH}(s)$. Thus, the linkage between the time-domain TDT measured step response function $w_{CH}(t)$ and frequency-domain VNA measured S_{21} parameter is established. Similarly, the TDR measured step response $w_r(t)$ can be transformed to complex s-domain via Laplace transformation as $W_r(s)$. Then the S_{11} parameter is related to $W_r(s)$ via $S_{11}(s) = sW_r(s)$.

In summary, time-domain impulse response, step response, complex s-domain transfer function, and s-parameters are interchangeable. We have introduced the mathematical procedures to carry out the transformations from one form to another, or from one domain to another domain. Accordingly, VNA-measured S-parameters and TDR- and TDT-measured step responses are interchangeable with similar mathematical procedures or transformations.

10.3.3. Generic Channel Model

Without getting involved in the details of the channel electrical or optical properties, a generic and scalable model for a channel is probably the one based on zeros and poles of the channel subsystem.

Consider an LTI system that can be specified with linear differential equations. In the S-plane, its transfer function can be represented in a rational form:

Equation 10.15

$$\begin{aligned} H_{CH}(s) &= K \frac{s^M + a_{M-1}s^{M-1} + \dots + a_0}{s^N + b_{N-1}s^{N-1} + \dots + b_0} \\ &= K \frac{\prod_{m=1}^M (s + z_m)}{\prod_{n=1}^N (s - p_n)} \end{aligned}$$

where N and M denote the number of poles and zeros, respectively, and this is an Nth-order system.

A channel is implemented with a physical medium. Therefore, its transfer function must comply with a couple physical rules:

- It must be causal. In other words, the region of convergence (ROC) is right to the rightmost pole.[\[10\]](#) Another way to define a causal system is that no output can be observed before an input is launched.
- It must be stable. In other words, all the poles are located on the left half of the S-plane (not including the imaginary axis), and the number of poles is greater than or equal to the number of zeros.

It is not intuitive to grasp the physical essence of the generic Nth-order channel model. So we start with the simplest first-order and

second-order models as the building blocks to gain some insights. Other high-order models can be obtained by using the cascading rules of many lower-order transfer functions to build an expected higher-order transfer function.^[11]

We will focus on the denominator of the rational model shown in [equation 10.15](#). If there is a single pole, it must be real and negative, and we have a factor of $(s - p_n)$ in the denominator (the first-order model). If there are complex poles, they must come as a complex conjugate pair, and we have a factor of

Equation 10.16

$$(s - p_n)(s - p_n^*) = s^2 + 2\zeta\omega_n s + \omega_n^2$$

in the denominator. * denotes the complex conjugate, ω_n is the natural frequency, and ζ is the damping factor (the second-order model). The details of the first- and second-order transfer functions are studied in detail in the next two sections.

10.3.3.1. A First-Order Analytical Model

A first-order rational model with one pole is expressed by the following:

Equation 10.17

$$H_{CH}(s) = K \frac{1}{s - p_n}, \quad ROC$$

$$L \downarrow \uparrow L^{-1}$$

$$h_{CH}(t) = K e^{p_n t}, \quad t \geq 0$$

$$w_{CH}(t) = \frac{K}{-p_n} (1 - e^{p_n t}), \quad t \geq 0$$

where $h_{CH}(t)$ and $w_{CH}(t)$ denote the impulse and step responses, respectively, and $K = -p_n$.

$$\tau = \frac{1}{(-p_n)}$$

Following the classic RC implementation of this transfer function, the time constant can be written as corner frequency can be written as

Equation 10.18

$$f_{3dB} = \frac{1}{2\pi\tau} = -\frac{p_n}{2\pi}$$

and the break frequency is at $2\pi f_{3dB}$. Beyond this frequency, the magnitude response follows the "20 dB per decade" asymptote.

[Figure 10.9](#) shows the frequency domain magnitude and phase responses (Bode plot), and [Figure 10.10](#) shows the time-domain impulse and step responses.

Figure 10.9. A one-pole model: Magnitude and phase responses in the frequency domain.

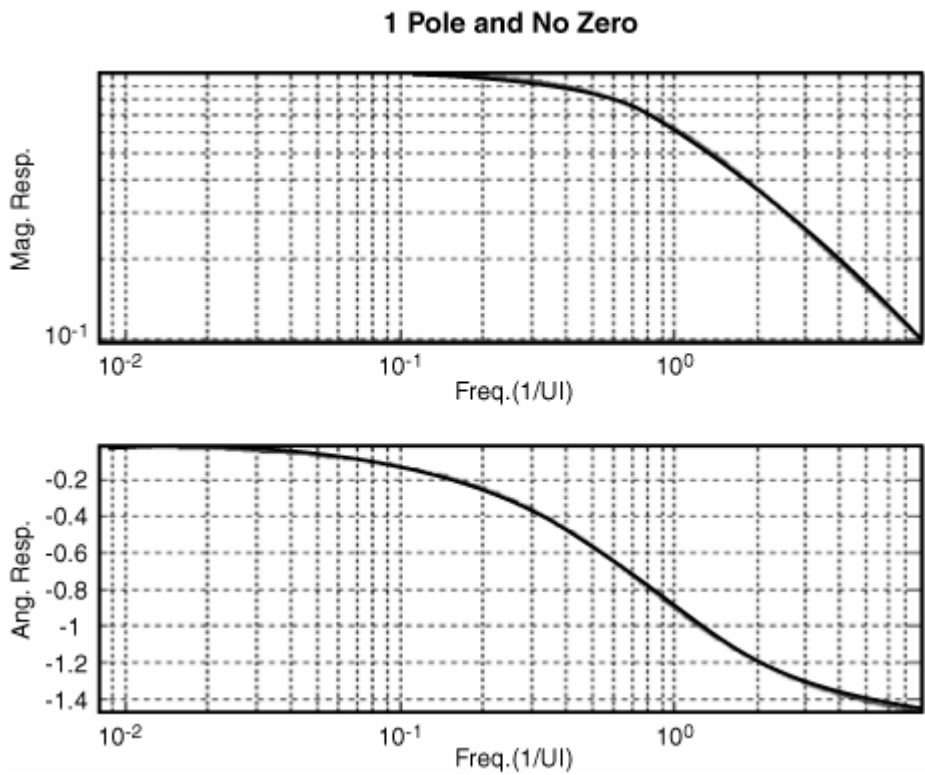
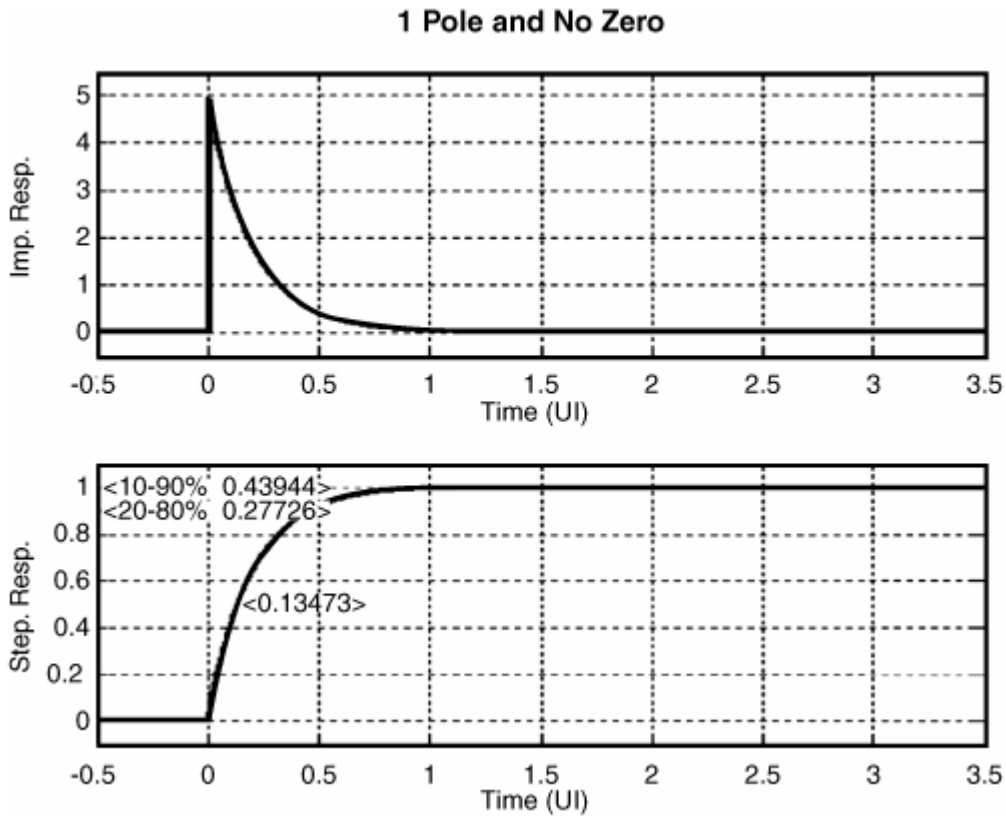


Figure 10.10. A one-pole model: Impulse and step responses in the time domain.



Now we have put the generic pole and zero-based model in terms of a close-form first-order model, or its frequency-domain transfer function, or time-domain impulse or step response.

10.3.3.2. A Second-Order Analytical Model

A second-order two-pole analytical model can be expressed as follows:

Equation 10.19

$$H_{CH}(s) = \frac{K}{(s - p_n)(s - p_k)}, \text{ ROC}$$

$$L \downarrow \uparrow L^{-1}$$

for $p_n \neq p_k$,

$$h_{CH}(t) = KA \left(e^{p_n t} - e^{p_k t} \right), \quad t \geq 0$$

$$w_{CH}(t) = -KA \left(\frac{1 - e^{p_n t}}{p_n} - \frac{1 - e^{p_k t}}{p_k} \right), \quad t \geq 0$$

for $p_n = p_k = \omega_n$,

$$h_{CH}(t) = Kt e^{p_n t}, \quad t \geq 0$$

$$w_{CH}(t) = 1 - e^{p_n t} + p_n t e^{p_n t}, \quad t \geq 0$$

$$A = \frac{1}{p_n - p_k}$$

where $h_{CH}(t)$ and $w_{CH}(t)$ denote the impulse and step responses, respectively. $K = p_n p_k$ and

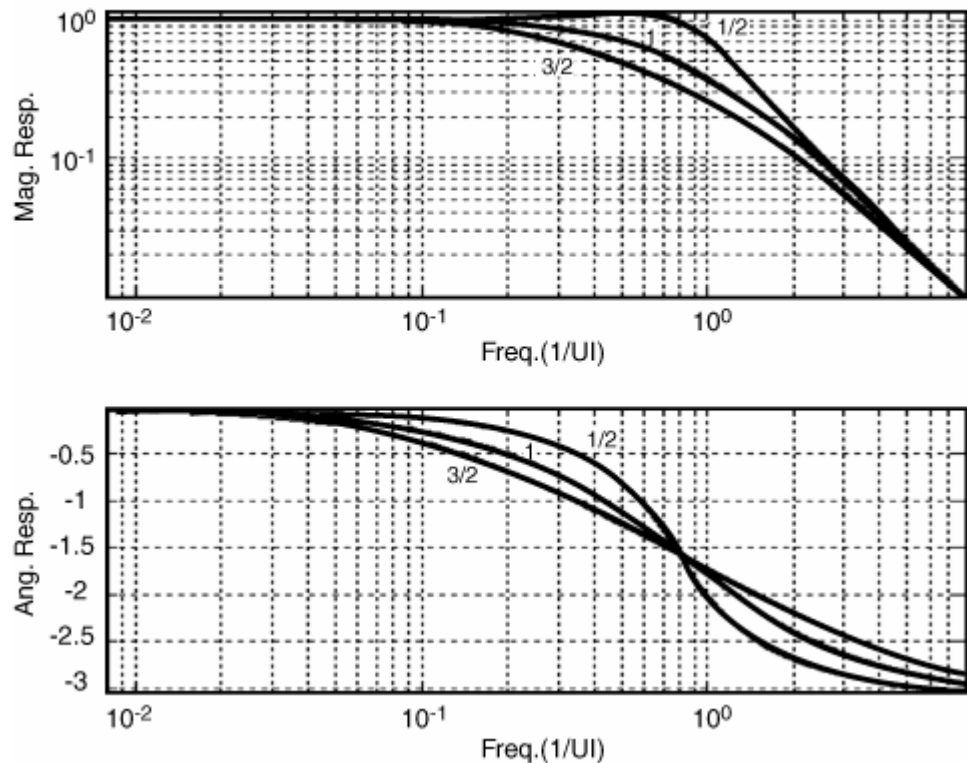
Following the classic RLC implementation of this transfer function, the underdamped natural frequency can be written as

$\omega_n = \sqrt{p_n p_k}$, and the damping factor can be written as $\zeta = -\frac{p_n + p_k}{\omega_n}$. We can also define the quality factor as $Q = \frac{1}{2\zeta}$. It is important to notice that the 3 dB corner frequencies are dependent on the damping factor, and the break frequency is at ω_n , which is independent of the damping factor.

We will illustrate three distinct second-order transfer functions with different damping factors: underdamped $\zeta < 1$, critically damped $\zeta = 1$, and overdamped $\zeta > 1$. [Figure 10.11](#) shows the magnitude and phase responses of the transfer functions in the frequency domain (Bode plots) for those three cases.

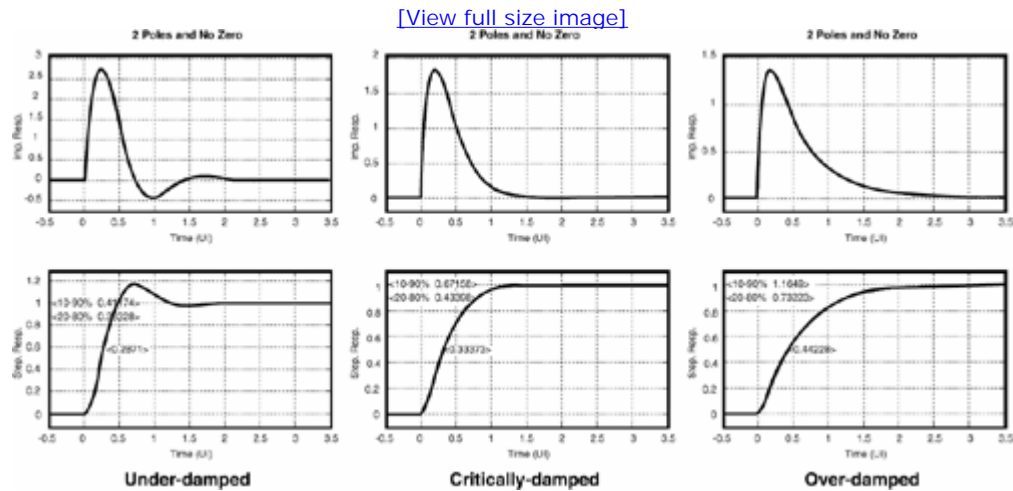
Figure 10.11. A two-pole model (underdamped, critically damped, and overdamped cases): Magnitude (upper panel) and phase responses (lower panel) in the frequency domain.

2 Poles and No Zero



Time-domain impulse and step responses can be estimated according to [equation 10.18](#) and are shown in [Figure 10.12](#).

Figure 10.12. A two-pole model (underdamped, critically damped, and overdamped cases): Impulse (upper panel) and step responses (lower panel) in the time domain.



With these two fundamental channel transfer functions, any arbitrary even or odd order channel transfer function can be built with the cascading rules.

User name: CSU San Diego

Book: Jitter, Noise, and Signal Integrity at High-Speed

Section: Chapter 10. Modeling and Analysis for Jitter and Signaling Integrity for High-Speed Links

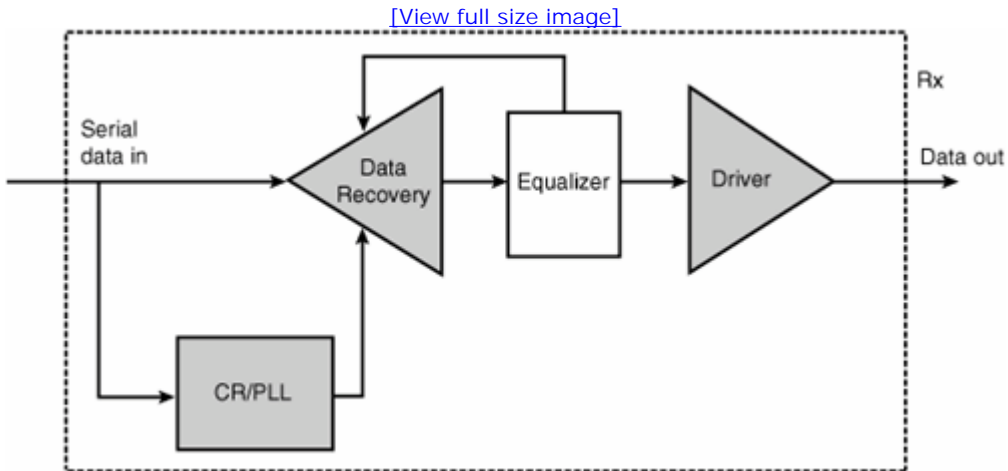
No part of any chapter or book may be reproduced or transmitted in any form by any means without the prior written permission for reprints and excerpts from the publisher of the book or chapter. Redistribution or other use that violates the fair use privilege under U.S. copyright laws (see 17 USC107) or that otherwise violates these Terms of Service is strictly prohibited. Violators will be prosecuted to the full extent of U.S. Federal and Massachusetts laws.

Information Theory Computer Science Mike Peng Li Prentice Hall Jitter, Noise, and Signal Integrity at High-Speed

10.4. Receiver Modeling and Analysis

A generic receiver subsystem block diagram was shown in [Figure 9.4 of Chapter 9](#). Because our primary emphasis in this section is on receiver signaling and jitter performance, we will focus on noise-sensitive data sampling, voltage driver or amplifier, and timing jitter-sensitive components of clock recovery. [Figure 10.13](#) is a simplified block diagram for a receiver.

[Figure 10.13. A simplified block diagram for a receiver.](#)



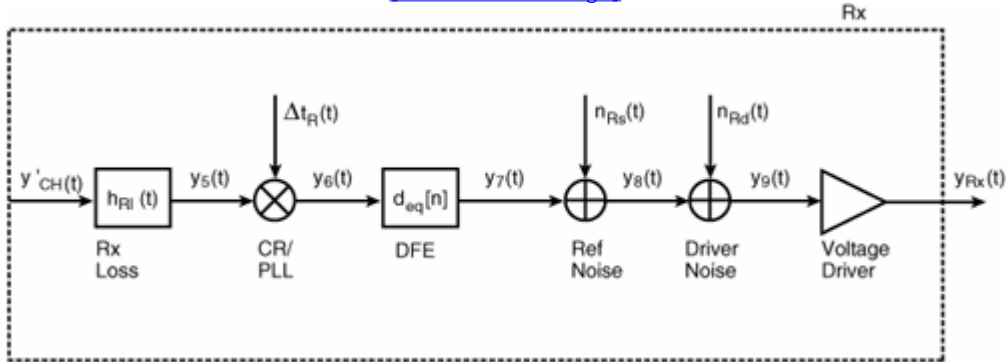
In this simplified receiver subsystem block diagram, the incoming serial data is split into two signal paths. One goes to the clock recovery unit that typically is implemented by a PLL, and the other goes to the data recovery or sampling unit. A feedback system is formed between equalization and data sampling. The direct inputs into the data sampling are recovered clock and serial incoming data. The feedback input is the equalizer's output. In addition to providing clock timing, clock recovery also tracks the low-frequency jitter associated with the incoming serial data. The purpose of the equalization is to compensate for or correct the incoming data signal distortion or ISI due to the lossy channel. The receiver can implement both linear and adaptive feedback equalization circuits. The feedback equalization is often called decision feedback equalization (DFE). The coefficients for a linear equalizer are fixed, and the DFE coefficients can be either fixed or adaptive, offering better flexibility. In the end, the data signal with channel lossy effect of ISI compensated may be fed to a voltage driver or amplifier to generate a required bit voltage level at the receiver output.

The channel output $y_{CH}(t)$ is the input for the receiver. The signal input is defined at the receiver's input pin. The on-chip loss impulse response $h_{RI}(t)$ is introduced to capture the chip package and on-chip interconnect loss effects. It is then split. One goes to the clock recovery, and the other goes to the data recovery or data sampling. Because we have already covered the linear equalizer for the transmitter, we will focus on only the DFE equalizer for the receiver, realizing that both linear and DFE are possible for receiver equalization. Because the recovered clock edges also move around trying to synchronize their phases with the low-frequency jitter associated with the data bits, it also has jitter relative to the ideal bit clock or jitter-free clock. Its effect can be modeled as the jitter

phase modulation denoted as $\Delta t_R(t)$ to the data signal timing. The infinite impulse response (IIR) type of filter for DFE has coefficient series of $\{d_m\}$. The reference voltage for the data sampling can have noise associated with it, and we denote it as $n_{RS}(t)$. In the last stage, the recovered digital data may be driven or amplified to a designated amplitude or power level. The amplitude noise generated by a driver or amplifier is denoted as $n_{RD}(t)$. Figure 10.14 shows the block diagram of the receiver subsystem behavior model we plan to use.

Figure 10.14. A receiver behavior model block diagram.

[View full size image]



The receiver behavior model is a "mixed-signal" approach, similar to the transmitter one. Signal input is more like an analog signal at the receiver input due to the channel loss effect. The on-chip interconnect, parasitic, and packaging effects are first handled by the loss impulse response function. Jitter is introduced through phase modulation to emulate the clock recovery phase tracking. It cancels some of the phase jitter associated with the incoming data signal. Sampling voltage reference noise and voltage driver or amplifier effects are also included. However, it is worth pointing out that only sampling voltage reference affects the link BER. Voltage noise after the data sampling does not affect the link BER.

If an impedance mismatch exists between the channel output port and the receiver input front end, the reflection occurs. In analogy to the transmitter reflection handling, we will assume that the reflection coefficient at the boundary between the channel and the receiver front end is $\rho_{rr}(s)$ (the same as S_{22}) and is frequency-dependent. We denote its inverse Laplace transformation as $\rho_{rr}(t)$. Then the signal at the output of the transmitter is

Equation 10.20

$$\dot{y}_{CH}(t) = y_{CH}(t) - \rho_{rr}(t) * y_{CH}(t)$$

when reflection is considered. If there is no reflection—namely, $\rho_{rr}(t) = 0$ —equation 10.20 returns to $y_{CH}(t)$.

10.4.1. Receiver Loss

The effect of the receiver on-chip loss on the input signal is expressed by the convolution operation of the following:

Equation 10.21

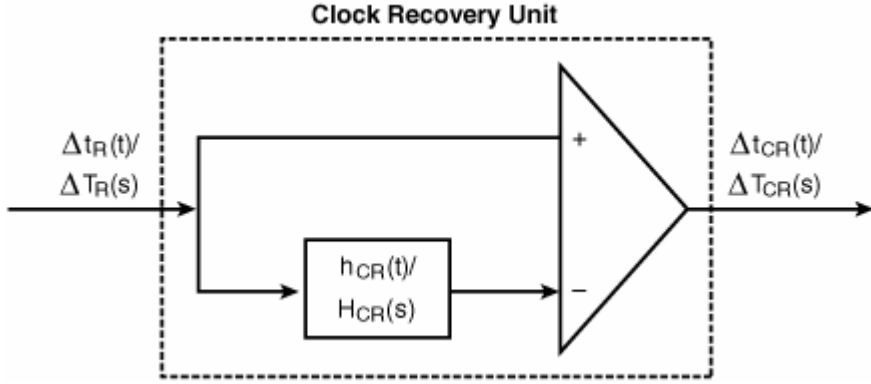
$$y_5(t) = \dot{y}_{CH}(t) * h_{RL}(t)$$

where $y'_{CH}(t)$ is the receiver input signal, and $h_{RL}(t)$ is the impulse response for the receiver on-chip loss considering package, interconnect, and parasitic effects.

10.4.2. Receiver Clock Recovery

We assume that the s-domain transfer function for the clock recovery circuit is $H_{CR}(s)$ and that its corresponding time-domain impulse response function is $h_{CR}(t)$. We will treat the input signal $y_5(t)$ timing in terms of the superimposition of the ideal timing nT_0 and phase jitter $\Delta t_R(t)$ phase modulation—namely, $t = nT_0 + \Delta t_R(t)$. The phase jitter modulated to the timing of the signal after the clock recovery depends on the clock recovery transfer function in a form that is shown in Figure 10.15.

Figure 10.15. Clock recovery jitter tracking behavior model.



The clock recovery and data sampling input form a difference function between data and clock. Therefore, the phase jitter on the data signal at the data sampling input is given by the following equation in the s-domain:

Equation 10.22

$$\Delta T_{CR}(s) = \Delta T_R(s) [1 - H_{CR}(s)]$$

The second term in the equation reflects the difference function. The time-domain relationship can be found by taking the inverse Laplace transformation of this equation. It becomes the following:

Equation 10.23

$$\Delta t_{CR}(t) = \Delta t_R(t) * [\delta(t) - h_{CR}(t)]$$

For most clock recovery circuits, their transfer functions $H_{CR}(s)$ are low-pass functions. For example, a PLL clock recovery has a low-pass transfer function. Therefore, $[1 - H_{CR}(s)]$ is a high-pass function. The phase jitter modulation to the data signal is high-pass filtered after the clock recovery circuit. The data waveform timing after the clock recovery is as follows:

Equation 10.24

$$y_6(t) = y_5(nT_0 + \Delta t_{CR}(t)) = y_5(nT_0 + \Delta t_R(t) * [\delta(t) - h_{CR}(t)])$$

Compared with the jitter at the clock recovery input $\Delta t_R(t)$, the jitter after the clock recovery at the sampling input $\Delta t_{CR}(t)$ is attenuated at low frequencies. As such, the broadband jitter of DJ, RJ, and TJ is smaller for $\Delta t_{CR}(t)$ compared with for $\Delta t_R(t)$ in general.

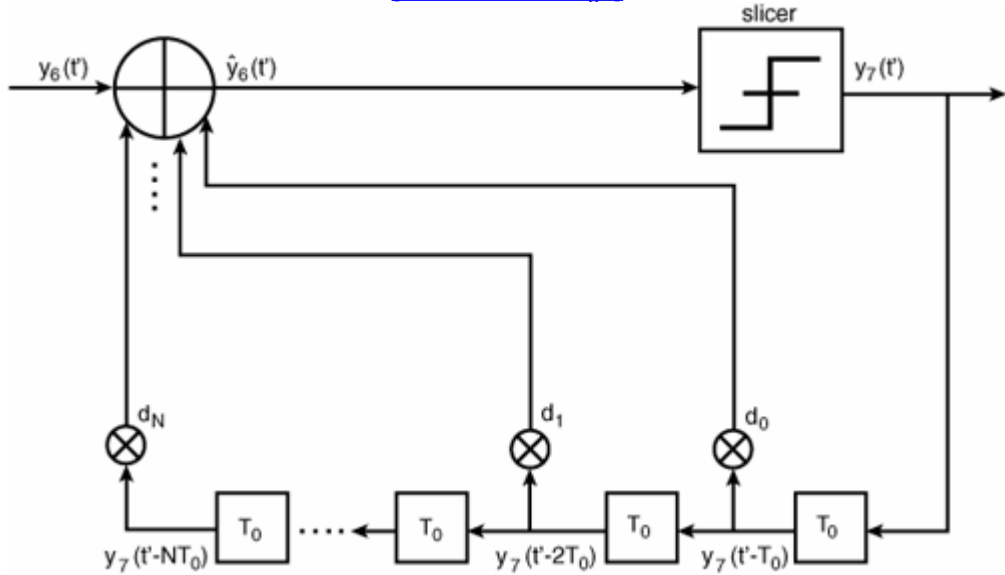
10.4.3. Receiver Equalization

The two basic receiver equalization methods are linear equalization and DFE. The mechanism for a receiver linear equalization is similar to that in the transmitter. The goal of a receiver equalization is to remove the ISI distortion caused by the lossy channel. For a linear and nonadaptive equalization, the taps coefficients must be predetermined. Thus, the channel's variability must be small for a linear equalization to work well. A clear advantage that a receiver equalization has over a transmitter equalization is that it allows feedback types of equalization to be implemented, such as DFE, due to the observability readily available at the receiver. A DFE equalizer can be designed to accommodate a wider range of channel variability. Therefore, DFE is widely used in receiver equalization. That is our focus for receiver equalization.^{[12], [13], [14], [15], [16]}

There are many different implementations for a DFE equalization, just as there are many IIR filter implementations. A typical N-tap DFE implementation is shown in Figure 10.16. Compared with a conventional IIR filter, a DFE has a new slicer that is basically a digital decoder. The signal at the output of a slicer is completely in digital form. A slicer removes the noise from all the feedback paths, offering better noise performance and stability for DFE feedback compared with a straight IIR filter.

Figure 10.16. An Rx DFE implementation using an N-tap IIR filter.

[View full size image]



The relationship between an Rx DFE equalization output and its input, as well as the feedback tap coefficients, are given by the following equation:

Equation 10.25

$$\begin{aligned} y_7(t') &= y_6(t') + d_1 y_7(t - T_0) + d_2 y_7(t - 2T_0) + \dots + d_N y_7(t - NT_0) \\ &= y_6(t') + \sum_{i=1}^N d_i y_7(t - iT_0) \end{aligned}$$

Note that we use a different timing notation of $t' = nT_0 + \Delta t_{CR}(t)$ to accommodate the clock recovery jitter tracking effect for the DFE timing. t' represents the dynamic timing provided by the clock recovery that tracks the low-frequency jitter. Most DFE discussions ignore the clock recovery jitter tracking effect in the consideration.

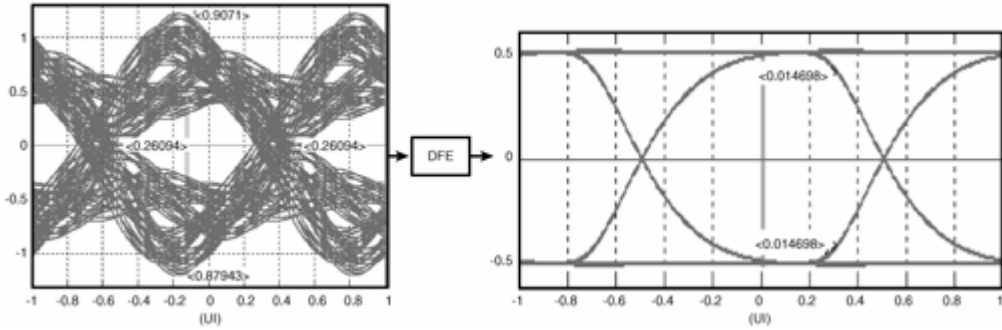
DFE tap coefficients can be predetermined if the channel loss is static or adaptive if the channeling is dynamic or time-varying, such as crosstalk-significant or temperature-sensitive channels. When DFE coefficients are predetermined, channel S-parameters, or impulse response/step response, need to be known, similar to Tx linear equalization. For adaptive equalization, digital control circuits need to be added. For adaptive DFE, the tap coefficients typically are determined by minimizing the difference between the slice input ($\hat{Y}_6(t')$) and output ($y_7(t')$). There are many minimization methods, such as least mean square (LMS), zero forcing, and steepest descent, to name a few.^{[13], [14], [16]}

Compared with Tx equalization, Rx DFE provides adaptive equalization capability on a per-bit basis, with better dynamic range, fine-tuned resolution, and flexibility in tap coefficient dynamic adjusting. The Rx DFE limitation may include lack of direct measurable to verify the DFE tap coefficients, posing challenges in DFE verification and testing. Also, DFE equalization is based on the data bits voltage information after (post-cursor) the current bit (cursor). Therefore, it cannot compensate for the channel distortion effect at times ahead (precursor) of the current bit. Such a limitation does not apply to the Tx equalization. In general, to compensate for both "precursor" and "postcursor" effects, a system design including both Tx linear and Rx DFE equalizations is a common practice.

Figure 10.17 shows an example of an eye opening with a receiver DFE equalization. The nearly closed eye diagram becomes a wide-open eye diagram after receiver DFE equalization.

Figure 10.17. The effect of receiver DFE on a nearly closed eye diagram.

[View full size image]



10.4.4. Amplitude Modulation for Receiver Reference Voltage Noise

Receiver data sampling determines the logical level of the received data bits at a sampling time and reference voltage level. Therefore, the reference voltage accuracy affects the accuracy of the logic bit determination. We will model the inaccuracy of the reference voltage as amplitude noise and denote it as $n_{Rs}(t)$. The interaction between $n_{Rs}(t)$ and the incoming digital waveform is additive and can be treated as "amplitude" modulation or amplitude perturbation. As in the case for the transmitter, this amplitude modulation can be expressed as follows:

Equation 10.26

$$y_8(t) = y_7(t) + n_{Rs}(t)$$

10.4.5. Amplitude Modulation for Receiver Driver Voltage Noise

Due to the channel loss, a voltage driver is commonly used in the receiver to boost the signal level so that the data bits can be correctly detected logically. While an amplifier within the voltage driver can increase the signal level, it can also generate amplitude noise at the same time. We denote the driver amplification associated noise as $n_{Rd}(t)$. Mathematically, we will treat driver amplitude noise as a small signal perturbation similar to the voltage reference noise. This additive noise modulation term relates the input with the output for the driver voltage noise through the following:

Equation 10.27

$$y_9(t) = y_8(t) + n_{Rd}(t)$$

Equations 10.26 and 10.27 can be combined to eliminate intermediate variable $y_8(t)$, and it gives rise to a signal relationship, including the effects of those two different types of noise sources. The following is the equation:

Equation 10.28

$$y_9(t) = y_7(t) + n_{Rs}(t) + n_{Rd}(t)$$

10.4.6. Receiver Driver

As in the case of the transmitter, a voltage driver or optical driver may be used in the last stage of the receiver to boost the signal. Again, we will model this last-stage driver as an ideal analog-to-digital converter (ADC) that generates the waveform at a certain voltage level or optical power level. We represent this ideal ADC as a linear amplification using the following:

Equation 10.29

$$y_{Rx}(t) = By_9(t)$$

where B is the voltage or power gain through the driver. This equation gives an "end-to-end" model for the receiver recovered waveform. Because this is the last stage of the link signaling, it is also the final "end-to-end" signal output for the link.

Similar to the Tx modeling, the signal outputs at various observing or testing points are in a cascading form. In other words, the output of the previous subsystem is the input of the current subsystem. With all the receiver's subsystems, it is now even more complex and lengthy to write a single equation to represent the "end-to-end" signaling relationship between transmitter digital input at the starting point and the receiver recovered signal at the receiver ending point. However, this relationship can be achieved through cascading of the chain relationships we have developed.

As soon as the waveform or amplitude time function is obtained for the receiver output, the corresponding eye diagram and BER CDF function can be built accordingly. In turn, the eye opening, total jitter, DJ, and RJ can be analyzed and obtained with the methods introduced in [Chapters 5](#) and [6](#).

URL <http://access.proquest.safaribooksonline.com/9780132429610/ch10lev1sec4>

User name: CSU San Diego

Book: Jitter, Noise, and Signal Integrity at High-Speed

Section: Chapter 10. Modeling and Analysis for Jitter and Signaling Integrity for High-Speed Links

No part of any chapter or book may be reproduced or transmitted in any form by any means without the prior written permission for reprints and excerpts from the publisher of the book or chapter. Redistribution or other use that violates the fair use privilege under U.S. copyright laws (see 17 USC107) or that otherwise violates these Terms of Service is strictly prohibited. Violators will be prosecuted to the full extent of U.S. Federal and Massachusetts laws.

Information Theory Computer Science Mike Peng Li Prentice Hall Jitter, Noise, and Signal Integrity at High-Speed

10.5. Summary

This chapter introduced the link system and subsystem behavior modeling by applying LTI theory and superimposition rules for signaling, jitter, and noise. The method is generic, without the need for detailed knowledge of circuit implementation. Yet it is still based on the general physics of the circuit implementations so that it is not a pure mathematical abstraction.

For the transmitter, its subsystems of digital data bit formation, equalization (both pre-emphasis and de-emphasis), timing jitter phase modulation due to the reference clock or PLL, amplitude noise modulation due to amplification, on-chip interconnect and package loss, voltage or power driver, and reflections due to the impedance or reflection index mismatch were discussed and modeled. Signal waveform at the output of each subsystem is expressed in terms of the physical parameters or characteristics of its previous accumulative subsystems with LTI cascading. With the waveform at the transmitter output, the corresponding eye opening or closure, jitter, and noise can be estimated.

For the channel, channel modeling and characterization using LTI theory were discussed in detail. Loss, crosstalk, and reflection effects were considered and modeled. Determination and characterization for the channel impulse response, step response, and S-parameters were discussed. In particular, the interrelationships between these items were discussed and quantified. The signal waveform at the channel's output in terms of its properties of impulse response, step response, or S-parameters was discussed.

For the receiver, its subsystems of on-chip package and interconnect loss, clock recovery output timing and jitter tracking, equalization (both linear and DFE), amplitude modulations due to reference voltage and amplification noise, and voltage or power driver were discussed and modeled. Reflections due to the impedance or refraction index mismatch between the channel and the receiver input front-end were discussed and modeled. Similar to transmitter and channel modeling, signal waveform at the output of each receiver subsystem was expressed in terms of the physical parameters or characteristic functions of its previous accumulative subsystems with LTI cascading. With the waveform at the receiver output, the corresponding eye opening or closure, jitter, and noise can be estimated and analyzed. Note that eye opening or closure, jitter, and noise of the receiver are in fact for the entire link in our signal cascading modeling.

URL <http://access.proquest.safaribooksonline.com/9780132429610/ch10lev1sec5>

User name: CSU San Diego

Book: Jitter, Noise, and Signal Integrity at High-Speed

Section: Chapter 10. Modeling and Analysis for Jitter and Signaling Integrity for High-Speed Links

No part of any chapter or book may be reproduced or transmitted in any form by any means without the prior written permission for reprints and excerpts from the publisher of the book or chapter. Redistribution or other use that violates the fair use privilege under U.S. copyright laws (see 17 USC107) or that otherwise violates these Terms of Service is strictly prohibited. Violators will be prosecuted to the full extent of U.S. Federal and Massachusetts laws.

Information Theory Computer Science Mike Peng Li Prentice Hall Jitter, Noise, and Signal Integrity at High-Speed

Endnotes

1. E. Lee and D. Messerschmitt, *Digital Communications*, Kluwer Academic Publishers, 1995.
2. A. X. Widmer et al., "Single-chip 4*500MBd CMOS Transceiver," IEEE Int. Solid-State Circuits Conf., pp 126–127, Feb. 1996.
3. B. Casper et al., "8 Gb/s SBD link with on-die waveform capture," IEEE Journal Solid-State Circuits, vol. 38, no. 12, pp. 2111–2120, Dec. 2003.
4. B. Casper et al., "An accurate and efficient analysis method for multi-Gb/s chip-to-chip signaling schemes," in IEEE Symp. VLSI Circuits Dig. Tech. Papers, pp. 54–57, June 2002.
5. V. Stojanovic and M. Horowitz, "Modeling and analysis of high-speed links," IEEE Custom Integrated Circuits Conference, pp. 589–594, Sept. 2003.
6. A. Sanders, M. Resso, and J. D'Ambrosia, "Channel compliance testing utilizing novel statistical eye methodology," Designcon, 2004.
7. M. Aoyama et al., "0.85 PW, 33 fs laser pulse generation from a Ti:sapphire laser system," Lasers and Electro-Optics (CLEO) Conference, 2003.
8. Agilent, "S-parameter design," Application Notes AN 154, 1990.
9. David M. Pozar, *Microwave Engineering*, Third Edition, John Wiley & Sons, Inc., 2005.
10. A. V. Oppenheim, A. S. Willsky, and I. Young, *Signals and Systems*, Chapters 4 and 9, Prentice-Hall, Inc., 1983.
11. J. Sun and M. Li, "A generic test path and DUT model for datacom ATE," IEEE International Test Conference, 2003.
12. R. Payne et al., "A 6.25-Gb/s binary transceiver in 0.13/splmu/m CMOS for serial data transmission across high loss legacy backplane channels," IEEE J. Solid-State Circuits, vol. 40, no. 12, pp. 2646–2657, Dec. 2005.
13. V. Sotjanovic et al., "Adaptive equalization and data recovery in a dual-mode (PAM2/4) serial link transceiver," IEEE Symposium on VLSI Circuits, June 2004.
14. J. E. Jaussi et al., "An 8 Gb/s source-synchronous I/O link with adaptive equalization, offset cancellation and clock deskew," in IEEE Int. Solid-State Circuits Conf., Dig. Tech. Papers, vol. 1, pp. 246–247, Feb. 2004.
15. K. Ksishna et al., "A 5Gb/s NRZ transceiver with adaptive equalization for backplane transmission," in IEEE Int. Solid-State Circuits Conf., Dig. Tech. Papers, vol. 1, pp. 64–65, Feb. 2005.
16. J. Zerbe et al., "Comparison of adaptive and non-adaptive equalization methods in high-performance backplanes," IEC DesignCon, 2005.

URL <http://access.proquest.safaribooksonline.com/9780132429610/ch10lev1sec6>

User name: CSU San Diego

Book: Jitter, Noise, and Signal Integrity at High-Speed

No part of any chapter or book may be reproduced or transmitted in any form by any means without the prior written permission for reprints and excerpts from the publisher of the book or chapter. Redistribution or other use that violates the fair use privilege under U.S. copyright laws (see 17 USC107) or that otherwise violates these Terms of Service is strictly prohibited. Violators will be prosecuted to the full extent of U.S. Federal and Massachusetts laws.

Information Theory Computer Science Mike Peng Li Prentice Hall Jitter, Noise, and Signal Integrity at High-Speed

11. Testing and Analysis for Jitter and Signaling Integrity for High-Speed Links

This chapter focuses on testing aspects of jitter and signaling for an I/O link system. Link signaling and its governing roles in determining test requirements and methodologies are discussed first. Then specific test requirements and methods are introduced for link subsystems of transmitter (Tx) output, channel output, receiver (Rx) input and tolerance, PLL output, and reference clock output within the context of leading link architectures. The importance of the roles for clock recovery (CR) and associated jitter transfer function (JTF), equalization (EQ), jitter components, and statistical samples in testing jitter and signaling are emphasized. System-level tests such as loopback and associated I/O built-in self-test (BIST) for jitter and signal integrity are also introduced.

URL <http://access.proquest.safaribooksonline.com/9780132429610/ch11>

User name: CSU San Diego

Book: Jitter, Noise, and Signal Integrity at High-Speed

Section: Chapter 11. Testing and Analysis for Jitter and Signaling Integrity for High-Speed Links

No part of any chapter or book may be reproduced or transmitted in any form by any means without the prior written permission for reprints and excerpts from the publisher of the book or chapter. Redistribution or other use that violates the fair use privilege under U.S. copyright laws (see 17 USC107) or that otherwise violates these Terms of Service is strictly prohibited. Violators will be prosecuted to the full extent of U.S. Federal and Massachusetts laws.

Information Theory Computer Science Mike Peng Li Prentice Hall Jitter, Noise, and Signal Integrity at High-Speed

11.1. Link Signaling and Its Impact on Testing

Chapter 9, "Jitter and Signal Integrity Mechanisms for High-Speed Links," introduced two leading link architectures in terms of their clock recovery circuits: the data-driving clock recovery architecture (see Figure 9.1) and the data- and reference clock-driven or common clock architecture (see Figure 9.2). For any serial data link signaling, clock recovery circuit (CRC) is a mandatory element because no in-rate clock is sent from transmitter to receiver. Thus, in testing the serial link, clock recovery must be considered as a necessary test requirement. We will call those types of link signaling with clock recovery the nominal serial link. As the data rate keeps increasing, advanced signaling techniques in addition to clock recovery are needed, such as transmitter and/or receiver equalizations. We will call those types of link signaling with both clock recovery and equalization circuits the advanced serial links. Then both nominal and advanced link signaling are discussed within the frameworks of data-driven and common clock link architectures.

11.1.1. Testing Implications for Nominal Link Signaling

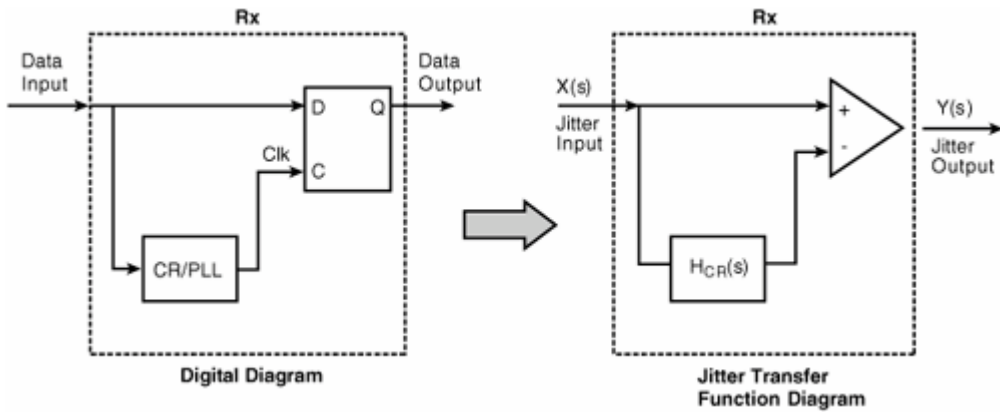
The single most important subsystem in the receiver for jitter or signaling testing is probably clock recovery for nominal link signaling. Clock recovery can have many functions. From a digital circuit point of view, clock recovery generates a clock for the receiver to sample the input data stream. From a jitter and signaling point of view, clock recovery tracks the low-frequency jitter associated with the incoming data stream.

11.1.1.1. Clock Recovery and Jitter Transfer Function (JTF)

The observables or reference points for testing a serial link and its subsystems are commonly defined at the transmitter output, the reference clock output, and the receiver input.^{[1], [2], [3], [4]} However, the ultimate goal of good link performance is to achieve the desired overall system BER at the receiver where the clock recovery physically resides. Thus, clock recovery characteristics directly affect the BER performance of the link system. As discussed for Figure 10.15 in Chapter 10, "Modeling and Analysis for Jitter and Signaling Integrity for High-Speed Links," the phase difference between the data stream and the recovered clock determines the total jitter or eye closure at the receiver data sampling flip-flop. This implies a clock-to-data "difference function" for testing jitter, as illustrated in Figure 11.1.

Figure 11.1. Receiver digital block diagram and jitter transfer function diagram.

[\[View full size image\]](#)



The phase difference between the data input and the clock input defines a "difference function" for the jitter seen at the receiver. The eye closure or jitter relevant to the receiver BER needs to undergo this difference function. In the complex s-domain, the jitter input X (s) and output Y(s) relationship can be expressed as follows:

Equation 11.1

$$Y(s) = X(s)[1 - H_{CR}(s)]$$

and the jitter transfer function is defined as follows:

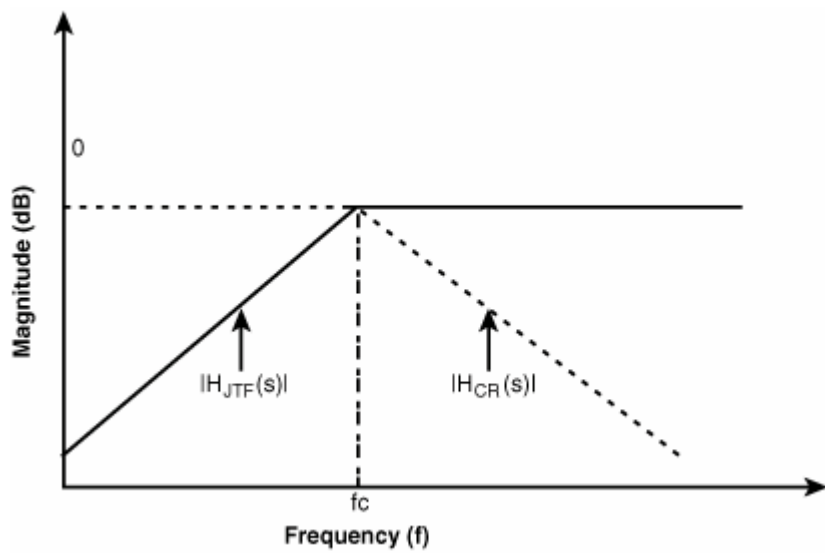
Equation 11.2

$$H_{JTF} = [1 - H_{CR}(s)]$$

A couple points are worth emphasizing for equation 11.1. First, the transfer function concept applies well to the waveform or eye diagram seen by the receiver. In that context, X(s) is the input signal waveform, and Y(s) is the output signal waveform. Second, the transport delay between data path and clock recovery path is assumed to be negligible in equations 11.1 and 11.2. It is a good design goal to maintain a small transport delay between data and clock for the receiver. However, if the transport delay is too big to ignore, a delay term of $\exp(-sT_d)$ needs to be added in front of the $H_{CR}(s)$ for those two equations, where T_d is the transport delay.

Most of the clock recovery circuits, such as PLL-based clock recovery, have a low-pass transfer function. In other words, $H_{CR}(s)$ is a low-pass function. Therefore, the jitter transfer function $H_{JTF}(s)$ is a high-pass function. The relationship and characteristics for $H_{CR}(s)$ and $H_{JTF}(s)$ are shown in Figure 11.2.

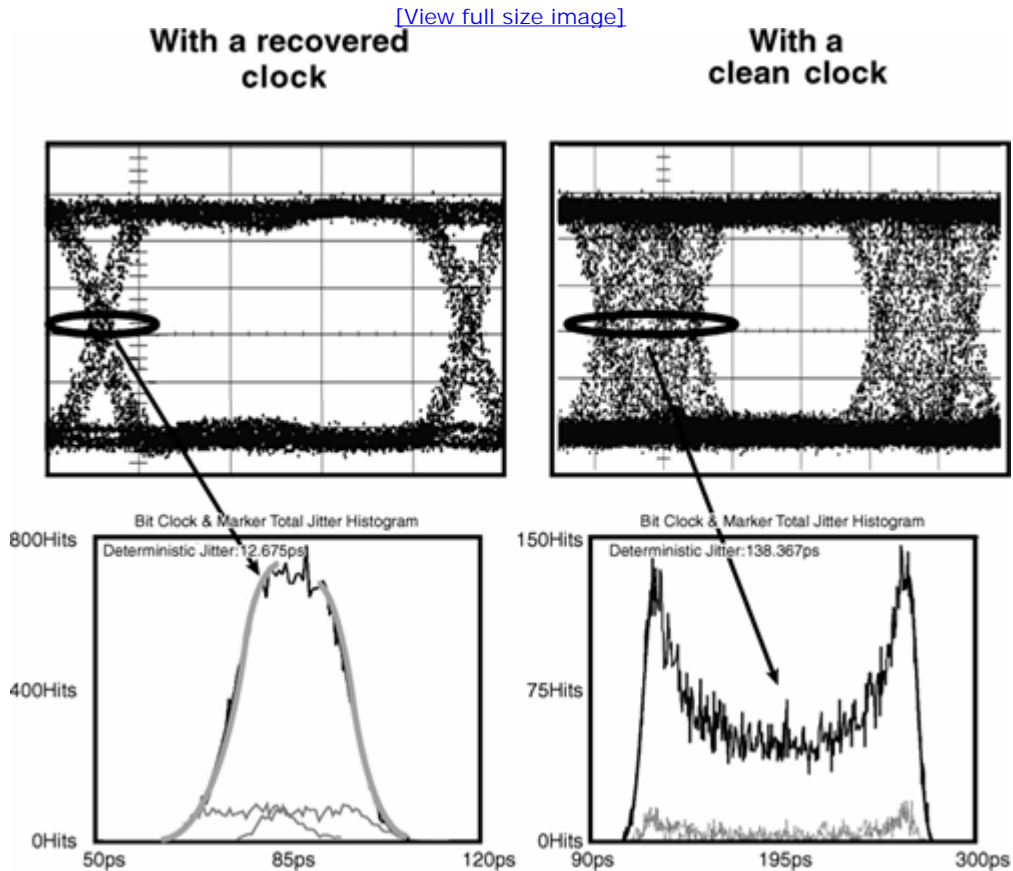
Figure 11.2. Transfer functions for clock recovery $H_{CR}(s)$ and jitter transfer function $H_{JTF}(s)$.



11.1.1.2. Jitter Transfer Function (JTF) and Link Testing

When a transmitter is tested, for the purpose of either jitter or signal output, receiver JTF must be considered. Jitter and signaling need to be linked to the system BER that is closely related to receiver clock recovery. The jitter transfer function input $X(s)$ can be the transmitter output or the channel output at the receiver input. In other words, when transmitter output is tested, a reference receiver is assumed at the end of the link with an ideal lossless channel assumption. Because the receiver jitter transfer function is a high-pass function, low-frequency jitter at the transmitter output is attenuated, and its contribution to the system BER is reduced. Thus, with proper design of clock recovery, the link system can allow the transmitter to have a certain amount of low-frequency jitter, enabling the use of low-cost components that can be intrinsically noisy or jittery. In turn, using clock recovery reduces the cost of making the high-speed link while still maintaining high performance. Figure 11.3 shows a transmitter signal eye diagram and jitter test with and without compliance clock recovery.

Figure 11.3. Eye diagram and jitter test with and without compliance clock recovery.



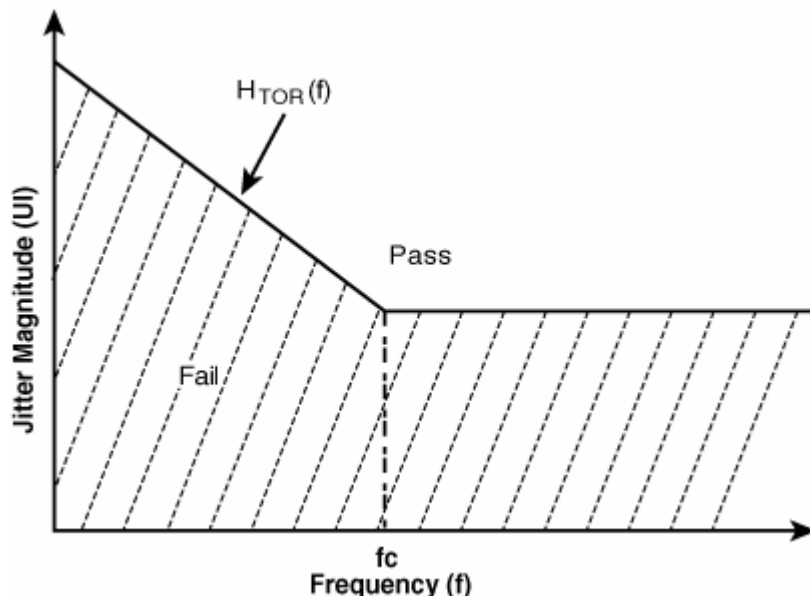
In addition to signal input sensitivity, an important test aspect is the receiver jitter tolerance, and that is directly related to its clock recovery and jitter tolerance function. The goal is to make sure that the receiver clock recovery is properly designed and can track low-frequency jitter. Because the clock tracks or attenuates low-frequency jitter, this is equivalent to saying that the receiver can tolerate more low-frequency jitter than high-frequency jitter. Thus, a receiver jitter tolerance mask is defined as the complement of the jitter transfer function. Denoting the receiver tolerance frequency mask as $H_{TOR}(f)$, we have the following:

Equation 11.3

$$H_{TOR}(f) = \frac{1}{|H_{JTF}(s)|}$$

Graphically, the jitter tolerance function looks like Figure 11.4.

Figure 11.4. Jitter tolerance mask function and pass/fail criteria.



The receiver tolerance mask typically is defined as corresponding to the 10^{-12} BER for a given set of frequency and magnitude for the sweeping periodic jitter. Thus, the mask value is the lower-limit boundary for the applied periodic jitter. If the amount of periodic jitter that a receiver can tolerate is less than the mask value, the receiver fails the tolerance test. Conversely, if the amount of periodic jitter that a receiver can tolerate is larger than the mask value, the receiver passes the tolerance test.

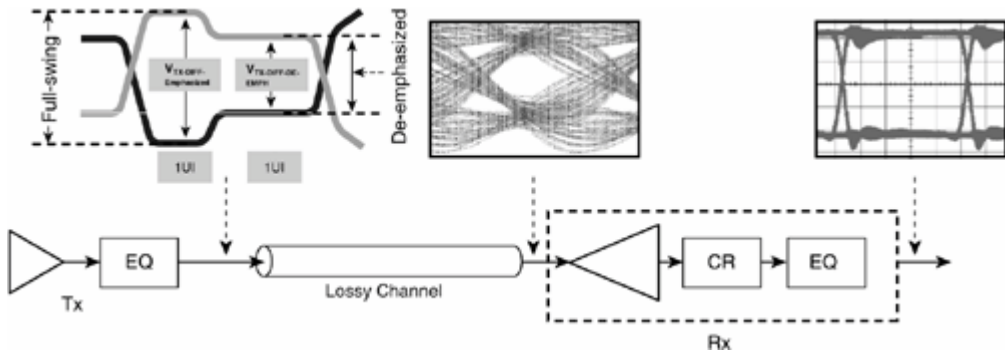
In addition to the JTF derived from the receiver clock recovery, the jitter and signal eye diagram test also must obey the statistical rules. This is so that the total timing jitter eye closure and amplitude noise eye closure satisfy the BER requirement commonly set at 10^{-12} —a stringent requirement implying a long test time if direct test is enforced. The next section discusses the test implications for the advanced link architecture using various equalization techniques in addition to clock recovery.

11.1.2. Testing Implications for Advanced Link Signaling

As discussed in Chapter 10, various equalization circuits have been developed to mitigate intersymbol interference (ISI) due to the lossy channel as the data rate keeps increasing. An equalization circuit can be implemented at the transmitter or receiver or both. Figure 11.5 shows advanced link signaling with both transmitter and receiver equalizations and the effect of equalization on signal quality before and after equalization.

Figure 11.5. An advanced serial link with both transmitter and receiver equalizations.

[\[View full size image\]](#)

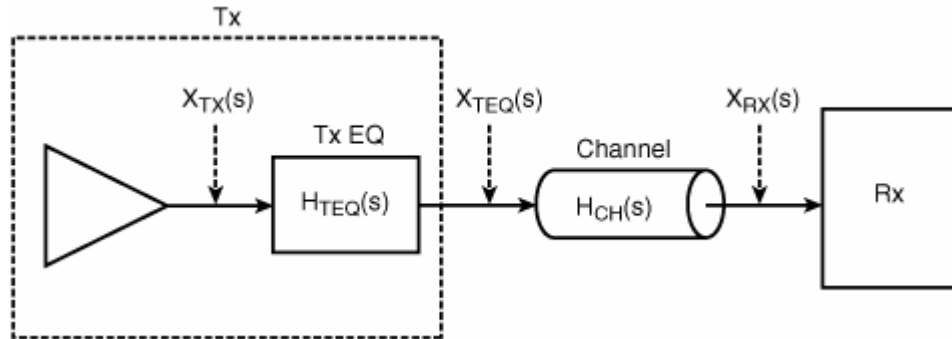


The commonly used equalizations at the transmitter are the linear types, and the commonly used equalizations at the receiver are adaptive decision feedback equalizations (DFEs). But linear and continuous linear types of equalizations may also be found in the receiver. If a linear transmitter equalization is implemented, its de-emphasis ratio must be significant at a higher data rate such that eye diagram or jitter at the transmitter output is not linked to what is seen at the receiver unless the channel effect is considered. In other words, the eye closure and jitter caused by the transmitter equalization must be removed in the test by considering channel loss effect, or full-swing bits and de-emphasized bits need to be tested separately against different compliance values. At higher data rates, the eye diagram at the receiver input is closed, and the conventional eye diagram test method becomes ineffective unless the receiver equalization is brought into the test consideration. These examples clearly show that equalization methods and channel loss characteristics must be incorporated into the jitter and signaling test for those links with advanced signaling where equalizations are mandatory. This section focuses on the test implications of equalizations. We will start with the transmitter equalization and then move to the receiver equalization. Note that the emerging test requirements associated with the equalization are an addition to, rather than a replacement for, the clock recovery JTF discussed in the nominal link signaling. The complete test requirement implications include effects from both clock recovery and equalization circuits.

11.1.2.1. Transmitter Equalization and Testing Implications

The essence of equalization is to correct or compensate for the waveform distortion caused by the lossy channel. If the equalization is implemented at the transmitter, the waveform at the receiver input should be the same as the waveform at the transmitter output, assuming that the compensation is perfect and that the channel has no impedance mismatch. This mechanism of transmitter equalization is illustrated in Figure 11.6.

Figure 11.6. A linear system diagram for Tx equalization.



An ideal Tx output waveform is represented by $X_{TX}(s)$ in the complex s-domain. The transfer function for the Tx equalization is represented by $H_{TEQ}(s)$, and its output is $X_{TEQ}(s)$. The lossy channel transfer function is $H_{CH}(s)$, and its output or Rx input is back to $X_{RX}(s)$. If the compensation is perfect, $X_{TX}(s) = X_{RX}(s)$. Mathematically, we have the following relationships:

Equation 11.4

$$X_{TEQ}(s) = H_{TEQ}(s)X_{TX}(s)$$

and

Equation 11.5

$$X_{RX}(s) = H_{CH}(s)X_{TEQ}(s) = H_{CH}(s)H_{TEQ}(s)X_{TX}(s)$$

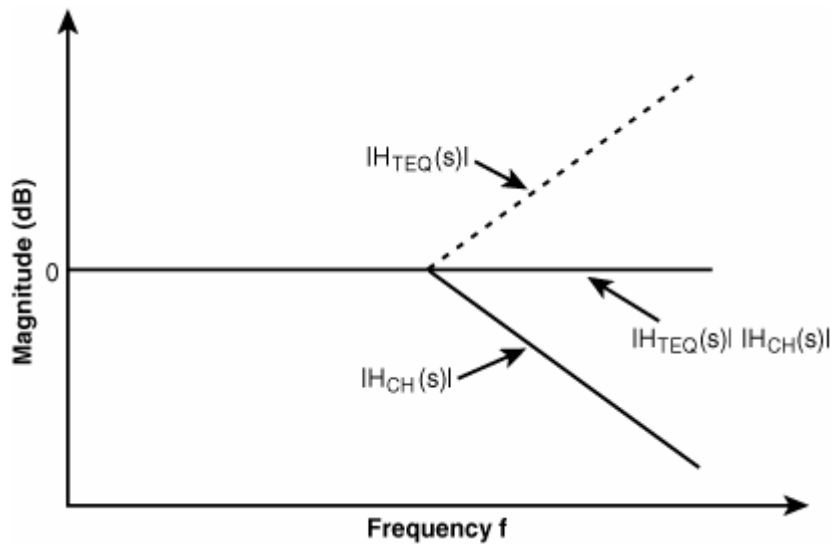
When the equalization is perfect, the product of transmitter equalization and channel transfer functions must be 1 to keep [equation 11.5](#) true, because $X_{TX}(s) = X_{RX}(s)$. Then we have

Equation 11.6

$$H_{TEQ}(s) = \frac{1}{H_{CH}(s)}$$

[Equation 11.6](#) says that for perfect transmitter equalization, its transfer function should be the reciprocal of the channel transfer function. This is a generic guideline for designing transmitter equalization. If $H_{CH}(s)$ is a low-pass function, as most of the lossy channels are, $H_{TEQ}(s)$ needs to be magnified at the high frequency. Such a reciprocal relationship is shown qualitatively in [Figure 11.7](#).

Figure 11.7. The relationship between transfer functions.



For a transmitter with equalization, we can measure $X_{TEQ}(s)$. However, what the receiver cares about or sees is $X_{RX}(s)$. Therefore, we need to transfer the observable $X_{TEQ}(s)$ to $X_{RX}(s)$, the waveform that the receiver sees. This can be done through [equation 11.4](#). We obtain the following:

Equation 11.7

$$X_{RX}(s) = \frac{X_{TEQ}(s)}{H_{TEQ}(s)}$$

For a transmitter test with equalization, the equalization transfer function needs to be defined and used in [equation 11.7](#). This is a new requirement for testing transmitter output, including waveform, jitter, and BER. The transmitter equalization transfer function needs to be built into the measurement instrument or tester.

The advantage of transmitter jitter or signal out mapping to the receiver through the transmitter equalization transfer function is that full-swing and de-emphasize bits do not need to be treated separately, simplifying the test's complexity. Another plausible method is to test full-swing and to de-emphasize bits separately and ensure that they meet the compliance eye mask accordingly. This method is not as simple and straightforward as the first method.

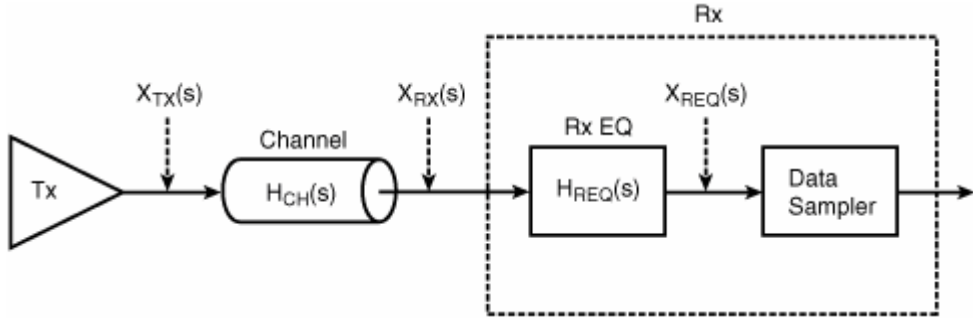
Although we've emphasized the importance of transferring $X_{TEQ}(s)$ to $X_{RX}(s)$ for testing jitter and signaling from the receiver

perspective, $X_{TEQ}(s)$ is still useful for verifying that the equalization transfer function $H_{TEQ}(s)$ is properly implemented.

11.1.2.2. Receiver Equalization and Testing Implications

If the equalization is implemented at the receiver, the waveform at the equalization output or sampling flip-flop input is the same as the waveform at the transmitter output, assuming that the equalization or compensation is perfect. Again, here we focus on the channel loss and assume that there is no impedance mismatch from transmitter to channel and from channel to receiver. The mechanism of receiver equalization is illustrated in [Figure 11.8](#) using the LTI theorem.

[Figure 11.8. An LTI diagram for Rx equalization.](#)



Similar to the case of transmitter equalization, the ideal Tx output waveform is represented by $X_{TX}(s)$. The lossy channel transfer function is $H_{CH}(s)$, and its output or Rx input is $X_{RX}(s)$. The transfer function for the Rx equalization is represented by $H_{REQ}(s)$, and its output is $X_{REQ}(s)$. If the compensation is perfect, $X_{REQ}(s) = X_{TX}(s)$. Mathematically, we have the following relationships:

[Equation 11.8](#)

$$X_{RX}(s) = H_{CH}(s)X_{TX}(s)$$

and

[Equation 11.9](#)

$$X_{REQ}(s) = H_{REQ}(s)X_{RX}(s) = H_{REQ}(s)H_{CH}(s)X_{TX}(s)$$

The product of receiver equalization and channel transfer functions must be 1 for [equation 11.9](#) to be true if the equalization is perfect. In other words, $X_{REQ}(s) = X_{TX}(s)$. Under such a condition, we have the following:

[Equation 11.10](#)

$$H_{REQ}(s) = \frac{1}{H_{CH}(s)}$$

[Equation 11.10](#) says that for a perfect receiver equalization, its transfer function should be the reciprocal of the channel transfer function. This is a generic guideline for designing a receiver equalization. If $H_{CH}(s)$ is a low-pass function, as most of the lossy channel is, $H_{REQ}(s)$ needs to be magnified at the high frequency. The characteristics of $H_{REQ}(s)$ are similar to $H_{TEQ}(s)$ for transmitter equalization. The properties shown in [Figure 11.7](#) for $H_{TEQ}(s)$ can also apply to $H_{REQ}(s)$.

The observable at the receiver input is $X_{RX}(s)$. At a higher data rate, $X_{RX}(s)$ is highly distorted and its corresponding eye diagram is closed, making the eye diagram an ineffective signal jitter and integrity metric at the receiver input. Meanwhile, the receiver or link BER is determined by the waveform $X_{REQ}(s)$ at the equalization output or data sampler input. To link the observable to the receiver BER, we need to transfer $X_{RX}(s)$ to $X_{REQ}(s)$ at the receiver sampler input. This can be done through [equation 11.9](#). We obtain the

following:

Equation 11.11

$$X_{REQ}(s) = \frac{X_{RX}(s)}{H_{REQ}(s)}$$

For channel output or receiver input test with a receiver equalization, the equalization transfer function needs to be defined and used in [equation 11.11](#). This is a new requirement for testing channel output (manifesting jitter and signaling properties for transmitter and channel), including waveform, jitter, and BER. The receiver equalization transfer function needs to be built into the measurement instrument or tester for channel output or receiver input test.

Unlike the transmitter output $X_{TEQ}(s)$ after its equalization, the receiver waveform $X_{REQ}(s)$ is not accessible or measurable from outside unless a special design is made to deliver this signal to the receiver output pin. The verification for the receiver equalization transfer function $H_{REQ}(s)$ generally is achieved with receiver tolerance testing. However, it is not easy to verify the exact shape of $H_{REQ}(s)$ or its tap coefficients if it is implemented with a digital filter unless a BIST circuit is implemented in the receiver.[\[5\]](#)

A natural question to ask would be what the testing implications are for a link with both transmitter and receiver equalization implemented. In that case, the transmitter and receiver test is the same as in the case where either of them is implemented. However, the equalization and channel transfer functions satisfy the following:

Equation 11.12

$$H_{TEQ} H_{REQ}(s) = \frac{1}{H_{CH}(s)}$$

for a perfect equalization.

In reality, however, it is rather rare to find such an approach due to the circuit complexity, power consumption, and overall cost. In practice, when the channel loss is not severe, transmitter equalization is commonly used because of its implementation simplicity and ease of testing. When the channel loss is severe, receiver equalization is commonly used because it is easy to make receiver equalization be adaptive.

URL <http://access.proquest.safaribooksonline.com/9780132429610/ch11lev1sec1>

User name: CSU San Diego

Book: Jitter, Noise, and Signal Integrity at High-Speed

Section: Chapter 11. Testing and Analysis for Jitter and Signaling Integrity for High-Speed Links

No part of any chapter or book may be reproduced or transmitted in any form by any means without the prior written permission for reprints and excerpts from the publisher of the book or chapter. Redistribution or other use that violates the fair use privilege under U.S. copyright laws (see 17 USC107) or that otherwise violates these Terms of Service is strictly prohibited. Violators will be prosecuted to the full extent of U.S. Federal and Massachusetts laws.

Information Theory Computer Science Mike Peng Li Prentice Hall Jitter, Noise, and Signal Integrity at High-Speed

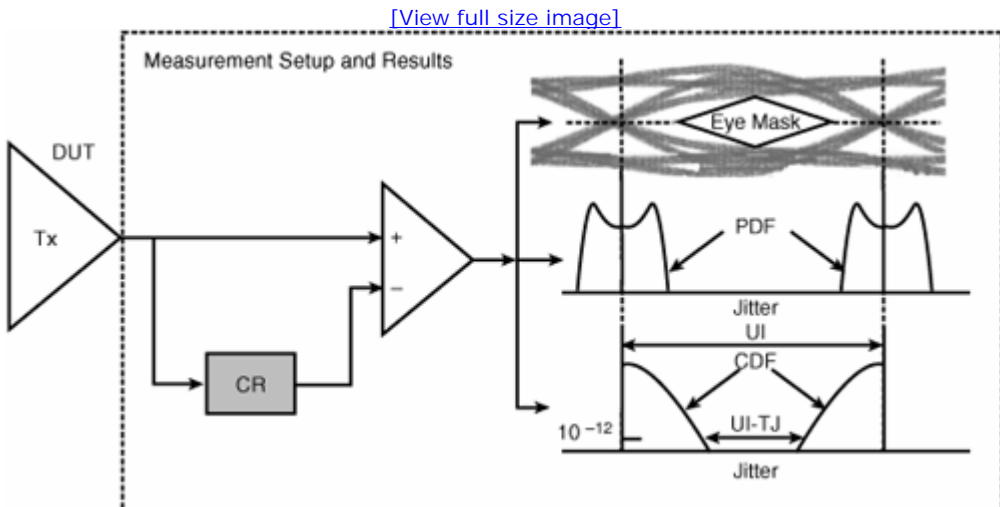
11.2. Transmitter Output Testing

Depending on the goal of testing, the test requirements and associated methods can be different. For serial link subsystem/component testing, an important requirement is the interoperability and system BER. Therefore, jitter and signaling at the transmitter output should be tested against a reference receiver and reference channel if equalization is used in the transmitter or receiver. As discussed in the preceding section, the test implications of nominal and advanced link signaling are different. Therefore, we will discuss the testing requirements and methods for those two distinct kinds of link signaling.

11.2.1. Transmitter Testing with Nominal Serial Link Signaling

The best representation for testing transmitter jitter and signaling statistically is probably the eye diagram. However, the reference clock used to construct the eye diagram should be the recovered clock complying with the characteristics of the receiver for a given serial link architecture or standard specification. A diamond-shaped eye mask corresponding to $\text{BER} = 10^{-12}$ is commonly used to define the corresponding zone boundary. Any voltage versus time sample of waveform falling into the zone causes a bit failure. The testing setup, eye diagram, and 10^{-12} eye mask are shown in Figure 11.9. This test method applies well to transmitter testing for both data-driven and common clock serial links, discussed in Chapter 9. In the case of common clock link architecture, the reference clock used to test the transmitter needs to be clean or jitter-free.

Figure 11.9. Transmitter test setup results when there is no equalization.



With the measured eye diagram, or jitter PDF and noise PDF, jitter and noise analysis can be conducted based on the methods introduced in Chapters 5 and 6. An eye diagram or waveform also gives the voltage versus time value measurements on one or many UIs. From that information, measurements for peak-to-peak and common mode voltage, rise/fall time, and overshoot/undershoot can be

obtained. Note that TJ and TN at BER = 10^{-12} can be achieved based on either in-situ measurement or RJ Gaussian modeling extrapolation. In-situ measurement has better accuracy but takes much more testing time. The model-based method takes less testing time but may suffer from accuracy problems if the distribution at lower probability deviates from Gaussian or the PDF at higher probability.

Many test and measurement platforms can measure waveform, eye diagram, jitter PDF, and BER CDF, including sampling oscilloscope (SO), real-time oscilloscope (RTO), time interval analyzer (TIA), and bit error rate test (BERT). Or a platform has combinations of some or all of them. The capability, functionality, and performance vary depending on the specific model. Refer to the websites of specific test and measurement vendors for details. Here we focus on only the general testing requirements and methodologies.

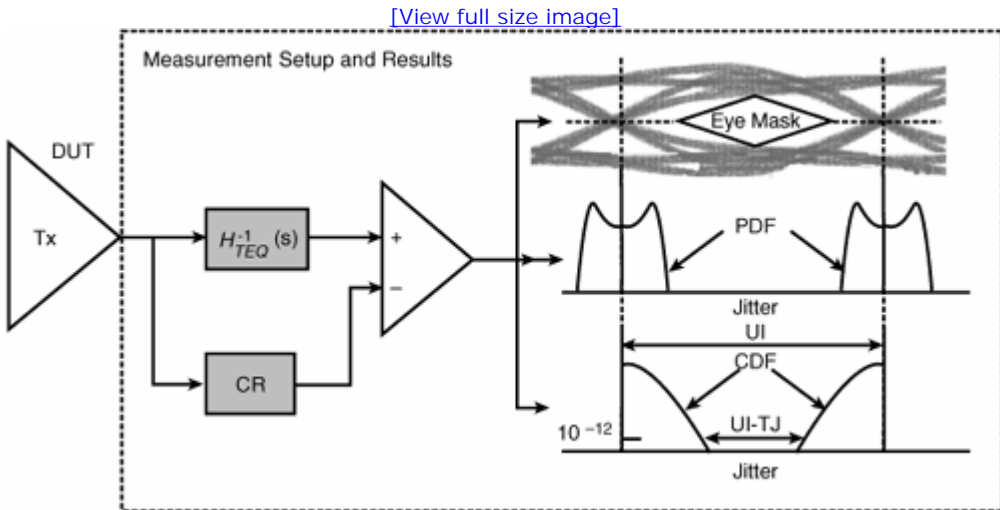
11.2.2. Transmitter Testing with Advanced Serial Link Signaling

The transmitter testing discussed in the preceding section is for a nominal serial link in which no equalization is implemented. In the case in which equalization is implemented, the transmitter testing needs to accommodate the new testing requirements imposed by the equalization. Furthermore, the new testing requirements differ depending on whether the equalization is implemented at the transmitter or receiver and what type of equalization is chosen. This section discusses transmitter testing when equalization is implemented at the transmitter or at the receiver. Clock recovery requirements will be carried out.

11.2.2.1. Link Signaling with Transmitter Equalization

The commonly implemented transmitter equalization is the de-emphasizing via a linear filter, as discussed in [section 10.2 of Chapter 10](#). A valid testing method is required to build in the transfer functions for the clock recovery and inverse transmitter equalization ($1/H_{TEQ}$ (s), given by [equation 11.7](#)) in the test setup. In this case, only one eye diagram needs to be tested, along with its jitter PDF and CDF. The corresponding test setup is shown in [Figure 11.10](#).

[Figure 11.10. Transmitter test setup with equalization built in.](#)

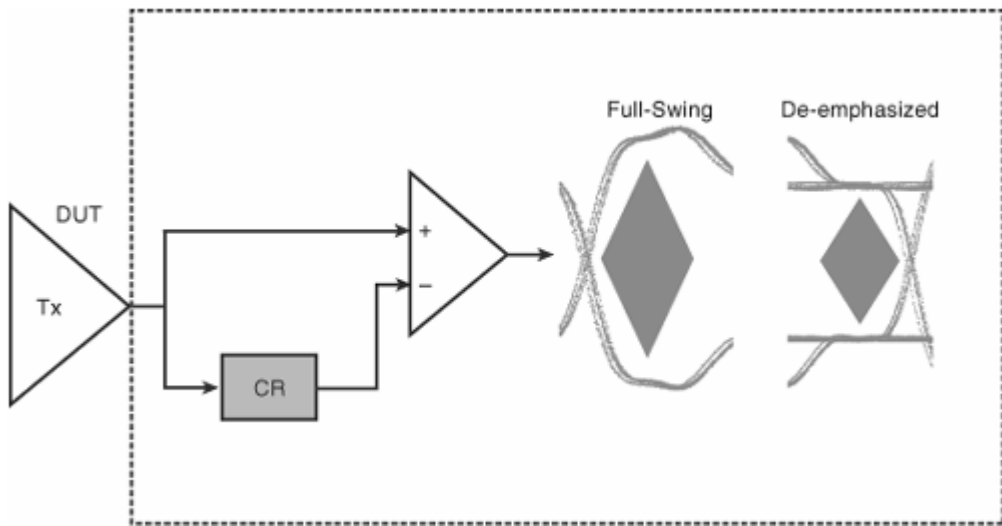


This method has only one eye diagram to deal with. Voltage values and rise/fall times can be determined from the waveform or eye diagram. From the eye diagram, jitter PDF or BER CDF is obtained, along with the DJ, RJ, and TJ.

Another test method is to ensure that the full-swing and de-emphasized voltages will satisfy their respective and different targeting values. You can group the full-swing bits and de-emphasized bits separately and construct two eye diagrams. Thus, two eye masks are associated with each type of eye diagram for the test. The main difference between these two eye masks is the eye height. The test method for this method is shown in [Figure 11.11](#).

[Figure 11.11. Transmitter test setup with equalization built into the eye masks.](#)

[\[View full size image\]](#)



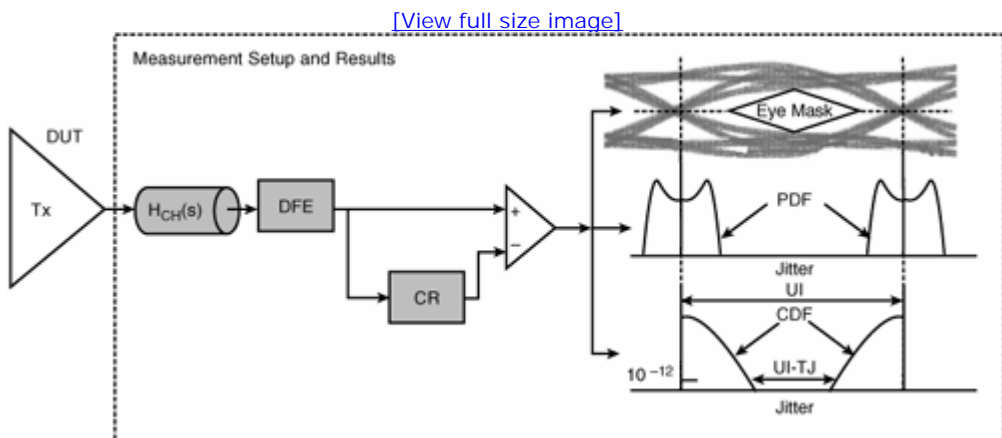
In this method, transmitter equalization is built into the two eye masks for full-swing and de-emphasized eye diagrams. Accordingly, each eye diagram has two sets of voltage, rise/fall time, DJ, RJ, and TJ values. This method is not as simple and straightforward as the first method.

11.2.2.2. Link Signaling with Receiver Equalization

As mentioned, equalization can also be implemented on the receiver side. DFE is a commonly used receiver equalization method. To test a transmitter with a receiver equipped with a DFE, the functionality of the DFE must be built into the measurement instrument. A concept similar to the "golden PLL" defined in the Fibre Channel standard^[4] can be established for DFE to define the number of taps and tap coefficients for the DFE so that it is a "golden DFE." Thus, a reference receiver for the measurement instrument has well-defined transfer functions for clock recovery and equalization DFE. Tap coefficients define a transfer function for a DFE implementation.

The purpose of a DFE is to correct or compensate for the ISI caused by the lossy channel, as we have mentioned in Chapter 9 and 10. But a transmitter's test or reference point typically is at its output pin. Therefore, a reference channel is also needed to emulate the lossy channel effect. As discussed in section 10.3 of Chapter 10, a reference channel can be represented in terms of its impulse response, step response, or S_{21} parameter/s-domain transfer function. Considering all those requirements, a transmitter test for an advanced serial link with a DFE receiver has the testing setup shown in Figure 11.12.

Figure 11.12. Transmitter test setup and results when the receiver has DFE equalization.



In this case, a measurement instrument must have three function blocks: channel transfer function, DFE, and clock recovery. They can be implemented by true hardware circuits or signal processing software. The lossy channel creates the closed eye through attenuation and ISI effects. The DFE then compensates for some of the ISI effect and opens the eye. In the last stage, the clock recovery tracks the low-frequency jitter and opens the eye further. In the end, the receiver sampler sees an open eye corresponding to a low BER. With the measured jitter PDF or BER CDF, DJ, RJ, and TJ can be estimated. With the waveform or eye diagram, the voltage level and rise/fall time are readily measurable.

Again, those test methods apply well to transmitter testing for both data-driven and common clock serial links. In the case of common clock link architecture, the reference clock used to test the transmitter needs to be clean or jitter-free.

URL <http://access.proquest.safaribooksonline.com/9780132429610/ch11lev1sec2>

User name: CSU San Diego

Book: Jitter, Noise, and Signal Integrity at High-Speed

Section: Chapter 11. Testing and Analysis for Jitter and Signaling Integrity for High-Speed Links

No part of any chapter or book may be reproduced or transmitted in any form by any means without the prior written permission for reprints and excerpts from the publisher of the book or chapter. Redistribution or other use that violates the fair use privilege under U.S. copyright laws (see 17 USC107) or that otherwise violates these Terms of Service is strictly prohibited. Violators will be prosecuted to the full extent of U.S. Federal and Massachusetts laws.

Information Theory Computer Science Mike Peng Li Prentice Hall Jitter, Noise, and Signal Integrity at High-Speed

11.3. Channel and Channel Output Testing

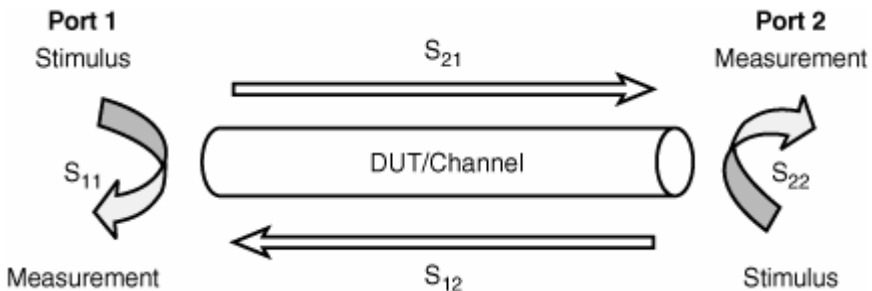
A channel itself is passive in nature. It is a signal carrier, but it neither generates nor receives a signal. Frequency-dependent loss for a copper-based channel causes signal degradation and ISI. Meanwhile, dispersion property for a fiber also causes signal degradation and ISI. The channel property itself is insufficient to determine the signal property at its output. Signal launch conditions must be known to determine signal and jitter properties at the channel output. The critical input signal properties include, but are not limited to, data pattern, voltage/power level, data rate, rise/fall times, and transmitter impedance and its match with the channel impedance. This section discusses two channel testing methods. One is S-parameter based, and the other is channel testing with a reference transmitter.

11.3.1. S-Parameter-Based Channel Testing

As introduced in [section 10.3 of Chapter 10](#), channel characteristics can be determined by either time-domain impulse response or step response, or frequency-domain S-parameter or transfer function. The results from those three different methods are interchangeable. Because the interaction between signal input and channel response becomes linear multiplication in the frequency domain, we will use S-parameters to illustrate the testing method, realizing that the same results can also be achieved by using other equivalent time-domain methods.

To fully characterize a single channel (a two-port system), complete S-parameters need to be measured, constituting 2x2 S-parameters, as shown in [equation 10.11](#). To measure an S-parameter for single-ended signaling, both stimulus and measurement are needed for a channel's two ports. In the frequency domain, the stimulus is commonly a programmable sinusoidal generator, and the measurement is commonly a tuned receiver that can measure both amplitude and phase of the response. Four pairs of measurements are needed to derive the complete S-parameters. A functional measurement block diagram is shown in [Figure 11.13](#).

Figure 11.13. A stand-alone test channel with an S-parameter measurement.



In general, all four S-parameters are needed to estimate the signal's properties at its output given the input signal properties. For the high-speed channel, it is possible to make the transmitter S_{11} (sometimes called transmitter return loss) match or be close to the channel's S_{11} so that no reflection at the boundary occurs between the transmitter and the channel. The same can be true for the receiver end S_{22} (or receiver return loss). Under those conditions, the dominant parameter is S_{21} when trying to estimate the jitter and signaling at the port 2 output when the signal is launched at its port 1 input. If the reference transmitter signal at the channel input is defined, the

signal at its output can be estimated in analogy to [equation 11.8](#):

Equation 11.13

$$X_{OCH}(s) = S_{21}(s)X_{ICH}(s)$$

$X_{ICH}(s)$ and $X_{OCH}(s)$ are the channel's input and output, respectively. Note that S_{21} is essentially the channel transfer function $H_{CH}(s)$ introduced in previous sections. Here $X_{ICH}(s)$ should be viewed as the reference transmitter input signal.

With the waveform at the receiver input $X_{OCH}(s)$ and the waveform at the reference transmitter output $X_{ICH}(s)$, it is possible to establish a threshold function for the S_{21} parameter based on [equation 11.13](#) as follows:

Equation 11.14

$$S_{21}(s) = \frac{X_{OCH}(s)}{X_{ICH}(s)} = S_0(s)$$

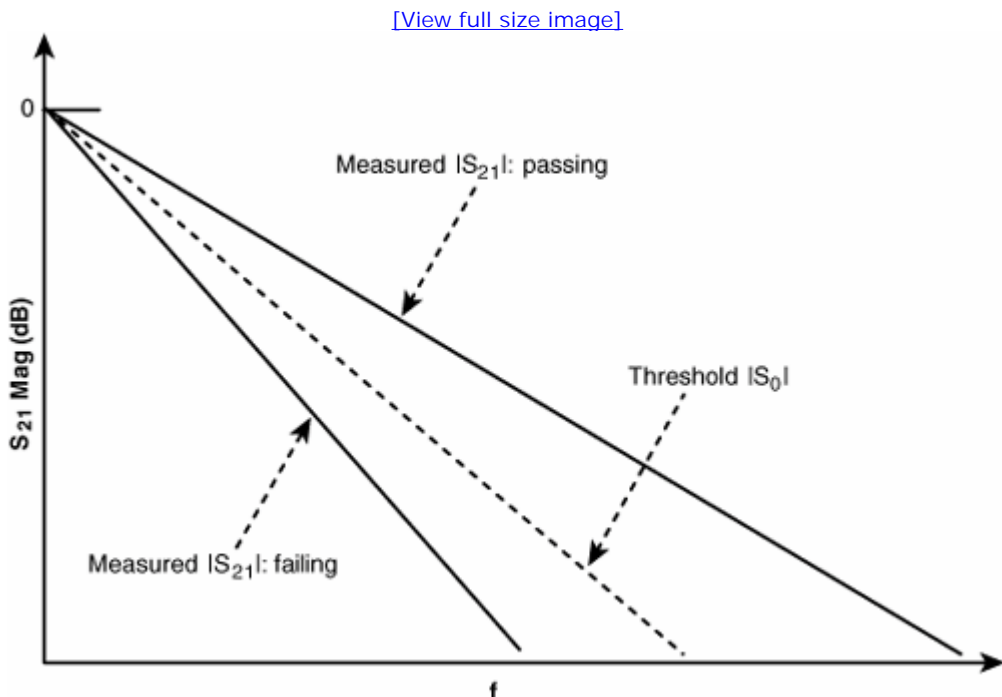
Thus, it is possible to define a threshold function S_0 so that if the measured S_{21} parameter is better than S_0 , the signaling and jitter at the channel output are better than that expected from the specification requirement. However, it is hard to establish a lower limit for S_{21} , because an S-parameter is a complex function containing both magnitude and phase. To enable setting a lower limit for S_{21} , a linear phase or constant group delay assumption is used so that only the magnitude part of the S-parameter needs to be considered. Under this consideration or approximation, a lower limiter for the S_{21} magnitude can be established as follows:

Equation 11.15

$$|S_{21}(s)| \geq |S_0(s)|$$

Graphically, the channel pass/fail test criteria can be illustrated as shown in [Figure 11.14](#).

Figure 11.14. S-parameter-based channel pass/fail test.

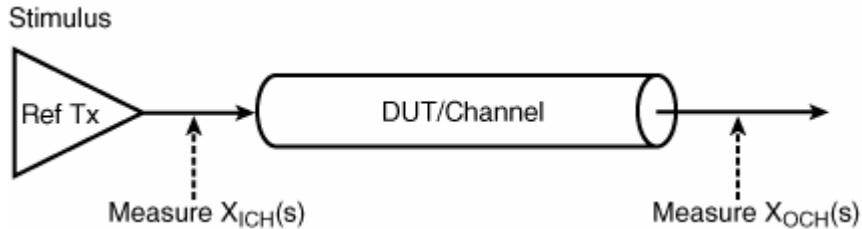


By considering the magnitude only, a pass-fail method based on the threshold S-parameter can be established for a channel stand-alone test, given the transmitter signal and jitter launch conditions. This is a simple and handy method to test the channel. However, because the phase is assumed to be constant or linear, such a method suffers from inaccuracy when the channel under test has a nonlinear phase. Some high-speed I/O standards use the general concept of this method to specify and test the channel, such as Serial ATA^[6] and Gigabit Ethernet (GBE).^[7] Refer to those documents for more details.

11.3.2. Channel Testing with a Reference Transmitter

The testing or compliance points for a link system are often defined at the transmitter output and the channel output or receiver input. To determine whether a channel complies with the specification requirement, another method is to use a reference transmitter in the form of actual hardware. The foundation for this idea is shown in [equation 11.14](#). By generating and measuring the reference transmitter output $X_{ICH}(s)$, and by measuring the channel output $X_{OCH}(s)$, the S_{21} can be determined through [equation 11.14](#). The measurement setup for this method is illustrated in [Figure 11.15](#).

Figure 11.15. Channel test with a reference transmitter.



After the S_{21} is obtained using this method, you can determine whether it passes or fails a compliance channel threshold S_0 similar to the procedure illustrated in [Figure 11.14](#). $X_{ICH}(s)$ and $X_{OCH}(s)$ can be measured through the time-domain measurement of signal waveform $x_{ICH}(t)$ and $x_{OCH}(t)$ and corresponding Laplace transformations. Note that $x_{ICH}(t)$ and $x_{OCH}(t)$ need to be real-time measurements to reserve the phase information.

URL <http://access.proquest.safaribooksonline.com/9780132429610/ch11lev1sec3>

User name: CSU San Diego

Book: Jitter, Noise, and Signal Integrity at High-Speed

Section: Chapter 11. Testing and Analysis for Jitter and Signaling Integrity for High-Speed Links

No part of any chapter or book may be reproduced or transmitted in any form by any means without the prior written permission for reprints and excerpts from the publisher of the book or chapter. Redistribution or other use that violates the fair use privilege under U.S. copyright laws (see 17 USC107) or that otherwise violates these Terms of Service is strictly prohibited. Violators will be prosecuted to the full extent of U.S. Federal and Massachusetts laws.

Information Theory Computer Science Mike Peng Li Prentice Hall Jitter, Noise, and Signal Integrity at High-Speed

11.4. Receiver Testing

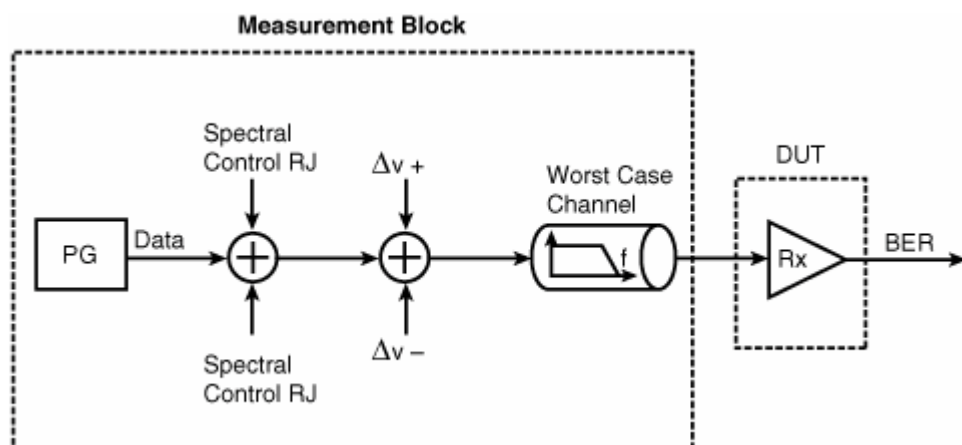
The goal of receiver tolerance testing is to ensure that the receiver under test can operate well even under worst-case signaling conditions. The challenge is to create or emulate the worst-case signal input to the receiver with its jitter and noise coming from the rest of the link subsystems. The key is to stress the receiver with the worst-case signaling and jitter input condition or conditions. When determining worst-case signaling and jitter, there are three important aspects to consider: amplitude/voltage stressing, timing/jitter stressing, and spectral contents stressing. Amplitude/voltage stressing is relatively straightforward. It simply tests the receiver when the input amplitude/voltage swing is at the lowest value. For timing/jitter stressing, various jitter types, including DJ (DCD and PJ) and RJ from the transmitter, and DDJ and BUJ from the channel, need to be considered. They are governed by the signaling and jitter properties of the transmitter and channel combined. Spectral contents have become an increasingly important consideration. Not only are the jitter components and corresponding magnitude required, but their spectral characteristics also need to be considered. How small an input signal amplitude or voltage is allowed depends on how low the receiver sensitivity is. The worst-case jitter composition, including its magnitude and spectral contents, also depends on the receiver equalization and clock recovery capabilities. Typically, the worst-case signaling and jitter condition is derived from the jitter and voltage budget allocated for each subsystem. Each subsystem is bounded in terms of its signal and jitter properties and is optimized for overall link interoperability and BER performance.

This section discusses receiver testing under nominal and advanced link signaling. Then we will discuss receiver internal jitter testing and determination, a new topic in receiver testing.

11.4.1. Rx Testing with Nominal Link Signaling

To accommodate the three key requirements for receiver testing—amplitude/voltage stressing, timing/jitter stressing, and spectral control/stressing—Figure 11.16 shows a general testing setup.

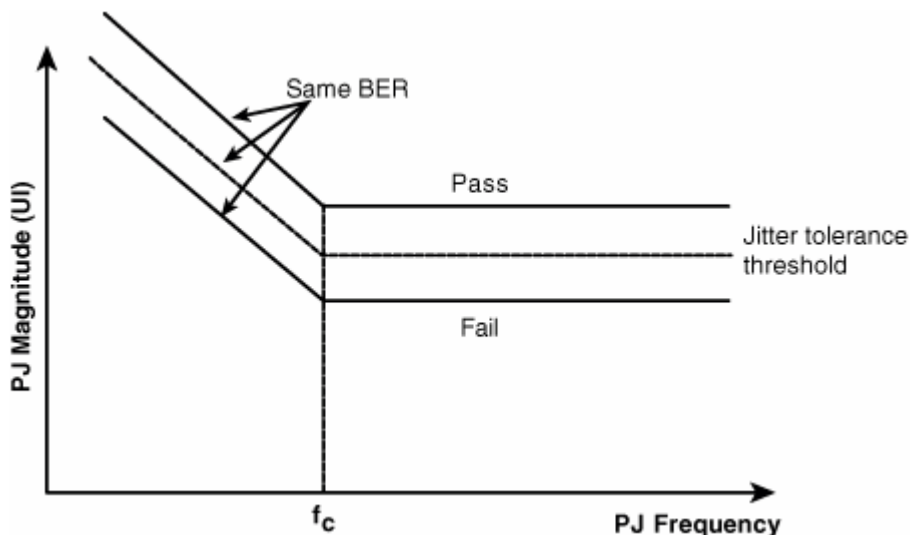
Figure 11.16. The receiver testing measurement setup for a data-driven architecture.



The programmable pattern generator (PG) is needed to generate the required data rate, data pattern, pulse width, rise/fall time, and voltage levels. With nominal link signaling, no transmitter equalization is used. Thus, the generator does not have to output full-swing and de-emphasis bits for the data pattern. DJ and RJ with controlled spectral contents are then modulated to the data signal. The DJ and RJ should emulate the jitter types and characteristics of the worst-case transmitter. Then common mode noise may be added to the signal because it is an important source for the differential signal. Then a worst-case lossy channel with crosstalk needs to be present at the last stage of stressing signal generation. Note that [Figure 11.16](#) is the functional block diagram and that the functionality can be implemented in many ways. When the worst-case signal is applied to the receiver's input, the BER is measured. It needs to be below the targeting value, typically set at 10^{-12} or lower.

The BER test is a system test because it cannot tell which subsystem has a problem when the receiver fails a test—unless the test receiver is the only device under test (DUT) and the rest of the subsystems are known to be good. Thus, other tests may be called for receiver characterization and debug in addition to the BER test. An example is clock recovery jitter track testing. Clock recovery tracks or attenuates the low-frequency jitter associated with the incoming signal. Clock recovery tracking can be tested by using a PJ (a subcomponent of DJ). The procedure involves sweeping its frequency and varying its magnitude so that a constant BER is achieved. When the PJ magnitude as a function of its frequency is plotted, the receiver clock recovery jitter tolerance function is determined. A typical clock recovery has a jitter tolerance function that looks like [Figure 11.17](#).

Figure 11.17. Receiver clock recovery jitter tolerance test results.



The testing result typically is compared to a golden clock recovery jitter tolerance curve. For second-order PLL-based clock recovery, a typical tolerance curve has a -40 dB/decade slope below the PLL corner frequency f_c . The negative slope manifests the PLL phase error transfer function of a high-pass with a 40 /decade slope below its corner frequency f_c (see [equation 11.3](#)). Jitter tolerance and jitter transfer function are complementary. If a receiver can attenuate more low-frequency jitter, this is equivalent to saying that it can tolerate more low-frequency jitter. When the tolerance curve measured is above the threshold curve, it is passing results, because the receiver can tolerate more than is required or expected. However, when the tolerance curve measured is below the threshold curve, it is failing, because the receiver can tolerate less than is required or expected.

11.4.2. Rx Testing with Advanced Link Signaling

Equalization is used with advanced link signaling. However, the receiver testing setup and method still are similar to that illustrated in [Figure 11.16](#), with the similar goal of covering amplitude/voltage stressing, timing/jitter stressing, and spectral control/stressing. Nevertheless, attention needs to be paid to a few new aspects of receiver advanced signaling with equalization.

As you know, for link signaling with transmitter equalization, the full-swing and de-emphasis bits need to be generated at appropriate voltage levels. It is critical for the PG to have full-swing and de-emphasis bit generation capability. For link signaling with receiver equalization, the worst-case lossy channel with significant crosstalk creation is critical to stress the receiver equalizer and have good test fault coverage.

Equalization or the lack thereof has little impact on the clock recovery jitter tolerance test. The clock recovery jitter tolerance test method introduced for nominal link signaling applies well to the case of advanced link signaling.

11.4.3. Receiver Internal Jitter Testing

In determining the link jitter budget, jitter allocation for its subsystems of transmitter, channel, receiver, and reference clock are all given. Transmitter, channel, and reference clock all have direct jitter output and can be measured and verified directly. For the receiver, the only observable is the BER, yet the receiver stress test does not give rise to the receiver internal jitter information directly. Thus, receiver internal jitter verification and test is an open question until [8].

The method developed in [8] for testing/determining the Rx internal jitter takes advantage of the independence between the receiver external jitter (all the link jitter except the Rx jitter) and receiver internal jitter. By using dual-Dirac as the DJ PDF model, and Gaussian as the RJ PDF model, the math can be further simplified and linearized. By applying a different amount of jitter in a controlled and calibrated way and observing the BER at the receiver output, receiver internal jitter can be determined by solving a set of linear equations.

This mechanism can be illustrated by using equation 5.25 of the Q factor definition. Based on equation 5.25, and having $t_s = 0.5$ UI, we get the following:

Equation 11.16

$$2\operatorname{erfc}^{-1}\left(\frac{1}{\rho}\beta(0.5UI, D, \sigma)\right) \approx \frac{UI - D}{\sqrt{2}\sigma}$$

where ρ is the transition density and β is the BER. Assume that Rx internal DJ and RJ are D_i and σ_i , respectively, and non-Rx or external DJ and RJ are D_e and σ_e , respectively. Then we have

Equation 11.17

$$D = D_i + D_e$$

and

Equation 11.18

$$\sigma = \sqrt{\sigma_i^2 + \sigma_e^2}$$

where D and σ are overall DJ peak-to-peak and RJ sigma present at the Rx sampling flip-flop input. We will demonstrate the method with RJ stressing. Under RJ stressing, external jitter DJ (D_e) is kept at a small constant, and RJ (σ_e) is known and programmable.

Because equation 11.16 is a linear equation with two variables, we need to create two different test conditions so that those two variables can be determined through jointly solving two linear equations.

Assume that Rx is tested under two different sets of jitter test conditions. Condition 1 has DJ D_e and RJ σ_{e1} , resulting in a BER measurement of β_1 . Condition 2 has DJ D_e and RJ σ_{e2} , resulting in a BER measurement of β_2 . Jitter values may be chosen such that β_1 and β_2 are higher than 10^{-12} —say, 10^{-6} —to have a shorter test time. Using equation 11.16, we have

Equation 11.19

$$\frac{UI - (D_i + D_e)}{\sqrt{(\sigma_i^2 + \sigma_{e1}^2)}} \approx 2\sqrt{2}\operatorname{erfc}^{-1}\left(\frac{1}{\rho}\beta_1\right) = Q_1$$

for test condition 1 and

Equation 11.20

$$\frac{UI - (D_i + D_e)}{\sqrt{(\sigma_i^2 + \sigma_{e2}^2)}} \approx 2\sqrt{2}erfc^{-1}\left(\frac{4}{\rho}\beta_2\right) = Q_2$$

for test condition 2. Here Q_1 and Q_2 are Q factors for these two jitter conditions.

Solving [equations 11.19](#) and [11.20](#) jointly, we can determine Rx internal DJ (D_i) and RJ (σ_i) uniquely in terms of known quantities of Q_1 , Q_2 , σ_{e1} , and σ_{e2} :

Equation 11.21

$$D_i = UI - D_e - Q_1 Q_2 \sqrt{\frac{(\sigma_{e1}^2 - \sigma_{e2}^2)}{Q_2^2 - Q_1^2}}$$

and

Equation 11.22

$$\sigma_i = \sqrt{\frac{Q_1^2 \sigma_{e1}^2 - Q_2^2 \sigma_{e2}^2}{Q_2^2 - Q_1^2}}$$

Clearly $Q_1 \neq Q_2$ is needed to avoid the singularities in [equations 11.21](#) and [11.22](#). As soon as the Rx internal DJ (D_i) and RJ (σ_i) have been determined, the Rx BER under the external targeting or compliance jitter condition represented by D_c and σ_c can be estimated by the BER estimation equation [5.12](#) in terms of both internal and external targeting jitter (D_c and σ_c) in the following form:

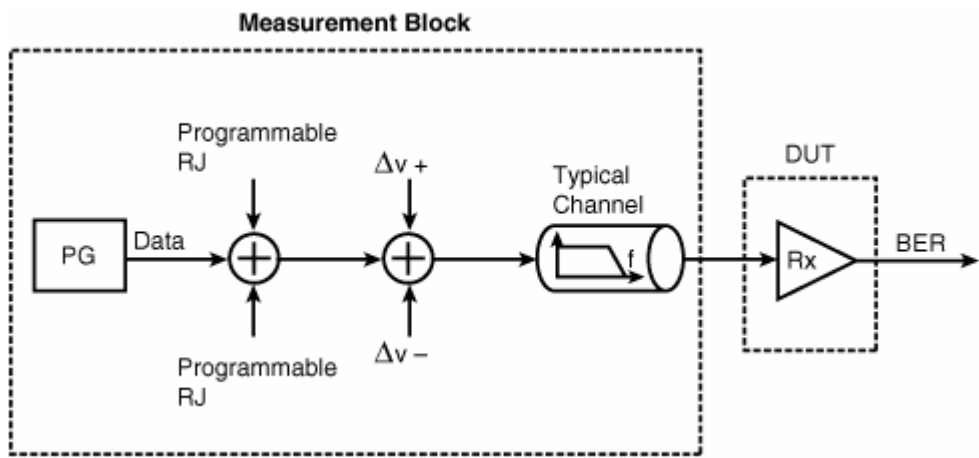
Equation 11.23

$$BER(t_{s0}, D_c, \sigma_c) \approx \rho \left(erfc \left(\frac{t_{s0} - \frac{D_i + D_c}{2}}{\sqrt{2(\sigma_i^2 + \sigma_c^2)}} \right) + erfc \left(\frac{UI - t_{s0} - \frac{D_i + D_c}{2}}{\sqrt{2(\sigma_i^2 + \sigma_c^2)}} \right) \right)$$

where t_{s0} is the optimal sampling time and typically is set at 0.5 UI.

[Figure 11.18](#) shows the experimental setup for the Rx internal jitter determination through external RJ stressing.

Figure 11.18. An experimental setup for Rx internal jitter testing/determination.



We have demonstrated the Rx internal DJ and RJ determination via RJ stressing. However, the same results can be achieved by DJ stressing or receiving sampling time shifting if Rx offers that type of controllability. Refer to [8] for more details on these two different stressing methods.

URL <http://access.proquest.safaribooksonline.com/9780132429610/ch11lev1sec4>

User name: CSU San Diego

Book: Jitter, Noise, and Signal Integrity at High-Speed

Section: Chapter 11. Testing and Analysis for Jitter and Signaling Integrity for High-Speed Links

No part of any chapter or book may be reproduced or transmitted in any form by any means without the prior written permission for reprints and excerpts from the publisher of the book or chapter. Redistribution or other use that violates the fair use privilege under U.S. copyright laws (see 17 USC107) or that otherwise violates these Terms of Service is strictly prohibited. Violators will be prosecuted to the full extent of U.S. Federal and Massachusetts laws.

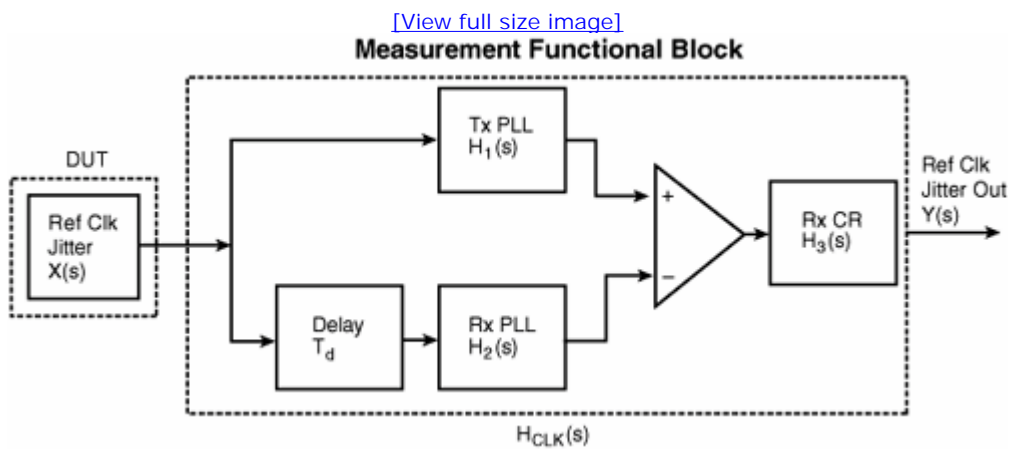
Information Theory Computer Science Mike Peng Li Prentice Hall Jitter, Noise, and Signal Integrity at High-Speed

11.5. Reference Clock Testing

Reference clock testing traditionally has been done with metrics such as period jitter and cycle-to-cycle jitter (see Chapter 7, "Clock Jitter"). These metrics are meaningful and appropriate within the context of a synchronized system, in which a global clock is used and period is used as the fundamental timing reference. Within the context of serial data communication, the fundamental timing reference used is the instantaneous clock edge time, coupled with the architecture of the receiver clock and data recovery. It is conceivable that both period jitter and cycle-to-cycle jitter are not appropriate metrics for quantifying the performance of the reference clock used in the serial data communication. In fact, it has been found that the reference clock device passes the period jitter or cycle-to-cycle jitter conventional requirement but fails in the actual serial link system.^[9] Thus, new metrics or estimation methods are needed to quantify jitter for the reference clock used in common clock serial data communication in which the reference clock performance needs to be independently specified.

The starting point is the common clock architecture illustrated in Figure 9.2 in Chapter 9. What matters here is the jitter or eye closure caused at the receiver sampling flip-flop due to the reference clock. Assuming that the reference clock phase jitter is $X(s)$, and the phase jitter at the receiver's sampling flip-flop is $Y(s)$, the relationship between $X(s)$ and $Y(s)$ can be estimated based on the LTI functional block diagram shown in Figure 11.19.

Figure 11.19. Reference jitter testing within a common clock architecture.



The following things happen to the reference clock. First, the reference clock signal is split into two paths. One goes to the transmitter, and the other goes to the receiver. When the reference clock goes to the transmitter, its phase jitter is modified by the transmitter multiplication PLL (represented by $H_1(s)$). Similarly, its phase jitter is modified by the receiver multiplication PLL (represented by $H_2(s)$) in parallel. The path to the transmitter and receiver may not necessarily be the same. Also, a transport delay (T_d) occurs between the transmitter signal path and receiver signal path. Furthermore, the split reference clock phase jitters are combined as a difference function at the receiver. Last, the combined phase jitter goes through a jitter transfer function $H_3(s)$ of the clock recovery at the receiver.

Mathematically, the relationship between $X(s)$ and $Y(s)$ can be represented by the following equation:

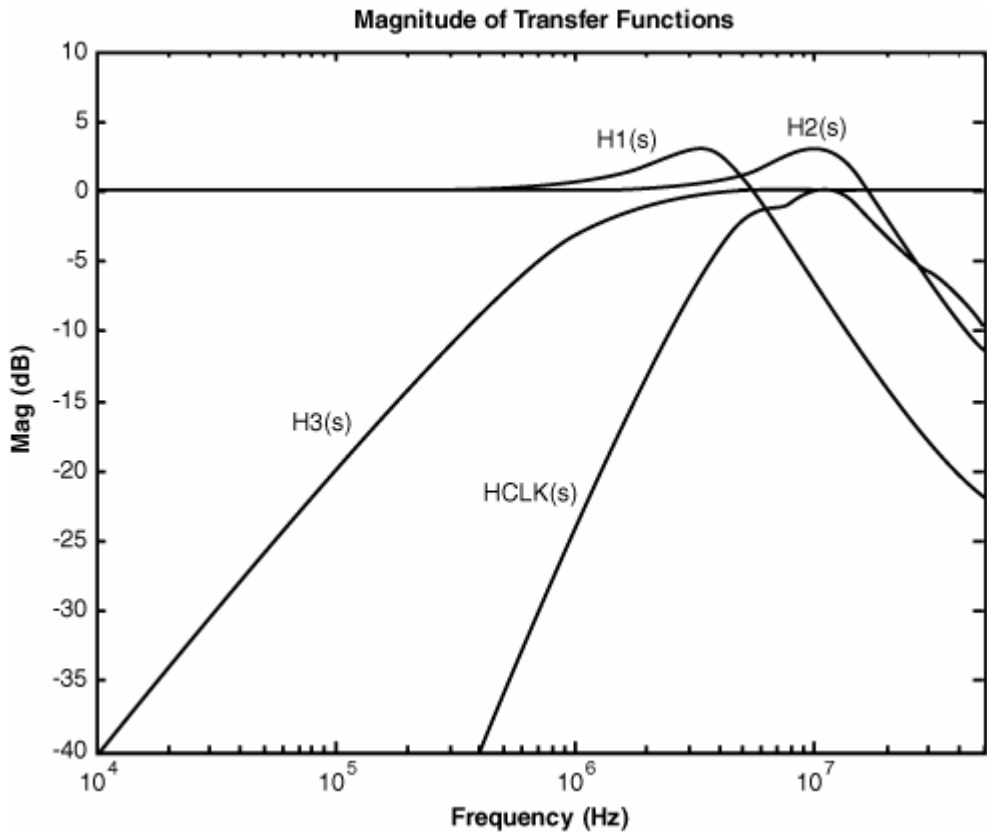
Equation 11.24

$$Y(s) = [(H_1(s) - e^{-sT_d} H_2(s)) H_3(s)] X(s) = H_{CLK}(s) X(s)$$

Clearly, the key to estimating reference clock jitter is its jitter transfer function $H_{CLK}(s)$, governed by the common clock link architecture and properties of the subsystems. Its characteristics depend on the properties of transmitter PLL $H_1(s)$, receiver PLL $H_2(s)$, receiver clock recovery jitter transfer function $H_3(s)$, and propagation delay T_d .

Figure 11.20 shows transfer functions of $H_1(s)$, $H_2(s)$, $H_3(s)$, and $H_{CLK}(s)$ for the common clock link system. The 3 dB frequencies for $H_1(s)$, $H_2(s)$, and $H_3(s)$ are 7 MHz, 22 MHz, and 1 MHz, respectively. Notice that $H_{CLK}(s)$ is a band-pass function, with its peak occurring between 7 and 22 MHz. It implies that only the jitter spectral contents within the 7 to 22 MHz range contribute the most to the receiver BER.

Figure 11.20. Jitter transfer functions for PLLs, clock recovery, and reference clock.

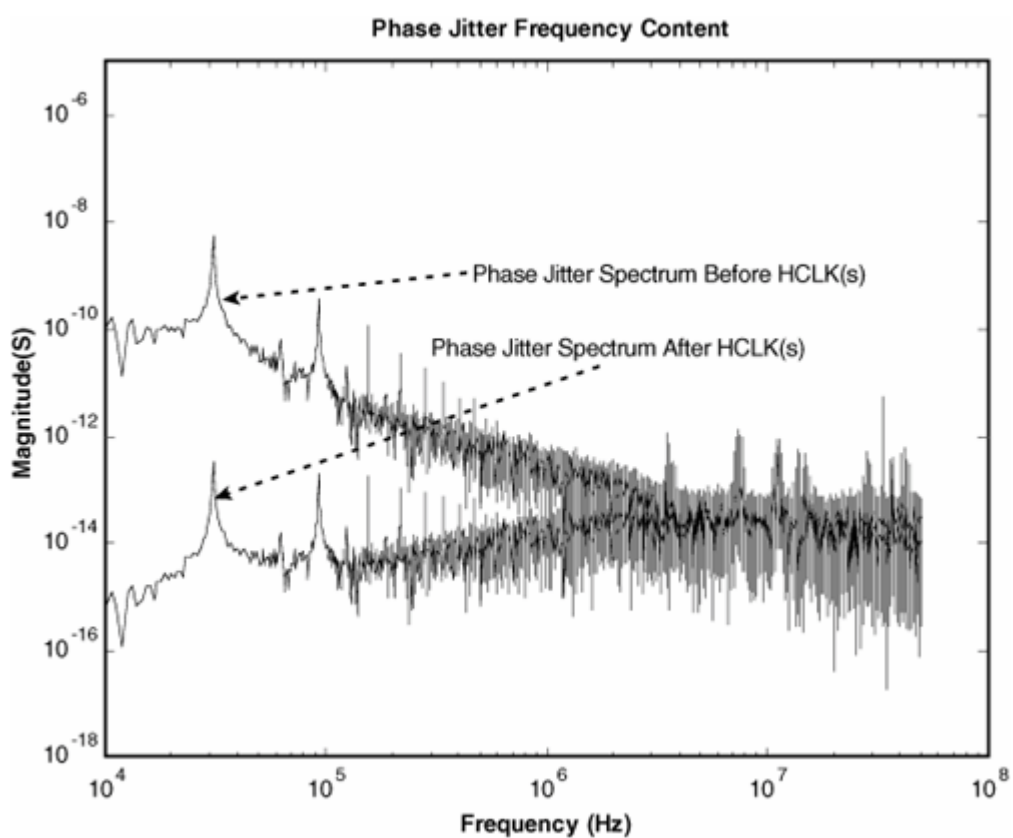


To test the reference clock used in the common clock link architecture, we need to measure phase jitter ($X(s)$) from the reference clock and then apply the jitter transfer function $H_{CLK}(s)$ according to [equation 11.24](#). The implementation of $H_{CLK}(s)$ can be done with software signal processing given that complete reference clock raw phase jitter time record $x(t)$ or spectrum $X(s)$ is available, or hardware circuits. Clearly software approaches offer versatility, scalability, and low-cost advantages.

It would be nice to put [equation 11.24](#) and reference clock testing into perspective. Figure 11.21 shows the phase jitter spectrum $X(s)$ before transfer function $H_{CLK}(s)$ is applied, and phase jitter spectrum $Y(s)$ after the transfer function $H_{CLK}(s)$ has been applied. It is clear that the shape of $Y(s)$ resembles the shape of $H_{CLK}(s)$.

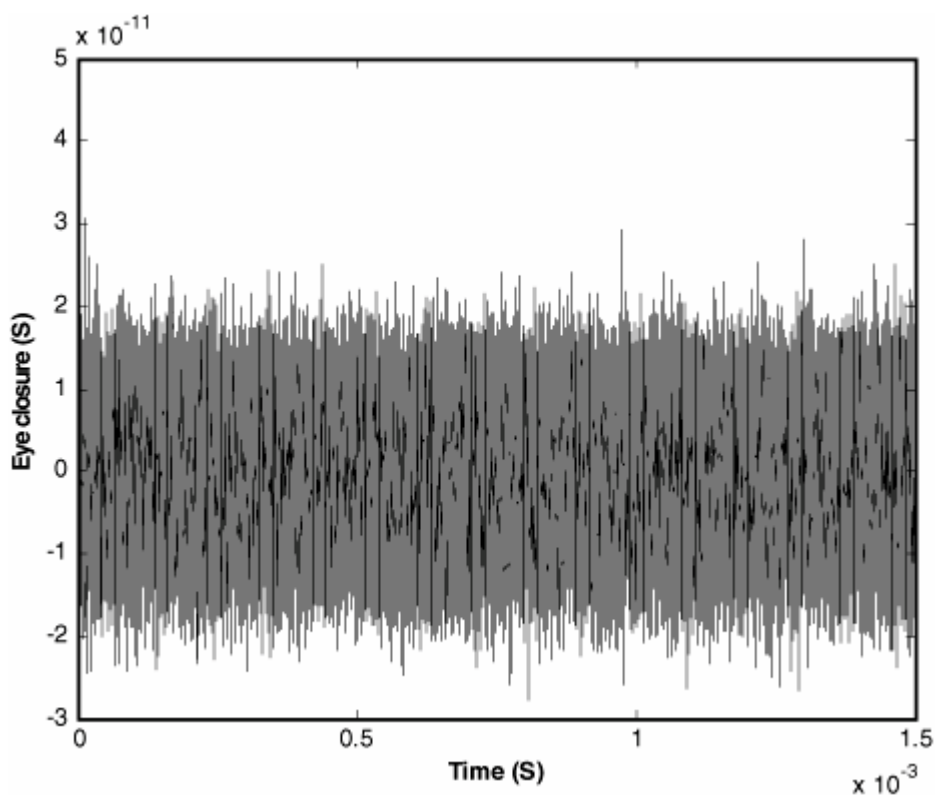
Figure 11.21. Phase jitter spectrum before and after the reference clock jitter transfer function.

[\[View full size image\]](#)



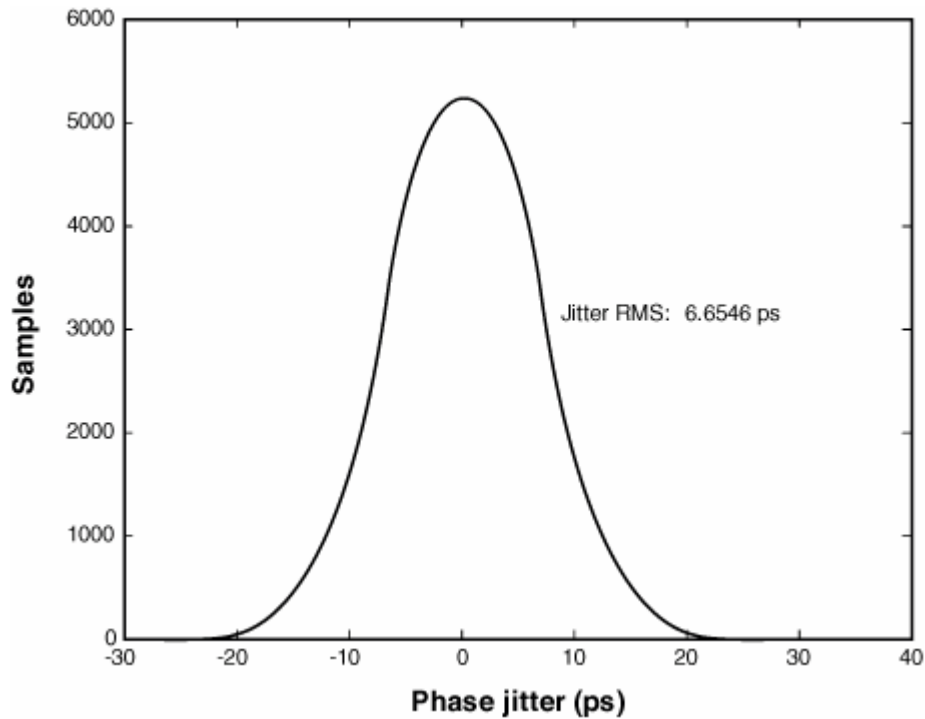
After $Y(s)$ is obtained, its time-domain counterpart $y(t)$ can be estimated via inverse Laplace transformation. The resulting $y(t)$ is shown in Figure 11.22.

Figure 11.22. Phase jitter in the time domain after the reference clock jitter transfer function.



With the phase jitter time record $y(t)$, the corresponding jitter histogram or PDF can be estimated. It is shown in Figure 11.23.

Figure 11.23. The phase jitter histogram after the reference clock jitter transfer function.



With the jitter histogram/PDF, statistical parameters such as rms, pk-pk (at a given probability), and mean can be estimated. In this example, the rms is estimated as 6.65 ps. Further readings on common clock architecture and reference clock testing can be found in [9], [10], [11].

URL <http://access.proquest.safaribooksonline.com/9780132429610/ch11lev1sec5>

User name: CSU San Diego

Book: Jitter, Noise, and Signal Integrity at High-Speed

Section: Chapter 11. Testing and Analysis for Jitter and Signaling Integrity for High-Speed Links

No part of any chapter or book may be reproduced or transmitted in any form by any means without the prior written permission for reprints and excerpts from the publisher of the book or chapter. Redistribution or other use that violates the fair use privilege under U.S. copyright laws (see 17 USC107) or that otherwise violates these Terms of Service is strictly prohibited. Violators will be prosecuted to the full extent of U.S. Federal and Massachusetts laws.

Information Theory Computer Science Mike Peng Li Prentice Hall Jitter, Noise, and Signal Integrity at High-Speed

11.6. PLL Testing

PLL testing has received more attention recently for high-speed links, such as common clock link architecture. This is because the transfer function for the transmitter multiplication PLL ($H_1(s)$) and receiver multiplication PLL ($H_2(s)$) needs to be confined to ensure the interoperability of the link system (see [Figure 11.19](#) and [equation 11.24](#)^{[1], [2], [6]}). This section introduces two PLL testing methods: the nonstimulus jitter variance function-based method covered in detail in [Chapter 8](#), "PLL Jitter and Transfer Function Analysis," and the traditional stimulus-based PLL test method.

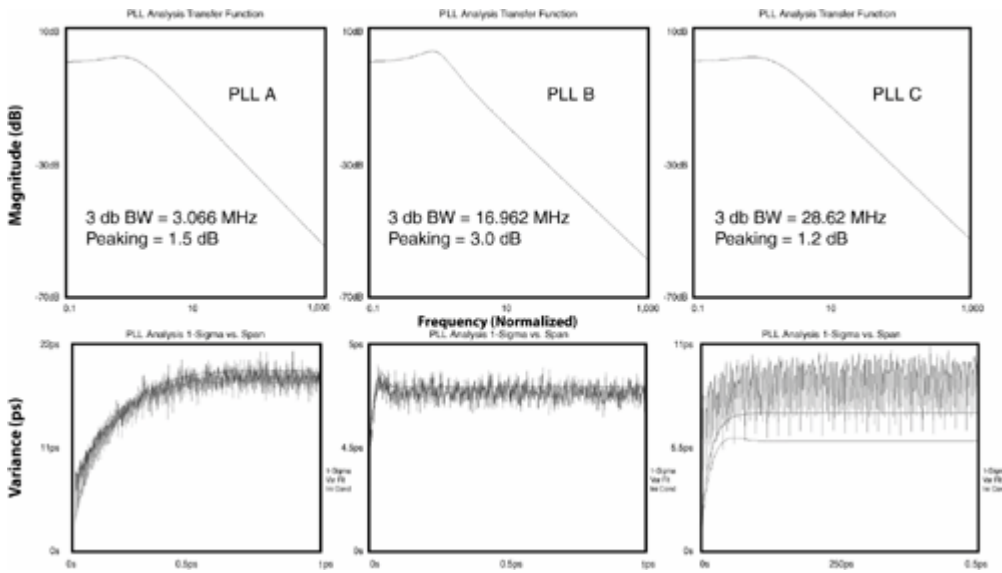
11.6.1. Non-Stimulus-Based Method

[Chapter 8](#) was dedicated to the new PLL testing method based on PLL jitter variance function measurement and analysis. This method uses the PLL internal jitter/noise as the "free" stimulus to measure the PLL characteristics (see [Figure 8.11](#) for the measurement setup for this method). As already demonstrated, such a method does not require a stimulus modulation signal generator; it measures the complete complex s-domain transfer function $H(s)$. With the transfer function measured, other related PLL characteristic functions (such as Bode function/plot and pole/zero location plot) and characteristic parameters (such as peaking and 3 dB frequency, locking time, and pull-in time) are readily obtainable.

The majority of PLL circuits used in clock recovery and clock multiplication are a second-order type of PLL that can be completely described by its 3 dB frequency and peaking parameters (or damping factor and natural frequency parameters). Thus, the PLL can be specified and tested through the two important parameters shown in [Figure 11.24](#)^{[1], [2], [6]},

Figure 11.24. PLL transfer function measurement using a variance function, nonstimulus method (see [Chapter 8](#)) for three different PLLs. 3 dB frequency and peaking are shown for each one.

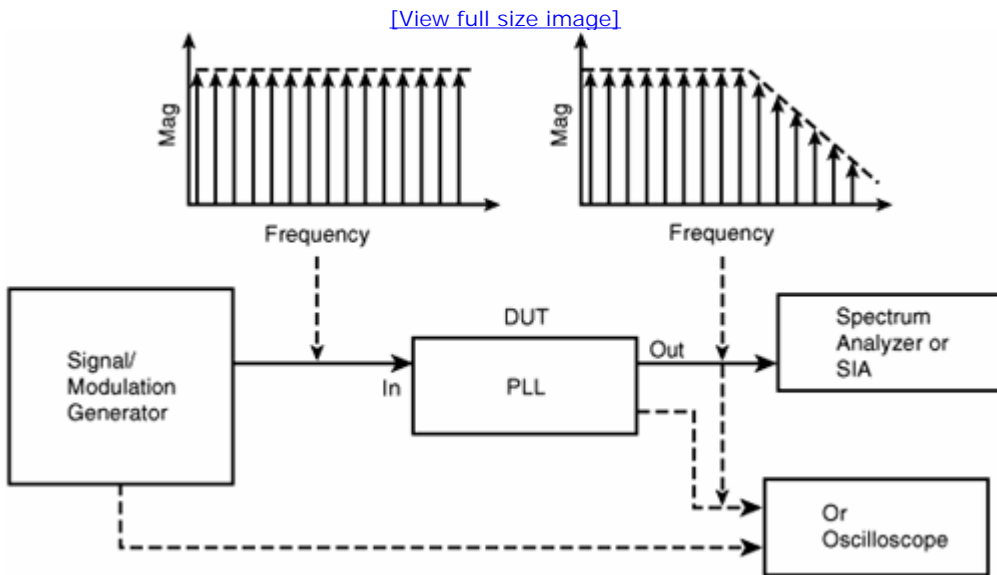
[\[View full size image\]](#)



11.6.2. Stimulus-Based Method

PLL testing using a modulation signal generator has been around for some time (see [12]). The working mechanism is straightforward. A data or clock signal with phase-modulated sinusoidal is fed to the PLL input. The sinusoidal modulation magnitude and frequency are first measured at the PLL's input. Then, at the PLL's output, the magnitude and frequency of the sinusoidal are measured again. This procedure is repeated with another sinusoidal at a different frequency. After the sinusoidal is swept through the interested frequency range, the ratio of the sinusoidal magnitude at the PLL output to that at the PLL input can be calculated. This magnitude ratio versus frequency function gives the PLL transfer magnitude function— $|H(s)|$. A typical test setup for this method is shown in Figure 11.25.

Figure 11.25. PLL transfer function measurement setup with a modulation signal generator as the stimulus.



To make the diagram less complex, we show only the measurement for the output. The measurement for the input is similar. The sinusoidal can be measured by a spectrum analyzer (SA) or time interval analyzer (TIA), or a sampling oscilloscope (SO) or real-time oscilloscope (RTO). In the case of an SO, a trigger signal is needed from the generator. This method is subject to the modulation signal generator capability, including resolution, modulation depth, and range. Most modulation generators today can go up to only 50 MHz. If a PLL 3 dB frequency is beyond this maximum frequency, this method cannot measure it.

User name: CSU San Diego

Book: Jitter, Noise, and Signal Integrity at High-Speed

Section: Chapter 11. Testing and Analysis for Jitter and Signaling Integrity for High-Speed Links

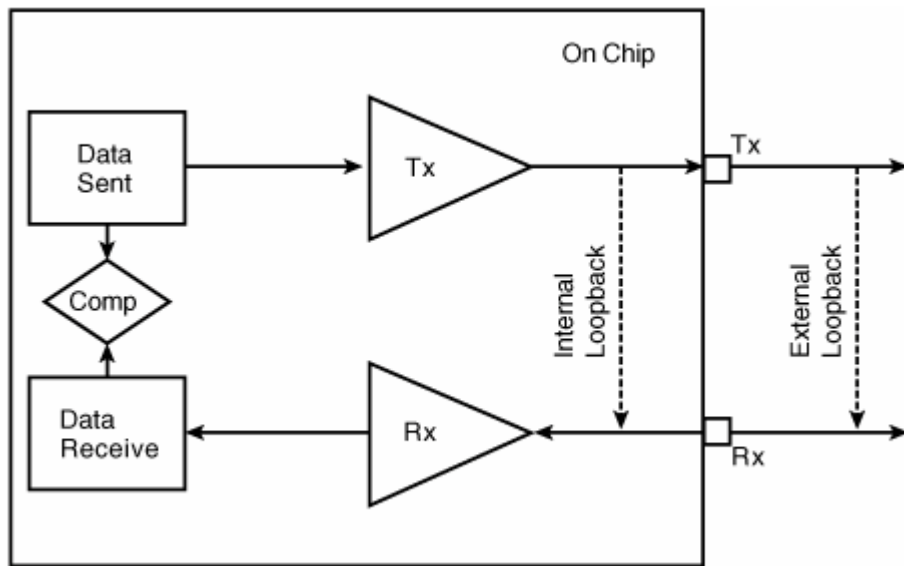
No part of any chapter or book may be reproduced or transmitted in any form by any means without the prior written permission for reprints and excerpts from the publisher of the book or chapter. Redistribution or other use that violates the fair use privilege under U.S. copyright laws (see 17 USC107) or that otherwise violates these Terms of Service is strictly prohibited. Violators will be prosecuted to the full extent of U.S. Federal and Massachusetts laws.

Information Theory Computer Science Mike Peng Li Prentice Hall Jitter, Noise, and Signal Integrity at High-Speed

11.7. Loopback Testing

We have introduced test methods for the link subsystems of transmitter, receiver, channel, reference clock, and PLL. These methods commonly use laboratory instruments to carry out the tests. A communication device, such as a serializer/deserializer (SERDES) chip, has both transmitter pins and receiver pins. Thus, an obvious way to test whether transmitter and receiver work together correctly is to connect the transmitter output to receiver input and check the logic bits sent and received. Such a method of connecting transmitter to receiver for testing is called a loopback test. A loopback test can be traced to the first telephone or telegraph communication system. Figure 11.26 shows the basic concept. Note that "Comp" represents the logical comparison between bits sent and received.

Figure 11.26. Block diagram of the basic concept of loopback testing.



Being easy to conduct and low cost (no external instruments are needed) are the major advantages of loopback tests. In recent years, the number of I/O pins on a complex system on chip (SOC) can be as high as 200, with the data rate in the range of multiple Gb/s. Testing all those I/Os in parallel for advanced SOCs is almost impossible for the laboratory instruments because of their limited number of channels (fewer than four is typical) and relatively high per-channel cost. Testing is also very challenging for automated test equipment (ATE) because of the signal integrity issues related to the test interfaces (such as loadboard and socket) and relatively high per-channel cost. Here the cost is relative to the simple, straightforward loopback. Thus, the loopback test method has its useful roles in testing complex SOCs with many multiple Gb/s I/Os. The loopback path can be either built into the chip or through external wires or cables.

Even though the loopback method offers simplicity and low cost, it has many limitations. First, it is a functional test, so it cannot test jitter or signal integrity without adding measurement circuits to the conventional SERDES devices. Second, when a loopback test

detects a failure, it cannot tell whether the failure comes from the transmitter, or the receiver, or both. In other words, loopback has very limited diagnostic test capability. Finally, a direct loopback test has limited fault coverage unless additional test circuits are built into the I/O circuits (such as design for test (DFT) or built-in self-test (BIST)) or added externally, as shown in [Figure 11.26](#).

Extra test circuits or resources are needed to overcome the limitations of the loopback test method. For example, with the jitter injection circuits, required jitter and spectrum can be injected at the loopback path, as shown in [Figure 11.26](#). Therefore, the worst-case test conditions can be created, and the fault coverage can be enhanced. In a second example, with the controllability and programmability built in for the receiver sampling time, voltage level, TJ, and TN at a given BER level can be measured. In a third example, by building in a known-good reference transmitter or receiver, a loopback test can be extended to test jitter and signal integrity for a transmitter or receiver. It is conceivable that loopback, together with DFT- and BIST-related circuits, can also provide comprehensive and high fault coverage test solutions, compared with the conventional off-chip and external test method and hardware. However, given the cost and complexity constraints for on-chip test circuits, it is likely that their accuracy will fall behind the laboratory instrument. Also, when all the DFT or BIST circuits needed are built into the I/O circuits, verifying that they are working correctly and accurately can be very challenging. The cost of the enhanced loopback with additional DFT and BIST circuits may not be significantly cheaper. Thus, when it comes to choosing an appropriate test method for testing a high-speed link and its subsystems, cost constraints and test objectives (such as design verification, characterization, diagnostics/debug, and high-volume production) should all be considered so that an optimal solution can be selected.

URL <http://access.proquest.safaribooksonline.com/9780132429610/ch11lev1sec7>

User name: CSU San Diego

Book: Jitter, Noise, and Signal Integrity at High-Speed

Section: Chapter 11. Testing and Analysis for Jitter and Signaling Integrity for High-Speed Links

No part of any chapter or book may be reproduced or transmitted in any form by any means without the prior written permission for reprints and excerpts from the publisher of the book or chapter. Redistribution or other use that violates the fair use privilege under U.S. copyright laws (see 17 USC107) or that otherwise violates these Terms of Service is strictly prohibited. Violators will be prosecuted to the full extent of U.S. Federal and Massachusetts laws.

Information Theory Computer Science Mike Peng Li Prentice Hall Jitter, Noise, and Signal Integrity at High-Speed

11.8. Summary

This chapter was dedicated to testing aspects of the serial link. It covered the link subsystem or component test for transmitter, channel, receiver, reference clock, and multiplication or clock recovery PLL, as well as link system test with loopback.

We started with the link signaling techniques that are critical for high-speed serial links—clock recovery and equalization. They are essential means to keep the overall link jitter in line with the UI decrease as the data rate keeps increasing. Meanwhile, they govern the testing requirements, and methodologies for high-speed links use those signaling techniques. We discussed the test requirements or implications in two signaling categories. The first is the link with clock recovery and is called nominal link signaling. The second is the link with both clock recovery and equalization; it is called advanced link signaling. The first reflects the link at data rates of about 1 Gb/s, and the second reflects the link at data rates of about 2.5 Gb/s and above, for copper-based channels. For a link with clock recovery, the key is the jitter transfer function (JTF), which must be used to build the reference receiver for transmitter and channel testing. JTF is also used to build the jitter mask for receiver clock recovery test. For a link with both clock recovery and equalization, the reference receiver must include both clock recovery and equalization functionalities. Transfer function for the equalization is developed similar to that for JTF for the clock recovery. Transfer functions for both clock recovery and equalization are then used to establish the testing implications for links with advanced signaling. Different implementations for transmitter equalization, receiver equalization, and combined transmitter and receiver equalization are discussed.

We then moved to the link subsystem. We started with the transmitter test because this is where the signal starts. Just as in the link signaling and test requirements section, we discussed the transmitter test methods for nominal link signaling and advanced signaling. For the nominal signaling, the measurement instrument must have the required clock recovery and associated JTF capability built in. The clock recovery can be implemented in hardware or software that is a unique feature for testing. For the advanced signaling, the measurement instrument must have the required equalization and clock recovery and associated JTF capabilities built in. The equalization and clock recovery can be implemented in the form of either hardware or software. Signal waveform, eye diagram, and BER need to be measured under the appropriate clock recovery and equalization conditions. We also discussed an alternative method to accommodating the transmitter equalization by splitting full-swing and de-emphasis bits and constructing two corresponding eye diagrams and using different eye masks derived from the equalization transfer function.

The signal from the transmitter goes to the channel, so we discussed channel testing. We introduced two channel testing methods: with channel stand-alone and channel with a reference transmitter. The stand-alone method used the S-parameter to quantify the channel characteristics. We also pointed out that the S-parameter can be converted to time-domain functions of impulse or step response functions using the LTI theorem and inverse Laplace transformation. A channel compliance test method based on the magnitude mask function for the S-parameter was introduced, and its limitation of ignoring phase information was discussed. The channel with a reference transmitter testing method measures the channel inputs and output waveform and derives the channel S-parameter in either the complex s-domain or time domain via LTI Laplace transformations.

The signal at the output of a channel goes to the receiver, so we discussed receiver testing for both nominal and advanced signaling scenarios. A generic receiver test setup and methodology were presented. We emphasized the three key aspects of receiver testing: amplitude/noise stressing, timing/jitter stressing, and spectral content stressing. The key subsystems to test in a receiver are clock recovery, equalization such as DFE, and data sampler. With each jitter or noise stressing, its components of deterministic, random, periodic, bounded, and uncorrelated aspects need to be considered for good test fault coverage. The spectral content for jitter or noise is another important test requirement for receiver testing, just as in the case of transmitter testing. Not only a specific jitter or noise component, but also a specific frequency range, needs to be generated. For the clock recovery test, jitter tolerance with a compliance mask as a function of frequency was introduced. We pointed out that the worst-case stress condition for a receiver test can have many causes due to many possible combinations between amplitude/noise, timing/jitter, and spectral stresses. Thus, to have good fault

coverage for receiver testing, the number of trials can be exhaustive. Last, we discussed a newly developed, but dearly needed, method to test for and determine the receiver internal intrinsic DJ and RJ. The end of the section introduced a complete set of jitter component tests for the link.

For a data-driven link architecture, all its subsystems of transmitter, channel, and receiver need to be tested. However, for the common clock link architecture, a new reference clock subsystem needs to be covered or added. We pointed out that the conventional jitter metrics for a reference clock such as period jitter or cycle-to-cycle jitter are no longer sufficient as a valid metric for testing reference clock within a common clock link architecture, such as those used in the PCI Express link. What is needed is the phase jitter within a certain frequency band, with the lower and higher 3 dB frequencies depending on the multiplication PLLs in the transmitter and receiver, respectively. The reference clock testing method introduced requires obtaining the phase jitter and then applying the requirement band-pass filter function in either the time or frequency domain in the second step. In the third step, time-domain phase jitter after the band-pass filter function is achieved and is used to construct the final jitter PDF, DJ, RJ, or rms calculation. The method can be implemented with software signal processing or hardware filter and delay circuits.

The band-pass filter function for testing the reference clock is derived from the system transfer functions of the two PLLs used in transmitter and receiver clock multiplications in common clock link architecture. The parameters of 3 dB frequency and peaking for those PLLs need to be tested and verified. Thus, we introduced PLL testing after reference clock testing. We introduced two PLL testing methods. The first was the newly developed, non-stimulus-based method. It measures the PLL output jitter autocorrelation or variance function and derives its system transfer function, as well as the associated 3 dB frequency and peaking, or damping factor and natural frequency. The second was the conventional, stimulus-based method that uses the sweeping sinusoidal at the PLL input and measures the corresponding at the PLL output. By calculating the magnitude ratio of output sinusoidal to input sinusoidal over a range of frequencies, the magnitude transfer function is determined. From that, the 3 dB frequency and peaking can be determined. The advantages and limitations of each method were discussed.

After finishing all the subsystem testing, we moved to loopback testing, a commonly used system test for communication links. We started by introducing the basic concept of loopback. We pointed out that even though loopback is simple, low-cost, and doesn't require external measurement instruments, it also has limitations. It can't test jitter and signal integrity, it can't separate the failure of transmitter from receiver, and it lacks good worst-case testing generation, and it has limited fault coverage. These are the major limitations of a simple loopback test method without adding extra testing circuits and resources. We discussed that although the limitations of the loopback testing method may be eased by adding circuits, the accuracy and cost may be the new concerns and remain challenging. In the end, when you choose a test method for a high-speed link and its components, test requirements, conditions, performance, cost, and coverage goals all need to be considered to derive a rational selection.

URL <http://access.proquest.safaribooksonline.com/9780132429610/ch11lev1sec8>

User name: CSU San Diego

Book: Jitter, Noise, and Signal Integrity at High-Speed

Section: Chapter 11. Testing and Analysis for Jitter and Signaling Integrity for High-Speed Links

No part of any chapter or book may be reproduced or transmitted in any form by any means without the prior written permission for reprints and excerpts from the publisher of the book or chapter. Redistribution or other use that violates the fair use privilege under U.S. copyright laws (see 17 USC107) or that otherwise violates these Terms of Service is strictly prohibited. Violators will be prosecuted to the full extent of U.S. Federal and Massachusetts laws.

Information Theory Computer Science Mike Peng Li Prentice Hall Jitter, Noise, and Signal Integrity at High-Speed

Endnotes

1. PCI Express 1.1 Base Specification, 2005, <http://www.pcisig.com/specifications/pciexpress/base>.
2. PCI Express 2.0 Base Specification, 2006, <http://www.pcisig.com/specifications/pciexpress/base>.
3. FB DIMM Link Signaling Specification, Rev. 0.8, JEDEC, 2005, <http://www.jedec.org/download/>.
4. Fibre Channel (FC) Standards, <http://www.t11.org/index.htm>.
5. M. Lin and K. T. Cheng, "Testable Design for Adaptive Linear Equalizer in High-Speed Serial Links," IEEE International Test Conference, 2006.
6. Serial ATA International Organization, Serial ATA Revision 2.5, 2005, <http://www.sata-io.org>.
7. Gigabit Ethernet (GBE) 802.3 Standard, <http://grouper.ieee.org/groups/802/3/>.
8. M. Li and J. Chen, "New Methods for Receiver Internal Jitter Measurements," IEEE International Test Conference, 2007.
9. M. Li, A. Martwick, G. Talbot, and J. Wilstrup, "Transfer Functions for the Reference Clock Jitter in a Serial Link: Theory and Applications," International Test Conference (ITC), 2004.
10. M. Li, "Jitter and Signaling Test for High-Speed Links," an invited paper, IEEE Customer Integrated Circuits Conference (CICC), 2006.
11. PCI Express Jitter and BER white paper (II), 2005, http://www.pcisig.com/specifications/pciexpress/technical_library.
12. R. E. Best, *Phase-Locked Loops: Design, Simulation, and Applications*, Fourth Edition, McGraw-Hill, 1999.

URL <http://access.proquest.safaribooksonline.com/9780132429610/ch11lev1sec9>

User name: CSU San Diego

Book: Jitter, Noise, and Signal Integrity at High-Speed

No part of any chapter or book may be reproduced or transmitted in any form by any means without the prior written permission for reprints and excerpts from the publisher of the book or chapter. Redistribution or other use that violates the fair use privilege under U.S. copyright laws (see 17 USC107) or that otherwise violates these Terms of Service is strictly prohibited. Violators will be prosecuted to the full extent of U.S. Federal and Massachusetts laws.

Information Theory Computer Science Mike Peng Li Prentice Hall Jitter, Noise, and Signal Integrity at High-Speed

12. Book Summary and Future Challenges

This short chapter reviews what you have learned about jitter, noise, and signal integrity, and what foreseen challenges are ahead of us as data rates keep increasing. We will start with the book summary, followed by the future challenges.

URL <http://access.proquest.safaribooksonline.com/9780132429610/ch12>

User name: CSU San Diego

Book: Jitter, Noise, and Signal Integrity at High-Speed

Section: Chapter 12. Book Summary and Future Challenges

No part of any chapter or book may be reproduced or transmitted in any form by any means without the prior written permission for reprints and excerpts from the publisher of the book or chapter. Redistribution or other use that violates the fair use privilege under U.S. copyright laws (see 17 USC107) or that otherwise violates these Terms of Service is strictly prohibited. Violators will be prosecuted to the full extent of U.S. Federal and Massachusetts laws.

Information Theory Computer Science Mike Peng Li Prentice Hall Jitter, Noise, and Signal Integrity at High-Speed

12.1. Book Summary

Now that you have read all the chapters, the architecture and logical flow of the book have become obvious. [Chapter 1](#) was a high-level overview of the fundamentals of jitter, noise, and signal integrity. It introduced basic concepts of jitter and noise source, jitter and noise separation into deterministic and random components at the first layer, and components at the second and third layers of the jitter or noise component tree. Then we discussed jitter, noise, and signal integrity from the perspectives of statistics, link system, and historical evolution and advancement.

Because jitter and noise are statistical signals, some fundamental statistics and signal theory are required to give quantitative and rigorous descriptions of and estimations for them. As such, [Chapter 2](#) was dedicated to two major math topics that are essential for jitter, noise, and signal integrity: statistical signaling and linear system theory. The statistical signaling portion discussed random signaling process, sampling, estimator, and spectral analysis. The linear system portion covered linear time-invariant (LTI), statistical estimation, and spectral analysis within an LTI. The first portion set the stage for the advanced jitter, noise, and signal integrity discussion. The second portion provided a foundation for a quantitative handling of jitter, noise, and signal integrity within a link system.

Equipped with the basic jitter and noise concepts and definitions, as well as the necessary statistical signaling and LTI theory, [Chapter 3](#) discussed all the jitter components quantitatively in terms of their probability distribution function (PDF) and power-spectral density (PSD). Deterministic components caused by duty cycle distortion (DCD), intersymbol interference (ISI), and crosstalk, and random components caused by Gaussian and high-order $1/f^{\alpha}$ noise, were covered for jitter and noise. In the end, the relationship between component PDF and total PDF was given via convolution operation, assuming that all the component PDFs are independent, a reasonable assumption in practice.

Having learned the PDFs and PSDs for all the jitter and noise components, [Chapter 4](#) moved on to build the comprehension and complex method to handle jitter, noise, and bit error rate (BER) cumulative distribution function (CDF) in multiple dimensions. The relationships between jitter, noise, and BER were discussed in terms of joint PDF, eye diagram, and BER CDF contour. The two-dimensional treatment for jitter, noise, and BER provided the necessary comprehension and accuracy for their quantification and estimation.

[Chapters 3](#) and [4](#) covered jitter, noise, and BER in a "bottom-up" or "forwarding" approach. We started from the component PDFs and tried to find a way to estimate the total PDF when all the components are present. Or we started from jitter and noise PDFs and tried to find a way to estimate the BER CDF contour or eye diagram contour when both effects are considered or included. This is opposed to when only one is considered or included, as in most of the analyses found in the literature. This bottom-up or forwarding approach is commonly used or encountered in modeling and simulations for jitter, noise, and BER where the physical properties for jitter and signal components are known or assumed ahead of time. You can calculate or estimate the overall total PDF or BER CDF in one or multiple dimensions based on the governing math or models. Conversely, jitter, noise, and BER can be handled through a "top-down" or "backward" approach. We start from total PDF and try to determine component PDFs. Or we start from a BER contour or eye diagram contour and tried to find a way to estimate component PDF for both jitter and noise at the same time. The top-down approach is more relevant to jitter and noise measurement or testing in which both total PDF and CDF, as well as component PDFs, need to be measured and determined. The initial state of the top-down approach is "high entropy," in which all the information is mixed and integrated and we try to separate it. This is relatively hard compared to the bottom-up approach, because some information may be lost in a high-entropy state. Because of these considerations, [Chapters 5](#) and [6](#) were dedicated to various jitter and noise separation methods.

[Chapter 5](#) focused on jitter separation based on either its corresponding total PDF or BER CDF. Most of the discussions concerned jitter, but they can be applied to noise component separation in a similar way. The widely accepted tailfit method was discussed in detail, supported by simulation results. The starting distribution function for the tailfit was based on either jitter PDF or CDF. The key signatures that make jitter separation possible in the statistical domain are that random jitter PDF is Gaussian and deterministic jitter is

bounded. In the CDF domain, this means that the CDF for random jitter is an integrated Gaussian or a well-defined error function. Although the simple "tailfit" method gives RJ random jitter (RJ) PDF and its corresponding sigma value, it gives only the DJ peak-to-peak (pk-pk) value. Thus, a deconvolution method was developed in [Chapter 5](#) to determine the DJ PDF in addition to the DJ pk-pk from tailfit. Thus, a complete solution to determine DJ and RJ PDFs was provided in [Chapter 5](#). We pointed out the limitations of any statistical-domain-based jitter separation method. For example, it is hard to determine second- or third-layer jitter components such as data-dependent jitter (DDJ), duty cycle distortion (DCD) jitter, intersymbol interference (ISI) jitter, and periodic jitter (PJ) in general from a total jitter PDF or CDF.

[Chapter 6](#) discussed jitter separation in both the time and frequency domains. Multiple jitter separation methods were introduced for each jitter component. For DDJ, DCD, and ISI, separation methods based on jitter real-time record or jitter spectrum were discussed. For PJ, RJ, and crosstalk or bounded uncorrelated jitter (BUJ) separation, three different methods based on jitter time variance function, jitter spectrum, and jitter PSD were presented. The recent emerging jitter component of pulse width shrinkage (PWS) was introduced, and its relationship to DCD and ISI was discussed. The different jitter separation methods were compared and summarized, along with their advantages and limitations. If you know the lower-layer jitter components, higher-layer jitter components can be readily estimated. Thus, DJ, RJ, and TJ can be estimated with the knowledge of lower-layer jitter components using the methods introduced in [Chapter 6](#).

After [Chapter 6](#), basic jitter, noise, signal integrity theorems, and newly developed analysis theorem and algorithms were introduced and were ready to be applied to solve practical problems. There are two types of applications in which jitter, noise, and signal integrity are critical: clock signal and data signal. A clock signal is commonly associated with a clock generator such as a phase-locked loop (PLL). A data signal typically is involved in a high-speed link that is composed of a data transmitter, channel, and data receiver. Therefore, we dedicated [Chapter 7](#) to clock jitter and [Chapter 8](#) to PLL jitter and transfer function analysis. PLL is related to clock jitter, as well as data jitter, because it is widely used in the transmitter and receiver for high-speed links. After clock jitter and PLL analysis, we moved to advanced topics of link jitter, noise, and BER. We started with jitter, noise, and signal integrity mechanisms within a link in [Chapter 9](#), followed by jitter, noise, and signal integrity modeling in [Chapter 10](#). Then jitter, noise, and signal integrity testing were covered in [Chapter 11](#) to give complete coverage, from the physical mechanism, to modeling and simulation, and then to testing and validation. So the flow of the book from basic theory to newly developed algorithms, and then to nominal applications and advanced applications, is logical and clear.

[Chapter 7](#) started with the definition of clock jitter and its role and impact on synchronous and asynchronous systems. We pointed out that jitter accumulates longer in an asynchronous system than in a synchronous system. Accordingly, we discussed three different jitter types—phase jitter, period jitter, and cycle-to-cycle jitter—covering the basic definition, mathematical representation, and interrelationship between them in both the time and frequency domains, and their usage models. Phase jitter accumulates long and is applicable to asynchronous systems such as serial link systems. Period jitter over one period is applicable to synchronous systems such as synchronous global parallel input/output (I/O) bus link systems. Last, because phase jitter and phase noise are closely related metrics and are widely used in the digital domain and radio-frequency (RF) domain, respectively, we discussed their interrelationships and mapping functions from one metric to another and vice versa.

After clock jitter, [Chapter 8](#) moved to PLL and its associated jitter. The focus here was on PLL characteristics and its linkage to jitter performance. We started with basic PLL modeling and analysis in both the time and frequency domains. The PLL functional analysis covered various transfer functions and parametric analyses for tracking and acquisition parameters. With basic knowledge of a PLL system, as well as related modeling and analysis theorems and algorithms, we moved to PLL jitter modeling and analysis, which require both PLL and jitter fundamentals. PSD or variance is the function that links the PLL and jitter characteristics. A relationship between jitter PSD at the PLL output and input was described. A novel algorithm that lets you determine PLL characteristic functions and internal PSDs was developed from analyzing and modeling its output jitter PSD. Equipped with the PLL and jitter modeling and analysis theorems and novel algorithms, we applied them to commonly encountered PLLs of the second and third order. A complete analysis and test for each type of PLL covering functional, parametric, and jitter PSD were presented in detail.

With knowledge of clock jitter, PLL, and its jitter modeling and analysis, we moved to discussing jitter, noise, and signal integrity in high-speed serial links, an advanced and more complex topic.

We dedicated [Chapter 9](#) to the jitter, noise, and signal integrity mechanisms and root sources for high-speed link systems. We started with two leading link architectures of data-driven and common clock and their corresponding working mechanisms. Then we zoomed in on architecture, jitter, noise, and signal integrity physical mechanisms for the subsystems of transmitter, receiver, channel, and reference clock. For the transmitter, the major jitter source of reference clock jitter and voltage driver noise were discussed. For the receiver, jitter from the clock recovery circuit and data sampler was the major focus. For the channel, various losses in both copper and optical-based channels were covered. For the reference clock, jitter due to PLL or crystal oscillator, as well as spread-spectrum clocking (SSC), were presented. In the end, we discussed the link jitter budget method using the RJ root-sum-square (RSS) method to ensure the link's interoperability and overall BER performance.

With the architectures for the entire link system and the subsystems, as well as the producing physical mechanisms for jitter, noise, and signal integrity, we were ready to discuss quantitative modeling and analysis in [Chapter 10](#). Jitter, noise, and signaling modeling and analysis methods were presented for link subsystems of transmitter, receiver, and channel within the framework of LTI system theory. Using the cascading property of the LTI theorem, signal, jitter, and noise at the channel and receiver outputs are readily obtainable given the transmitter output/channel input and the channel and receiver transfer functions. Important subsystems of equalization and clock recovery (CR) were included in the modeling. For the equalization, both transmitter and receiver equalizations were considered. The modeling and analysis methods introduced in this chapter can give estimations for most of today's advanced serial links, and they are scalable to future link advancements and generations because they are LTI-based.

After covering the link modeling and analysis theorem and method, we moved to the test and validation aspects for high-speed links in [Chapter 11](#). We started with the test implications and requirements from the link architectures and topologies operating mechanisms, with a focus on clock recovery and equalization. We divided link signaling into two classes: nominal with clock recovery only, and advanced with both clock recovery and equalization. We presented testing requirements and methods accordingly. Transmitter and receiver testing methods for both nominal and advanced link signaling were covered, along with stand-alone channel, reference clock, and PLL test methods. Last, system test methods such as loopback testing were discussed. Complete testing coverage for both link system and subsystem were presented.

URL <http://access.proquest.safaribooksonline.com/9780132429610/ch12lev1sec1>

User name: CSU San Diego

Book: Jitter, Noise, and Signal Integrity at High-Speed

Section: Chapter 12. Book Summary and Future Challenges

No part of any chapter or book may be reproduced or transmitted in any form by any means without the prior written permission for reprints and excerpts from the publisher of the book or chapter. Redistribution or other use that violates the fair use privilege under U.S. copyright laws (see 17 USC107) or that otherwise violates these Terms of Service is strictly prohibited. Violators will be prosecuted to the full extent of U.S. Federal and Massachusetts laws.

Information Theory Computer Science Mike Peng Li Prentice Hall Jitter, Noise, and Signal Integrity at High-Speed

12.2. Future Challenges

This book has presented both fundamental and up-to-date theorems for jitter, noise, and signaling integrity. However, the subject that we aimed at is a moving target. Data rates will only get faster, and the jitter, noise, and signal integrity challenges will only get more challenging.^[1]

We will talk about the challenges of data rate increases while maintaining cost effectiveness. The challenges will be discussed from the perspectives of fundamental theorems, link architecture/topology, modeling and analysis methods, and testing and validation methods.

The fundamental theorems and analysis methodologies for jitter, noise, and signal integrity that we have presented in this book will continue to hold as we move to higher data rates, but they may be insufficient. Today's jitter or noise separation methods are all based on stationary statistics. The current methods of separating jitter into DJ and RJ solely based on bounded or unbounded jitter distribution may not be comprehensive enough for the future. For example, crosstalk or electromagnetic interference (EMI)-induced jitter is likely to be nondeterministic, nonstationary, and nonrepeating. New methods to separate jitter into this new category will provide better precision and comprehension for jitter separation. Furthermore, today's jitter separation is largely based on jitter signal properties, rather than jitter root causes or physical properties. For diagnostic or debugging purposes, it will be better to develop jitter or noise separation methods based on the root causes or physical properties so that we can quantify how much jitter is caused by crosstalk, EMI, reflection, thermal noise, 1/f noise, and so on.

On the link architecture side, new developments are expected because most of the advances will be in integrated circuits, leaving channel materials unchanged for some time to maintain the overall low link cost. Moreover, low cost implies that relatively noisy or jittery components will be used for the link transmitter, receiver, and reference clock. Meanwhile, the same or a better BER performance metric still needs to be maintained. To resolve the conflict between cost and performance requirements, new and (most likely) complex architectures are expected to be developed. These new architectures for higher data rates will have a common goal—to reduce the jitter seen at the receiver data sampling point. The common clock architecture is one example. Another is the forwarding clock architecture considered by JEDEC for its FB DIMM II.^[2] Although the exact implementation or topology can differ, any successful architecture should be able to maintain the phase correlation between data and clock at the receiver so that their phase difference is kept to a minimum. At the subsystem level, equalization will continue to play an important role in reducing the receiver eye closure due to the lossy channel. Advanced equalizations at the transmitter, receiver, or both are expected. However, complexity and the order of the equalization filter will likely be constrained by power consumption and testability difficulties. With the new link architecture, equalization, and clocking scheme, new modeling and test requirements will be imposed.

On the jitter, noise, and signal integrity modeling and analysis side, new methods will need to be able to accommodate the new requirements imposed by the new link architectures and subsystem advancements. However, to provide better accuracy and comprehension, fully digital, per-edge-based modeling methods are needed to quantify the nonlinear subsystems such as digital clock recovery and digital DFE equalization. Also, most link models today are system-level behavior models, in which jitter and noise properties are assumed rather than directly drawn from circuit simulation. A tight coupling between the link system-level behavior model and the subsystem circuit physical model is needed to provide better accuracy and consistency. Furthermore, to cover worst-case link signaling, Monte Carlo methods will need to be used.

Testing and validation methods will continue to progress according to link system and subsystem advancements. The reference transmitter and receiver for testing and validation will become even more complicated than what we have defined today, manifesting in ever-increasing complexity in transmitter and receiver circuits. With the forwarding clock architecture, receiver input and tolerance testing will become two-port rather than the conventional one-port. At higher data rates, the effects of test interface, such as test fixture, socket, or load-load, cannot be ignored and need to be removed, de-embedded, or compensated for from the test results to maintain the accuracy and test margin. As data rates keep increasing, the total available jitter budget for the link 1 unit interval (UI) will continue to

decrease. Guarantee by design can be very challenging given the process variation and its impact on jitter-sensitive parameters, such as peaking and 3 dB frequency for PLLs used in the link. This will lead to the need for some sort of high-volume production (HVM) testing to cover jitter, noise, and signal integrity to ensure a good manufacturing yield. The requirements for and goals of HVM testing differ from the design verification and compliance tests. Also, the methods developed for design verification may be too expensive, too good, or too slow for HVM testing. Testing may be distributed to both on-chip and off-chip to achieve the best optimization for the overall cost, throughput, test coverage, and yield. The accuracy of the test equipment will get even better, with jitter noise flow within the sub-picosecond range for a 10 Gbps.^[3]

We would like to point out that we have discussed only some of the challenges—not all of them. Although we intended to cover most of the major challenges, our view is subjective. In any case, it is generally believed that jitter, noise, and signal integrity is an evolving subject. There will be ample space for new theorems, algorithms, and methodologies to be invented and developed as data rates, link architectures, and subsystem circuits keep increasing or advancing.

URL <http://access.proquest.safaribooksonline.com/9780132429610/ch12lev1sec2>

User name: CSU San Diego

Book: Jitter, Noise, and Signal Integrity at High-Speed

Section: Chapter 12. Book Summary and Future Challenges

No part of any chapter or book may be reproduced or transmitted in any form by any means without the prior written permission for reprints and excerpts from the publisher of the book or chapter. Redistribution or other use that violates the fair use privilege under U.S. copyright laws (see 17 USC107) or that otherwise violates these Terms of Service is strictly prohibited. Violators will be prosecuted to the full extent of U.S. Federal and Massachusetts laws.

Information Theory Computer Science Mike Peng Li Prentice Hall Jitter, Noise, and Signal Integrity at High-Speed

Endnotes

1. International Technology Roadmap for Semiconductors (ITRS) reports, 2007 revision, <http://www.itrs.net/>.
2. FB DIMM II Link Signaling Specification, draft, JEDEC, 2006.
3. M. Li, "Multiple GHz and Gb/s ICs Testing Challenges and Solutions from Design to Production," Proceedings of the 4th International Conference on Semiconductor Technology, Semicon China, 2005.

URL <http://access.proquest.safaribooksonline.com/9780132429610/ch12lev1sec3>

User name: CSU San Diego

Book: Jitter, Noise, and Signal Integrity at High-Speed

No part of any chapter or book may be reproduced or transmitted in any form by any means without the prior written permission for reprints and excerpts from the publisher of the book or chapter. Redistribution or other use that violates the fair use privilege under U.S. copyright laws (see 17 USC107) or that otherwise violates these Terms of Service is strictly prohibited. Violators will be prosecuted to the full extent of U.S. Federal and Massachusetts laws.

Index

[[SYMBOL](#)] [[A](#)] [[B](#)] [[C](#)] [[D](#)] [[E](#)] [[F](#)] [[G](#)] [[H](#)] [[I](#)] [[J](#)] [[K](#)] [[L](#)] [[M](#)] [[N](#)] [[O](#)] [[P](#)] [[Q](#)] [[R](#)] [[S](#)] [[T](#)] [[U](#)] [[V](#)] [[W](#)] [[X](#)] [[Z](#)]

2-D (two-dimensional) Gaussian distribution

3-D BER function

URL <http://access.proquest.safaribooksonline.com/9780132429610/Index>

User name: CSU San Diego

Book: Jitter, Noise, and Signal Integrity at High-Speed

No part of any chapter or book may be reproduced or transmitted in any form by any means without the prior written permission for reprints and excerpts from the publisher of the book or chapter. Redistribution or other use that violates the fair use privilege under U.S. copyright laws (see 17 USC107) or that otherwise violates these Terms of Service is strictly prohibited. Violators will be prosecuted to the full extent of U.S. Federal and Massachusetts laws.

Index

[SYMBOL] [A] [B] [C] [D] [E] [F] [G] [H] [I] [J] [K] [L] [M] [N] [O] [P] [Q] [R] [S] [T] [U] [V] [W] [X] [Z]

advanced link signaling, receiver testing

advanced serial link signaling, transmitter testing

AM (amplitude modulation)

amplitude deviation

amplitude modulation (AM)

for receiver driver voltage noise, LTI

for receiver reference voltage noise, LTI

amplitude noise [See also [noise](#).]

amplitude noise PDF

convolution

eye diagrams

arbitrary DJ PDF, deconvolution simulations

architecture

clock recovery architecture

link system architecture

channel

channel material and characteristics

jitter budget

performance factors

subsystem architecture

reference clock

transmitter

associative property, LTI properties

asynchronized systems, clock jitter

autocorrelation function, statistical estimators for LTI systems

averaged PWS and DDJ

averages, statistical estimates

URL <http://access.proquest.safaribooksonline.com/9780132429610/index>

User name: CSU San Diego

Book: Jitter, Noise, and Signal Integrity at High-Speed

No part of any chapter or book may be reproduced or transmitted in any form by any means without the prior written permission for reprints and excerpts from the publisher of the book or chapter. Redistribution or other use that violates the fair use privilege under U.S. copyright laws (see 17 USC107) or that otherwise violates these Terms of Service is strictly prohibited. Violators will be prosecuted to the full extent of U.S. Federal and Massachusetts laws.

Index

[SYMBOL] [A] [B] [C] [D] [E] [F] [G] [H] [I] [J] [K] [L] [M] [N] [O] [P] [Q] [R] [S] [T] [U] [V] [W] [X] [Z]

band-pass filter function

BER (bit error rate)

historical overview of

jitter and 2nd

noise and 2nd

TJ, comparing

BER CDF

DJ variation error

jitter separation

DJ PDF estimation

tailfit method

TJ estimation

straightforward dual-Dirac method

variation given DJ PDFs

bit error mechanisms

bit error rate

historical overview of

jitter and 2nd

noise and 2nd

TJ, comparing

bit errors

bode plots, PLLs

bounded uncorrelated jitter (BUJ) 2nd

PDF

spectrum

budgets, jitter budget (link systems)

BUJ (bounded uncorrelated jitter) 2nd

PDF

spectrum

BUJ separation

Fourier spectrum

PSD

time-domain variance function

URL <http://access.proquest.safaribooksonline.com/9780132429610/index>

User name: CSU San Diego

Book: Jitter, Noise, and Signal Integrity at High-Speed

No part of any chapter or book may be reproduced or transmitted in any form by any means without the prior written permission for reprints and excerpts from the publisher of the book or chapter. Redistribution or other use that violates the fair use privilege under U.S. copyright laws (see 17 USC107) or that otherwise violates these Terms of Service is strictly prohibited. Violators will be prosecuted to the full extent of U.S. Federal and Massachusetts laws.

Index

[SYMBOL] [A] [B] [C] [D] [E] [F] [G] [H] [I] [J] [K] [L] [M] [N] [O] [P] [Q] [R] [S] [T] [U] [V] [W] [X] [Z]

cascading property, LTI properties

Cauchy-Schwartz inequality

CD (chromatic dispersion)

CDF (Cumulative Distribution Function), distribution

independent variables

multidimensional CDF

random variables

statistical random processes

central limiting theory

challenges, future challenges

channel

LTI

channel LTI modeling

channel transfer functions

generic channel models

testing

reference transmitters

s-parameter-based channel testing

channel (link system architecture)

channel material and characteristics

copper-based channels

crosstalk

optical fiber-based channels

reflection

channel LTI modeling

channel transfer functions, LTI

impulse responses

s-parameters

unit step responses

characteristic parameters

second-order PLL analysis

third-order PLL analysis

characteristics

channel characteristics

copper-based channels

crosstalk

optical fiber-based channels

reflection

characterization, jitter

Chebyshev Inequality, statistical estimates

chromatic dispersion, optical fiber-based channels

chromatic dispersion (CD)

clock jitter

asynchronous systems

defined

synchronized systems

clock recovery (CR)

JTF (Jitter Transfer Function)

clock recovery architecture

clock recovery circuit (CRC)

communication systems

commutative property, TI properties

comparing

conventional PLL analysis methods

time and frequency domain jitter separation methods

components

jitter

noise

conditional probability, random variables

continuous variables

convergence

of estimator

sampling and estimation

conversion

phase jitter to phase noise

phase noise to phase jitter

convolution

amplitude noise PDFs

for jitter PDFs

copper-based channels

dielectric loss

skin effect

copper-based communication

copper-based crosstalk

correlation, statistical estimates

CR (clock recovery)

CRC (clock recovery circuit)

cross-phase modulation (XPM)

crosstalk

channels

electrical crosstalk

optical crosstalk

copper-based crosstalk

fiber-based crosstalk

cycle-to-cycle jitter

interrelationships

frequency domain

time domain

URL <http://access.proquest.safaribooksonline.com/9780132429610/index>

User name: CSU San Diego

Book: Jitter, Noise, and Signal Integrity at High-Speed

No part of any chapter or book may be reproduced or transmitted in any form by any means without the prior written permission for reprints and excerpts from the publisher of the book or chapter. Redistribution or other use that violates the fair use privilege under U.S. copyright laws (see 17 USC107) or that otherwise violates these Terms of Service is strictly prohibited. Violators will be prosecuted to the full extent of U.S. Federal and Massachusetts laws.

Index

[SYMBOL] [A] [B] [C] [D] [E] [F] [G] [H] [I] [J] [K] [L] [M] [N] [O] [P] [Q] [R] [S] [T] [U] [V] [W] [X] [Z]

data-dependent jitter (DDJ) 2nd

averaged PWS and
DCD (duty cycle distortion)
estimation for RC LTI systems
model for
simulations

DCD (duty cycle distortion)

DDJ separation

DCD (duty cycle distortion) jitter, DDJ (data-dependent jitter)

DDJ (data-dependent jitter) 2nd

averaged PWS and
DCD (duty cycle distortion)
estimation for RC LTI systems
model for
simulations

DDJ separation

DCD and ISI separation
Fourier spectrum
jitter time function

debugging jitter

decision feedback equalizations (DFEs) 2nd

deconvolution

DJ PDF determination
jitter separation PDFs
simulations
arbitrary DJ PDF
triangular DJ PDF
theory

deterministic jitter (DJ) 2nd

DDJ (data-dependent jitter)
DCD (duty cycle distortion)
estimation for RC LTI systems
model for
simulations 2nd
variation error, BER CDF

deterministic noise (DN)

device under test (DUT)

DFEs (decision feedback equalizations) 2nd

DFT (Discrete Fourier Transformation)
diagnostics, jitter
dielectric loss, copper-based channels
direct FT spectrum, jitter as a function of frequency
direct observables, jitter separation
Discrete Fourier Transformation (DFT)
discrete variables
distribution, random variables
 CDF (Cumulative Distribution Function)
 CDF versus PDF
 multidimensional PDF (Probability Density Function)
 PDF (Probability Density Function) 2nd
distributive property, LTI properties
DJ (deterministic jitter) 2nd
 DDJ (data-dependent jitter)
 DCD (duty cycle distortion)
 estimation for RC LTI systems
 model for
 simulations
 variation error, BER CDF
DJ model, straightforward dual-Dirac method 2nd
DN (deterministic noise)
Domains, statistical domains (jitter separation)
DUT (device under test)
duty cycle distortion (DCD)
duty cycle distortion (DCD) jitter

URL <http://access.proquest.safaribooksonline.com/9780132429610/index>

User name: CSU San Diego

Book: Jitter, Noise, and Signal Integrity at High-Speed

No part of any chapter or book may be reproduced or transmitted in any form by any means without the prior written permission for reprints and excerpts from the publisher of the book or chapter. Redistribution or other use that violates the fair use privilege under U.S. copyright laws (see 17 USC107) or that otherwise violates these Terms of Service is strictly prohibited. Violators will be prosecuted to the full extent of U.S. Federal and Massachusetts laws.

Index

[SYMBOL] [A] [B] [C] [D] [E] [F] [G] [H] [I] [J] [K] [L] [M] [N] [O] [P] [Q] [R] [S] [T] [U] [V] [W] [X] [Z]

electrical crosstalk, channels

electrical reflection, channels

EMI (electromagnetic interference)

reducing in reference clock

ergodic random processes

estimating jitter energy within certain frequency bands

estimation

central limiting theory

peak-to-peak estimations

PWS

sample estimators and convergence

estimator, convergence of

expectation, statistical estimates

eye diagrams

amplitude noise PDFs

for jitter PDFs

URL <http://access.proquest.safaribooksonline.com/9780132429610/Index>

User name: CSU San Diego

Book: Jitter, Noise, and Signal Integrity at High-Speed

No part of any chapter or book may be reproduced or transmitted in any form by any means without the prior written permission for reprints and excerpts from the publisher of the book or chapter. Redistribution or other use that violates the fair use privilege under U.S. copyright laws (see 17 USC107) or that otherwise violates these Terms of Service is strictly prohibited. Violators will be prosecuted to the full extent of U.S. Federal and Massachusetts laws.

Index

[SYMBOL] [A] [B] [C] [D] [E] [F] [G] [H] [I] [J] [K] [L] [M] [N] [O] [P] [Q] [R] [S] [T] [U] [V] [W] [X] [Z]

f⁻² jitter

PSD

FEXT

fiber-based communication

fiber-based crosstalk

filter coefficients

first-order analytical model, generic channel models

flick noise

FM (frequency modulation)

four-wave mixing (FWM)

Fourier spectrum

DDJ separation

PJ, RJ, and BUJ separation

Fourier Transformation (FT)

frequency, time-frequency domain jitter separation

jitter as a function of frequency

direct FT spectrum

jitter PSD

jitter as a function of time

frequency domain, interrelationships (cycle-to-cycle jitter)

frequency-domain analysis, LTI systems

frequency-domain modeling, PLLs

frequency-domain PSD-based methodology, third-order PLL analysis

frequency modulation (FM)

FT (Fourier Transformation)

functional analysis, PLLs

bode plots

impulse/step responses

phase and magnitude responses

poles and zeros

future challenges

FWM (four-wave mixing)

URL <http://access.proquest.safaribooksonline.com/9780132429610/index>

User name: CSU San Diego

Book: Jitter, Noise, and Signal Integrity at High-Speed

No part of any chapter or book may be reproduced or transmitted in any form by any means without the prior written permission for reprints and excerpts from the publisher of the book or chapter. Redistribution or other use that violates the fair use privilege under U.S. copyright laws (see 17 USC107) or that otherwise violates these Terms of Service is strictly prohibited. Violators will be prosecuted to the full extent of U.S. Federal and Massachusetts laws.

Index

[SYMBOL] [A] [B] [C] [D] [E] [F] [G] [H] [I] [J] [K] [L] [M] [N] [O] [P] [Q] [R] [S] [T] [U] [V] [W] [X] [Z]

Gaussian distribution

Gaussian jitter

PDF

PSD

generic channel models

first-order analytical model

second-order analytical model

generic two-dimensional PDFs

GM (multiple Gaussian)

URL <http://access.proquest.safaribooksonline.com/9780132429610/index>

User name: CSU San Diego

Book: Jitter, Noise, and Signal Integrity at High-Speed

No part of any chapter or book may be reproduced or transmitted in any form by any means without the prior written permission for reprints and excerpts from the publisher of the book or chapter. Redistribution or other use that violates the fair use privilege under U.S. copyright laws (see 17 USC107) or that otherwise violates these Terms of Service is strictly prohibited. Violators will be prosecuted to the full extent of U.S. Federal and Massachusetts laws.

Index

[SYMBOL] [A] [B] [C] [D] [E] [F] [G] [H] [I] [J] [K] [L] [M] [N] [O] [P] [Q] [R] [S] [T] [U] [V] [W] [X] [Z]

higher-order jitter processes, f^{-2}

PDF

PSD

historical overview of jitter, noise, BER and signal integrity

URL <http://access.proquest.safaribooksonline.com/9780132429610/index>

User name: CSU San Diego

Book: Jitter, Noise, and Signal Integrity at High-Speed

No part of any chapter or book may be reproduced or transmitted in any form by any means without the prior written permission for reprints and excerpts from the publisher of the book or chapter. Redistribution or other use that violates the fair use privilege under U.S. copyright laws (see 17 USC107) or that otherwise violates these Terms of Service is strictly prohibited. Violators will be prosecuted to the full extent of U.S. Federal and Massachusetts laws.

Index

[SYMBOL] [A] [B] [C] [D] [E] [F] [G] [H] [I] [J] [K] [L] [M] [N] [O] [P] [Q] [R] [S] [T] [U] [V] [W] [X] [Z]

IC (integrated circuit)

IFT (inverse Fourier Transformation)

implementation algorithm

total jitter PDF

tail PDF identification

tailfitting

impulse responses, channel transfer functions

LTI

PLLs

independent variables

CDF

PDF

integrated circuit (IC)

internal jitter testing, receiver testing

interrelationships

cycle-to-cycle jitter

frequency domain

time domain

intersymbol interference (ISI) 2nd

intrinsic jitter

intrinsic noise

flick noise

shot noise

thermal noise

inverse FT (IFT)

ISI (intersymbol interference) 2nd

ISI separation, DDJ separation

URL <http://access.proquest.safaribooksonline.com/9780132429610/index>

User name: CSU San Diego

Book: Jitter, Noise, and Signal Integrity at High-Speed

No part of any chapter or book may be reproduced or transmitted in any form by any means without the prior written permission for reprints and excerpts from the publisher of the book or chapter. Redistribution or other use that violates the fair use privilege under U.S. copyright laws (see 17 USC107) or that otherwise violates these Terms of Service is strictly prohibited. Violators will be prosecuted to the full extent of U.S. Federal and Massachusetts laws.

Index

[SYMBOL] [A] [B] [C] [D] [E] [F] [G] [H] [I] [J] [K] [L] [M] [N] [O] [P] [Q] [R] [S] [T] [U] [V] [W] [X] [Z]

jitter

BER and 2nd

BUJ [See **BUJ (bounded uncorrelated jitter)**.]

clock jitter

asynchronized systems

defined

synchronized systems

components

cycle-to-cycle jitter

interrelationships

DCD (duty cycle distortion)

DJ (deterministic jitter)

DDJ (data-dependent jitter)

Gaussian jitter

historical overview of

PDF

PSD

overall jitter PDFs

convolution for

eye diagrams

PDF

periodic jitter 2nd

phase jitter

PJ [See **PJ (periodic jitter)**.]

PLLs

phase jitter PSD

variance and PSD

PSD

RJ (random jitter) 2nd

f⁻² jitter

Gaussian jitter

PDF

PSD

second-order PLL analysis 2nd

sources of

intrinsic jitter

nonintrinsic jitter

transfer function in serial data communication

translation from noise

jitter and transfer function analysis, third-order PLL analysis

jitter budget, link systems

jitter energy, estimating within certain frequency bands

jitter PDF

- convolution for
- eye diagrams

jitter PSD, jitter as a function of frequency

jitter separation

- BER CDF
- DJ PDF estimation
 - tailfit method* 2nd
 - TJ estimation*
- direct observables
 - PDFs*
- DJ PDF determination through deconvolution
- tailfit method
 - BER CDF*
 - Monte Carlo simulations*
 - PDF with statistical noise*
 - results*
 - theory for total jitter PDF*
 - "transformed" BER CDF
- statistical domain
- straightforward dual-Dirac method
 - accuracy* 2nd
 - BER CDF*
 - total jitter PDF*

time-frequency domain jitter separation [See [time-frequency domain jitter separation](#).]

"transformed" BER CDF

- tailfit method* 2nd

jitter time function, DDJ separation

joint probability, random variables

JTF (Jitter Transfer Function)

- clock recovery
- link testing

URL <http://access.proquest.safaribooksonline.com/9780132429610/index>

User name: CSU San Diego

Book: Jitter, Noise, and Signal Integrity at High-Speed

No part of any chapter or book may be reproduced or transmitted in any form by any means without the prior written permission for reprints and excerpts from the publisher of the book or chapter. Redistribution or other use that violates the fair use privilege under U.S. copyright laws (see 17 USC107) or that otherwise violates these Terms of Service is strictly prohibited. Violators will be prosecuted to the full extent of U.S. Federal and Massachusetts laws.

Index

[SYMBOL] [A] [B] [C] [D] [E] [F] [G] [H] [I] [J] [K] [L] [M] [N] [O] [P] [Q] [R] [S] [T] [U] [V] [W] [X] [Z]

kurtosis

URL <http://access.proquest.safaribooksonline.com/9780132429610/index>

User name: CSU San Diego

Book: Jitter, Noise, and Signal Integrity at High-Speed

No part of any chapter or book may be reproduced or transmitted in any form by any means without the prior written permission for reprints and excerpts from the publisher of the book or chapter. Redistribution or other use that violates the fair use privilege under U.S. copyright laws (see 17 USC107) or that otherwise violates these Terms of Service is strictly prohibited. Violators will be prosecuted to the full extent of U.S. Federal and Massachusetts laws.

Index

[SYMBOL] [A] [B] [C] [D] [E] [F] [G] [H] [I] [J] [K] [L] [M] [N] [O] [P] [Q] [R] [S] [T] [U] [V] [W] [X] [Z]

Laplace Transformation [See [LT \(Laplace Transformation\)](#).]

law of large numbers

linear system theory

 LTI properties

associative property

cascading property

commutative property

distributive property

 LTI systems

frequency-domain analysis

time-domain analysis

linear time-invariant (LTI) theory

 channel

 channel LTI modeling

 channel transfer functions

 generic channel models

 receiver

amplitude modulation for receiver driver voltage noise

amplitude modulation for receiver reference voltage noise

clock recovery

drivers

equalization

loss

 transmitter

digital data bits

drivers

equalization

jitter phase modulation

loss

noise amplitude modulation

link signaling

 loopback testing

 PLLs

 non-stimulus-based method, PLL testing

 receiver

advanced link signaling

internal jitter testing

nominal link signaling

receiver equalization
reference clock testing
stimulus-based method, PLL testing
testing

advanced link signaling

nominal link signaling

transmitter equalization

link system architecture

channel
channel material and characteristics
jitter budget
performance factors
receiver (Rx)
reference clock
subsystem architecture
transmitter
performance factors
subsystem architecture

link testing, JTF (Jitter Transfer Function)

loopback testing

LT (Laplace Transformation)

LTI (linear time-invariant)

channel
channel LTI modeling
channel transfer functions
generic channel models
receiver
amplitude modulation for receiver driver voltage noise
amplitude modulation for receiver reference voltage noise
clock recovery
drivers
equalization
loss
transmitter
digital data bits
drivers
equalization
jitter phase modulation
loss
noise amplitude modulation

LTI properties

associative property
cascading property
commutative property
distributive property

LTI systems

frequency-domain analysis
output autocorrelation function
output PSD
PSD (power spectrum density)
statistical estimators
autocorrelation function
mean
square-mean
time-domain analysis

User name: CSU San Diego

Book: Jitter, Noise, and Signal Integrity at High-Speed

No part of any chapter or book may be reproduced or transmitted in any form by any means without the prior written permission for reprints and excerpts from the publisher of the book or chapter. Redistribution or other use that violates the fair use privilege under U.S. copyright laws (see 17 USC107) or that otherwise violates these Terms of Service is strictly prohibited. Violators will be prosecuted to the full extent of U.S. Federal and Massachusetts laws.

Index

[SYMBOL] [A] [B] [C] [D] [E] [F] [G] [H] [I] [J] [K] [L] [M] [N] [O] [P] [Q] [R] [S] [T] [U] [V] [W] [X] [Z]

magnitude responses, PLLs

mean

statistical estimators, for LTI systems

medium [See [channel](#).]

models

DDJ (data-dependent jitter)

first-order analytical model

generic channel models

second-order analytical model

moderately damped PLLs

moments, statistical estimates

Monte Carlo simulations, tailfit method

PDF with statistical noise

results

multidimensional CDF

multidimensional PDF (Probability Density Function), distribution (random variables)

multiple-Gaussian (MG)

URL <http://access.proquest.safaribooksonline.com/9780132429610/index>

User name: CSU San Diego

Book: Jitter, Noise, and Signal Integrity at High-Speed

No part of any chapter or book may be reproduced or transmitted in any form by any means without the prior written permission for reprints and excerpts from the publisher of the book or chapter. Redistribution or other use that violates the fair use privilege under U.S. copyright laws (see 17 USC107) or that otherwise violates these Terms of Service is strictly prohibited. Violators will be prosecuted to the full extent of U.S. Federal and Massachusetts laws.

Index

[SYMBOL] [A] [B] [C] [D] [E] [F] [G] [H] [I] [J] [K] [L] [M] [N] [O] [P] [Q] [R] [S] [T] [U] [V] [W] [X] [Z]

NEXT

noise [See also [amplitude noise](#).]

- BER and 2nd
- components
- defined
- historical overview of
- intrinsic noise
 - flick noise*
 - shot noise*
 - thermal noise*
- overall amplitude noise PDF
 - convolution*
 - eye diagrams*
- periodic noise
- phase noise
- sources of
 - intrinsic noise*
 - nonintrinsic noise*
- translating to timing jitter

noise analysis

- PLLs
- phase jitter PSD
- variance and PSD

nominal link signaling

- receiver testing
- testing

nominal serial link signaling, transmitter testing

nonintrinsic jitter

nonintrinsic noise

- crosstalk
- copper-based crosstalk
- fiber-based crosstalk
 - DCD (duty cycle distortion)*
 - ISI (intersymbol interference)*

User name: CSU San Diego

Book: Jitter, Noise, and Signal Integrity at High-Speed

No part of any chapter or book may be reproduced or transmitted in any form by any means without the prior written permission for reprints and excerpts from the publisher of the book or chapter. Redistribution or other use that violates the fair use privilege under U.S. copyright laws (see 17 USC107) or that otherwise violates these Terms of Service is strictly prohibited. Violators will be prosecuted to the full extent of U.S. Federal and Massachusetts laws.

Index

[SYMBOL] [A] [B] [C] [D] [E] [F] [G] [H] [I] [J] [K] [L] [M] [N] [O] [P] [Q] [R] [S] [T] [U] [V] [W] [X] [Z]

observables, direct observables (jitter separation)

optical crosstalk, channels

optical fiber-based channels

chromatic dispersion

polarization mode dispersion

optical reflection, channels

output autocorrelation function, LTI systems

output PSD, LTI systems

overall jitter PDF

overdamped PLLs

parametric analysis

URL <http://access.proquest.safaribooksonline.com/9780132429610/index>

User name: CSU San Diego

Book: Jitter, Noise, and Signal Integrity at High-Speed

No part of any chapter or book may be reproduced or transmitted in any form by any means without the prior written permission for reprints and excerpts from the publisher of the book or chapter. Redistribution or other use that violates the fair use privilege under U.S. copyright laws (see 17 USC107) or that otherwise violates these Terms of Service is strictly prohibited. Violators will be prosecuted to the full extent of U.S. Federal and Massachusetts laws.

Index

[SYMBOL] [A] [B] [C] [D] [E] [F] [G] [H] [I] [J] [K] [L] [M] [N] [O] [P] [Q] [R] [S] [T] [U] [V] [W] [X] [Z]

parametric analysis

moderately damped PLLs

overdamped PLLs

PLLs

underdamped PLLs

pattern generator (PG)

PDF (Probability Density Function)

amplitude noise PDF

convolution

eye diagrams

BER CDF variation

generic two-dimensional PDFs

jitter separation

for BUJ

versus CDF

convolution for

Distribution, random variables 2nd

DJ PDF determination through deconvolution

tailfit method [See **tailfit method**.]

overall jitter PDF

eye diagrams

f^{-2} jitter

for Gaussian jitter

independent variables

jitter

multidimensional PDF

for multiple PJs (periodic jitter)

for single PJ (periodic jitter)

statistical random processes

sum of two statistical variables

TJ PDFs

total jitter PDF, straightforward dual-Dirac method

for two PJs (periodic jitter)

peak-to-peak estimations

peak-to-peak value

performance factors

receiver (Rx)

transmitter

period jitter**periodic jitter (PJ) 2nd**

- PDF for multiple PJs
- PDF for single PJ
- PDF for two PJs
- spectrum for multiple PJs
- spectrum for single PJ
- spectrum for two PJs

periodic noise and jitter**PG (pattern generator)****phase interpolator (PI)****phase jitter**

- from phase noise conversion
- to phase noise conversion

phase jitter PSD, PLLs

phase-locked loops [See **PLLs (phase-locked loops)**.]

phase modulation (PM)**phase noise**

- from phase jitter conversion
- to phase jitter conversion

phase responses, PLLs**PI (phase interpolator)****PJ (periodic jitter) 2nd**

- PDF for multiple PJs
- PDF for single PJ
- PDF for two PJs
- spectrum for multiple PJs
- spectrum for single PJ
- spectrum for two PJs

PJ separation

- Fourier spectrum
- PSD
- time-domain variance function

PLLs (phase-locked loops) 2nd

- bode plots
- comparison with conventional PLL analysis methods
- frequency-domain modeling
- functional analysis
- impulse/step responses

phase and magnitude responses

poles and zeros

jitter

variance and PSD

moderately damped PLL

noise analysis

phase jitter PSD

variance and PSD

overdamped PLLs

parametric analysis 2nd

overview

phase jitter PSD

second-order analysis

characteristic parameters

jitter and transfer function analysis

system transfer function

testing

non-stimulus-based method

stimulus-based method

third-order PLL analysis

characteristic parameters
jitter and transfer function analysis
system transfer function
time-domain modeling
underdamped PLLs, parametric analysis

PM (phase modulation)

PMD (polarization mode dispersion)

optical fiber-based channels

poles, PLLs

power spectrum density (PSD)

BUJ separation
DDJ separation
 f^{-2} jitter
for Gaussian jitter
jitter
LTI systems
output autocorrelation function
output PSD
PJ separation
RJ spectrum
statistical random processes
variance, PLLs jitter and noise analysis
Wiener-Kinchine theorem

probability

conditional probability
joint probability
random variables
statistical independence

properties

associative property
cascading property
commutative property
distributive property
LTI properties

PSD (power spectrum density)

BUJ separation
DDJ separation
 f^{-2} jitter
for Gaussian jitter
jitter
LTI systems
output autocorrelation function
output PSD
PJ separation
RJ spectrum
statistical random processes
variance, PLLs jitter and noise analysis
Wiener-Kinchine theorem

PWS (pulse width shrinkage)

averaged PWS and DDJ
defined
estimation

User name: CSU San Diego

Book: Jitter, Noise, and Signal Integrity at High-Speed

No part of any chapter or book may be reproduced or transmitted in any form by any means without the prior written permission for reprints and excerpts from the publisher of the book or chapter. Redistribution or other use that violates the fair use privilege under U.S. copyright laws (see 17 USC107) or that otherwise violates these Terms of Service is strictly prohibited. Violators will be prosecuted to the full extent of U.S. Federal and Massachusetts laws.

Index

[SYMBOL] [A] [B] [C] [D] [E] [F] [G] [H] [I] [J] [K] [L] [M] [N] [O] [P] [Q] [R] [S] [T] [U] [V] [W] [X] [Z]

Q-factor

BER

DJ PDF estimation

URL <http://access.proquest.safaribooksonline.com/9780132429610/index>

User name: CSU San Diego

Book: Jitter, Noise, and Signal Integrity at High-Speed

No part of any chapter or book may be reproduced or transmitted in any form by any means without the prior written permission for reprints and excerpts from the publisher of the book or chapter. Redistribution or other use that violates the fair use privilege under U.S. copyright laws (see 17 USC107) or that otherwise violates these Terms of Service is strictly prohibited. Violators will be prosecuted to the full extent of U.S. Federal and Massachusetts laws.

Index

[SYMBOL] [A] [B] [C] [D] [E] [F] [G] [H] [I] [J] [K] [L] [M] [N] [O] [P] [Q] [R] [S] [T] [U] [V] [W] [X] [Z]

radio frequency (RF) 2nd

random Gaussian jitter (RGJ)

random Gaussian noise (RGN)

random high-order jitter (RHJ)

random higher-order noise (RHN)

random jitter (RJ) 2nd

f^{-2} jitter

PDF

PSD

Gaussian jitter

PDF

PSD

random noise (RN)

random processes

relationships between

statistical estimators for

statistical random processes

CDF

ergodic random processes

PDF

single power and power spectrum density (PSD)

SSS (strict-sense stationary)

WSS (wide-sense stationary)

random variables

continuous variables

discrete variables

distribution functions

CDF (Cumulative Distribution Function)

CDF versus PDF

multidimensional PDF (Probability Density Function)

PDF (Probability Density Function)

probability and

conditional probability

joint probability

statistical independence

RC LTI systems, DDJ estimation

receiver

LTI

amplitude modulation for receiver driver voltage noise
amplitude modulation for receiver reference voltage noise
receiver clock recovery
receiver drivers
receiver equalization
receiver loss
testing

receiver (Rx), testing

- advanced link signaling
- internal jitter testing
- nominal link signaling

receiver (Rx) (link system architecture)

- performance factors
- subsystem architecture

receiver clock recovery, LTI

receiver drivers, LTI

receiver equalization

- link signaling
- LTI
- testing

receiver loss, LTI

reducing EMI, reference clock

reference clock

- testing

reference transmitters, channel testing

references

reflection

- channels
- electrical reflection
- optical reflection

reflection coefficient, channel transfer functions

relationships between random processes

RF (radio frequency) 2nd

RGJ (random Gaussian jitter)

RGN (random Gaussian noise)

RHJ (random high-order jitter)

RHN (random higher-order noise)

RJ (random jitter) 2nd

- f^{-2} jitter
- PDF
- PSD

- Gaussian jitter
- PDF
- PSD

RJ (random jitter) separation

- Fourier spectrum
- PSD
- time-domain variance function

RMS (root-mean-square)

RN (random noise)

RSS, jitter budgets

URL <http://access.proquest.safaribooksonline.com/9780132429610/index>

User name: CSU San Diego

Book: Jitter, Noise, and Signal Integrity at High-Speed

No part of any chapter or book may be reproduced or transmitted in any form by any means without the prior written permission for reprints and excerpts from the publisher of the book or chapter. Redistribution or other use that violates the fair use privilege under U.S. copyright laws (see 17 USC107) or that otherwise violates these Terms of Service is strictly prohibited. Violators will be prosecuted to the full extent of U.S. Federal and Massachusetts laws.

Index

[SYMBOL] [A] [B] [C] [D] [E] [F] [G] [H] [I] [J] [K] [L] [M] [N] [O] [P] [Q] [R] [S] [T] [U] [V] [W] [X] [Z]

s-parameter-based channel testing

s-parameters, channel transfer functions (LTI)

SA (spectrum analyzer) 2nd

sampling

central limiting theory

sample estimators and convergence

SBS (stimulated Brillouin scattering)

second-order analytical model, generic channel models

second-order PLL analysis

characteristic parameters

jitter and transfer function analysis

system transfer function

separation

ISI separation, from DDJ

jitter separation [See [jitter separation](#).]

RJ (random jitter) separation

Fourier spectrum

PSD

time-domain variance function

serial data communication, jitter transfer function

SG (single-Gaussian)

Shannon, Claude

shot noise

signal integrity

historical overview of

signal-to-noise-ratio (SNR)

signaling

advanced serial link signaling, transmitter testing

nominal serial link signaling, transmitter testing

simulations

DDJ (data-dependent jitter)

jitter and transfer function analysis, third-order PLL analysis

single-Gaussian (SG)

single power, statistical random processes

skewness

skin effect, copper-based channels

slicers

SNR (signal-to-noise-ratio)

sources

- of jitter
 - intrinsic jitter*
 - nonintrinsic jitter*
- of noise
 - intrinsic noise*
 - nonintrinsic noise*

spectral analysis

- CDF
- PDF

spectrum

- for BUJ
 - direct FT spectrum, jitter as a function of frequency
 - Fourier spectrum
- for multiple PJs (periodic jitter)
- PJ, RJ, and BUJ spectrum
- for single PJ (periodic jitter)
- for two PJs (periodic jitter)

spectrum analyzer (SA) 2nd**square-mean, statistical estimators for LTI systems****SRS (stimulated Raman scattering)****SSS (strict-sense stationary)****standard deviation****static timing reference****statistical domain, jitter separation****statistical estimates**

- Chebyshev Inequality
- correlation
- expectation or average
- moments
- variance

statistical estimators

- LTI systems
 - autocorrelation function*
 - mean*
 - square-mean*
- for random processes
 - statistical independence, random variables

statistical noise, PDFs (Monte Carlo simulations)**statistical random processes**

- CDF
- ergodic random processes
- PDF
 - single power and power spectrum density (PSD)
 - SSS (strict-sense stationary)
 - WSS (wide-sense stationary)

statistical variables, PDF (sum of)**step responses, PLLs****stimulated Brillouin scattering (SBS)****stimulated Raman scattering (SRS)****straightforward dual-Dirac method, jitter separation**

- accuracy
- BER CDF
- total jitter PDF

strict-sense stationary (SSS) random process**subsystem architecture**

- receiver (Rx)
- transmitter

synchronized systems, clock jitter

system transfer function

second-order PLL analysis

third-order PLL analysis

URL <http://access.proquest.safaribooksonline.com/9780132429610/index>

User name: CSU San Diego

Book: Jitter, Noise, and Signal Integrity at High-Speed

No part of any chapter or book may be reproduced or transmitted in any form by any means without the prior written permission for reprints and excerpts from the publisher of the book or chapter. Redistribution or other use that violates the fair use privilege under U.S. copyright laws (see 17 USC107) or that otherwise violates these Terms of Service is strictly prohibited. Violators will be prosecuted to the full extent of U.S. Federal and Massachusetts laws.

Index

[SYMBOL] [A] [B] [C] [D] [E] [F] [G] [H] [I] [J] [K] [L] [M] [N] [O] [P] [Q] [R] [S] [T] [U] [V] [W] [X] [Z]

tail PDF identification

tailfit method

BER CDF

implementation algorithm

tail PDF identification

tailfitting

Monte Carlo simulations

PDF with statistical noise

results

theory for total jitter PDF

"transformed" BER CDF

tailfitting

taps

testing

channels

reference transmitters

s-parameter-based channel testing

link signaling

advanced link signaling

nominal link signaling

loopback testing

PLLs

non-stimulus-based method

stimulus-based method

receiver

advanced link signaling

internal jitter testing

nominal link signaling

receiver equalization

reference clock testing

transmitter equalization

transmitter output testing

advanced serial link signaling

nominal serial link signaling

thermal noise

third-order PLL analysis

characteristic parameters

jitter and transfer function analysis

- system transfer function
- TIA (time interval analyzer)**
- time and frequency domain jitter separation methods, comparing
- time domain, interrelationships (cycle-to-cycle jitter)
- time-domain analysis, LTI systems
- time-domain measurements, jitter
- time-domain modeling, PLLs
- time-domain variance function-based methodology, PLLs
- time-domain variance functions**
 - BUJ separation
 - PJ separation
 - RJ spectrum
- time-frequency domain jitter separation**
 - jitter as a function of frequency
 - direct FT spectrum*
 - jitter PSD*
 - jitter as a function of time
- time interval analyzer (TIA)**
- timing deviation**
- timing jitter [See [jitter](#).]**
- TJ, BER (comparing)**
- TJ estimation, BER CDF**
- TJ PDF**
- TN (total noise)**
- total jitter PDF**
 - implementation algorithm
 - tail PDF identification*
 - tailfitting*
 - straightforward dual-Dirac method
 - theory for
- total noise (TN)**
- transfer function analysis, second-order PLL analysis**
- "transformed" BER CDF, jitter separation (tailfit method)
- translation of noise to timing jitter**
- transmitter**
 - LTI
 - transmitter digital data bits
 - transmitter drivers
 - transmitter equalization
 - transmitter jitter phase modulation
 - transmitter loss
 - transmitter noise amplitude modulation
- transmitter (link system architecture)**
 - performance factors
 - subsystem architecture
- transmitter digital data bits, LTI**
- transmitter drivers, LTI**
- transmitter equalization**
 - link signaling
 - LTI
 - testing
- transmitter jitter phase modulation, LTI**
- transmitter loss, LTI**
- transmitter noise amplitude modulation, LTI**
- transmitter output testing**
 - advanced serial link signaling
 - nominal serial link signaling
- triangular DJ PDF, deconvolution simulations**
- two-dimensional (2-D) Gaussian distribution**

URL <http://access.proquest.safaribooksonline.com/9780132429610/index>

User name: CSU San Diego

Book: Jitter, Noise, and Signal Integrity at High-Speed

No part of any chapter or book may be reproduced or transmitted in any form by any means without the prior written permission for reprints and excerpts from the publisher of the book or chapter. Redistribution or other use that violates the fair use privilege under U.S. copyright laws (see 17 USC107) or that otherwise violates these Terms of Service is strictly prohibited. Violators will be prosecuted to the full extent of U.S. Federal and Massachusetts laws.

Index

[SYMBOL] [A] [B] [C] [D] [E] [F] [G] [H] [I] [J] [K] [L] [M] [N] [O] [P] [Q] [R] [S] [T] [U] [V] [W] [X] [Z]

underdamped PLLs, parametric analysis

unit step responses, channel transfer functions (LTI)

URL <http://access.proquest.safaribooksonline.com/9780132429610/Index>

User name: CSU San Diego

Book: Jitter, Noise, and Signal Integrity at High-Speed

No part of any chapter or book may be reproduced or transmitted in any form by any means without the prior written permission for reprints and excerpts from the publisher of the book or chapter. Redistribution or other use that violates the fair use privilege under U.S. copyright laws (see 17 USC107) or that otherwise violates these Terms of Service is strictly prohibited. Violators will be prosecuted to the full extent of U.S. Federal and Massachusetts laws.

Index

[SYMBOL] [A] [B] [C] [D] [E] [F] [G] [H] [I] [J] [K] [L] [M] [N] [O] [P] [Q] [R] [S] [T] [U] [V] [W] [X] [Z]

variables

independent variables, PDF and CDF
random variables, probability and

variance, PSD

PLLs jitter and noise analysis
statistical estimates

variation error, BER CDF (DJ PDFs) 2nd

vector network analyzer (VNA)

verification, jitter and transfer function analysis (third-order PLL analysis)

VNA (vector network analyzer)

URL <http://access.proquest.safaribooksonline.com/9780132429610/index>

User name: CSU San Diego

Book: Jitter, Noise, and Signal Integrity at High-Speed

No part of any chapter or book may be reproduced or transmitted in any form by any means without the prior written permission for reprints and excerpts from the publisher of the book or chapter. Redistribution or other use that violates the fair use privilege under U.S. copyright laws (see 17 USC107) or that otherwise violates these Terms of Service is strictly prohibited. Violators will be prosecuted to the full extent of U.S. Federal and Massachusetts laws.

Index

[SYMBOL] [A] [B] [C] [D] [E] [F] [G] [H] [I] [J] [K] [L] [M] [N] [O] [P] [Q] [R] [S] [T] [U] [V] [W] [X] [Z]

wavelength division multiplexing (WDM)

WDM (wavelength division multiplexing)

wide-sense stationary (WSS) random process

Wiener-Kinchine theorem

WSS (wide-sense stationary)

URL <http://access.proquest.safaribooksonline.com/9780132429610/index>

User name: CSU San Diego

Book: Jitter, Noise, and Signal Integrity at High-Speed

No part of any chapter or book may be reproduced or transmitted in any form by any means without the prior written permission for reprints and excerpts from the publisher of the book or chapter. Redistribution or other use that violates the fair use privilege under U.S. copyright laws (see 17 USC107) or that otherwise violates these Terms of Service is strictly prohibited. Violators will be prosecuted to the full extent of U.S. Federal and Massachusetts laws.

Index

[SYMBOL] [A] [B] [C] [D] [E] [F] [G] [H] [I] [J] [K] [L] [M] [N] [O] [P] [Q] [R] [S] [T] [U] [V] [W] [X] [Z]

XPM (cross-phase modulation)

URL <http://access.proquest.safaribooksonline.com/9780132429610/index>

User name: CSU San Diego

Book: Jitter, Noise, and Signal Integrity at High-Speed

No part of any chapter or book may be reproduced or transmitted in any form by any means without the prior written permission for reprints and excerpts from the publisher of the book or chapter. Redistribution or other use that violates the fair use privilege under U.S. copyright laws (see 17 USC107) or that otherwise violates these Terms of Service is strictly prohibited. Violators will be prosecuted to the full extent of U.S. Federal and Massachusetts laws.

Index

[\[SYMBOL\]](#) [\[A\]](#) [\[B\]](#) [\[C\]](#) [\[D\]](#) [\[E\]](#) [\[F\]](#) [\[G\]](#) [\[H\]](#) [\[I\]](#) [\[J\]](#) [\[K\]](#) [\[L\]](#) [\[M\]](#) [\[N\]](#) [\[O\]](#) [\[P\]](#) [\[Q\]](#) [\[R\]](#) [\[S\]](#) [\[T\]](#) [\[U\]](#) [\[V\]](#) [\[W\]](#) [\[X\]](#) [\[Z\]](#)

[zeros, PLLs](#)

URL <http://access.proquest.safaribooksonline.com/9780132429610/index>